Development of reverse *N*-substituted fosmidomycin analogs as *P. falciparum* 1-deoxy-D-xylulose 5-phosphate reductoisomerase inhibitors

Inaugural dissertation

for the attainment of the title of doctor
in the Faculty of Mathematics and Natural Sciences
at the Heinrich Heine University Düsseldorf

presented by

Mona Mahmoud

From Egypt

Düsseldorf, 2024

Published by permission of the Faculty of Mathematics and Natural Sciences

at Heinrich Heine University Düsseldorf

Supervisor: Prof. Dr. Thomas Kurz

Co-supervisor: Prof. Dr. Holger Gohlke

Date of the oral examination: 12.04.2024

Printed with the support of the German Academic Exchange Service (DAAD)

Affidavit

I declare under oath that I have produced my thesis independently and without any undue assistance from third parties considering the “Principles for the Safeguarding of Good Scientific Practice” at Heinrich Heine University Düsseldorf. The presented dissertation has not been submitted to another faculty. So far, I have not attempted to earn a doctoral degree (neither successfully nor unsuccessfully).

Düsseldorf,

Mona Mahmoud

The presented dissertation was conducted under the supervision of Prof. Dr. Thomas Kurz from April 2019 to March 2023 at the Institute for Pharmaceutical and Medicinal Chemistry, Heinrich Heine University Düsseldorf.

Acknowledgment

First of all, I want to thank God “Allah” for enlightening my path and introducing me to the best people who helped initiate and complete this work.

Words can never express my deepest gratitude and appreciation to Prof. Dr. Thomas Kurz for his continuous supervision, support, patience, motivation, and enthusiasm during my studies. His guidance helped me in all the research and writing of this thesis. I am grateful to you, Thomas, for providing me with the chance to work in your research team, without you, this work would never have come to light.

I am extending my sincere gratitude to Prof. Holger Gohlke for accepting my co-supervision and for our successful collaboration.

I want to thank the German Egyptian Research Long-Term Scholarship (GERLS) program, funded by the Egyptian Ministry of Higher Education and Scientific Research (MHESR) and the German Academic Exchange Service (DAAD), for funding my stay in Germany and for the financial support, which undoubtedly contributed to the completion of this work. Special thanks to Mrs. Iman Al-Rashdan for always being there trying to solve all my problems.

Let me take the opportunity to thank former and current research group members who supported me in completing my PhD. Alex, Beate, Chris, Fabian, Franzi, Hendric, Leandro, Marc, Olli, Petra, Saskia, Stefan, Talea, Vitalij, and Yodi. I owe you a massive debt of gratitude for creating such a nurturing environment of solidarity in the lab. I will always fondly remember our inspiring discussions about science and current affairs. Special thanks to Beate for her endless support from day one in Germany. Without your support, it would not be easy.

In addition, I would like to express my gratitude to Maria Beuer, Mohanad Aian, Prof. Dr. Klaus Schaper, Peter Behm, Dr. Peter Tommes, and Gabriele Zerta from HHU CeMSA (HHU Center of Molecular and Structural Analytics) and Elemental Analysis for performing the analyses of my compounds.

Many thanks to the group of Prof. Markus Fischer, particularly Dr. Boris Illarionov, for the hard work you have put into the biological evaluation of my compounds in the enzymatic assay against different DXR orthologs and your timely and ever-constructive feedback throughout our collaboration.

I am grateful to Dr. rer. nat Jana Held and Dr. Laís de Carvalho for screening my compounds against *P. falciparum* and our stimulating discussions.

Special thanks go to Prof. Nobutada Tanake and Sana Takada for conducting crystal structure studies on the *Pf*DXR enzyme.

I would like to express my deep gratitude to my research group at the National Research Center (NRC) in Egypt, especially to Prof. Dr. Hoda El-Diwani, for her invaluable support, without which I would not have reached this point.

Finally, I would like to thank my lovely husband, Alaa, for his continued love, support, encouragement, and understanding, which helped me finish this work. Also, special thanks go to my daughters, Lama and Lina; you have made me stronger, better, and more fulfilled than I could have imagined. I love you to the moon and back.

I am immensely grateful to my parents, sisters, brother, family, and friends, especially Sara Metry, for their dedication and support through good and bad times.

Table of contents

1. List of Abbreviation

Å	Angstrom
ACN	Acetonitrile
ACT	Artemisinin-based Combination Therapy
ADME	Absorption, Distribution, Metabolism, and Excretion
Bn	Benzyl
Boc	*tert*-Butoxycarbonyl
br	Broad
calcd.	Calculated
°C	Celsius
δ	Chemical Shift
CO_2	Carbon dioxide
conc.	Concentrated
CQ	Chloroquine
crt	Chloroquine-resistance transporter
cytB	Cytochrome b
d	Doublet
DCM	Dichloromethane
dd	Douplet of douplets
DDT	Dichlorodiphenyltrichloroethane
DHA	Dihydroartemisinin
dhfr	Dihydrofolate reductase
DIPEA	*N*,*N*-Diisopropylethylamine
DMEM	Dulbecco´s Modified Eagle´s Medium
DMF	*N*,*N*-Dimethylformamide
DMSO-*d6*	Deuterated dimethyl sulfoxide
DMSO	Dimethyl sulfoxide
DOXP	1-Deoxy-D-xylulose-5-phosphate
DTT	Dithiothreitol
DXR	1-Deoxy-D-xylulose-5-phosphate reductoisomerase
*Ec*DXR	Escherichia coli 1-deoxy-D-xylulose-5-phosphate reductoisomerase
ED	Electron-donation.
e.g.	Exempli gratia (Latin: for example)
ELISA	Enzyme-linked immunosorbent assay
Eq.	Equivalents
ESI	Electrospray ionization
ESI-MS	Electrospray ionization-Mass spectroscopy

Et	Ethyl
EtOAc	Ethyl acetate
et al.	Et alii (Latin: and others)
TEA	Triethylamine
EW	Electron-withdrawing
FV	Food Vacuole
g	Gram(s)
GlpT	Glycerol-3-phosphate Transporter
G6PD	Glucose-6-phosphate dehydrogenase
h	Hour(s)
HA	Hydroxamic acid
HATU	1-[Bis(dimethylamino)methylene]-1H-1,2,3-triazolo[4,5-b]pyridinium-3-oxide hexafluorophosphate
HEPES	4-(2-Hydroxyethyl)-1-piperazineethanesulfonic acid
HepG2	Human hepatocyte carcinoma cell line
hept	Heptet
HPLC	High-performance liquid chromatography
HRMS	High-resolution mass spectrometry
HRP2	Histidine-rich protein 2
HTS	High-throughput screening
Hz	Hertz
IC_{50}	Half maximal inhibitory concentration
In situ	Latin: in position
In vacuo	Latin: in a vacuum
In vitro	Latin: in glass
In vivo	Latin: within the living
IPP	Isopentenyl Diphosphate
J	Coupling constant (Hz)
K13	Kelsh 13
K_2CO_3	Potassium carbonate
$KMnO_4$	Potasium permenganate
Lb	Lysogeny Broth
m	Multiplet
M	Molar
MACS	Magnetic column separation
MDR	Multidrug-resistant
Me	Methyl
MeOD-*d4*	Deuterated methanol
MEP	2-C-methyl-D-erythritol-4-phosphate

mg	Milligram
µM	Micromole
min	Minute(s)
mL	Milliliter(s)
mM	Milimole
mmol	Millimole(s)
MMV	Medicines for Malaria Venture
$MnCl_2$	Manganese(II) chloride
MoA	Mechanism of action
mp.	Melting point
MS	Mass Spectrometry
Mtb	*Mycobacterium tuberculosis*
*Mtb*DXR	*Mycobacterium tuberculosis* 1-Deoxy-D-xylulose-5-phosphate reductoisomerase
MVA	Mevalonic acid
m/z	Mass to charge ratio
NaCl	Sodium chloride
NADPH	Nicotinamide Adenine Dinucleotide Phosphate (reduced form)
$NaHCO_3$	Sodium hydrogen carbonate
NaN_3	Sodium azide
NaOH	Sodium hydroxide
n-BuLi	*n*-Butyllithium
n.d.	Not determined
NHPI	*N*-hydroxyphthalimide
Ni^{+2}	Nickel
nM	Nanomole
NMP	Non-mevalonate Pathway
NMR	Nuclear magnetic resonance
p	Pentet
P. berghei	*Plasmodium berghei*
PCR	Polymerase Chain Reaction
P. cynomolgi	*Plasmodium cynomolgi*
PDB	Protein Data Bank
P. falciparum	*Plasmodium falciparum*
*Pf*3D7	Chloroquine-sensitive *P. falciparum* laboratory strains
PfATP4	*Plasmodium falciparum* ATPase 4
*Pf*Dd2	Multidrug-resistant *P. falciparum* laboratory strains
Pfdhfr	*P. falciparum* dihydrofolate reductase
Pfdhodh	*P. falciparum* pyrimidine biosynthetic enzyme

Pfdhps	*P. falciparum* dihydropteroate synthase
*Pf*DXR	*Plasmodium falciparum*-1-deoxy-D-xylulose-5-phosphate reductoisomerase
*Pf*EMP1	*P. falciparum* Erythrocyte Membrane Protein 1
PfPI4K	*Plasmodium falciparum* Phosphatidylinositol 4-Kinase
*Pf*mdr	*P. falciparum* multidrug resistance
Pgh	P-glycoprotein pump
pH	Potential hydrogen
Ph	Phenyl
P. knowlesi	*Plasmodium knowlesi*
Plasmodium spp	*Plasmodium* species
P. malariae	*Plasmodium malariae*
P. ovale	*Plasmodium ovale*
P.o. Curtis	*Plasmodium ovale Curtis*
P.o. wallikeri	*Plasmodium ovale wallikeri*
POM	Pivaloyloxymethyl
ppm	Parts Per Million
pREP4	Bacterial plasmid with p15A origin and lacI gene for regulating expression from pQE vectors
P. vivax	*Plasmodium vivax*
q	Quartet
quant.	Quantitative
RBCs	Red Blood Cells
RDT	Rapid diagnostic test
RPMI-1640	Roswell Park Memorial Institute
r.t.	Room temperature
s	Singlet
SAR	Structure-Activity Relationship
SDS-PAGE	Sodium dodecyl-sulfate polyacrylamide gel electrophoresis
SI	Selectivity index
S_{N2}	Nucleophilic substitution reaction
SP	Sulfadoxine-pyrimethamine
t	Triplet
TCP	Target Candidate Profiles
TES	Therapeutic efficacy studies
TFA	Trifluoroacetic acid
THF	Tetrahydrofuran
TLC	Thin Layer Chromatography
TMSBr	Trimethylsilyl bromide
TPP	Target Product Profiles

Tris hydrochloride	Tris (hydroxymethyl) aminomethane (THAM) hydrochloride
tt	Triplet of triplets
UV	Ultraviolet
WHO	World Health Organization

2. Introduction

2.1 Malaria

Infectious diseases are recognized to be one of the leading cause of death in third-world countries, especially among young children.[1] In these countries, malaria still poses a serious threat to human life and is considered one of the most severe and life-threatening diseases, threatening nearly half of the world's population (Figure 1). The World Malaria Report 2022 documented 247 million malaria cases worldwide, with 619,000 deaths.[2] In the same year, Africa alone carried the highest share of malaria burden, with 95% of all malaria cases. Furthermore, in areas of continuous malaria transmission, children under five years of age and pregnant women represent the highest morbidity and mortality rates.[2]

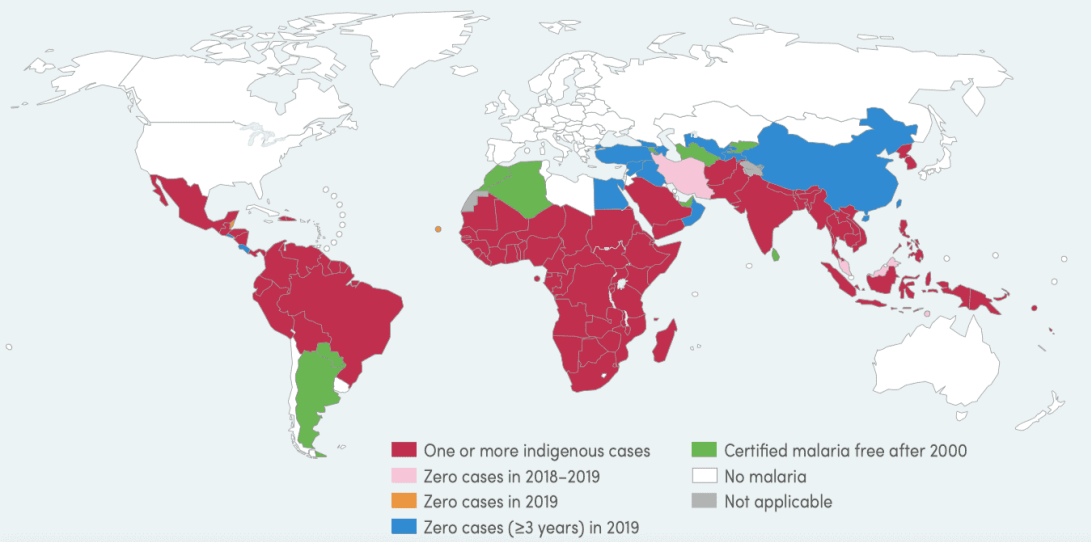

Figure 1: Malaria threats map 2021 WHO.[3]

2.1.1 The Parasite

Malaria is a life-threatening mosquito-borne disease caused by protozoan parasites of the genus *Plasmodium*. Six parasite species cause malaria in humans: (1) *Plasmodium falciparum*, which causes malaria tropica; (2) *Plasmodium malaria*, which causes malaria quartan; (3) *Plasmodium ovale*, which causes malaria tertian; (4) *Plasmodium vivax* which causes malaria tertian; (5) *Plasmodium knowles*; and (6) *Plasmodium cyonomolgi*.[4–11]

(1) P. falciparum: the most prevalent species in sub-Saharan Africa and can also be found in other malarious tropical areas worldwide. Most of the malaria-related morbidity and mortality are associated with *P. falciparum* infection. Approximately 1,200 African children <5 years of age died each day after *P. falciparum* infection. *P. falciparum* is commonly associated with severe malaria as well as complications related to malaria during pregnancy.[12,13]

(2) P. vivax: the second most significant species and accounts for most malaria cases in Southeast Asia and Latin America.[14,15] *P. vivax* can form hypnozoites (a dormant liver stage) in infected patients, leading to relapse of clinical symptoms months or years after initial infection.[14]

***(3) P. ovale*:** found in West Africa and Asia. Two genetically different sub-species exist, *P.o. Curtis* and *P.o. wallikeri*. *P. ovale* bears the added complication of a dormant liver stage, leading to clinical symptoms months or even years after the initial infection.[16]

***(4) P. malariae*:** can be found all over the world, but it is particularly common in West Africa. It represents only a small percentage of mild infections. However, chronic infection with *P. malariae* may result in splenomegaly or renal damage.[5,17]

***(5) P. knowlesi*:** was initially considered a parasite of non-human primates. However, it was discovered that it could cause malaria in humans, which leads to severe and fatal malaria complications. The reasons for the emergence and mode of transmission of *P. knowlesi* in humans remain unclear.[18–21]

(6) *P. cynomolgi*: is found throughout Southeast Asia, where it circulates among various macaque monkey species. *P. cynomolgi,* a simian malaria parasite, possesses biological and genetic characteristics similar to those of *P. vivax*. Although the infection of humans with *P. cynomolgi* was considered exceedingly rare, many natural human infections have been documented in recent years.[9–11]

Mixed infections between *Plasmodium* spp. were reported in people living in disease-endemic areas. For example, mixed disease between *P. falciparum* and *P. vivax* represents up to 10-30% of the cases in areas where both parasites are prevalent. Co-infections with other species, such as *P. ovale* and *P. malariae,* were also observed. These co-infections pose additional complications for parasite elimination.[22]

2.1.2 The *plasmodium* life cycle

Malaria is a hematoprotozoan parasitic infection caused by a unicellular eukaryotic organism that cannot survive outside host(s) and belongs to the Apicomplexa phylum.[23] Malaria has a complex life cycle that involves two hosts: humans, where asexual multiplication occurs, and female Anopheles mosquitoes, where sexual reproduction of the parasite occurs (Figure 2). A malaria-infected female *Anopheles* mosquito transmits the sporozoites of the *Plasmodium* spp. parasite to the bloodstream of malaria's next victim during a blood meal. These sporozoites rapidly invade liver cells, where they mature into schizonts, from which several thousand merozoites develop. Following this initial replication in the liver (exoerythrocytic schizogony), the infected liver cell bursts, releasing the merozoites into the bloodstream, where they undergo asexual multiplication in the erythrocytes (erythrocytic schizogony). Blood-stage parasites are responsible for the clinical symptoms of the disease, which develop 4-8 days after the initial invasion. Since the merozoite replication cycle within the red blood cells lasts 36-72 hours, frequent episodes of fever occur in time intervals of 36-72 hours when the infected red blood cells lyse, releasing endotoxins.[24–26] The trigger is unknown, but some merozoites differentiate into sexual male and female gametocytes. The male microgametocytes and female macrogametocytes are concentrated on skin capillaries and taken up by the mosquito during another blood meal. The process by which parasites multiply inside a mosquito is called the sporogonic cycle. In the mosquito's gut, the male and

female gametocytes fuse, generating diploid zygotes, which become motile and elongate into ookinetes. The ookinetes invade the midgut wall of the mosquito, where they develop into oocysts. Oocysts undergo cycles of meiotic division and form sporozoites, which move from the mosquito's abdomen to its salivary glands. Inoculating the sporozoites into a new human host perpetuates the malaria life cycle. In both *P. vivax* and *P. ovale* species of malaria, the invasion of red blood cells by the merozoites can be delayed for several months or even years after the initial infection. This delay can cause a relapse if the dormant form of the parasite, known as hypnozoites, is not effectively treated.[27,28]

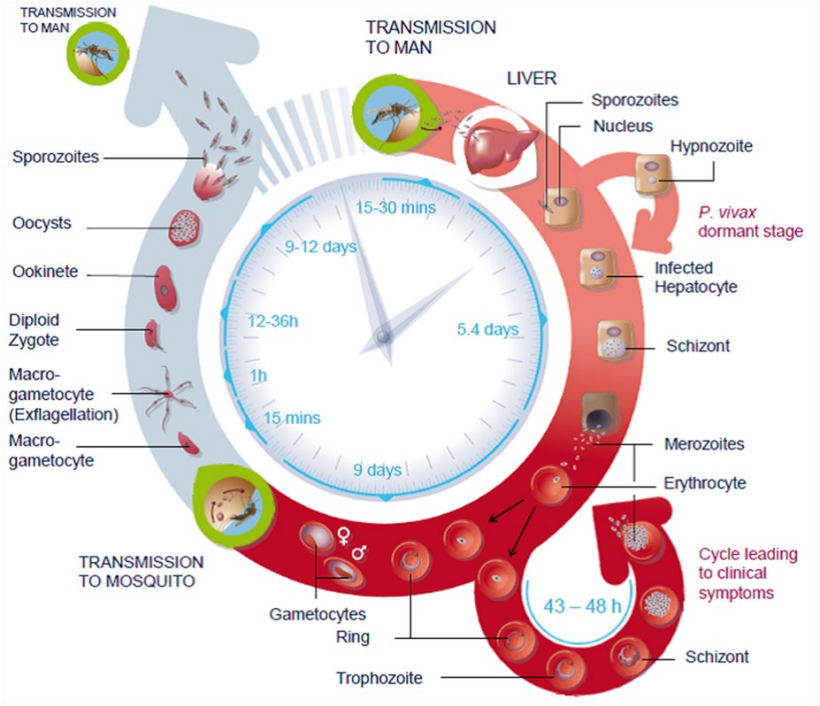

Figure 2: The *plasmodium* spp. Life cycle. (Medicines for Malaria Venture (MMV)).[27]

To evade immune system recognition, several *Plasmodium* species utilize variations on the surface of the infected red blood cells (RBCs).[29] After *P. falciparum* infection, overexpression of the var genes, which encode the erythrocyte membrane protein 1 (*PfEMP1*), occurs (Figure 3). *PfEMP*1 is thought to play a vital role in the virulence associated with *P. falciparum* infection. RBCs carrying *PfEMP*1 on their surface stick to capillary walls, facilitating further binding with uninfected cells, helping the parasite spread to other RBCs, and bringing about the fatal symptoms of *P. falciparum* malaria. In addition, infected RBCs are prevented from circulating through the spleen, where they would be subjected to host immune cell attack and removal from circulation.[30]

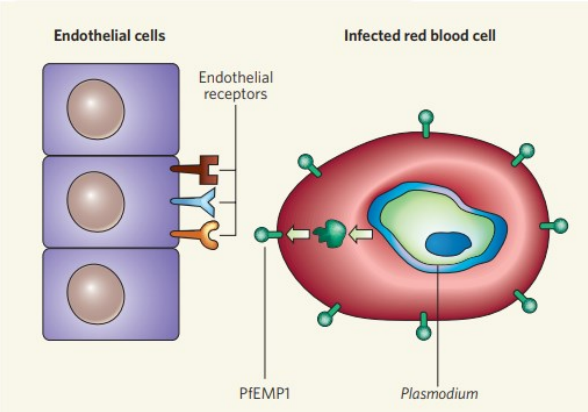

Figure 3: Red blood cell infected with *plasmodium falciparum* taken from BORST et al.[30] Reproduced with permission from Springer Nature, Nature 2006, 439 (7079), 926–927.

2.1.3 Clinical presentation

The clinical presentation of *Plasmodium spp.* infection can vary substantially depending on the species and host factors. The level of host protective immunity acquired through past parasite exposure can help decrease symptoms severity and reduce the risk of severe malaria.[31–33] Malaria infection can be categorized as uncomplicated or severe (complicated). Uncomplicated malaria infection is an acute febrile illness with typical initial symptoms, including high fever, chills, headache, myalgias, and arthralgias. In children, digestive symptoms like vomiting and diarrhea are usually common. These symptoms manifest suddenly after the hemolysis of invaded red blood cells. *P. falciparum* infections are the most likely to progress to severe (complicated infection) potentially fatal forms if not treated in 24 hours. Complicated malaria, though less frequent, can also be caused by *Plasmodium vivax* or *Plasmodium knowlesi* infections. Severe infection is characterized by severe anemia and various multi-organ damage manifestations, including cerebral malaria, neurological abnormalities, acute renal failure, or acute respiratory distress. Severe malaria complications are due to capillaries' obstruction caused by infected red blood cells.[28,34]

2.1.4 Diagnosis and prevention

2.1.4.1 Diagnosis

The WHO considers fever and the presence of parasites in the patient blood as diagnostic criteria for *Plasmodium* spp infection.[35] A microscopic examination of Giemsa-stained blood smears remains the gold standard for malaria infection diagnosis. However, parasite infection can also be identified by (1) Fluorescence microscopy of parasite nuclei stained with acridine orange,[36,37] (2) Rapid diagnostic test (RDT),[35] in which various test kits are used to detect malaria parasite antigens and (3) Polymerase chain reaction (PCR) based assay.[35,38]

2.1.4.2 Prevention

Preventing *Plasmodium* infection relies mainly on mosquito vector control and the development of effective vaccines.[35]

2.1.4.2.1 Mosquito (vector) control

Methods used to control malarial parasite vectors include the following:

1. The widespread use of insecticides against mosquitoes, such as dichlorodiphenyltrichloroethane (DDT), larvicides, and endectocides such as ivermectin.[39]
2. Using insecticide-impregnated bed nets to prevent parasite contact with humans. [39]
3. Disruption of mosquito breeding grounds.

2.1.4.2.2 Vaccines

An effective malaria vaccine would be an efficient tool to encounter the enormous socioeconomic burden caused by malaria. Unlike viruses and bacteria, *Plasmodium* spp is a large-genome microorganism with a very complex life cycle in which different sets of parasite antigens are exposed to the immune system during various stages of parasite invasion. Therefore, developing an effective malaria vaccine is very challenging.[40] However, the fact that adults living in high-transmission malarious areas could acquire partial protective immunity after frequent re-exposure "concomitant immunity" indicates that vaccination is possible.

Various malaria vaccine candidates were developed (Figure 4),[41–43] these vaccines target mainly three stages in the malaria parasite life cycle: (i) pre-erythrocytic stage (sporozoite/hepatic), (ii) erythrocytic stage (asexual), (iii) sexual stage (transmission-blocking). An ideal malaria vaccine would ultimately prevent the first stages of parasite development, blocking further stages from developing and preventing transmission.

On 6 October 2021, the WHO recommended RTS,S/AS01 (Mosquirix), a vaccine developed by GlaxoSmithKline (GSK), as the first approved malaria vaccine for preventing *P. falciparum* malaria in children aged between 6 weeks and 17 months living in regions with moderate to high transmission.[35,44] The RTS,S is a pre-erythrocytic vaccine designed to stimulate the immune system to prevent the parasite infection of liver cells, where it can multiply, reenter the bloodstream, and infect red blood cells, causing the disease symptoms. Data from the pilot studies showed that RTS,S/AS01 has a favorable safety profile and can significantly reduce severe, life-threatening malaria with 30-40% efficacy.[44,45]

R21/Matrix-M™ vaccine (R21/MM), manufactured by Oxford University, has shown high efficacy against malaria, with an initial clinical trial showing a 77% efficacy rate.[46] The R21/MM vaccine is the first to meet the WHO's goal of at least 75% efficacy against malaria.[47] Based on the efficacy and safety profile of the R21/MM vaccine in the phase IIb trials, in April 2023, Ghana's Food and Drugs Authority was the first to approve the R21 vaccine for young children. Following Ghana's decision, Nigeria has also approved the R21 vaccine. However, the safety and effectiveness of the R21/MM are still under assessment by the WHO for final approval.[43]

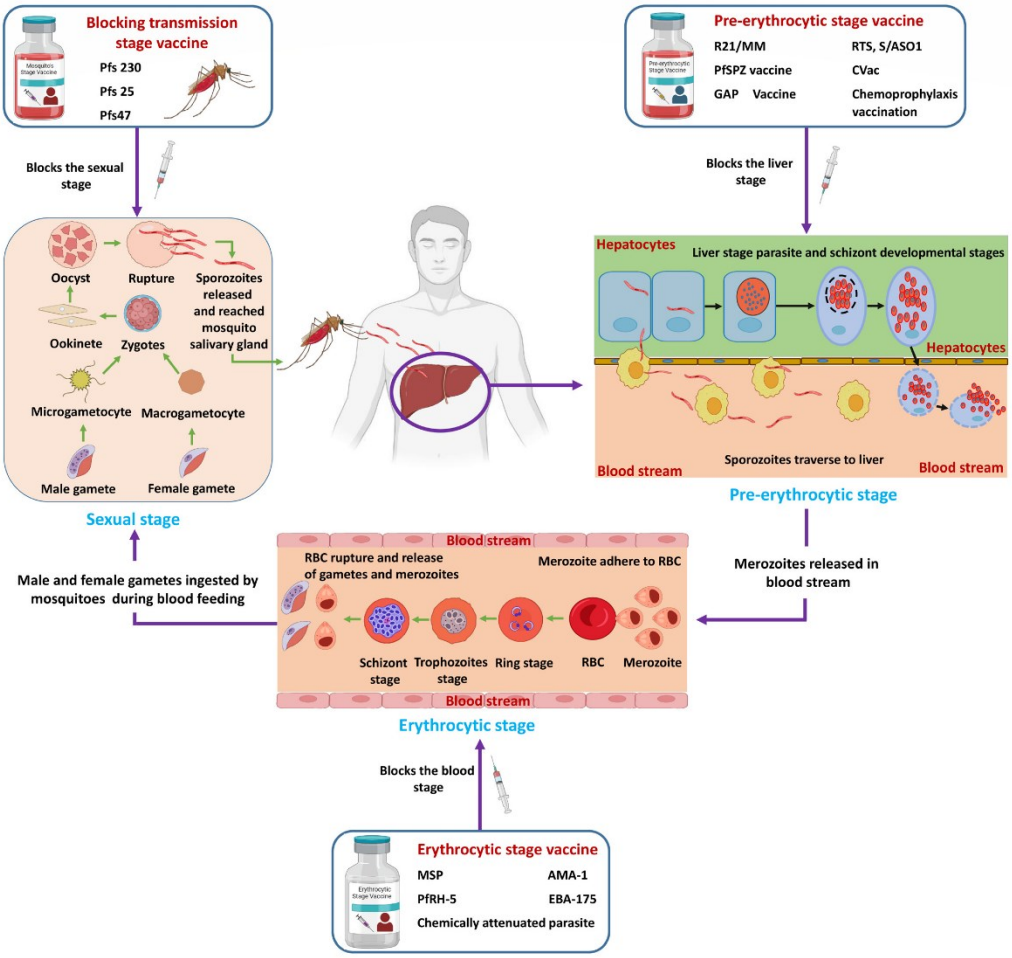

Figure 4: Current state and different stages of development of human malaria vaccines. Used without modifications from SIDDIQUI *et al.*[43]

2.1.5 Prophylaxis and treatment of malarial infection

2.1.5.1 Antimalarial drugs

Most currently used antimalarial drugs target the erythrocytic stage of malaria infection, which causes the symptoms. Antimalarial drugs are grouped into four main classes: quinoline derivatives, antifolate, artemisinin derivatives, and antimicrobials. Some of the well-known antimalarial chemical classes, their mode of action, and side effects are presented in Table 1.[34,48–50]

Table 1: Some well-known anti-malarial chemical classes.

Class	Category	Drug (Year of Development)	Therapeutic Use	Side Effect	Mechanism of action
Quinoline derivatives	Cinchona alkaloid	Quinine! (1820)	Treatment of *P. falciparum* infection and severe malaria, usually combined with other medications to shorten the course of treatment and minimize adverse effects.	Hypoglycemia, Cinchonism, and hypotension	These drugs interfere with hemoglobin digestion by accumulating in the *plasmodium* parasite's food vacuole (FV). Additionally, they prevent the subsequent polymerization of hem to non-toxic haemozoin by forming drug-haemozoin complexes and/or by adhering to the crystals' developing faces.[51]
	4-aminoquinoline	Chloroquine (1940)	non-falciparum malaria because of the emergence of chloroquine resistance *P. falciparum* strains.	Accumulate in retinal and melanin, resulting in rash, itching, hair loss, headache, and GIT disturbances.	
		Amodiaquine! (1948)	As a partner drug in ACT to treat some cases of chloroquine resistance *P. falciparum* strains.	Hepatitis and myelotoxicity. It was withdrawn from therapeutic use because of its side effects.	
		Piperaquine! (1960)	Resistance has diminished its usage as monotherapy. Used as partner drug with dihydroartemisinin in ACT.	Headache, dizziness, and GIT disturbances.	
	8-Aminoquinoline	Primaquine (1950)	Prophylaxis and radical cure of *P. vivax* and *P. ovale*. gametocytocidal for *P. falciparum.*	Hemolytic anemia in G6PD deficiency	
		Tafenoquine (1978)	Prophylaxis and radical cure of *P. vivax* and *P. ovale*. gametocytocidal for *P. falciparum.*	Hemolytic anemia in G6PD deficiency	
	Aryl aminoalcohol	Mefloquine*! (1970)	Prophylaxis and partner drug in ACT to treat *P. falciparum.* Its usage is limited because of the severe side effects.	Depression, psychosis, nightmares	
		Lumefantrine! (1976)	Combined with artemether in ACT.	Headache, anorexia, dizziness.	
		Halofantrine* (1980)	Due to its cardiotoxicity, its use has decreased over time. It is now only used to cure severe and resistant forms of malaria, but only in patients who are known to be free from heart disease.	Cardiac toxicity	

Table 1: Continued

Class	Category	Drug (Year of Development)	Therapeutic Use	Side Effect	Mechanism of action
Artemisinin	Sesquiterpene lactone endoperoxides	Artemether Artesunate Dihydroartemisinin	ACT; treatment of severe malaria, chloroquine resistant malaria, and complicated *P. falciparum*.	Have an excellent safety profile. Long-term use may cause nausea, vomiting, abdominal pain, itching, and fever.	The Endoperoxide bridge in its molecule appears to interact with heme iron in the parasite and generates oxygen radicals. The resulting free radical selectively binds to membrane proteins, causes lipid peroxidation, damages the endoplasmic reticulum, inhibits protein synthesis, and ultimately results in the lysis of the parasite.[52]
Antifolate	Diaminopyrimidine	Pyrimethamine*! (1950)	Used only in combination with other drugs for the treatment of falciparum malaria. Pyrimethamine use decreased due to resistance.	Nausea, rashes, megaloblastic anemia, and granulocytopenia	Block the folate biosynthetic pathway in the parasite.[53] Pyrimethamine and proguanil inhibit *dhfr* enzyme. Atovaquone: Interferes with electron flow in aerobic respiration, which results in the collapse of the mitochondrial membrane and, finally, cell apoptosis.[54,55]
	Sulfonamides	Sulfadoxine! (1960)	Sulfadoxine is no longer used alone as an antimalarial drug.	Exfoliative dermatitis, Stevens-Johnson syndrome. Because of its side effects	
	Biguanide	Proguanil! (1945)	Combined with artesunate as ACT for treatment of chloroquine-resistant parasite strains. Proguanil is combined with Atovaquone (1991) to treat *P. falciparum*	Alopecia, aphthous ulceration, nausea, and gastric irritation Atovaquone side effects: diarrhea, vomiting, GIT disturbances, headache, rashes, and fever.	
Antimicrobial	Tetracycline	Doxycycline! And tetracycline!	Slow-acting antimalarials combined with quinine to treat uncomplicated *P. falciparum* resistance to quinine. Doxycycline is used as chemoprophylaxis.	GIT disturbances.	Inhibit DNA replication and protein synthesis inside the apicoplast of *Plasmodium* species.[56]
	Lincisamide	Clindamycin!			

*Drugs rendered ineffective due to the development of resistant strains or the emergence of undesirable side effects.
! Drugs used only in combination with other agents.

2.1.5.2 Chemoprevention and chemoprophylaxis

2.1.5.2.1 Chemoprevention

Seasonal malaria chemoprevention campaigns are an effective strategy commonly used to reduce malaria in regions of a seasonal malaria epidemic.[35,57] The objective is to prevent malarial illness in children and pregnant women by intermittent administration of preventive treatment courses to maintain the antimalarial drug concentrations in the blood during the malaria season.[35,58] WHO recommends a combination of sulfadoxine, pyrimethamine, and amodiaquine as a chemopreventive combination in areas with highly seasonal malaria transmission. Also, a 3-day course of artemisinin-based combination (ACTs, dihydroartemisinin (DHA), and piperaquine) was found to be effective in preventing malaria in high-risk groups (Figure 5).[59,60]

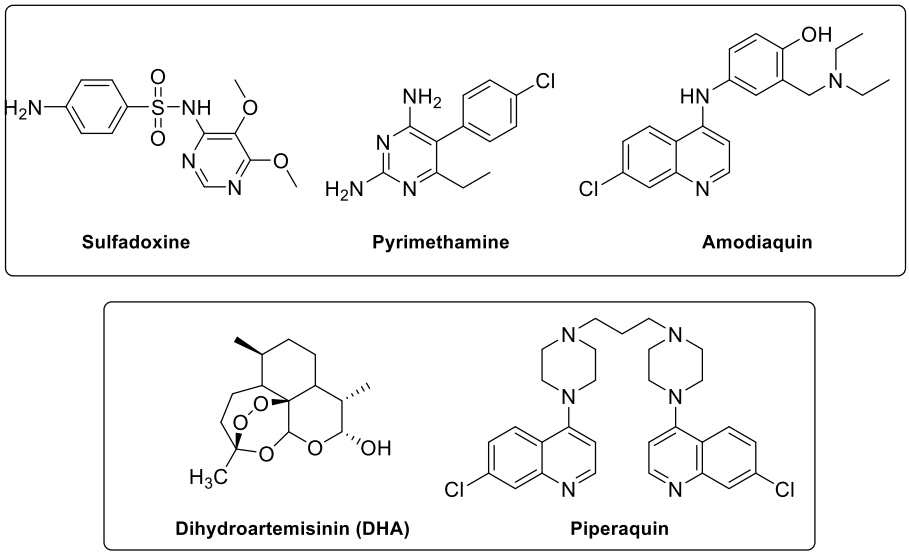

Figure 5: Structure of chemopreventive drugs.

2.1.5.2.2 Chemoprophylaxis

Chemoprophylaxis is an alternative strategy in which antimalaria medicines, given at prophylactic doses, are temporarily used to protect subjects entering an endemic area. In order to avoid the potential emergence of drug resistance, the WHO emphasizes, when possible, that drugs used for chemophylaxis or chemoprotection should differ from the first-line treatment used in the same region.[35,58] Also, the used drugs need an excellent safety profile as they are given to healthy people. The WHO recommends three 'gold-standard' drugs for chemoprotection: a daily dose of atovaquone-proguanil, doxycycline, and a weekly dose of mefloquine. [49,61] The Atovaquone/proguanil combination was first approved for medical use in the United States in 2000. Since 2011, it has been sold under the brand name Malarone®, among others, and is mainly used to prevent malaria.[62] Although it is not typically used to treat malaria, it is used in some countries to treat uncomplicated malaria infections. The use of mefloquine is now limited because it is associated with severe side effects. Moreover, mefloquine should be avoided in neuropsychiatric patients (Figure 6).[49]

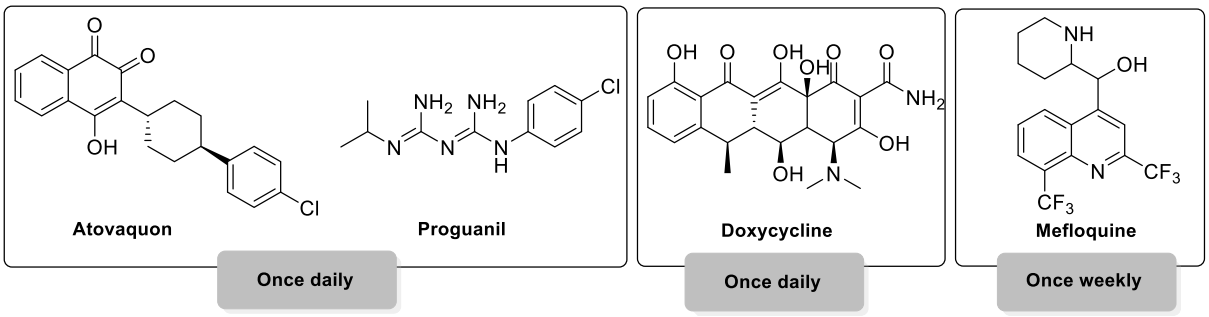

Figure 6: Structure of chemoprotective agents.

2.1.5.3 Treatment

Because of the sophistication within the life cycle of *Plasmodium* parasite, there is no single drug that can fully eradicate all species of malaria parasites or effectively treat the various manifestations of the disease that occur in different patient populations. Thus, a combination of drugs is frequently given simultaneously to efficiently combat malarial infection and to make resistance development difficult. Antimalarial dosing must be tailored to every condition based on the geographic location of the infection, the *Plasmodium* species, and the disease severity (Figure 7).[35,63] The drug choice is usually guided more by drug resistance frequencies than species differences. During pregnancy, the therapeutic options are limited to the drugs known to be safe for both the mother and the fetus, and different regimens are needed.

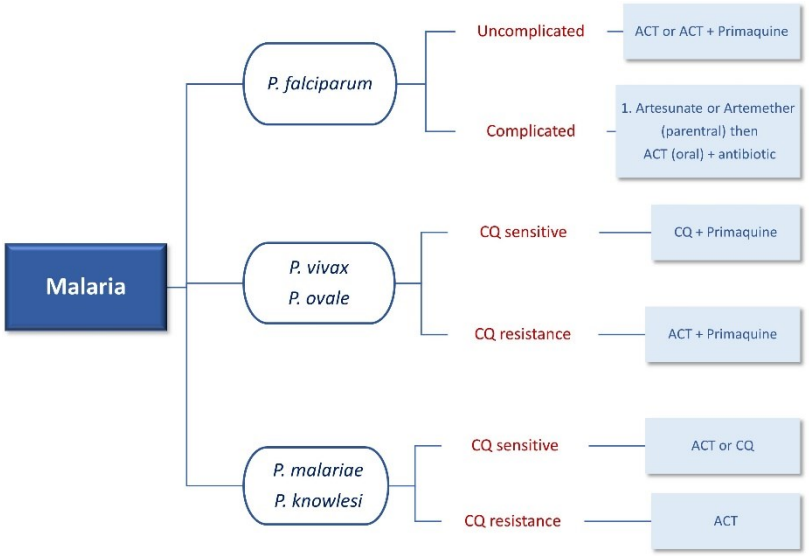

Figure 7: Malaria treatment options.

2.1.5.3.1 Treatment of uncomplicated malaria as recommended by the WHO

- Treatment of *P. falciparum* infections

The WHO recommends six different ACTs [64,65] (Figure 8) to treat uncomplicated *P. falciparum* infections.[35,66] Owing to its high lipophilicity, artemisinin itself could not be used in the approved combination. Instead, semisynthetic derivatives are used, namely, dihydroartemisinin (DHA), artesunate, or artemether. One of the most well-known combinations is artemether and lumefantrine, which is sold under different brand names, of

which Coartem® is the most recognized. Coartem® tablets came into medical use in 1992 and are indicated for treating acute uncomplicated *P. falciparum* infections not treatable with chloroquine.[67,68] The artesunate–pyronaridine combination (Pyramax®) is used for the treatment of uncomplicated *P. falciparum* and *P. vivax* infections when other combinations fail.[66] The combination is generally well tolerated; however, it is not recommended for patients suffering from severe liver or kidney diseases.[69] Also, Pyramax® is not generally recommended in early pregnancy.[69] Eurartesim® is the brand name of the piperaquine/dihydroartemisinin combination. Eurartesim® is used to treat uncomplicated *P. falciparum* and *P.vivax* malaria infections. The combination was approved in 2011 for medical use in Europe.[70] In addition to the ACTs, a single dose of primaquine should be added to the antimalarial regimen in low transmission areas to reduce infection transmission.[35,71]

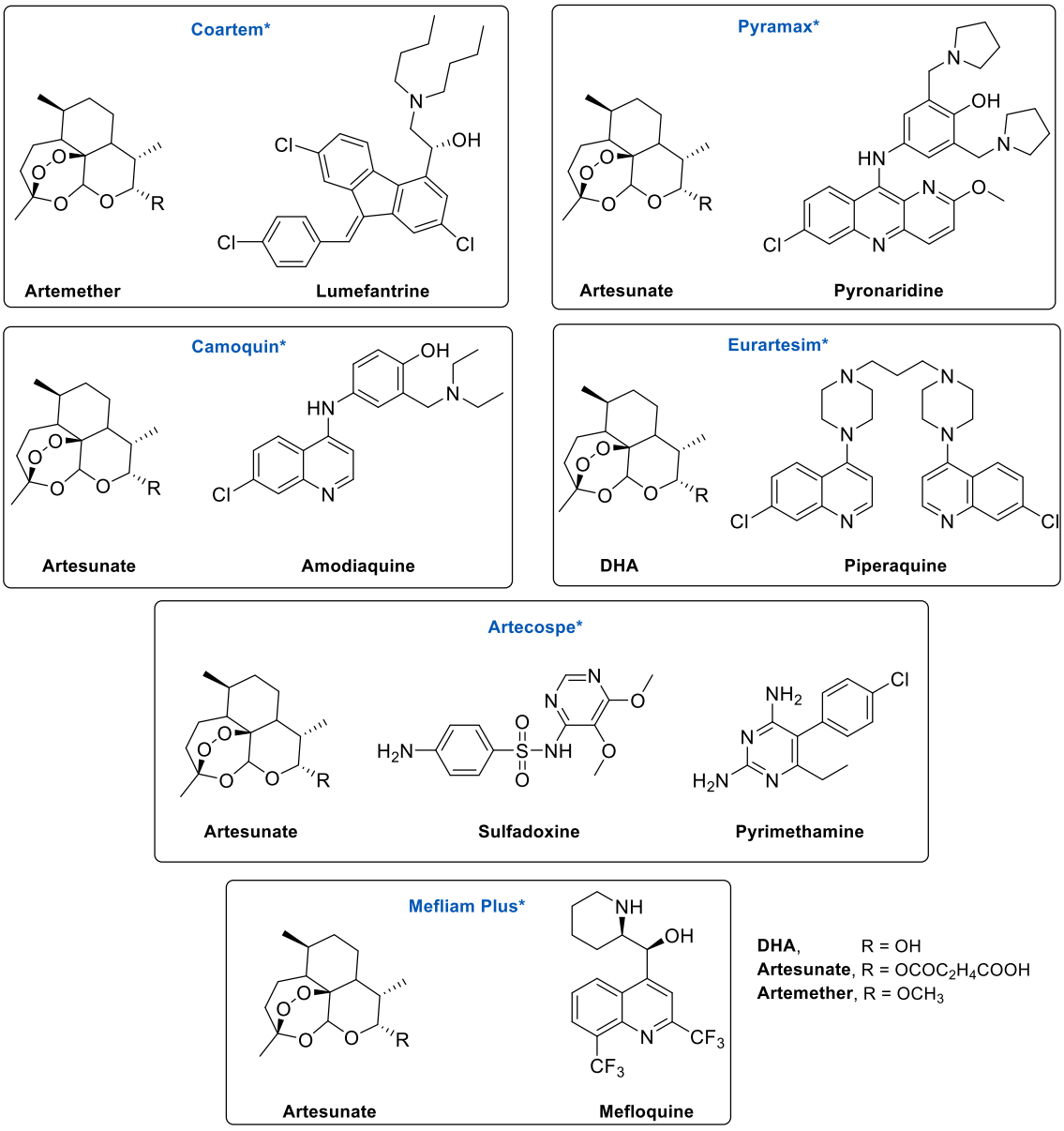

Figure 8: Artemisinin-based combination therapies (ACTs). Trade names are colored blue. * Other trade names are available.

- Treatment of *P. vivax* infections

Chloroquine (CQ) resistant *P. vivax* is becoming increasingly widespread, particularly in Asia. *P. vivax* infections in these areas should be treated with an ACT. Relapses of *P. vivax* malaria present a challenge in malaria control, so primaquine or tafenoquine is added to the treatment protocol to prevent relapses that could occur years after primary infection. However, the used primaquine dose and administration frequency should be guided by the patient's glucose-6-phosphate dehydrogenase (G6PD) enzyme activity to avoid complications. [35,71]

2.1.5.3.2 Treatment of severe malaria

In severe malaria, parenteral administration of an artemisinin derivative is used for at least 24 hours. When parenteral artesunate and artemether are unavailable, intramuscular quinine should be used. This is then followed by a complete 3-day course of an oral ACT once the patient can tolerate oral medicines. This combination is used to ensure a complete cure and prevent the development of resistance to the artemisinin derivatives. Children under six years of age with severe malaria should receive rectal artesunate if injectable treatment cannot be provided.[35,71]

2.1.6 Resistance to antimalarial drugs

Parasite resistance is the ability of the parasite to survive and multiply despite the administration of an adequate dose of appropriate treatment. Over the years, most antimalarial drugs have lost efficacy. Resistance against chloroquine (CQ), the mainstay of malaria chemotherapy for many years, is widely reported and has resulted in limiting its therapeutic efficacy.[48,72] Also, antifolates proved ineffective in many endemic areas. Declining clinical efficacy has also affected many other antimalarial drugs, including sulfadoxine-pyrimethamine (SP),[48,73,74] quinine, and mefloquine. Artemisinin and ACT partial resistance (defined as a prolonged time for parasite clearance from blood after an adequate dose administration) was recently confirmed.[75,76] Cross-resistance profiles between several treatment classes were reported as well.[77]

Present knowledge indicates that several genetic events are correlated with the molecular mechanisms that strengthen resistance to antimalarial drugs (Table 2).[71,78,79] These genetic alterations are mutations or changes in a copy number of genes encoding or relating to the drug's parasite target or influx/efflux pumps that affect the intraparasitic concentration of the drugs.[80] For example, resistance to aryl amino alcohols (e.g., mefloquine) in *P. falciparum* resulted from amplification in the *Pf*mdr (*Pf* multidrug resistance) gene, which encodes an ATP-dependent p-glycoprotein pump (*Pgh*) chargeable for the transport of hydrophobic substances.[81,82] In addition, single point mutations within the gene *cytB,* coding for cytochrome b, confer resistance to atovaquone [82,83] or the gene encoding dihydrofolate reductase (*dhfr*),[82] resulted in pyrimethamine resistance, were reported. In *P. falciparum*, a mutation in the *P. falciparum* dihydropteroate synthase (*Pfdhps*) and *P. falciparum* dihydropteroate reductase (*Pfdhfr*) genes is involved in the reduced drug susceptibility to sulfadoxine and pyrimethamine, respectively.[82,84,85] Whole-genome sequencing of the artemisinin-resistant parasite revealed mutation within the Kelch 13 (*K13*) propeller protein related to the artemisinin resistance in clinical and field isolates.[78,86]

Pre-prediction of the emergence and spread of resistance against current antimalarials and newly introduced compounds enable the research and medical communities to plan malaria control strategies that may delay the emergence of resistance. The worldwide database on antiprotozoal efficacy and resistance was initiated in 2000 to facilitate reporting on the status of antiprotozoal effectiveness in malaria-endemic countries. This database contains extracted information from reports of therapeutic efficacy studies (TES) and surveys of molecular markers on antiprotozoal resistance conducted by several research institutes and governmental and non-governmental organizations.[78]

Table 2: *P. falciparum* drug resistance markers

Drug	***P.falciparum* resistance marker**	**Protein function**
Artemisinin derivatives	*k13*, Kelch protein K13	Scaffold protein that may be involved in maintaining phosphatidylinositol-3-phosphate levels
Amodiaquine	*crt*,chloroquine-resistance transporter and *mdr1*	Drug metabolite transporter super-family of electrochemical potential-driven transporters
Mefloquine	*mdr1*	Drug metabolite transporter superfamily of electrochemical potential-driven transporters

2.1.7 The drug discovery and development pipeline

Considering the persistently high annual malaria deaths and the rapid emergence of resistance against almost all available antimalarial drugs, continuing efforts toward discovering a more efficient antimalarial chemotherapy is necessary.[78] In 1999, the most extensive, non-profitable, antimalarial discovery project, the Medicines for Malaria Venture (MMV), was established in Switzerland to partner with universities and pharmaceutical companies in the fight against malaria.[87] Figure 9 shows MMV's global portfolio of new antimalarial drugs, including the most promising candidates to be used in malaria therapy.[87] Promising compounds are identified mainly through four approaches: design of alternative analogs to available drugs, target-based screening, rational drug design, and phenotypic screening.[88]

To date, phenotypic screening is the most successful approach to delivering preclinical candidates. The potential for the identified compounds to act as new antimalarial drug candidates is defined by the MMV Target Product Profiles (TPP) and Target Candidate Profiles (TCP) to be (i) their novel modes of action, which enhances their ability to overcome known resistant mechanisms; (ii) being effective in a single dose against severe malaria;(iii) possess activity against multiple life cycle stages of *P. vivax* and *P. ovale* to prevent relapse; and (iv) have prophylactic activity, preventing initial infection by killing the sporozoites and exo-erythrocytic schizonts and blocking transmission either by targeting gametocytes or the insect vector (endectocides). The compounds should also pose good safety profile, especially for small children and pregnant women.[89–91]

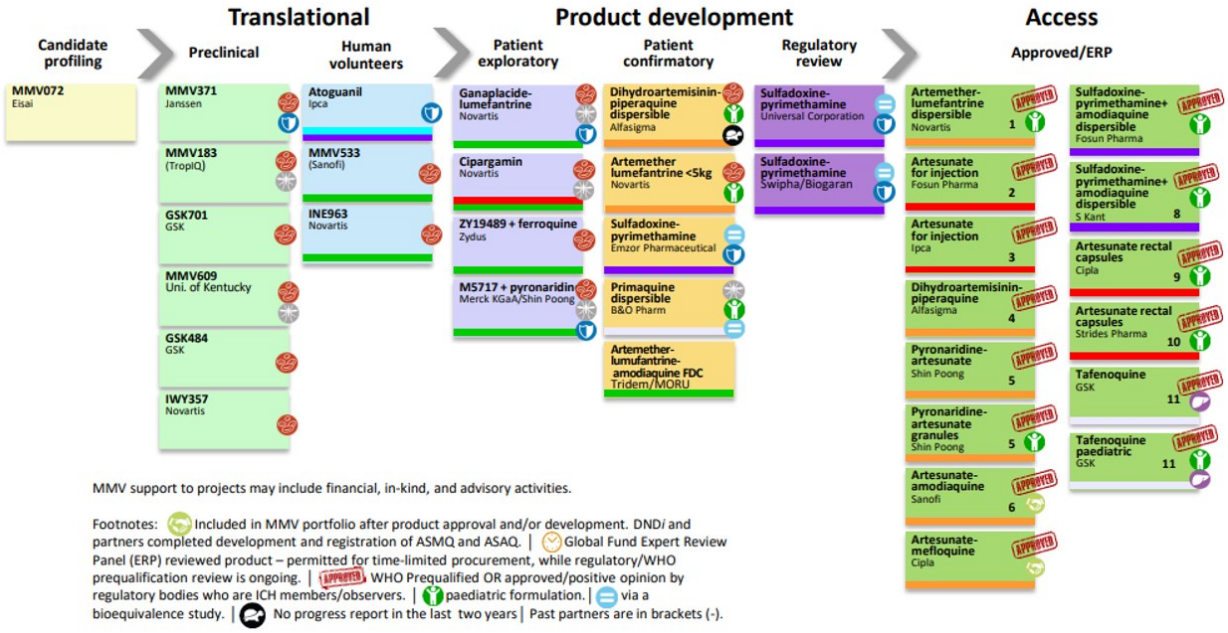

Figure 9: The global portfolio of new antimalarial medicines organized by (MMV, May 2022).[87]

As shown in Figure 9, several artemisinin derivatives were approved for the treatment of uncomplicated or severe *P. falciparum* infections, either alone or in combination with other known antimalarial drug classes. Also, in recent years, new candidates with a new mechanism of action have reached clinical trials either alone or in combination with other drugs (Figure 10). These substances include OZ439 (artefenomel),[92–97] KAF156 (Ganaplacide),[87,98–101] KAE609 (cipargamin),[87,102–105] DSM265,[87,106–109] MMV (390048),[110–112] SJ733,[87,113–115] P218,[87,116–118] and DDD107498 (DDD-498).[119]

OZ439 (artefenomel) is an orally active, fully synthetic peroxide that possesses fast-acting, curative, and transmission-blocking ability and is active against artemisinin-resistant *P. falciparum* parasites.[92,93] The precise mode of action (MoA) for OZ439 has yet to be discovered, but it's believed that oxidative stress plays a significant role. Artefenomel is investigated as a single-dose cure in combination with either DSM265, piperaquine, or ferroquine as a possible non-ACT combination.[94] Artefenomel with ferroquine, a new 4-aminoquinoline without cross-resistance with known 4-aminoquinoline, is processing in phase IIa clinical trial.[94–96] OZ439 and ferroquine principally target the asexual blood-stage parasites. Phase I and II trials of OZ439/DSM265 combination in *P. falciparum* infected healthy volunteers showed satisfactory safety, tolerability, and promising antimalarial activity.[97]

Ganaplacide (KAF156) is a novel imidazolopiperazine that targets both asexual and sexual blood stages as well as the liver stages of the parasite.[98–100] Ganaplacide is active against most *Plasmodium* species, including drug-resistant parasites. Phase II study of ganaplacide with lumefantrine in adults with acute *P. vivax* or *P. falciparum* malaria showed the ability of this combination to clear parasite infections superior to all currently available antimalarial drugs without evident safety concerns.[87,100] In 2023, Novartis and MMV have decided to start a large Phase III trial to compare the efficacy of ganaplacide/lumefantrine to the efficacy of the artemether/lumefantrine combination in treating patients with acute uncomplicated *P. falciparum* infection.[101]

Cipargamin (KAE609) is poised to begin phase IIb investigations.[87,102] KAE609, developed by Novartis in collaboration with MMV, is a highly potent, fast-acting, schizonticidal, synthetic spiroindolone that is safe and well-tolerated.[104] KAE609 is a novel compound that acts through the inhibition of *PfATP4*. *PfATP4* is a transporter found on the parasite's plasma membrane that plays a crucial role in regulating the levels of Na^+ and H^+ ions within the parasite. Inhibition of this channel increases Na^+ levels and pH, leading to swelling, rigidity, and fragility of the parasite, thereby contributing to parasite clearance and intrinsic parasite killing.[105] Studies showed that Cipargamin is equally effective as artesunate against *P. falciparum* and *P. vivax* isolates.[102,103]

DSM265 is a novel triazolopyrimidine that shows efficacy against both blood and liver stages of *P. falciparum* and drug-resistant parasite isolates.[106,107] DMS265 is a selective inhibitor of the *P. falciparum* pyrimidine biosynthetic enzyme *P. falciparum* dihydroorotate dehydrogenase (*Pfdhodh*).[108,109] DSM265 showed the ability to maintain its serum concentration at a level higher than its minimum parasiticidal concentration in humans for eight days. It also showed efficacy as a treatment and chemoprotective agent in phase IIa clinical trials.[87,106,107]

The 2-aminopyridine MMV390048 possesses the potential to act as a transmission-blocking drug and possesses excellent prophylactic activity against *Plasmodium cynomolgi in vivo*.[110,111] MMV 390048 inhibits the *Plasmodium falciparum* Phosphatidylinositol 4-Kinase (*PfPI4K*). This inhibition affects the asexual liver, blood, and sexual gametocyte stages. MMV390048 is currently in phase IIa clinical trials in Ethiopia.[87,112]

SJ733 is a dihydroisoquinoline that potently suppressed parasitemia in both *P. berghei* and *P. falciparum* mouse models.[113] This molecule, like KAE609, arrests parasite motility and blocks intracellular parasite replication by inhibiting the *P. falciparum* cation transporting ATPase, *PfATP4*. This elucidation of its MoA, along with high oral bioavailability and good safety profile with no cytotoxicity, supports the continued development of this molecule as a possible new therapy for malaria.[87,114,115]

P218 is evaluated in controlled human malaria infection cohorts in phase I testing.[116] P218 (Figure 10) is an antifolate drug identified by examining the co-crystal structures of *Pfdhfr* and their substrates. The novel mechanism of binding to *Pfdhfr* allows P218 to beat the resistance that has emerged from the utilization of pyrimethamine. P218 also showed significant selectivity for binding to malarial dihydrofolate reductase (*dhfr*) over human *dhfr*. P218 demonstrated potent *in vitro* antiplasmodial and *in vivo* antimalarial activity. The preclinical assessment of P218 displayed satisfactory safety profiles and suitable pharmacological and metabolic profiles to warrant further consideration for clinical development.[87,117,118]

DDD107498 (DDD-498) inhibits *P. falciparum* elongation factor 2, thereby blocking protein synthesis. DDD107498 (DDD-498) exhibits remarkable effectiveness against all stages of the parasite's life cycle.[119] In March 2023, Merck started a phase II trial of DDD107498 to treat acute malarial infection.

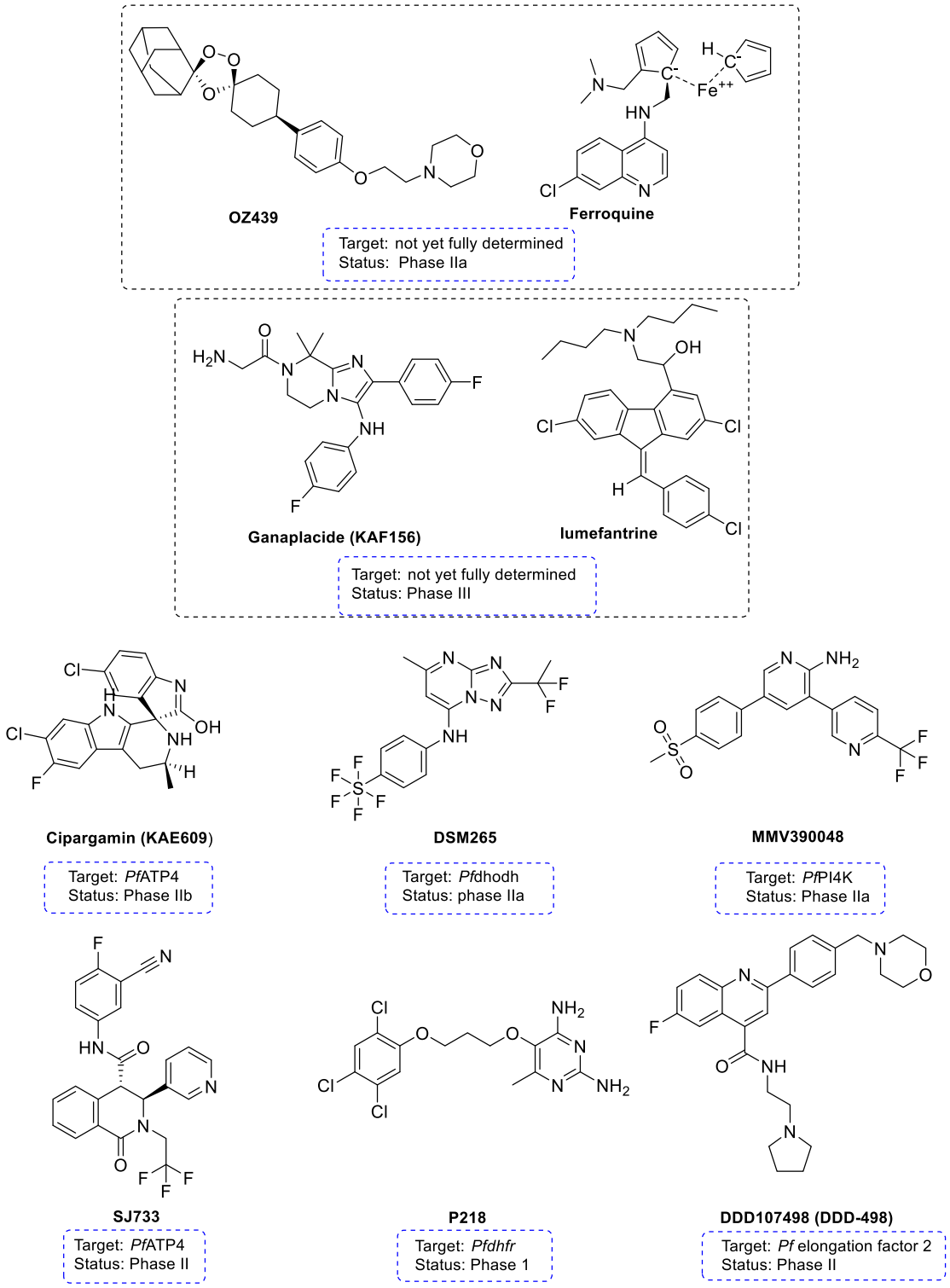

Figure 10: Structures of the clinical candidates and related compounds.

2.2 Over 40 Years of Fosmidomycin Drug Research: A Comprehensive Review and Future Opportunities

Published in: *Pharmaceuticals* **2022**, *15*, 1553.

Impact Factor: 5.215 (2022-2023)

https://doi.org/10.3390/ph15121553

Contribution: 20%

pharmaceuticals

MDPI

Review

Over 40 Years of Fosmidomycin Drug Research: A Comprehensive Review and Future Opportunities

Talea Knak [1,†], Mona A. Abdullaziz [1,†], Stefan Höfmann [1,†], Leandro A. Alves Avelar [1], Saskia Klein [1], Matthew Martin [2], Markus Fischer [3], Nobutada Tanaka [4] and Thomas Kurz [1,*]

1 Institut für Pharmazeutische und Medizinische Chemie, Heinrich Heine University Düsseldorf, Universitätsstraße 1, 40225 Düsseldorf, Germany
2 Initiative for Science & Society, Duke University, 140 Science Drive, Durham, NC 27708, USA
3 Institut für Pharmazie, Universität Hamburg, Bundesstrasse 45, 20146 Hamburg, Germany
4 School of Pharmacy, Kitasato University, 5-9-1 Shirokane, Minato-ku, Tokyo 108-8641, Japan
* Correspondence: thomas.kurz@hhu.de
† These authors contributed equally to this work.

Abstract: To address the continued rise of multi-drug-resistant microorganisms, the development of novel drugs with new modes of action is urgently required. While humans biosynthesize the essential isoprenoid precursors isopentenyl diphosphate (IPP) and dimethylallyl diphosphate (DMAPP) via the established mevalonate pathway, pathogenic protozoa and certain pathogenic eubacteria use the less well-known methylerythritol phosphate pathway for this purpose. Important pathogens using the MEP pathway are, for example, *Plasmodium falciparum*, *Mycobacterium tuberculosis*, *Pseudomonas aeruginosa* and *Escherichia coli*. The enzymes of that pathway are targets for antiinfective drugs that are exempt from target-related toxicity. 2*C*-Methyl-D-erythritol 4-phosphate (MEP), the second enzyme of the non-mevalonate pathway, has been established as the molecular target of fosmidomycin, an antibiotic that has so far failed to be approved as an anti-infective drug. This review describes the development and anti-infective properties of a wide range of fosmidomycin derivatives synthesized over the last four decades. Here we discuss the DXR inhibitor pharmacophore, which comprises a metal-binding group, a phosphate or phosphonate moiety and a connecting linker. Furthermore, non-fosmidomycin-based DXRi, bisubstrate inhibitors and several prodrug concepts are described. A comprehensive structure–activity relationship (SAR) of nearly all inhibitor types is presented and some novel opportunities for further drug development of DXR inhibitors are discussed.

Keywords: DXR/IspC inhibitor; fosmidomycin; malaria; *Plasmodium falciparum*; *Mycobacterium tuberculosis*; PfDXR

Citation: Knak, T.; Abdullaziz, M.A.; Höfmann, S.; Alves Avelar, L.A.; Klein, S.; Martin, M.; Fischer, M.; Tanaka, N.; Kurz, T. Over 40 Years of Fosmidomycin Drug Research: A Comprehensive Review and Future Opportunities. *Pharmaceuticals* **2022**, *15*, 1553. https://doi.org/10.3390/ph15121553

Academic Editors: Gabriela Hrckova and Gustavo Henrique Goulart Trossini

Received: 28 October 2022
Accepted: 5 December 2022
Published: 14 December 2022

1. Introduction

The rapid spread of multi-drug-resistant (MDR) strains of pathogenic bacteria and parasites poses a global threat to human health. Thus, new drugs addressing unique therapeutic targets are urgently needed. Since its discovery in the early 1990s [1] by Rohmer et al., the 2*C*-methyl-D-erythritol 4-phosphate (MEP) pathway is accepted as an attractive, and for the treatment of malaria validated, target for the development of new anti-infective drugs. The MEP pathway is essential in several clinically relevant pathogens such as *Mycobacterium tuberculosis*, *Escherichia coli* (*E. coli*) and apicomplexan parasites including *Plasmodium* spp., and *Toxoplasma* spp., but is absent in mammals, fungi, archaebacteria and most Gram-positive bacteria such as *Streptococci* and some *Staphylococci* [1–6]. Over the course of seven enzymatic reactions, the MEP pathway leads to isopentenyl diphosphate (IPP) and dimethylallyl diphosphate (DMAPP), precursors to the isoprenoids. Since the enzymes of the MEP pathway have no human orthologs, target-related toxicity is not to be expected [7,8]. However, no MEP inhibitor has so far been approved as an anti-infective drug.

Fosmidomycin (**1**) and FR9000098 (**2**) were first described in 1978 as antibiotics and herbicides (Figure 1) [9–11]. Twenty years later, they were identified as inhibitors of 1-deoxy-D-xylulose-5-phosphate reductoisomerase (DXR), the second and rate-limiting enzyme of the MEP pathway [12–14].

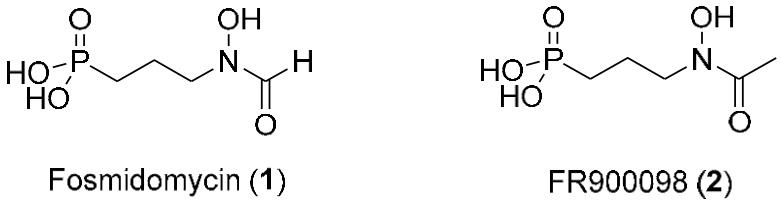

Figure 1. Structural formula of the natural product fosmidomycin (**1**) and its acetyl analog FR900098 (**2**).

The phosphono-hydroxamic acids **1** and **2** possess potent antibacterial and antiparasitic properties. Unfortunately, the main shortcoming of both lead structures **1** and **2** are their unfavorable pharmacokinetic properties, mainly insufficient membrane permeability due to the charged phosphonate and the polar hydroxamate moiety and the short half-life time [15,16].

Over more than 40 years, significant efforts to improve the anti-infective properties have led to hundreds of novel DXR inhibitors based on the lead structures fosmidomycin (**1**) and FR900098 (**2**). In this review, we outline the physicochemical, pharmacokinetic and anti-infective properties of the parent compounds **1** and **2** as well as their efficacy spectra against various bacterial and parasitic pathogens. A short section of this review is dedicated to recent results of fosmidomycin (**1**) in human clinical trials. In addition, an overview of both the historical and recent development of novel DXR inhibitors with a particular focus on their activity against various pathogenic organisms and their structure–activity relationships (SARs) are also included.

2. Discovery and Evaluation of Fosmidomycin (1) and Related Natural Products

In 1978, fosmidomycin (**1**, FR-31564) and FR900098 (**2**) were first described as a new class of antibiotics isolated from *Streptomyces lavendulae* and *Streptomyces rubellomurinus* [9,17]. The biosynthesis of FR900098 (**2**) has been completely elucidated, whereas, for fosmidomycin (**1**), only the biosynthesis of the putative precursor FR32863 (**IV**, Figure 2) is known [18–20]. Over the past four decades, the antiparasitic and antibacterial activities of **1** and **2** were determined, analyzed, and improved by various research groups. Alongside **1** and **2**, additional phosphono-hydroxamic acids were discovered by the Fujisawa Pharmaceutical Co., Ltd. (Figure 2) [21].

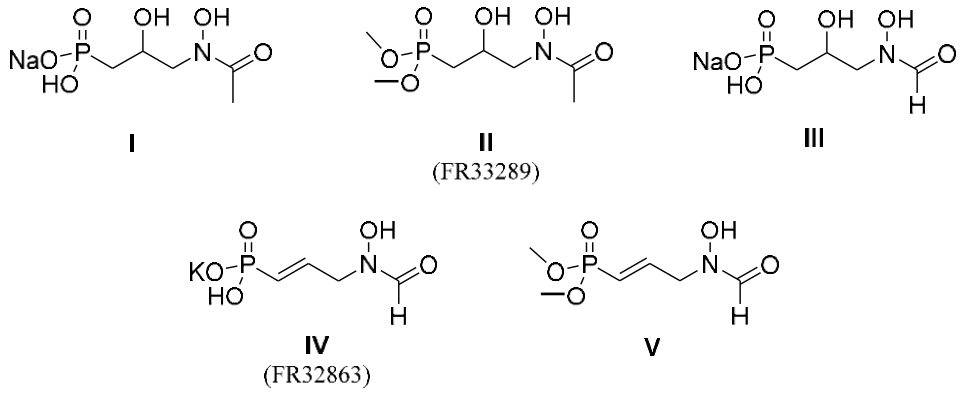

Figure 2. Additional phosphono-hydroxamic acids published by the Fujisawa Pharmaceutical Co., Ltd. [21].

In a 1978 patent, Fujisawa Pharmaceutical Co., Ltd. described the first synthesis of both **1** and **2** as shown in Scheme 1 [10]. The four-step synthesis consists of the alkylation of an *N,O*-diprotected hydroxylamine (**VI**) with 1,3-dibromopropane, followed by a Michaelis-Becker reaction of propyl bromide **VII** with dibutyl phosphonate to give the protected phosphonic ester (**VIII**). After the removal of the protecting groups, the free hydroxylamine (**IX**) was formylated and acetylated producing the natural compounds (**1**) and (**2**).

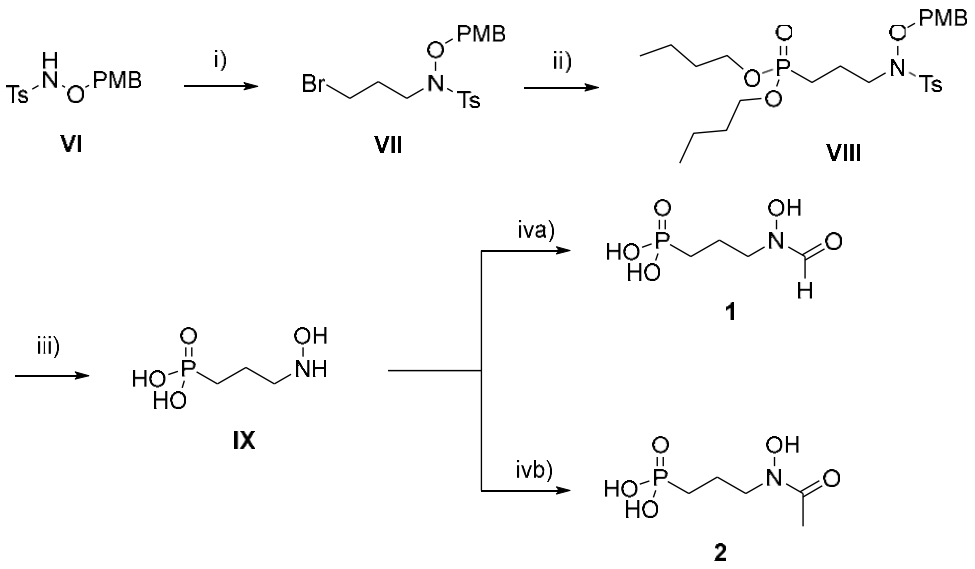

Scheme 1. (**i**) 1. Na, EtOH, 70 °C, 1.5 h, 2. 1,3-dibromopropane, 2 h, rt to reflux, (**ii**) 1. NaH, benzene, dibutyl phosphonate, reflux, 3.5 h, 2. **VII**, reflux, 5.6 h (**iii**) 6 N HCl, acetic acid, 20 h, reflux (**iva**) 1. formic acid, acetic anhydride, 1.1 h, 0 to 5 °C, 2. NH_3 (28 % aq. sol.), (**ivb**) acetic anhydride, water, rt, 1.5 h, Ts = tosyl, PMB = p-methoxybenzyl.

In 1989, Shigi identified fosmidomycin as an antibiotic inhibiting isoprenoid biosynthesis [22]. Towards the end of the millennium, in 1998, fosmidomycin (**1**) and FR900098 (**2**) were identified as selective inhibitors of *Ec*DXR by Kuzuyama et al. [12]. Additionally, in a Science publication in 1999 Jomaa and coworkers described fosmidomycin (**1**) as a *Pf* DXR inhibitor, inhibiting the growth of *P. falciparum* and also possessing curative properties in mice infected with *Plasmodium vinckei* [13]. In 2002, Kremsner and coworkers conducted a small-scale clinical trial of fosmidomycin for the treatment of uncomplicated malaria in adults, laying the foundation for further clinical trials [23].

2.1. Anti-Infective Activity of Fosmidomycin

Fosmidomycin inhibits a broad spectrum of pathogens which rely on the MEP pathway for the biosynthesis of DMAPP IPP. These pathogens include the apicomplexans *P. falciparum* (*Pf*) and *Toxoplasma gondii* (*Tg*) as well as bacteria [24]. The majority of pathogens use the MEP pathway, which includes Gram-negative bacteria such as *E. coli* (*Ec*) [25], *Acinetobacter baumannii* [26], *Klebsiella pneumonia* [26], *Pseudomonas aeruginosa* [27] and Gram-positive bacteria, including certain species of *Staphylococcus* [28]. Some bacteria use both, the MEP and the mevalonate pathway, for the synthesis of DMAPP and IPP, with the mevalonate pathway being a more recent addition to some species [29]. Pathogens that feature both pathways include *Listeria monocytogenes* and some species of *Streptomyces* [28]. In contrast, examples of pathogenic bacteria that exclusively use the mevalonate pathway includes Gram-positive genus of *Streptococcus* and the Gram-negative genus of *Borrelia* [28,30]. The application of fosmidomycin is limited to species that solely rely on the non-mevalonate pathway for isoprenoid synthesis.

To date, the DXRs of *P. falciparum*, *E. coli* and *M. tuberculosis* (*Mt*) are the best-studied enzymes. As a result, most synthesized fosmidomycin analogs have been tested against at

least one of these enzymes, in addition to cellular assays. Additional information about the efficacies of **1** and **2** against these pathogens can be found in the Supplementary Materials (Table S1).

Although the enzyme catalytic sites are highly conserved across pathogens [31,32], whole-cell activities for inhibitors differ greatly due to significant distinctions among the organisms as a whole, including different localization of the DXR enzymes. In bacteria, the enzyme resides in the cytosol, whereas the homologs in parasites are located in the apicoplast, a plastid-like cell organelle accommodating a variety of biosynthetic pathways [24]. Uptake mechanisms of fosmidomycin also differ among pathogens. In *E. coli*, a cAMP-dependent glycerol 3-phosphate transporter facilitates an effective drug uptake resulting in bacterial death.

In contrast, *M. tuberculosis* lacks a similar transporter, making the bacteria intrinsically resistant to fosmidomycin as the inhibitor cannot penetrate the cell wall via passive diffusion [33]. Additionally, the cell wall of *Mt* contains highly lipophilic mycolic acids, which prevent cell wall penetration of polar drugs, including fosmidomycin, in typically used concentrations [33]. For human erythrocytes infected with *Pf*, a parasite-induced pathway known as the new permeability pathway was proposed to be most likely responsible for drug uptake [15]. Treatment of *Pf* with fosmidomycin resulted in reduced amounts of MEP pathways metabolites and their resulting isoprenoids [34]. Parasite growth is inhibited in the first cell cycle after haemoglobin digestion and DNA replication has been initiated [35].

2.1.1. Parasites

In vitro and in vivo, the *Pf* parasites infect human erythrocytes for asexual reproduction. Besides the erythrocyte membrane, the parasitophorous vacuole membrane (PVM) and the plasmodium cell membrane must also be overcome. Inside the *Plasmodium* parasite, DXR is localized in the apicoplast which contains additional four membrane layers (Figure 3) [36].

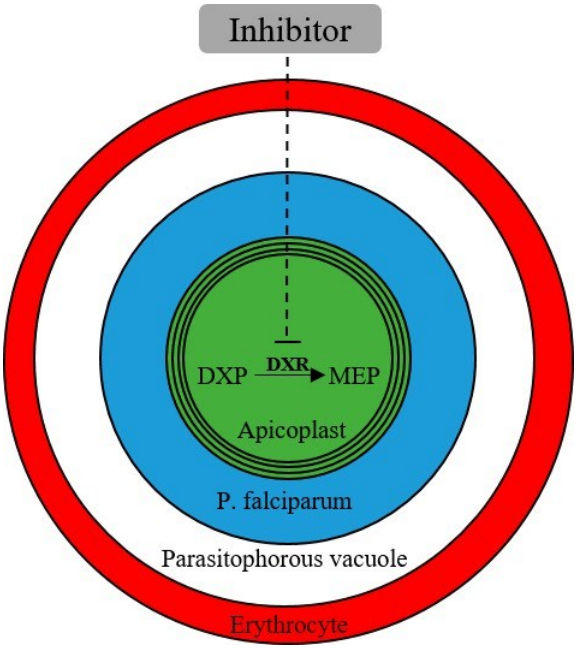

Figure 3. Passage of DXR inhibitors across seven membranes in *Plasmodium*-infected erythrocytes. Adapted with permission from *J. Med. Chem.* 2015, 58, 4, 2025–2035 [37]. Copyright 2022 American Chemical Society.

Fosmidomycin is able to kill *Pf* pathogens (IC_{50} = 0.81 μM) [37], but not *Toxoplasma gondii*. In both pathogens, the DXR enzyme is located in the Apicoplast. Nevertheless, fosmidomycin seems to be unable to penetrate the membranes of *T. gondii* while penetration

through *Pf* membranes is possible [15]. A likely cause for fosmidomycin's inability to act upon *T. gondii* is the lack of the glycerol-3-phosphate transporter (*GlpT*), which is known to be responsible for fosmidomycin uptake in *E. coli* and other pathogens [34]. Interestingly, strains of *T. gondii* engineered to express GlpT are susceptible to fosmidomycin. Enzyme assays performed on *T. gondii* DXR have shown, that both fosmidomycin (K_i = 90 nM) and FR900098 (K_i = 48 nM) are potent inhibitors [34], paving the way for fosmidomycin-based treatments if the permeability issues can be overcome by structural modification [15].

Babesia orientalis is a tick-borne apicomplexan parasite and the cause of water buffalo babesiosis. While humans are not affected by this pathogen, its eradication is of interest as it causes considerable economic loss, especially in China. Fosmidomycin was able to limit the growth of *B. orientalis*, with the treatment of the pathogen leading to a significant reduction in relative growth [38]. Similar results were reported in *B. bigemina* and *B. bovis*, with clearance achievable in 3 days and 4 days, respectively. Both parasite species were incapable of growth after in vitro treatment with fosmidomycin, suggesting that fosmidomycin may be an effective drug for the treatment of bovine babesiosis [39].

Eimeria tenella causes eimeriosis in poultry and poses a major threat to food security. Impairment of parasitic growth required higher concentrations of fosmidomycin compared to *P. falciparum* to be statistically significant [40]. The poor efficacy of fosmidomycin was attributed to different factors, including inactivation of the active drug, poor permeability, and/or efflux of the drug. Taking similar results from *T. gondii* and the absence of the MEP pathway in the *Cryptosporidium* genus altogether into consideration these findings imply heterogeneity among apicomplexan parasites [40].

2.1.2. Gram-Positive Bacteria

The *Staphylococcus* genus is unique in that it features species that rely on either pathway for isoprenoid synthesis. Fosmidomycin inhibited the growth of *S. schleiferi* (MIC = 0.5–8 µg/mL) and *S. pseudintermedius* (MIC = 0.5–1 µg/mL) which are associated with household animal infections and both possess all enzymes of the non-mevalonate pathway. However, fosmidomycin could not cure infections with *S. aureus*, *S. epidermidis* and *S. lugdenensis,* which lack the *dxr* gene [28,41]. These findings contradicted earlier reports of fosmidomycin and FR900098 having shown activity against *S. aureus* [42]. A recent publication by Edwards et al. showed that fosmidomycin is indeed inactive against *S. aureus*. Edwards et al. also laid out a resistance mechanism towards fosmidomycin in *S. schleiferi* and *S. peudintermedius*, mediated by mutations lowering the function of GlpT and leading to decreased drug uptake into the aforementioned pathogens [43].

2.1.3. Gram-Negative Bacteria

The Gram-negative bacterium *E. coli* is often considered to be a model organism for anti-bacterial drug research, but a survey conducted on clinical isolates in 2018 showed that 58% of samples were resistant to current treatment options [44]. Fosmidomycin is a moderate agent against the K12 strain of *E. coli* (MIC = 12.5 µM) [45]. While fosmidomycin showed potent enzyme inhibitory activity against the wild type of *Ec*DXR (IC_{50} = 0.03 µM), several mutations have been observed that decreased activity by up to 10-fold [25]. A fosmidomycin resistance gene (*fsr*) was also originally discovered in *Ec*, most likely encoding for an efflux pump that increased resistance by more than 30-fold. This efflux pump seems to be specific for fosmidomycin and does not act upon other antibiotics apart from trimethoprim [46,47]. It could be shown that *E. coli* can grow even after the deletion of the genes encoding for DXS and DXR. Rodríguez-Concepción and coworkers described that in the case of *dxs* deletion, mutations in the *ribB* and *aceE* genes lead to enzymes capable of supplying DXP. A mechanism for survival of DXR deletion has yet to be postulated and is of great interest to elucidate a new possible way of fosmidomycin resistance [48,49].

Strains of the *Burkholderia* genus, pathogens related to opportunistic infections of the respiratory tract in cystic fibrosis patients, were mostly resistant to both fosmidomycin and FR900098 as well as other conventional antibiotics [50]. Resistance was mostly attributed to

insufficient retention of inhibitors within bacterial cells, caused by the upregulation of *fsr*. This resistance could be partially circumvented by the addition of glucose-6-phosphate to the medium, prompting an increase of genes related to glycerol-3-phosphate uptake into bacterial cells, thus facilitating FR900098 (**2**) uptake [50]. A combination of fosmidomycin and colistin reduced the MIC of colistin by up to 64-fold in clinical isolates of *B. multivorans*, an effect that could be attributed to increased membrane permeability [51].

Francisella tularensis is a Gram-negative bacterium and the cause of tularemia, a zoonotic disease transmitted by rodents and lagomorphs [52]. Jawaid et al. showed that fosmidomycin reduced in vitro growth of *F. tularensis* subspecies *novicida* by inhibition of *F. tularensis* DXR (MIC = 136 μM) [53]. Clinical isolates of *Francisella* were resistant to β-lactam antibiotics due to the expression of β-lactamases and spontaneously occurring resistance to fosmidomycin has also been described. Similar to *S. schleiferi* and *S. pseudintermedius*, this resistance was mediated by mutations in the GlpT gene [52].

The causative agent of the plague, *Yersinia pestis*, garnered attention over its potential applications for bioterrorism [54] and the 2017 plague outbreak in Madagascar [55]. The disease mostly manifests in two forms: the bubonic and pneumonic plague [55]. Both fosmidomycin (IC_{50} = 0.71 μM) and FR900098 (IC_{50} = 0.23 μM) showed submicromolar inhibitory activity [56]. Both agents lacked the ability to inhibit the growth of *Y. pestis*, even though uptake of fosmidomycin was likely mediated by a transport protein homologous to the *E. coli* GlpT transporter [57].

Acinetobacter baumannii is a Gram-negative bacterium and the cause of a plethora of nosocomial infections, including soft-tissue infections, pneumonia, septicemia, and urinary tract infections [58]. Treatment of emerging multidrug-resistant *A. baumannii* infections often requires reserve antibiotics such as carbapenems in combination with colistin or an aminoglycoside. Fosmidomycin (IC_{50} = 47 nM) and FR900098 (IC_{50} = 24 nM) both exhibited nanomolar activity against *Ab*DXR but only FR900098 showed activity against selected *A. baumannii* strains in a whole-cell assay [26]. Resistance to fosmidomycin and FR900098 in certain *A. baumannii* strains was theorized to be based on a lack of GlpT uptake or poor permeability.

The Gram-negative bacterium *Klebsiella pneumoniae* naturally resides on the skin as well as in the nasopharyngeal and intestinal tracts of both humans and mammals. *K. pneumoniae* is opportunistically pathogenic and a leading cause of nosocomial infections. The pathogen is not inherently resistant to antibiotics but is known for its ability to acquire multidrug resistance plastids [59]. Both fosmidomycin (IC_{50} = 20 nM) and FR900098 (IC_{50} = 23 nM) showed equal nanomolar activity in an enzyme assay, with fosmidomycin also exhibiting weak activity in a whole-cell assay (MIC = 64–128 mg/L). The superior activity of fosmidomycin over its acetyl derivate (MIC = 256 mg/L) may be attributed to a more facile uptake via the GlpT [26].

In addition to the above-listed pathogens, fosmidomycin and FR900098 have been tested against other bacteria listed in Table S1 of the Supplementary Materials. Information on those pathogens is limited, though noteworthy examples include *Bacillus anthracis* and *Pseudomonas aeruginosa*.

2.2. Pharmacokinetic Profile of Fosmidomycin

Fosmidomycin and FR900098 both contain a phosphonic acid group, which is connected via a propyl linker to *N*-formylated (**1**) or *N*-acetylated (**2**) hydroxylamine moieties, leading to highly polar, water-soluble and stable compounds. Due to its dianionic structure in a physiological medium, the phosphonate group (pK_{a1} = 2.2, pK_{a2} = 6.7) [60], is mainly responsible for the excellent aqueous solubility of both compounds. The high water solubility on the other hand results in unfavorable permeability [61,62], as well as a comparatively short plasma half-life of approximately 1.87 h due to rapid renal excretion [63]. The absorption half-life of fosmidomycin via a one-compartment model was determined at 0.4 to 1.1 h [64]. No metabolites of **1** are known and the active agent is excreted renally [65]. An advantageous trait of **1** and **2** is their low cytotoxicity as determined in a mouse model.

In addition to these early findings more recent clinical trials have confirmed the generally low toxicity of fosmidomycin paving the way for further clinical trials in humans [66,67].

In vivo studies in humans best fit with a one-compartment model and first-order absorption and elimination of fosmidomycin [67]. Plasma protein binding is typically low for a hydrophilic therapeutic agent at about 1% [67]. No mutagenic potential has been reported for fosmidomycin, although the formation of an *N*-substituted hydroxylamine upon hydrolysis is theoretically possible [68]. Hydroxylamines have been reported to have mutagenic potential [69]. Fosmidomycin is typically administered two to four times per day with an upper daily dose of 3600 mg per day [67]. Expectedly, the fluctuation of fosmidomycin's plasma concentrations is lower if smaller doses are administered more frequently compared to larger doses over a larger interval. More frequent applications of smaller doses also result in higher minimum plasma concentrations at a steady state. The mode of action of fosmidomycin seems to be time-dependent rather than concentration-dependent [64]. This finding suggests more frequent applications are required to maintain consistently high plasma concentrations of the drug.

2.3. Clinical Trials from 1985 to 2018

Since its discovery, fosmidomycin has been the subject of several clinical trials, both as a standalone therapeutic and in combination with other approved antimalarials or antibiotics. In 1985, fosmidomycin phase I and phase II clinical trials for the treatment of urinary tract infections were conducted [70,71]. However, the study was discontinued for unknown reasons. In their third edition of the guidelines of malaria treatment, the WHO classifies treatments with a cure rate of 90% as acceptable [72]. A 2015 meta-analysis by Fernandes et al. pooled the data of ten clinical trials studying fosmidomycin, of which six were pediatric studies and the remaining four were involving adults [73]. Trials employing **1** as a single therapeutic agent failed to produce acceptable cure rates by the WHO's standards [73]. More recent trials are focused on fosmidomycin combinations, for example with the antibiotic clindamycin for which Wiesner et al. showed a synergistic effect [66]. While most studies involved this combination, an approach that made use of artesunate instead of clindamycin is also included [73]. The meta-analysis showed that the combination of fosmidomycin with a second antimalarial led to a cure rate of 85% (95% CI: 71–98%) on day 28 in children and 70% (95% CI: 40–100%) respectively in adults. **1** proved to be a safe antimalarial, with adverse events mainly limited to gastrointestinal disturbance [73]. However, isolated cases of haematological changes such as neutropenia have been reported by Borrmann et al. [74]. A temporary hiatus in the clinical evaluation of fosmidomycin may be attributed to a 2012 trial by Lanaspa et al. that only produced a 43% cure rate on day 28 (95% CI: 27–59%) for children under the age of three [75]. In 2018; Mombo-Ngoma et al. published the results of a Gambon-based study involving fosmidomycin in combination with piperaquine [76]. The aim of this phase II study was to demonstrate the efficacy, tolerability and safety of the combination as a treatment of *P. falciparum* infections in both children and adults. The cure rate on day 28 across all age groups was reported to be 83.8% (95% CI: 75.1–90.5%). In addition to adverse effects concerning the gastrointestinal and respiratory tract, two out of the 100 enrolled patients showed a prolonged QT interval of >500 msec [76]. None of the completed trials produced cure rates that can be considered acceptable by the WHO's standards, although the cure rate of 85% in children as determined in the meta-analysis by Fernandes et al. comes close [73]. Because the dosage of fosmidomycin is already high, further increasing the dose for fosmidomycin alone may not be feasible and may not result in better cure rates. In vitro, a decrease in Vγ9/Vδ2 T cell response, which can detect (*E*)-4-hydroxy-3-methylbut-2-enyl pyrophosphate (HMB-PP) as a key intermediary of the MEP pathway, has been observed. The significance of this observation has not yet been assessed in vivo [77]. Fosmidomycin's shortfall in efficacy underlines the necessity of either inclusion of an additional antimalarial into existing fosmidomycin-based combination therapies or the introduction of structural modifications to fosmidomycin to improve cure rates.

As of February 2022, there are no ongoing fosmidomycin clinical trials listed on ClinicalTrial.gov, though the Deutsche Malaria GmbH recently announced a trial of triple therapy using fosmidomycin, clindamycin and artesunate. The trial will be supported by the EU Malaria Fund and aims to enroll more than 5000 patients, making it the largest single trial of fosmidomycin in humans [78]. No timeline or further updates regarding this study have been published.

3. 1 Targeting the Deoxy-D-xylulose-5-phosphate Reductoisomerase (DXR)

The MEP pathway begins with the synthesis of 1-deoxy-D-xylulose 5-phosphate (DXP) from two glycolytic intermediates, pyruvate (**X**) and glyceraldehyde 3-phosphate (**XI**) catalyzed by DXP synthase (DXS), concluding with the production of IPP and DMAPP after six catalytic steps (Figure 4) [79].

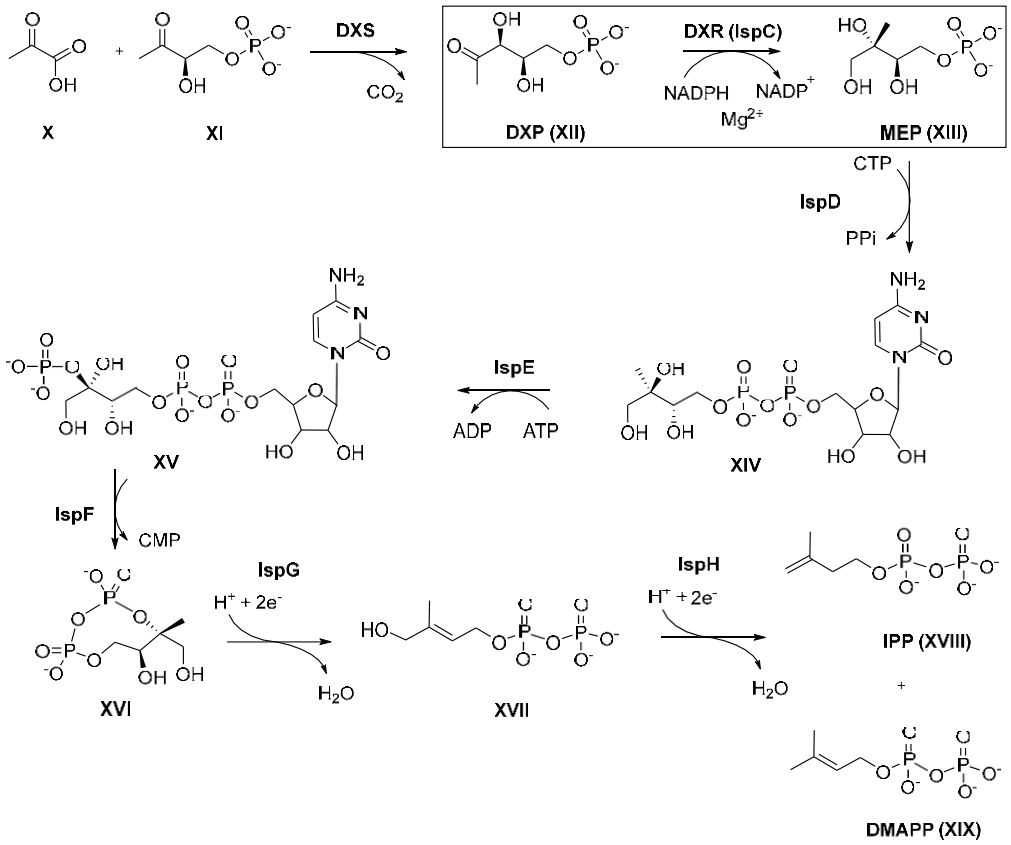

Figure 4. The MEP pathway leading to the isoprenoid precursors isopentenyl diphosphate (**XVII, IPP**) and dimethylallyl diphosphate (**XIX, DMAPP**) via an IspC/DXR-catalysed conversion of 1-deoxy-D-xylulose 5-phosphate (**XII, DXP**) to 2-C-methyl-D-erythritol 4-phosphate (**XIII, MEP**).

In the second step 1-deoxy-D-xylulose 5-phosphate reductoisomerase (DXR/IspC), a homodimer catalyzes the intramolecular rearrangement and reduction of DXP (**XII**) to MEP (**XIII**) [80]. The complex conversion of DXP to MEP requires the presence of the cofactor NADPH and a bivalent metal ion, e.g., Mg^{2+} or Mn^{2+} [81].

At least two possible reaction mechanisms (Figure 5) have been proposed for the DXR-catalyzed isomerization of **XII** to 2-C-methyl-D-erythrose 4-phosphate **(XII c)**. One reaction mechanism for the formation of intermediate **XIIc** is based on an α-ketol-rearrangement, in which the C3 hydroxyl group of **XII** is deprotonated, followed by a subsequent 1,2-alkyl shift. The C3-C4 carbon-carbon bond is cleaved in a way that C4 can thereafter attack the carbonyl C2. The 1-hydroxy 2-ethyl phosphate translocates to the C2 position, forming **XIIc** [82,83].

An alternative approach is a stepwise retro-aldol/aldol-mechanism [82–84]. In the retro-aldol step, the oxidation of the C4 carbon atom of **XII** causes a C-C bond break between C3 and C4, whereby a hydroxyacetone enolate **XIIa** and an aldehyde phosphate **XIIb** are formed as intermediates [85,86]. In the following aldolization step, the hydroxyacetone enolate **XIIa** attacks the aldehyde phosphate **XIIb**, forming **XIIc** in an electrophilic attack. A new bond is formed between the C2 carbon atom of the enolate and the C1 atom of the aldehyde phosphate **XIIb**. In the last step, **XIIc** is reduced to MEP **XIII** by NADPH.

MEP is the substrate of IspD, which catalyzes the reaction with cytidine 5′-triphosphate (CTP) to give methylerythritol cytidyl diphosphate (**XIV**). Subsequently, the C2 hydroxyl group of **XIV** is phosphorylated by IspE using ATP as a phosphate donor. The resulting phosphate ester 4-diphosphocytidyl-2-C-methyl-D-erythritol-2-phosphate (**XV**) is then cyclized by IspF to 2-C-methyl-D-erythritol-2,4-cyclodiphosphate (**XVI**). In the following step, IspG catalyzes the reductive dehydratisation and ring opening to yield 4-hydroxy-3-methyl-butenyl 1-diphosphate (**XVII**). Finally, the reductive dehydroxylation of **XVII** provides both isopentenyl diphosphate (IPP, **XVIII**) and dimethylallyl diphosphate (DMAPP, **XIX**) [79].

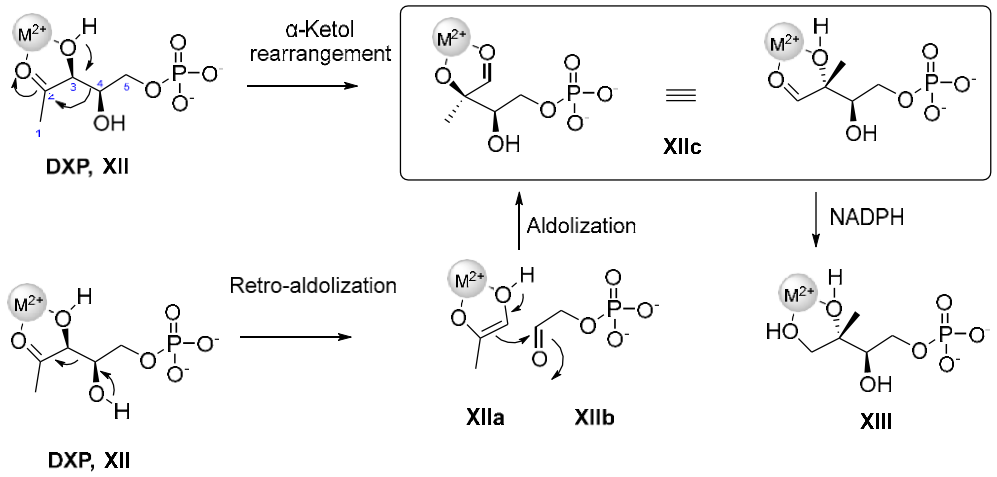

Figure 5. Two conceivable mechanisms for the enzymatic mode of action of DXR involving a divalent metal cation M^{2+} (grey sphere) and NADPH [87]. Used with permission of EUREKA SCIENCE, from Targeting the MethylErythritol Phosphate(MEP) Pathway for Novel Antimalarial, Antibacterial and Herbicidal Drug Discovery: Inhibition of 1-Deoxy-D-Xylulose-5-Phosphate Reductoisomerase (DXR) Enzyme, Nidhi Singh, Volume 13, Issue 11, 2007; permission conveyed through Copyright Clearance Center, Inc.

3.1. Crystal Structures of DXR

1-Deoxy-D-xylulose 5-phosphate reductoisomerase (DXR) is present in more than 400-annotated (Swiss-Prot) entries in the Uniprot database. These entries consist primarily of bacteria with some examples of eucaryota. The length of the amino acid (aa) sequence varies from 356 aa in *Campylobacter jejuni* to 488 in *Plasmodium falciparum* (Figure 6A) [88]. Presently, the DXR structures of *E. coli* (*Ec*DXR), *P. falciparum* (*Pf* DXR), and *M. tuberculosis* (*Mt*DXR) have been more thoroughly characterized and studied [89,90].

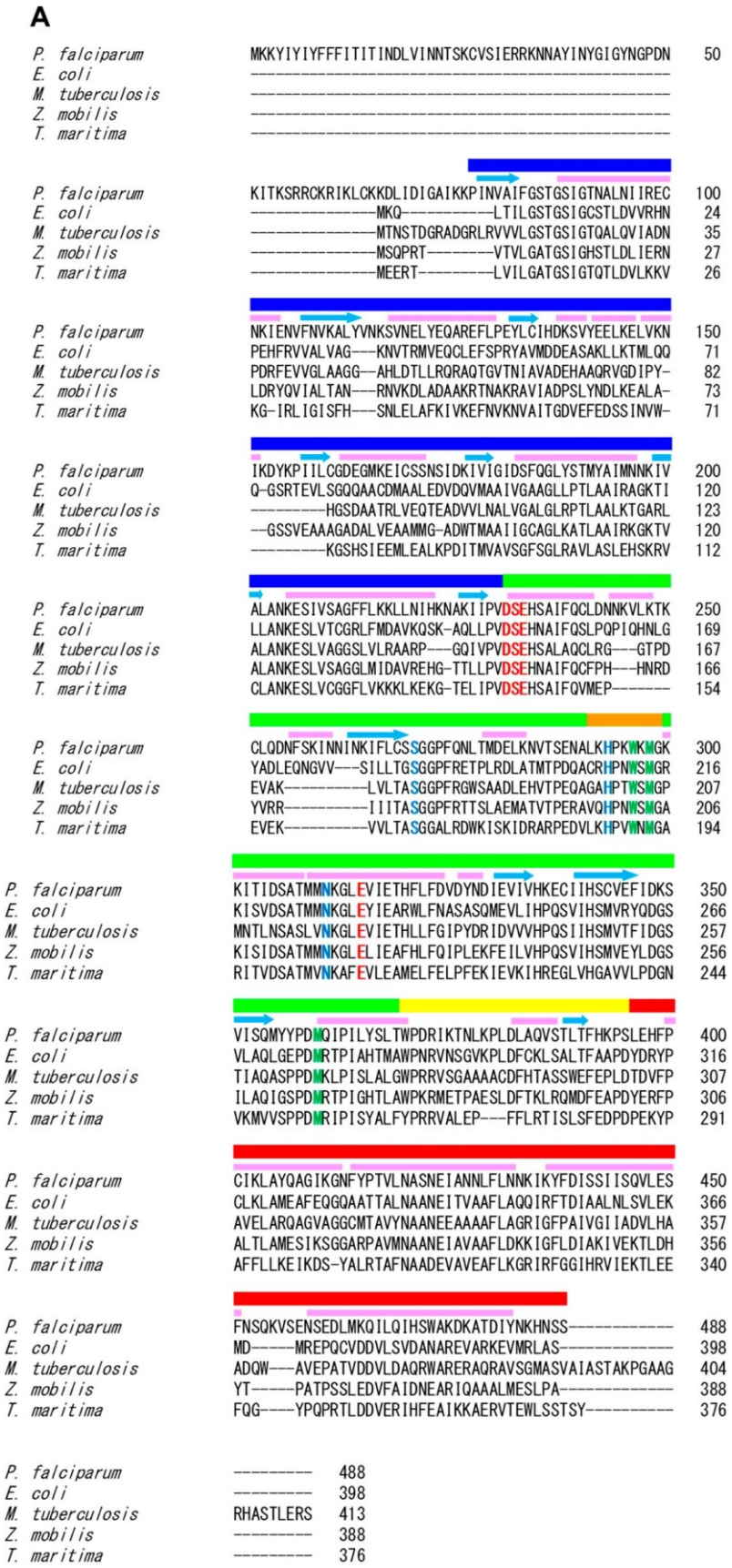

Figure 6. *Cont.*

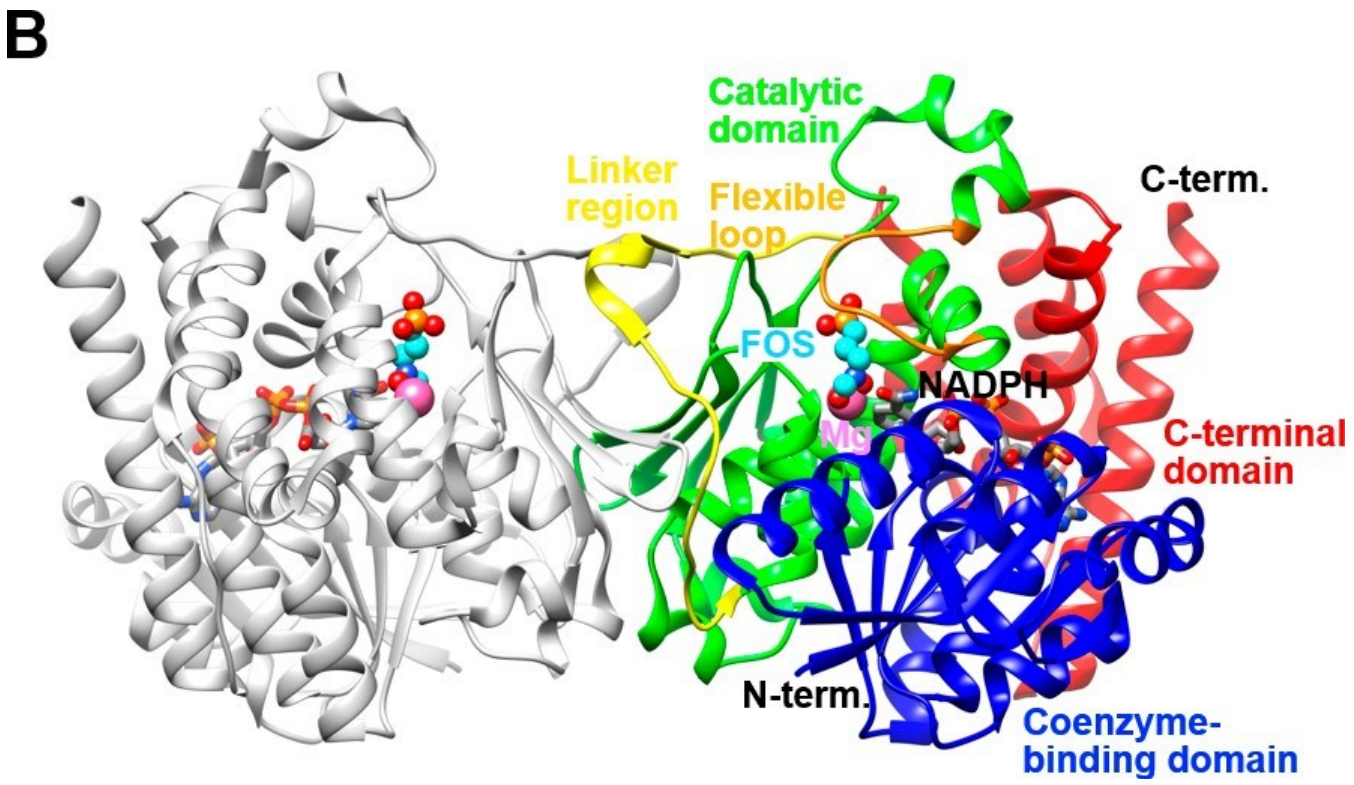

Figure 6. (**A**): Amino acid sequence alignment of bacterial and parasitic DXRs. Residues involved in phosphate/phosphonate-, linker-, and metal and hydroxamate-binding are highlighted in blue, green, and red, respectively. The colored ribbons above the sequence alignment represent the respective domains in *Pf* DXR: the NADPH-binding (blue), catalytic (green), and C-terminal (red) domains. The linker region and flexible loop in the catalytic domain are colored yellow and orange, respectively. The pink bars and cyan arrows represent the secondary structure elements, namely, α-helices and β-strands, respectively; (**B**): The overall structure of the quaternary (enzyme-NADPH-metal-inhibitor) complex of *Pf* DXR (PDB 3AU9) [91]. Three domains, a linker region, and a flexible loop in the catalytic domain of one subunit are colored as in (**A**). The other subunit is colored grey. The bound fosmidomycin (FOS) and NADPH molecules are shown as ball-and-stick (cyan) and stick (grey) models, respectively. The bound magnesium ions are shown as sphere models (pink).

DXRs are homodimers. The subunit of DXR consists of two large domains separated by a cleft containing a deep pocket, a linker region, and a C-terminal domain (Figure 6B). One of the large domains is the N-terminal NADPH binding domain and the other is the catalytic domain which provides the groups necessary for catalysis (metal and substrate binding). The N-terminal NADPH-binding domain is connected to a catalytic domain. The N-terminal domain (NTD) comprises the first 150 amino acids. The structural organization of the NTD resembles the Rossman fold, which is found in proteins showing interactions with dinucleotides. This region shows high similarity among orthologues *Ec*DXR, *Mt*DXR and *Pf*DXR.

The central catalytic domain comprises 125 amino acids and due to the metal-based mechanism of catalysis, acidic amino acids responsible for the binding of the divalent metal are found in this domain (Figure 6A). Another important characteristic of the substrate-binding site is the flexibility of the domains, a feature necessary for the complex enzymatic process involving both a divalent cation and NADPH. In DXR crystals, the relative position of the NADPH-binding and catalytic domains exhibits different conformations depending on the presence of co-crystallized ligands, cofactors, and substrates. These conformations are highly dependent on the position of a flexible loop located at the entrance of the substrate-binding site, causing the catalytic site to be in a closed, open, or super-open

state [31,91,92]. The connection between the catalytic domain and the C-terminal domain is made via a sequence of around 30 amino acids known as the linker region. In the crystal structures of DXR, the linker region as well as a β-strand of the catalytic domain from each subunit are involved in the dimer interface. The C-terminal domain of DXR is formed by a four-helix bundle motif, showing a high degree of flexibility and no interface of contact between the dimer subunits [31,92,93].

An analysis of the similarity between the orthologues *Ec*DXR, *Mt*DXR, and *Pf* DXR using BLAST revealed that *Ec*DXR shares 40% amino acid sequence identity with *Mt*DXR and 37% with *Pf* DXR, while *Mt*DXR and *Pf* DXR share 34% identity [89]. Despite the sequence identity of the proteins ranging from 34% to 40%, the overall three-dimensional arrangement of the enzymes co-crystalized with both cofactors is similar [31]. The major part of the dissimilar regions occupies solvent-exposed areas.

The first *Ec*DXR crystal structure was independently determined in 2002 by the Stubbs group (PDB 1K5H) [31] and the Ohsawa group (PDB 1JVS) [94]. The structure of *Mt*DXR was first solved in 2006 [95] and *Pf* DXR in 2011 [91]. Since then, solid efforts by several groups led to the obtention of crystal structures of DXR from different organisms. Currently, 77 DXR crystal structures from twelve organisms, with or without cofactors and/or substrates/inhibitors, are deposited in the Protein Data Bank (PDB) (Table S2, Supplementary Materials). The crystal structures of DXR co-crystallized with inhibitors in the catalytic site provided key information on both the active site architecture and the binding mode of NADPH, DXP, and inhibitors.

Active Site

Since DXR from *P. falciparum* is an attractive target for inhibitor design, we have used it for our analysis of both the active site and binding mode of fosmidomycin (1, Figure 6B). However, due to the N-terminal insertion of ca. 70 amino acids in *Pf* DXR (Figure 6A), the residue number of *Pf* DXR significantly differs from other DXRs. So, in the following description, *Ec*DXR numbering is shown in parentheses.

The substrate-binding cavity of DXR is highly conserved in all organisms and consists mainly of three regions: a positively charged phosphate/phosphonate binding pocket, a hydrophobic region around the linker backbone, and a metal binding pocket [31,32]. Note that the residues involved in inhibitor binding described below are conserved among DXRs (Figure 6A). The substrate and substrate-analogous inhibitors bind to the cleft of the catalytic domain and induce a conformational change that tether the N-terminal and the catalytic domains in the closed conformation. Concomitantly with the movement of the catalytic domain, the C-terminal domain also shows a closed conformation. In addition, the flexible loop (residues 291–299 in *Pf* DXR, colored orange in Figure 6) in the catalytic domain adopts a conformation that allows it to function as a lid over the active site. The highly conserved residues Trp296 (212), Met298 (214), and Met360 (276) form a barrier between the active site and the solvent. The indole ring of Trp296 (212) provides the key hydrophobic interaction with the alkyl chain of the substrate and the backbone of fosmidomycin, which lies parallel within a distance of 4 Å. The acidic residues Asp231 (150), Glu233 (152), and Glu315 (231) are conserved at the active site and coordinate the divalent metal cation essential for enzyme activity. Met298 (214), Met360 (276), and the nicotinamide ring of NADPH also contribute to the formation of the hydrophobic binding pocket. The phosphonic acid moiety of fosmidomycin is bound similarly to the phosphate group of DXP in *Ec*DXR, forming hydrogen bonds with Ser270 (186) and Asn311 (227). The phosphonate group also forms a hydrogen bond with His293 (209). The hydroxamic acid moiety of fosmidomycin coordinates the divalent metal cation that is bound by the side chains of Asp231 (150), Glu233 (152), and Glu315 (231). The hydroxamate group also interacts with Ser232 (151) and Asn311 (227) (Figure 7).

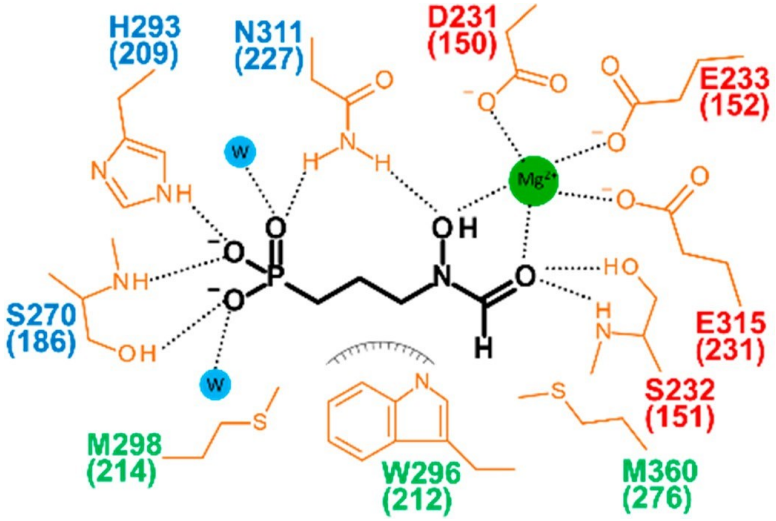

Figure 7. The binding mode of fosmidomycin in the active site of *Pf* DXR. Residues involved in the inhibitor binding are colored as in Figure 6A. The number in the parentheses indicates the residue number for the equivalent residue of *Ec*DXR.

The hydroxamic acid moiety of fosmidomycin (**1**) mimics the hydroxyl ketone structure and the phosphonic acid the monoalkyl phosphonate structure of DXP (**XII**, Figure 8A). Therefore, the substrate analog fosmidomycin binds in the active site with a comparable binding mode. Fosmidomycin acts as a slow, tight-binding competitive inhibitor with the substrate while acting uncompetitively towards the cofactor NADPH [84]. Based on the structure and interaction of fosmidomycin and its analogs with the binding site of DXR, this class of inhibitors can be described by a pharmacophore model presented in Figure 8B.

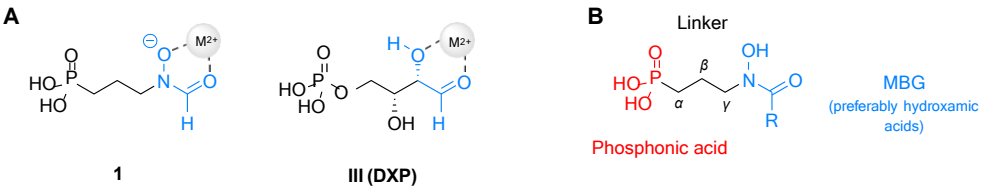

Figure 8. (**A**) Binding of **1** and natural substrate DXP (**III**) to a metal ion, represented by a grey sphere. (**B**) Simplified pharmacophore model of fosmidomycin-based DXR inhibitors MGB: Metal-binding group.

4. Structural Modifications of Fosmidomycin and FR900098

Based on the pharmacophore model defined in the previous section (Figure 8B), modifications of fosmidomycin and FR900098 will be discussed. These structural changes to both lead structures were introduced to overcome their poor pharmacokinetic properties and to especially improve the permeability. To assess structure–activity relationships (SAR), a wide array of structural modifications will be presented as well as their impact on the anti-infective activity. Docking studies and co-crystal structures are included to further illustrate this SAR.

4.1. Modifications of the Retro-Hydroxamate Moiety

Chemically, fosmidomycin is often described as a retro-hydroxamate. More specifically, with respect to the hydroxamate moiety, fosmidomycin is an *N*-substituted formohydroxamic acid. Regarding fosmidomycin analogs, the term reverse fosmidomycin derivative is commonly used for analogs, where the carbonyl group of the reversed hydroxamic acid is attached to the propyl linker and not to the nitrogen. The hydroxamic acid (HA) functionality is a common bidentate metal binding group (MBG) capable of chelating metal cations such as Zn^{2+}, Fe^{2+}, Fe^{3+}, Mg^{2+} and Mn^{2+} in the active sites of metalloenzymes [96]. The

chelation of the catalytically essential metal cation (Mg^{2+} or Mn^{2+}) in the active site of DXR by the retro-hydroxamate group of fosmidomycin is essential to its anti-infective effects.

4.1.1. Inversion of the Retro-Hydroxamate Moiety

The concept of reversing the orientation of the hydroxamate moiety was pioneered by the Rohmer group which synthesized compounds **3** and **4** (Figure 9) as analogs of fosmidomycin and FR900098. Both reverse analogs exhibited inhibitory activity comparable to that of fosmidomycin against *Ec*DXR with IC_{50} values of 0.17 (**3**) and 0.05 µM (**4**), respectively [97]. One year later, Woo et al. showed that compound **3** is a slower *Synechocystis* DXR binder in comparison to fosmidomycin [98]. In 2010, Zinglé et al. demonstrated that the superior *Ec*DXR inhibition of **4** was attributed to the hydrophobic interaction between the *N*-methyl group and the indole of Trp212 of *Ec*DXR [99]. Homolog **5** with an ethyl residue showed two orders of magnitude decrease in activity compared to **4** **[99]**.

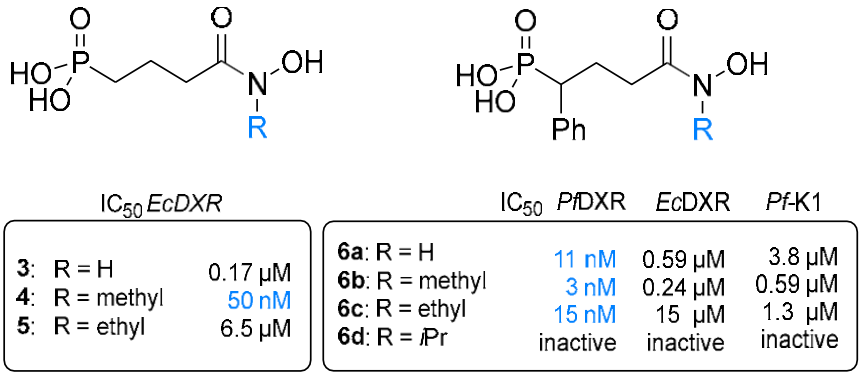

Figure 9. Structures, antibacterial, and antiplasmodial activities of the reverse fosmidomycin analogs **3**–**6**.

In parallel, reverse fosmidomycin analogs with a phenyl substituent in the *α*-position of the propyl linker were reported by Kurz and co-workers (**6a**–**d**, Figure 9). *α*-Phenyl analog (**6a**) served as a lead compound for the reverse inhibitor type. Furthermore, the compounds were decorated with small alkyl substituents (Me, Et, *i*Pr) at the hydroxamic acid nitrogen. The *N*-methylated carba analog **6b** was the most active inhibitor in the first reverse series, outperforming fosmidomycin and FR900098 in *Ec*DXR and *Pf* DXR inhibition with IC_{50} values of 0.24 µM and 3 nM, respectively. Enzyme inhibition data demonstrated that the strength of *Ec*DXR and *Pf* DXR inhibition decreased as the size of the substituent on the hydroxamic acid nitrogen increased. While the *N*-methyl-substituted DXR inhibitor **6b** is a potent *Pf* growth inhibitor, the *N*-ethyl substituted derivative **6c** already showed a 5-fold reduction in cellular antiplasmodial activity against *Pf* -K1. The bulkier *N*-isopropyl group of compound **6d** led to a loss of inhibitory activity against the *Pf* DXR and *Ec*DXR enzymes and *Pf*-K1 [100,101].

4.1.2. Alteration of the Acyl Moiety and Replacement of the Hydroxamic Acid Moiety

In order to create beneficial hydrophobic interactions in the hydrophobic sub-pockets of *Ec* and *Pf* DXR, Giessmann et al. [102] and Ortmann et al. [103] replaced the formyl group of fosmidomycin with aliphatic and aromatic acyl residues (**7, 8**, Figure 10). Within these series, the pentafluoro benzoyl derivative (**7c**) and the 4-phenoxybutanamide analog (**8b**) were the most active representatives with IC_{50} values of 1.3 (**7c**) and 1.0 µM (**8b**) against *Ec*DXR [102,103]. Flexible docking studies suggested that the acyl residues of compounds **7a**–**e** prevented the formation of the preferred geometry of the hydroxamate-metal complex [103].

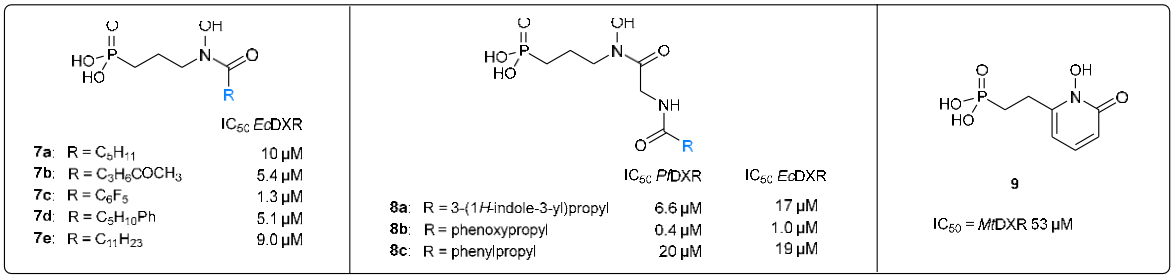

Figure 10. Structures and biological activities of compounds **7**–**9** with modified MBGs.

Andaloussi et al. developed the *N*-hydroxypyridone **9** (Figure 10) as an MBG [104], which only showed very weak *Mt*DXR enzyme inhibition with an IC_{50} value of 53 µM and no in vitro growth inhibition of *Mt* [104].

To confirm the importance of the hydroxamic acid functionality, the hydroxamic acid MBG was replaced with various amide moieties (**10a**–**e**, Figure 11) [102,105]. The IC_{50} values of amides **10a**–**e** against *Ec*DXR was > 30 µM. This was also demonstrated for fosmidomycin and FR900098 by Woo et al. who replaced the *N*-hydroxyl group of the retro-hydroxamate moiety with a methyl group in compounds **11a**, **b** (Figure 11) resulting in a complete loss of inhibitory activity against *Synechocystis* DXR [98]. Chofor et al. reported a series of *ortho*-substituted arylamide derivatives (**12a**–**c**, Figure 11) [16]. These *ortho*-substituents were expected to contribute to the chelation of the active site metal cation. However, none of the synthesized derivatives **12a**–**c** inhibited *Ec*DXR and *Mt*DXR at a concentration of 100 µM nor the growth of *Pf* -K1 parasites in human erythrocytes. According to Chofor et al., the low flexibility of the amide bond might be responsible for the lack of metal-binding and, therefore, inhibitory activity [16].

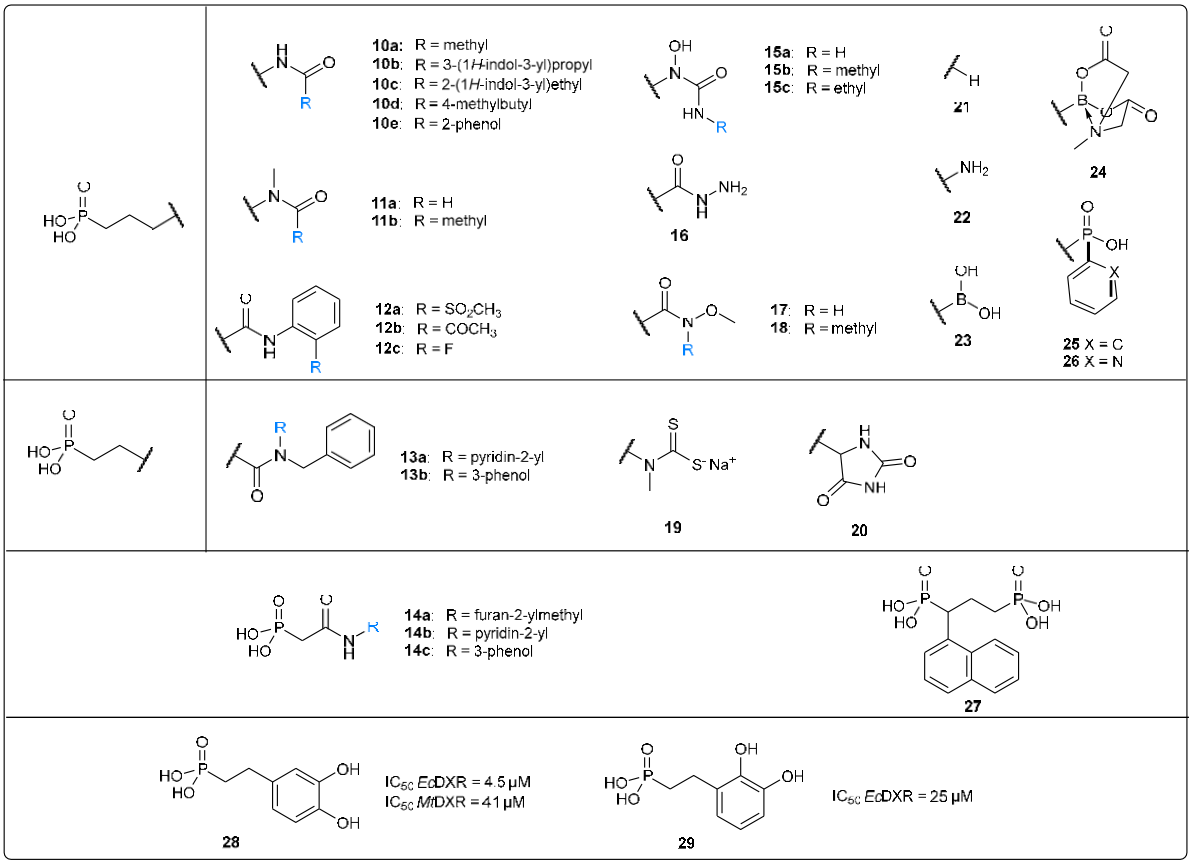

Figure 11. Structures and biological activities of analogs **10**–**29** with alternative chelating functionalities.

Kaye and colleagues studied the replacement of the hydroxamate MBG with a variety of *N*-arylalkyl substituted amides (**13a, b**, Figure 11), in which the benzyl group was intended to occupy the hydrophobic sub-pocket of the substrate binding site. However, the synthesized analogs **13a, b** were completely inactive against the *Pf* DXR enzyme [106]. Secondly, they introduced aryl and heteroaryl carboxamide groups (**14a–c**, Figure 11) in addition to shortening the propyl linker, but these modifications also led to inactive analogs [107,108].

Further work on replacing the hydroxamate MBG with different nitrogen-containing metal chelating moieties such as hydroxyureas (**15a–c**), hydrazide (**16**), *O*-methylated hydroxamate (**17**, **18**), dithiocarbamate (**19**) or hydantoin (**20**) functionalities (Figure 11) was performed [109]. For the hydroxyureas (**15a–c**) results regarding antiplasmodial or antibacterial activity have not been published [109]. Furthermore, the potential metal chelators **16–20** did not display any inhibitory activity towards *Ec*DXR. The authors suggested that the protonation of the hydrazide group of **16** under the assay's conditions (pH = 7.5) could explain the loss of its chelation capability. In the case of **19**, the authors reported decomposition of the dithiocarbamate moiety under the conditions of the enzyme assay [110]. The negligible *Mt*DXR inhibition of **20** is not surprising given that the hydantoin moiety of derivative **20** is not an established MBG [104]. Mercklé et al. showed that, as expected, the removal of the hydroxamic acid MBG as in the propyl phosphonic acid **21** and the aminopropyl phosphonic acid **22** (Figure 11) resulted in a complete loss of activity towards *Ec*DXR [105]. Mancini reported a chemically interesting derivative with a boronic acid unit as a potential MBG (**23**, Figure 11), though it was inactive in the *Ec*DXR enzyme assay. Prodrug **24** (Figure 11) to boronic acid **23** showed negligible activity towards *E. coli* [111]. Additionally, phosphinic acids with an aryl (**25**) or heteroaryl residues (**26**) were synthesized, but not evaluated against DXR (Figure 11) [112]. Furthermore, the bisphosphonic acid (**27**) was also inactive against DXR of *Ec*, *Pf* and *Mt* (Figure 11) [93]. The two catechol derivatives with a 3,4-catechol (**28**) and 2,3-catechol moiety (**29**) stood in contrast to the previously mentioned inactive derivatives (Figure 11). Compound **28** was at least weakly active against *Mt*DXR (IC_{50} = 41 µM) but no in vitro growth inhibition of *Mt* was observed. Interestingly, when tested against *Ec*DXR, the 2,3-catechol derivative **29** (IC_{50} = 25 µM) was weaker than the 3,4-catechol analog **28** (IC_{50} = 4.5 µM). These results confirmed the importance of the position of the two catechol hydroxyl groups for sufficient metal coordination [110,113].

So far, all attempts to replace the hydroxamate group with alternative chelating groups greatly reduced or resulted in a complete loss of inhibitory activity. The above-summarized results illustrate the predominant role of the hydroxamic acid MBG in DXR inhibitors.

4.1.3. Development of Bisubstrate Inhibitors

Since the adenosine-binding pocket of the cofactor NADPH returned a good score on a druggability test conducted by Hirsch and coworkers [114], a new bisubstrate inhibitor approach has been explored, aimed at simultaneously targeting the substrate and cofactor binding sites of DXR.

Guided by an *Mt*DXR fosmidomycin co-crystal structure, the Dowd group was the first to develop a series of fosmidomycin analogs aimed to occupy both binding pockets. Two series of compounds, fosmidomycin-like hydroxamic acids with large acyl residues (**30a–d**, Figure 12) and arylalkoxyamides (**31a–d**, termed *O*-linked bisubstrate inhibitors, Figure 12), were synthesized as potential bisubstrate inhibitors. While none of the derivatives was more active than fosmidomycin against *Mt*DXR, compounds **30a** and **30b** showed at least weak IC_{50} values of 18 and 27 µM. Docking experiments suggested that compound **30a** could interact with *Mt*DXR via an alternative non-bisubstrate mode of binding. So far, the Dowd group concluded that the hydroxamic acids **30a, b** are more potent *Mt*DXR inhibitors than the arylalkoxyamide derivatives (**31a, b**) [41,115]. Later on, compound **30a** was tested for its ability to inhibit the *Pf* DXR enzyme, but the compound showed only moderate activity with an IC_{50} of 1.34 µM [115,116].

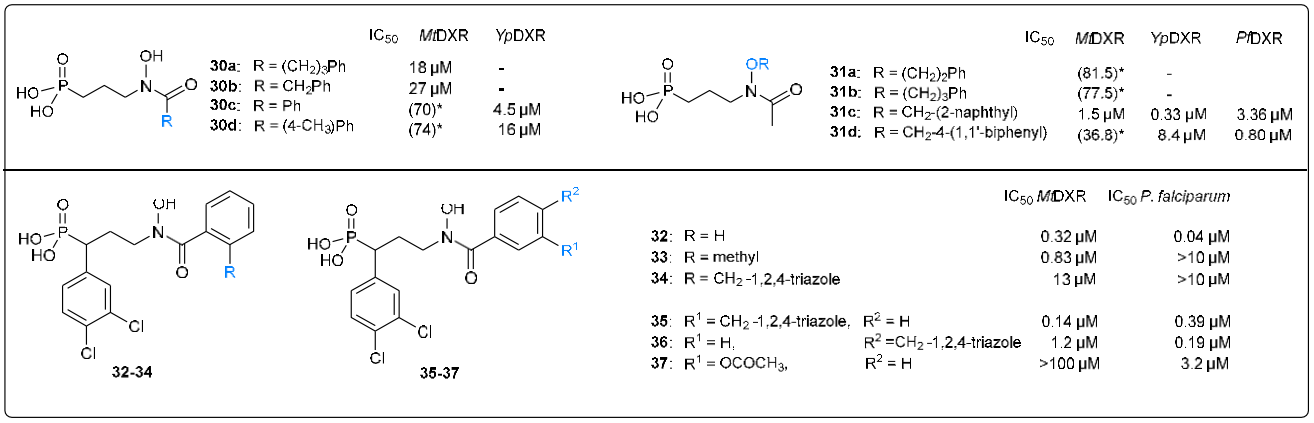

Figure 12. Biological activities of the potential bisubstrate inhibitors **30**–**37**. Values marked with * indicate the percentage of inhibition at 100 µM.

To improve the antibacterial activity and confirm that both hydroxamic acid and arylalkyloxyamide analogs can act as DXR bisubstrate inhibitors a larger series of hydroxamic acids (**30c, d**, Figure 12) and arylalkyloxyamides (**31c, d**, Figure 12) was developed by San Jose et al. [41]. When tested against *Mt*DXR, the most active compound was the arylalkyloxyamide **31c** with an IC_{50} value of 1.5 µM. However, **31c** and **31d** required concentrations of ≥200 µg/mL to be effective against *Mt*, while compound **31d** inhibited the growth of *Mt* at 25–50 µg/mL [41]. With an IC_{50} value of 0.33 µM against *Yp*DXR, compound **31c** was the most potent analog. Therefore, the authors suggested that a free hydroxamic acid functionality to strongly chelate the metal cation is not necessary for *Yp*DXR inhibition in the case of these potential bisubstrate inhibitors [41]. To assess whether **30c** and **31c** are bisubstrate inhibitors, Lineweaver-Burk analysis of **30c** and **31c**, tested against *Mt*DXR and *Yp*DXR, respectively, indicated that both compounds competitively inhibit NADPH and DXP. In 2021 Girma et al. tested alkoxyamides **31c, d** for their activity against *Pf* DXR. **31d** showed superior activity to **31c** with an IC_{50} of 0.80 to 3.36 µM, respectively. To determine the mechanism of inhibition of **31d**, Lineweaver-Burk analysis against *Pf* DXR enzyme was also performed. **31d** showed the lowest inhibition constant (K_i) with respect to both the substrate DXP and the cofactor NADPH. This finding demonstrated that **31d** is a bisubstrate inhibitor of *Pf*DXR [116].

The retro-hydroxamate **32** (Figure 12) showed submicromolar inhibitory activity towards *Mt*DXR (IC_{50} = 0.32 µM) in addition to potent in vitro growth inhibition in a *Pf* parasite assay (IC_{50} = 0.04 µM). A co-crystal structure of **32** in complex with *Mt*DXR in the presence of NADPH (PDB 3ZHY) showed that the terminal phenyl ring binds close to the NADPH binding site at a distance of 3.5–3.7 Å of the NADPH nicotinamide ring. In this position, the terminal phenyl ring can also interact with Met267. Inspired by the crystal structure, additional substituents were introduced at different positions on the phenyl ring, aimed at reaching the cofactor-binding pocket (**32**–**34**, Figure 12). The presence of methyl (**32**) or 1,2,4-triazole **(33)** substituents in the *ortho*-position of the phenyl moiety did not improve the inhibition. Isomers **35** and **36** (Figure 12) featuring the 1,2,4-triazole substituent in the *meta*- and *para*-position displayed enhanced inhibitory activity against *Mt*DXR compared to **34**, with IC_{50} values of 0.14 µM (**35**) and 1.2 µM (**36**).

In contrast, the introduction of the phenol ester substituent in compound **37** (Figure 12) resulted in a complete loss of activity towards *Mt*DXR. The strong in vitro growth inhibition of compounds **35** and **36** in a *Pf* growth assay and their potent *Mt*DXR inhibition suggested that the terminal triazole moiety might be involved in specific interactions with the DXR binding site [117]. Current efforts to develop DXR bisubstrate inhibitors provided novel compounds with heterogenous biological activities, with some inhibitors (**32**, **35**) showing very promising *Mt*DXR inhibition and antiplasmodial in vitro activity. Analog **37** showed that larger residues within the NADPH binding site are tolerated. This provides an

interesting starting point for the development of further inhibitors of this class. To further elucidate the binding modes of potential bisubstrate inhibitors, co-crystallization with an occupied NADPH binding site is required.

4.2. Modifications of the Propyl Linker

Earlier studies already highlighted the importance of the phosphonic acid and hydroxamate groups and a well-defined linker length between both pharmacophores. In contrast, the linker modifications provided a wide spectrum of options for further improvements of anti-infective activity against various microorganisms. The synthesized derivatives are structurally diverse. These modifications encompass alterations of the linker length (**38**–**41**), insertion of a double bond (**42**–**46**) or hetero atoms (**47**–**54**), restriction of the linker flexibility (**55**–**60**) and substitution of the linker in the *α*-, *β*- and *γ*-position.

4.2.1. Linker Length Variation

In an initial effort to determine the ideal linker length, the Fujisawa Pharmaceutical Co., Ltd. was the first to explore modifications of the carbon backbone. However, the shortened ethylene analogs **38** did not show any antibacterial activity against, e.g., *P. aeruginosa* (Figure 13) [118]. The Dowd group synthesized a series of FR900098 analogs with two to five methylene units separating the MBG and phosphonic acid moiety (**39a–c**, Figure 13) [119]. The results showed that compounds with chain lengths of two, four or five methylene groups weakly inhibited *Mt*DXR at 100 µM (74-86%) [119]. Later, Zinglé et al. prepared reverse fosmidomycin (**3**) and reverse FR900098 (**4**) homologs bearing a shortened ethylene (**40a, 41a**, Figure 13) or extended butylene linker (**40b, 41b**, Figure 13). The derivatives with an ethylene linker were weakly active (**41a**) or lacked activity (**40a**) against *Ec*DXR, while the reduction was less drastic for the butylene homologs (**40b, 41b**), with IC_{50} values of 0.27 and 0.11 µM, respectively [99].

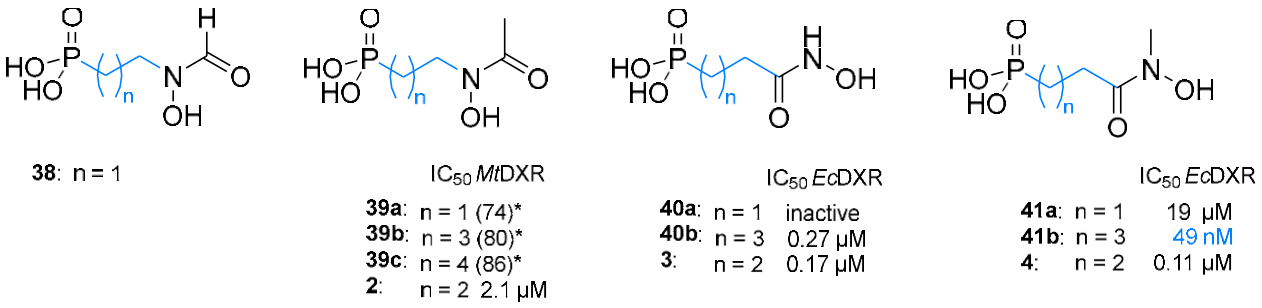

Figure 13. Biological activities of analogs **38**–**41.** Values marked with * indicate the percentage of inhibition at 100 µM.

4.2.2. α,β-Unsaturated Propenyl Linker

FR32863 (**IV**), a natural antibiotic isolated from *Streptomyces lavendulae* in 1980, is the dehydro-congener of fosmidomycin (**1**). FR32863 and its acetylated analog **42** showed activity similar to **1** and **2** against a panel of Gram-negative bacteria including *P. aeruginosa* [21,118]. Biological evaluation showed that FR32863 is an excellent inhibitor of *Pf* DXR (IC_{50} = 9 nM) that also potently inhibits the growth of *Pf* 3D7 with an IC_{50} of 19 nM. Compound **42** was further active against *Mt*DXR with an IC_{50} of 1.1 µM. Based on these results, Devreux synthesized *Z*- (**43a–e**, **44d**) and *E*-configured (**44a–c**, Figure 13) *α,β*-unsaturated DXR inhibitors with additional substituents in the *α*-position and tested them against *Ec*DXR [119]. The *Z*-configured *α*-bromo derivative **44d** was the most active compound, displaying a submicromolar IC_{50} value of 0.45 µM. Furthermore, the *E*-configured.

Analogs (**44a–c**) were active in the micromolar range (IC_{50} = 5.5–16 µM), while the *Z*-configured derivatives **43a–e** were inactive. This suggested that the relative *trans*-conformation of the phosphonic acid and hydroxamate moiety towards each other is essential for activity. However, the combination of an *α*-substituent and an *α, β*-unsaturated linker constrained

the rotational freedom, thus leading to reduced activity against *Ec*DXR [120]. The Dowd group also designed and synthesized a series of FR32863 (**IV**) analogs **45** and **46a–d** (Figure 14). Although, none of the derivatives exceeded the activity of FR32863 against *Pf* DXR, compounds **45** and **46a–c** showed moderate inhibitory activity in vitro with IC_{50} of 2.1–14 µM [121].

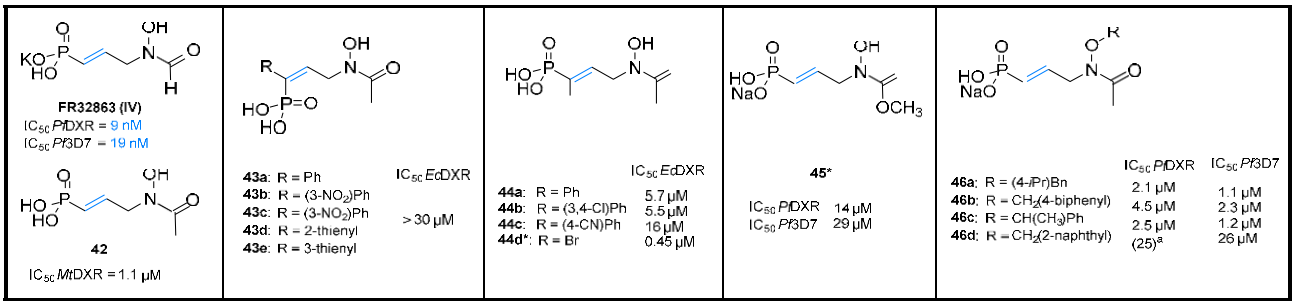

Figure 14. Biological activity of the fosmidomycin and FR900098 derivatives (**42–46**) with an *α,β*-unsaturated linker. * Ammonium salts were prepared. [a] Values in parentheses are the percent remaining enzyme activity at 100 µM.

4.2.3. Oxa Analogs

Fosfoxacin (**47**, Figure 15), the naturally occurring phosphate congener and *α*-oxa analog of fosmidomycin as well as fosfoxacin's acetyl analog (**48**), are more potent inhibitors of *Synechocystis* DXR compared to fosmidomycin [122]. These results encouraged Haemers et al. to synthesize a series of *β*- and *γ*-oxa-isosteres (**49–54**, Figure 15) as the electronegative oxygen might increase the acidity of the phosphonic acid and hydroxamic acid moiety. While compounds **49** and **50** are *β*-oxa-isosteres of fosmidomycin and FR900098, respectively, analogs **51–54** are reverse derivatives. The results showed that the *β*-oxa analogs **49–52** are more active *Ec*DXR inhibitors than the *γ*-counterparts (hydroxycarbamates) **53** and **54**. The *β*-oxa isosteres **50** and **52** were almost as potent as FR900098 displaying IC_{50} values of 87 nM (**50**) and 72 nM (**52**) against *Ec*DXR and submicromolar activity against strain *Pf*3D7 [123].

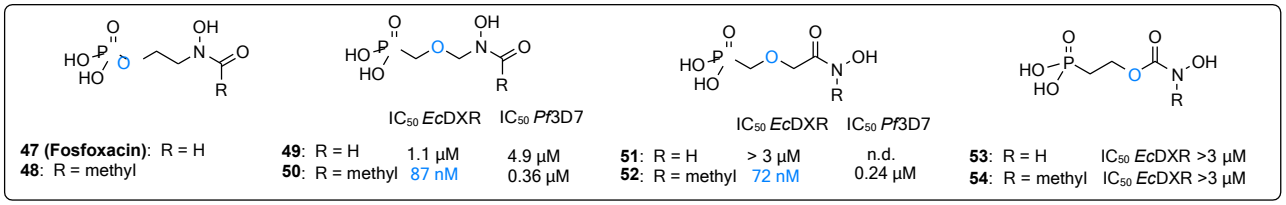

Figure 15. Structure and biological activity of the oxa analogs **47**–**54**.

4.2.4. Conformationally Restricted Analogs

In 2006, the Van Calenbergh group incorporated a cyclopropyl (**55–57**, Figure 16) [124] and cyclopentyl (**58–59**, Figure 16) [125] ring into the linker to restrict rotational freedom. The racemic *trans*-cyclopropyl *N*-acetyl analog **55** resulted in submicromolar inhibition of *Ec*DXR with an IC_{50} of 0.16 µM, while the enantiomerically pure (1*R*,2*S*)-**55** showed enhanced activity (IC_{50} = 50 nM) that was comparable to fosmidomycin. Additionally, (1*R*,2*S*)-**55** was similarly active compared to fosmidomycin (IC_{50} = 0.32 µM) in an in vitro *Pf* 3D7 assay. The replacement of the acetyl moiety of (1*R*,2*S*)-**55** by a formyl moiety (**56**) reduced the activity against *Ec*DXR and *Pf*3D7 by approximately 6-fold.

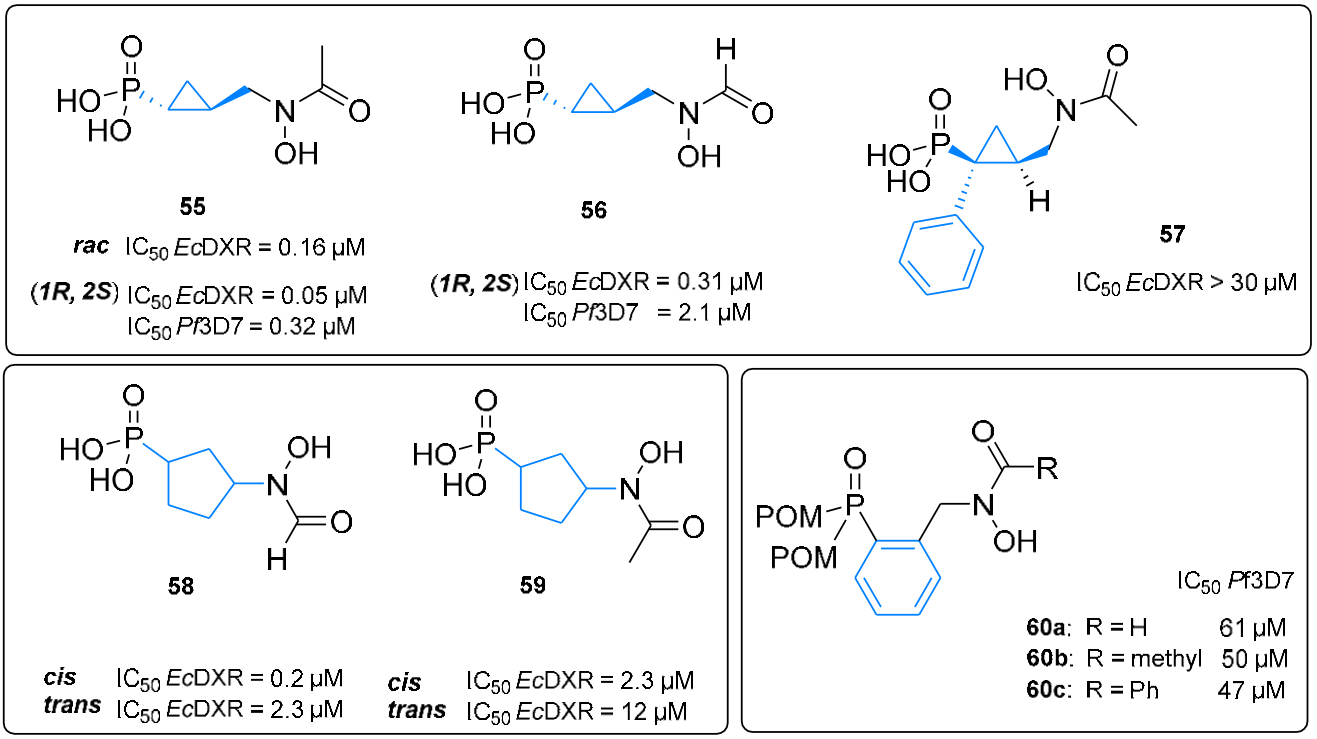

Figure 16. Biological activity of conformationally restricted analogs **55**–**60**.

The racemic mixture of an *α*-phenyl substituted *cis*-cyclopropyl derivative (**57**) was inactive towards *Ec*DXR. Unfortunately, it is not clear whether the loss of activity was caused by the bulky *α*-phenyl moiety or by the *cis*-conformation of the phosphonic acid and hydroxamate moieties [124]. Haemers et al. gave some insights regarding the preferred configuration of restricted analogs as they synthesized the *cis*- and *trans*-cyclopentyl derivatives of fosmidomycin (**1**) and FR900098 (**2**). The *cis* isomers of **58** and **59** (IC_{50} values of 0.20 and 2.3 µM, respectively) were more active than their *trans*-isomers (IC_{50} values of 2.3 and 12 µM, respectively).

One year later, the synthesis and antiplasmodial activity of three conformationally restrained aromatic analogs **60a–c** (Figure 16) were reported by Walter and colleagues. The analogs **60a–c** were tested as bis(pivaloyloxymethyl) (POM) ester prodrugs and the POM prodrugs of **1** and **2** were prepared for direct comparison. While the POM-prodrugs of **1** and **2** were moderately active against *Pf* 3D7 (IC_{50} = 0.4–2.1 µM), the activity of the corresponding rigidized analogs (**60a–c**) was very weak [126].

4.3. α-, β- and γ-Substituted Fosmidomycin Analogs

4.3.1. α-Phenyl and α-Biaryl-Substituted Analogs

To date, most attempts to improve the anti-infective properties of fosmidomycin are related to the substitution and modification of the *α*-position of the propyl linker (Figure 17) [45,125,127–131]. The first chain-substituted derivatives were decorated with an *α*-phenyl-substituent and were synthesized and patented in 2005 by Kurz et al. [132]. The diethanolammonium salt of *α*-phenyl-fosmidomycin (**61**, Figure 17) was the first inhibitor to exceed the antiplasmodial activity of FR900098 (**61** IC_{50} = 0.4 µM and FR900098 IC_{50} = 0.8 µM) against *Pf*Dd2.

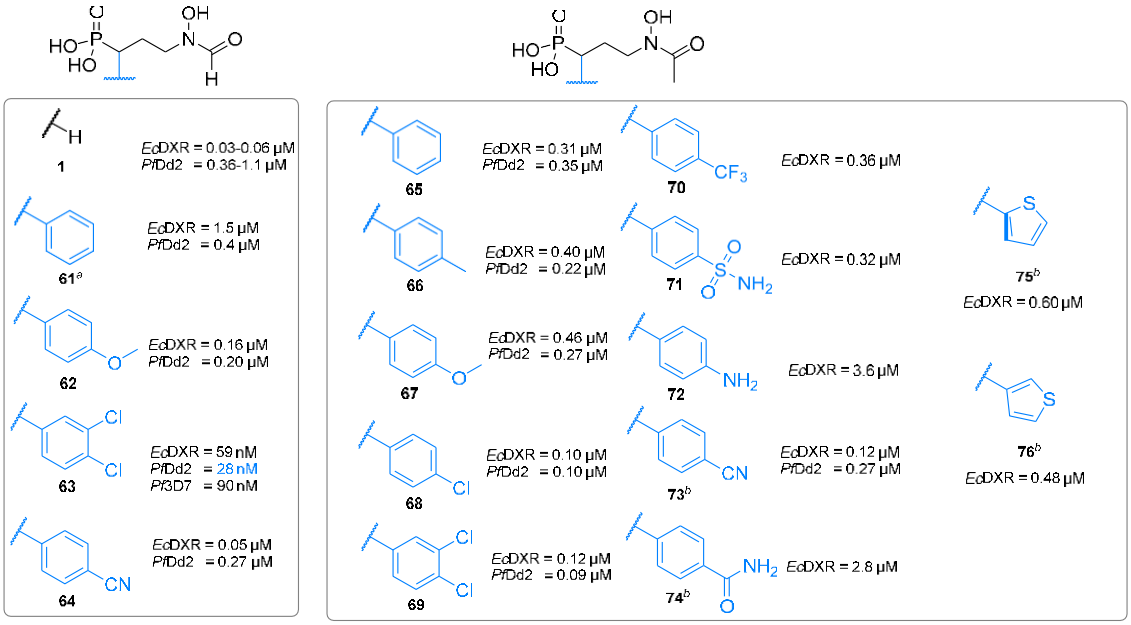

Figure 17. Antibacterial and antiplasmodial activities of α-phenyl derivatives (**61**–**76**). [a] Diethanolammonium salt was prepared. [b] Ammonium salts were prepared.

In 2006 and 2007, Van Calenbergh and coworkers presented a comprehensive series of *α*-phenyl substituted analogs with electron-rich and electron-deficient substituents at the phenyl moiety (**62**–**74**, Figure 17) [130]. The authors aimed to investigate the influence of lipophilicity and electronic properties with respect to their inhibitory activity against *Ec*DXR and the *Pf* Dd2 strain [45]. Whereas several *α*-phenyl-substituted compounds of this series showed slightly lower inhibitory activity than lead structures fosmidomycin (**1**) and FR900098 (**2**) against *Ec*DXR, the inhibition of *Pf* growth (Dd2 and 3D7 strains) was consistently superior. The authors suggested the 3,4-dichlorophenyl unit of the derivatives **63** and **69** increased the lipophilicity and facilitated entry into *P. falciparum* cells and/or enabled more selective interactions with *Pf* DXR. The *α*-3,4-dichlorophenyl substituted analog **63** was a milestone in lead optimization, as it was the first inhibitor which exceeded the potency of **2**, with an IC_{50} value of 59 nM against *Ec*DXR. In addition, **63** exhibited potent in vitro activity with IC_{50} values of 28 and 90 nM against *Pf* Dd2 and *Pf* 3D7 strains, respectively. Unfortunately, *Pf*DXR inhibition was not reported [45].

In accordance with previous studies [45], the potency of the most active *N*-acetyl-(4-cyano)phenyl analog **73** was exceeded by its *N*-formyl analog **64**. Furthermore, both compounds exceeded **1** and **2** in an antiplasmodial growth assay (IC_{50} = 0.27 μM) using intraerythrocytic stages of the *Pf* D2d strain [130]. A 2-thienyl and 3-thienyl analog (**75**–**76**, Figure 17) exhibited submicromolar activity (IC_{50} = 0.48–0.60 μM) as well, which confirmed that thiophene can be used in this case as a phenyl bioisoster [130].

Achieving whole-cell activity for fosmidomycin-like DXR inhibitors against *M. tuberculosis* is particularly challenging as *Mt* lacks the GlpT-type transporters, responsible for inhibitor uptake in other bacteria.

In 2011, FR900098 (**2**) was first tested against *Mt*DXR by the Karlén group [128]. Although significant *Mt*DXR inhibition was observed, no antimycobacterial activity was detected. In response, the Karlén group developed more lipophilic inhibitors based on the work of Van Calenbergh and Kurz [120,130,131,133]. Both research groups demonstrated that *α*-phenyl substituents increased the activity of *Pf* and *Ec*DXR inhibitors. Employing the same strategy, the Karlén group synthesized several *α*-phenyl derivatives with different substituents in the *ortho*-position of the phenyl moiety, *α*-biaryl derivatives, and inhibitors with bicyclic ring systems in the *α*-position (**77**–**91**, Figure 18) [128,129]. The *ortho*-substitution of the *α*-phenyl moiety completely reduced the activities of the inhibitors against *Mt*DXR.

Docking experiments proposed possible clashes between the *ortho*-substituents and the enzyme, which could explain the loss of activity. Furthermore, none of the derivatives (**77**–**91**, Figure 18) inhibited the growth of *Mt* H37Rv. The inhibitors with bulky moieties in the α-position (**84**–**88**) inhibited *Mt*DXR with IC_{50} values between 1.5 and 27 μM. The α-4-(pyridine-3-yl)phenyl analog (**89**) exhibited the best activity against *Mt*DXR (IC_{50} = 0.8 μM), which is comparable to the α-3,4-dichlorophenyl derivate (**90**, IC_{50} = 0.7 μM). No correlation between calculated logP and IC_{50} values of this compound series (**77**–**91**) was found. Docking experiments of **89** with *Mt*DXR suggested that the biaryl moiety of **89** interacts with the flexible loop formed by Gly198-Met208 (Figure 19). This possible interaction provided the basis for further inhibitor optimizations.

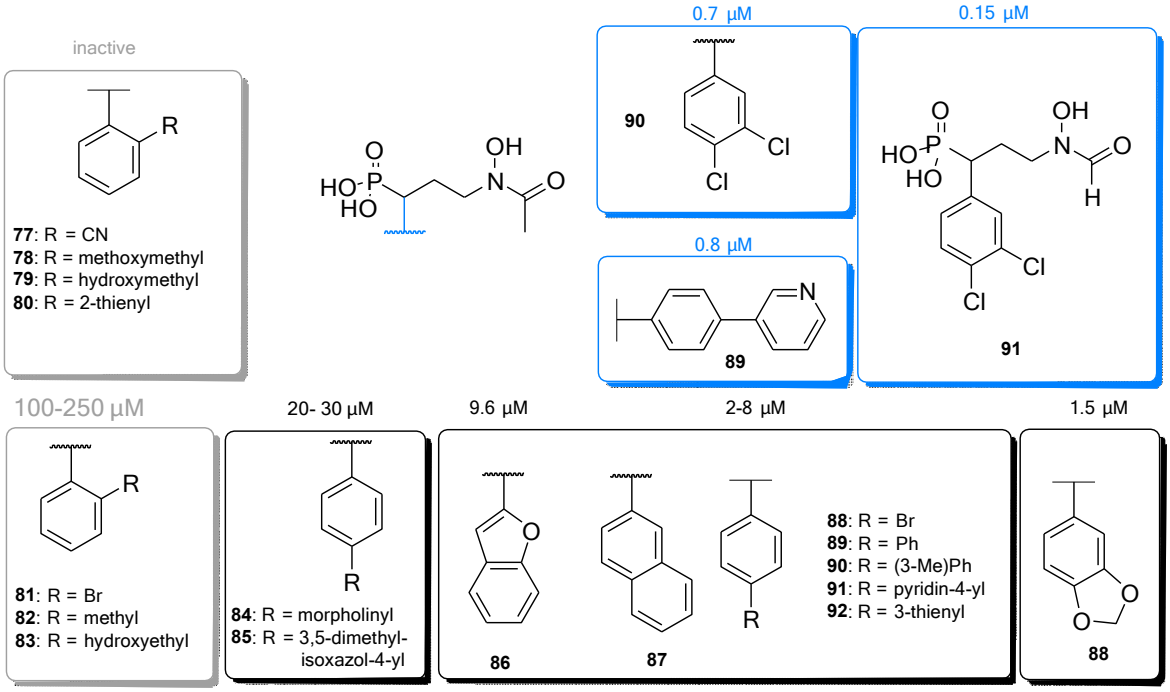

Figure 18. Structure–activity relationship of α-substituted FR900098 analogs **77**–**90**, the *N*-formyl analog **91** and their activity against *Mt*DXR.

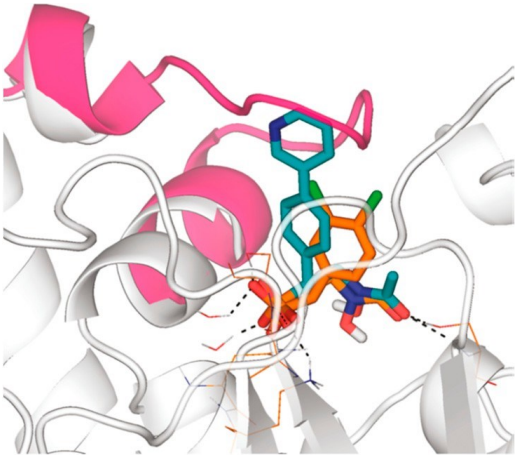

Figure 19. Compound **89** (turquoise carbon atoms) docked in the X-ray structure of *Mt*DXR in complex with 3 orange carbon atoms (PDB code 2Y1G) [128]. The Gly198-Met208 flap (colored in pink) from the 2JVC structure representing *Mt*DXR bound to fosmidomycin (**1**). Reprinted with permission from *J. Org. Chem. 2011, 76, 21, 8986–8998* [129]. Copyright 2022 American Chemical Society.

4.3.2. α-Halogenated Phosphonic Acid Derivatives

Verbrugghen et al. [127] tried to mimic the acidity of the phosphate group of fosfoxacin (**47**, Section 4.2.3) with *α*-chloro (**92**) and *α*-fluoro (**93**) phosphonic acid moieties (Figure 20). Additionally, the group conducted P^{31}-NMR-titrations of FR900098 and its *α*-chloro and fluoro analogs (**92, 93**). This experiment revealed that the decreased pKa_2 value of the phosphonic acid moiety of both analogs ($pKa_2 \sim 6$ vs. $pKa_2 \sim 7.35$ for **2**) is isoacidic to a monoalkyl phosphate group. The corresponding SAR data led to the conclusion that DXR inhibitors with a dianionic phosphonate group are more potent inhibitors than the corresponding monoprotonated phosphonate anions (further explanations are discussed in Section 5) [98,104,127,134].

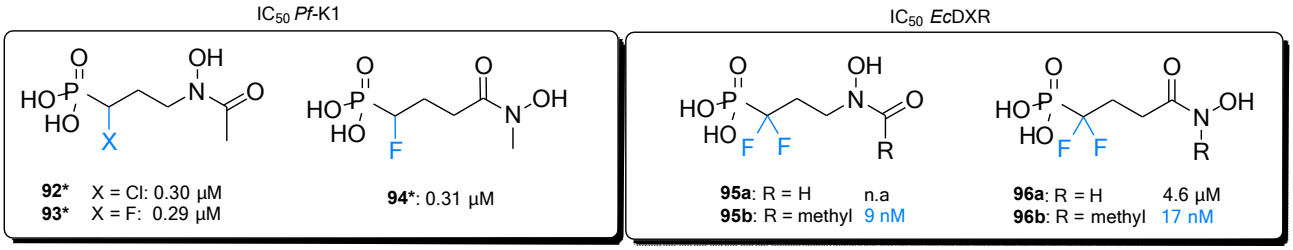

Figure 20. Biological activities of α-halogenated phosphonic acid derivatives (**92**–**96**). * Ammonium salts were prepared.

Furthermore, the Van Calenbergh group synthesized the *α*-fluoro analog (**94**) of the reverse FR900098 [127]. The three racemic compounds (**92**–**94**) were screened for their activity against asexual blood stages of *Pf* and found to inhibit their growth with IC_{50} values in the micromolar range (IC_{50} = 0.29–0.31 µM), surpassing the activity of FR900098 (IC_{50} = 0.42 µM). Both fluorinated analogs (**93**–**94**) were further evaluated in the *Plasmodium berghei* (GFP ANKA strain) mouse model by intraperitoneal (i.p.) application of high doses (50 mg/kg) for 5 consecutive days. Chloroquine (CQ) eradicated parasitemia after 4 days post-infection, while FR900098 only led to 93% suppression of parasitemia. Compared to the reference substances CQ and FR9800098, the in vivo activity of **93** (88%) and **94** (85%) was slightly weaker on day 4. In summary, **93** and **94** exhibited significant in vivo antimalarial activity at day 4 after i.p. application, but none of the monohalogenated DXR inhibitors (**93**–**94**) demonstrated curative antimalarial activity [127]. This was an important outcome and provided a starting point to investigate inhibitors with further substitutions at the *α*-methylene group.

Recently, Dreneau et al. extended the mono *α*-halogenation into difluorination synthesizing the *α,α*-difluorophosphonic acid derivatives of fosmidomycin and FR9000098 (**95a, b**, Figure 20) as well as their reverse analogs (**96a, b**, Figure 20). The difluorinated analogs were tested for their inhibitory activity against *Ec*DXR and a fosmidomycin-resistant *E. coli* (FosR) strain [135]. Against *Ec*DXR, the *N*-acylated and *N*-methylated derivatives (**95b**, **96b**) showed excellent IC_{50} values of 9 and 17 nM, respectively. Therefore, the potency of **95b** and **96b** is in the same range as fosmidomycin and FR900098. In contrast, the non-methylated difluoromethylene compound **96a** was significantly less efficient than its *N*-methylated congener **96a** (IC_{50} = 4.6 µM) against *Ec*DXR. The same observation was made in the *E. coli* growth inhibition assay paper determined with the disc diffusion method, where **96a** was inactive, while **95b** and **96b** effectively inhibited bacterial growth. Moreover, no spontaneous resistance to these compounds occurred in *E. coli* as was observed for fosmidomycin [136]. This increase in activity was attributed to the formation of phosphonate dianions under test conditions. The isoacidic nature and the isosteric geometry of the fluorinated phosphonic moiety, together with improved electrostatic and van der Waals interactions, are possible explanations for the pronounced activity. None of the derivatives could prevent the growth of the fosmidomycin-resistant *E. coli* strain FosR, in which the GlpT transporter is dysfunctional and did not facilitate the uptake of

these inhibitors. This suggested that uptake of inhibitors **95a, b** and **96a, b** relied on an active transport mechanism by intact and functioning GlpT transporters. In summary, the introduction of two fluorine atoms in the α-position of the linker improved *Ec*DXR inhibition significantly and enhanced the antimicrobial activity compared to phosphate analogs (**47**, **48**) or non-fluorinated lead structures in *E. coli* (**1**–**4**, Figure 9).

4.3.3. Structurally Diverse Substituents in the α-Position

The promising results obtained with the α-phenyl substituted DXR inhibitors (Section 4.3.1), encouraged the Van Calenbergh group to extend the scope of α-substituents to benzamido (**97**), a phenylurea moiety (**98**), methoxy (**99**), phenoxy (**100**), substituted 1,2,3-triazolyl groups (**101a–c**), azido (**102**) and a hydroxyl group (**103**, all Figure 21) [137]. Of the structurally diverse inhibitors, only the α-azido derivative (**102**) and the α-hydroxy derivative (**103**) showed pronounced *Ec*DXR inhibition. The electron-rich α-triazole derivatives (**101a–c**) did not inhibit *Ec*DXR and only moderately suppressed the growth of *Pf* -K1. This behavior was postulated by the authors to be caused by the inability of the triazole ring to form π–π interactions with Trp211. Later, a reverse analog (**104**, Figure 21) was synthesized and showed weak inhibition of *Pf* and *Ec*DXR with IC_{50} values of 9–11 µM [138].

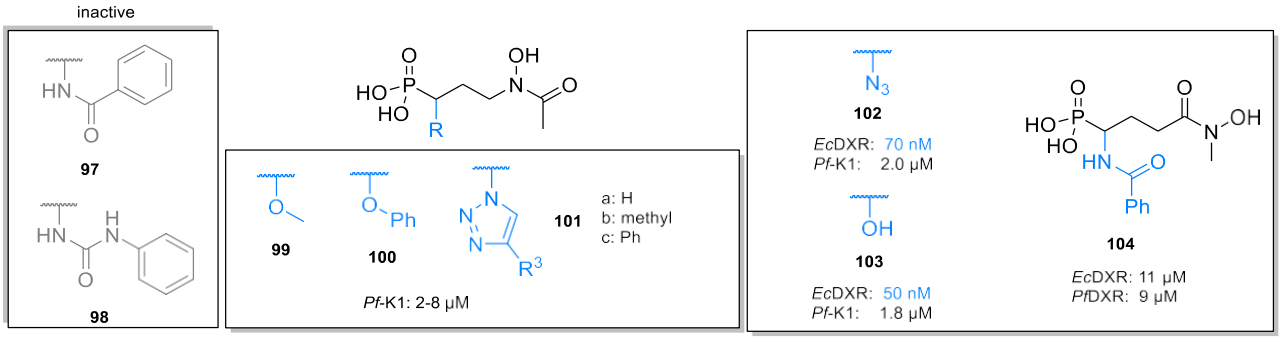

Figure 21. Biological data of structurally diverse α-substituted analogs **97**–**104**.

The α-pyridinyl-substituted fosmidomycin analogs (**105a, b** and **106a, b**, Figure 22) were designed by Xue et al. [139] and assessed with respect to their inhibitory potential against *Ec*DXR, *Pf* DXR, *Pf* Dd2 and *Pf* 3D7 (data of the latter not shown). The pyridine-containing derivatives **105a, b** and **106a, b** showed similar IC_{50} values to fosmidomycin when tested against *Ec*DXR (IC_{50} = 35–87 nM vs. IC_{50} (**1**) = 34 nM), while being 2-fold more active than fosmidomycin towards *Pf* DXR (IC_{50} = 2-13 nM vs. IC_{50} (**1**) = 21 nM). The antiplasmodial activity of the four compounds was stronger compared to fosmidomycin. Similar to fosmidomycin, the four pyridine derivatives (**105a, b** and **106a, b**) exhibited no cytotoxicity against human noncancerous fibroblast WI-38 cells (>300 µM) resulting in extraordinarily high selectivity indices of >1700.

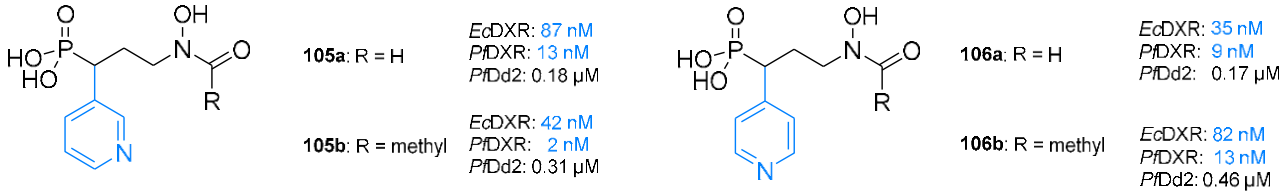

Figure 22. Rational design of α-pyridinyl DXR-inhibitors **105a, b** and **106a, b**. K_i values are given in µM (black) or nM (blue) against *Ec*DXR, *Pf*DXR and *Pf*Dd2.

To elucidate the interactions between **106b** and *Pf* DXR, the crystal structure in complex with NADPH and Mn^{2+} was solved and analyzed (Figure 23). In the crystal structure, the backbone of **106b** showed similar interactions to previously analyzed DXR inhibitors with α-phenyl substituents (e.g., **66**, Figure 17) [32,94,140,141]. In addition, the pyridine

nitrogen atom formed a hydrogen bond with the thiol group of Cys338. This interaction is not possible for the unsubstituted phenyl analog **66** and is thus a conceivable explanation for the weaker activity of **66** compared to **106b**.

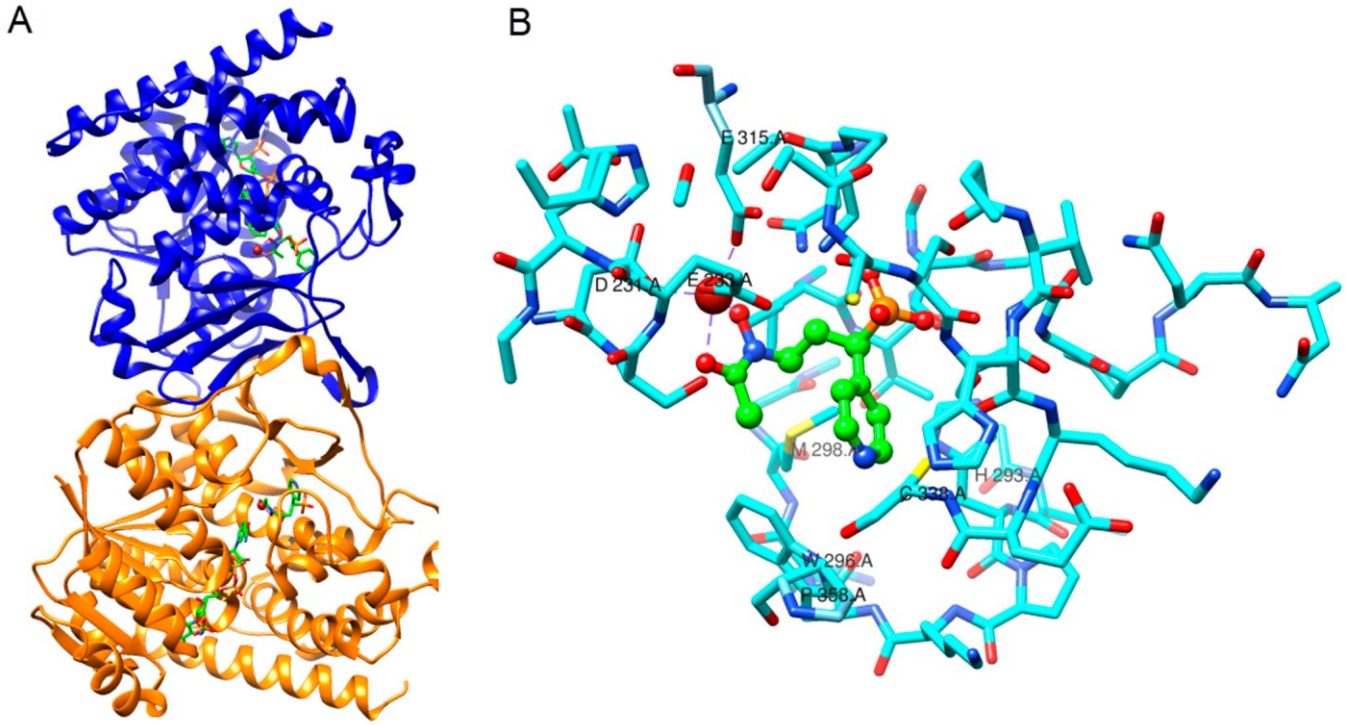

Figure 23. (**A**) overall structure of *Pf* DXR in complex with Mn^{2+} (brown sphere), **106b** (green) and NADPH. (**B**) Close-up view of the active site of *Pf* DXR:**106b**. Reproduced from Xue et al. (PDB: 4GAE [139].

4.3.4. α-Substituted Reverse Carba Analogs

Focusing on reverse fosmidomycin analogs, Kurz and coworkers broadly investigated the effects of the substitution at the *α*-position of the propyl linker [93,100,101]. The comprehensive biological data of *α*-substituted reverse analogs (**107–111**) are summarized in Figure 24. Several reverse carba analogs (**107b, 108a, 109** and **110a, b, 111b**) inhibited *Pf* DXR with IC_{50} values in the low nanomolar range and outperformed fosmidomycin. The IC_{50} values against *Ec*DXR are 1–3 orders of magnitude higher than the corresponding IC_{50} values for *Pf* DXR, but comparable to fosmidomycin. This finding is of significant importance since *Ec*DXR was initially used as a surrogate for *Pf* DXR inhibition due to its difficult production and handling [100]. Kurz and coworkers concluded based on this series that *α*-phenyl derivatives with a free or *N*-methylated hydroxamic acid **(107a, b)** moiety are very promising derivatives for further drug development [93,100,101]. Introduction of electron-withdrawing chloro- and fluoro-substituents (**109, 110a, b**) led to excellent inhibitors of *Pf* DXR (IC_{50} = 3–4 nM), while electron-donating groups (**111**) decreased activity (Figure 24). Derivative **110b** was furthermore a potent inhibitor of *Pf* Dd2 in vitro (IC_{50} = 40 nM).

Interestingly, the in vivo efficacy of the difluorophenyl derivative **110a** (application of 80 mg/kg i.p. for 5 days) in a *P. berghei* ANKA mouse model at day 5 post-infection was almost similar to fosmidomycin. Compounds **110a** and **110b** reduced the percentage of infected erythrocytes significantly (89% and 78%, respectively), but the effect on mice survival was less pronounced, and no curative antimalarial activity was observed [100].

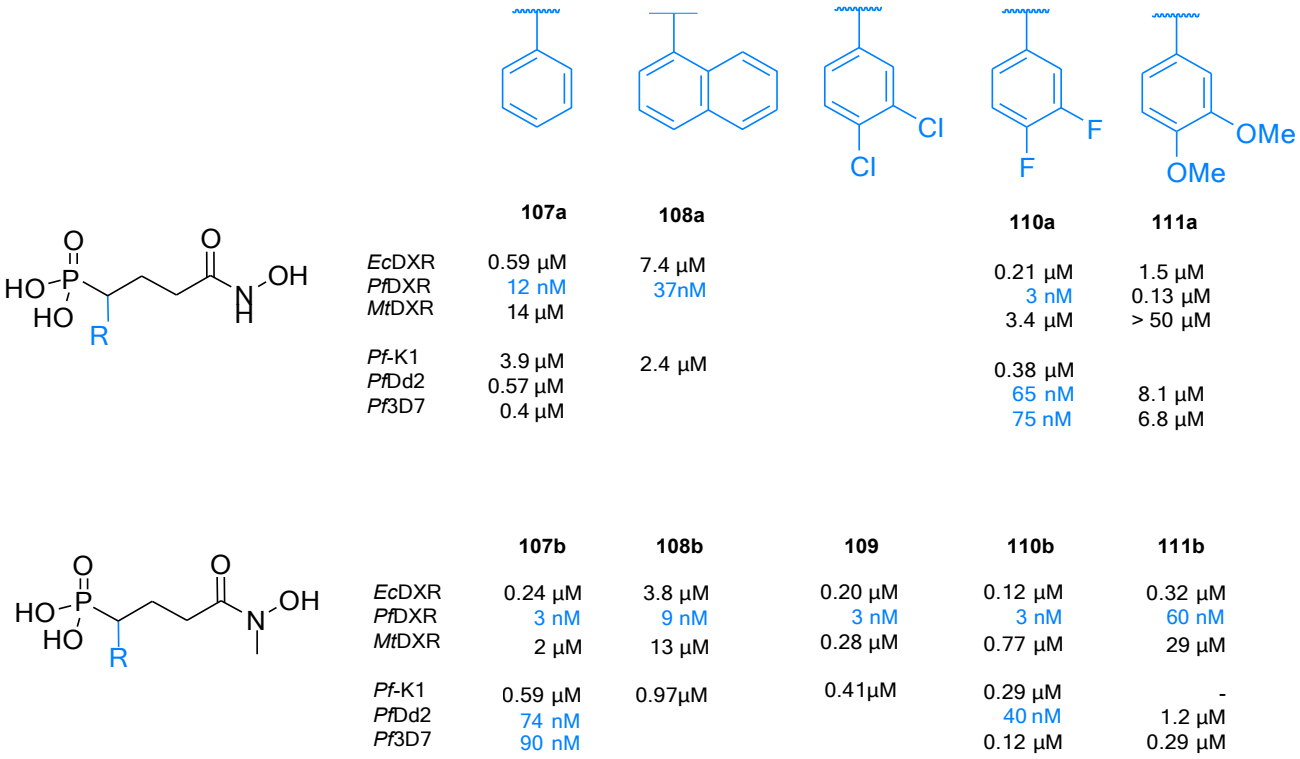

Figure 24. Biological data of α-substituted reverse fosmidomycin analogs (**105**–**109**).

Moreover, the X-ray crystal structure of *Ec*DXR in complex with fosmidomycin and Mn^{2+} (Figure 25) revealed that fosmidomycin fits perfectly into the closed conformation of the catalytic site, whereas the difluorophenyl ring of **110b** would clash with the flexible loop region and therefore binds to the open conformation of the catalytic site.

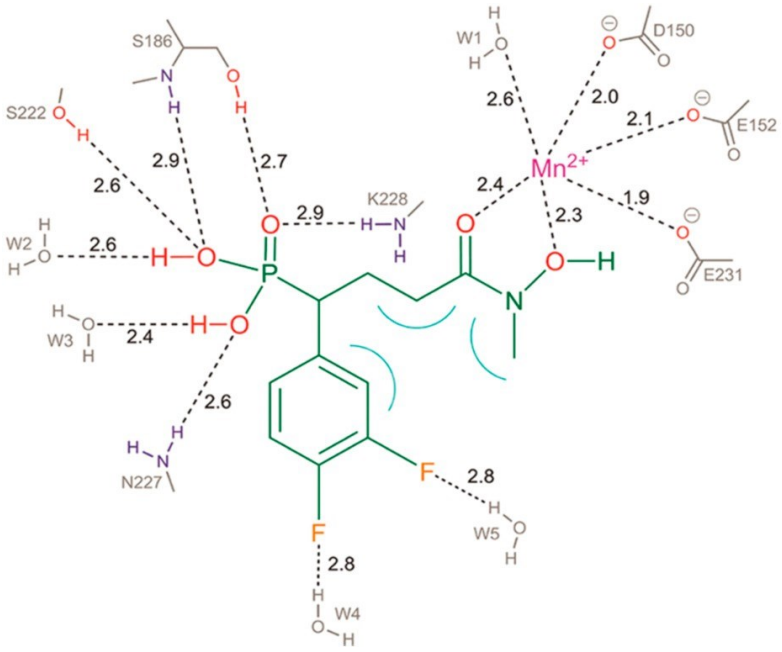

Figure 25. Schematic overview between **110b** (green) and the active site of *Ec*DXR. Intramolecular van der Waals interactions (light blue) between the *N*-methyl group with the difluorophenyl ring and the linker atoms of **110b**. Distances are in Å [100]. Reprinted with permission from *J. Med. Chem.* 2011, 54, 6796–6802 [100]. Copyright 2022 American Chemical Society.

4.3.5. Reverse α-Substituted Oxa, Thia and Aza Analogs

Based on the promising *α*-phenyl-substituted reverse carba analogs, Kurz and coworkers developed bioisosteric *α*-substituted *β*-thia and *β*-oxa analogs (**112–115**, Figure 26) [93,138,142,143]. Compounds **112–115** were tested against *Pf, Mt* and *Ec*DXR enzymes as well as in antiplasmodial growth assays towards *Pf* Dd2 and *Pf* 3D7. The *β*-oxa analogs with an unsubstituted hydroxamic acid group (**113**) were at least 2 orders of magnitude less potent than their *N*-methylated analogs **112a–h** in all DXR enzymes and *Pf* growth assays. Derivatives **112a–h** were good to excellent inhibitors of *Pf* DXR (IC_{50} = 12–65 nM), but were less efficient in *Pf* growth assays (IC_{50} = 0.2 µM–1.3 µM). These results indicated that the *N*-methylation of the hydroxamic acid moiety is often beneficial for potent antiplasmodial in vitro activity of *α*-phenyl-substituted reverse analogs. The positive impact of *N*-methyl substitution was later confirmed for the *β*-thia-analogs (**115a–h**) as the non-methylated derivatives **114a–f** were in general less efficient compared to the *N*-methyl-substituted analogs. Analysis of the crystal structures of *N*-methylated derivatives showed, that the methyl group forms beneficial van der Waals interactions [100,138].

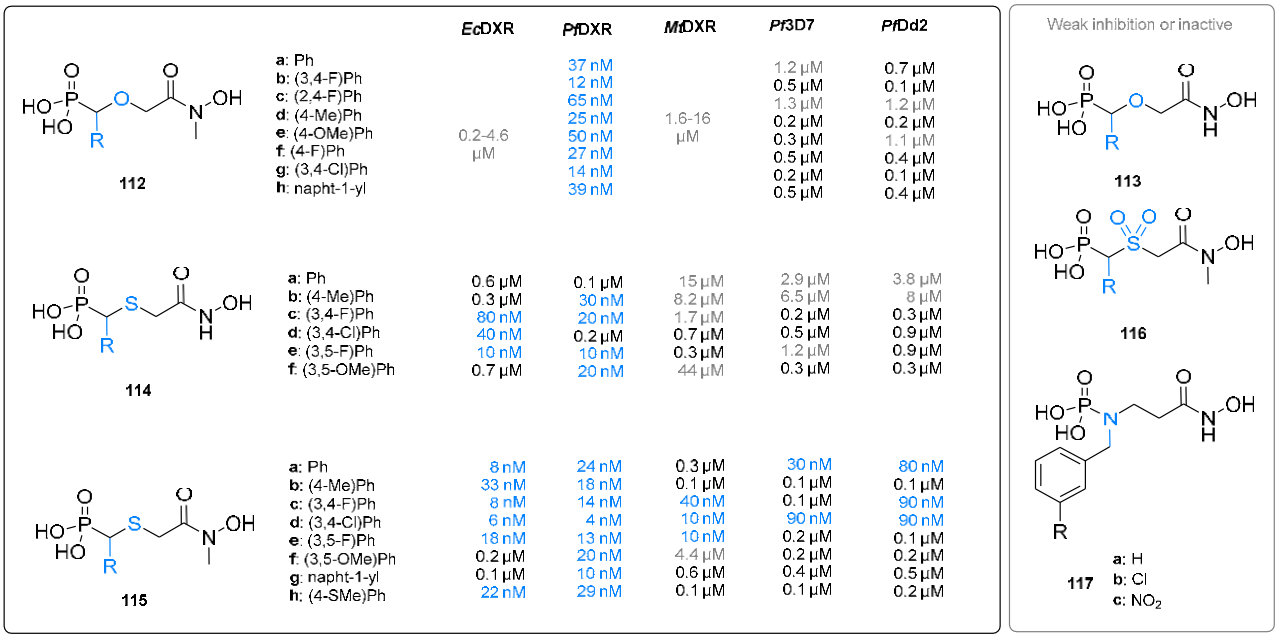

Figure 26. Antibacterial and antiplasmodial activity of thia (**112+113**), oxa (**114+115**), sulfone (**116**) and aza (**117**) analogs.

Furthermore, carba, oxa and thia analogs showed potent inhibitory activity towards the DXRs of *E. coli*, *P. falciparum* and *M. tuberculosis* (Figures 17 and 26). The thia-analogs **115a–h** were more active against *Ec*DXR and *Mt*DXR than the carba analogs (**107b–111b**, Figure 24) while the carba derivatives displayed the strongest activity against *Pf* DXR. The oxa analogs (**112a–h, 113**) demonstrated the weakest inhibitory activity against all tested DXR enzymes.

The higher activity of the thia analogs was explained by the interaction of the large polarizable sulfur atom with the highly conserved Met298 of the flexible loop. In oxa analogs, the considerably smaller electronegative oxygen atom would lead to a repulsive effect, while the carbon atom does not interact with the enzyme [138]. Kunfermann et al. identified the remarkable enantioselectivity of thia analog **115a** towards *Pf* DXR [138]. The highly active *S*-(+)-enantiomer of **115a** gave a IC_{50} of 9 nM, whereas the *R*-(−) enantiomer was virtually inactive with an IC_{50} of >10 µM. This was confirmed by the co-crystallization of the *S*-(+)-isomer of **115a** with *Pf* DXR. In addition, the *α*-3,4-dichlorophenyl-substituted derivative **115d** showed excellent inhibition of all tested DXR enzymes (*Ec, Mt, Pf*) with excellent IC_{50} values of 5-10 nM. In a later publication, the thioethers were oxidized

to their corresponding sulfones with the general structure **116** (Figure 26). The sulfone derivatives were 2–3 orders of magnitude weaker inhibitors than their corresponding thioethers in respect to the three enzyme orthologs. The majority of the sulfone derivatives showed no significant inhibition of *Pf* 3D7 growth in vitro. One exception is the α-3,5-dimethoxy substituted sulfone derivative (structure not shown), which displayed at least moderate antiplasmodial in vitro activity [143]. Adeyemi et al. recently synthesized a series of *α*-benzyl analogs (**117a–c**, Figure 26), where the benzyl residues were attached to a nitrogen atom instead of the sp^3-hybridized *α*-carbon atom of the propyl linker, resulting in phosphoramidate analogs of reverse FR900098. The *α*-benzyl derivatives (**117a–c**) were non-cytotoxic to the mammalian cells, but only weakly active or inactive against *P. falciparum*. Docking studies suggested that the benzyl substituent would not fit into the substrate binding site of *Pf*DXR due to its size and conformational constraint [144].

4.3.6. β- and γ-Substituted Analogs

Compared to *α*-substituted DXR inhibitors, there are fewer *β*- and *γ*-substituted DXR inhibitors available due to their more difficult synthetic accessibility. Earlier in the development of fosmidomycin analogs, Geffken and coworkers synthesized some moderately to weakly active POM-prodrugs of **1** and **2** with *γ*-methyl and *γ*-phenyl substitution (**118–119**, Figure 27) [133]. While the POM-prodrug of **1** inhibited 100% growth of the *Pf* 3D7 strain at 100 μM, the activity for *γ*-methyl (**118a, b**) and *γ*-phenyl (**119a, b**) derivatives dropped to or below 60% growth inhibition. The weak antiplasmodial activity was attributed to the *γ*-methyl and *γ*-phenyl residues which could interfere with the interaction between the hydroxamic acid moiety and the divalent cation in the active site of DXR [133].

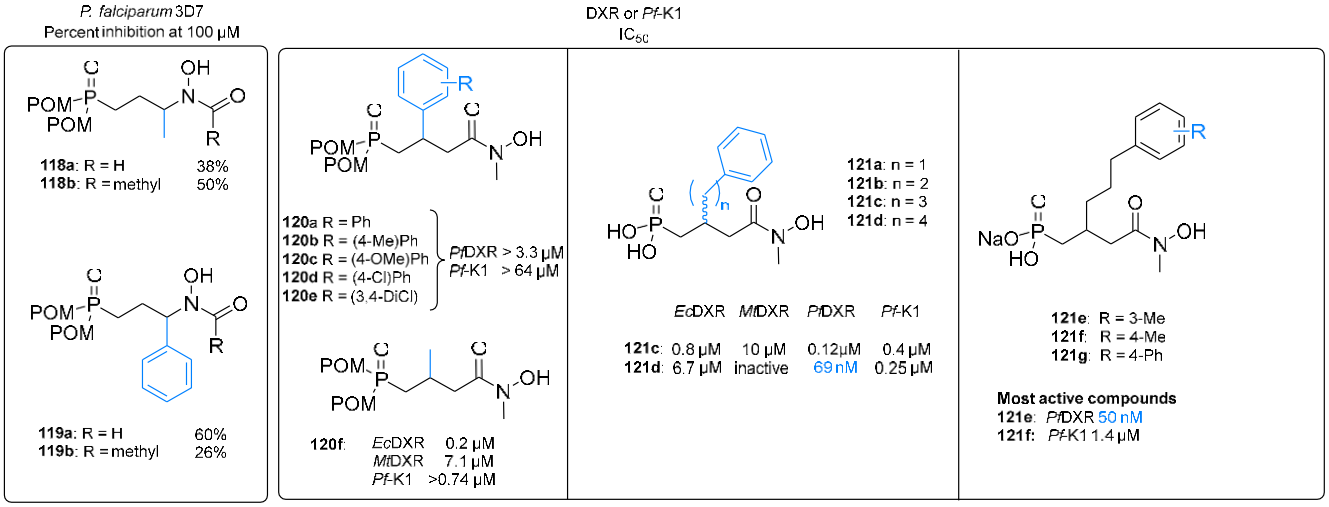

Figure 27. Antiplasmodial activity of β- and γ-substituted analogs (**118**–**121**).

Van Calenbergh and coworkers [145] introduced aryl (**120a–e**, Figure 27), alkyl (**120f**), and aryl alkyl substituents (**121a–d**) at the *β*-position of lead structure **4** (Figure 9).

If a *β*-aryl moiety (**120a–e**) is directly attached to the carbon linker, the derivatives are weak to poor inhibitors of *Ec, Pf* and *Mt*DXR. The reduction in inhibitory activity was lower in the *β*-methyl substituted analog (**120f**), but still significant. A small activity improvement was observed for inhibitors with arylalkyl residues in the *β*-position (**121a–d**). For example, compound **121c** with a phenyl-propyl residue inhibited *Ec*DXR and *Pf* DXR with IC_{50} values of 0.8 and 0.1 μM, respectively. In contrast, the *β*-phenyl-butyl derivative **121d** was more active against *Pf*DXR with an IC_{50} of 69 nM, surpassing the inhibitory activity of fosmidomycin. However, **121d** was less active towards *Ec*DXR and inactive against *Mt*DXR.

X-ray structures of **121c** and **121d** in complex with *Pf* DXR revealed that the longer, more flexible phenyl alkyl residues led to different flap structures in the case of *Pf*DXR.

The β-phenyl residues of these compounds are in a boomerang shape and able to interact with their own *N*-methylated hydroxamic acid moiety as well as with Trp296 through an acyl-group-to-ring interaction. Additionally, the X-ray structures revealed that the *R*-enantiomer is primarily bound to the enzyme.

Expanding their prior work, van Calenbergh and coworkers synthesized a series of β-arylpropyl derivatives (**121e**–**g**, Figure 27) bearing various substituted phenyl moieties [146]. The introduction of a methyl group in the 3-position in the case of **121e** improved inhibitory activity to 50 nM against *Ec*DXR compared to the unsubstituted phenyl ring (**121c**). An improvement of *Pf* -K1 inhibition was realized by the introduction of a methyl group in the 4-position of the phenyl ring (**121f**), leading to an IC_{50} value of 1.4 µM. The replacement of the phenyl moiety with a biphenyl substituent (**121g**) slightly decreased inhibitory activity against *Pf* DXR (IC_{50} = 1.6 µM) while significantly reducing inhibitory activity against *Pf* -K1 (IC_{50} > 64 µM). X-ray structure analysis of **121e** and other members of this series revealed that upon inhibitor binding the flap covering the active site was disordered resulting in key interactions of Trp296 with **1** and **2** being no longer possible.

5. Phosphonic Acid Isosteres and Bioisosteres

Fosfoxacin (**47**), first isolated from *P. fluorescens* in 1990 [122], is the phosphate bioisoster of fosmidomycin (Figure 15). In 2006, fosfoxacin (**47**) and its acetylated congener **48** (Figure 15) were first synthesized by Woo et al. and identified as more potent inhibitors of *Synechocystis* DXR than **1** (K_i **47** = 19 nM and K_i **48** = 2 nM vs. K_i **1** = 57 nM, data not shown in Figure 28) [98]. Munier et al. [147] continued investigating the replacement of the phosphonic acid moiety of **1**–**4** (Figure 9) by a phosphate moiety and evaluated the antibacterial efficacy of bioisosteres **47**–**48** and **122**–**123** against DXRs of *E. coli* and *M. smegmatis* (Figure 28, data for *M. smegmatis* not presented). The organic phosphates **123** (IC_{50} = 46 nM) and **48** (IC_{50} = 77 nM) inhibited *Ec*DXR in a similar range as fosmidomycin (IC_{50} = 42 nM) but are still 12–20-fold weaker inhibitors than **2** (IC_{50} = 4 nM, Figure 1). Surprisingly, the formyl analog **47** and the non-methylated hydroxamic acid analog **122** are only moderate to weak inhibitors of *Ec*DXR (IC_{50} = 0.34 µM and 2.6 µM, respectively). Furthermore, **47**–**48** and **122**–**123** were tested in bacterial growth assays but were less effective than **1** and **2** (Figure 1) in *Ec* and a fosmidomycin-resistant *Ec* strain (FosR). In general, it was unexpected that all phosphonic acid derivatives were more potent than their phosphate analogs because phosphate derivatives should fit better into the phosphate-binding site of DXR [147,148].

Fujisawa Pharmaceutical Co., Ltd., performed one of the earliest attempts to replace the phosphonic acid with a phosphinic acid group (**124**–**125**, Figure 28). However, both phosphinic acid analogs (**124**–**125**) were less active against selected Gram-negative bacteria than **1** and **2** **[118]**.

Perruchon et al. [134] retained the phosphonic acid group and synthesized biologically stable monoalkyl phosphonates (**126**–**133**, Figure 28) that are not rapidly cleaved by phosphatases [149,150]. To further investigate the possible presence of an extended binding region, compounds (**131**–**133**, Figure 28) were synthesized [134]. Indeed, the activity against *Ec*DXR increased with the chain length of the alkyl residue (IC_{50} = 50 µM for **126** with methyl group vs. IC_{50} = 2.1 µM for **130** with isopentyl group), suggesting the presence of the proposed lipophilic binding region. However, the alkyl monoesters showed no measurable antiplasmodial activity (IC_{50} > 10 µM) with the exception of the arylethyl monoesters (**131**–**133**), which showed weak inhibitory activities against *Pf* Dd2 strains (IC_{50} = 5–6 µM). In summary, it was demonstrated that both hydroxy groups of the phosphonic acid moiety are mandatory for potent inhibitory activity and all synthesized derivatives displayed low in vitro inhibitory activity against *Pf*Dd2 and *Ec*DXR.

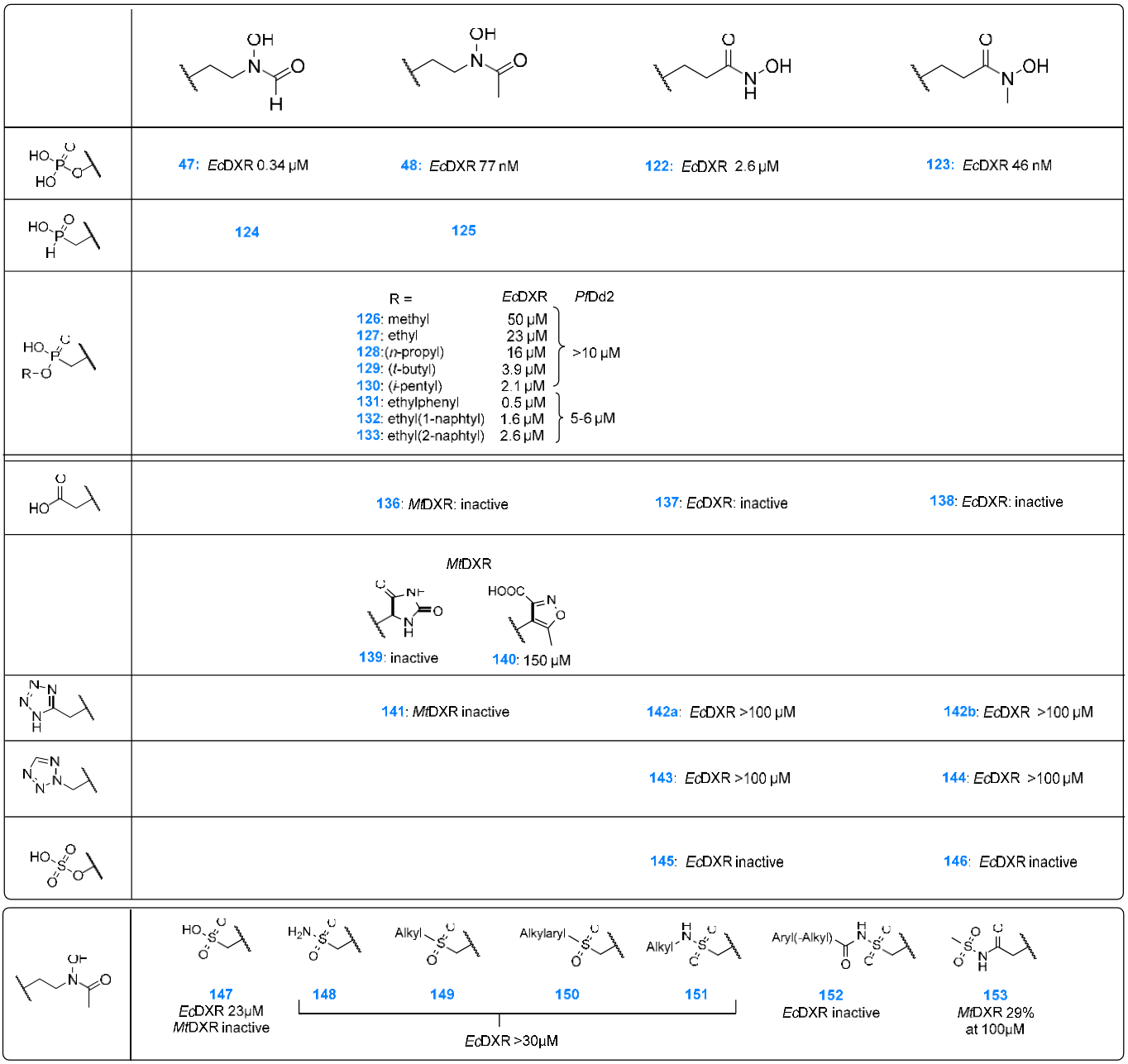

Figure 28. Biological data of phosphonic acid isosteres. Light blue: hydroxamate moiety. Grey: hydroxamic acid moiety. a: R = H. b: R = methyl. n.d. = not determined. Fosmidomycin (**1**) as a reference compound.

Furthermore, different research groups replaced the phosphonic acid group with isosteric groups, which are summarized in the second half of Figure 28. Derivatives with a carboxylic acid moiety (**136–138**, Figure 28) were inactive against *Synechocystis*, *Ec* or *Mt* DXR [98,99,151]. A possible explanation for the loss of inhibitory activity resulting from the phosphonic acid replacement is the planar geometry of a carboxylic acid moiety compared to the pyramidal geometry of the phosphonic acid group.

In 2011, Andaloussi et al. [104] tried to identify less polar *Mt*DXR inhibitors, which can penetrate the highly lipophilic cell wall by replacing the phosphonate with carboxylic acid bioisosters (**139–141**, Figure 28). Only the isoxazole carboxylic acid analog (**140**) showed negligible *Mt*DXR inhibition with an IC_{50} of 150 µM (IC_{50} **1** = 0.08 µM), while the hydantoin (**139**) and C-substituted tetrazoles (**141**) showed no inhibition [104]. Nguyen-

Trung et al. [152] developed analogous *C*- and *N*-substituted tetrazole derivatives (**142–144**, Figure 28), which demonstrated no inhibitory activity towards *Ec*DXR. The loss of activity was explained by the planar rigid structure of the tetrazole, which could disrupt several potential interactions between the heterocycle and various amino acids in the active site of DXR. The authors hypothesized that **142–144** were unable to occupy the hydroxamate and phosphonic acid binding sites simultaneously.

In addition, several working groups studied the importance of the phosphonic acid pharmacophore by replacing this moiety with charged and uncharged sulfur-containing functional groups.

The mono alkyl sulfate analogs (**145–146**), sulfonic acid (**147**) and sulfamate analog **148** (Figure 28) were weak or inactive against *Ec*DXR [98,99,151], likely due to their different abilities to form hydrogen-bond interactions compared to the phosphonic acid moiety [153]. Perruchon et al. [134] synthesized derivatives with polar, but uncharged, sulfone or sulfonamide moieties (**149–151**, Figure 28). Both groups contain two oxygen atoms which could act as hydrogen bond acceptors and form hydrogen-bond networks with Ser186, Ser222, Asn227 and Lys228, akin to the interactions of the phosphonic acid group. Furthermore, Perruchon et al. analyzed the surface of the phosphonic acid binding site and identified a small sub-pocket that eventually permits the attachment of small additional residues. The sulfone derivatives with small alkyl (**149**) and arylalkyl moieties (**150**) can only act as hydrogen bond acceptors, while the N-H moiety of the sulfonamide (**150**) might form hydrogen bonds with Ser186 and Ser222 due to their side-chain flexibility, which allows rotational and conformational changes. However, no derivative showed inhibitory activity against *Ec*DXR (Figure 28). In 2015, Gadakh et al. [154] continued the efforts regarding possible replacements for the phosphonic acid pharmacophore by modifying the unsubstituted sulfonamide moiety. The authors synthesized four *N*-acylated sulfonamides with methyl, phenyl, benzyl and phenylethyl residues (**151**, Figure 28). Even though molecular modelling results indicated the occupation of a larger hydrophobic pocket like for the arylethyl esters (**131–133**), the compounds with an *N*-acyl sulfonamide moiety (**152**, Figure 28) were completely inactive against *Ec*DXR. At least, 29% inhibition of *Mt*DXR was observed for the *N*-(methylsulfonyl)amide (**153**, Figure 28) at a concentration of 100 μM. A possible explanation for the lack of activity of compounds **151–153** could be the strong delocalization of the negative charge weakening the hydrogen bond network in the phosphate-binding site.

In summary, derivatives with sulfamate or *N*-substituted tetrazole derivatives as neutral molecules, as well as carboxylic acid, sulfonate and *C*-substituted tetrazole derivatives as monoprotonic acids and mono- and diesters of the phosphonic acid moiety do not inhibit DXR enzymes.

The data presented underscore the importance of two negatively charged groups which are present in the (monoalkyl)phosphate and the phosphonate moiety. However, differences between phosphonate and phosphate-based inhibitors (**47–48** and **122–123**) observed in antimicrobial growth assays could be related to the cell wall and/or membrane penetration and chemical/metabolic stability. Interestingly, the fact that phosphate-based derivatives (**47–48**) inhibited *Ec* growth indicated that highly hydrophilic phosphates can penetrate into cells, likely via the glycerol 3-phosphate transporter (GlpT) and/or the hexose 6-phosphate (UhpT) transporter [155–157]. This hypothesis is supported by the lack of inhibition observed in a fosmidomycin-resistant *Ec* strain in which GlpT/UhpT transporters are not active [158]. Besides this, the metabolic instability of organic phosphates due to their cleavage and inactivation by phosphatases is well described and can contribute to the different activities of phosphates compared to the phosphonic acid-based inhibitors [98]. Consequently, further investigation by several groups concentrated on the synthesis of phosphonic acid prodrugs and derivatives.

6. Conclusions Regarding Structure–Activity Relationship

The hydroxamate and retro-hydroxamate moiety are thus far the only suitable MBGs that result in potent DXR inhibitory activity. Inhibitors with hydroxamate and retro-

hydroxamate MBGs showed comparable activity and no enhanced selectivity for specific bacteria or parasites. All analogs with (bio)isosteric replacements for these groups were only weakly active or inactive (Figure 29). The tight structure–activity relationship was also demonstrated for the phosphonic acid moiety. Only the naturally occurring monoalkylphosphate fosfoxacin (**47**) and the phosphate analogs **48**, and **122**–**123** (Figure 15) showed comparable or slightly superior activity against DXRs compared with fosmidomycin. All other tested di- and monoprotonic acids (carboxylates, sulfonates, phosphonic acids) as well as non-dissociating moieties (sulfamates, *N*-substituted tetrazoles) showed no DXR inhibition. Furthermore, it has been demonstrated that both hydroxy groups of the phosphonic acid moiety are essential for potent inhibitory activity.

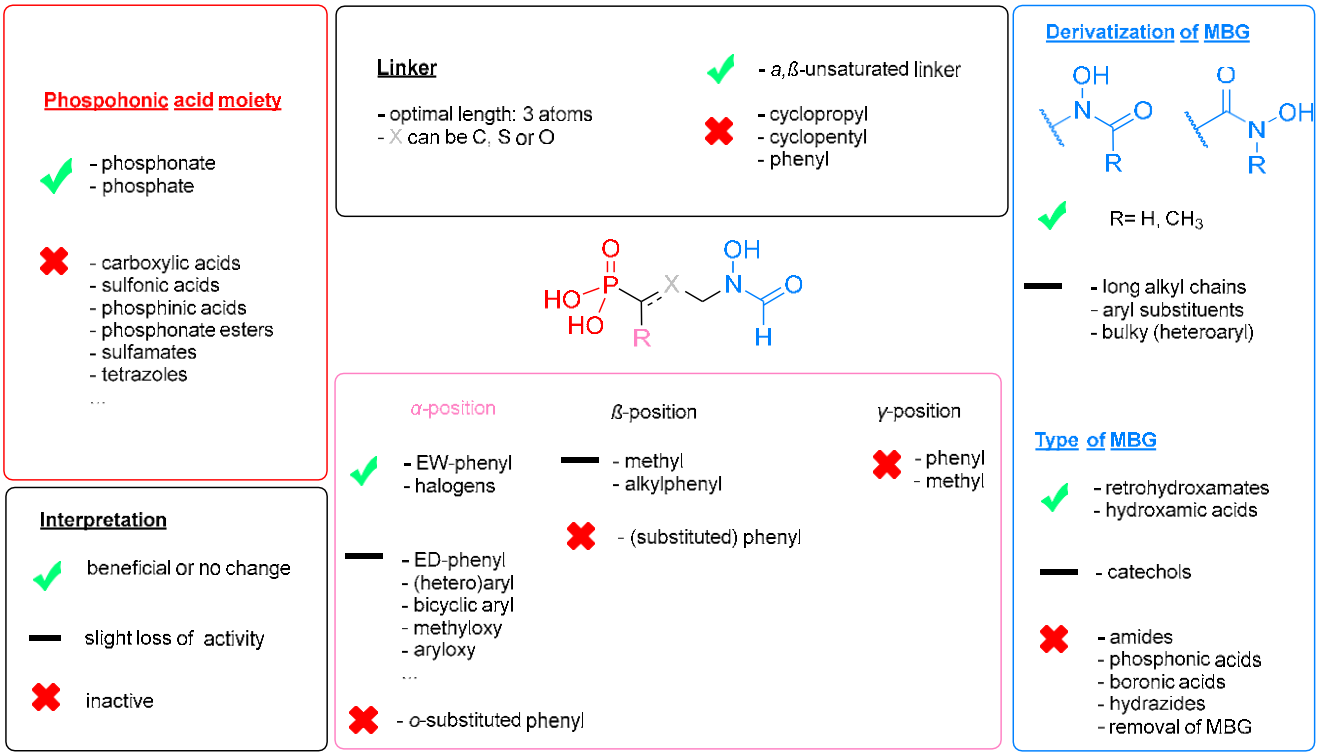

Figure 29. Structure–activity relationship (SAR) of fosmidomycin derivatives. EW = electron withdrawing, ED = electron donating, o = ortho, MBG = metal binding group.

To optimize the linker, several structurally diverse inhibitors were synthesized: The optimal linker consists of three atoms being classified as α-, β- and γ-atoms, which in most inhibitors are carbon atoms. Nitrogen atoms in the α-position and oxygen atoms in the γ-position were not tolerated, while β-oxa analogs were partly tolerated. However, a sulfur atom in the β-position of the linker (**115**, Figure 26), led to the most potent known inhibitors and showed increased selectivity for *Mt*DXR. The majority of conformationally restricted linkers were not tolerated. Two exceptions are a trans-configured cyclopropyl linker (**55**, Figure 16), which displayed similar activity as fosmidomycin (**1**), and an unsaturated propenyl linker as in FR32863 (**IV**, Figure 2), which was active in the nanomolar range.

In the α position electron-withdrawing chlorine and fluorine atoms increased activity and the acidity of the phosphonate moiety. Furthermore, α-phenyl substituents, especially with electron-withdrawing residues in *para*- and *meta*-position such as fluorine (**110a, b**, Figure 24 and **114c, 115c**, Figure 26), were beneficial. β- and γ- substituted analogs are scarce and these types of modifications are mostly not well tolerated.

Despite the promising anti-infective activity of DXR inhibitors in vitro, to date, none of the inhibitors exhibited significant curative antimalarial in vivo activity in infectious

mouse models. However, among emerging diverse inhibitors, some derivatives showed excellent DXR enzyme inhibition in the low nanomolar range.

7. Prodrugs of Fosmidomycin and Its Analogs

Phosphonic acid groups in drugs and drug candidates are often associated with unfavorable and challenging physicochemical and ADME properties. Despite their stability towards phosphatases, the membrane permeability and subsequent cellular uptake of small molecules containing phosphonic acid groups are often insufficient [159–161]. The poor membrane permeability of phosphonic acids is due to their anionic nature at physiological pH. To mask the anionic structure and to overcome the limitation described above, various types of phosphonic acid prodrugs were and are still under development. The overall goal of this prodrug concept is to enable efficient oral administration of phosphonic acid-based small molecules.

Particularly challenging organisms include *Mt* due to its highly lipophilic mycolic acid-containing cell wall, and parasites with apicoplasts, in which the DXR enzyme is located. In *Pf* erythrocyte models, prodrugs need to pass seven membranes and the exact compartment of bioactivation is not known [36]. To date, all in vivo studies with DXR inhibitors have been conducted with mice infected with *Plasmodia*.

To mask the highly polar phosphonic acid moiety of fosmidomycin and its analogs and to achieve in vivo efficacy against malaria, established prodrug concepts commonly used for antiviral drugs were employed. These concepts include lipophilic phosphonate esters, e.g., tenofovir disoproxil (Viread, 2001) [162] containing a bis-POC (isopropyloxycarbonyloxymethyl) moiety and adefovir dipivoxil (Hepsera, 2002) [163] with a bis-POM (pivaloyloxymethyl) moiety, aryloxyphosphoramidate (e.g., remdesivir, sofosbuvir) [161,164–167], aryloxyphosphonamidate prodrugs (e.g., tenofovir alafenamide) [162,168,169] phosphobisamidates [170], cyclic esters and monoalkylphosphonates [163].

7.1. Lipophilic Phosphonic Acid Esters

Aiming to overcome the poor permeability and absorption as well as the relatively short half-life time of fosmidomycin and FR900098 (Figure 1) [61,62], several groups developed phosphonic acid prodrugs to increase oral bioavailability and in vivo efficacy. Most prodrug moieties increase the lipophilicity of the phosphonic acid group. The different structure types of lipophilic prodrugs presented in the following chapters are summarized in Figure 30.

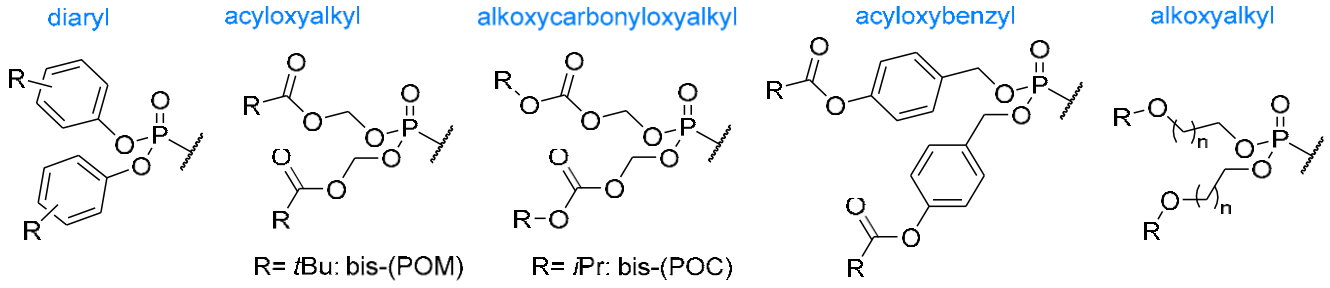

Figure 30. Lipophilic phosphonate prodrugs used for fosmidomycin and its analogs.

7.1.1. Ester Prodrugs of Fosmidomycin and FR900098

In 2001, the first in vivo studies with FR900098 (**2**, Figure 1) and its diaryl ester prodrugs were conducted by Wiesner et al. (**154a–c**, Figure 31). While a significant increase in the in vivo antimalarial efficacy for the bis(4-methoxyphenyl) diester prodrug (**154c**) was observed, no curative properties have been detected [171].

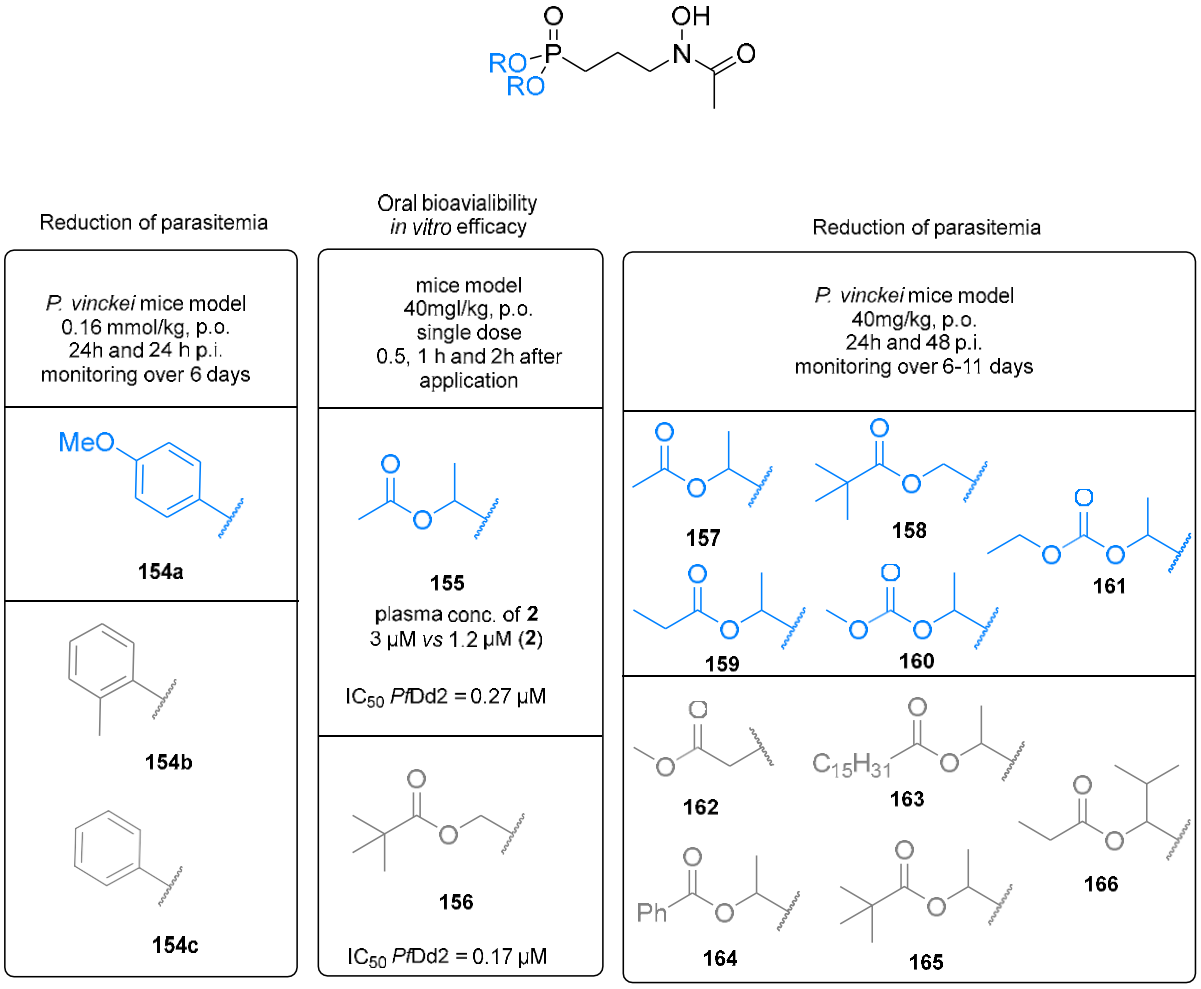

Figure 31. Results of in vivo studies of lipophilic FR900098 (**2**) esters. Blue indicates improvement and grey reduction of efficacy/plasma concentration of the prodrug compared to parent compound **2**. p.o. = per os, p.i. = postinfection.

Due to toxicity concerns for the liberated phenols upon bioconversion, alternative lipophilic phosphonic acid derivatives such as acyloxyalkyl and alkoxycarbonyloxyethyl esters (Figure 30) of FR900098 (**2**) have been synthesized by the Schlitzer group. These derivatives were designed to reduce toxicity while increasing bioavailability and antimalarial in vivo activity [172–174]. Initial investigations documented an improved in vitro antiplasmodial activity of the FR900098-prodrug **155** against *Pf* 3D7 and Dd2 strains as well as increased oral bioavailability. To prove the bioconversion of **155** and verify oral bioavailability, 40 mg/kg of ester prodrug **155** and **2** were orally administered to mice. **2** showed a plasma concentration of 1.2 µM after 30 min while application of **155** led to an improved plasma concentration of 3 µM of **2** after cleavage of the prodrug moiety by plasma esterases. The plasma levels of **155** and **2** were below the detection limit 2 h after application underlining the poor pharmacokinetic properties of **2** and its prodrugs [173].

Following up on this concept, the Schlitzer group synthesized further bis[(acyloxy)alkyl] (**157–159, 162–166**, Figure 31) and bis[(alkoxycarbonyloxy) ethyl] ester (**160–161**) prodrugs of **2** and tested them in a *P. vinckei* mouse model over 6 to 11 days. Even though the prodrug **158** was more active than its parent compound **2**, the formation of formaldehyde from the dioxymethylene group was classified as unfavorable. In contrast, prodrugs containing a 1,1-dioxyethylene group (**157, 159–161, 163–165**) released less problematic acetaldehyde during bioactivation.

The most promising derivative **157** was tested in vivo and compared with FR900098. 10 mg/kg of **157** showed the same activity as 40 mg/kg of FR900098, while higher dosages up to 40 mg/kg of **157** exceeded the efficacy of FR900098 after 8 days [174]. Although the in vivo efficacy of **2** has been improved through the development of prodrugs, further improvements are necessary in order to provide candidates with curative properties.

In 2017, Courtens et al. [175] described acyloxybenzyl and alkoxyalkyl phosphonate ester prodrugs of the reverse FR900098 **(167–168**, Figure 32). The acyloxybenzyl prodrugs **167a–e** surpassed the inhibitory activity of fosmidomycin against *Pf*-K1 (IC_{50} (**1**) = 1.7 µM) and *Mt* H37Ra strains (IC_{50} (**1**) > 64 µM). Among the tested compounds, the acetyl ester **167a** was the weakest inhibitor, while **167c** and **167e** were highly active derivatives (IC_{50} = 0.4 µM) against *Mt*. However, prodrugs **167a–e** showed cytotoxic effects in the MRC-5 fibroblast cell line. In contrast to alkyloxymethyl prodrugs, acyloxybenzyl prodrugs release the reactive electrophile quinone methide during bioactivation, which could be the reason for the observed cytotoxicity [175]. The synthesized monoalkoxyalkyl phosphonates (**168a–d**) were not active against *Mt*, but the antiplasmodial activity of dodecyl **168c** and hexadecyl analog **168d** exceeded the efficacy of fosmidomycin. The authors hypothesized that the long alkyl chains could improve passive diffusion. The Dowd group elucidated the activity of phosphonate ester as potential prodrugs of **2** against a panel of Gram-positive (*B. anthracis*, *E. faecalis*, *S. aureus* (MSSA and MRSA)) and Gram-negative bacteria (*Acinetobacter* and *E. coli*) as well as *Mt* (Figure 33) [42]. Consistent with previous results with dialkyl ester prodrugs, the prodrugs **169, 173** and **175** showed weak or reduced activity against these bacteria (for results of all tested bacteria, see Uh et al. [42]), which was expected due to insufficient bioactivation of small aliphatic dialkylphosphonates.

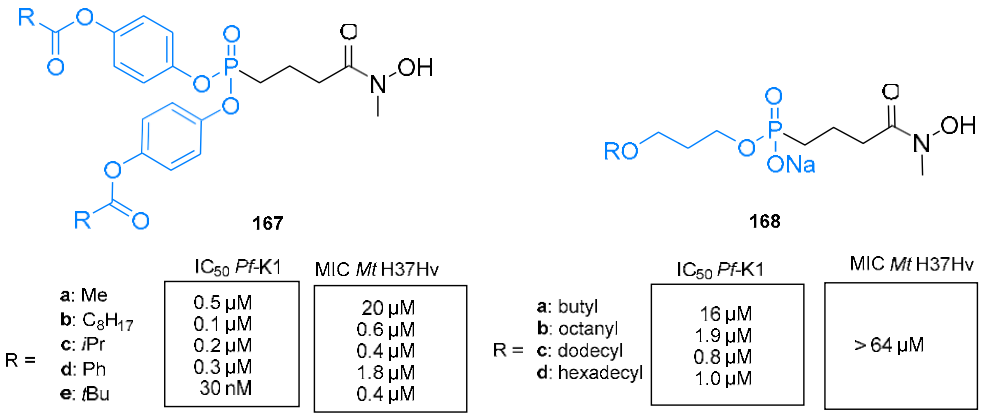

Figure 32. Antiplasmodial and antimycobacterial activity of acyloxybenzyl (**157**) and alkoxyalkyl phosphonate ester prodrugs (**158**).

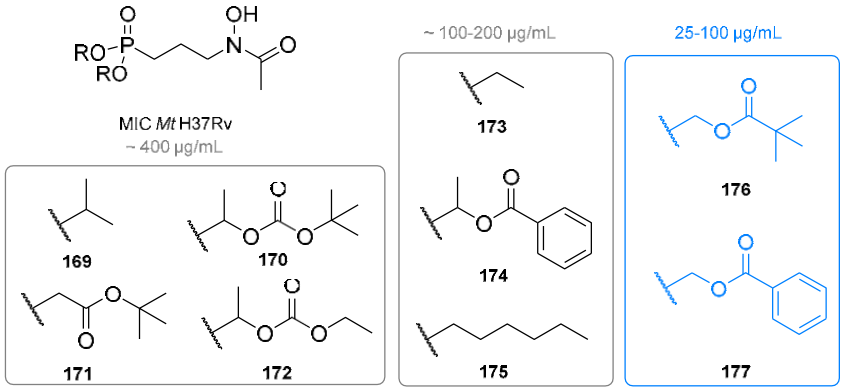

Figure 33. Inhibitory activity of different FR900098 prodrugs (**169–177**) against *M. tuberculosis* H37Rv in growth assay.

The bis-POM ester (**176**) (MIC = 50–100 µg/mL) and the bis-[benzoyloxymethyl] ester (**177**) (MIC = 25–100 µg/mL) were moderately active against *Mt* H37Rv. In general, the antimycobacterial activity increases with the size of the prodrug moiety [42]. In *Mt*, the uptake of hydrophilic DXR inhibitors does not occur via the GlpT transporter due to its absence. Consequently, the effectiveness of the prodrugs **176** and **177** mainly relies on their lipophilicity, which enables penetration of the membranes by passive diffusion. Moreover, it was hypothesized that prodrugs **176** and **177** circumvent resistance caused by *glpT* mutations observed in bacteria where uptake of DXR inhibitors is reliant on the GlpT. The second observation made in this study is that ester prodrugs of primary alcohols (**176, 177**) are more active than esters prodrugs of secondary alcohols (**170**, **172, 174**). It was hypothesized that cellular esterases are unable or only partially able to hydrolyze substrates with a substituted acyl moiety [42,176].

In 2012, Ponaire et al. reported further acyloxymethyl phosphonate prodrugs of **3** and **4** (**178–180**, Figure 34) and tested their activity in an *M. smegmatis* growth assay using a paper disc diffusion method with a concentration of 400 nmol/disk. (Figure 34) [177]. The phosphonic acids **1** and **2** inhibited the growth of *M. smegmatis,* whereas the prodrugs **178a–c** showed no growth inhibition. Prodrugs of *N*-methylated DXR inhibitors (**180a–c**) moderately inhibited mycobacterial growth. The *n*-propionyloxymethyl prodrug **180a** was more active than the lipophilic POM (**180b**) and benzoyloxymethyl (**180c**) prodrugs [178]. This suggested that the uptake of bulky and rigid prodrugs might be restricted. As the most active prodrug **180a** contained an *n*-propionyloxymethyl moiety, the *n*-propionyloxymethyl prodrugs of **1** and **2** were prepared (**179a, b**). However, **179a, b** demonstrated no growth inhibitory effects.

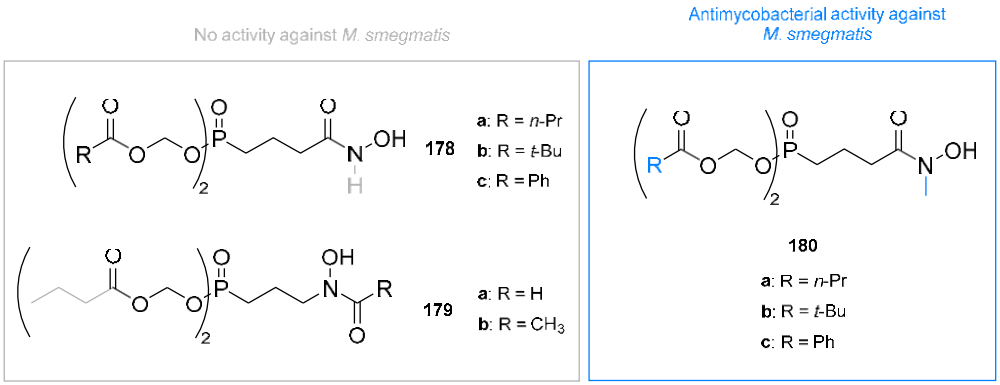

Figure 34. Antimycobacterial activity of prodrugs (**178**–**180**) against M. smegmatis determined by paper disc diffusion method.

7.1.2. Ester Prodrugs of Fosmidomycin Analogs

Haemers et al. synthesized the *β*-oxa isostere of **4** (**54**, Figure 15) and the corresponding POM-prodrug (**181**, Figure 35), which showed a 4-fold improvement in in vitro efficacy against *Pf* 3D7 compared to the parent compound **54** [123]. The Dowd group designed and synthesized POM prodrugs (**182a, b**) of the natural product FR32863 (**IV**) and the acetylated analog **42** (Figure 35). Both prodrugs (**182a, b**) Prodrug **182a** was identified as a potent inhibitor of *Pf* growth with an IC_{50} of 13 nM [179].

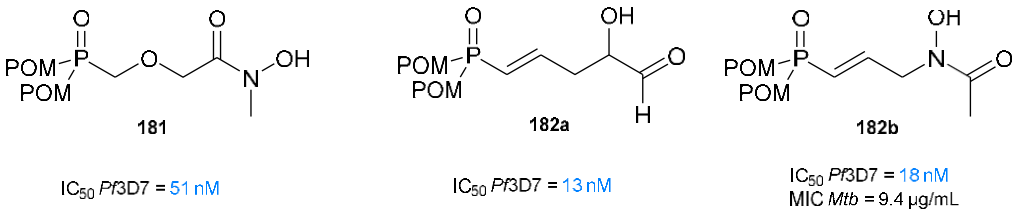

Figure 35. Structure and antiplasmodial activity of prodrugs **181** and **182**.

The POM prodrug **182a** was further evaluated for in vivo efficacy in a *P. berghei*-infected mouse model of malaria, where groups of mice were infected with luciferase-based blood-stage *P. berghei* ANKA (PbA). Prodrug **182a** reduced parasitemia in the mice treated with a dose of 20 mg/kg for 5 days. Moreover, **182a** was well tolerated and showed no evidence of cytotoxicity in vitro [121]. The POM-prodrug **182b** was only tested in vitro in an *Mt* growth assay and compared to parent compound **45** (Figure 14) increased the MIC from >200 μg/mL to 9.4 μg/mL [119].

In 2006, Schlüter et al. published a series of α-benzylated POM-prodrugs shown in Figure 36. These prodrugs contain benzyl (**183**), 2,5-dimethyl-benzyl (**184**), 3,4-dichlorobenzyl (**185**), 4-methoxybenzyl (**186**) and (5,6,7,8)tetrahydronaphthalen-eylmethyl (THN) (**187**–**188**) substituents in the α-position of the propyl linker (Figure 36). While the prodrugs with a 3,4-dichlorobenzyl (**185**) moiety retained most of their antiplasmodial activity (59% inhibition at 1 μM) compared to **1** and **2** (32% and 71% at 1 μM), all other bulky substituents at the phenyl moiety drastically reduced antiplasmodial potency [131]. Schlüter et al. expanded the SAR analysis of the substitution pattern in the α-position by comparing the antiplasmodial activities of a number of α-alkyl-substituted (methyl, dimethyl, ethyl, *n*-propyl and *i*-propyl) inhibitors (**189, 191**–**194**) with POM-prodrugs of **1** and **2** (Figure 36) [131] The α-methyl-substituted prodrugs (**189a, b**) exerted significant antiplasmodial activity (IC_{50} = 0.7 μM), while longer alkyl chains led to a considerable loss of antimalarial activity (less than 50% *Pf* growth inhibition at 25 μM, data and structures not shown). The α-phenyl derivatives (**190a, b**) exhibited similar antiplasmodial activity to (**189a, b**). Extending this concept, the *N*-acetylated and *N*-formylated derivatives with α-hydroxymethyl (**195a, b**) and fluorinated α-phenyl substituents (**196**–**198**) were prepared and evaluated. The α-hydroxymethyl moiety compromised the inhibitory effects and reduced activities of inhibitors with IC_{50} values of 6.7 μM for **195a** and 3.7 μM for **195b**. The presence of the α-2,6-dimethyl-phenyl group in **198a** led to reduced activity. In contrast, the introduction of an α-3,4-difluoro phenyl substituent (**196a**) increased the potency towards *Pf* compared to the analog bearing an unsubstituted phenyl ring (43.7% inhibition @ 0.5 μM for **196a** vs. 39% for **190a** with an α-phenyl substituent) [133].

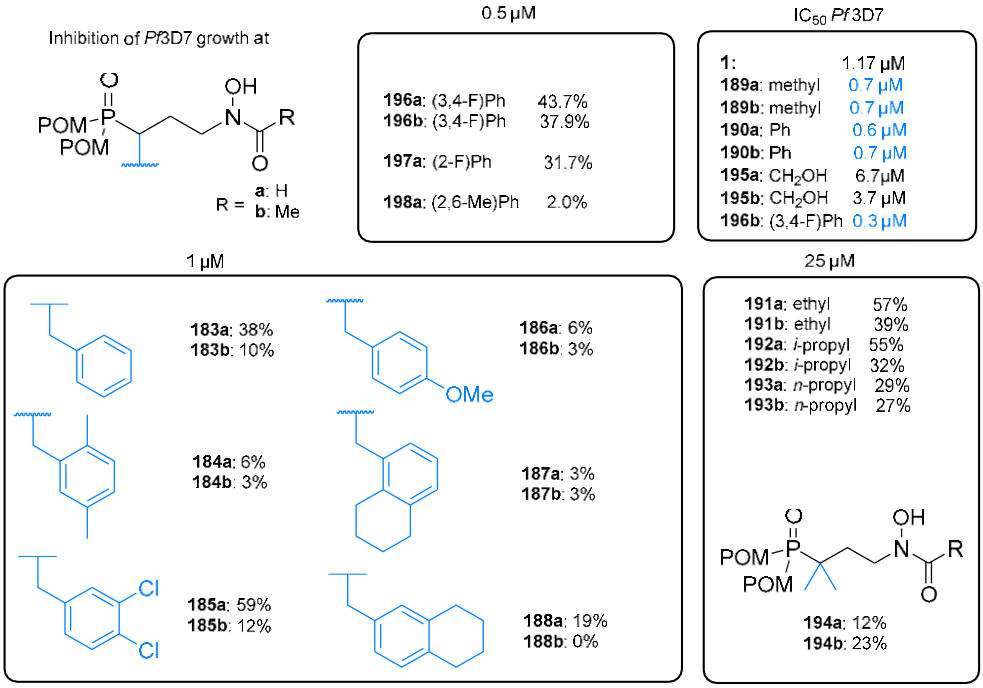

Figure 36. Antiplasmodial activity of α-benzyl and α-alkyl analogs **183**–**198**. Derivatives were screened for their inhibition of *P. falciparum* 3D7 growth at 0.5, 1 and 25 μM.

The Kurz group also synthesized phosphonate ester prodrugs of reverse *β*-oxa and carba analogs with a 3,4-difluorophenyl substituent in the *α*-position of the linker (**110a**, **110b** and **114b**, Figure 37). The phosphonic acid group of the inhibitors **110a**, **110b** and **114b** was masked with *n*-butyloxycarbonyloxymethyl (**A**), POC (**B**) and POM (**C**) prodrug moieties (Figure 37). All prodrugs of this series (**199–205**, Figure 37) were excellent to potent inhibitors of *Pf* 3D7 and Dd2 with IC_{50} values between 8 and 49 nM and were more potent than their respective parent compounds (IC_{50} = 0.075–0.54 µM) [37]. Significant growth inhibition was achieved by the introduction of the POM prodrug moiety unit into the *β*-oxa analog **205** with an IC_{50} value of 13 nM against *Pf* 3D7. **205** was more than 40-fold more active than the parent compound **114b** (IC_{50} value of 0.54 µM). The antiplasmodial activity of **114b** was further surpassed by the carba analog **203** with an excellent IC_{50} value of 8 nM. The inhibitors with an *n*-butyloxycarbonyloxymethyl prodrug unit (**A**) outperformed the inhibitors with a POC prodrug unit (**B**), which could be due to less steric hindrance during enzymatic or chemical cleavage. Notably, the *n*-butyloxycarbonyloxymethyl (**199**, **200**, **201**) and POM (**205**) prodrugs exhibited the same antiplasmodial potency (IC_{50} = 13–39 nM) in a whole-cell assay as their parent phosphonic acids **110a, b** and **114b** in a *Pf* DXR enzyme assay. Finally, it should be mentioned that, to date, no prodrugs of the highly active reverse thia analogs were synthesized, which could be an interesting strategy, especially for *Mt* drug research.

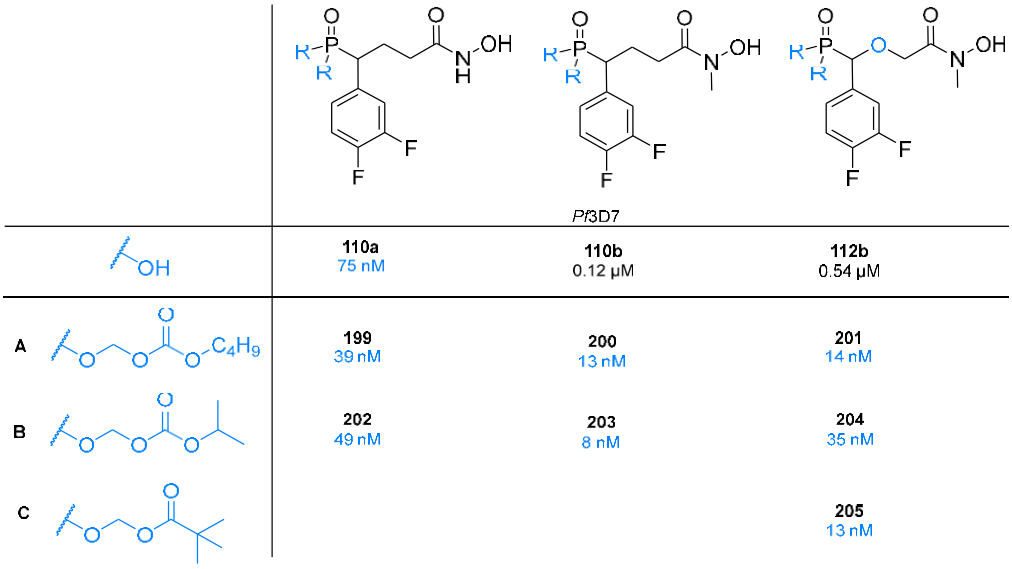

Figure 37. Antiplasmodial activity of parent compounds (**110a**, **110b**, **114b**) and prodrugs (**199**–**205**) against *Pf*3D7.

Faísca Phillips et al. [180] combined several concepts that increased antiplasmodial activity and synthesized the rigidized 1-hydroxy-piperidin-2-one analogs **206** and 1-hydroxy-azepan-2-one **207** (Figure 38). In accordance with the design, the cyclic POM-prodrug **208** surpassed the activity of fosmidomycin, FR900098, and its POM-prodrug (IC_{50} = 72 nM) against *Pf*Dd2.

An interesting example of an intramolecular cyclic phosphonate is the potential prodrug **208** synthesized by Andaloussi et al. (Figure 38) [128]. While the parent compound with a free phosphonic acid (**83**, Figure 18) showed 36% growth inhibition of *Mt*DXR at 100 µM, the cyclic ester was 3-fold less active and showed little activity. Both compounds lacked activity against *Mt* H37Ra.

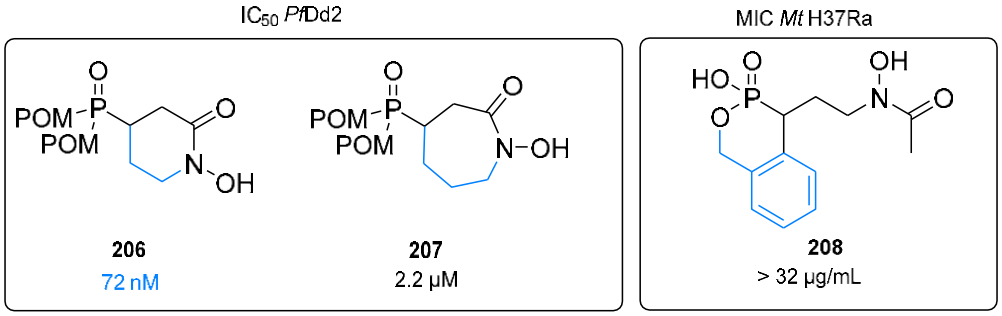

Figure 38. Inhibitory activity of rigidized prodrugs **206**–**208** against *Pf*Dd2 or *Mt* H37Ra.

7.2. Double Prodrugs

In 2012 and 2015 Kurz and collaborators also published the first double ester prodrugs of the reverse α-3,4-difluorophenyl-substituted DXR inhibitors (**108b** and **112b**, see Section 4.3.5) containing acyloxymethyl or alkoxycarbonyloxymethyl phosphonate prodrug moieties. [127] Since the penetration of several membranes is necessary to reach the target DXR in the plasmodial apicoplast, the hydroxy group of the hydroxamic acid moiety was also masked by acetate, pivalate, carbonate and carbamate (Figure 39) [37]. By masking the phosphonic acid and hydroxamate structures concurrently, the calculated log *p* values increased significantly (log *p* = −2.5 for **1** vs. log *p* > 2.5 for all double prodrugs) [37].

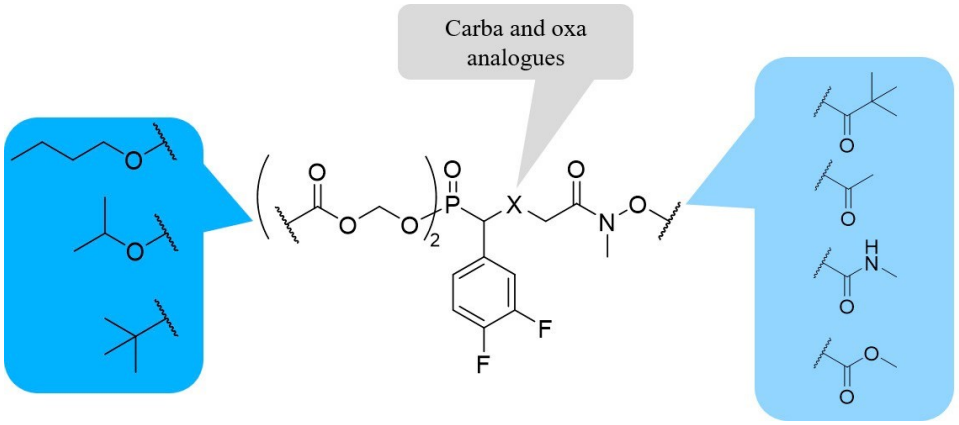

Figure 39. Schematic overview of reverse α-3,4-difluorophenyl-substituted β-oxa and carba analogs.

As expected, none of the double prodrugs inhibited *Pf* DXR. Surprisingly, despite the nanomolar antiplasmodial in vitro activity against *Pf* Dd2 (IC_{50} = 4–70 nM) and 3D7 (IC_{50} = 8–20 nM) no significant in vivo antimalarial activity in a *P. berghei* and a humanized SCID *P. falciparum* mouse model was observed.

By combining the concept of POM-phosphonate prodrugs with different hydroxamic acid prodrugs such as carboxylic acid esters, carbonates and carbamates, the Van Calenbergh group synthesized novel double prodrugs (**209**–**219**, Figure 40). The biological evaluation of this series was performed via whole-cell assays against *Pf* -K1 and *Mt* H37Rv or H37Ra [181]. Although, the majority of compounds (**209**–**214, 217**–**219**) did not inhibit *Mt* growth, prodrugs with a 2-nitrofuran (**215**) and 2-nitrothiophene (**216**) moiety were weak *Mt* H37Rv inhibitors with MIC of 12.5 µM. The authors hypothesized that **215** and **216** are bioreductive prodrugs. Unfortunately, significant cytotoxicity of **215** and **216** against MRC-5 fibroblasts was observed, diminishing their selectivity indices to approximately 2. The carbonate prodrug **219** and the nonanoyloxybenzyl ester prodrug **218** showed low activity against *Pf*-K1, while the ester prodrugs **210**–**212** were equipotent to fosmidomycin. The *N*-benzyl substituted carbamate prodrug **209** was the only retro-hydroxamate to surpass

the activity of its parent compound **180b** (IC_{50} of **209** = 0.64 µM vs. IC_{50} of **180b** = 0.73 µM). To date, no in vivo data of these double prodrugs have been published.

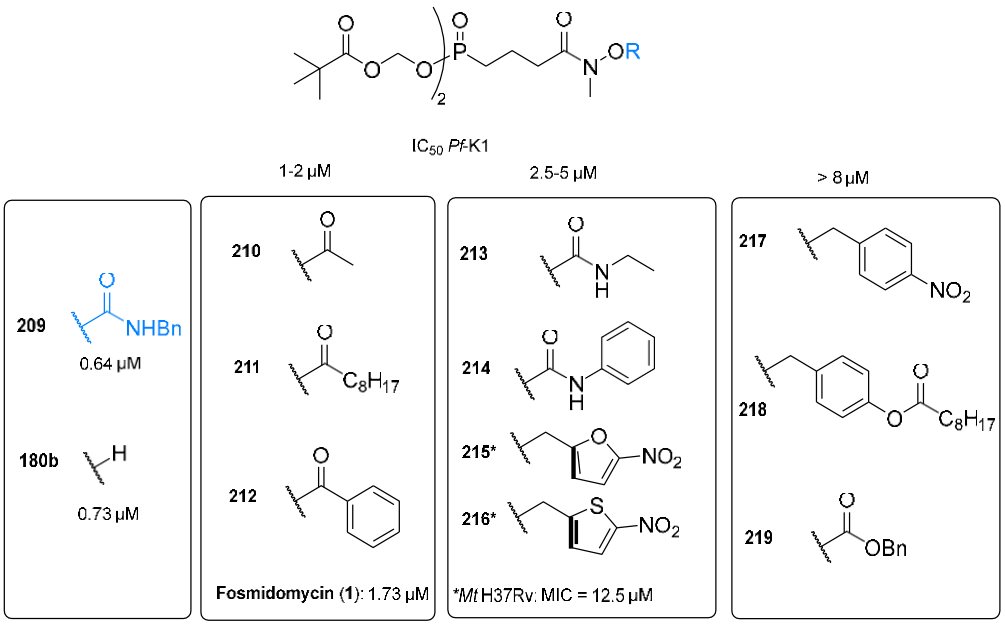

Figure 40. Antiplasmodial activity of double prodrugs **209**–**219** against asexual blood stages of *Pf* -K1 (IC_{50} in µM) and *Mt* H37Rv (MIC in µM).

In conclusion, while the bioconversion of the POC- and POM-prodrug is well studied, further studies regarding the bioactivation of hydroxamate prodrugs in vitro and in vivo are required.

7.3. Amino Acid Esters and Phosphonamidate Prodrugs

A third prodrug strategy, that is already well-studied and applied to improve pharmacokinetic properties in hepatitis and HIV therapies is the phosphonoamidate prodrug concept. Aryloxyphosphoramidate prodrugs that are currently in clinical use are sofosbuvir (Sovaldi, 2013) [166,167] and remdesivir (Veklury, 2020) [161] while tenofovir alafenamide (Vemlidy, 2015) [168] is the only aryloxyphosphonamidate in clinical use.

The Calenbergh group published two series of amino acid-based reverse N-methyl-fosmidomycin derivatives (**220**–**223**) and their in vitro inhibitory activity was tested against *Mt* H37Rv and asexual blood stages of *Pf* -K1 (Figure 41) [182,183]. In the first series, they focused solely on the conversion of the phosphonate moiety into bis-phosphonamidate prodrugs. These modifications were performed by varying amino acid residues (**220a**–**f**). Only the *L*-lysine-based bis-phosphonamidate prodrug (**220e**) showed submicromolar activity against *Pf* (IC_{50} = 0.96 µM), while the other derivatives showed activity similar to fosmidomycin. The *L*-tyrosine **222a** (IC_{50} = 0.23 µM) and *N*-acetyl-tyrosine **222b** (IC_{50} = 0.31 µM) prodrugs showed improved inhibition of *Pf* -K1 growth in comparison with fosmidomycin (IC_{50} = 1.73 µM). According to the authors, the likely protonation of **222a** at physiological pH did not appear to affect the uptake into red blood cells. Against the H37Rv wild-type strain of *Mt*, only the *L*-leucine **221b** and *L*-alanine **220f** based prodrugs exhibited weak activity with MIC values of 50 and 20 µM, respectively. The other derivatives did not show activity, which might be attributed to a lack of uptake. Furthermore, **220e** and **222b** were evaluated in a *P. berghei* malaria mouse model with a dose of 50 mg/kg applied intraperitoneally for 5 consecutive days. Compound **220e** failed to show a reduction of parasitemia post-infection, probably due to chemical/metabolic stability or insufficient bioactivation, while **222b** was able to initially reduce parasitaemia at day 4 (82% suppression). However, the in vivo activity was reduced stepwise after 7 days (66%) and reached 50% of suppression after 14 days.

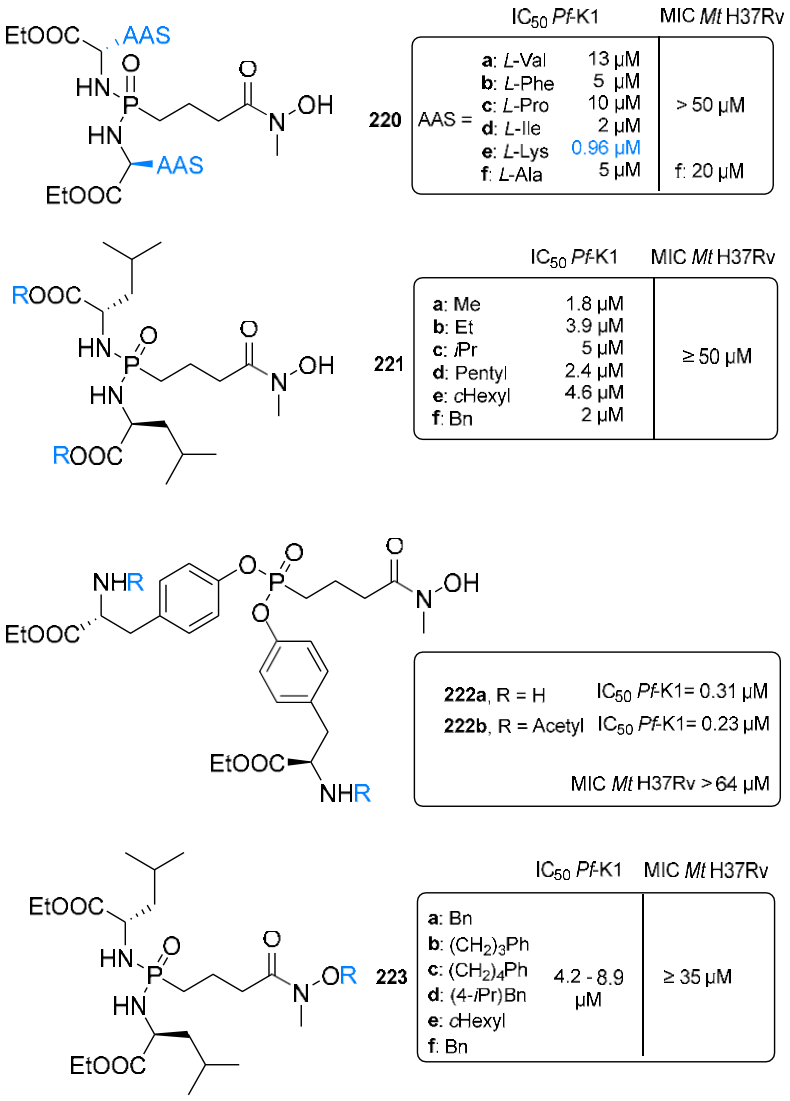

Figure 41. Biological data of amino acid-based prodrugs **220a–f**, **221a–f**, **222a–b**, and **223a–f** against asexual blood stages of *Pf*-K1 (IC_{50} in µM) and *Mt* H37Rv (MIC in µM). AAS = Amino acid side chain.

The α-3,4-dichlorophenyl substitution of reverse fosmidomycin derivatives is a key structural element responsible for potent DXR inhibition and anti-infective in vitro activity [100]. Based on this successful modification, the *L*-alanine ethyl ester and *N*-acetyl *L*-tyrosine ethyl ester prodrugs (structures not shown) have been synthesized. Both derivatives lacked antiplasmodial activity, while the parent α-3,4-dichlorophenyl compound (**109**) exhibited nanomolar activity [37].

The Dowd group recently published arylalkyloxyamide analogs of **2** which potentially act as bisubstrate inhibitors for the natural substrate DXP and the NADPH cofactor [41]. Van Calenbergh and coworkers combined these findings with their phosphodiamidate prodrug strategy and developed prodrugs with improved penetration capabilities due to increased lipophilicity [183]. The promising whole-cell antimycobacterial activity of *L*-leucine ethyl ester phosphondiamidate (**221b**) was used as a starting point for further modification combined with different *N*-alkoxy residues (**223a–g**, Figure 41). All tested derivatives were less active against *Pf* -K1 (IC_{50} = 4.2–8.9 µM) compared to fosmidomycin (IC_{50} = 1.73 µM) and less active than **220f** against the nonvirulent *Mt* H37Ra strain. These derivatives were inactive against H37Rv *Mt*, but cytotoxicity against MRC-5 fibroblasts was significant.

In summary, the phosphobisamidate prodrug **220f** exhibited moderate in vitro activity against *Mt* H37Hv strains, whereas fosmidomycin was inactive, suggesting that this prodrug strategy may allow permeation through the highly lipophilic *Mt* cell wall. The combination of a phosphodiamidate prodrug and arylalkyloxyamide moieties (**223a–g**) was unsuccessful. In *Pf,* the tyrosine ester strategy was more promising than the phosphodiamidate strategy as *N*-acetyl- and *L*-tyrosine esters (**222a, b**) were the most active compounds.

In 2019, Munier et al. synthesized aryl phosphoramidate prodrugs of fosfoxacin (**47**) and its *N*-methylated analog **48** bearing an *L*-alanine methyl ester and a 4-methoxyphenyl moiety (Figure 42) [184].

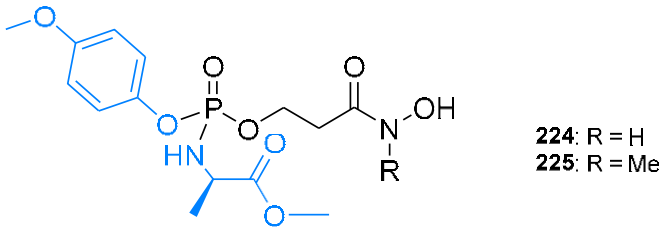

Figure 42. Structures of aryl phosphoramidate prodrugs of fosmidomycin (**224**) and FR900098 (**225**).

Both compounds (**224**–**225**) did not inhibit the growth of *E. coli* and *M. smegmatis* at the highest concentration of 400 nmol/disc in a paper disc diffusion assay. The authors demonstrated that **225** was not stable in the buffer used during the 48 h assay. Furthermore, the bioconversion into fosfoxacin was determined via incubation with carboxypeptidase Y (CPY), which catalyzes the hydrolyses of the carboxylic acid ester as the first step in bioactivation. While the results are not meaningful for **225** due to its instability in the buffer, **224** was completely converted to the amino acyl phosphoramidate intermediate with a half-life time of 20 h [184]. This new prodrug strategy for DXRi is interesting and should be used for phosphonic acid analogs, as this moiety is more stable compared to the phosphate moiety of the fosfoxacin analogs.

In summary, the Van Calenbergh group successfully implemented the synthesis of a new prodrug type for DXR inhibitor discovery. However, significant in vivo activity was not achieved. To date, none of the applied prodrugs concepts presented in this chapter led to curative properties of the parent DXR inhibitors. However, the opportunities are not yet exhausted, and a combination with other concepts and the development of bisubstrate inhibitors may help accomplish the desired curative in vivo activity.

8. Fosmidomycin Conjugates and Hybrids

Sparr et al. addressed the poor permeability of fosmidomycin analogs by facilitating cellular uptake via a carrier. Cell-penetrating peptides (CPPs), e.g., polycationic oligoarginins are able to transport physiologically active compounds across membranes and act as a carrier or delivery vehicle [185–188]. The authors synthesized a salt of fosmidomycin and 6-carboxyfluorescein (FAM) labeled octaarginine amide in a 4-to-1 ratio (**226**, Figure 43). For the second target molecule, octaarginine was attached to the retrohydroxamate group of diethyl phosphonate ester of FR900098 using a glutaric acid linker (**227**, Figure 43). First, the activity against asexual blood-stage *Pf* 3D7 in comparison to fosmidomycin was determined. While the covalent conjugate **227** was less active than fosmidomycin, the salt **226** was 40-fold more active (IC_{50} = 4 nM). It was demonstrated that the FAM-octaarginine alone is no plasmodial growth inhibitor at concentrations up to 100 µM, suggesting the improved activity of **226** is caused by enhanced uptake rather than synergistic effects. In contrast, neither fosmidomycin nor salt **226** inhibited the growth of *T. gondii* (strain RH) in infected human foreskin fibroblasts (HFF). The authors demonstrated that this is due to the inability of both compounds to cross the parasite's membranes.

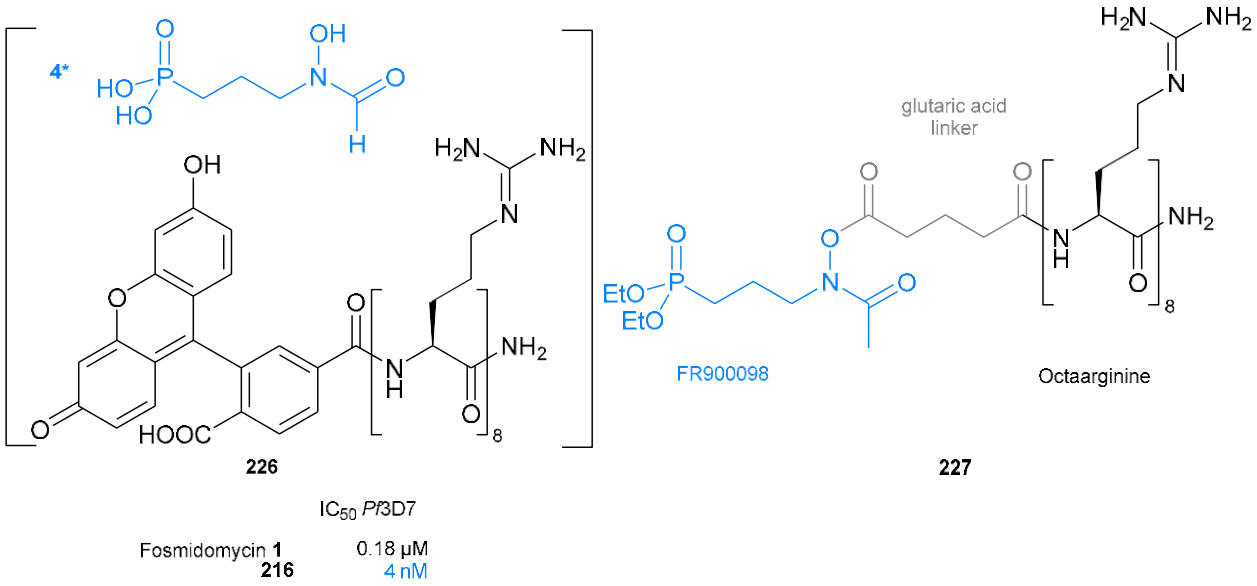

Figure 43. Structure and antiplasmodial activity of fosmidomycin (**226**) and FR900098 (**227**) octaarginine conjugates.

It has been demonstrated that artemisinin–spermidine conjugates were up to 10-fold more active against the chloroquine-sensitive *Pf*3D7 strain [189]. This inspired Palla et al. to synthesize fosmidomycin conjugates and hybrids using the following fragments: the diethyl phosphonate ester of fosmidomycin (blue), a propyl carboxylic acid linker (grey) attached to the fosmidomycin hydroxamate nitrogen, a second linker (black), and the second pharmacophore (green). The artemisinin (ART) conjugates used the polyamines spermidine (**228**) or homospermidine (**229**) as a second linker, while the desalkylchloroquin (DCQ) hybrids were connected via an ethylenediamine (**230**) or piperazine (**231**) linker (Figure 44).

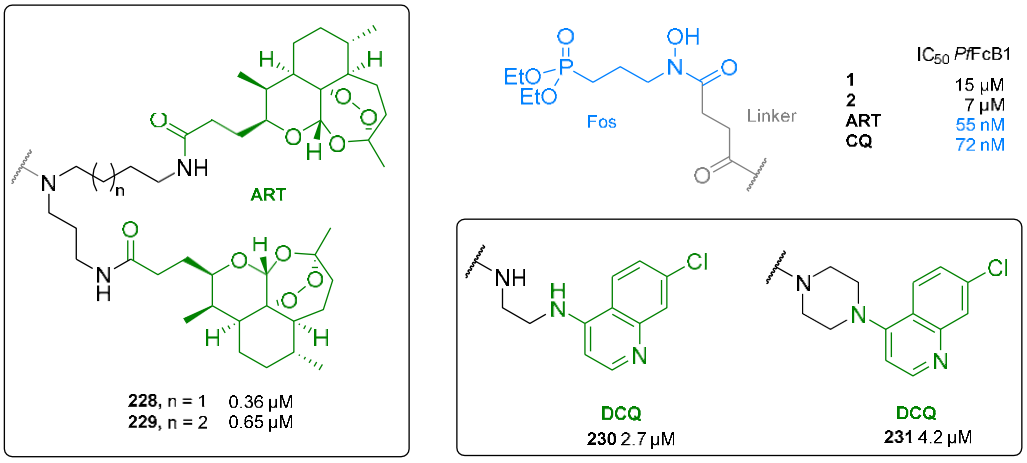

Figure 44. Antiplasmodial activities of artemisinin (ART)-conjugates **228**–**229** and desalkylchloroquin (DCQ) hybrids (**230**–**231**) against chloroquine-resistant *P. falciparum* FcB1 strain with ART and CQ as references.

Compared to the diethyl phosphonate ester of fosmidomycin (structure not shown), which was completely inactive towards *P. falciparum* FcB1, the artemisinin conjugates **228** and **229** exhibited potent activity with IC_{50} values of 0.36 and 0.65 µM, respectively. However, these values are one order of magnitude higher than the IC_{50} value of artemisinin (IC_{50} = 55 nM). Compared to **228** and **229**, the DCQ hybrids **230** and **231** were active in the

low micromolar range, but are still less active than the parent compound chloroquine. As demonstrated in this and previous studies, the phosphonic acid moiety of fosmidomycin is crucial for activity against DXR and its alkyl esters are not cleaved by plasma esterases. This suggests that the fosmidomycin pharmacophore of the reported conjugates is also inactive against DXR. Consequently, the potency of **228**–**231** in the conducted plasmodial growth assay is likely caused by the pharmacological effect of the second drug (ART, DCQ).

To compensate for the poor physicochemical properties of fosmidomycin, the novel concepts of covalent and noncovalent attachment to drug delivery vehicles as well as drugs-conjugates and hybrid molecules have been demonstrated to be sufficient, but not well examined for DXR inhibitors. These first explorative studies were auspicious and provide opportunities for further improvement, e.g., application of more labile linker units for drug delivery vehicles for complete drug release or the use of DXR inhibitors bearing a free phosphonic acid moiety or proven ester prodrugs instead of stable dialkyl phosphonate esters. Furthermore, DXR assays must be conducted to elucidate if the inhibitory effect of the drug-drug and hybrid conjugates can be attributed to DXR inhibition and/or other target-based effects.

9. DXR-Inhibitors Not Based on Fosmidomycin

Non-fosmidomycin-based DXR inhibitors are herein defined as molecules that inhibit the isolated enzyme but do not follow the classical pharmacophore of fosmidomycin and reverse analogs. The number and success of these inhibitors have so far been limited. Due to the similarity of nitrogen-containing bisphosphonates to DMAPP and its antimalarial activity, Yajima et al. screened a library of bisphosphonic acid derivatives and identified compounds **232** and **233** as moderate DXR inhibitors with IC_{50} values of 4 and 7 µM, respectively (Figure 45). Interestingly, the crystal structures of **232** showed that the bisphosphonic acid group acts as the metal chelator and does not occupy the phosphonic acid pocket [190].

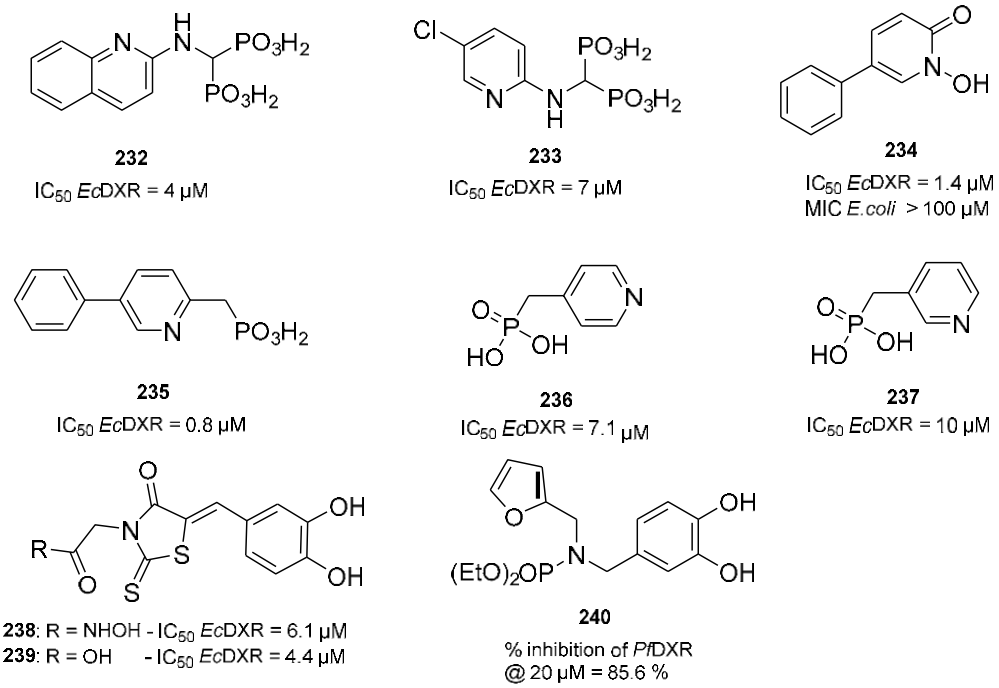

Figure 45. Structure and biological data of non-fosmidomycin-based DXR inhibitors **232**–**240**.

Aiming to increase the lipophilicity of bisphosphonic acid-based inhibitor **232**, Deng et al. tested phenyl and benzyl derivatives containing different cyclic metal-binding moieties against *Ec*DXR, including inhibitor **234** (Figure 45). Among the tested compounds, 1-hydroxypyridin-2(*1H*)-one **234** inhibited *Ec*DXR at low micromolar concentrations (IC_{50} = 1.4 µM) [113]. To expand on the concept that an increase in lipophilicity is

beneficial to the design of DXR inhibitors, the authors synthesized a series of arylphosphates containing electron-deficient aromatic moieties. Compounds containing pyridine rings (**236** and **237**, Figure 45) were active in micromolar concentrations, while compound **235** (Figure 45) inhibited the enzyme at submicromolar concentrations (**235** IC_{50} = 0.8 μM) [191]. The *Ec*DXR cocrystal structure demonstrated that the phosphonic acid group of **235** occupied the phosphate binding site of DXP and is not interacting with the catalytic metal (Figure 46).

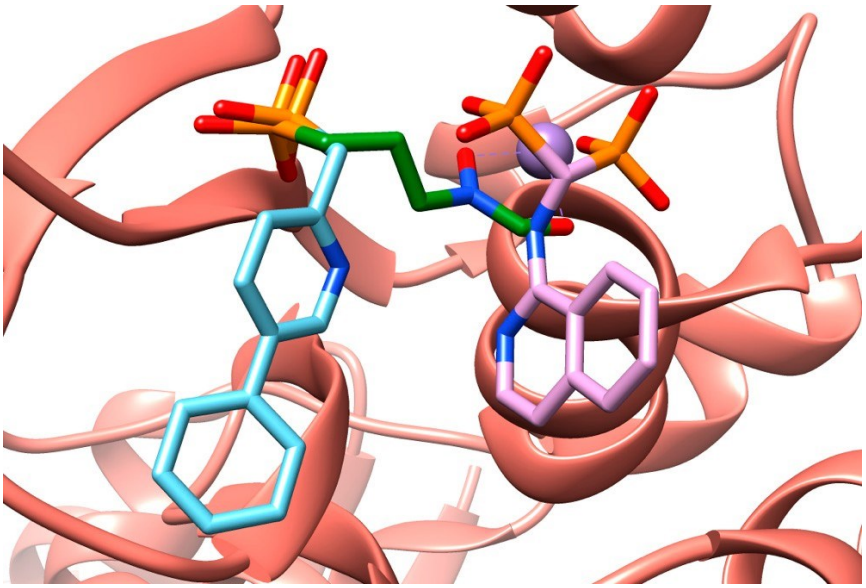

Figure 46. Superposition of fosmidomycin (green) PDB 1ONP, compound **235** (blue) PDB 3ANM and compound **232** (pink) PDB 1T1R in the structure of *Ec*DXR (salmon) PDB 1ONP.

To design a molecule that can interact with the catalytic metal ion and occupy the NADPH binding site, Zinglé et al. synthesized catechol-rhodanine-based DXR inhibitors. The compounds were found to be promiscuous inhibitors due to the formation of aggregates. With the inclusion of a detergent in the assay media, compounds **238** and **239** (Figure 45) showed inhibition at micromolar concentrations (**238** IC_{50} = 6.1 μM and **239** IC_{50} = 4.4 μM). Alteration of NADPH concentration in the assay did not alter the inhibition of **238** and **239**, suggesting that the compounds indeed did not interact with the NADPH recognition site [192].

More recently, in silico studies identified *N*-substituted phosphoramidate derivatives with a free phosphonic acid as potential DXR inhibitors. However, only the corresponding phosphonic acid esters were tested against the enzyme and compound **240** (Figure 45) was the most active compound of this series [193].

Theaflavins have been found to be non-competitive inhibitors of DXR. Theaflavin-3,3′-digallate (**241**, Figure 47) showed IC_{50} of 14.9 μM [194]. Docking studies suggested the compounds interact with the entrance of the substrate-binding site, supporting its non-orthosteric inhibition. A recent high throughput screening (HTS) campaign to identify inhibitors of the MEP pathway focusing on IspC and IspD used LOPAC (Library of Pharmacologically Active Compounds), a mixed library of 1280 commercial compounds, and 150 natural products [195]. The result of this work was the identification of novel chemical scaffolds as DXR inhibitors **241–246** shown in Figure 47. However, no experimental validation of these scaffolds has been conducted.

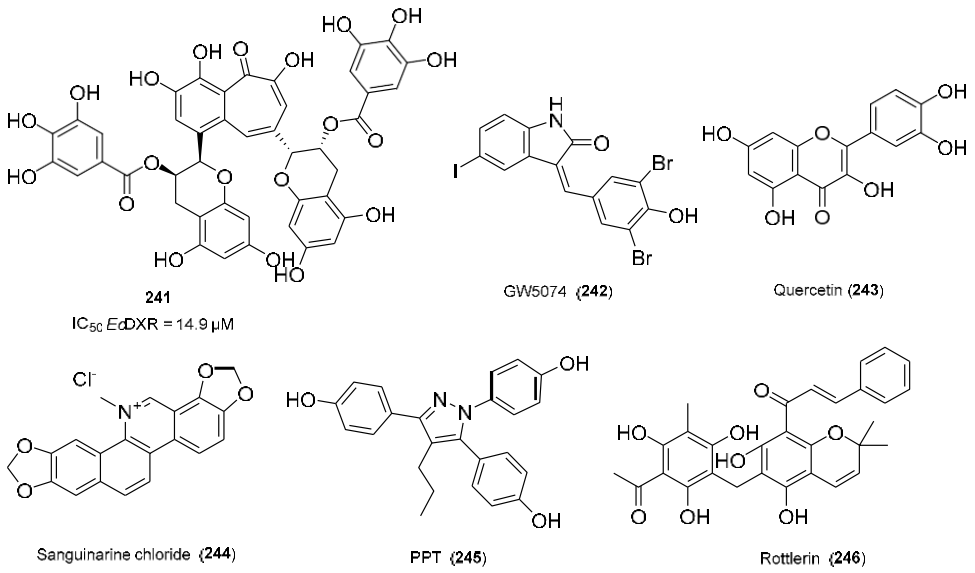

Figure 47. Structures of natural products (**241**–**246**) that potentially act as DXR inhibitors. Lead structures for the design of DXRi identified via HTS by Haymond et al. [195].

10. Summary

The importance of the MEP pathway for the development of anti-infective drugs has been demonstrated by target- and cell-based assays in animal models and clinical trials with fosmidomycin. The majority of DXR inhibitor development focused on the structural optimization of the natural products fosmidomycin (**1**) and FR900098 (**2**). Both natural compounds potently inhibited the DXR enzymes of a panel of pathogenic bacteria and parasites such as *E. coli*, *M. tuberculosis,* and *P. falciparum*.

Different design strategies have been employed to optimize the inhibitor profile and thereby pharmacokinetic (PK) and pharmacodynamic (PD) properties of **1** and **2**. The most promising analogs reported are α-phenyl and α-fluoro-substituted derivatives, which exhibited low nanomolar activity towards the DXR enzymes of *P. falciparum* and *M. tuberculosis*. However, this success was only in part transferred to whole-cell activity, and the in vivo efficacy of fosmidomycin has never been exceeded by an analog. The main shortcomings of **1** and **2** are their insufficient membrane permeability due to the charged phosphonic acid group and the short half-life as demonstrated by several unsatisfactory clinical trials.

To enhance the permeability of **1**, **2**, and their analogs, which are present as phosphonate anions at physiological pH of 7.4, several phosphonate prodrug concepts were applied, including lipophilic ester and phosphonamidate prodrugs. Some mono and double prodrugs showed significantly improved antiparasitic and antibacterial activity compared to their parent compounds. However, even nanomolar in vitro activity could not be translated into potent or, at best, curative in vivo properties.

Recent results suggest that addressing the hydrophobic subpocket within the substrate binding site or the NADPH binding site (e.g., the adenosine-binding pocket) are promising strategies toward more lipophilic and druglike DXR inhibitors. However, so far, the postulated bisubstrate inhibitors have not been validated by co-crystal structures with DXR enzymes. Bisubstrate inhibitors are recent developments in the field of DXR inhibitors, and thus their potential may not have been fully explored.

In more than 40 years of fosmidomycin drug research, no new highly active structure types have been developed based on numerous DXR crystal structures or discovered in drug screening approaches. A few examples of innovative drug design concepts have been used, including the conjugation of fosmidomycin to cell-penetrating-peptides (CPP) or fragments of other antimalarials. These concepts have so far not yielded improved anti-infectives, leaving room for further optimization. Since competitive catalytic site

inhibitors of the phosphonohydroxamic acid type have not shown the expected in vivo efficacy, possible strategies include the development of small molecules with more druglike properties such as allosteric DXR inhibitors or DXR dimerization inhibitors. It remains to be seen whether the application of novel prodrug concepts from the field of antivirals will be more successful than the concepts used to date.

Despite the widespread distribution of the MEP pathway, significant antiparasitic activity has only been achieved against *Plasmodia*, but even here, no inhibitors with curative properties in animal models have been developed. Various studies revealed that the antiplasmodial properties of DXR inhibitors are more pronounced than their antibacterial effects, although several bacterial DXRs are inhibited with nanomolar IC_{50} values. Among the bacterial pathogens, studies with *M. tuberculosis* dominate, while studies with Gram-negative bacteria are underrepresented. To improve the antibacterial properties of fosmidomycin analogs, the design of siderophore conjugates to target resistant Gram-negative bacteria is another promising opportunity as demonstrated by the recently approved antibiotic Cefiderocol (Fetroja, 2020).

In conclusion, since no further clinical studies with fosmidomycin as an antibiotic have been carried out since 1985, it cannot currently be assessed whether fosmidomycin could gain importance as a reserve antibiotic against certain bacteria. Current data provide hardly any arguments for the suitability of fosmidomycin for this purpose. Although approval for the treatment of Malaria could not be achieved so far, fosmidomycin in combination with approved antimalarials showed promising in vivo activity in humans with curative potential. On the other hand, the required repeat application of high doses of fosmidomycin and unimprovable cure rates as a standalone antimalarial are both unsatisfactory. As novel clinical studies with fosmidomycin in combination with clindamycin and artesunate are set to begin in 2022, fosmidomycin-based combination therapy for malaria is still possible. In our view, the DXR enzyme and the MEP pathway remain viable targets for anti-infective drug research, not only because of the vital importance of isoprenoids for the survival of pathogens, but also due to the pathway's widespread prevalence and its absence in mammals.

Supplementary Materials: The following supporting information can be downloaded at: https://www.mdpi.com/article/10.3390/ph15121553/s1. In this file, we describe obtained IC_{50} or MIC values of fosmidomycin (**1**) and FR900098 (**2**) for all tested microorganisms and the PDB codes from DXR crystal structures. Table S1: Antiparasitic and antibiotic data of fosmidomycin (**1**) and FR900098 (**2**) obtained from enzyme assays and growth inhibition assays; Table S2: Existing co-crystal structures of DXR enzymes.

Author Contributions: Data curation and writing—original draft preparation, T.K. (Talea Knak), M.A.A., S.H., L.A.A.A., S.K. and N.T.; writing—review and editing, T.K. (Talea Knak), M.A.A., S.H., L.A.A.A., S.K., M.F., M.M., N.T. and T.K. (Thomas Kurz); visualization, T.K. (Talea Knak), M.A.A., S.H., L.A.A.A., S.K. and N.T.; supervision, T.K. (Thomas Kurz); project administration, T.K. (Talea Knak), M.A.A., S.H. and T.K. (Thomas Kurz). All authors have read and agreed to the published version of the manuscript.

Funding: T. Knak, T. Kurz and S.H. are funded in part by the Deutsche Forschungsgemeinschaft—270650915 (Research Training Group GRK 2158, TP2d to SB). M.A.A. receives funding from The Egyptian Ministry of Higher Education and Scientific Research (MHESR) and the German Academic Exchange Service (DAAD) (GERLS Scholarship 91705741).

Institutional Review Board Statement: Not applicable.

Informed Consent Statement: Not applicable.

Data Availability Statement: Data sharing not applicable.

Acknowledgments: We want to acknowledge the Institute of Pharmaceutical and Medicinal Chemistry at Heinrich-Heine-University, Düsseldorf. Especially, we are grateful for Adelbert Bacher's valuable suggestions and our fruitful discussions.

Conflicts of Interest: The authors have no relevant affiliations with any organization or entity with a financial interest in or financial conflict with a subject matter or materials discussed in the manuscript apart from those disclosed and thus declare that there is no conflict of interests.

Abbreviations

ADME, absorption, distribution, metabolism, and excretion; BLAST, Basic Local Alignment Search Tool; DMAPP, dimethylallyl diphosphate; CPY, carboxypeptidase Y; DXP, 1-deoxy-D-xylulose-5-phosphate; DXR, 1-deoxy-D-xylulose-5-phosphate reductoisomerase; DXRi, 1-deoxy-D-xylulose-5-phosphate reductoisomerase inhibitor; Ec, *Escherichia coli*; *fsr*, fosmidomycin resistance gene; GlpT, glycerol-3-phosphate transporter; IPP, isopentenyl diphosphate; IspC, 1-deoxy-D-xylulose-5-phosphate reductoisomerase; IspD, 4-diphosphocytidyl-2C methyl-D-erythritol synthase; IspE, 4-diphosphocytidyl-2C-methyl-D-erythritol kinase; IspF, 2C-methyl-D-erythritol 2,4-cyclodiphosphate synthase; IspG, 2C-methyl-D-erythritol 2,4-cyclodiphosphate reductase; IspH, 1-hydroxy-2-methyl-2-(E)-butenyl-4-diphosphate reductase; HA, hydroxamic acid; HTS, high throughput screening; MBG, metal binding group; MDR, multidrug resistance; MEP, 2C-methyl-d-erythritol- 4-phosphate pathway; MRC-5, Medical Research Council cell strain 5; MRSA, methi- cillin -resistant *Staphylococcus aureus*; MSSA, methicillin-sensitive *Staphylococcus aureus*; Mt, *Mycobacterium tuberculosis*; NHP, N-hydroxypyridone; n.i., no inhibition; NMP, non-mevalonate pathway; PDB, protein database; Pf, *Plasmodium falciparum*; Pf3D7, chloroquine-sensitive *plasmodium* falciparum strain 3D7; PfDd2, multiresistant strain *plasmodium falciparum* strain Dd2; Pf-K1, *Plasmodium falciparum* strain K1, a chloroquine- and pyrimethamine-resistant strain; PMB, p-methoxybenzyl; POC, isopropyloxycarbonyloxymethyl; POM, pivaloyloxymethyl; QSAR, quantitative structure–activity relationship; R, residue; SAR, structure–activity relationship; SCID, severe combined immunodeficiency; ssp., subspecies; THN, (5,6,7,8)-tetrahydronaphthaleneylmethyl; UhpT, hexose 6-phosphate transporter; Yp, *Yersinia pestis*.

References

1. Rohmer, M.; Knani, M.; Simonin, P.; Sutter, B.; Sahm, H. Isoprenoid Biosynthesis in Bacteria: A Novel Pathway for the Early Steps Leading to Isopentenyl Diphosphate. *Biochem. J.* **1993**, *295*, 517–524. [CrossRef] [PubMed]
2. Disch, A.; Schwender, J.; Müller, C.; Lichtenthaler, H.K.; Rohmer, M. Distribution of the Mevalonate and Glyceraldehyde Phosphate/Pyruvate Pathways for Isoprenoid Biosynthesis in Unicellular Algae and the Cyanobacterium *Synechocystis* PCC 6714. *Biochem. J.* **1998**, *333*, 381–388. [CrossRef] [PubMed]
3. Arigoni, D.; Sagner, S.; Latzel, C.; Eisenreich, W.; Bacher, A.; Zenk, M.H. Terpenoid Biosynthesis from 1-Deoxy-D-xylulose in Higher Plants by Intramolecular Skeletal Rearrangement. *Proc. Natl. Acad. Sci. USA* **1997**, *94*, 10600–10605. [CrossRef] [PubMed]
4. Schwender, J.; Zeidler, J.; Gröner, R.; Müller, C.; Focke, M.; Braun, S.; Lichtenthaler, F.W.; Lichtenthaler, H.K. Incorporation of 1-Deoxy-D-Xylulose into Isoprene and Phytol by Higher Plants and Algae. *FEBS Lett.* **1997**, *414*, 129–134. [CrossRef]
5. Cvejić, J.H.; Rohmer, M. CO_2 as Main Carbon Source for Isoprenoid Biosynthesis via the Mevalonate-independent Methylerythritol 4-Phosphate Route in the Marine Diatoms *Phaeodactylum tricornutum* and *Nitzschia ovalis*. *Phytochemistry* **2000**, *53*, 21–28. [CrossRef]
6. Eberl, M.; Hintz, M.; Reichenberg, A.; Kollas, A.-K.; Wiesner, J.; Jomaa, H. Microbial Isoprenoid Biosynthesis and Human γδ T Cell Activation. *FEBS Lett.* **2003**, *544*, 4–10. [CrossRef]
7. Coppens, I. Targeting Lipid Biosynthesis and Salvage in Apicomplexan Parasites for Improved Chemotherapies. *Nat. Rev. Microbiol.* **2013**, *11*, 823–835. [CrossRef]
8. Hunter, W.N. The Non-Mevalonate Pathway of Isoprenoid Precursor Biosynthesis. *J. Biol. Chem.* **2007**, *282*, 21573–21577. [CrossRef]
9. Okuhara, M.; Kuroda, Y.; Goto, T.; Okamoto, M.; Terano, H.; Kohsaka, M.; Aoki, H.; Imanaka, H. Studies on New Phosphonic Acid Antibiotics. I. FR-900098, Isolation and Characterization. *J. Antibiot.* **1980**, *33*, 13–17. [CrossRef]
10. Kamiya, T.; Hashimoto, M.; Hemmi, K.; Takeno, H. Hydroxyaminohydrocarbonphosphonic Acids. U.S. Patent US4206156A, 3 June 1980.
11. Patterson, D.R. Herbicidal Hydroxyamino Phosphonic Acids and Derivatives. U.S. Patent US4693742A, 15 September 1987.
12. Kuzuyama, T.; Shimizu, T.; Takahashi, S.; Seto, H. Fosmidomycin, a Specific Inhibitor of 1-Deoxy-D-Xylulose 5-Phosphate Reductoisomerase in the Nonmevalonate Pathway for Terpenoid Biosynthesis. *Tetrahedron Lett.* **1998**, *39*, 7913–7916. [CrossRef]
13. Jomaa, H.; Wiesner, J.; Sanderbrand, S.; Altincicek, B.; Weidemeyer, C.; Hintz, M.; Türbachova, I.; Eberl, M.; Zeidler, J.; Lichtenthaler, H.K.; et al. Inhibitors of the Nonmevalonate Pathway of Isoprenoid Biosynthesis as Antimalarial Drugs. *Science* **1999**, *285*, 1573–1576. [CrossRef] [PubMed]

14. Zeidler, J.; Schwender, J.; Müller, C.; Wiesner, J.; Weidemeyer, C.; Beck, E.; Jomaa, H.; Lichtenthaler, H. Inhibition of the Non-Mevalonate 1-Deoxy-D-Xylulose-5-Phosphate Pathway of Plant Isoprenoid Biosynthesis by Fosmidomycin. *Z. Für Nat. C* **1998**, *53*, 980–986. [CrossRef]
15. Baumeister, S.; Wiesner, J.; Reichenberg, A.; Hintz, M.; Bietz, S.; Harb, O.S.; Roos, D.S.; Kordes, M.; Friesen, J.; Matuschewski, K.; et al. Fosmidomycin Uptake into *Plasmodium* and *Babesia*-Infected Erythrocytes Is Facilitated by Parasite-Induced New Permeability Pathways. *PLoS ONE* **2011**, *6*, e19334. [CrossRef] [PubMed]
16. Chofor, R.; Risseeuw, M.D.P.; Pouyez, J.; Johny, C.; Wouters, J.; Dowd, C.S.; Couch, R.D.; Van Calenbergh, S. Synthetic Fosmidomycin Analogues with Altered Chelating Moieties Do Not Inhibit 1-Deoxy-D-Xylulose 5-Phosphate Reductoisomerase or *Plasmodium falciparum* Growth in Vitro. *Molecules* **2014**, *19*, 2571–2587. [CrossRef]
17. Iguchi, E.; Okuhara, M.; Kohsaka, M.; Aoki, H.; Imanaka, H. Studies on New Phosphonic Acid Antibiotics. II. Taxonomic Studies on Producing Organisms of the Phosphonic Acid and Related Compounds. *J. Antibiot.* **1980**, *33*, 19–23. [CrossRef]
18. Parkinson, E.I.; Erb, A.; Eliot, A.C.; Ju, K.-S.; Metcalf, W.W. Fosmidomycin Biosynthesis Diverges from Related Phosphonate Natural Products. *Nat. Chem. Biol.* **2019**, *15*, 1049–1056. [CrossRef]
19. Eliot, A.C.; Griffin, B.M.; Thomas, P.M.; Johannes, T.W.; Kelleher, N.L.; Zhao, H.; Metcalf, W.W. Cloning, Expression, and Biochemical Characterization of *Streptomyces rubellomurinus* Genes Required for Biosynthesis of Antimalarial Compound FR900098. *Chem. Biol.* **2008**, *15*, 765–770. [CrossRef]
20. Johannes, T.W.; DeSieno, M.A.; Griffin, B.M.; Thomas, P.M.; Kelleher, N.L.; Metcalf, W.W.; Zhao, H. Deciphering the Late Biosynthetic Steps of Antimalarial Compound FR-900098. *Chem. Biol.* **2010**, *17*, 57–64. [CrossRef]
21. Kuroda, Y.; Okuhara, M.; Goto, T.; Okamoto, M.; Terano, H.; Kohsaka, M.; Aoki, H.; Imanaka, H. Studies on New Phosphonic Acid Antibiotics. IV. Structure Determination of FR-33289, FR-31564 and FR-32863. *J. Antibiot.* **1980**, *33*, 29–35. [CrossRef]
22. Shigi, Y. Inhibition of Bacterial Isoprenoid Synthesis by Fosmidomycin, a Phosphonic Acid-containing Antibiotic. *J. Antimicrob. Chemother.* **1989**, *24*, 131–145. [CrossRef]
23. Missinou, M.A.; Borrmann, S.; Schindler, A.; Issifou, S.; Adegnika, A.A.; Matsiegui, P.B.; Binder, R.; Lell, B.; Wiesner, J.; Baranek, T.; et al. Fosmidomycin for Malaria. *Lancet* **2002**, *360*, 1941–1942. [CrossRef] [PubMed]
24. Nair, S.C.; Brooks, C.F.; Goodman, C.D.; Sturm, A.; McFadden, G.I.; Sundriyal, S.; Anglin, J.L.; Song, Y.; Moreno, S.N.; Striepen, B. Apicoplast Isoprenoid Precursor Synthesis and the Molecular Basis of Fosmidomycin Resistance in *Toxoplasma gondii*. *J. Exp. Med.* **2011**, *208*, 1547–1559. [CrossRef]
25. Armstrong, C.M.; Meyers, D.J.; Imlay, L.S.; Freel Meyers, C.; Odom, A.R. Resistance to the Antimicrobial Agent Fosmidomycin and an FR900098 Prodrug through Mutations in the Deoxyxylulose Phosphate Reductoisomerase Gene (dxr). *Antimicrob. Agents Chemother.* **2015**, *59*, 5511–5519. [CrossRef] [PubMed]
26. Ball, H.S.; Girma, M.B.; Zainab, M.; Soojhawon, I.; Couch, R.D.; Noble, S.M. Characterization and Inhibition of 1-Deoxy-d-Xylulose 5-Phosphate Reductoisomerase: A Promising Drug Target in *Acinetobacter baumannii* and *Klebsiella pneumoniae*. *ACS Infect. Dis.* **2021**, *7*, 2987–2998. [CrossRef] [PubMed]
27. Altincicek, B.; Hintz, M.; Sanderbrand, S.; Wiesner, J.; Beck, E.; Jomaa, H. Tools for Discovery of Inhibitors of the 1-Deoxy-D-Xylulose 5-Phosphate (DXP) Synthase and DXP Reductoisomerase: An Approach with Enzymes from the Pathogenic Bacterium *Pseudomonas aeruginosa*. *FEMS Microbiol. Lett.* **2000**, *190*, 329–333. [CrossRef]
28. Misic, A.M.; Cain, C.L.; Morris, D.O.; Rankin, S.C.; Beiting, D.P.; Fey, P.D. Divergent Isoprenoid Biosynthesis Pathways in *Staphylococcus* Species Constitute a Drug Target for Treating Infections in Companion Animals. *mSphere* **2016**, *1*, e00258-16. [CrossRef]
29. Lange, B.M.; Rujan, T.; Martin, W.; Croteau, R. Isoprenoid Biosynthesis: The Evolution of Two Ancient and Distinct Pathways Across Genomes. *Proc. Natl. Acad. Sci. USA* **2000**, *97*, 13172–13177. [CrossRef]
30. Van Laar, T.A.; Lin, Y.-H.; Miller, C.L.; Karna, S.L.R.; Chambers, J.P.; Seshu, J. Effect of Levels of Acetate on the Mevalonate Pathway of *Borrelia burgdorferi*. *PLoS ONE* **2012**, *7*, e38171. [CrossRef]
31. Reuter, K.; Sanderbrand, S.; Jomaa, H.; Wiesner, J.; Steinbrecher, I.; Beck, E.; Hintz, M.; Klebe, G.; Stubbs, M.T. Crystal Structure of 1-Deoxy-D-xylulose-5-phosphate Reductoisomerase, a Crucial Enzyme in the Non-mevalonate Pathway of Isoprenoid Biosynthesis. *J. Biol. Chem.* **2002**, *277*, 5378–5384. [CrossRef]
32. Mac Sweeney, A.; Lange, R.; Fernandes, R.P.M.; Schulz, H.; Dale, G.E.; Douangamath, A.; Proteau, P.J.; Oefner, C. The Crystal Structure of *E.coli* 1-Deoxy-D-Xylulose-5-Phosphate Reductoisomerase in a Ternary Complex with the Antimalarial Compound Fosmidomycin and NADPH Reveals a Tight-Binding Closed Enzyme Conformation. *J. Mol. Biol.* **2005**, *345*, 115–127. [CrossRef]
33. Brown, A.C.; Parish, T. Dxr is Essential in *Mycobacterium tuberculosis* and Fosmidomycin Resistance is Due to a Lack of Uptake. *BMC Microbiol.* **2008**, *8*, 1–9. [CrossRef] [PubMed]
34. Cai, G.; Deng, L.; Xue, J.; Moreno, S.N.J.; Striepen, B.; Song, Y. Expression, Characterization and Inhibition of *Toxoplasma gondii* 1-Deoxy-D-Xylulose-5-Phosphate Reductoisomerase. *Bioorg. Med. Chem. Lett.* **2013**, *23*, 2158–2161. [CrossRef] [PubMed]
35. Howe, R.; Kelly, M.; Jimah, J.; Hodge, D.; Odom, A.R. Isoprenoid Biosynthesis Inhibition Disrupts *Rab5* Localization and Food Vacuolar Integrity in *Plasmodium falciparum*. *Eukaryot. Cell* **2013**, *12*, 215–223. [CrossRef] [PubMed]
36. Botté, C.Y.; Dubar, F.; McFadden, G.I.; Maréchal, E.; Biot, C. *Plasmodium falciparum* Apicoplast Drugs: Targets or Off-Targets? *Chem. Rev.* **2012**, *112*, 1269–1283. [CrossRef] [PubMed]
37. Brücher, K.; Gräwert, T.; Konzuch, S.; Held, J.; Lienau, C.; Behrendt, C.; Illarionov, B.; Maes, L.; Bacher, A.; Wittlin, S.; et al. Prodrugs of Reverse Fosmidomycin Analogues. *J. Med. Chem.* **2015**, *58*, 2025–2035. [CrossRef]

38. He, L.; He, P.; Luo, X.; Li, M.; Yu, L.; Guo, J.; Zhan, X.; Zhu, G.; Zhao, J. The MEP Pathway in *Babesia orientalis* Apicoplast, a Potential Target for Anti-Babesiosis Drug Development. *Parasites Vectors* **2018**, *11*, 452. [CrossRef]
39. Sivakumar, T.; Aboulaila, M.; Khukhuu, A.; Iseki, H.; Alhassan, A.; Yokoyama, N.; Igarashi, I. In Vitro Inhibitory Effect of Fosmidomycin on the Asexual Growth of *Babesia bovis* and *Babesia bigemina*. *J. Protozool. Res.* **2008**, *18*, 71–78.
40. Clastre, M.; Goubard, A.; Prel, A.; Mincheva, Z.; Viaud-Massuart, M.C.; Bout, D.; Rideau, M.; Velge-Roussel, F.; Laurent, F. The Methylerythritol Phosphate Pathway for Isoprenoid Biosynthesis in *Coccidia*: Presence and Sensitivity to Fosmidomycin. *Exp. Parasitol.* **2007**, *116*, 375–384. [CrossRef]
41. San Jose, G.; Jackson, E.R.; Haymond, A.; Johny, C.; Edwards, R.L.; Wang, X.; Brothers, R.C.; Edelstein, E.K.; Odom, A.R.; Boshoff, H.I.; et al. Structure–Activity Relationships of the MEPicides: N-Acyl and O-Linked Analogs of FR900098 as Inhibitors of Dxr from *Mycobacterium tuberculosis* and *Yersinia pestis*. *ACS Infect. Dis.* **2016**, *2*, 923–935. [CrossRef]
42. Uh, E.; Jackson, E.R.; San Jose, G.; Maddox, M.; Lee, R.E.; Lee, R.E.; Boshoff, H.I.; Dowd, C.S. Antibacterial and Antitubercular Activity of Fosmidomycin, FR900098, and Their Lipophilic Analogs. *Bioorg. Med. Chem. Lett.* **2011**, *21*, 6973–6976. [CrossRef]
43. Edwards, R.L.; Heueck, I.; Lee, S.G.; Shah, I.T.; Miller, J.J.; Jezewski, A.J.; Mikati, M.O.; Wang, X.; Brothers, R.C.; Heidel, K.M.; et al. Potent, Specific MEPicides for Treatment of Zoonotic *Staphylococci*. *PLoS Pathog.* **2020**, *16*, e1007806. [CrossRef] [PubMed]
44. Ropponen, H.-K.; Richter, R.; Hirsch, A.K.H.; Lehr, C.-M. Mastering the Gram-negative Bacterial Barrier—Chemical Approaches to Increase Bacterial Bioavailability of Antibiotics. *Adv. Drug Deliv. Rev.* **2021**, *172*, 339–360. [CrossRef] [PubMed]
45. Haemers, T.; Wiesner, J.; Poecke, S.V.; Goeman, J.; Henschker, D.; Beck, E.; Jomaa, H.; Calenbergh, S.V. Synthesis of α-Substituted Fosmidomycin Analogues as Highly Potent *Plasmodium falciparum* Growth Inhibitors. *Bioorg. Med. Chem. Lett.* **2006**, *16*, 1888–1891. [CrossRef] [PubMed]
46. Fujisaki, S.; Ohnuma, S.; Horiuchi, T.; Takahashi, I.; Tsukui, S.; Nishimura, Y.; Nishino, T.; Kitabatake, M.; Inokuchi, H. Cloning of a Gene from *Escherichia coli* that Confers Resistance to Fosmidomycin as a Consequence of Amplification. *Gene* **1996**, *175*, 83–87. [CrossRef]
47. Nishino, K.; Yamaguchi, A. Analysis of a Complete Library of Putative Drug Transporter Genes in *Escherichia coli*. *J. Bacteriol.* **2001**, *183*, 5803–5812. [CrossRef] [PubMed]
48. Sauret-Güeto, S.; Urós, E.M.; Ibáñez, E.; Boronat, A.; Rodríguez-Concepción, M. A Mutant Pyruvate Dehydrogenase E1 Subunit Allows Survival of *Escherichia coli* Strains Defective in 1-Deoxy-D-Xylulose 5-Phosphate Synthase. *FEBS Lett.* **2006**, *580*, 736–740. [CrossRef]
49. Perez-Gil, J.; Uros, E.M.; Sauret-Güeto, S.; Lois, L.M.; Kirby, J.; Nishimoto, M.; Baidoo, E.E.; Keasling, J.D.; Boronat, A.; Rodriguez-Concepcion, M. Mutations in *Escherichia coli aceE* and *ribB* Genes Allow Survival of Strains Defective in the First Step of the Isoprenoid Biosynthesis Pathway. *PLoS ONE* **2012**, *7*, e43775. [CrossRef]
50. Messiaen, A.S.; Verbrugghen, T.; Declerck, C.; Ortmann, R.; Schlitzer, M.; Nelis, H.; Van Calenbergh, S.; Coenye, T. Resistance of the *Burkholderia cepacia* Complex to Fosmidomycin and Fosmidomycin Derivatives. *Int. J. Antimicrob. Agents* **2011**, *38*, 261–264. [CrossRef]
51. Malott, R.J.; Wu, C.-H.; Lee, T.D.; Hird, T.J.; Dalleska, N.F.; Zlosnik, J.E.A.; Newman, D.K.; Speert, D.P. Fosmidomycin Decreases Membrane Hopanoids and Potentiates the Effects of Colistin on *Burkholderia multivorans* Clinical Isolates. *Antimicrob. Agents Chemother.* **2014**, *58*, 5211–5219. [CrossRef]
52. Mackie, R.; McKenney, E.; van Hoek, M. Resistance of *Francisella Novicida* to Fosmidomycin Associated with Mutations in the Glycerol-3-Phosphate Transporter. *Front. Microbiol.* **2012**, *3*, 226. [CrossRef]
53. Jawaid, S.; Seidle, H.; Zhou, W.; Abdirahman, H.; Abadeer, M.; Hix, J.H.; van Hoek, M.L.; Couch, R.D. Kinetic Characterization and Phosphoregulation of the *Francisella tularensis* 1-Deoxy-D-Xylulose 5-Phosphate Reductoisomerase (MEP Synthase). *PLoS ONE* **2009**, *4*, e8288. [CrossRef] [PubMed]
54. Biological and Chemical Terrorism: Strategic Plan for Preparedness and Response. Recommendations of the CDC Strategic Planning Workgroup. *MMWR Recomm. Rep.* **2000**, *49*, 1–14.
55. Nguyen, V.K.; Parra-Rojas, C.; Hernandez-Vargas, E.A. The 2017 Plague Outbreak in Madagascar: Data Descriptions and Epidemic Modelling. *Epidemics* **2018**, *25*, 20–25. [CrossRef]
56. Haymond, A.; Johny, C.; Dowdy, T.; Schweibenz, B.; Villarroel, K.; Young, R.; Mantooth, C.J.; Patel, T.; Bases, J.; San Jose, G.; et al. Kinetic Characterization and Allosteric Inhibition of the *Yersinia pestis* 1-Deoxy-D-xylulose 5-phosphate Reductoisomerase (MEP Synthase). *PLoS ONE* **2014**, *9*, e106243. [CrossRef] [PubMed]
57. Ball, H.S.; Girma, M.; Zainab, M.; Riley, H.; Behrendt, C.T.; Lienau, C.; Konzuch, S.; Avelar, L.A.A.; Lungerich, B.; Soojhawon, I.; et al. Inhibition of the *Yersinia pestis* Methylerythritol Phosphate Pathway of Isoprenoid Biosynthesis by α-Phenyl-Substituted Reverse Fosmidomycin Analogues. *ACS Omega* **2020**, *5*, 5170–5175. [CrossRef]
58. Michalopoulos, A.; Falagas, M.E. Treatment of *Acinetobacter* Infections. *Expert Opin. Pharmacother.* **2010**, *11*, 779–788. [CrossRef] [PubMed]
59. Tzouvelekis, L.S.; Markogiannakis, A.; Psichogiou, M.; Tassios, P.T.; Daikos, G.L. Carbapenemases in *Klebsiella pneumoniae* and Other Enterobacteriaceae: An Evolving Crisis of Global Dimensions. *Clin. Microbiol. Rev.* **2012**, *25*, 682–707. [CrossRef]
60. Głowińska, A.; Trochimczuk, A.W. Polymer-Supported Phosphoric, Phosphonic and Phosphinic Acids—From Synthesis to Properties and Applications in Separation Processes. *Molecules* **2020**, *25*, 4236. [CrossRef]
61. Kuemmerle, H.P.; Murakawa, T.; De Santis, F. Pharmacokinetic Evaluation of Fosmidomycin, a New Phosphonic Acid Antibiotic. *Chemioterapia* **1987**, *6*, 113–119.
62. Murakawa, T.; Sakamoto, H.; Fukada, S.; Konishi, T.; Nishida, M. Pharmacokinetics of Fosmidomycin, a New Phosphonic Acid Antibiotic. *Antimicrob. Agents Chemother.* **1982**, *21*, 224–230. [CrossRef]
63. Wiesner, J.; Borrmann, S.; Jomaa, H. Fosmidomycin for the Treatment of Malaria. *Parasitol. Res.* **2003**, *90*, S71–S76. [CrossRef] [PubMed]

64. Ruangweerayut, R.; Looareesuwan, S.; Hutchinson, D.; Chauemung, A.; Banmairuroi, V.; Na-Bangchang, K. Assessment of the Pharmacokinetics and Dynamics of Two Combination Regimens of Fosmidomycin-Clindamycin in Patients with Acute Uncomplicated *Falciparum* Malaria. *Malar. J.* **2008**, *7*, 225. [CrossRef] [PubMed]
65. Tsuchiya, T.; Ishibashi, K.; Terakawa, M.; Nishiyama, M.; Itoh, N.; Noguchi, H. Pharmacokinetics and Metabolism of Fosmidomycin, a New Phosphonic Acid, in Rats and Dogs. *Eur. J. Drug Metab. Pharmacokinet.* **1982**, *7*, 59–64. [CrossRef] [PubMed]
66. Wiesner, J.; Henschker, D.; Hutchinson, D.B.; Beck, E.; Jomaa, H. In Vitro and In Vivo Synergy of Fosmidomycin, a Novel Antimalarial Drug, with Clindamycin. *Antimicrob. Agents Chemother.* **2002**, *46*, 2889–2894. [CrossRef] [PubMed]
67. Na-Bangchang, K.; Ruengweerayut, R.; Karbwang, J.; Chauemung, A.; Hutchinson, D. Pharmacokinetics and Pharmacodynamics of Fosmidomycin Monotherapy and Combination Therapy with Clindamycin in the Treatment of Multidrug Resistant *Falciparum* Malaria. *Malar. J.* **2007**, *6*, 70. [CrossRef]
68. Wiesner, J.; Ziemann, C.; Hintz, M.; Reichenberg, A.; Ortmann, R.; Schlitzer, M.; Fuhst, R.; Timmesfeld, N.; Vilcinskas, A.; Jomaa, H. FR-900098, an Antimalarial Development Candidate that Inhibits the Non-Mevalonate Isoprenoid Biosynthesis Pathway, Shows no Evidence of Acute Toxicity and Genotoxicity. *Virulence* **2016**, *7*, 718–728. [CrossRef]
69. Uppala, R.; Arthanareeswari, M. Determination of Hydroxylamine Genotoxic Impurity by Derivatization in Penicillamine Drug Substance by GCHS-MS. *Mater. Today Proc.* **2021**, *34*, 506–509. [CrossRef]
70. Kuemmerle, H.P.; Murakawa, T.; Soneoka, K.; Konishi, T. Fosmidomycin: A New Phosphonic Acid Antibiotic. Part I: Phase I Tolerance Studies. *Int. J. Clin. Pharmacol. Ther. Toxicol.* **1985**, *23*, 515–520.
71. Wiesner, J.; Reichenberg, A.; Hintz, M.; Ortmann, R.; Schlitzer, M.; Van Calenbergh, S.; Borrmann, S.; Lell, B.; Kremsner, P.G.; Hutchinson, D.; et al. Fosmidomycin as an Antimalarial Agent. In *Isoprenoid Synthesis in Plants and Microorganisms*; Bach, T., Rohmer, M., Eds.; Springer: New York, NY, USA, 2012.
72. World Health, O. *Guidelines for the Treatment of Malaria*, 3rd ed.; World Health Organization: Geneva, Switzerland, 2015.
73. Fernandes, J.F.; Lell, B.; Agnandji, S.T.; Obiang, R.M.; Bassat, Q.; Kremsner, P.G.; Mordmüller, B.; Grobusch, M.P. Fosmidomycin as an Antimalarial Drug: A Meta-Analysis of Clinical Trials. *Future Microbiol.* **2015**, *10*, 1375–1390. [CrossRef]
74. Borrmann, S.; Lundgren, I.S.; Oyakhirome, S.; Impouma, B.; Matsiegui, P.; Adegnika, A.; Issifou, S.; Kun, J.; Hutchinson, D.; Wiesner, J.; et al. Fosmidomycin plus Clindamycin for Treatment of Pediatric Patients Aged 1 to 14 Years with *Plasmodium falciparum* Malaria. *Antimicrob. Agents Chemother.* **2006**, *50*, 2713–2718. [CrossRef]
75. Lanaspa, M.; Moraleda, C.; Machevo, S.; González, R.; Serrano, B.; Macete, E.; Cisteró, P.; Mayor, A.; Hutchinson, D.; Kremsner, P.G.; et al. Inadequate Efficacy of a New Formulation of Fosmidomycin-Clindamycin Combination in Mozambican Children Less than Three Years Old with Uncomplicated *Plasmodium falciparum* Malaria. *Antimicrob. Agents Chemother.* **2012**, *56*, 2923–2928. [CrossRef] [PubMed]
76. Mombo-Ngoma, G.; Remppis, J.; Sievers, M.; Zoleko Manego, R.; Endamne, L.; Kabwende, L.; Veletzky, L.; Nguyen, T.T.; Groger, M.; Lötsch, F.; et al. Efficacy and Safety of Fosmidomycin–Piperaquine as Nonartemisinin-Based Combination Therapy for Uncomplicated *Falciparum* Malaria: A Single-Arm, Age De-Escalation Proof-of-Concept Study in Gabon. *Clin. Infect. Dis.* **2017**, *66*, 1823–1830. [CrossRef] [PubMed]
77. Eberl, M.; Oldfield, E.; Herrmann, T. Immuno-Antibiotics: Targeting Microbial Metabolic Pathways Sensed by Unconventional T Cells. *Immunother. Adv.* **2021**, *1*, 1–12. [CrossRef] [PubMed]
78. Deutsche Malaria Gesellschaft GmbH. DMG Receives Financing from European Union Malaria Fund. Available online: https://www.dmg-deutschemalaria.com/news/eu-malaria-fund-financing/ (accessed on 14 September 2021).
79. Zhao, L.; Chang, W.C.; Xiao, Y.; Liu, H.W.; Liu, P. Methylerythritol Phosphate Pathway of Isoprenoid Biosynthesis. *Annu. Rev. Biochem.* **2013**, *82*, 497–530. [CrossRef] [PubMed]
80. Kuzuyama, T.; Takahashi, S.; Watanabe, H.; Seto, H. Direct Formation of 2-C-Methyl-D-Erythritol 4-Phosphate from 1-Deoxy-D-Xylulose 5-Phosphate by 1-Deoxy-D-Xylulose 5-Phosphate Reductoisomerase, a New Enzyme in the Non-Mevalonate Pathway to Isopentenyl Diphosphate. *Tetrahedron Lett.* **1998**, *39*, 4509–4512. [CrossRef]
81. Chellapandi, P.; Prathiviraj, R.; Prisilla, A. Deciphering Structure, Function and Mechanism of *Plasmodium* IspD Homologs from Their Evolutionary Imprints. *J. Comput. Aided Mol. Des.* **2019**, *33*, 419–436. [CrossRef]
82. Hoeffler, J.-F.; Tritsch, D.; Grosdemange-Billiard, C.; Rohmer, M. Isoprenoid Biosynthesis via the Methylerythritol Phosphate Pathway. Mechanistic Investigations of the 1-Deoxy-D-Xylulose 5-Phosphate Reductoisomerase. *Eur. J. Biochem.* **2002**, *269*, 4446–4457. [CrossRef]
83. Wong, U.; Cox, R. The Chemical Mechanism of D-1-Deoxyxylulose-5-Phosphate Reductoisomerase from *Escherichia coli*. *Angew. Chem.* **2007**, *46*, 4926–4929. [CrossRef]
84. Koppisch, A.T.; Fox, D.T.; Blagg, B.S.J.; Poulter, C.D.E. *coli* MEP Synthase: Steady-State Kinetic Analysis and Substrate Binding. *Biochemistry* **2002**, *41*, 236–243. [CrossRef]
85. Proteau, P.J. 1-Deoxy-D-xylulose 5-Phosphate Reductoisomerase: An Overview. *Bioorg. Chem.* **2004**, *32*, 483–493. [CrossRef]
86. Argyrou, A.; Blanchard, J.S. Kinetic and Chemical Mechanism of *Mycobacterium tuberculosis* 1-Deoxy-D-xylulose-5-phosphate Isomeroreductase. *Biochemistry* **2004**, *43*, 4375–4384. [CrossRef] [PubMed]
87. Singh, N.; Cheve, G.; Avery, M.; McCurdy, C. Targeting the Methyl Erythritol Phosphate (MEP) Pathway for Novel Antimalarial, Antibacterial and Herbicidal Drug Discovery: Inhibition of 1-Deoxy-D-Xylulose-5-Phosphate Reductoisomerase (DXR) Enzyme. *Curr. Pharm. Des.* **2007**, *13*, 1161–1177. [CrossRef] [PubMed]
88. The UniProt, C. UniProt: The Universal Protein Knowledgebase in 2021. *Nucleic Acids Res.* **2021**, *49*, D480–D489. [CrossRef] [PubMed]

89. Johnson, M.; Zaretskaya, I.; Raytselis, Y.; Merezhuk, Y.; McGinnis, S.; Madden, T.L. NCBI BLAST: A Better Web Interface. *Nucleic Acids Res.* **2008**, *36*, W5–W9. [CrossRef] [PubMed]
90. McWilliam, H.; Li, W.; Uludag, M.; Squizzato, S.; Park, Y.M.; Buso, N.; Cowley, A.P.; Lopez, R. Analysis Tool Web Services from the EMBL-EBI. *Nucleic Acids Res.* **2013**, *41*, W597–W600. [CrossRef] [PubMed]
91. Umeda, T.; Tanaka, N.; Kusakabe, Y.; Nakanishi, M.; Kitade, Y.; Nakamura, K.T. Molecular Basis of Fosmidomycin's Action on the Human Malaria Parasite *Plasmodium falciparum*. *Sci. Rep.* **2011**, *1*, 9. [CrossRef] [PubMed]
92. Henriksson, L.M.; Unge, T.; Carlsson, J.; Aqvist, J.; Mowbray, S.L.; Jones, T.A. Structures of *Mycobacterium tuberculosis* 1-Deoxy-D-Xylulose-5-Phosphate Reductoisomerase Provide New Insights into Catalysis. *J. Biol. Chem.* **2007**, *282*, 19905–19916. [CrossRef]
93. Konzuch, S.; Umeda, T.; Held, J.; Hähn, S.; Brücher, K.; Lienau, C.; Behrendt, C.T.; Gräwert, T.; Bacher, A.; Illarionov, B.; et al. Binding Modes of Reverse Fosmidomycin Analogs Toward the Antimalarial Target IspC. *J. Med. Chem.* **2014**, *57*, 8827–8838. [CrossRef]
94. Yajima, S.; Nonaka, T.; Kuzuyama, T.; Seto, H.; Ohsawa, K. Crystal Structure of 1-Deoxy-D-Xylulose 5-Phosphate Reductoisomerase Complexed With Cofactors: Implications of a Flexible Loop Movement Upon Substrate Binding. *J. Biochem.* **2002**, *131*, 313–317. [CrossRef]
95. Henriksson, L.M.; Björkelid, C.; Mowbray, S.L.; Unge, T. The 1.9 A Resolution Structure of *Mycobacterium tuberculosis* 1-Deoxy-D-Xylulose 5-Phosphate Reductoisomerase, a Potential Drug Target. *Acta Crystallogr. Sect. D Biol. Crystallogr.* **2006**, *62*, 807–813. [CrossRef]
96. Codd, R. Traversing the coordination chemistry and chemical biology of hydroxamic acids. *Coord. Chem. Rev.* **2008**, *252*, 1387–1408. [CrossRef]
97. Kuntz, L.; Tritsch, D.; Grosdemange-Billiard, C.; Hemmerlin, A.; Willem, A.; Bach, T.J.; Rohmer, M. Isoprenoid Biosynthesis as a Target for Antibacterial and Antiparasitic Drugs: Phosphonohydroxamic Acids as Inhibitors of Deoxyxylulose Phosphate Reducto-Isomerase. *Biochem. J.* **2005**, *386*, 127–135. [CrossRef] [PubMed]
98. Woo, Y.-H.; Fernandes, R.P.M.; Proteau, P.J. Evaluation of Fosmidomycin Analogs as Inhibitors of the *Synechocystis sp.* PCC6803 1-Deoxy-D-Xylulose 5-Phosphate Reductoisomerase. *Bioorg. Med. Chem.* **2006**, *14*, 2375–2385. [CrossRef]
99. Zinglé, C.; Kuntz, L.; Tritsch, D.; Grosdemange-Billiard, C.; Rohmer, M. Isoprenoid Biosynthesis via the Methylerythritol Phosphate Pathway: Structural Variations around Phosphonate Anchor and Spacer of Fosmidomycin, a Potent Inhibitor of Deoxyxylulose Phosphate Reductoisomerase. *J. Org. Chem.* **2010**, *75*, 3203–3207. [CrossRef]
100. Behrendt, C.T.; Kunfermann, A.; Illarionova, V.; Matheeussen, A.; Pein, M.K.; Gräwert, T.; Kaiser, J.; Bacher, A.; Eisenreich, W.; Illarionov, B.; et al. Reverse Fosmidomycin Derivatives Against the Antimalarial Drug Target IspC (Dxr). *J. Med. Chem.* **2011**, *54*, 6796–6802. [CrossRef]
101. Behrendt, C.T.; Kunfermann, A.; Illarionova, V.; Matheeussen, A.; Gräwert, T.; Groll, M.; Rohdich, F.; Bacher, A.; Eisenreich, W.; Fischer, M.; et al. Synthesis and Antiplasmodial Activity of Highly Active Reverse Analogues of the Antimalarial Drug Candidate Fosmidomycin. *ChemMedChem* **2010**, *5*, 1673–1676. [CrossRef] [PubMed]
102. Giessmann, D.; Heidler, P.; Haemers, T.; Van Calenbergh, S.; Reichenberg, A.; Jomaa, H.; Weidemeyer, C.; Sanderbrand, S.; Wiesner, J.; Link, A. Towards New Antimalarial Drugs: Synthesis of Non-Hydrolyzable Phosphate Mimics as Feed for a Predictive QSAR Study on 1-Deoxy-D-Xylulose-5-Phosphate Reductoisomerase Inhibitors. *Chem. Biodivers.* **2008**, *5*, 643–656. [CrossRef]
103. Ortmann, R.; Wiesner, J.; Silber, K.; Klebe, G.; Jomaa, H.; Schlitzer, M. Novel Deoxyxylulosephosphate-Reductoisomerase Inhibitors: Fosmidomycin Derivatives with Spacious Acyl Residues. *Arch. Der Pharm.* **2007**, *340*, 483–490. [CrossRef]
104. Andaloussi, M.; Lindh, M.; Björkelid, C.; Suresh, S.; Wieckowska, A.; Iyer, H.; Karlén, A.; Larhed, M. Substitution of the Phosphonic Acid and Hydroxamic Acid Functionalities of the DXR Inhibitor FR900098: An attempt to Improve the Activity Against *Mycobacterium Tuberc*. *Bioorg. Med. Chem. Lett.* **2011**, *21*, 5403–5407. [CrossRef]
105. Mercklé, L.; Andrés-Gómez, A.D.; Dick, B.; Cox, R.; Godfrey, C. A Fragment-Based Approach to Understanding Inhibition of 1-Desoxy-D-Xylulose-5-Phosphate Reductoisomerase. *ChemBioChem* **2005**, *6*, 1866–1874. [CrossRef]
106. Adeyemi, C.M.; Faridoon; Isaacs, M.; Mnkandhla, D.; Hoppe, H.C.; Krause, R.W.M.; Kaye, P.T. Synthesis and Antimalarial Activity of N-Benzylated (N-Arylcarbamoyl)alkylphosphonic Acid Derivatives. *Bioorg. Med. Chem.* **2016**, *24*, 6131–6138. [CrossRef] [PubMed]
107. Bodill, T.; Conibear, A.C.; Blatch, G.L.; Lobb, K.A.; Kaye, P.T. Synthesis and Evaluation of Phosphonated N-Heteroarylcarboxamides as DOXP-Reductoisomerase (DXR) Inhibitors. *Bioorg. Med. Chem.* **2011**, *19*, 1321–1327. [CrossRef] [PubMed]
108. Bodill, T.; Conibear, A.C.; Mutorwa, M.K.; Goble, J.L.; Blatch, G.L.; Lobb, K.A.; Klein, R.; Kaye, P.T. Exploring DOXP-Reductoisomerase Binding Limits Using Phosphonated N-Aryl and N-Heteroarylcarboxamides as DXR Inhibitors. *Bioorg. Med. Chem.* **2013**, *21*, 4332–4341. [CrossRef]
109. Kurz, T.; Geffken, D.; Wackendorff, C. Hydroxyurea analogues of Fosmidomycin. *Z. Für Nat.* **2003**, *58*, 106–110. [CrossRef]
110. Zinglé, C.; Kuntz, L.; Tritsch, D.; Grosdemange-Billiard, C.; Rohmer, M. Modifications Around the Hydroxamic Acid Chelating Group of Fosmidomycin, an Inhibitor of the Metalloenzyme 1-Deoxyxylulose 5-Phosphate Reductoisomerase (DXR). *Bioorg. Med. Chem. Lett.* **2012**, *22*, 6563–6567. [CrossRef] [PubMed]
111. Mancini, G.; Bouda, M.; Gamrat, J.M.; Tomsho, J.W. Synthesis and Antimicrobial Evaluation of γ-Borono Phosphonate Compounds in *Escherichia coli* and *Mycobacterium smegmatis*. *ACS Omega* **2019**, *4*, 14551–14559. [CrossRef]
112. Montel, S.; Midrier, C.; Volle, J.-N.; Braun, R.; Haaf, K.; Willms, L.; Pirat, J.-L.; Virieux, D. Functionalized Phosphanyl-Phosphonic Acids as Unusual Complexing Units as Analogues of Fosmidomycin. *Eur. J. Org. Chem.* **2012**, *2012*, 3237–3248. [CrossRef]
113. Deng, L.; Sundriyal, S.; Rubio, V.; Shi, Z.-Z.; Song, Y. Coordination Chemistry Based Approach to Lipophilic Inhibitors of 1-Deoxy-D-Xylulose-5-Phosphate Reductoisomerase. *J. Med. Chem.* **2009**, *52*, 6539–6542. [CrossRef]

114. Masini, T.; Kroezen, B.S.; Hirsch, A.K.H. Druggability of the Enzymes of the Non-Mevalonate-Pathway. *Drug Discov. Today* **2013**, *18*, 1256–1262. [CrossRef]
115. San Jose, G.; Jackson, E.R.; Uh, E.; Johny, C.; Haymond, A.; Lundberg, L.; Pinkham, C.; Kehn-Hall, K.; Boshoff, H.I.; Couch, R.D.; et al. Design of Potential Bisubstrate Inhibitors Against *Mycobacterium tuberculosis* (Mtb) 1-Deoxy-D-Xylulose 5-Phosphate Reductoisomerase (Dxr)—Evidence of a Novel Binding Mode. *MedChemComm* **2013**, *4*, 1099–1104. [CrossRef]
116. Girma, M.B.; Ball, H.S.; Wang, X.; Brothers, R.C.; Jackson, E.R.; Meyers, M.J.; Dowd, C.S.; Couch, R.D. Mechanism of Action of N-Acyl and N-Alkoxy Fosmidomycin Analogs: Mono- and Bisubstrate Inhibition of IspC from *Plasmodium falciparum*, a Causative Agent of Malaria. *ACS Omega* **2021**, *6*, 27630–27639. [CrossRef] [PubMed]
117. Jansson, A.M.; Więckowska, A.; Björkelid, C.; Yahiaoui, S.; Sooriyaarachchi, S.; Lindh, M.; Bergfors, T.; Dharavath, S.; Desroses, M.; Suresh, S.; et al. DXR Inhibition by Potent Mono- and Disubstituted Fosmidomycin Analogues. *J. Med. Chem.* **2013**, *56*, 6190–6199. [CrossRef] [PubMed]
118. Hemmi, K.; Takeno, K.; Hashimoto, M.; Kamiya, T. Studies on Phosphonic Acid Antibiotics. IV. Synthesis and Antibacterial Activity of Analogs of 3-(N-Acetyl-N-hydroxyamino)-propylphosphonic Acid (FR-900098). *Chem. Pharm. Bull.* **1982**, *30*, 111–118. [CrossRef] [PubMed]
119. Jackson, E.R.; San Jose, G.; Brothers, R.C.; Edelstein, E.K.; Sheldon, Z.; Haymond, A.; Johny, C.; Boshoff, H.I.; Couch, R.D.; Dowd, C.S. The Effect of Chain Length and Unsaturation on *Mtb* Dxr Inhibition and Antitubercular Killing Activity of FR900098 Analogs. *Bioorg. Med. Chem. Lett.* **2014**, *24*, 649–653. [CrossRef]
120. Devreux, V.; Wiesner, J.; Jomaa, H.; Van der Eycken, J.; Van Calenbergh, S. Synthesis and Evaluation of α,β-Unsaturated α-Aryl-substituted Fosmidomycin Analogues as DXR Inhibitors. *Bioorg. Med. Chem. Lett.* **2007**, *17*, 4920–4923. [CrossRef]
121. Wang, X.; Edwards, R.L.; Ball, H.; Johnson, C.; Haymond, A.; Girma, M.; Manikkam, M.; Brothers, R.C.; McKay, K.T.; Arnett, S.D.; et al. MEPicides: α,β-Unsaturated Fosmidomycin Analogues as DXR Inhibitors against Malaria. *J. Med. Chem.* **2018**, *61*, 8847–8858. [CrossRef]
122. Katayama, N.; Tsubotani, S.; Nozaki, Y.; Harada, S.; Ono, H. Fosfadecin and Fosfocytocin, New Nucleotide Antibiotics Produced by Bacteria. *J. Antibiot.* **1990**, *43*, 238–246. [CrossRef]
123. Haemers, T.; Wiesner, J.; Giessmann, D.; Verbrugghen, T.; Hillaert, U.; Ortmann, R.; Jomaa, H.; Link, A.; Schlitzer, M.; Van Calenbergh, S. Synthesis of β- and γ-Oxa Isosteres of Fosmidomycin and FR900098 as Antimalarial Candidates. *Bioorg. Med. Chem.* **2008**, *16*, 3361–3371. [CrossRef]
124. Devreux, V.; Wiesner, J.; Goeman, J.L.; Van der Eycken, J.; Jomaa, H.; Van Calenbergh, S. Synthesis and Biological Evaluation of Cyclopropyl Analogues of Fosmidomycin as Potent Plasmodium falciparum Growth Inhibitors. *J. Med. Chem.* **2006**, *49*, 2656–2660. [CrossRef]
125. Haemers, T.; Wiesner, J.; Busson, R.; Jomaa, H.; Van Calenbergh, S. Synthesis of α-Aryl-Substituted and Conformationally Restricted Fosmidomycin Analogues as Promising Antimalarials. *Eur. J. Org. Chem.* **2006**, *2006*, 3856–3863. [CrossRef]
126. Kurz, T.; Schlueter, K.; Pein, M.; Behrendt, C.T.; Bergmann, B.; Walter, R.D. Conformationally Restrained Aromatic Analogues of Fosmidomycin and FR900098. *Arch. Der Pharm.* **2007**, *340*, 339–344. [CrossRef] [PubMed]
127. Verbrugghen, T.; Cos, P.; Maes, L.; Van Calenbergh, S. Synthesis and Evaluation of α-Halogenated Analogues of 3-(Acetylhydroxyamino)propylphosphonic Acid (FR900098) as Antimalarials. *J. Med. Chem.* **2010**, *53*, 5342–5346. [CrossRef] [PubMed]
128. Andaloussi, M.; Henriksson, L.M.; Więckowska, A.; Lindh, M.; Björkelid, C.; Larsson, A.M.; Suresh, S.; Iyer, H.; Srinivasa, B.R.; Bergfors, T.; et al. Design, Synthesis, and X-ray Crystallographic Studies of α-Aryl Substituted Fosmidomycin Analogues as Inhibitors of *Mycobacterium tuberculosis* 1-Deoxy-D-Xylulose 5-Phosphate Reductoisomerase. *J. Med. Chem.* **2011**, *54*, 4964–4976. [CrossRef] [PubMed]
129. Nordqvist, A.; Björkelid, C.; Andaloussi, M.; Jansson, A.M.; Mowbray, S.L.; Karlén, A.; Larhed, M. Synthesis of Functionalized Cinnamaldehyde Derivatives by an Oxidative Heck Reaction and their Use as Starting Materials for Preparation of *Mycobacterium tuberculosis* 1-Deoxy-D-Xylulose-5-Phosphate Reductoisomerase Inhibitors. *J. Org. Chem.* **2011**, *76*, 8986–8998. [CrossRef] [PubMed]
130. Devreux, V.; Wiesner, J.; Jomaa, H.; Rozenski, J.; Van der Eycken, J.; Van Calenbergh, S. Divergent Strategy for the Synthesis of α-Aryl-Substituted Fosmidomycin Analogues. *J. Org. Chem.* **2007**, *72*, 3783–3789. [CrossRef] [PubMed]
131. Schlüter, K.; Walter, R.D.; Bergmann, B.; Kurz, T. Arylmethyl Substituted Derivatives of Fosmidomycin: Synthesis and Antimalarial Activity. *Eur. J. Med. Chem.* **2006**, *41*, 1385–1397. [CrossRef] [PubMed]
132. Kurz, T.; Geffken, D.; Kaula, U. Phosphororganische Verbindungen und deren Verwendung. DE10356410A1, 23 June 2005.
133. Kurz, T.; Schlüter, K.; Kaula, U.; Bergmann, B.; Walter, R.D.; Geffken, D. Synthesis and Antimalarial Activity of Chain Substituted Pivaloyloxymethyl Ester Analogues of Fosmidomycin and FR900098. *Bioorg. Med. Chem.* **2006**, *14*, 5121–5135. [CrossRef] [PubMed]
134. Perruchon, J.; Ortmann, R.; Altenkämper, M.; Silber, K.; Wiesner, J.; Jomaa, H.; Klebe, G.; Schlitzer, M. Studies Addressing the Importance of Charge in the Binding of Fosmidomycin-like Molecules to Deoxyxylulosephosphate Reductoisomerase. *ChemMedChem* **2008**, *3*, 1232–1241. [CrossRef]
135. Dreneau, A.; Krebs, F.S.; Munier, M.; Ngov, C.; Tritsch, D.; Lièvremont, D.; Rohmer, M.; Grosdemange-Billiard, C. α,α-Difluorophosphonohydroxamic Acid Derivatives Among the Best Antibacterial Fosmidomycin Analogues. *Molecules* **2021**, *26*, 5111. [CrossRef] [PubMed]
136. Chekan, J.R.; Cogan, D.P.; Nair, S.K. Molecular Basis for Resistance Against Phosphonate Antibiotics and Herbicides. *MedChemComm* **2016**, *7*, 28–36. [CrossRef]

137. Verbrugghen, T.; Vandurm, P.; Pouyez, J.; Maes, L.; Wouters, J.; Van Calenbergh, S. Alpha-Heteroatom Derivatized Analogues of 3-(Acetylhydroxyamino)propyl Phosphonic Acid (FR900098) as Antimalarials. *J. Med. Chem.* **2013**, *56*, 376–380. [CrossRef] [PubMed]
138. Kunfermann, A.; Lienau, C.; Illarionov, B.; Held, J.; Gräwert, T.; Behrendt, C.T.; Werner, P.; Hähn, S.; Eisenreich, W.; Riederer, U.; et al. IspC as Target for Antiinfective Drug Discovery: Synthesis, Enantiomeric Separation, and Structural Biology of Fosmidomycin Thia Isosters. *J. Med. Chem.* **2013**, *56*, 8151–8162. [CrossRef] [PubMed]
139. Xue, J.; Diao, J.; Cai, G.; Deng, L.; Zheng, B.; Yao, Y.; Song, Y. Antimalarial and Structural Studies of Pyridine-Containing Inhibitors of 1-Deoxyxylulose-5-phosphate Reductoisomerase. *ACS Med. Chem. Lett.* **2013**, *4*, 278–282. [CrossRef] [PubMed]
140. Steinbacher, S.; Kaiser, J.; Eisenreich, W.; Huber, R.; Bacher, A.; Rohdich, F. Structural Basis of Fosmidomycin Action Revealed by the Complex with 2-C-Methyl-D-Erythritol 4-Phosphate Synthase (IspC). Implications for the Catalytic Mechanism and Anti-Malaria Drug Development. *J. Biol. Chem.* **2003**, *278*, 18401–18407. [CrossRef]
141. Yajima, S.; Hara, K.; Iino, D.; Sasaki, Y.; Kuzuyama, T.; Ohsawa, K.; Seto, H. Structure of 1-Deoxy-D-Xylulose 5-Phosphate Reductoisomerase in a Quaternary Complex with a Magnesium Ion, NADPH and the Antimalarial Drug Gosmidomycin. *Acta Crystallogr. Sect. F Struct. Biol. Cryst. Commun.* **2007**, *63*, 466–470. [CrossRef]
142. Brücher, K.; Illarionov, B.; Held, J.; Tschan, S.; Kunfermann, A.; Pein, M.K.; Bacher, A.; Gräwert, T.; Maes, L.; Mordmüller, B.; et al. α-Substituted β-Oxa Isosteres of Fosmidomycin: Synthesis and Biological Evaluation. *J. Med. Chem.* **2012**, *55*, 6566–6575. [CrossRef]
143. Lienau, C.; Gräwert, T.; Alves Avelar, L.A.; Illarionov, B.; Held, J.; Knaab, T.C.; Lungerich, B.; van Geelen, L.; Meier, D.; Geissler, S.; et al. Novel Reverse Thia-Analogs of Fosmidomycin: Synthesis and Antiplasmodial Activity. *Eur. J. Med. Chem.* **2019**, *181*, 111555. [CrossRef]
144. Adeyemi, C.M.; Hoppe, H.C.; Isaacs, M.; Klein, R.; Lobb, K.A.; Kaye, P.T. Synthesis of N-Substituted Phosphoramidic Acid Esters as "Reverse" Fosmidomycin Analogues. *Tetrahedron* **2019**, *75*, 2371–2378. [CrossRef]
145. Chofor, R.; Sooriyaarachchi, S.; Risseeuw, M.D.P.; Bergfors, T.; Pouyez, J.; Johny, C.; Haymond, A.; Everaert, A.; Dowd, C.S.; Maes, L.; et al. Synthesis and Bioactivity of β-Substituted Fosmidomycin Analogues Targeting 1-Deoxy-D-Xylulose-5-Phosphate Reductoisomerase. *J. Med. Chem.* **2015**, *58*, 2988–3001. [CrossRef]
146. Sooriyaarachchi, S.; Chofor, R.; Risseeuw, M.D.P.; Bergfors, T.; Pouyez, J.; Dowd, C.S.; Maes, L.; Wouters, J.; Jones, T.A.; Van Calenbergh, S.; et al. Targeting an Aromatic Hotspot in *Plasmodium falciparum* 1-Deoxy-D-Xylulose-5-Phosphate Reductoisomerase with β-Arylpropyl Analogues of Fosmidomycin. *ChemMedChem* **2016**, *11*, 2024–2036. [CrossRef]
147. Munier, M.; Tritsch, D.; Krebs, F.; Esque, J.; Hemmerlin, A.; Rohmer, M.; Stote, R.H.; Grosdemange-Billiard, C. Synthesis and Biological Evaluation of Phosphate Isosters of Fosmidomycin and Analogs as Inhibitors of *Escherichia coli* and *Mycobacterium smegmatis* 1-Deoxyxylulose 5-Phosphate Reductoisomerases. *Bioorg. Med. Chem.* **2017**, *25*, 684–689. [CrossRef] [PubMed]
148. Meyer, O.; Grosdemange-Billiard, C.; Tritsch, D.; Rohmer, M. Isoprenoid Biosynthesis via the MEP Pathway. Synthesis of (3R,4S)-3,4-Dihydroxy-5-Oxohexylphosphonic Acid, an Isosteric Analogue of 1-Deoxy-D-Xylulose 5-Phosphate, the Substrate of the 1-Deoxy-D-Xylulose 5-Phosphate Reducto-isomerase. *Org. Biomol. Chem.* **2003**, *1*, 4367–4372. [CrossRef] [PubMed]
149. Freeman, S.; Ross, K.C. 3 Prodrug Design for Phosphates and Phosphonates. In *Progress in Medicinal Chemistry*; Ellis, G.P., Luscombe, D.K., Eds.; Elsevier: Amsterdam, The Netherlands, 1997; Volume 34, pp. 111–147.
150. Krise, J.P.; Stella, V.J. Prodrugs of Phosphates, Phosphonates, and Phosphinates. *Adv. Drug Deliv. Rev.* **1996**, *19*, 287–310. [CrossRef]
151. Kurz, T.; Geffken, D.; Wackendorff, C. Carboxylic Acid Analogues of Fosmidomycin. *Z. Für Nat.* **2003**, *58*, 457–461. [CrossRef]
152. Nguyen-Trung, A.T.; Tritsch, D.; Grosdemange-Billiard, C.; Rohmer, M. Synthesis of Tetrazole Analogues of Phosphonohydroxamic Acids: An Attempt to Improve the Inhibitory Activity Against the DXR. *Bioorg. Med. Chem. Lett.* **2013**, *23*, 1643–1647. [CrossRef]
153. Macchiarulo, A.; Pellicciari, R. Exploring the Other Side of Biologically Relevant Chemical Space: Insights into Carboxylic, Sulfonic and Phosphonic Acid Bioisosteric Relationships. *J. Mol. Graph. Model.* **2007**, *26*, 728–739. [CrossRef]
154. Gadakh, B.; Pouyez, J.; Wouters, J.; Venkatesham, A.; Cos, P.; Van Aerschot, A. N-Acylated Sulfonamide Congeners of Fosmidomycin Lack Any Inhibitory Activity Against DXR. *Bioorg. Med. Chem. Lett.* **2015**, *25*, 1577–1579. [CrossRef]
155. Island, M.D.; Wei, B.Y.; Kadner, R.J. Structure and Function of the *uhp* Genes for the Sugar Phosphate Transport System in *Escherichia coli* and *Salmonella typhimurium*. *J. Bacteriol.* **1992**, *174*, 2754–2762. [CrossRef]
156. Lemieux, M.J.; Huang, Y.; Wang, D.-N. Glycerol-3-Phosphate Transporter of *Escherichia coli:* Structure, Function and Regulation. *Res. Microbiol.* **2004**, *155*, 623–629. [CrossRef]
157. Sakamoto, Y.; Furukawa, S.; Ogihara, H.; Yamasaki, M. Fosmidomycin Resistance in Adenylate Cyclase Deficient (cya) Mutants of *Escherichia coli*. *Biosci. Biotechnol. Biochem.* **2003**, *67*, 2030–2033. [CrossRef]
158. Hemmerlin, A.; Tritsch, D.; Hammann, P.; Rohmer, M.; Bach, T.J. Profiling of Defense Responses in *Escherichia coli* Treated with Fosmidomycin. *Biochimie* **2014**, *99*, 54–62. [CrossRef] [PubMed]
159. Halpern, L. The Transfer of Inorganic Phosphorous Across the Red Cell Membrane. *J. Biol. Chem.* **1936**, *114*, 747–770. [CrossRef]
160. Leibman, K.C.; Heidelberger, C. The Metabolism of P^{32}-Labelled Ribonucleotides in Tissue Slices and Cell. *J. Biol. Chem.* **1955**, *216*, 823–830. [CrossRef] [PubMed]
161. Wiemer, A.J. Metabolic Efficacy of Phosphate Prodrugs and the Remdesivir Paradigm. *ACS Pharmacol. Transl. Sci.* **2020**, *3*, 613–626. [CrossRef]
162. De Clercq, E. Tenofovir Alafenamide (TAF) as the Successor of Tenofovir Disoproxil Fumarate (TDF). *Biochem. Pharmacol.* **2016**, *119*, 1–7. [CrossRef]
163. Hostetler, K.Y. Alkoxyalkyl Prodrugs of Acyclic Nucleoside Phosphonates Enhance Oral Antiviral Activity and Reduce Toxicity: Current State of the Art. *Antivir. Res.* **2009**, *82*, A84–A98. [CrossRef]

164. Spinner, C.D.; Gottlieb, R.L.; Criner, G.J.; Arribas López, J.R.; Cattelan, A.M.; Soriano Viladomiu, A.; Ogbuagu, O.; Malhotra, P.; Mullane, K.M.; Castagna, A.; et al. Effect of Remdesivir vs Standard Care on Clinical Status at 11 Days in Patients With Moderate COVID-19: A Randomized Clinical Trial. *JAMA* **2020**, *324*, 1048–1057. [CrossRef]
165. Goldman, J.D.; Lye, D.C.B.; Hui, D.S.; Marks, K.M.; Bruno, R.; Montejano, R.; Spinner, C.D.; Galli, M.; Ahn, M.Y.; Nahass, R.G.; et al. Remdesivir for 5 or 10 Days in Patients with Severe COVID-19. *N. Engl. J. Med.* **2020**, *383*, 1827–1837. [CrossRef]
166. Smolders, E.J.; Jansen, A.M.E.; Ter Horst, P.G.J.; Rockstroh, J.; Back, D.J.; Burger, D.M. Viral Hepatitis C Therapy: Pharmacokinetic and Pharmacodynamic Considerations: A 2019 Update. *Clin. Pharmacokinet.* **2019**, *58*, 1237–1263. [CrossRef]
167. Kirby, B.J.; Symonds, W.T.; Kearney, B.P.; Mathias, A.A. Pharmacokinetic, Pharmacodynamic, and Drug-Interaction Profile of the Hepatitis C Virus NS5B Polymerase Inhibitor Sofosbuvir. *Clin. Pharmacokinet.* **2015**, *54*, 677–690. [CrossRef]
168. Scott, L.J.; Chan, H.L.Y. Tenofovir Alafenamide: A Review in Chronic Hepatitis B. *Drugs* **2017**, *77*, 1017–1028. [CrossRef] [PubMed]
169. Agarwal, K.; Fung, S.K.; Nguyen, T.T.; Cheng, W.; Sicard, E.; Ryder, S.D.; Flaherty, J.F.; Lawson, E.; Zhao, S.; Subramanian, G.M.; et al. Twenty-Eight Day Safety, Antiviral Activity, and Pharmacokinetics of Tenofovir Alafenamide for Treatment of Chronic Hepatitis B Infection. *J. Hepatol.* **2015**, *62*, 533–540. [CrossRef] [PubMed]
170. Mackman, R.L. Anti-HIV Nucleoside Phosphonate GS-9148 and Its Prodrug GS-9131: Scale Up of a 2′-F Modified Cyclic Nucleoside Phosphonate and Synthesis of Selected Amidate Prodrugs. *Curr. Protoc. Nucleic Acid Chem.* **2014**, *56*, 10–14. [CrossRef] [PubMed]
171. Reichenberg, A.; Wiesner, J.; Weidemeyer, C.; Dreiseidler, E.; Sanderbrand, S.; Altincicek, B.; Beck, E.; Schlitzer, M.; Jomaa, H. Diaryl Ester Prodrugs of FR900098 with Improved in Vivo Antimalarial Activity. *Bioorg. Med. Chem. Lett.* **2001**, *11*, 833–835. [CrossRef] [PubMed]
172. Wiesner, J.; Ortmann, R.; Jomaa, H.; Schlitzer, M. Double Ester Prodrugs of FR900098 Display Enhanced in-Vitro Antimalarial Activity. *Arch. Der Pharm.* **2007**, *340*, 667–669. [CrossRef]
173. Ortmann, R.; Wiesner, J.; Reichenberg, A.; Henschker, D.; Beck, E.; Jomaa, H.; Schlitzer, M. Acyloxyalkyl Ester Prodrugs of FR900098 With Improved in Vivo Anti-Malarial Activity. *Bioorg. Med. Chem. Lett.* **2003**, *13*, 2163–2166. [CrossRef]
174. Ortmann, R.; Wiesner, J.; Reichenberg, A.; Henschker, D.; Beck, E.; Jomaa, H.; Schlitzer, M. Alkoxycarbonyloxyethyl Ester Prodrugs of FR900098 With Improved in vivo Antimalarial Activity. *Arch. Der Pharm.* **2005**, *338*, 305–314. [CrossRef]
175. Courtens, C.; Risseeuw, M.; Caljon, G.; Cos, P.; Van Calenbergh, S. Acyloxybenzyl and Alkoxyalkyl Prodrugs of a Fosmidomycin Surrogate as Antimalarial and Antitubercular Agents. *ACS Med. Chem. Lett.* **2018**, *9*, 986–989. [CrossRef]
176. Jackson, E.R.; Dowd, C.S. Inhibition of 1-Deoxy-D-Xylulose-5-phosphate Reductoisomerase (Dxr): A Review of the Synthesis and Biological Evaluation of Recent Inhibitors. *Curr. Top. Med. Chem.* **2012**, *12*, 706–728. [CrossRef]
177. Ponaire, S.; Zinglé, C.; Tritsch, D.; Grosdemange-Billiard, C.; Rohmer, M. Growth Inhibition of *Mycobacterium smegmatis* by Prodrugs of Deoxyxylulose Phosphate Reducto-Isomerase Inhibitors, Promising Anti-Mycobacterial Agents. *Eur. J. Med. Chem.* **2012**, *51*, 277–285. [CrossRef]
178. Liu, J.; Barry, C.E., III; Besra, G.S.; Nikaido, H. Mycolic Acid Structure Determines the Fluidity of the Mycobacterial Cell Wall. *J. Biol. Chem.* **1996**, *271*, 29545–29551. [CrossRef]
179. Edwards, R.L.; Brothers, R.C.; Wang, X.; Maron, M.I.; Ziniel, P.D.; Tsang, P.S.; Kraft, T.E.; Hruz, P.W.; Williamson, K.C.; Dowd, C.S.; et al. MEPicides: Potent Antimalarial Prodrugs Targeting Isoprenoid Biosynthesis. *Sci. Rep.* **2017**, *7*, 8400. [CrossRef] [PubMed]
180. Faísca Phillips, A.M.; Nogueira, F.; Murtinheira, F.; Barros, M.T. Synthesis and Antimalarial Evaluation of Prodrugs of Novel Fosmidomycin Analogues. *Bioorg. Med. Chem. Lett.* **2015**, *25*, 2112–2116. [CrossRef] [PubMed]
181. Courtens, C.; Risseeuw, M.; Caljon, G.; Maes, L.; Cos, P.; Martin, A.; Van Calenbergh, S. Double Prodrugs of a Fosmidomycin Surrogate as Antimalarial and Antitubercular Agents. *Bioorg. Med. Chem. Lett.* **2019**, *29*, 1232–1235. [CrossRef] [PubMed]
182. Courtens, C.; Risseeuw, M.; Caljon, G.; Maes, L.; Martin, A.; Van Calenbergh, S. Amino Acid Based Prodrugs of a Fosmidomycin Surrogate as Antimalarial and Antitubercular Agents. *Bioorg. Med. Chem.* **2019**, *27*, 729–747. [CrossRef] [PubMed]
183. Courtens, C.; Risseeuw, M.; Caljon, G.; Cos, P.; Martin, A.; Van Calenbergh, S. Phosphonodiamidate Prodrugs of N-Alkoxy Analogs of a Fosmidomycin Surrogate as Antimalarial and Antitubercular Agents. *Bioorg. Med. Chem. Lett.* **2019**, *29*, 1051–1053. [CrossRef] [PubMed]
184. Munier, M.; Tritsch, D.; Lièvremont, D.; Rohmer, M.; Grosdemange-Billiard, C. Synthesis and Biological Evaluation of Aryl Phosphoramidate Prodrugs of Fosfoxacin and its Derivatives. *Bioorg. Chem.* **2019**, *89*, 103012. [CrossRef]
185. Langel, Ü. *Cell-Penetrating Peptides: Processes and Applications*; CRC Press: Boca Raton, FL, USA, 2002; p. 424.
186. Pujals, S.; Fernández-Carneado, J.; López-Iglesias, C.; Kogan, M.J.; Giralt, E. Mechanistic Aspects of CPP-Mediated Intracellular Drug Delivery: Relevance of CPP Self-Assembly. *Biochim. Biophys. Acta Biomembr.* **2006**, *1758*, 264–279. [CrossRef]
187. Kamena, F.; Monnanda, B.; Makou, D.; Capone, S.; Patora-Komisarska, K.; Seebach, D. On the Mechanism of Eukaryotic Cell Penetration by α- and β-Oligoarginines—Targeting Infected Erythro cytes. *Chem. Biodivers.* **2011**, *8*, 1–12. [CrossRef]
188. Samuel, B.U.; Hearn, B.; Mack, D.; Wender, P.; Rothbard, J.; Kirisits, M.J.; Mui, E.; Wernimont, S.; Roberts, C.W.; Muench, S.P.; et al. Delivery of Antimicrobials into Parasites. *Proc. Natl. Acad. Sci. USA* **2003**, *100*, 14281–14286. [CrossRef]
189. Chadwick, J.; Jones, M.; Mercer, A.E.; Stocks, P.A.; Ward, S.A.; Park, B.K.; O'Neill, P.M. Design, Synthesis and Antimalarial/Anticancer Evaluation of Spermidine Linked Artemisinin Conjugates Designed to Exploit Polyamine Transporters in *Plasmodium falciparum* and HL-60 Cancer Cell Lines. *Bioorg.Med. Chem.* **2010**, *18*, 2586–2597. [CrossRef] [PubMed]
190. Yajima, S.; Hara, K.; Sanders, J.M.; Yin, F.; Ohsawa, K.; Wiesner, J.; Jomaa, H.; Oldfield, E. Crystallographic Structures of Two Bisphosphonate:1-Deoxyxylulose-5-Phosphate Reductoisomerase Complexes. *J. Am. Chem. Soc.* **2004**, *126*, 10824–10825. [CrossRef] [PubMed]

191. Deng, L.; Endo, K.; Kato, M.; Cheng, G.; Yajima, S.; Song, Y. Structures of 1-Deoxy-D-Xylulose-5-Phosphate Reductoisomerase/Lipophilic Phosphonate Complexes. *ACS Med. Chem. Lett.* **2011**, *2*, 165–170. [CrossRef] [PubMed]
192. Zinglé, C.; Tritsch, D.; Grosdemange-Billiard, C.; Rohmer, M. Catechol-Rhodanine Derivatives: Specific and Promiscuous Inhibitors of *Escherichia coli* Deoxyxylulose Phosphate Reductoisomerase (DXR). *Bioorg. Med. Chem.* **2014**, *22*, 3713–3719. [CrossRef]
193. Adeyemi, C.M.; Hoppe, H.C.; Isaacs, M.; Mnkandhla, D.; Lobb, K.A.; Klein, R.; Kaye, P.T. Synthesis and Anti-Parasitic Activity of N-Benzylated Phosphoramidate Mg^{2+}-Chelating Ligands. *Bioorg. Chem.* **2020**, *105*, 104280. [CrossRef]
194. Hui, X.; Yue, Q.; Zhang, D.D.; Li, H.; Yang, S.Q.; Gao, W.Y. Antimicrobial Mechanism of Theaflavins: They Target 1-Deoxy-D-Xylulose 5-Phosphate Reductoisomerase, the Key Enzyme of the MEP Terpenoid Biosynthetic Pathway. *Sci. Rep.* **2016**, *6*, 38945. [CrossRef]
195. Haymond, A.; Dowdy, T.; Johny, C.; Johnson, C.; Ball, H.; Dailey, A.; Schweibenz, B.; Villarroel, K.; Young, R.; Mantooth, C.J.; et al. A High-Throughput Screening Campaign to Identify Inhibitors of DXP Reductoisomerase (IspC) and MEP Cytidylyltransferase (IspD). *Anal. Biochem.* **2018**, *542*, 63–75. [CrossRef]

3.Previous work on developing potent DXR inhibitors

With the spread of multidrug-resistant *Plasmodium* species, the need for new, improved therapeutics to reduce malaria deaths and the discovery of new drug targets remain an urgent research goal. The isoprenoid precursors isopentenyl diphosphate (IPP) and dimethylallyl diphosphate (DMAPP) are essential in several human pathogens like *Plasmodium falciparum (P. falciparum)*, *Mycobacterium tuberculosis* (*M. tuberculosis*) and *Escherichia coli* (*E. coli*), where they are synthesized through the methyl-D-erythritol phosphate (MEP) pathway known as non-mevalonate pathway.[120–123] Humans use the long-known mevalonate pathway to synthesize the same isoprenoid precursors.[124,125] The absence of MEP in humans makes it an attractive pathway for discovering novel anti-infective drug candidates.[126]

The enzyme 1-deoxy-D-xylulose 5-phosphate reductoisomerase (DXR) catalyzes the isomerization and reduction of 1-deoxy-D-xylulose-5-phosphate (DOXP) to 2-*C*-methyl-D-erythritol-4-phosphate (MEP). This reaction is considered rate-limiting in isoprenoid synthesis by the MEP pathway. DXR requires NADPH and a divalent metal cation for its enzymatic activity.[127,128] and is considered a clinically validated drug target in anti-infective drug discovery.[127,128]

Fosmidomycin (**1**) is structurally similar to the DXR's natural substrate (DOXP) and acts as a potent inhibitor of *the Pf*DXR enzyme.[127] **1** also showed potent *in vitro* and *in vivo* antiplasmodial activity.[127] Unfortunately, fosmidomycin (**1**) does not fit fully as a novel antimalarial drug because of its unfavorable pharmacokinetic properties (e.g., short plasma half-life) and physicochemical properties (high hydrophilicity). For example, fosmidomycin deprotonation at physiological pH is responsible for its insufficient membrane permeability, which is a common reason for low oral bioavailability.[129,130] Thus, novel analogs with enhanced activity and pharmacokinetic profiles are needed. Considerable efforts were made to improve the efficacy of fosmidomycin by modifying either the phosphonate group, which mimics the monophosphate group in DOXP (**A**), the hydroxamate group, which chelates the bivalent metal ion (**B**), or the linker (**C**) connecting them (Figure 11). Since SAR studies on fosmidomycin highlighted the importance of these groups for both appropriate binding and good inhibition of DXR enzyme (Section 2.2), new approaches are needed to develop potent DXR inhibitors. One approach to improve the anti-infective capabilities of fosmidomycin is by increasing the binding affinity of the new analogs by targeting novel binding pockets in the DXR enzyme.

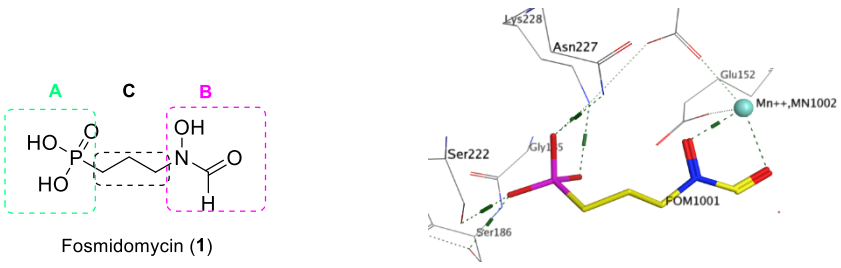

Figure 11: Structure and binding interactions of fosmidomycin (**1**) in *Ec*DXR enzyme PDB: 1ONP.[131]

The first attempt was made by KURZ et al., who examined the impact of introducing substitution at the α-position of the propyl linker on DXR inhibition. *α*-Phenyl-fosmidomycin (**2**, Figure 12) was the first chain-substituted

DXR inhibitor to show improved antiplasmodial activity against *Pf*Dd2 strains (IC_{50} = 0.4 µM) compared to fosmidomycin.[132] Next, the promising results obtained with α-phenyl-fosmidomycin and its analogs encouraged KURZ and co-workers to study the effect of introducing α-substituents on the linker of reverse fosmidomycin analogs. The results showed that various reverse carba analogs with decorated α-phenyl-substituents are potent *Pf*DXR inhibitors (**3a,b-5a,b**) with IC_{50} values in the low nanomolar range (Figure 12). This strengthened the positive impact of the introduction of α-substituents on DXR inhibition activity.[133,134]

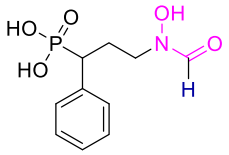

2*

*Pf*Dd2 IC_{50} = 0.4 µ*M*

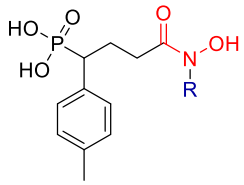

3

3a *Pf*DXR IC_{50} = 0.01 µM, *Pf*Dd2 IC_{50} = 0.25 µM
3b *Pf*DXR IC_{50} = 0.19 µM, *Pf*Dd2 IC_{50} = 2.80 µM

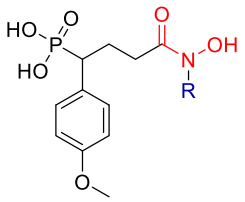

4

4a *Pf*DXR IC_{50} = 0.02 µM, *Pf*Dd2 IC_{50} = 0.30 µM
4b *Pf*DXR IC_{50} = 0.08 µM, *Pf*Dd2 IC_{50} = 3.60 µM

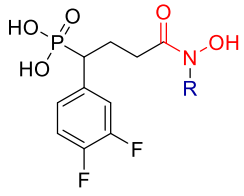

5

5a *Pf*DXR IC_{50} = 3 nM, *Pf*-K1 IC_{50} = 0.38 µM
5b *Pf*DXR IC_{50} = 3 nM, *Pf*-K1 IC_{50} = 0.29 µM

Figure 12: Structures, antiplasmodial, and *Pf*DXR inhibitory activity of compounds **2**, **3a,b**, **4a,b**, and **5a,b**. *Diethanolammonium salt was prepared. In pink, the hydroxamate metal binding group is highlighted. In red, the reverse hydroxamate metal binding group is highlighted.

Crystal structure of **4b** in *Pf*DXR (PDB: 3WQR, Figure 13a) indicates that **4b** is located in the active site cavity and has comparable molecular interactions, metal coordination abilities, and potential hydrogen-bond networks as observed for fosmidomycin in the fosmidomycin-*Pf*DXR complex (Figure 13b). The co-crystal structure showed that the α-MeO-Ph group is accommodated in a hydrophobic sub-pocket. Furthermore, the α-MeO-Ph group of **4b** destabilizes the active site flap, residues 291-299, resulting in a relatively open conformation. This unique conformation allowed the formation of additional space around the hydroxamic acid nitrogen, which was not present in the fosmidomycin structure (PDB: 3AU9).[135] Despite this open conformation, strong binding of **4b** to *Pf*DXR was enhanced by novel van der Waals interactions between the α-MeO-Ph group and the core of the active site sup-pocket. Moreover, the *N*-methyl group also enhanced the binding by forming an intramolecular interaction with the α-MeO-Ph ring and through the interaction with the side chain of Met360. These interactions opened up possibilities for designing potent DXR inhibitors by addressing other binding pockets in the DRX substrate binding site.[133]

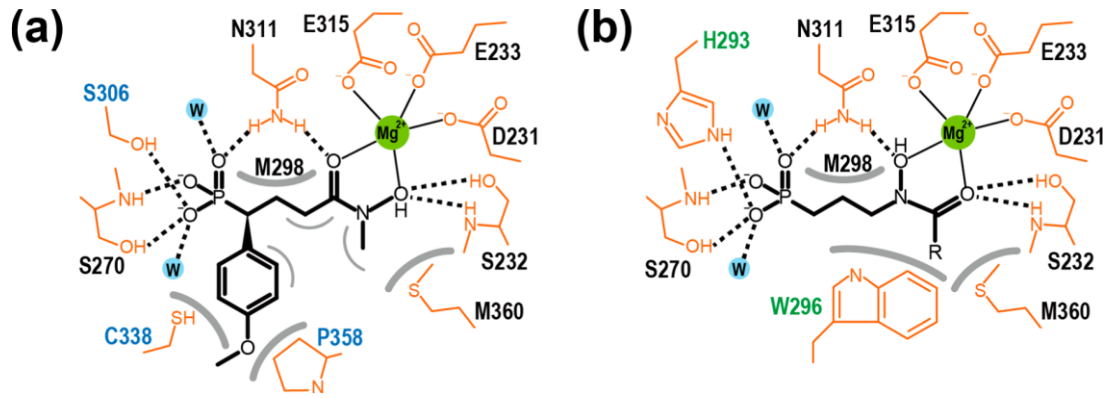

Figure 13: Schematic overview of the interactions of **4b** (a) and fosmidomycin (b) in the active site of *Pf*DXR. Intra- and intermolecular van der Waals contacts are shown as thin and thick gray arcs, respectively. Reprinted with permission from *J. Med. Chem*. 2014, 57, 8827−8838. Copyright 2023 American Chemical Society.[133]

The Kurz group also investigated the effect of introducing alkyl substituents in the hydroxamic acid nitrogen of the α-phenyl analogs **6a-d** as a second possibility to enhance the binding affinity to the substrate binding pocket. They have demonstrated that increasing the size of the alkyl substituents from methyl to ethyl group reduced both cellular and enzymatic activity (Figure 14). The bulkier *N*-isopropyl group even led to a loss of inhibitory activity against the *Pf*DXR enzyme and *Pf*-K1 strain.[134,136] The *N*-methyl substituted reverse analog **6b** showed the most potent *Pf*DXR inhibitory with IC_{50} of 3 nM, outperforming fosmidomycin (IC_{50} = 0.14 µM).

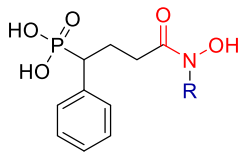

6a, R = H **6b**, R = Me **6c**, R = Et **6d**, R = *i*-Pr

*Pf*DXR IC_{50} [nm]	11	3	15	inactive

Figure 14: Structures and *Pf*DXR inhibition of **6a-d**. In red, the reverse hydroxamate metal binding functionality is highlighted.

Encouraged by the α-substituted analogs, the VAN CALENBERGH.[137] group conducted a study on the effects of introducing various substituents at the β-position of *N*-methyl-substituted reverse fosmidomycin analog (Figure 15). From the synthesized series, inhibitors with arylalkyl residues in the β-position showed the most potent activity (**7a-c**). Compound **7c**, for example, showed the strongest inhibition against *Pf*DXR with an IC_{50} of 69 nM. Crystallographic studies of **7b** and **7c** on the *Pf*DXR enzyme revealed novel binding modes to the enzyme. The phenylalkyl residues resulted in different flap structures in *Pf*DXR. The rearrangement of the flap produced favorable interactions between the phenyl ring of the inhibitors and the tryptophan residue (W296) of the active site flap. The enhanced activity of **7b** and **7c** is likely due to these binding site interactions (Figure 16).[137]

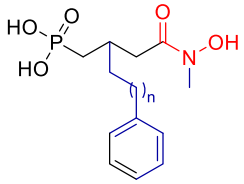

	7a, n = 1	**7b**, n = 2	**7c**, n = 3
*Pf*DXR IC_{50} [μM]	1.36	0.12	0.07

Figure 15: Structures, antiplasmodial, and *Pf*DXR inhibition of **7a-c**. In red, the hydroxamate metal binding functionality is highlighted; in blue, the arylalkyl residue is highlighted.

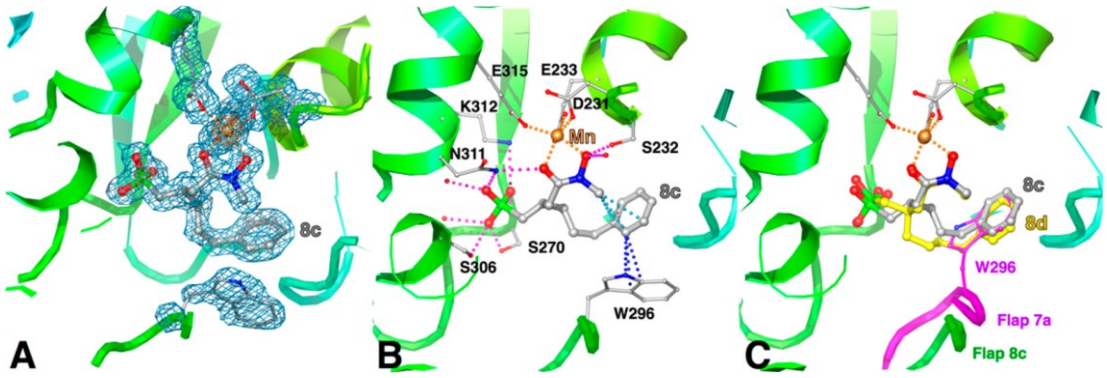

Figure 16: Crystal structure of *Pf*Dxr bound to **7b** and **7c**. Reprinted with permission from *J. Med. Chem.* 2015, 58, 7, 2988-3001. Copyright 2023 American Chemical Society.[137]

DXR enzyme comprises three distinct domains: the N-terminal domain, catalytic domain, and C-terminal domain. The N-terminal domain includes the NADPH binding site; the connector domain houses the enzymatic reaction; the C-terminal domain plays a crucial role in maintaining the highly conserved active site structure (Figure 17A).[138] In DXR, the nicotinamide-binding pocket of the cofactor NADPH is located adjacent to the substrate binding site (Figure 17B).[139] Moreover, the NADPH binding pocket gave a good score in the druggability studies performed by MASINI et al.[140]

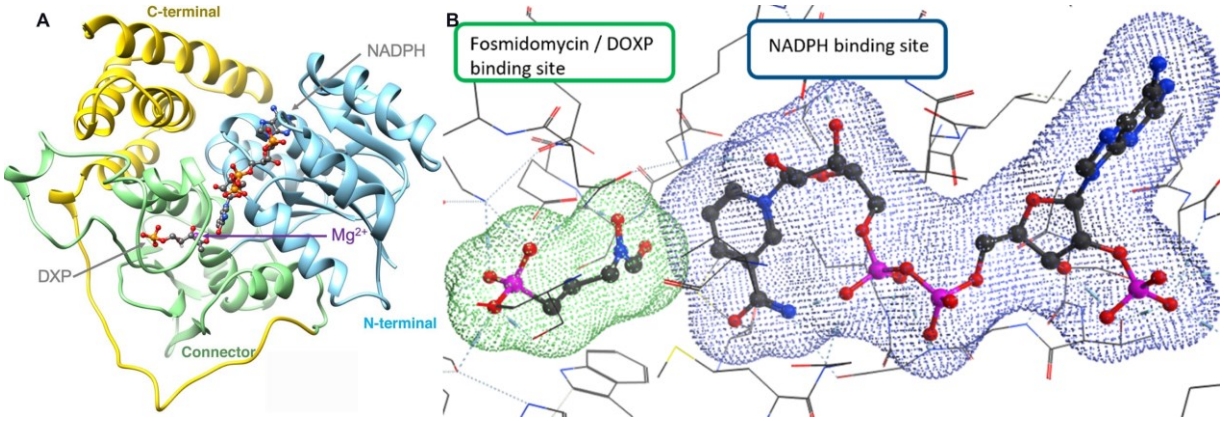

Figure 17: **A**) Representation of the DXR monomer structure. The N-terminal domain (colored blue), the catalytic domain (colored green), and the C-terminal domain (colored gold) are labeled. Reprinted with permission from *Journal of Computer-Aided Molecular Design* (2019) 33:927–940 Copyright 2023 Springer Nature.[138] **B**) NADPH and fosmidomycin/DOXP binding sites. Crystal structure of *Pf*DXR in a ternary complex with fosmidomycin and NADPH PDB: 3AU9.[135]

Based on these facts, the DOWD group was the first to develop a series of fosmidomycin analogs with different arylalkyl substituents on the *N*-hydroxy oxygen atom (arylalkoxyamide type, **9**) or the carbonyl carbon atom of the hydroxamate moiety (*N*-acyl type, **8**) to act as bisubstrate inhibitors of DXR enzyme.[141] These analogs were designed to simultaneously occupy the fosmidomycin/DOXP and NADPH binding pockets. Surprisingly, whereas these analogs bear large substituents on the hydroxamic acid group, they exhibited moderate to weak inhibitory activity against *Pf*DXR.[141,142] Inhibitors **8** and **9** were the most active analogs in the synthesized series. **8** and **9** inhibited *Pf*DXR with an IC_{50} of 1.34 and 3.36 µM, respectively (Figure 18). To assess whether **8** and **9** are bisubstrate inhibitors, Lineweaver-Burk analysis of **8** and **9** against *Pf*DXR was performed. The assay indicated that **9** had a competitive mode of inhibition relative to both the substrate and NADPH-binding sites, indicating a possible bisubstrate mode of inhibition. On the other hand, compound **8** showed a competitive mode of inhibition relative to the substrate and an uncompetitive mode of inhibition relative to NADPH. These results indicated that **8** had a non-bisubtrate binding mode. However, the hypothesized binding modes of **8** and **9** could not be supported by crystallographic evidence.

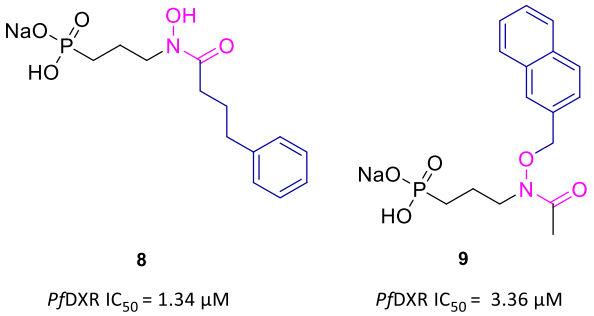

Figure 18: Structures and *Pf*DXR inhibitory activity of **8** and **9**. In pink, the hydroxamate metal binding functionality is highlighted; in blue, the groups targeting the NADPH site are highlighted.

JANSSON et al. also attempted to address the NADPH binding site by using compound **10a** as a lead compound (Figure 19).[143] **10a** showed potent *in vitro* growth inhibition in a *P. falciparum* parasite assay (IC_{50} = 0.04 µM). To further enhance the possibility of addressing the co-factor binding site, additional substituents were introduced at different positions on the phenyl ring of **10a**. Of the new series compound **10b** (Figure 19), bearing a 1,2,4-triazole substituent in the meta position, was the most active analog. However, **10b** displayed a five times reduction in antiplasmodial activity (IC_{50} = 0.19 µM) than **10a**. Despite their antiplasmodial activity, **10a** and **10b** were not evaluated against the *Pf*DXR enzyme. Furthermore, the bisubstrate binding mode was not confirmed with a co-crystal structure with *Pf*DXR enzyme.[143]

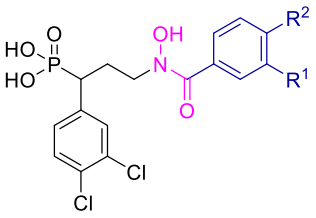

10a-c

	10a, R^1 = H; R^2 = H	**10b**, R^1 = H; R^2 = CH_2-1,2,4-triazole
Pf IC_{50} [µM]	0.04	0.19

Figure 19: Structures, *P. falciparum* inhibitionof **10a**, **10b**. In pink, the hydroxamate metal binding functionality is highlighted; in blue, the groups targeting the NADPH site are highlighted.

4. Aim of work

Based on the previous attempts to improve the DXR inhibitory activity by targeting new binding pockets in DXR enzyme, the current study aimed to design and synthesize high-affinity *Pf*DXR inhibitors while considering the need for increased lipophilicity. The compounds were designed to address new hydrophobic pockets in the substrate binding site or even to target the NADPH binding site in the N-terminal domain of the DXR enzyme. The potent *Pf*DXR inhibitor **6b** (IC_{50} = 3 nM, Figure 14, Section 3) was selected as the lead compound.[136] Since, up to our knowledge, the exact mode of binding of the previously reported potential bisubstrate inhibitors is unknown, determining the synthesized analogs' binding mode by co-crystal structures with *Pf*DXR enzyme was also planned in collaboration with the group of Prof. NOBUTADA TANAKA. For this purpose, different strategies were employed.

1- Amide and arylalkoxyamide analogs

The Dowd group doubted the importance of the free hydroxamate OH functionality.[141,142] They showed that the arylalkoxyamide **9** (Figure 18**,** Section 3) could moderately inhibit *Pf*DXR enzyme with IC_{50} of 3.36 µM. Lineweaver-Burk analysis of **9** against *Pf*DXR revealed a competitive mode of inhibition relative to both the substrate and NADPH-binding sites.[141,142] Encouraged by these results, the first part of this project aimed to investigate the feasibility of developing non-hydroxamate inhibitors by replacing the hydroxamate group of **6b** with alternative moieties like amide and alkoxyamide functionality (Figure 20). Different arylalkyl groups were introduced at the nitrogen atom of the amide group or the oxygen atom of the hydroxamic acid moiety (arylalkoxyamid analogs). The arylalkyl-substituted amide and arylalkoxyamide analogs were designed to enable the binding to either the NADPH binding site or the novel binding pockets but not to coordinate the divalent cation.

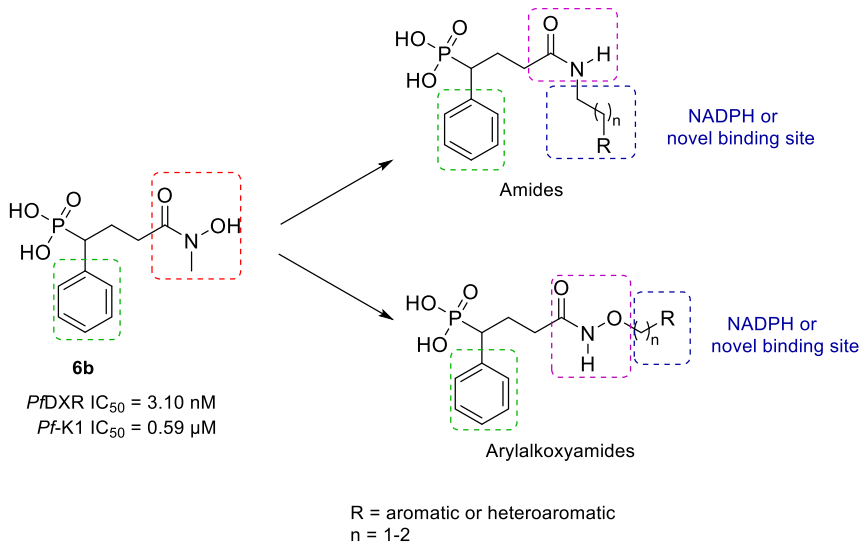

Figure 20: Design strategy of the amides and arylalkoxyamides compound library.

2- *N*-substituted hydroxamic acid analogs

The crystal structure of compound **4b** (Figure 13, Section 3) revealed the formation of a unique space around the nitrogen atom of the hydroxamic acid group, which was not present in the fosmidomycin *Pf*DXR co-crystal structure. This discovery prompted further investigation into the possibility of incorporating large substituents on the nitrogen atom of the hydroxamic acid group to fill the newly formed space. The objective of this part was to determine the impact of large substituents on DXR inhibitory activity. To explore this, various *N*-substituted hydroxamic acid analogs were proposed using **6b** as the lead structure. To ensure the divalent metal cation's coordination ability, the hydroxamic acid group of **6b** was retained unchanged. Included in this part, the optimum length of the alkyl chain needed to approach the hydrophobic sub-pockets in the substrate binding site was planned to be tested. (Figure 21).

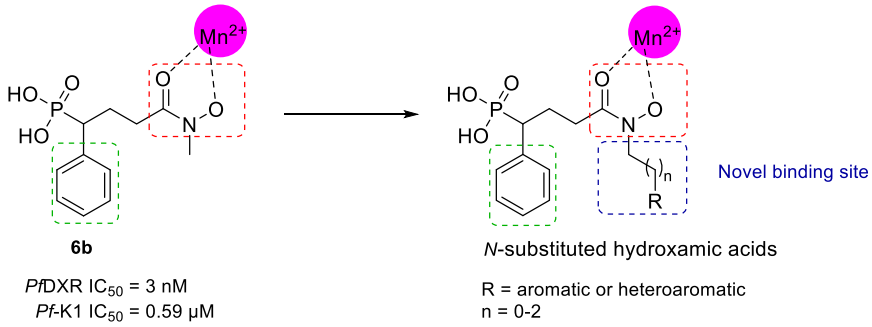

Figure 21: Design strategy of the *N*-substituted hydroxamic acids compound library.

3- Optimization of the most active inhibitor type

In order to gain new insights regarding the structure-activity relationships (SAR), iterative cycles of structural modifications to the most active inhibitor type were planned as the next optimization step.

4- Phosphonate prodrugs of representative inhibitors

The prodrug strategy has proven successful in improving permeation across biological membranes, thereby increasing the activity against intact pathogen cells and the *in vivo* activity. Indeed, BRÜCHER et al. showed that the *in vitro* efficacy of reverse fosmidomycin derivatives against asexual blood stages of *P. falciparum* could be enhanced by more than an order of magnitude by conversion of the hydrophilic phosphonate moiety into acyloxymethyl and alkoxycarbonyloxymethyl prodrugs.[144] As a final structural modification, we aimed to mask the polar phosphonic acid group as lipophilic ester prodrugs. Toward this goal, pivaloyloxymethyl (POM) phosphonate esters of selected *N*-substituted hydroxamic acid were designed (Figure 22).

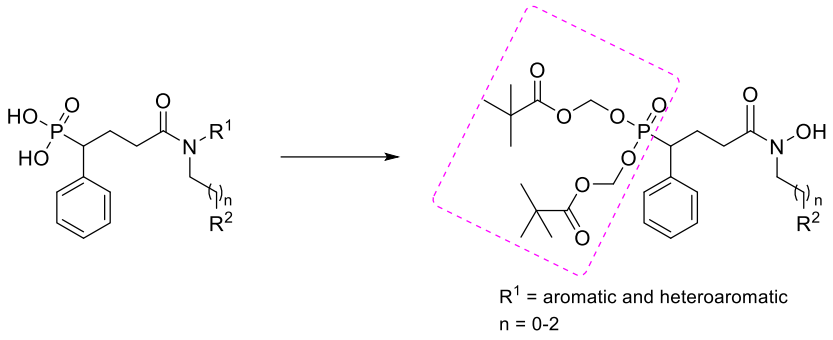

Figure 22: Design strategy of the POM esters.

5- Research strategy and collaboration partners

The synthesized phosphonic acids should first be tested in a target-based enzymatic assay to test their ability to inhibit *PfDXR* as our primary intention. Still, isozymes from other species were also considered. This evaluation was planned to be implemented in collaboration with the working group of Prof. FISCHER at the University of Hamburg. Also, evaluation of the compounds and the POM esters in phenotypic cell-based screening to assess their antiplasmodial activity against asexual blood stages of the malaria parasite by the working group of Dr. JANA HELD, Institute of Tropical Medicine, University of Tübingen was planned. Two *Plasmodium falciparum* strains were intended to be used, the chloroquine-sensitive *Pf*3D7 and the multidrug resistance *Pf*Dd2 strains.

To elucidate the exact binding mode of the compounds, co-crystal structures of the *PfDXR* enzyme with the most active analogs in the presence and absence of the cofactor (NADPH) were planned. The crystal structure studies were intended to be performed by Prof. NOBUTADA TANAKA, School of Pharmacy, Kitasato University (Figure 23). The information obtained from the *Pf*DXR inhibition assay and co-crystal structure studies served as a crucial benchmark for further structural optimization in subsequent cycles of structural modifications.

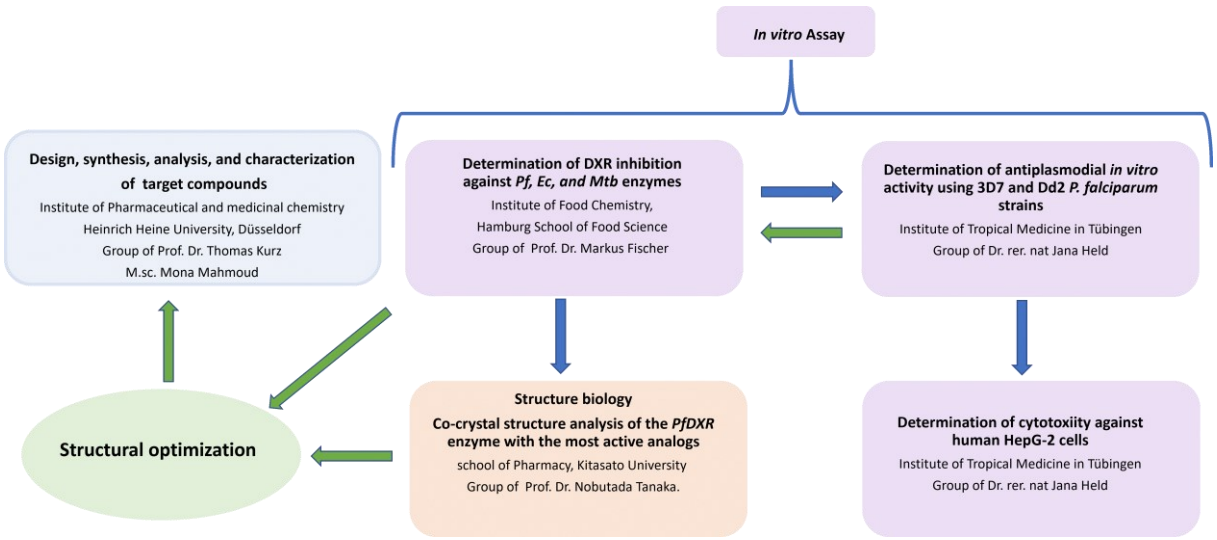

Figure 23: Collaboration partners and project structure

5. Results

5.1 DXR inhibitor synthesis

5.1.1 Synthesis of the starting materials

5.1.1.1 Synthesis of carboxylic acid **15**

The key intermediate carboxylic acid **15**, required for the synthesis of all inhibitor types, was synthesized according to the procedures reported by BEHRENDT et al.[136] Diethyl benzyl phosphonate **11** was chosen as the starting material. *C*-Alkylation of **11** with [2-(1,3-dioxolan-2-yl)ethyl]bromide (**12**) in the presence of *n*-butyllithium provided 1,3-dioxolane **13** in 93% yield. Acidic hydrolysis of compound **13** furnished the aldehyde **14**, which was oxidized to the corresponding carboxylic acid **15** by treatment with SeO_2 and H_2O_2 (Scheme 1).

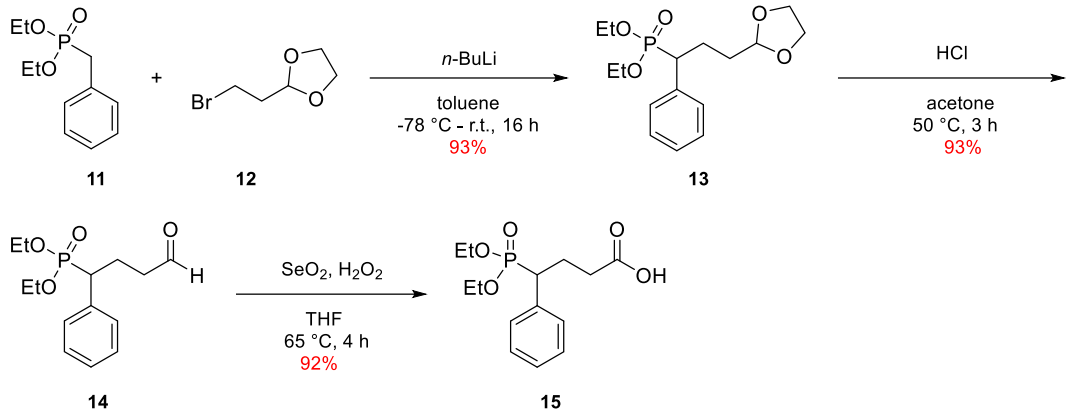

Scheme 1: Synthesis of the reverse carba analog **15**.

5.1.1.2 Synthesis of the *O*-substituted hydroxylamines

The *O*-substituted hydroxylamines needed for arylakoxyamide synthesis were obtained *via* a modified GABRIEL amine two-step synthesis strategy. For the synthesis of hydroxylamines **22a**,**b**, the oxazole **19a** and the thiazole **19b** intermediates were first prepared using the procedure of ZHAO et al. (Scheme 2).[145]

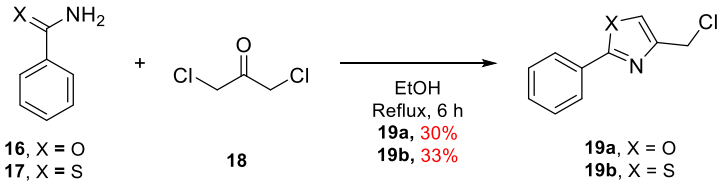

Scheme 2: Synthesis of heterocycles **19a** and **19b**.

The reaction is analogous to HANTZSCH-thiazole synthesis in which condensation of 1,3-dichloroacetone (**18**) with benzamide (**16**) or thiobenzamide (**17**) afforded the intermediates **IIa,b**. In the next step, cyclization of **IVa,b** produced the chloromethyl-substituted oxazole **19a** and thiazole **19b** in moderate yields.[145] The reaction mechanism is shown in Scheme 3.

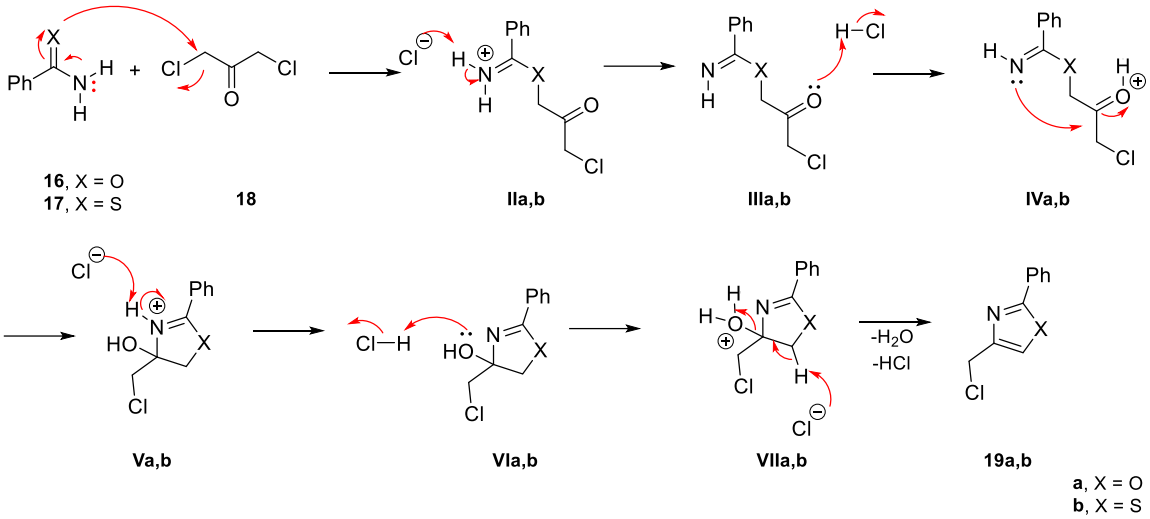

Scheme 3: HANTZSCH-thiazole reaction mechanism.

The phthaloyl-protected hydroxylamines **21a-h** were synthesized through the nucleophilic substitution of the chloromethyl-substituted oxazole **19a**, thiazole **19b**, and commercially available arylalkyl halides **19c-h** on *N*-hydroxyphthalimide (NHPI, **20**) using the literature procedure reported by ASFAHA et al.[146] Subsequently; the deprotection was performed through hydrazinolysis yielding the *O*-substituted hydroxylamines **22a-h** (Scheme 4).[146]

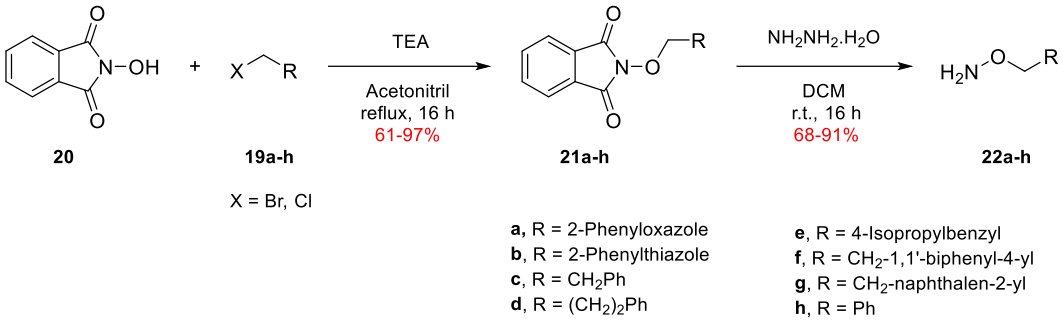

Scheme 4: Synthesis of the *O*-substituted hydroxylamines **22a-h**.

5.1.1.3 Synthesis of the *N*-substituted-*O*-benzyl-protected hydroxylamines

In order to synthesize *N*-substituted hydroxamic acids and to determine the optimal length to approach the new binding site, known **26a** and new **26b-e** *O*-benzyl-protected hydroxylamines with varying lengths of the alkyl chain and different aromatic groups were synthesized. The synthesis of the known *O*-benzylhydroxylamine (**22h**) was performed as shown in Scheme 4. Boc protection of **22h** was performed using Boc-anhydride in ethanol. The *N*-alkylation of **23** with arylalkyl halides **24a-e** in the presence of sodium hydride provided *N*-substituted benzyloxycarbamates **25a-e**. Finally, the removal of the Boc-protecting group was performed by using either 4 M HCl in dioxane to yield the *N*-substituted-*O*-Bn-protected hydroxylamines **26a**,**b** or 1:1 TFA/DCM mixture to yield the *N*-substituted-*O*-Bn-protected hydroxylamines **26c-e** (Scheme 5).[147]

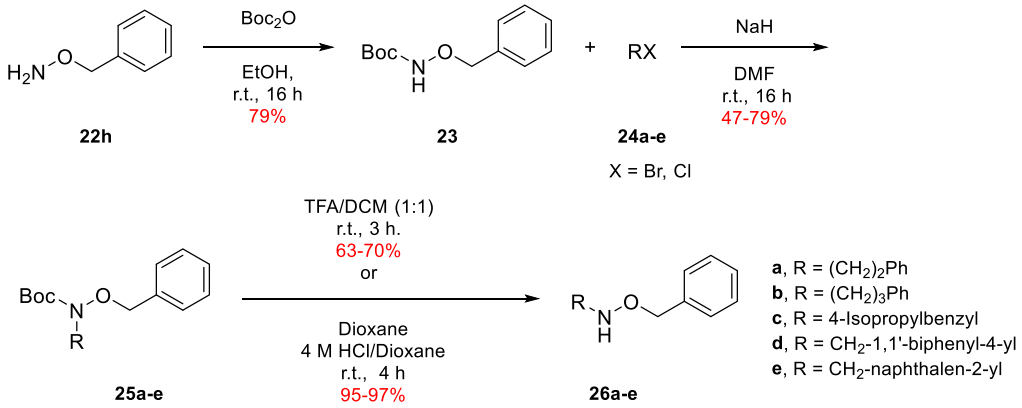

Scheme 5: Synthesis of the *N*-substituted-*O*-benzyl protected hydroxylamines **26a-e**.

5.1.2 Synthesis of amides, arylalkoxyamides, and *N*-substituted hydroxamic acid analogs

5.1.2.1 HATU coupling reaction

Coupling reactions were conducted using HATU (**VIII**) (Hexafluorophosphate Azabenzotriazole Tetramethyl Uronium) as an amide coupling reagent. The reaction mechanism of carboxylic acid activation by HATU and subsequent amide bond formation is summarized in Scheme 6. In the first step, the carboxylate anion **IX**, formed by deprotonation by an organic base (not shown), attacks HATU (**VIII**) to form the unstable *O*-acyl(tetramethyl)isouronium salt (**X**), and the 1-hydroxy-7-azabenzotriazole (OAt anion **XI)**. The OAt anion (**XI**) rapidly attacks the isouronium salt **X**, affording the OAt-active ester (**XII**) and liberating a stoichiometric quantity of tetramethylurea. The addition of a nucleophile, such as an amine, to the OAt-active ester afforded the acylated product **XIII**. HATU is used along with *N*,*N*-diisopropylethylamine (DIPEA), also known as Hünig's bases, or triethylamine (TEA) to form amide bonds.[148] Typically, DMF is used as a solvent, although other polar aprotic solvents can also be used.[149] Coupling of the carboxylic acid **15** with the synthesized *O*-substituted hydroxylamines **22a**-**g**, *N*-substituted-*O*-benzyl protected hydroxylamines **26a-e**, and different commercially available amines **27a-c** was performed using adapted procedure from literature.[149] The reactions were performed using DMF as a solvent and DIPEA as a base (Scheme 7). Target compounds were then purified using flash chromatography (on a prepacked silica cartridge) using DCM:30% methanol/DCM (100:0→70:30) as eluent. The purity of compounds **28a-g**, **29a-e**, and **30a-c** were determined by HPLC and was found to be >95%.

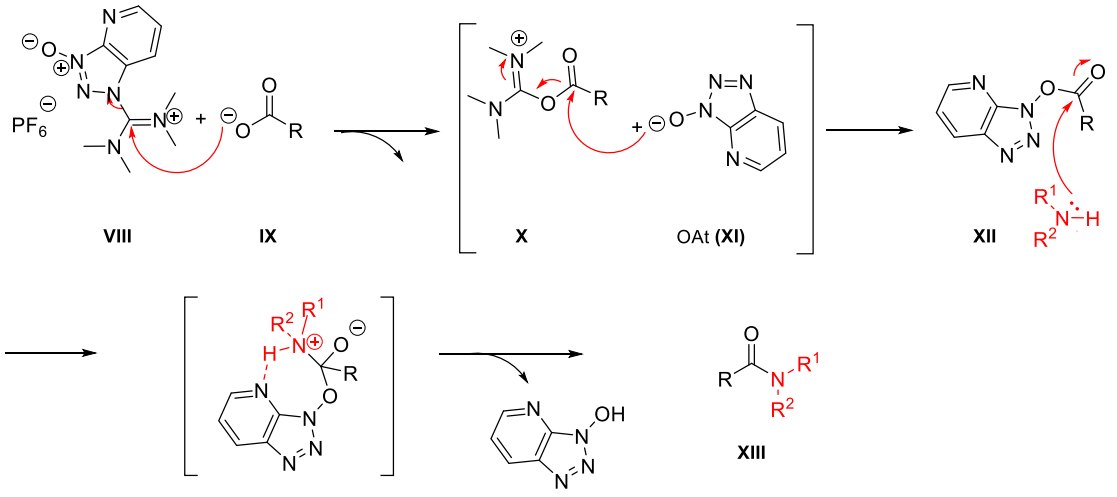

Scheme 6: HATU coupling reaction mechanism.

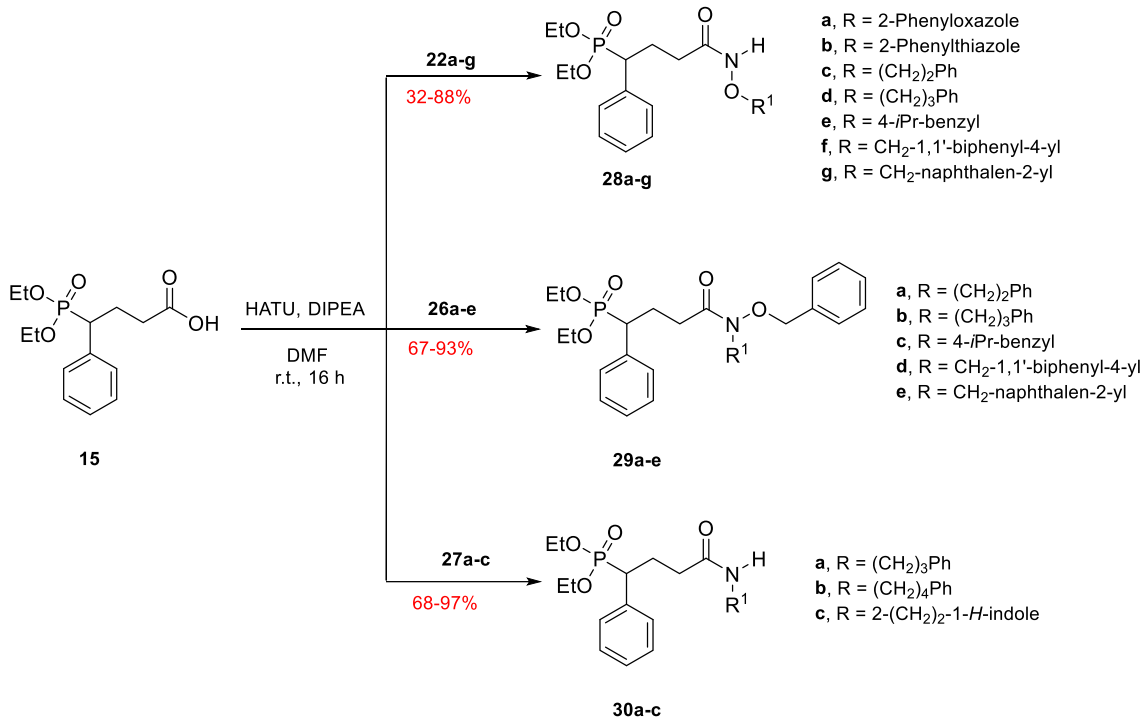

Scheme 7: Synthesis of compounds **28a-g**, **29a-e**, and **30a-c**.

The structures of the synthesized derivatives **28a-g**, **29a-e**, and **30a-c** were confirmed by ^{1}H-NMR and ^{13}C-NMR. An example of the ^{1}H-NMR spectrum is displayed in Figure 24 for compound **29b**. In the ^{1}H-NMR (300 MHz, DMSO), the signals of the aromatic hydrogen atoms for compound **29b** are between 7.39 – 7.23 ppm (10H) and 7.21 – 7.10 ppm (5H). The methylene group hydrogens of the benzyl group (CH$_2$Ph, signal 15 in spectrum, Figure 24) appear as a multiplet at 4.69 – 4.54 ppm. The methylene groups of the diethyl phosphonate ester functionality (CH$_2$CH$_3$) appear as two multiplets, each with 2 protons between 4.07 – 3.90 ppm and 3.88 – 3.65 ppm. An additional multiplet with 2H between 3.88 – 3.65 ppm belongs to one methylene group of the phenylpropyl moiety (CH$_2$CH$_2$CH$_2$Ph). Signal 7, generated by the hydrogen atom on the methine carbon atom (PCH), appears at 3.28 – 3.12 ppm and shows the splitting pattern of a doublet of doublets of doublets (ddd). The methylene hydrogens adjacent to the asymmetric center show a long-distance coupling with ^{31}P and appear as

two multiplet at 2.33 – 2.14 ppm (3H) and 2.08 – 1.90 ppm (1H). The two other methylene groups, which belong to the propyl linker of the phenylpropyl moiety, appears as one multiplet ($CH_2CH_2\underline{CH_2}Ph$) at 2.57 – 2.50 ppm and a pentet ($CH_2\underline{CH_2}CH_2Ph$) at 1.78 ($J$ = 7.3 Hz). Finally, the methyl groups of the ethyl ester moiety ($CH_2\underline{CH_3}$) appear as two triplets with J coupling of 7.0 at 1.19 and 1.01 ppm. ^{13}C-NMR (75 MHz, MeOD) spectrum of **29b** (Figure 25) revealed the presence of signals at δ 175.30 (C=O), 142.64, 136.40 (d, $J_{C\text{-}P}$ = 6.9 Hz), 135.64, 130.62 (d, $J_{C\text{-}P}$ = 6.8 Hz), 130.49, 129.90, 129.79 (d, $J_{C\text{-}P}$ = 2.6 Hz), 129.59, 129.40, 128.66 (d, $J_{C\text{-}P}$ = 3.2 Hz), 126.96, 77.04 (CH2, Bn group), 64.02 (d, $J_{C\text{-}P}$ = 7.2 Hz, $\underline{CH_2}CH_3$), 63.51 (d, $J_{C\text{-}P}$ = 7.4 Hz, $\underline{CH_2}CH3$), 45.66, 44.23 (d, $J_{C\text{-}P}$ = 138.1 Hz, P$\underline{CH}$), 33.89, 30.99 (d, $J_{C\text{-}P}$ = 16.2 Hz), 29.57, 25.64, 16.72 (d, $J_{C\text{-}P}$ = 6.0 Hz, $CH_2\underline{CH_3}$), and 16.53 (d, $J_{C\text{-}P}$ = 5.8 Hz, $CH_2\underline{CH_3}$) ppm confirming the structure.

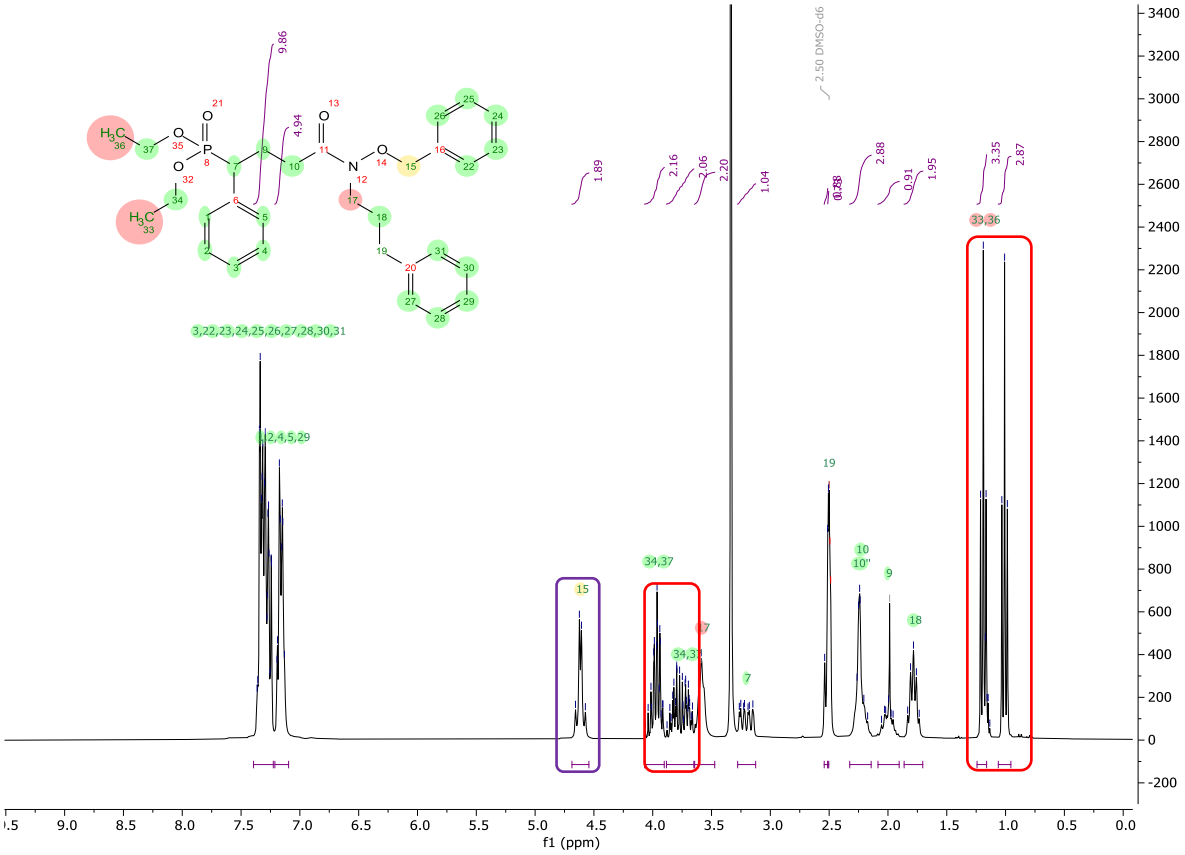

Figure 24: ^{1}H-NMR spectrum of compound **29b**. ^{1}H-NMR signals of the diethyl phosphonate group marked red. The methylene group hydrogens of the benzyl group are marked purple.

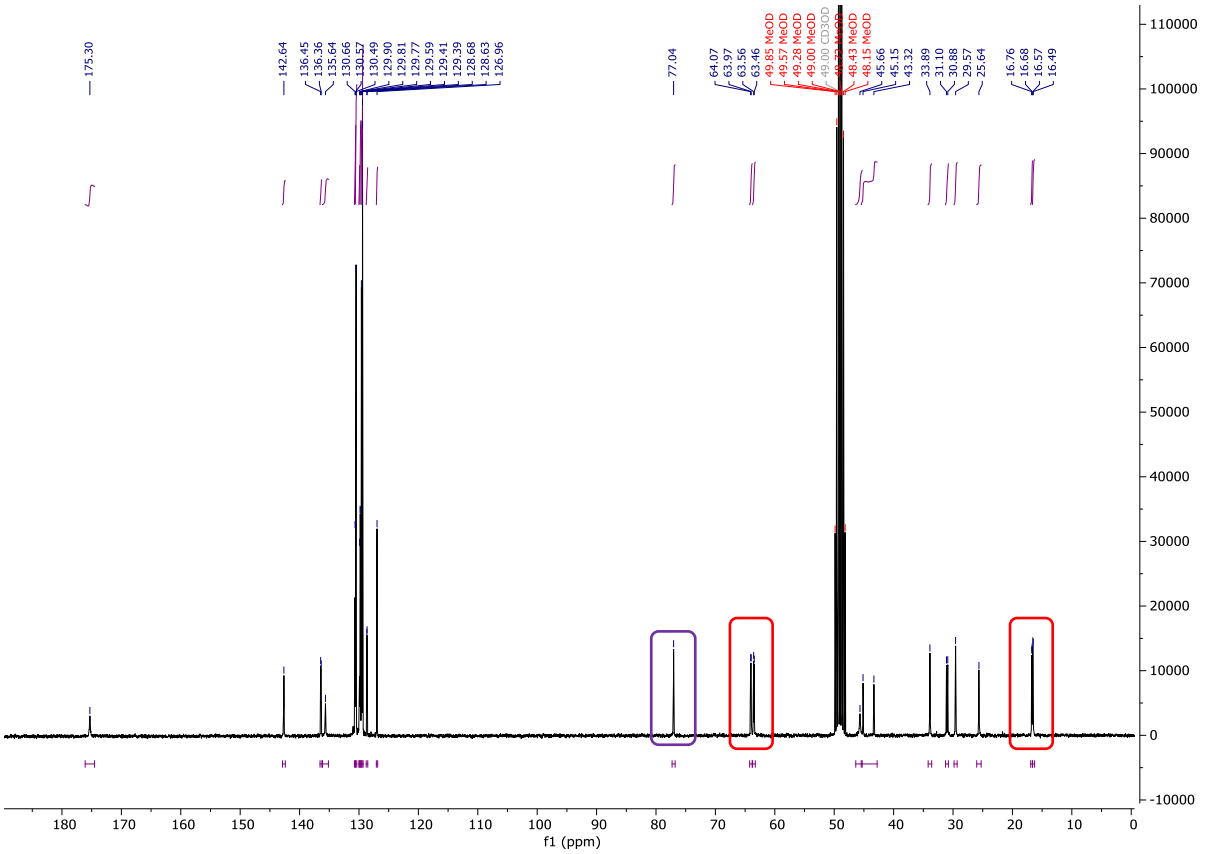

Figure 25: ^{13}C-NMR spectrum of compound **29b**. ^{13}C-NMR signals of the diethyl phosphonate group marked red. The methylene group hydrogens of the benzyl group are marked purple.

5.1.2.2 Conversion of the phosphonate esters to phosphonic acids

The trimethylsilyl bromide (TMSBr) mediated deprotection of the phosphonic acid diethyl ester moiety is the final step of the synthetic route in the case of the amide and arylalkoxyamide derivatives.[150] TMSBr has been widely used as a mild and efficient reagent for the conversion of ethyl phosphonates into phosphonic acids.[150] McKenna postulated a multistep dealkylation mechanism similar to the Arbuzov reaction (Scheme 8).[151] This mechanism was then supported by kinetic studies by Conibear.[152] Initially, rapid activation of the phosphonate ester by silylation is followed by dealkylation, where two ethyl groups are replaced by two trimethylsilyl groups (transesterification) to yield bis(trimethylsilyl)phosphonates. This is followed by hydrolysis of the bis(trimethylsilyl)phosphonates with water to obtain the phosphonic acids.[153]

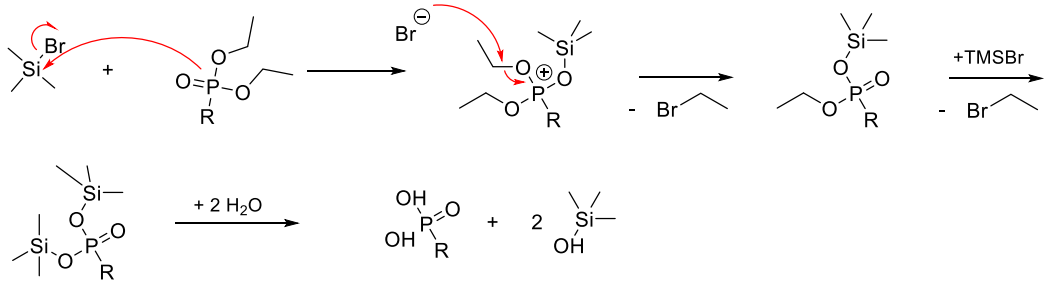

Scheme 8: Mechanism of phosphonate ester cleavage by TMSBr.

The deprotection of the phosphonic acid diethyl esters **28a-g**, **29a-e**, and **30a-c** was performed using microwave-assisted phosphonate ester cleavage.[154] TMSBr (2.00 eq) and a reaction time of 2 hours were required to drive

the reaction to completion. Due to the sensitivity of TMSBr to hydrolysis, the reaction must be carried out in dry solvents and under inert gas. The corresponding silyl esters were obtained after 2 h. Water was then added to liberate the free phosphonic acid (Scheme 9). Compounds **31e**, **31g**, and **32a-e** were then purified using reverse-phase chromatography water:acetonitrile (90:10→70:30)), whereas compounds **31c**, **31d**, **31f**, and **33a-c** were purified by the formation of the corresponding disodium salt. After purification, all compounds showed a purity of >95% in HPLC.

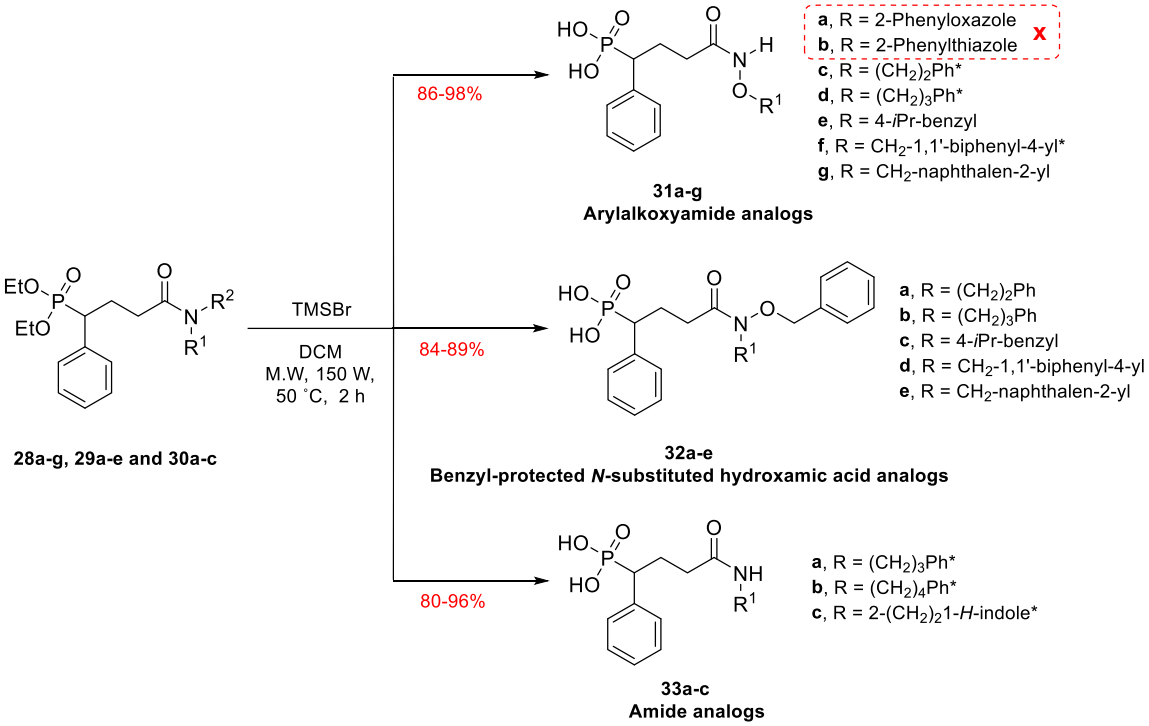

Scheme 9: Synthesis of arylalkoxyamide analogs **31a-g**, benzyl-protected *N*-substituted hydroxamic acid analogs **32a-e**, and amide analogs **33a-c**. * The compounds were prepared as disodium salt.

Surprisingly, the TMSBr treatment of the **28a** and **28b** provided carboxylic acid **15** and alkoxyamines **22a** and **22b**.

Spectral and analytical data confirmed the formation of compounds **31a-g**, **32a-e,** and **33a-c**. For example, ^{1}H-NMR spectrum of compound **32b** showed the disappearance of the two multiplets of the methylene groups of the diethyl phosphonate ester functionality ($\underline{CH_2}CH_3$) between 4.07 – 3.90 ppm and 3.88 – 3.65 ppm and the two triplets of the methyl groups of the ethyl ester moiety ($CH_2\underline{CH_3}$) at 1.19 and 1.01 ppm (Figure 26).^{13}C-NMR also confirmed the disappearance of diethyl phosphonate ester functionality (Figure 27)

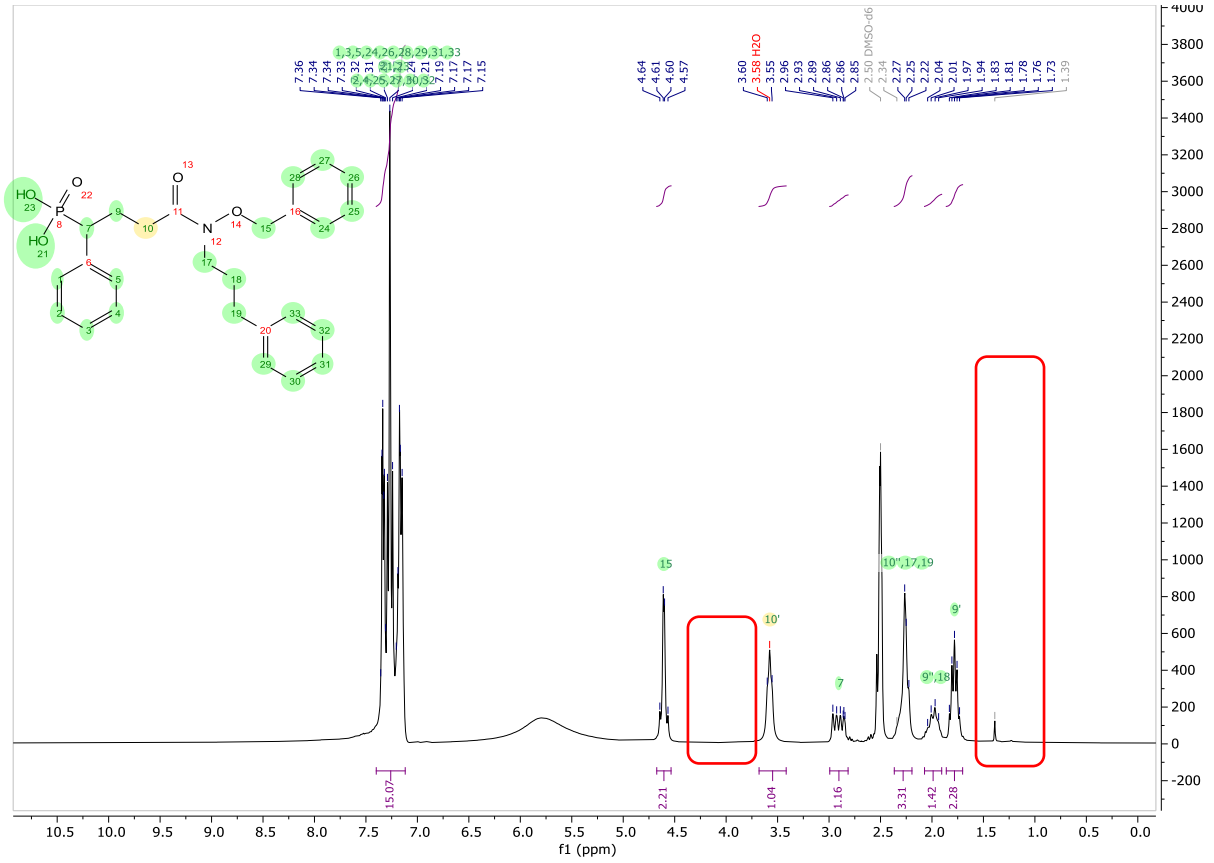

Figure 26: ^{1}H-NMR spectrum of compound **32b**. Red rectangles marked the normal region of the diethyl phosphonate group compared to Figure 24.

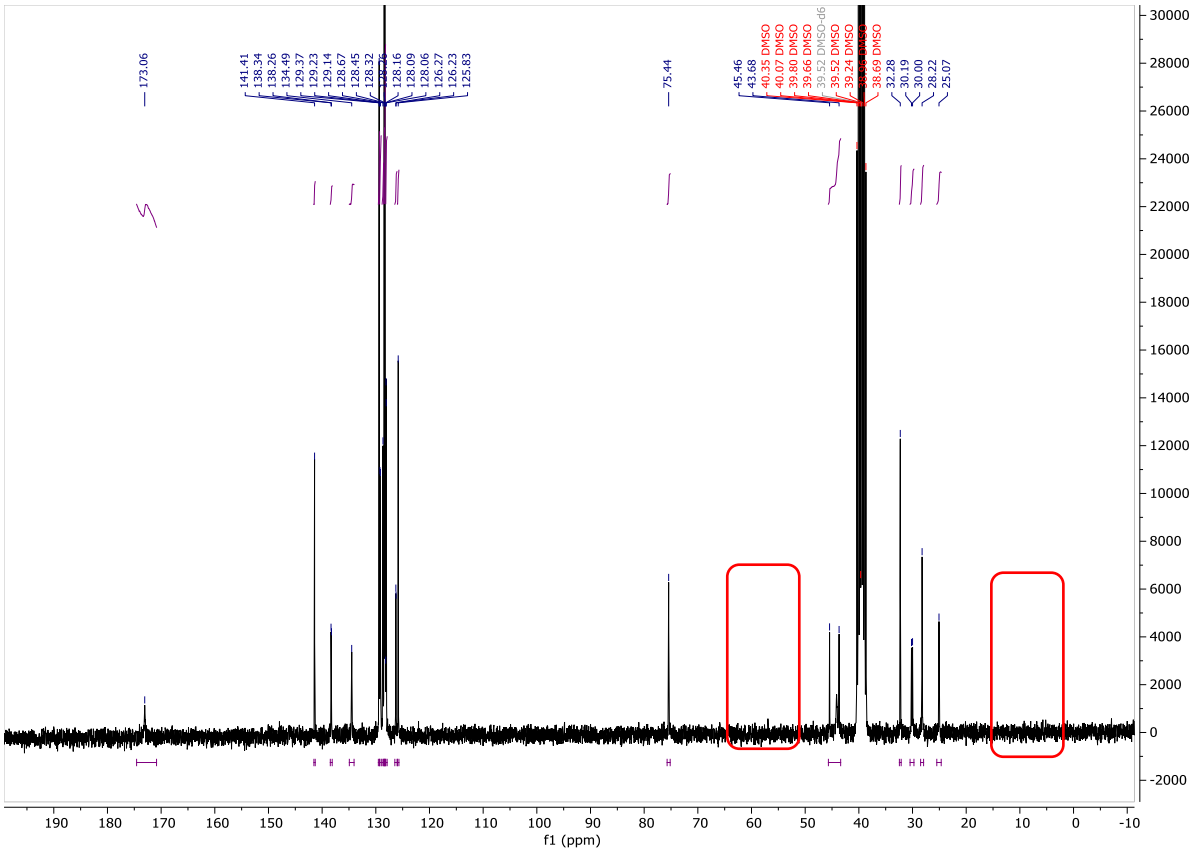

Figure 27: ^{13}C-NMR spectrum of compound **32b**. Red rectangles marked the normal region of the diethyl phosphonate group signals compared to Figure 25.

5.1.2.3 Removal of the benzyl-protecting group

As a final step for synthesizing the *N*-substituted hydroxamic acid analogs **34a-e**, the *O*-benzyl-protected compounds were deprotected by catalytic hydrogenation using Pd/C and H_2 under atmospheric pressure, as shown in Scheme 10. The crude products were purified by reverse phase flash chromatography (on a prepacked silica cartridge), using water:acetonitrile (90:10→80:20) as eluent. Compounds **34a-e** were obtained in a yield ranging from 80-99%. The purity of the *N*-substituted hydroxamic acid analogs **34a-e** were determined using HPLC and met the requirement for the planned biological testing >95.0%.

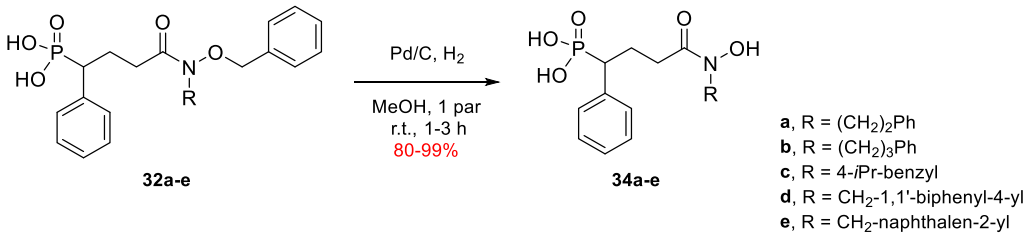

Scheme 10: Synthesis of the *N*-substituted hydroxamic acid analogs **34a-e**.

^{1}H-NMR spectrum of compound **34b** (Figure 28) revealed the disappearance of the methylene group hydrogens of the benzyl group at 4.69 – 4.54 ppm (CH$_2$Ph) and the disappearance of the signals of five aromatic hydrogen atoms between 7.39 – 7.23 ppm. Multiplicities of other ^{1}H-NMR signals of compound **34b** remain unchanged

compared to the phosphonic acid diethyl ester **29b** (Figure 24).[13]C-NMR (Figure 29) also confirmed the structure with the disappearance of the signal at 77.04 ppm (CH2, Bn group).

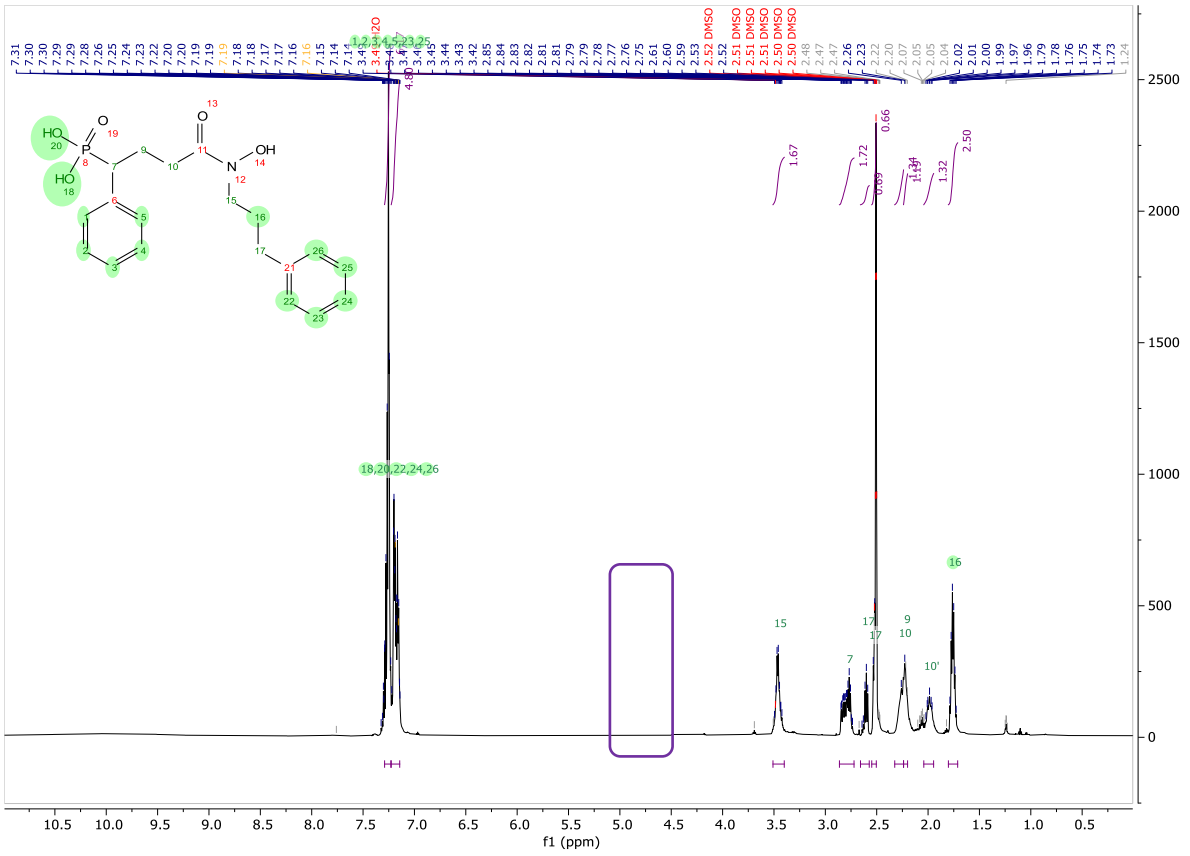

Figure 28: [1]H-NMR spectrum of compound **34b**. Purple rectangles marked the normal region of the methylene group hydrogens of the benzyl group compared to Figure 24

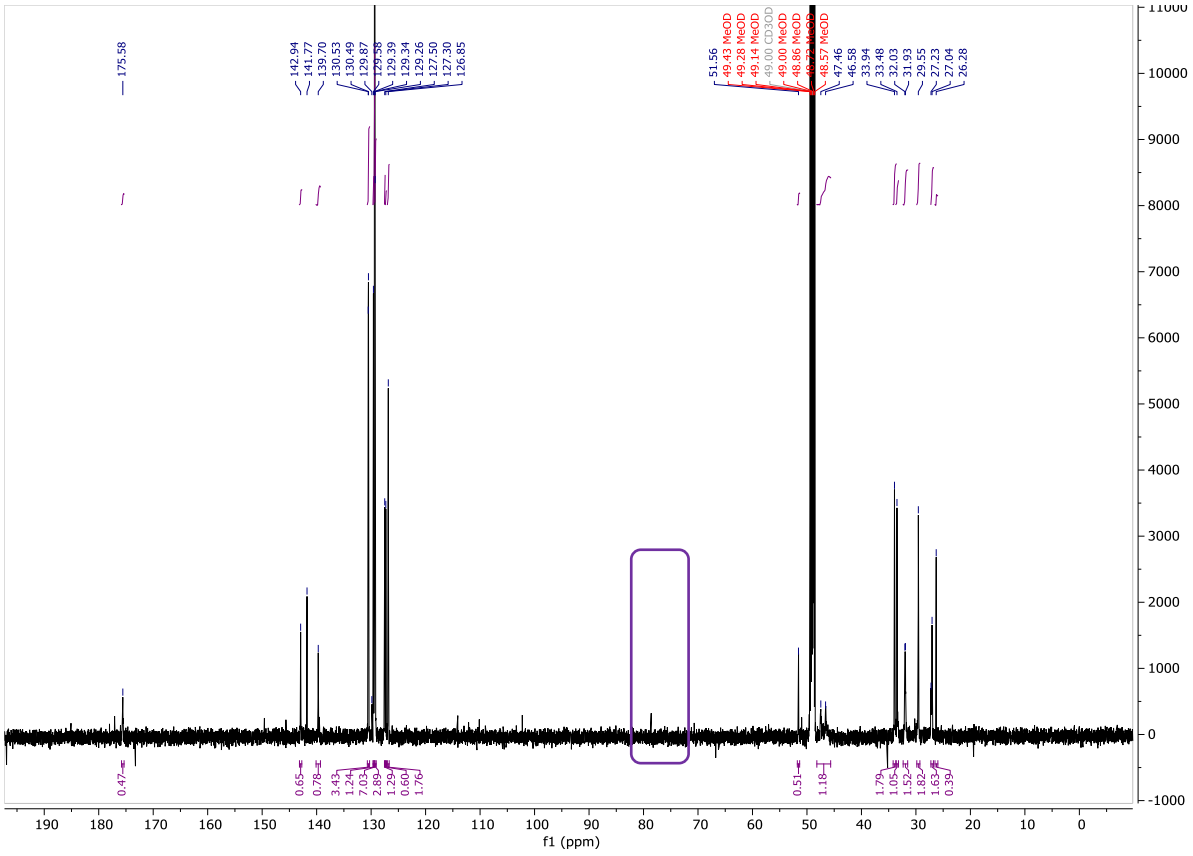

Figure 29: ^{13}C-NMR spectrum of compound **34b**. Purple rectangles marked the normal region of the methylene group carbon of the benzyl group compared to Figure 25.

To ensure the ^{1}H-NMR signal assignment for compound **34b**, ^{1}H, ^{1}H-COSY experiment was carried out, the result of which is given in Figure 30. Because of the coupling of the neighboring protons, which produce the resonance signals 7 and 9, the assignment made for signals 7 and 9 proves to be correct. The COSY NMR revealed that no pronounced coupling takes place between protons of signals 7 and 10. Moreover, the COSY spectrum also confirmed the coupling between the methylene protons (signal 16) and protons of two methylene groups, 15 and 17, thereby confirming the assignment of all aliphatic protons.

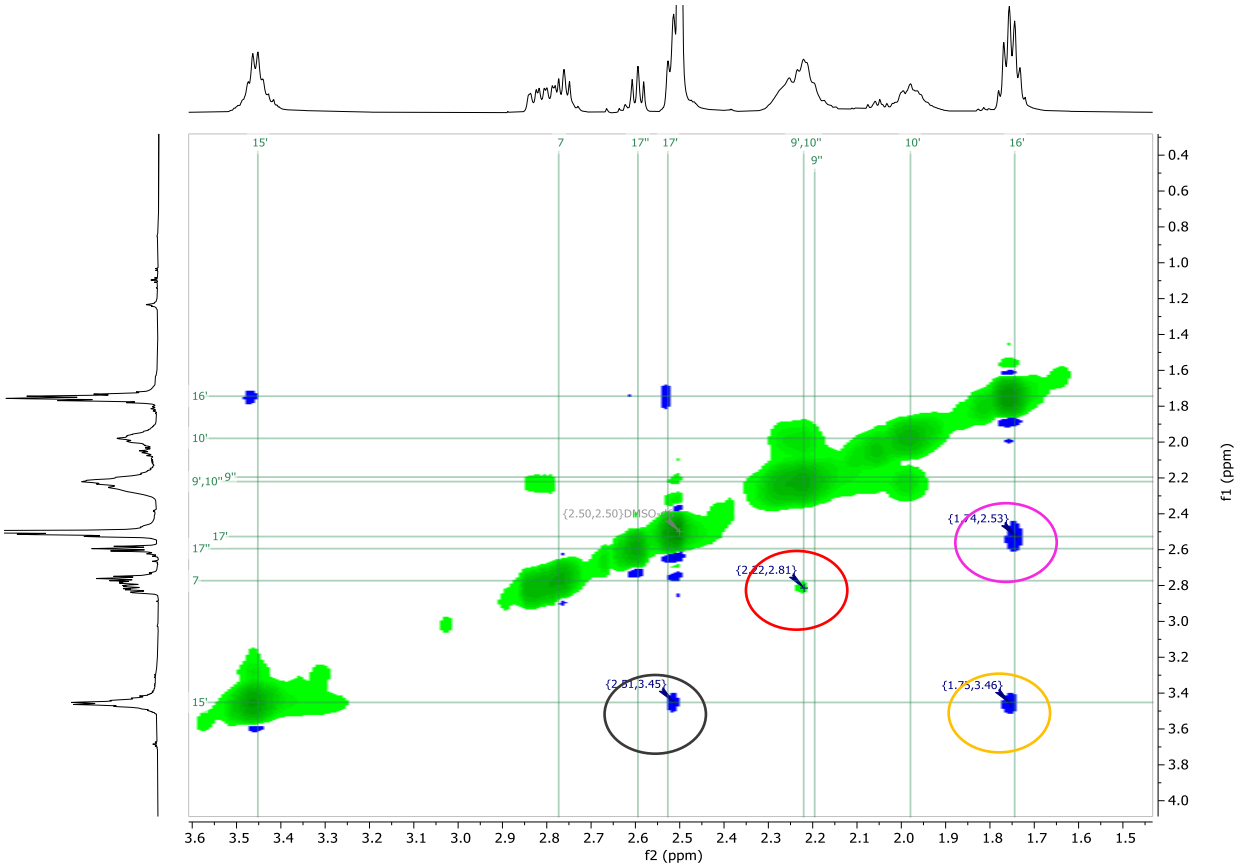

Figure 30: ^{1}H, ^{1}H-COSY NMR of compound **34b**. Point pointing to coupling between protons of the methylene signal 16 and methylene group 17 circled pink. Point pointing to coupling between protons of the methylene signal 16 and methylene group 15 circled orange. Point pointing to the coupling between protons of the methylene signal 17 and methylene group 15 circled gray. Point pointing to the coupling between the proton of the methine carbon (signal 7) and the methylene signal 9.

5.1.3 Synthesis of the nicotine amide analogs

Compounds bearing a nicotine amide moiety have been designed to mimic the 1,4-dihydropyridine group of the cofactor (NADPH). In addition, the nicotine amide group might increase the possibility of *H*-bonding interactions with the NADPH binding site (Figure 31).

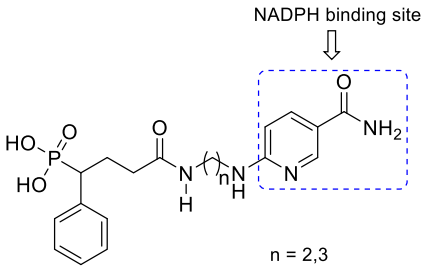

Figure 31: Schematic presentation of the nicotine amide mimics.

5.1.3.1 Synthesis of the 6-((aminoalkyl)amino)nicotinamides (**37a,b**)

The first step in the preparation of the nicotine amide analogs was the synthesis of the 6-((aminoalkyl)amino)nicotinamides (**37a,b**). The amination of the pyridine moiety *via* an aromatic nucleophilic substitution reaction of 6-chloronicotinamide (**35**) and different alkylene diamines **36a,b** (Scheme 11) was

performed using various test procedures (Table 3). The tested procedures showed that the synthesis could only be achieved using the microwave irradiation of **35** and the diamine in the presence of sodium bicarbonate as a base and isoamyl alcohol as a solvent.

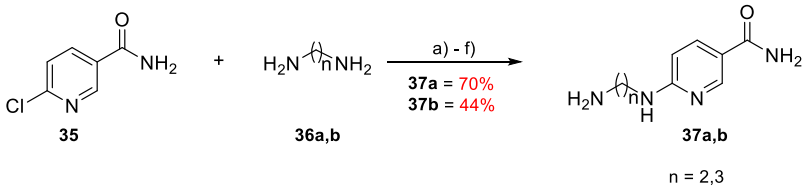

Scheme 11: Synthesis of the 6-((aminoalkyl)amino)nicotinamides **37a,b**.

Table 3: Reaction optimization conditions for synthesizing compounds **37a,b**.

Reaction	Base	Solvent	Temperature	Time	Yield
a)	2.0 eq. TEA	THF	r.t.	16 h	-
b)	2.0 eq. TEA	THF	60 ˚C	16 h	-
c)	5.0 eq. KOH	THF	60 ˚C	16 h	-
d)	5.0 eq. KOH	THF	Reflux	8 h	-
e)	1.2 eq. Na_2CO_3	DMF	100 ˚C	96 h	-
f)	1.2 eq. Na_2CO_3	Isoamyl alcohol	MW at 130 ˚C	2 h	45%

5.1.3.2 Synthesis of nicotine amide analogs **39a,b**

After the successful synthesis of **37a,b**, they were then used for the synthesis of **39a** and **39b** (Scheme 12).[136] The synthesis started with a HATU coupling reaction of the carboxylic acid **15** and the nicotine amides **37a,b** as described before (Section 5.1.2.1) to yield the corresponding diethyl phosphonate **38a,b**. Finally, ester cleavage was achieved using the procedure reported by BEHENDERT et al. (Scheme 12).[136] The diethyl phosphonates **38a,b** were reacted with 10.00 eq. of TMSBr in DCM. The corresponding silyl esters were hydrolyzed with water after 1 h of stirring at r.t. to liberate the corresponding phosphonic acids. **39a,b** were purified by reverse phase flash chromatography (on a prepacked silica cartridge), using water:acetonitrile (90:10→80:20) as eluent, and obtained with a purity of > 95.0%.

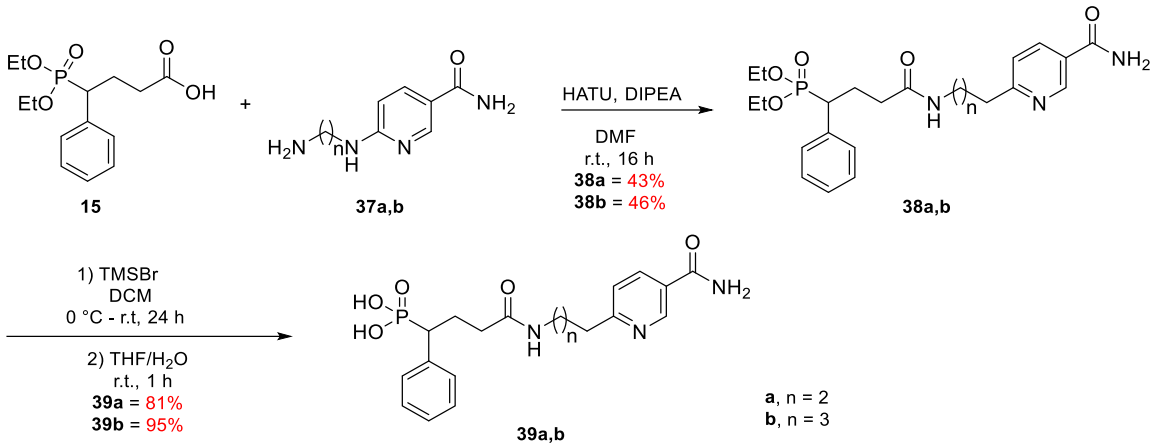

Scheme 12: Synthesis of the nicotine amide analogs **39a,b**.

5.1.4 Biological evaluation

5.1.4.1 Determination of DXR inhibition

To prove the mode of action and to evaluate the enzyme inhibition activity, the synthesized compounds and fosmidomycin (as reference compound) were screened first against DXR from *P. falciparum* (*Pf*DXR) using an enzyme assay reported previously by BEHRENDT et al..[134] For compounds that showed submicromolar *Pf*DXR inhibitory activity, they were further screened against *Escherichia coli* (*Ec*DXR) and *Mycobacterium tuberculosis* (*Mtb*DXR) DXR orthologs. The enzyme assays are based on the photometric determination of NADPH consumption, which is associated with the DXR-catalyzed reaction described earlier.[134] IC_{50} values were determined by nonlinear regression analysis using the program package Dynafit.[155] The curve shapes were closely similar in all cases.

Table 4 summarizes the DXR inhibition activity of the synthesized compounds. Replacing the metal-binding hydroxamic acid group with the amide or alkoxyamide groups led to the complete loss of inhibitory activity. This finding is attributed to the inability of these derivatives to chelate the divalent metal cation required for DXR catalytic activity. The *N*-substituted hydroxamic acid analogs displayed potent to moderate activity against *PfDXR* enzyme with IC_{50} between 0.030 and 1.3 µM. Of the *N*-substituted hydroxamic acids, compounds **34a** (IC_{50} = 0.064 µM) and **34b (**IC_{50} = 0.030 µM) were the most potent *Pf*DXR inhibitors, with an activity surpassing that of fosmidomycin (**1**, IC_{50} = 0.16 µM). Compound **34c** (4-*i*PrBn) displayed decreased but still significant inhibition of the enzyme with an IC_{50} value of 0.40 µM. Notably, the more rigid biphenyl and naphthyl analogs showed only weak enzyme inhibition activity. Based on their *Pf*DXR activity, **34a**, **34b**, and **34c** were chosen for further investigation and tested against *Mtb*DXR and *Ec*DXR. Whereas **34a** and **34c** were more active against *Pf*DXR than against *Ec*DXR, **34b** was almost equipotent against both *Pf*DXR and *Ec*DXR with IC_{50} 0.030 and 0.035 µM, respectively. It is worth noting that the compounds **34a-c** were 100-fold less potent against *Mtb*DXR when compared with their *Pf*DXR inhibition.

Table 4: DXR inhibition of arylalkoxyamides (**31c-g**), amides (**33a-c**), *N*-substituted hydroxamic acid analogs (**34a-e**) and, nicotine amide analogs **39a**,**b**.

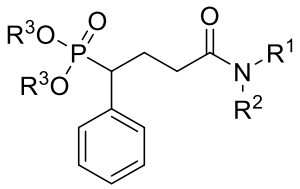

Cpd.no.	Structure			DXR IC_{50} (µM) [a]		
	R^1	R^2	R^3	*Pf*	*Ec*	*Mtb*
31c	H	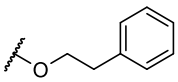	Na	n.d.	n.d.	n.d.
31d	H	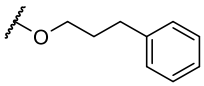	Na	52 ± 5	n.d.	n.d.
31e	H	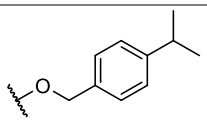	H	27.66 ±6.33	n.d.	n.d.
31f	H	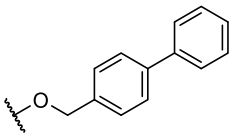	Na	n.d.	n.d.	n.d.
31g	H	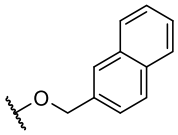	H	n.d.	n.d.	n.d.
33a	H	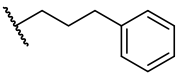	Na	> 500	n.d.	n.d.
33b	H	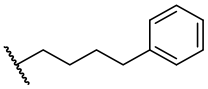	Na	n.d.	n.d.	n.d.
33c	H	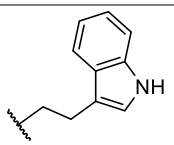	Na	n.d.	n.d.	n.d.
34a	OH	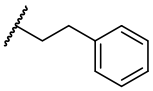	H	0.064 ± 0.011	0.48 ± 0.06	27 ± 4
34b	OH	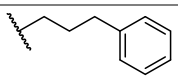	H	0.030 ± 0.007	0.035 ± 0.004	3.0 ± 0.2
34c	OH	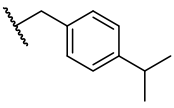	H	0.40 ± 0.09	0.61 ± 0.07	67 ± 1.0
34d	OH	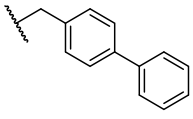	H	1.3 ± 0.2	9.7 ± 0.3	166 ± 16

34e	OH	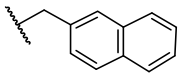	H	0.50 ± 0.03	7.9 ± 0.8	118 ± 20
39a	H	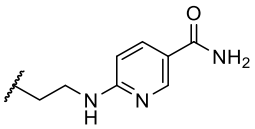	H	>500	n.d.	n.d.
39b	H	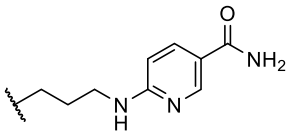	H	>500	n.d.	n.d.
Fosmidomycin				0.16	n.d.	n.d.

[a] Enzyme assay: values were calculated from eight or more data points. In general, two or three independent determinations were performed.[151] n.d., not determined. The purity of all tested compounds was >95%.

5.1.4.2 Determination of the antiplasmodial activity and cytotoxicity

The growth inhibitory effect of the compounds against asexual stage *P. falciparum* malaria parasites was measured. Specifically, chloroquine-sensitive (*Pf*3D7) and multidrug-resistant (*Pf*Dd2) *P. falciparum* strains were used. Parasite growth was monitored by measuring the expression of *P. falciparum* histidine-rich protein 2 by enzyme-linked immunosorbent assay as described previously by NOEDL et al.[156]

As shown in Table 4 and Table 5, good agreement was observed between the antiproliferative activity against the *P. falciparum* 3D7 and Dd2 strains and the inhibition of *Pf*DXR enzyme. Again, the arylalkoxyamides **31c-g** and the amides **33a-c** were also unable to inhibit the proliferation of the tested *P. falciparum* parasites. In accordance with the DRX inhibition, the *N*-substituted hydroxamic acid analogs compounds **34a** (*Pf*3D7 IC_{50} = 0.78 µM, *Pf*Dd2 IC_{50} = 0.73 µM) and **34b** (*Pf*3D7 IC_{50} = 0.55 µM, *Pf*Dd2 IC_{50} = 0.94 µM) were the most active representatives and exhibited antiplasmodial activity comparable to that of fosmidomycin (*Pf*3D7 IC_{50} = 0.88 µM, *Pf*Dd2 IC_{50} = 0.81 µM).

Finally, to ensure their parasite selectivity, inhibition of HepG2 cells were performed, and selectivity indices (ratio of the antiparasitic activity to the human cell toxicity), were calculated. As shown in Table 6, the hydroxamic acid analogs **34a-c** showed no cytotoxicity against HepG2 cell lines, with IC_{50} values > 1 mM. Thus, these compounds possess good *in vitro* parasite selectivity toward *P. falciparum.*

Table 5: *In vitro* antiplasmodial activity of arylalkoxyamides **31c-g**, amides **33a-c** *N*-substituted hydroxamic acid analogs **34a-e** and, nicotine amide analogs **39a**,**b**.

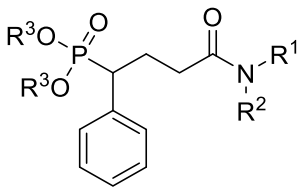

Cpd.no.	Structure			Antiplasmodial activity [a]	
	R^1	R^2	R^3	*Pf*3D7 IC_{50} (µM)	*Pf*Dd2 IC_{50} (µM)
31c	H	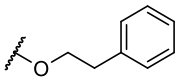	Na	>27.78	>27.78
31d	H	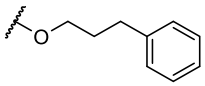	Na	>27.78	>27.78
31e	H	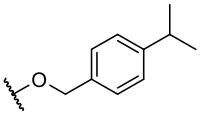	H	>27.78	>27.78
31f	H	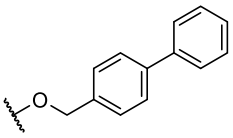	Na	>27.78	>27.78
31g	H	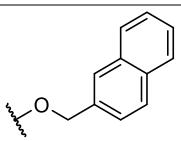	H	>27.78	>27.78
33a	H	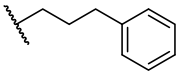	Na	>27.78	>27.78
33b	H	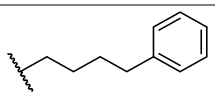	Na	>27.78	>27.78
33c	H	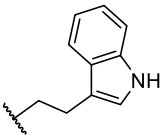	Na	>27.78	>27.78
34a	OH	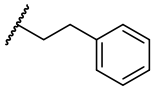	H	0.78 ±0.06	0.73 ±0.01
34b	OH	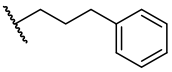	H	0.55 ±0.03	0.94 ±0.16
34c	OH	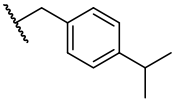	H	11.21 ± 0.74	9.16 ±10.07

34d	OH	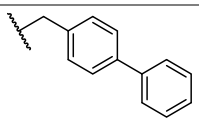	H	>27.78	>27.78
34e	OH	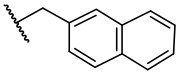	H	>27.78	>27.78
39a	H	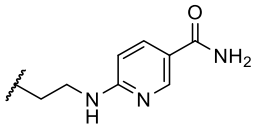	H	>27.78	>27.78
39b	H	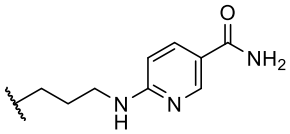	H	>27.78	>27.78
Fosmidomycin				0.88[c]	0.81[c]

[a] *In vitro* assay [155,157] values are the mean of at least two duplicate determinations. [b] Enzyme assay: values were calculated from eight or more data points. In general, two or three independent determinations were performed. [c] IC_{50} value according to ref 158.[158] n.d., not determined. The purity of all tested compounds was >95%.

Table 6: Cytotoxicity and selectivity indices of compounds **34a-c**.

Compound	**HepG-2 IC_{50} (µM) [a]**	***Pf*3D7 selectivity index [b]**	***Pf*Dd2 selectivity index [b]**
34a	>1000	>1277	>1366
34b	>1000	>1818	>1063
34c	>1000	>89	>109

[a] Cytotoxicity test with HepG-2 cells: values are the mean of two duplicate determinations. [b] Selectivity indices were calculated as the HepG-2 cell IC_{50}/*Pf*3D7 or *Pf*Dd2 IC_{50}; larger values indicate greater selectivity toward parasite activity.

5.2 Optimization of the *N*-phenylpropyl substituted hydroxamic acid **34b**

5.2.1 Strategy

In this project's first part, the synthesis and biological evaluation of different amide, arylalkoxyamide, and *N*-substituted hydroxamic acid analogs were described. Evaluation of the synthesized prototypes in target-based enzyme assay against *PfDXR* enzyme revealed that the synthesized arylalkoxyamides and amides might no longer be able to chelate the divalent metal cation, resulting in decreased DXR inhibitory activity. However, all the *N*-substituted hydroxamic acids inhibited the *Pf*DXR enzyme, with compounds **34a** and **34b** being the most active analogs with IC_{50} in a 2-digit nanomolar range (Figure 32). This observation was also confirmed by testing the ability of **34a** and **34b** to inhibit the proliferation of asexual blood stages of *P. falciparum* parasites (*Pf*3D7 IC_{50} = 0.73 and 0.55, *Pf*Dd2 IC_{50} = 0.78 and 0.94 µM, respectively). These results, in our hands, concede the importance of a free hydroxamic acid group for potent DXR inhibition.

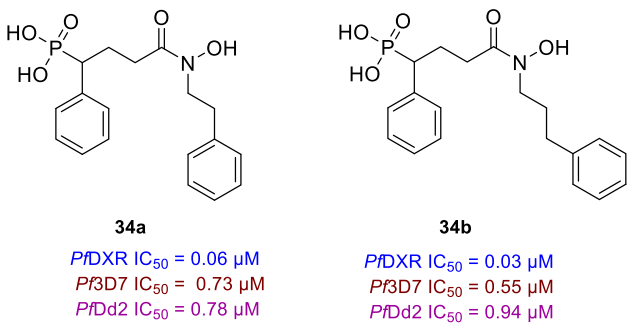

Figure 32: Structure of the most active *N*-substituted hydroxamic acid analogs **34a** and **34b**.

Based on the results obtained from this project's first part, we intended to go further with the understanding of the structure-activity relationship (SAR) by designing a new series of *N*-substituted hydroxamic acid analogs. Compound **34b** was chosen to serve as the lead for the second series (Figure 33).

Comparing the *Pf*DXR inhibitory activity of compounds **34a** and **34b**, the length of the alkyl chain between the nitrogen atom of the reverse hydroxamate functionality and the phenyl ring was found to be directly related to the DXR inhibitory activity of the compounds. Therefore, as a first modification on the structure of **34b**, new derivatives with a longer alkyl chain were synthesized to determine the optimal length that promotes appropriate interaction with the hydrophobic sub-pocket (Section 6).

The beneficial impact of the replacement of the α-phenyl ring of the linker with a more lipophilic electron-deficient 3,4-difluorophenyl moiety was demonstrated by our research group.[134] Accordingly, the introduction of the α-3,4-difluorophenyl group was also tested in this chapter. This modification was suggested to increase lipophilicity and enhance the hydrophobic interactions with the *Pf*DXR and *Ec*DXR enzymes. In the α-3,4-difluorophenyl analogs, the optimum length of the alkyl chain required to approach the hydrophobic sub-pocket was also explored.

Finally, the phenyl ring of the phenylpropyl moiety of **34b** was decorated with different substituents to determine the influence of lipophilicity, electronic, and steric properties on DXR inhibition.

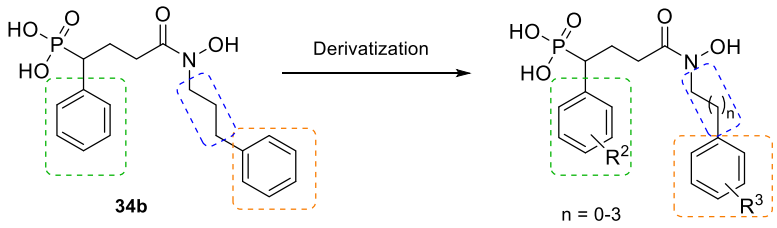

Figure 33: Design strategy of the second project compounds library.

5.2.2 Synthesis of *N*-substituted phenylbutyl and phenylpentyl hydroxamic acids **46a** and **46b**

The new derivatives **46a** with phenylbutyl and **46b** with phenylpentyl substituents on the nitrogen atom of the hydroxamic acid functionality were synthesized to determine the optimal length that promotes appropriate interaction with the druggable or hydrophobic pockets. The synthesis started with preparing the required *O*-benzyl-protected hydroxylamines **43a**,**b**. The preparation started with the synthesis of the commercially unavailable phenylalkyl chlorides **41a**,**b**. Compounds **41a**,**b** were synthesized via chlorination of corresponding alcohols **40a**,**b** using Appel reaction, adapted from literature (Scheme 13).[159]

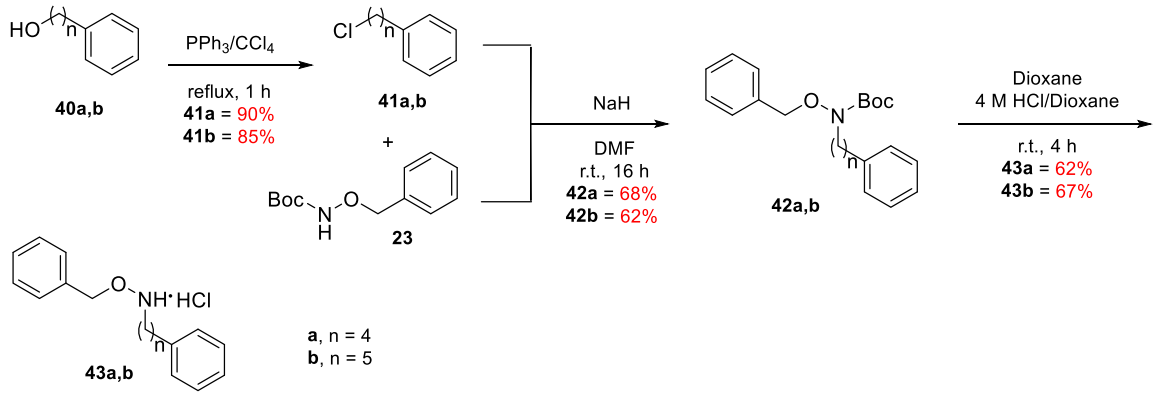

Scheme 13: Synthesis of *N*-substituted and *O*-Bn-protected hydroxylamines **43a,b**.

The Appel reaction begins with the halophilic substitution between triphenylphosphine (**XIV**) and carbon tetrachloride (**XV**), leading to the formation of phosphonium salt **XVI**. Deprotonation of the alcohol by the trichloromethyl anion **XVII** yields the alkoxide **XVIII**. The alkoxide's nucleophilic displacement of the chloride yields intermediate **XIX**. The halide reacts in an S_{N2} process, forming the alkyl halide **XX** and triphenylphosphine oxide **XXI**, as shown in Scheme 14.[160]

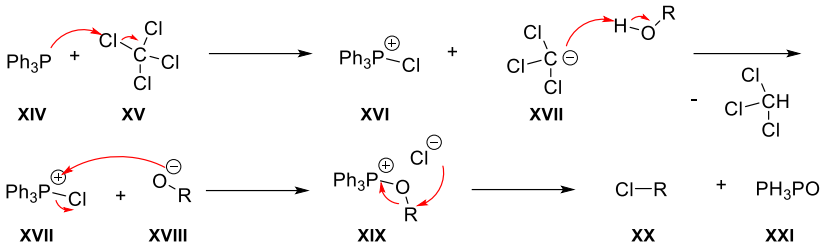

Scheme 14: Appel reaction mechanism.

The *N*-alkylation of *tert*-butyl (benzyloxy)carbamate **23** (detailed synthesis Scheme 5) with **41a**,**b** in the presence of sodium hydride provided the *N*-substituted benzyloxycarbamates **42a**,**b**. Finally, the removal of the Boc-protecting group using 4 M HCl in dioxane yielded the *N*-substituted *O*-benzyl-protected hydroxylamines **43a**,**b** (Scheme 13)**.** The *O*-benzyl-protected hydroxylamines **43a**,**b** were then coupled with carboxylic acid **15** using HATU and DIPEA in DMF to provide the benzyl-protected compounds **44a**,**b**. Treatment of the phosphonic acid diethyl esters **44a**,**b** with trimethylsilyl bromide (TMSBr) followed by hydrolysis with water provided the corresponding phosphonic acids **45a**,**b**. Finally, the benzyl-protecting groups were removed using Pd/C catalyzed hydrogenation, yielding the hydroxamic acids **46a**,**b** (Scheme 15). The details of this step are shown in section 5.1.2.3 in part 1 (Scheme 10). Compounds **46a**,**b** were purified by reverse phase flash chromatography (on a prepacked silica cartridge), using water:acetonitrile (90:10→80:20) as eluent and obtained in the required purity for biological testing >95%.

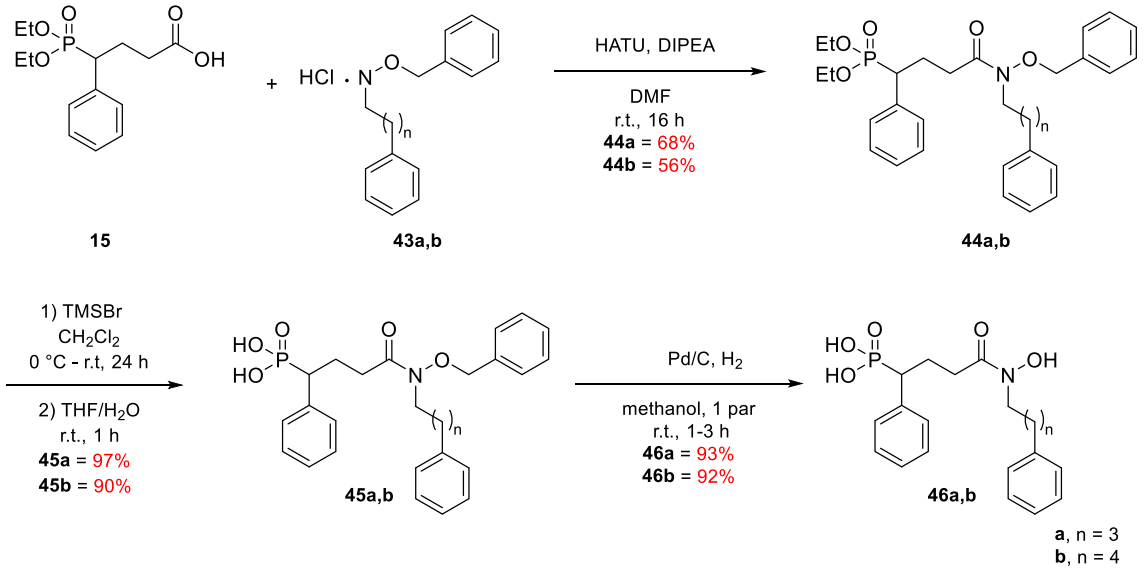

Scheme 15: Synthesis of compounds **46a,b**.

5.2.3 Synthesis of *N*-substituted hydroxamic acids with α-3,4-difluorophenyl substituent **55a-d**

The Michaelis–Arbuzov reaction is one of the most useful approaches for forming a C-P bond.[161] The reaction is a bimolecular nucleophilic substitution (S_{N2}) process between a trialkyl phosphite **XXII** and an alkyl halide **XXIII** (Scheme 16), promoted by heat, to form a pentavalent phosphorus species **XXIV**. The transformation is initiated

by the reaction of the nucleophilic trialkyl phosphite **XXII** with the electrophilic alkyl halide **XXIII** to give a phosphonium intermediate **XXIV** and a halide anion. A second reaction of the displaced halide anion with the phosphonium intermediate **XXIV** affords the phosphonate ester **XXV** along with an alkyl halide **XXVI**.[162]

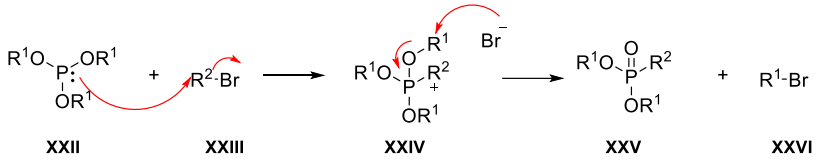

Scheme 16: Michaelis–Arbuzov reaction mechanism.

The Michaelis–Arbuzov reaction was used to synthesize the diethyl (3,4-difluorobenzyl)phosphonate (**49**). **49** was synthesized from triethyl phosphite (**47**), and 4-(bromomethyl)-1,2-difluorobenzene (**48**) using the procedure reported by LION et al.[163] **49** was then used as starting material for the synthesis of the carboxylic acid **52** using the procedures reported by BEHRENDET et al. (Scheme 17).[134] **52** was coupled with the synthesized hydroxylamines **26a**,**b** and **43a**,**b** and yielded compounds **53a-d** in a good yield (70-85%). Surprisingly, the reaction sequence utilized in Scheme 15 to obtain hydroxamic acids **46a**,**b** through phosphonic acid ester cleavage followed by catalytic hydrogenation was ineffective for the synthesis of phosphonic acids **55a-d**. Thus, to synthesize phosphonic acids **55a-d**, the benzyl-protecting group was initially eliminated through Pd/C-catalyzed hydrogenation, producing compounds **54a-d** with a good yield. Subsequently, the phosphonic acid ester groups of **54a-d** were cleaved using the method described by Behrendt et al., leading to the formation of phosphonic acids **55a-d** in 82-87% yield.[134] **55a-d** were purified by reverse phase flash chromatography (on a prepacked silica cartridge), using water:acetonitrile (90:10→80:20) as eluent and obtained with a purity of >95.0%.

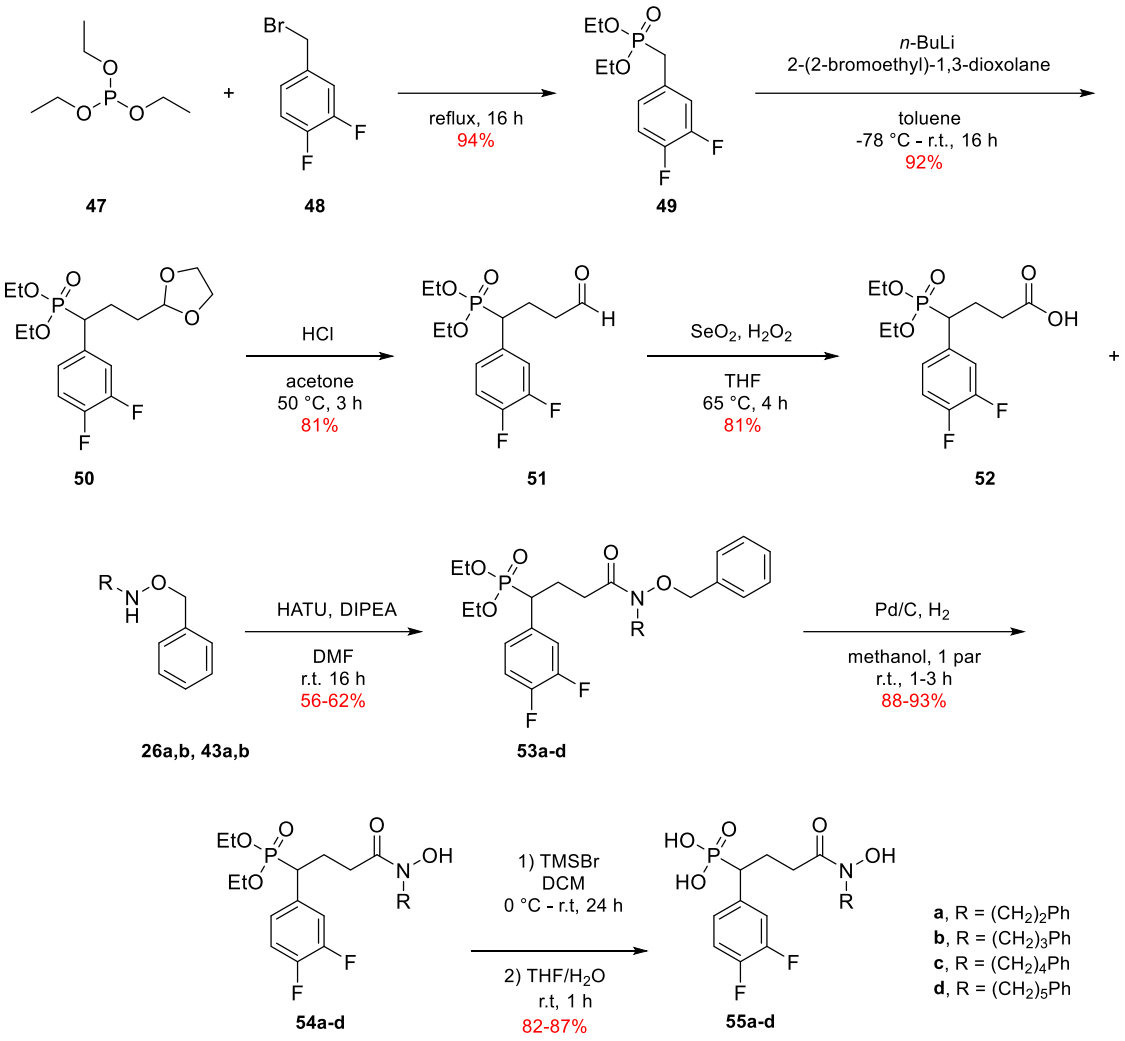

Scheme 17: Synthesis of the α-3,4-difluorophenyl analogs **55a-d**

5.2.4 Synthesis of α-phenyl analogs with substituents on the phenyl ring of the phenylpropyl group **63a-d** and **66**

The arylalkyl chlorides **58a-e** and their corresponding alcohols **57a-e** were not commercially available and, as such, were required to be synthesized. Therefore, as a first step for the preparation of **58a-e**, carboxylic acids **56a-e** were reduced to the corresponding primary alcohols **57a-e** using the procedure reported by PATEL et al. [164] Then the alcohols **57a-e** were converted to the phenylalkyl chlorides **58a-e** through the Apple reaction procedure described before.[159,165] An initial attempt to synthesize **58a** according to the method reported by Soo et al. failed.[166] The formed phenylalkyl chlorides were then used as starting material for the synthesis of the *N*-substituted *O*-benzyl-protected hydroxylamines **60a-e** (Scheme 18) as described before in Scheme 5 (Section 5.1.1.3).

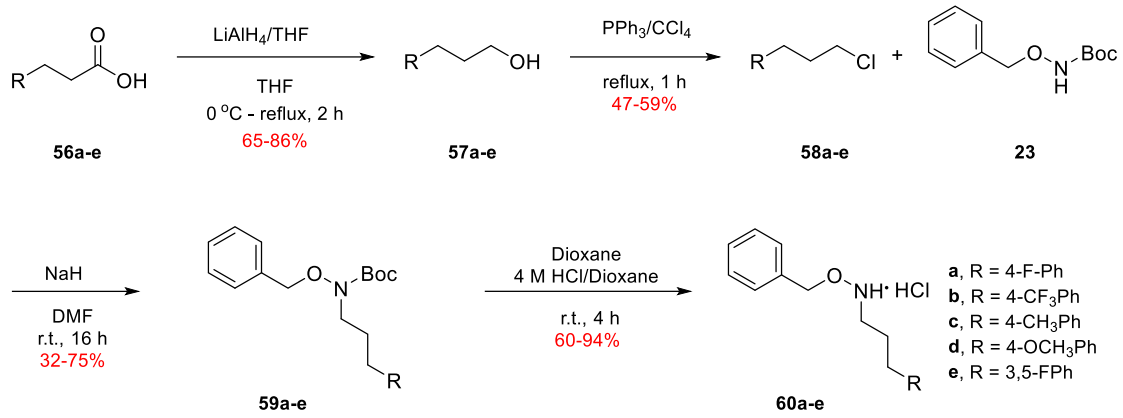

Scheme 18: Synthesis of the *N*-substituted *O*-benzyl-protected hydroxylamines **60a-e.**

The synthesized *N*-substituted *O*-benzyl-protected hydroxylamines **60a-e** were then coupled with carboxylic acid **15** to yield *N*-substituted benzyloxyamides **61a-d** (Scheme 19) and **64** (Scheme 20) in a good yield (70-85%). Synthesis of the *N*-substituted hydroxamic acids (**63a-d**, Scheme 19) was successful using the same deprotection sequence as used for the synthesis of **34a-e** (Scheme 10) and **46a**,**b** (Scheme 15).[136]

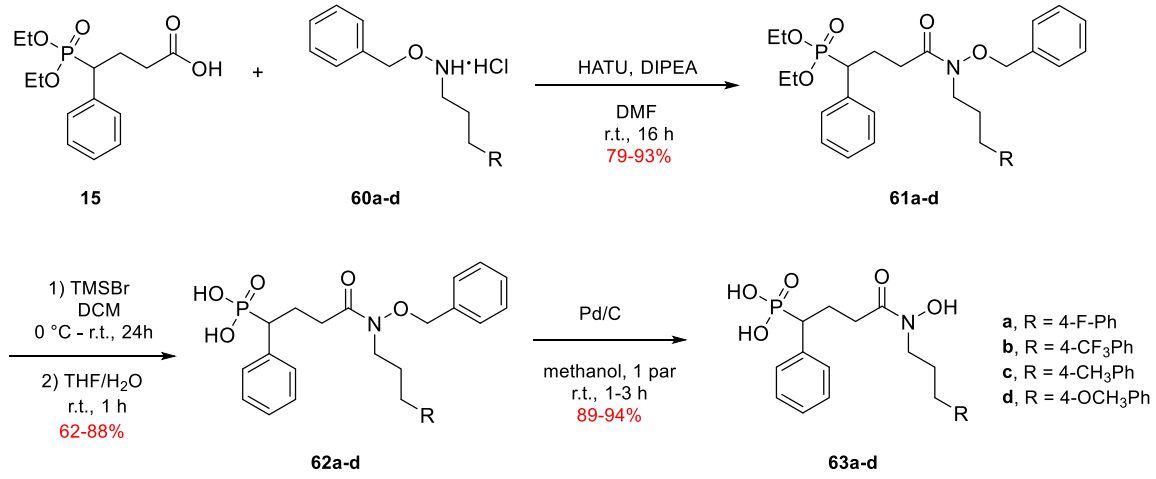

Scheme 19: Synthesis of the *N*-substituted hydroxamic acid analogs **63a-d**

The synthesis of the 3,5-diflurophenylpropyl analog **66** was achieved by starting with the benzyl-deprotection of **64** using Pd/C-catalyzed hydrogenation to yield compound **65** in a good yield. Finally, cleavage of the phosphonic acid ester moiety of **65** afforded the *N*-substituted hydroxylamine **66** (Scheme 20).[136]

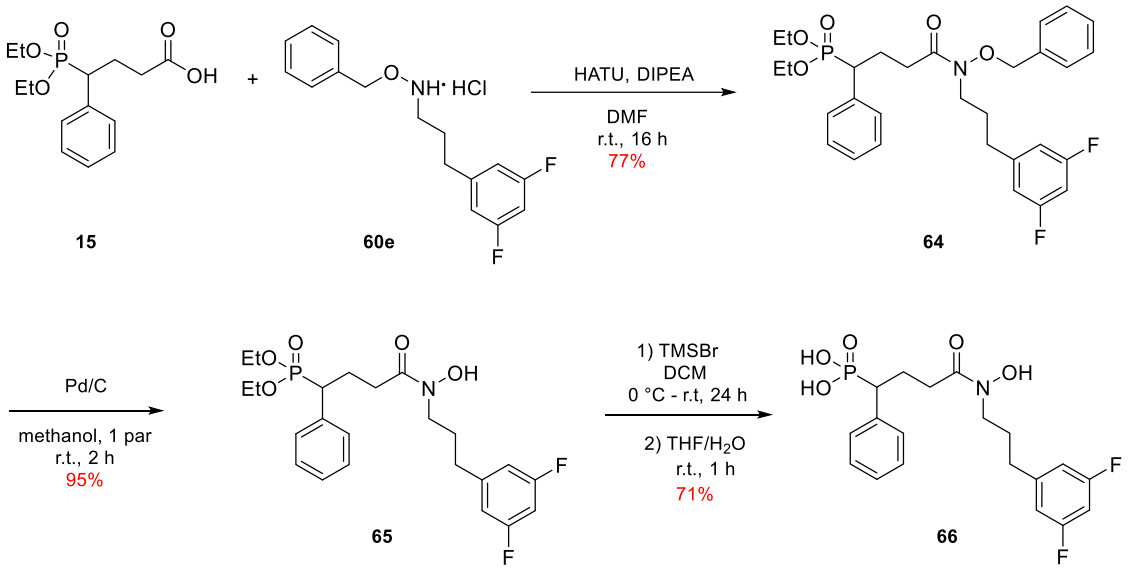

Scheme 20: Synthesis of the *N*-substituted hydroxamic acid analog **66**.

5.2.5 Biological evaluation

5.2.5.1 Determination of DXR inhibition

The phosphonohydroxamic acids **46a**,**b**, **55a-d**, **63a-d**, and **66** were evaluated as inhibitors of DXR from *P. falciparum* (*Pf*DXR) as our primary target, *Escherichia coli* (*Ec*DXR), and *Mycobacterium tuberculosis* (*Mtb*DXR) using a photometric assay that was described in section 5.1.4. The results are shown in Table 7.

Of the new compounds, compounds **46a**,**b**, **55b**,**d**, **63a**,**c**,**d**, and **66** showed approximately equal potency against *Ec*DXR (IC_{50} = 0.013-0.069 µM) and *Pf*DXR (IC_{50} = 0.018-0.044 µM) orthologs, whereas the compounds showed weaker activity against *Mtb*DXR ortholog (IC_{50} = 2.9-20 µM). The α-3,4-diflurphenyl compounds **55c** and **55d** were the most potent analogs in this series against *Pf*DXR IC_{50} = 0.017 (**55c**) and 0.018 µM (**55d**). Compound **55c** showed the most potent activity against *Ec*DXR with IC_{50} of 0.001 µM.

*Pf*DXR inhibitory data (Table 7) of the α-phenyl analogs showed that by extending the alkyl chain length as in phenylbutyl analog **46a** (IC_{50} = 0.035 µM) and phenylpentyl analog **46b** (IC_{50} = 0.029 µM), the *Pf*DXR inhibition remains unaffected compared with the phenylpropyl analog **34b** (IC_{50} = 0.030 µM). However, a slight improvement in the *Pf*DXR inhibition was observed by extending the alkyl chain length in α-3,4-diflurphenyl phenylpropyl analog **55c** (IC_{50} = 0.017 µM) and α-3,4-diflurphenyl phenylpentyl analog **55d** (IC_{50} = 0.018 µM) when compared with α-3,4-diflurphenyl phenylpropyl analog **55b** (IC_{50} = 0.028 µM).

Further consideration of the enzyme inhibitory activity, the α-3,4-diflurphenyl compounds **55b-d** showed an improvement in *Ec*DXR inhibitory activity (IC_{50} = 0.013-0.001 µM) compared with the α-phenyl analogs **34b** (IC_{50} = 0.035µM), (Table 5, section 5.1.4), **46a** (IC_{50} = 0.069µM), and **46b** (IC_{50} = 0.041 µM).

The influence of electronic and steric effects in DXR inhibition is tested with compounds **63a-d** and **66**. Comparing an electron-withdrawing group at the *p*-position (F, **63a**; CF_3, **63b**) and electron-donating group (CH_3, **63c**; OCH_3, **63d**) with the lead compound **34b** showed that electronic and steric effects on the phenyl ring do not

largely influence *Pf*DXR inhibition (IC_{50} = 0.019-0.044 µM) and *Ec*DXR inhibition (IC_{50} = 0.019-0.045 µM). The same observation was also noticed with the 3,5-diflurophenyl analog **66** *Pf*DXR IC_{50} = 0.030 µM, *Ec*DXR IC_{50} = 0.036 µM, and this strengthens the observation that substitution pattern on the phenyl ring of the phenylpropyl group does not largely influence the *Pf*DXR and *Ec*DXR inhibition. The effectiveness of *Mtb*DXR inhibition was found to depend on the type of substituents present. Small substituents at the *p*-position, such as F (**63a**) or CH_3 (**63c**), did not affect *Mtb*DXR inhibition. However, more bulky substituents at the *p*-position, such as CF_3 (**63b**) or OCH_3 (**63d**), resulted in a fourfold decrease in *Mtb*DXR inhibition compared to **34b**.

Table 7: DXR inhibition of compounds **46a**,**b**, **55a-d**, **63a-d**, and **66**.

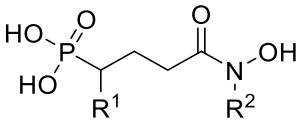

Cpd. no.	Structure		DXR IC_{50} (µM) [a]		
	R^1	R^2	*Pf*	*Ec*	*Mtb*
46a	Ph	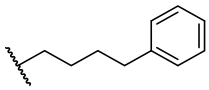	0.035 ± 0.003	0.069 ± 0.004	11 ± 1.0
46b	Ph	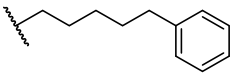	0.029 ± 0.001	0.041 ± 0.014	19 ± 1.0
55a	3,4-F-Ph	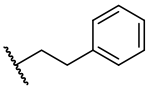	0.020 ± 0.003	0.13 ± 0.02	4.8 ± 0.05
55b	3,4-F-Ph	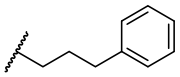	0.028 ± 0.002	0.013 ± 0.002	4.4 ± 0.1
55c	3,4-F-Ph	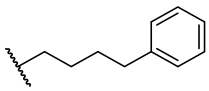	0.017 ± 0.002	0.001 ± 0.0001	1.5 ± 0.20
55d	3,4-F-Ph	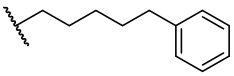	0.018 ± 0.002	0.013 ±-0.002	4.8 ± 0.35
63a	Ph	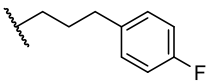	0.019 ±0.003	0.019 ± 0.002	2.9 ± 0.2
63b	Ph	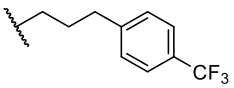	0.041 ± 0.003	0.13 ± 0.02	12.5 ± 1.0
63c	Ph	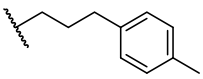	0.044 ± 0.004	0.022 ± 0.003	3.8 ± 0.01
63d	Ph	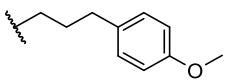	0.024 ± 0.004	0.045 ± 0.001	11 ± 1.0

66	Ph	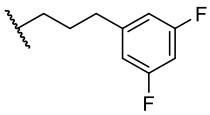	0.030 ± 0.003	0.036 ± 0.005	20 ± 2.0
34b	Ph	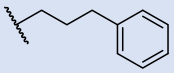	0.030 ± 0.007	0.035 ± 0.004	3.0 ± 0.2

[a] Enzyme assay: values were calculated from eight or more data points. In general, two or three independent determinations were performed.

5.2.5.2 Determination of the antiplasmodial activity and cytotoxicity

The antiproliferative potential of the study compounds **46a**,**b**, **55a-d**, **63a-d**, and **66** against asexual stage *P. falciparum* malaria parasites was also measured as described in part 1 section 5.1.4.2.

For compounds **55a**, **55b**, **63a**, **63c**, and **66,** the antiplasmodial activity displayed a good correlation with the *Pf*DXR inhibition activity. Besides, the antiplasmodial activity confirmed the conclusion that most of the induced modification on the structure of **34b**, except increasing the length of the alkyl chain, did not result in a significant variation of the antiproliferative activity against the *Pf*3D7and *Pf*Dd2 strains (Table 8).

A slight drop in antiplasmodial activity took place with the extension of the alkyl chain length (at the hydroxamic acid nitrogen) of the α-phenyl analogs **46a** (*Pf*3D7 IC_{50} = 3.70, *Pf*Dd2 IC_{50} = 3.53 µM) and **46b** (*Pf*3D7 IC_{50} = 5.59, *Pf*Dd2 IC_{50} = 3.95 µM) compared with **34b** (*Pf*3D7 IC_{50} = 0.55, *Pf*Dd2 IC_{50} = 0.94 µM). This outcome was also observed with the α-3,4-difluorophenyl analogs **55c** (*Pf*3D7 IC_{50} = 4.02, *Pf*Dd2 IC_{50} = 3.52) and **55d** (*Pf*3D7 IC_{50} = 4.60, *Pf*Dd2 IC_{50} = 4.56 µM) compared with **55b** (*Pf*3D7 IC_{50} = 1.25, *Pf*Dd2 IC_{50} = 0.99 µM).

The replacement of the α-phenyl ring with the more electron deficient 3,4-diflurophenyl group did not show any significant effect on the antiplasmodial activity compared with the α-phenyl analogs (**34a,b,** and **46a,b**). Compounds **55a-d** displayed good to moderate activity against the tested *P. falciparum* strains (*Pf*3D7 IC_{50} = 1.25-4.60, *Pf*Dd2 IC_{50} = 0.99-4.56 µM).

The introduction of different substituents on either the *p*-position of the phenyl ring of the phenylpropyl moiety, compounds **63a**, **63c**, and **63d**, or at the 3,5 positions, compound **66**, did not result in a significant change in the antiplasmodial activity (Table 8). However, the antiplasmodial activity of compound **63b** was drastically weaker (*Pf*3D7 IC_{50} = 16.71, *Pf*Dd2 IC_{50} = 25.74 µM).

Finally, to ensure their selectivity, inhibition of HepG2 were performed, and selectivity indices (ratio of the antiparasitic activity to the human cell toxicity), were calculated. The compounds showed no cytotoxicity against HepG2 cell lines, with IC_{50} values >1 mM. Thus, these compounds possess good selectivity indices against *P. falciparum*.

Table 8: *In Vitro* antiplasmodial activity, cytotoxicity against HepG-2 cells and SI of compounds **46a**,**b**, **55a-d**, **63a-d**, and **66**

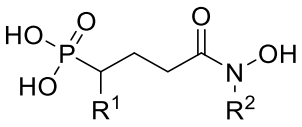

Cpd. no.	Structure		Antiplasmodial Activity [a]		Cytotoxicity	
	R^1	R^2	*Pf*3D7 IC_{50} (µM)	*Pf*Dd2 IC_{50} (µM)	*HepG-2* IC_{50} (µM)	*Pf*3D7 SI [b]
46a	Ph	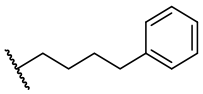	3.70 ± 1.94	3.53 ± 0.49	601.13	162.47
46b	Ph	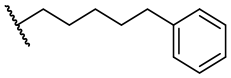	5.59 ± 0.85	3.95 ± 0.23	>1000	>179
55a	3,4-F-Ph	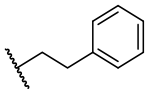	1.55 ± 0.05	1.76 ± 0.05	>1000	>645
55b	3,4-F-Ph	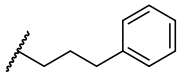	1.25 ± 0.08	0.99 ± 0.16	>1000	>800
55c	3,4-F-Ph	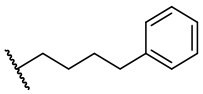	4.02 ± 0.06	3.52 ± 0.05	>1000	>250
55d	3,4-F-Ph	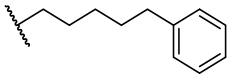	4.60 ± 0.16	4.56 ± 0.23	>1000	>217
63a	Ph	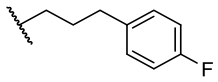	1.73 ± 0.09	3.67 ± 0.14	>1000	>578
63b	Ph	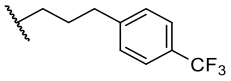	16.71 ± 1.05	25.74 ± 0.31	>1000	>60
63c	Ph	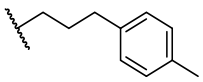	2.88 ± 1.21	2.88 ± 1.90	>1000	>347
63d	Ph	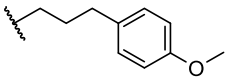	4.00 ± 1.47	1.81 ± 0.23	>1000	>250
66	Ph	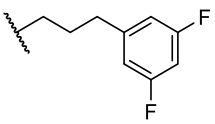	1.69 ± 0.18	2.62 ± 0.04	>1000	>591
34b	Ph	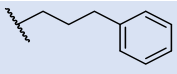	0.55 ±0.03	0.94 ±0.16	>1000	>1800

[a] *In vitro* assay: values are the mean of two duplicate determinations. [b] Selectivity Index (SI) shown as HepG-2 IC_{50}/ *Pf*3D7 IC_{50}. values larger than 1 indicate greater parasite selectivity.

5.3 Phosphonic acid prodrugs of selected inhibitors

5.3.1 Phosphonic acid ester prodrugs

Phosphonic acid groups in drugs and drug candidates are often responsible for insufficient membrane permeability and, subsequently, for poor cellular uptake.[167–169] The poor membrane permeability of phosphonic acids is due to their anionic nature at physiological pH. Masking the polar phosphonic acid group with lipophilic ester promoieties has proven successful in improving diffusion across biological membranes, thereby increasing the activity against intact pathogen cells and the *in vivo* activity. Particularly challenging are parasites with apicoplasts, which compartmentalize the DXR enzyme. Although the exact compartment of bioactivation is unknown,[170,171] hydrolysis of the promoiety by esterases inside the cell releases the active inhibitor (Figure 34).[144]

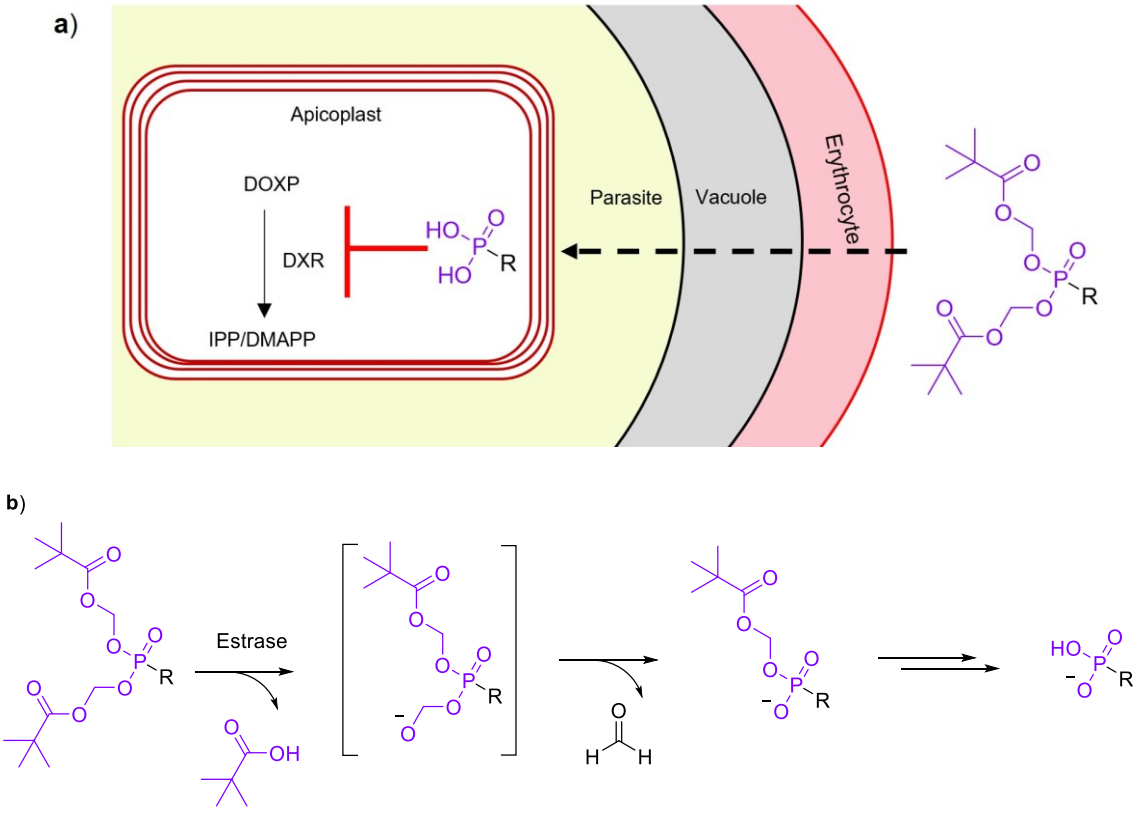

Figure 34: a) Passage and activation of a POM prodrug in *Plasmodium*-infected red blood cells modified from Brücher et al.[144] b) Bioactivation mechanism of POM prodrugs.

With the aim to improve penetration of the numerous biomembranes that the inhibitors must pass before reaching their target protein inside the apicoplast, the phosphonic acid motif of selected *N*-substituted hydroxamic acid analogs were modified using the bis-pivaloyloxymethyl (POM) ester moiety. The acyloxymethyl prodrugs, such as bis-pivaloyloxymethyl (POM), are among the most explored phosphonate promoieties.[171] Indeed, in 2015, Brücher et al. showed that the conversion of the phosphonate moiety into acyloxymethyl groups resulted in a pronounced improvement in the *in vitro* activity against asexual blood stages of *P. falciparum*, with IC_{50} values in the low nanomolar range.[144,171]

5.3.2 Synthesis of POM prodrugs **68a-d** and **72**

Scheme 21 shows the synthetic route to obtain the bis-pivaloyloxymethyl (POM) prodrugs **68a-d**. As starting materials, we selected phosphonic acids **32a-d**. The conversion into POM esters **68 a-d** was accomplished by treatment of **32a-d** with chloromethyl pivalate in the presence of triethylamine (TEA). After column chromatography with diethyl ether as eluent, all intermediates **67a-d** were obtained in good purity (96-99%). Catalytic hydrogenation of *O*-benzyl-protected precursors **67a-d** afforded the corresponding hydroxamic acids **68a-d** in 95-96% yield.[144]

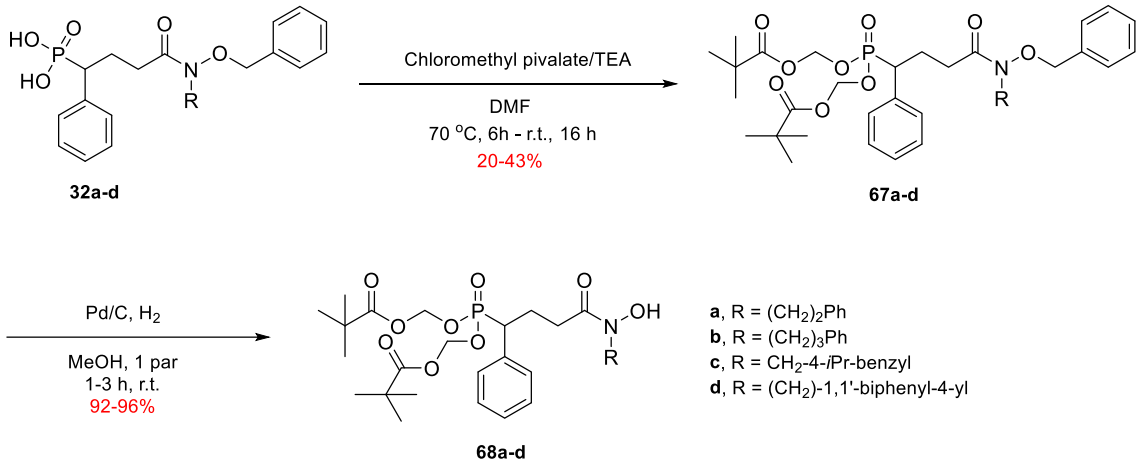

Scheme 21: Synthesis of the bis-pivaloyloxymethyl prodrugs (**68a-d**).

To use their antiplasmodial activity for comparison, the known POM prodrug **72** and its parent phosphonic acid **71** were synthesized starting from phosphonic acid **69** according to the procedure reported by BEHRENDT et al. (Scheme 22).[144,172]

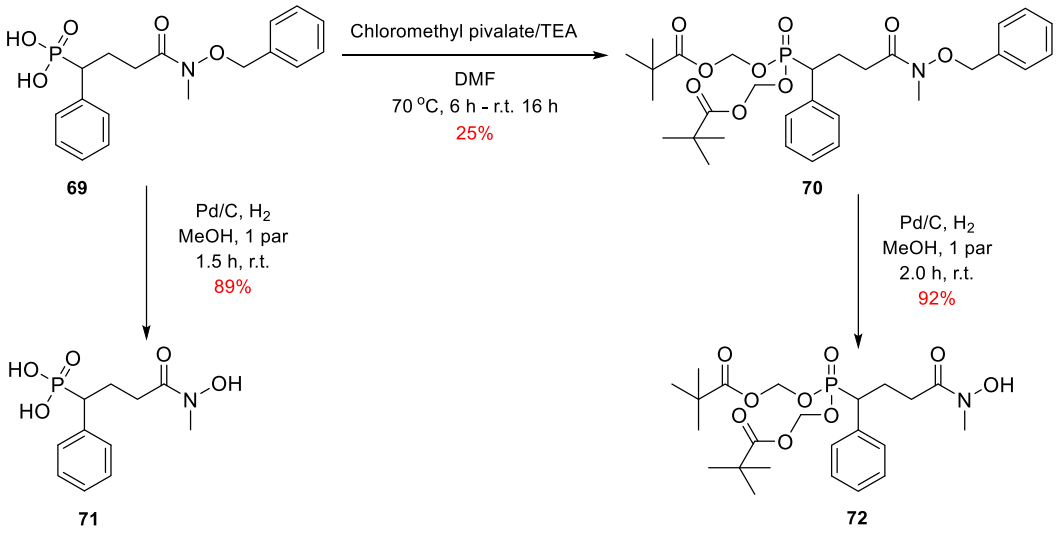

Scheme 22: Synthesis of the *N*-methyl hydroxamic acid **71** and POM prodrugs **72**.

5.3.3 Biological evaluation

5.3.3.1 Determination of antiplasmodial activity

The synthesized prodrugs **68a-d** were assayed for antiplasmodial activity against the chloroquine-sensitive (*Pf*3D7) and multidrug resistance (*Pf*Dd2) strains, as shown in section 5.1.4.2. Unexpectedly, except for prodrug **68d**, the prodrugs possessed weaker antiplasmodial activity (*Pf*3D7 IC_{50} = 3.04-28.11 and *Pf*Dd2 IC_{50} = 3.44 - 18.48 µM) against the tested *P. falciparum* strains than their parent phosphonic acids (Table 9).

Intending to understand the reason for the reduced antiplasmodial activity of the POM prodrugs, whether this is structurally related or related to the assay or the used parasitic cells, compound **72** and its parent phosphonic acid **71** were tested, and the results were used for comparison.

Testing compound **72** for its antiplasmodial activity showed a three times reduction of activity against the *Pf*3D7 strain than the phosphonic acid **71** (*Pf*3D7 IC_{50} = 1.01 and 0.33 µM, respectively). By contrast, the phosphonic acid **71** (*Pf*Dd2 IC_{50} = 0.27 µM) and the prodrug **72** (*Pf*Dd2 IC_{50} = 0.18 µM) showed approximately the same activity against the *Pf*Dd2 parasites. It is worth noting that the POM prodrug **72** was successful previously to induce a threefold improvement in antiplasmodial activity compared to its parent phosphonic acid **71** when tested against *Pf*K1 strain (*Pf*K1 IC_{50} = 0.17 and 0.48 µM, respectively).

Although the reason for this weaker activity is unknown, a possible explanation may be the lack of adequate activation of the POM prodrugs inside the cells to their corresponding phosphonic acids. Further evaluation of this hypothesis by performing a liquid chromatography–mass spectrometry (LC-MS), described recently by MIKATI et al., is still required.[173] This assay is used to quantify the POM prodrug activation inside the cells.

Table 9: *In vitro* antiplasmodial activity of DXR inhibitors **34a-d**, and **71** and prodrugs **68a-d**, and **72**.

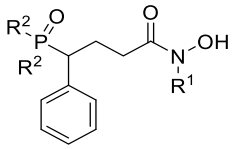

Cpd. no.	R		*Pf*3D7 IC_{50} (µM)	*Pf*Dd2 IC_{50} (µM)
	R^1	R^2		
34a	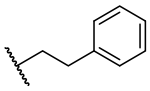	OH	0.78 ± 0.06	0.73 ± 0.05
34b	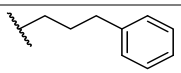	OH	0.55 ± 0.03	0.94 ± 0.16
34c	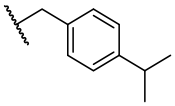	OH	11.20 ± 0.74	9.20 ± 0.17
34d	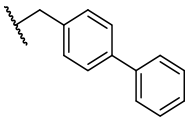	OH	>27.78	>27.78
71	CH_3	OH	0.33 ± 0.08	0.27 ± 0.02
68a	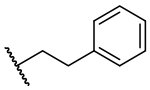	$OCH_2OCOtBu$	23.35 ± 0.92	11.25 ± 2.54
68b	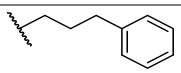	$OCH_2OCOtBu$	3.04 ± 0.34	3.44 ± 0.11
68c	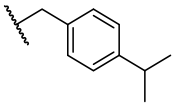	$OCH_2OCOtBu$	19.00 ± 4.72	12.60 ± 1.03
68d	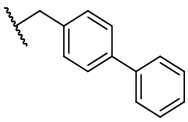	$OCH_2OCOtBu$	28.11 ± 4.86	18.48 ± 0.46
72	CH_3	$OCH_2OCOtBu$	1.01 ± 0.19	0.184 ± 0.04

Values are the mean of at least two duplicate determinations.[155,157]

6. Crystal structure analysis of 34b in *Pf*DXR

To determine the synthesized compounds' binding modes, the group of Prof. NOBUTADA TANAKA conducted a co-crystallization study of several *N*-substituted hydroxamic acids in the *Pf*DXR enzyme. The study revealed so far the successful co-crystalization of the most active compound, **34b**, in both quaternary and ternary complexes.

Co-crystallization of *Pf*DXR in quaternary complex, with NADPH, Mn^{2+}, and **34b** (Figure 35A), and ternary complex, with Mn^{2+} and **34b** (Figure 35B) afforded crystals with a resolution of 1.44 and 1.60 Å, respectively. The present crystal structures are the first quaternary and ternary complexes of *Pf*DXR with reverse fosmidomycin analogs bearing large substituents on the nitrogen atom of the reverse hydroxamic acid group. The high-resolution crystal structure analyses revealed that *Pf*DXR selectively bound the *S*-enantiomer compound **34b**. The X-ray structure analyses showed that the active site structures of both complexes are similar. In contrast, conformational differences are observed between the binding sites for the adenine moiety of NADPH between the quaternary and the ternary complexes. The active site structure of the quaternary complex showed no differences from those previously reported quaternary complexes of *Pf*DXR.[133] A structural overlay of the ternary complex with the quaternary complex (Figure 35C) documents the consistency of the ligand binding mode. Only the flexible loop, colored violet (residues 291−299), is slightly disordered. In both complexes, **34b** binds to the active site cavity. The molecular interaction between the core of **34b** (Phosphonic acid group, alkyl linker, and hydroxamic acid moiety) and *Pf*DXR is similar to the interaction between the α-*p*-CH_3-Phenyl substituted reverse fosmidomycin analog and *Pf*DXR, reported by KONZUCH et al.[133] The *N*-linked phenylpropyl moiety pointed toward a previously overlooked inhibitor binding site, not the nicotinamide binding site, of *Pf*DXR. In addition, an intramolecular interaction was observed between the first methylene group of the propyl linker and the α-phenyl ring. The propyl linker's second and third methylene groups are surrounded by the side chains of Trp296 and Met360 and the α-phenyl ring. Furthermore, the phenyl ring of the phenylpropyl moiety has contact with the binding site through van der Waals interactions with the side chain of Ser232, His341, and Pro358. These intramolecular and binding site interactions of the phenylpropyl moiety are thought to stabilize the binding of **34b** in the binding pocket.

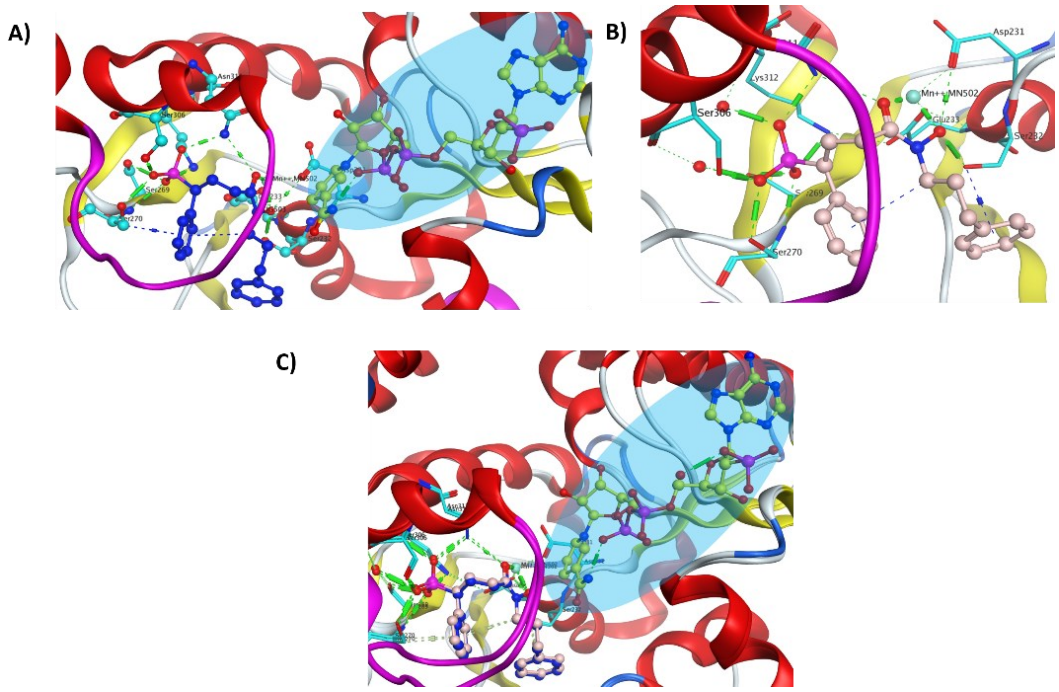

Figure 35: A) Close-up view of the active site of the quaternary complex of *Pf*DXR with bound **34b** in blue, Mn^{2+} in cyan, NADPH in yellow, and NADPH binding site highlighted in blue. (B) Close-up view of the active site of the ternary complex of *Pf*DXR with bound **34b** in pink Mn^{2+} in cyan. C) An overlay of quaternary and ternary complexes showed consistency of the ligand binding mode, whereas the flexible loop-colored violet (residues 291−299) is slightly disordered, NADPH binding site highlighted blue. The figure is created using the MOE software.

To examine the differences in binding interactions, a comparison of a possible hydrogen-bond network of the **34b** quaternary complex and the quaternary complex of *Pf*DXR complexed with α-*p*-CH_3-Ph was performed.[133] The phosphonate group of both **34b** and the α-*p*-CH_3-Ph analog forms a tight hydrogen-bond network with the main chain NH and side chain OH of Ser270, the side chain NH of Ser296, the side chain NH of Lys 312, the side chain NH of Asn311, the side chain OH of Ser306, and two water molecules (Figure 36). The reverse-hydroxamate group of the α-*p*-CH_3-Ph analog and **34b** coordinate the Mg^{2+} and Mn^{2+} ion, respectively, that is bound by residues Asp231, Glu233, and Glu315. Thus, the Mg^{2+} ion has a distorted trigonal bipyramidal geometry. The hydrogen-bond network of the reverse hydroxamic acid group with surrounding residues is essentially equivalent in both crystal structures. The α-phenyl ring of **34b** has van der Waals contacts with the side chains of Ser270 and Cys338, and similar interactions have been observed for the α-*p*-CH_3-Ph analog. The flexible loop region (residues291−299) in the **34b** complex also adopts the same open conformation as the α-*p*-CH_3-Ph analog.

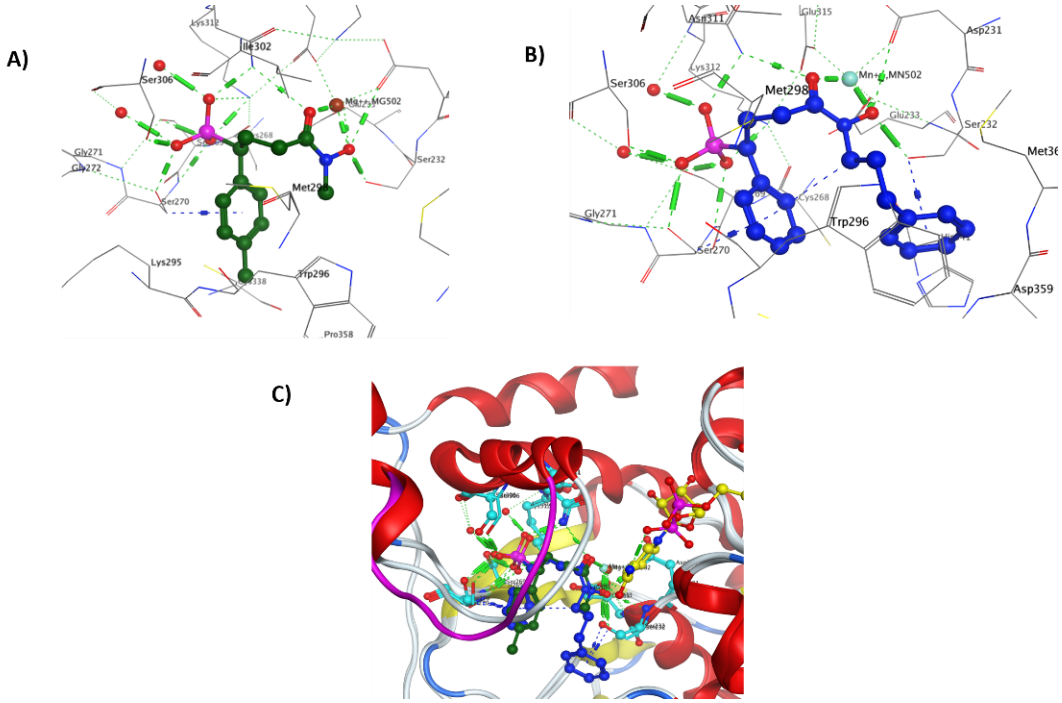

Figure 36: A structural comparison of the binding mode of α-*p*-CH_3-Ph analog (PDB: 3WQQ)[174] and that of **34b**. The bound inhibitor molecules are shown as ball-and-stick models. A) Schematic overview of the interactions of α-*p*-CH_3-Ph analog in dark green in the active site of *Pf*DXR Metal coordination and possible hydrogen bonds are shown as green dashed lines. Intra- and intermolecular and van der Waals contacts are shown as blue dashed lines. B) Schematic overview of the interactions of **34b** in blue, the active site of *Pf*DXR. Metal coordination and possible hydrogen bonds are shown as green dashed lines. Intra- and intermolecular contacts are shown as blue dashed lines. C) an overlay of the binding modes of α-*p*-CH_3-Ph and **34b** showed consistency of the binding behavior. The figure is created using the MOE software.

To conclude, from both crystal structures, with and without the NADPH cofactor, it is confirmed that **34b** did not act as bisubstrate inhibitors or interfere with the binding of the NADPH cofactor. In contrast, a new binding mode was identified that might help in designing more potent inhibitors.

7. Summary

Against the growing demand for new drugs to combat malaria, the enzyme 1-deoxy-D-xylulose-5-phosphate reductoisomerase (DXR) has emerged as a promising drug target. In most apicomplexan parasites (including *Plasmodium* species), most gram-negative and some gram-positive bacteria, DXR catalyzes the second step of IPP and DMAPP synthesis *via* the non-mevalonate pathway, which is absent in humans. Inhibitors of DXR can, therefore, be anticipated to exhibit activity against various protozoan and bacterial pathogens.

This thesis describes efforts to introduce new reverse fosmidomycin analogs as DXR inhibitors with new binding modes and potent antiplasmodial activity. Considering the reported attempts to target new binding pockets in DXR enzyme and the prevailing SAR covered in section 2.2,[171] the new compounds were designed to occupy hydrophobic pocket in DXR's substrate binding site or NADPH domains. Synthetic routes to these analogs were elaborated, and the compounds were evaluated in the working group of Prof. Dr. MARKUS FISCHER for their ability to inhibit *Pf*, *Ec,* and *Mtb* DXR orthologs. In addition, the antiproliferative potential of the synthesized compounds against two *P. falciparum* strains, *Pf*Dd2 and *Pf*3D7, was tested by the group of Dr. JANA HELD. Finally, the compounds were tested for their cytotoxicity against human HepG-2 cells to ensure parasite selectivity.

The project's initial phase studied the feasibility of synthesizing non-hydroxamic acid DXR inhibitors. Furthermore, this project was dedicated to the successful attempts to study the effect of the introduction of large substituents on the nitrogen atom of the hydroxamic acid group of compound **6b** on DXR inhibitory activity. The prepared arylalkoxyamides (**31c-g**) and amides (**33a-c**) were inferior in both DXR inhibition and antiplasmodial activity when compared to the *N*-substituted hydroxamic acid analogs (**34a-e**). These results reinforce the view that an intact hydroxamate or reverse-hydroxamate group is essential for ligating the divalent metal ion in DXR. From this series, compound **34b** was the most potent inhibitor. **34b** showed equal potency against *Pf*DXR and *Ec*DXR enzymes with IC_{50} in the subnanomolar range (*Pf*DXR IC_{50} = 0.030 µM, and *Ec*DXR IC_{50} = 0.035 µM). Furthermore, compound **34b** showed comparable activity to that of fosmidomycin against the tested *P. falciparum* strains (Figure 37).

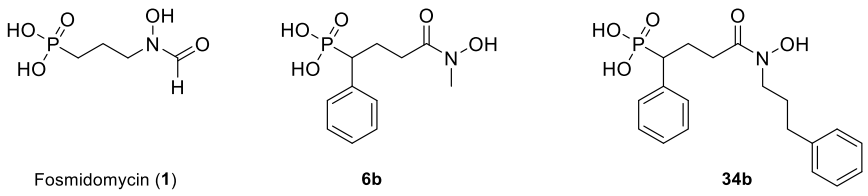

Figure 37: Structure, *Pf*DXR inhibition, and antiplasmodial activity of fosmidomycin, structure and *Pf*DXR inhibition of **6b**, and structure, DXR inhibition, and antiplasmodial activity of **34b**.

The work covered in the second part constitutes part of the efforts to optimize the structure of **34b**. A summary of the performed structural modifications is shown in Figure 38.

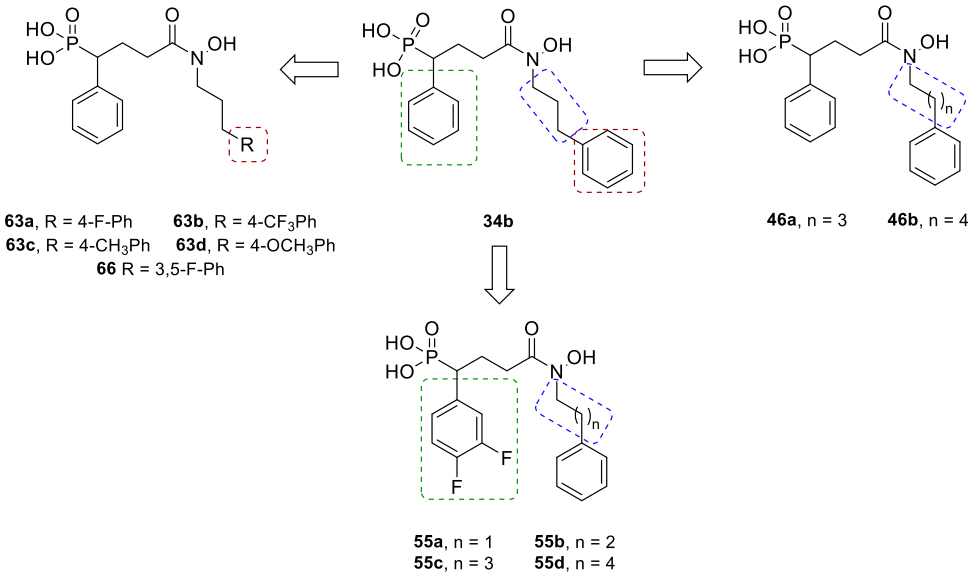

Figure 38: Structural optimization strategies of **34b.**

At first, the optimum length of the alkyl chain required to reach the new binding site was tested. Two compounds with phenylbutyl (**46a**) and phenylpentyl (**46b**) substituents at the hydroxamic acid nitrogen were synthesized. The *Pf*DXR inhibitory activity of **46a** (IC_{50} = 0.035 µM) and **46b** (IC_{50} = 0.029 µM) showed equal potency to that of **34b** (IC_{50} = 0.035 µM). On the other hand, the antiplasmodial activity of compounds **46a** (*Pf*3D7 IC_{50} = 3.70 and *Pf*Dd2 IC_{50} = 5.59 µM) and **46b** (*Pf*3D7 IC_{50} = 3.53 and *Pf*Dd2 IC_{50} =3.95 µM), revealed that with increasing the length of the alkyl chain, partial loss of antiplasmodial activity took place when compared with **34b** (Figure 39).

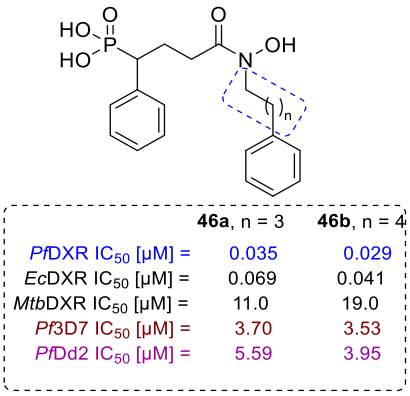

Figure 39: Structure, *Pf*DXR, and antiplasmodial activity of **46a** and **46b**.

Then, the phenyl ring in the α-position of the phosphonic acid group was replaced with a 3,4-diflurophenyl group (**55a-d**). This modification is known to increase the acidity of the phosphonic acid moiety, thereby leading to a stronger interaction with the phosphate binding site of DXR.[134] In the synthesized compounds **55b-d**, the introduction of α-3,4-difluorophenyl ring resulted in a slight improvement in *Pf*DXR inhibition compared with the α-phenyl analogs **34b** and **46a**,**b**. From the α-3,4-diflurphenyl compounds, **55c** and **55d** were the most potent analogs in this project against *Pf*DXR IC_{50} = 0.017 and 0.018 µM, respectively. Compound **55b** exhibited comparable *Pf*DXR inhibition IC_{50} = 0.028 µM to that of **34b** IC_{50} = 0.03 µM. Additionally, **55b** exhibited strong antiplasmodial activity against *Pf*3D7 IC_{50} = 1.25 µM and *Pf*Dd2 IC_{50} = 0.99 µM. This finding confirms the three-carbon spacer as the optimum alkyl chain length for the compound to display potency against both *Pf*DXR

and antiplasmodial activity (Figure 40). Compounds **55b-d** demonstrated superior *Ec*DXR inhibition with IC_{50} ranging from 0.001 to 0.013 µM when compared to α-phenyl analogs **34b** and **46a,b** (IC_{50} = 0.035-0.069 µM). Compound **55c** was this project's most potent EcDXR inhibitor (IC_{50} of 0.001 µM).

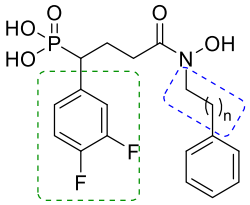

	55a, n = 1	**55b**, n = 2	**55c**, n = 3	**55d**, n = 4
*Pf*DXR IC_{50} [µM] =	0.020	0.028	0.017	0.018
*Ec*DXR IC_{50} [µM] =	0.13	0.013	0.001	0.013
*Mtb*DXR IC_{50} [µM] =	4.8	4.4	1.5	4.8
*Pf*3D7 IC_{50} [µM] =	1.55	1.25	4.02	4.60
*Pf*Dd2 IC_{50} [µM] =	1.76	0.99	3.52	4.56

Figure 40: Structure, *Pf*DXR, and antiplasmodial activity of d **55a-d**.

Finally, with the aim to explore the influence of lipophilicity, electronic and steric properties on DXR inhibition, compounds **63a-d** with *p*-substituted phenylpropyl groups and **66** with a 3,5-difluorosubstituted phenylpropyl group were prepared. Evaluation of these derivatives indicated that it is not trivial to increase either the affinity for *Pf*DXR (IC_{50} range of 0.019-0.044 µM) or the antiplasmodial activity (*Pf*3D7 IC_{50} range of 1.73-4.00 µM; *Pf*Dd2 IC_{50} range of 2.06-3.67 µM) by substituting the phenyl ring anticipated to occupy the new binding site (Figure 41). While this observation proved true for *Ec*DXR inhibition, *Mtb*DXR inhibition varied widely depending on the substituent type.

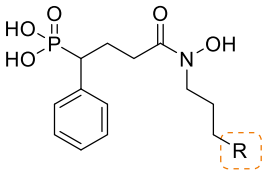

	63a, R = 4-F-Ph	**63c**, R = 4-CH_3Ph	**63d**, R = 4-OCH_3Ph	**66**, R = 3,5-F-Ph
*Pf*DXR IC_{50} [µM] =	0.019	0.044	0.024	0.030
*Ec*DXR IC_{50} [µM] =	0.019	0.022	0.045	0.036
*Mtb*DXR IC_{50} [µM] =	2.9	3.8	11	20
*Pf*3D7 IC_{50} [µM] =	1.73	2.88	4.00	1.69
*Pf*Dd2 IC_{50} [µM] =	3.67	2.88	2.06	2.62

Figure 41: Structure, *Pf*DXR, and antiplasmodial activity of **63a**, **63c, 63d,** and **66**.

The development of the pivaloyloxymethyl (POM) prodrugs **68a-d** to improve the cellular activity of selected analogs by masking the ionic nature of the phosphonic acid function at physiological pH was attempted in section 5.3. Unfortunately, the POM prodrugs were less active than their parent phosphonic acids. For example, compound **68b** showed a three-fold reduction in antiplasmodial activity against *Pf*3D7 strain (IC_{50} = 3.04 µM) and a seven-fold reduction against *Pf*Dd2 strain (IC_{50} = 3.44 µM) when compared with **34b** (Figure 42). Further evaluation of this discrepancy is needed for justification.

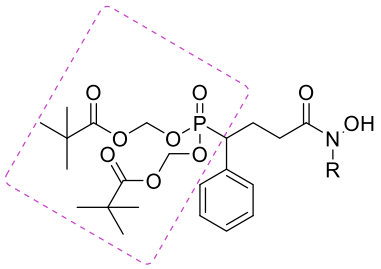

68a-d

	68a, R = $(CH_2)_2Ph$	**68b**, R = $(CH_2)_3Ph$	**68c**, R =4-*i*Pr-benzyl	**68d**, R = CH_2-1,1' biphenyl-4-yl
*Pf*3D7 IC_{50} [µM] =	23.35	3.04	19.00	28.11
*Pf*Dd2 IC_{50} [µM] =	11.25	3.44	12.60	18.48

Figure 42: Structure and antiplasmodial activity of **68a-d**.

The group of Prof. Nobutada Tanaka executed crystallographic studies of the *Pf*DXR with several *N*-substituted hydroxamic acid analogs. These studies resulted in the successful crystallization of compound **34b** both in ternary and quaternary complexes (section 6).

The novel X-ray structures of **34b** in *Pf*DXR showed that the active sites of both quaternary complex, with NADPH, Mn^{2+}, and **34b**, and ternary complex, with Mn^{2+} and **34b**, are similar. Additionally, the active site of the quaternary complex showed no deviations from the quaternary complexes of *Pf*DXR reported earlier.[133] In both complexes, **34b** binds to the active site cavity, and consistency of the binding mode was observed (Figure 43). The binding of compound **34b** phosphonic and hydroxamic acid moieties in *Pf*DXR is similar to the previously reported interaction between the α-*p*-CH_3-Phenyl substituted reverse fosmidomycin analog and *Pf*DXR. The *N*-linked phenylpropyl moiety showed a new inhibitor binding mode in previously overlooked hydrophobic sup-pocket in *Pf*DXR. It is believed that the *N*-linked phenylpropyl moiety plays a crucial role in stabilizing the binding of **34b** throw intramolecular interaction between the first methylene group of the propyl linker and the α-phenyl ring and the binding site van der Waals interaction of the side chain of Ser232, His341, and Pro358 with the phenyl ring. The crystal structures with and without the NADPH cofactor showed that **34b** adopted a new binding mode not observed before with known DXR inhibitors.

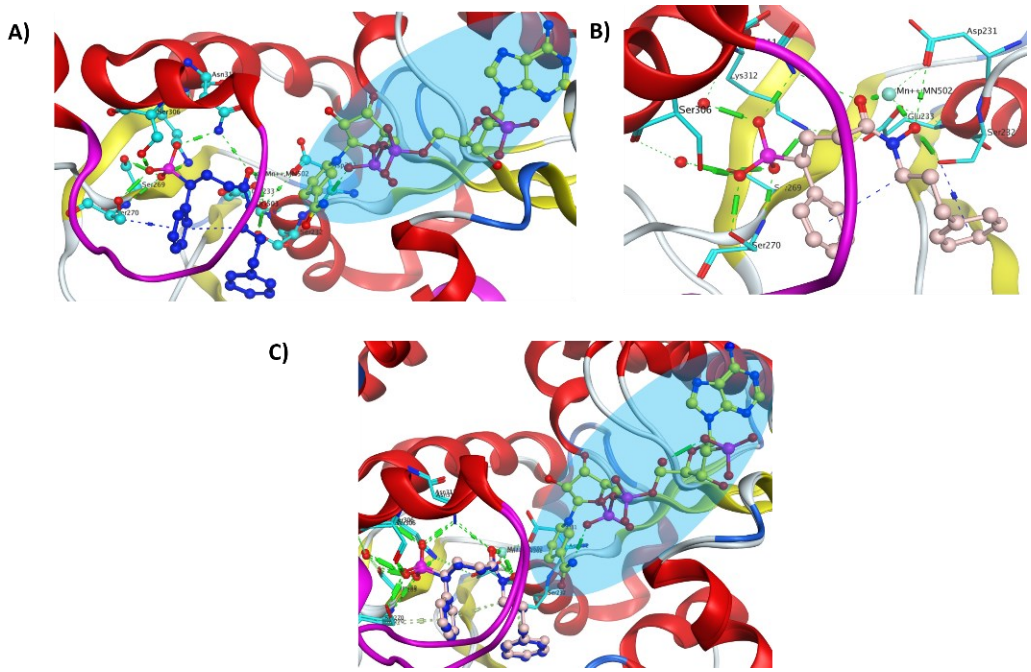

Figure 43: Binding interaction of **34b** in quaternary complex (A), ternary complex (B), and the overlay of both complexes (C). The figure is created using the MOE software.

The first outcome of this thesis offered the following conclusions for the SAR regarding *Pf*DXR inhibition and antiplasmodial activity against *Pf*3D7 and *Pf*Dd2, summarized in Figure 44.

1- The reverse *N*-substituted hydroxamic acid functionality is crucial for DXR inhibition, and the attempts to replace it with either the amide or alkoxyamide functionalities resulted in the loss of DXR inhibition and, therefore, the antiplasmodial activity.
2- A three-carbon alkyl chain between the nitrogen atom of the hydroxamic acid group and the phenyl ring is the optimum length for potent *Pf*DXR inhibition in connection with potent antiplasmodial activity.
3- The substitution of the phenyl ring of the phenylpropyl group with either an electron-withdrawing group (F, at the *p*-position, **63a**, or F at 3,5 positions, **66**) or an electron-donating group (OCH_3, **63d**, CH_3, **63c**, at the *p*-position) did not significantly impact both DXR inhibition and antiplasmodial activity. However, compound **63b** with (CF_3 at the *p*-position) showed weaker antiplasmodial activity when compared with compounds **63a**, **63c**, **63d**, and **66**.
4- Derivatives with phenyl ring (**34a**,**b**, and **46a**,**d**) or 3,4-difluorophenyl ring (**55a-d**) in α-position relative to the phosphonic acid function showed equal antiplasmodial activity. However, a slight improvement in the *Pf*DXR inhibition with the α-3,4-difluorophenyl analogs (**55a-d**) was observed.
5- The pivaloyloxymethyl (POM) prodrugs showed lower antiplasmodial activity than their parent phosphonic acids.

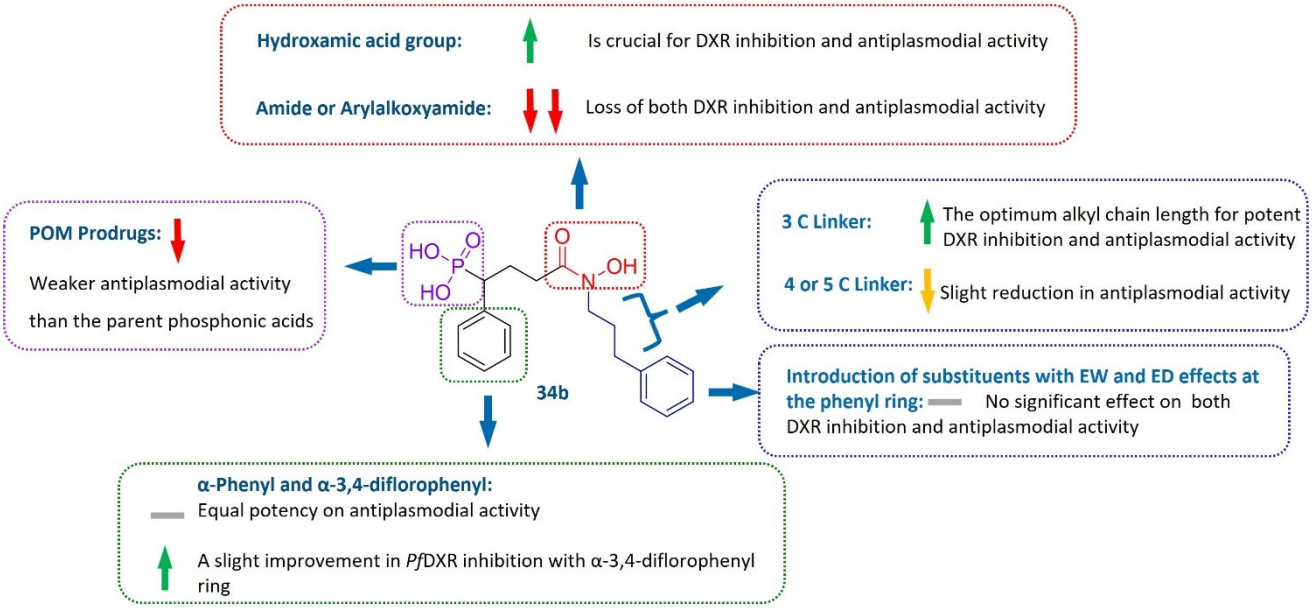

Figure 44: Summary of the Structure-Activity Relationship (SAR). EW: electron-withdrawing, ED: electron-donating.

An additional conclusion of this work regarding DXR inhibition is that the synthesized compounds exhibited weaker inhibition to *Mtb*DXR compared to *Pf*DXR and *Ec*DXR.

8. Experimental

8.1 General Information

8.1.1 Reaction, monitoring, and purification

Chemicals and solvents were purchased from commercial suppliers (Sigma-Aldrich, Acros Organics, TCI, Fluorochem ABCR, Alfa Aesar, J&K, Carbolution) and used without further purification. Dry solvents were obtained from Acros Organics. Ambient or room temperature corresponds to 22°C. The reaction progression was monitored using thin-layer-chromatography plates by Macherey Nagel (ALUGRAM Xtra SIL g/UV254). Visualization was achieved with ultraviolet irradiation (254 nm) or by staining with a $KMnO_4$-solution (9 g $KMnO_4$, 60 g K_2CO_3, 15 mL of a 5% aqueous NaOH-solution, and 900 mL demineralized water). Purification was either performed with a prepacked Silica cartridges (Acros, RediSep® Rf Normal Phase Silica) or (Acros, RediSep® Silver C18 Reversed Phase Silica) for flash column chromatography (Combi Flash Rf 200, TeleDyneIsco). Different eluent mixtures of solvents (*n*-hexane and EtOAc or DCM and methanol) served as the mobile phase for flash column chromatography and are stated in the experimental procedure. The microwave reactions were carried out in the Discover microwave reactor from CEM gmbH. A 10 mL thick-walled microwave tube sealed with a snap-on lid was used as the reaction vessel.

8.1.2 Analytics

An NMR-Spectrometer by Bruker (Bruker Avance III – 300 or Bruker Avance III - 600) were used to perform ^{1}H-, ^{13}C-NMR, and ^{31}P-NMR experiments. Chemical shifts are given in parts per million (ppm), relative to residual non-deuterated solvent peak (^{1}H-NMR: DMSO-*d6* (2.50), MeOD-*d4* (3.31); ^{13}C-NMR: DMSO-*d6* (39.52), MeOD-*d4* (49.15). Signal patterns are indicated as: singlet (s), doublet (d), doublet of doublets (dd), triplet (t), triplet of triplets (tt), quartet (q), doublet of quartets (dq), heptet (h), pentet (p) or multiplet (m). Coupling constants, *J*, are quoted to the nearest 0.1 Hz and are presented as observed. ESI-MS and ESI-HRMS were carried out using Bruker Daltonics UHR-QTOF maXis 4G (Bruker Daltonics) under electrospray ionization (ESI). LC-MS were carried out using Bruker Compass Data Analysis 4.2 under electrospray ionization (ESI). The characterizations mentioned above were carried out by the HHU Center of Molecular and Structural Analytics at Heinrich Heine University Düsseldorf (http://www.chemie.hhu.de/en/analytics-center-hhucemsa.html). Melting points were determined using a Büchi M-565 melting point apparatus. High-Performance Liquid Chromatography (HPLC)measurements were carried out on Varian ProStar 210 combined with the UV detector Varian ProStar 330 in the 220-254 nm range from Varian Inc. The stationary phase was the chromatography column Phenomenex Luna C-18 (2) particle size 5 µm (250 x 4.6 mm) with an upstream Phenomenex Security guard C-18 (4.0 mm x 3.0 mm). The measurements were carried out using the eluent gradient shown below (Table 10). Three methods were used for HPLC analysis:

Method A: flow rate: 1.00 mL/min; Eluent A: water + 0.1% TFA; Eluent B: acetonitrile + 0.1% TFA and UV absorption of 254 nm.

Method B: flow rate: 1.00 mL/min; Eluent A: water; Eluent B: acetonitrile and UV absorption of 254 nm.

Method C: flow rate: 1.00 mL/min; Eluent A: water + 0.1% TFA; Eluent B: acetonitrile + 0.1% TFA and UV absorption of 220 nm. The purity of all final compounds was 95% or higher.

Table 10: The solvent gradient for HPLC analysis.

Time/min	Water or Water + 0.1% TFA	ACN or ACN 0.1% TFA
0-0.50	90	10
0.5-20.0	90 ⟶ 0	10 ⟶ 100
20-30.0	0	100

8.2 Overview of target compounds

<table>
<tr>
<td>Arylalkoxyamide analogs
 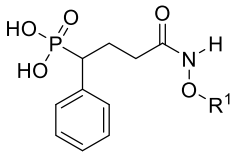
31c, R = $(CH_2)_2Ph$
31d, R = $(CH_2)_3Ph$
31e, R = 4-isopropylbenzyl
31f, R = CH_2-1,1'-biphenyl-4-yl
31g, R = CH_2-naphthalen-2-yl</td>
<td>Amide analogs
 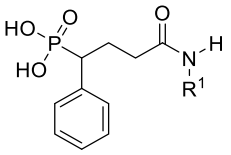
33a, R = $(CH_2)_3Ph$
33b, R = $(CH_2)_4Ph$
33c, R = 2-$(CH_2)_2$-1-*H*-indole</td>
</tr>
<tr>
<td>α-phenyl *N*-substituted hydroxamic acid analogs
 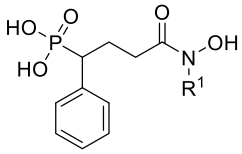
34a, R = $(CH_2)_2Ph$
34b, R = $(CH_2)_3Ph$
34c, R = 4-isopropylbenzyl
34d, R = CH_2-1,1'-biphenyl-4-yl
34e, R = CH_2-naphthalen-2-yl
46a, R = $(CH_2)_4Ph$
46b, R = $(CH_2)_5Ph$</td>
<td>Nicotinamide analogs
 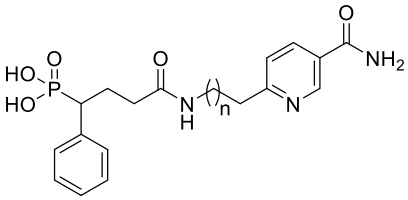
39a, n = 2
39b, n = 3</td>
</tr>
<tr>
<td>α-3,4-difluorophenyl *N*-substituted hydroxamic acid analogs
 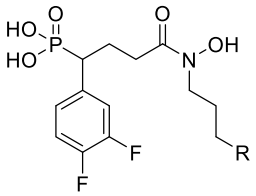
55a, R = $(CH_2)_2Ph$
55b, R = $(CH_2)_3Ph$
55c, R = $(CH_2)_4Ph$
55d, R = $(CH_2)_5Ph$</td>
<td>α-phenyl analogs with substituents on phenyl ring of the phenylpropyl group
 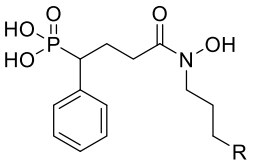
63a, R = 4-F-Ph
63b, R = 4-CF_3Ph
63c, R = 4-CH_3Ph
63d, R = 4-OCH_3Ph
66, R = 3,5-F-Ph</td>
</tr>
<tr>
<td colspan="2">Pivaloyloxymethyl (POM) prodrugs
 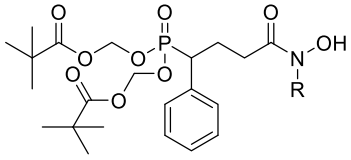
68a, R = $(CH_2)_2Ph$
68b, R = $(CH_2)_3Ph$
68c, R = CH_2-4-*i*PrPh
68d, R = (CH_2)-1,1biph
72 , R = CH_3</td>
</tr>
</table>

8.3 Synthesis procedures

8.3.1 Synthesis of starting materials

Synthesis of diethyl (3-(1,3-dioxolan-2-yl)-1-phenylpropyl)phosphonate (**13**)

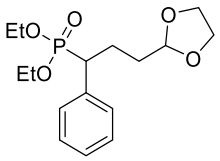

$C_{16}H_{25}O_5P$
[328.1440]

Dioxolane **13** was synthesized according to the procedure reported by BEHRENDT et al.[136]

All spectroscopic data are in agreement with published data.[136]

Diethyl (4-oxo-1-phenylbutyl)phosphonate (**14**)

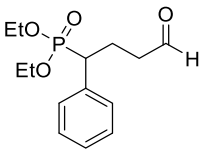

$C_{14}H_{21}O_4P$
[284.1177]

Aldehyde **14** was synthesized according to the procedure reported by BEHRENDT et al.[136]

All spectroscopic data are in agreement with published data.[136]

Synthesis of 4-(diethoxyphosphoryl)-4-phenylbutanoic acid (**15**)

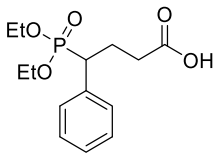

$C_{14}H_{21}O_5P$
[300.1127]

Carboxylic acid **15** was synthesized according to the procedure reported by BEHRENDT et al.[136]

All spectroscopic data are in agreement with published data.[136]

4-(Chloromethyl)-2-phenyloxazole (**19a**)

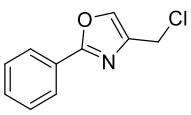

$C_{10}H_8ClNO$
[193.0294]

19a was synthesized according to the procedure reported by ZHAO et al.[145]

All spectroscopic data are in agreement with published data.[146,175]

4-(Chloromethyl)-2-phenylthiazole (**19b**)

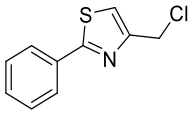

$C_{10}H_8ClNS$
[209.0066]

19b was synthesized according to the procedure reported by ZHAO et al.[145]

All spectroscopic data are in agreement with published data.[146,175]

2-((2-Phenyloxazol-4-yl)methoxy)isoindoline-1,3-dione (**21a**)

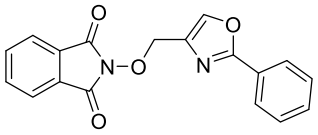

$C_{18}H_{12}N_2O_4$
[320.0797]

21a was synthesized from 4-(chloromethyl)-2-phenyloxazole (**19a**) according to the procedure reported by ASFAHA et al. [146]

All spectroscopic data were in agreement with literature.[146]

2-((2-Phenylthiazol-4-yl)methoxy)isoindoline-1,3-dione (**21b**)

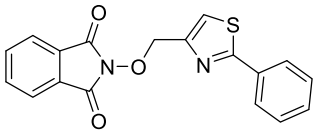

$C_{18}H_{12}N_2O_3S$
[336.0569]

21b was synthesized from 4-(chloromethyl)-2-phenylthiazole (**19b**) according to the procedure reported by ASFAHA et al. [146]

All spectroscopic data were in agreement with literature [146]

2-Phenethoxyisoindoline-1,3-dione (**21c**)

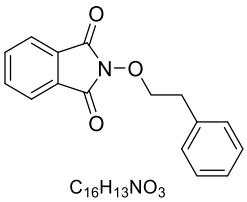

$C_{16}H_{13}NO_3$
[267.0895]

21c was synthesized from (2-bromoethyl)benzene (**19c**) according to the procedure reported by ASFAHA et al.[146]

All spectroscopic data were in agreement with literature.[146,176]

2-(3-Phenylpropoxy)isoindoline-1,3-dione (**21d**)

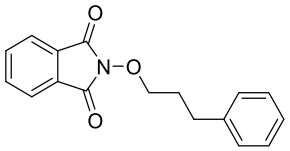

$C_{17}H_{15}NO_3$
[281.1052]

21d was synthesized from (3-bromopropyl)benzene (**19d**), according to the procedure reported by KIM et al.[177]

All spectroscopic data were in agreement with literature.[177]

2-((4-Isopropylbenzyl)oxy)isoindoline-1,3-dione (**21e**)

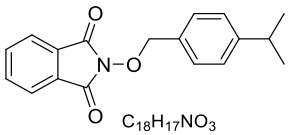

$C_{18}H_{17}NO_3$
[295.1208]

4-Isopropylbenzyl chloride (**19e**) (1.00 eq., 4.15 mmol, 0.70 g, 0.46 mL), *N*-hydroxyphthalimide (1.20 eq, 5.00 mmol, 0.815 g), and TEA (2.00 eq., 8.40 mmol, 0.84 g, 1.16 mL) were dissolved in 20 mL of acetonitrile and refluxed. After 16 h, the reaction mixture was poured into 100 mL of ice water. The obtained precipitate was separated by filtration and repeatedly washed with a saturated $NaHCO_3$ solution until the filtrate became colorless. The residue was recrystallized from ethanol to afford 0.9 g of **21e** (62%) as a white powder.

^{1}H-NMR (300 MHz, DMSO-*d6*) δ 7.85 (s, 4H), 7.47 – 7.38 (m, 2H), 7.31 – 7.23 (m, 2H), 5.12 (s, 2H), 2.89 (hept, J = 6.9 Hz, 1H), 1.19 (d, J = 6.9 Hz, 6H).

HPLC (Method C): Rt = 16.79 min, purity > 99.0%

mp.: 115.2 °C.

2-([1,1'-Biphenyl]-4-ylmethoxy)isoindoline-1,3-dione (**21f**)

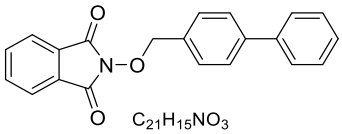

$C_{21}H_{15}NO_3$
[329.1052]

21f was synthesized from 4-(bromomethyl)-1,1'-biphenyl (**19f**) according to the procedure reported by ASFAHA et al. [146]

All spectroscopic data were in agreement with literature.[146,176]

2-(Naphthalen-2-ylmethoxy)isoindoline-1,3-dione (**21g**).

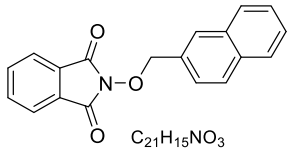

$C_{21}H_{15}NO_3$
[319.1208]

2-(Bromomethyl)naphthalene (**19g**) (1.00 eq., 4.16 mmol, 0.92 g), *N*-hydroxyphthalimide (1.20 eq, 5.00 mmol, 0.82 g) and TEA (2.00 eq., 8.32 mmol, 0.84 g, 1.16 mL) were dissolved in 20 mL of acetonitrile and refluxed. After 16 h, the reaction mixture was poured into 100 mL of ice water. The obtained precipitate was separated by filtration and repeatedly washed with a saturated $NaHCO_3$ solution until the filtrate became colorless. The residue was recrystallized from ethanol to afford 1.00 g of **21g** (89%) as a white powder.

All spectroscopic data are in agreement with published data. [176,178]

^{1}H-NMR (300 MHz, DMSO-*d6*) δ 8.02 (d, *J* = 1.7 Hz, 1H), 8.00 – 7.91 (m, 3H), 7.85 (s, 4H), 7.68 (dd, *J* = 8.4, 1.7 Hz, 1H), 7.59 – 7.50 (m, 2H), 5.33 (s, 2H).[176,178]

HPLC (Method A): Rt = 15.22 min, purity = 97.60%.

mp.: 188.7 °C.

2-(Benzyloxy)isoindoline-1,3-dione (**21h**)

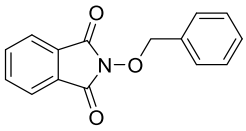

$C_{15}H_{11}NO_3$
[253.0739]

Benzyl chloride (**19h**) (1.00 eq., 16.6 mmol, 2.10 g, 1.91 mL), *N*-hydroxyphthalimide (1.20 eq, 19.92 mmol, 3.27 g), and TEA (2.00 eq., 33.2 mmol, 3.35 g, 4.61 mL) were dissolved in 70 mL of acetonitrile and refluxed. After 16 h, the reaction mixture was poured into 300 mL of ice water. The obtained precipitate was separated by filtration and repeatedly washed with a saturated $NaHCO_3$ solution until the filtrate became colorless. The residue was recrystallized from ethanol to afford 3.0 g of **21h** (60%) as a white powder.

All spectroscopic data are in agreement with published data.[179]

^{1}H-NMR (300 MHz, DMSO-*d6*) δ 7.85 (s, 4H), 7.55 – 7.48 (m, 2H), 7.44 – 7.36 (m, 3H), 5.17 (s, 2H).[179]

HPLC (Method A): Rt = 13.68 min, purity > 99.0%.

mp.: 146.4 °C, **Lit**.: 144.0 - 146.0 °C.[180]

O-((2-Phenyloxazol-4-yl)methyl)hydroxylamine (**22a**)

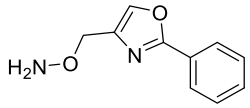

$C_{10}H_{10}N_2O_2$
[190.0742]

22a was synthesized from 2-((2-phenyloxazol-4-yl)methoxy)isoindoline-1,3-dione (**21a**) according to the procedure reported by ASFAHA et al. [146]

All spectroscopic data were in agreement with literature.[146]

O-((2-Phenylthiazol-4-yl)methyl)hydroxylamine (**22b**)

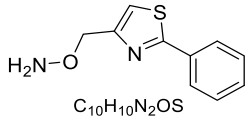

$C_{10}H_{10}N_2OS$
[206.0514]

22b was synthesized from 2-((2-phenylthiazol-4-yl)methoxy)isoindoline-1,3-dione (**21b**) according to the procedure reported by ASFAHA et al. [146]

All spectroscopic data were in agreement with literature. [146]

O-Phenethylhydroxylamine (**22c**)

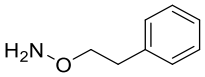

$C_8H_{11}NO$
[137.0841]

22c was synthesized from 2-phenethoxyisoindoline-1,3-dione (**21c**) according to the procedure reported by ASFAHA et al. [146]

All spectroscopic data were in agreement with literature.[146,176]

O-(3-Phenylpropyl)hydroxylamine (**22d**)

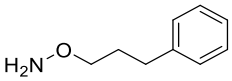

$C_8H_{11}NO$
[151.0997]

22d was synthesized from 2-(3-phenylpropoxy)isoindoline-1,3-dione **(21d)** according to the procedure reported by KIM et al.[177]

All spectroscopic data were in agreement with literature.[177]

O-(4-Isopropylbenzyl)hydroxylamine (**22e**)

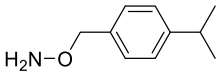

$C_{10}H_{15}NO$
165,1154

To a solution of 2-((4-isopropylbenzyl)oxy)isoindoline-1,3-dione (**21e**) (1.00 eq., 2.00 mmol, 0.59 g) in DCM (20 mL), hydrazine monohydrate (2.00 eq., 4.00 mmol, 0.20 g, 0.19 mL) was added. The mixture was stirred at r.t. for 16 h. After reaction completion, the mixture was filtered, and the filtrate was washed three times with a saturated solution of $NaHCO_3$ (3 x 10 mL) and two times with brine (2 x 10 mL). The organic phase was dried over Na_2SO_4, filtered, and the solvent evaporated under reduced pressure. The crude product was purified by flash chromatography (on a prepacked silica cartridge), using *n*-hexane:EtOAc (100:0→70:30) as eluent to afford 0.26 g of **22e** (79%) as a colorless oil.

All spectroscopic data are in agreement with published data.[181]

^{1}H-NMR (300 MHz, DMSO-*d6*) δ 7.28 – 7.15 (m, 4H), 6.00 (s, 2H), 4.52 (s, 2H), 2.87 (hept, J = 6.9 Hz, 1H), 1.19 (d, J = 6.9 Hz, 6H).[181]

HPLC (Method A): Rt = 8.16 min, purity = 97.4%

O-([1,1'-Biphenyl]-4-ylmethyl)hydroxylamine (**22f**)

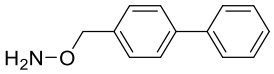

$C_{13}H_{13}NO$
199,0997

22f was synthesized from 2-([1,1'-biphenyl]-4-ylmethoxy)isoindoline-1,3-dione **(21f)** according to the procedure reported by ASFAHA et al. [146]

All spectroscopic data were in agreement with literature.[146,176]

O-(Naphthalen-2-ylmethyl)hydroxylamine (**22g**)

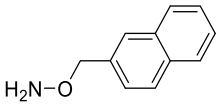

$C_{11}H_{11}NO$
173,0841

To a solution of 2-(naphthalen-2-ylmethoxy)isoindoline-1,3-dione (**21g**) (1.00 eq., 2.65 mmol, 0.80 g) in DCM (30 mL), hydrazine monohydrate (2.00 eq., 5.30 mmol, 0.27 g, 0.26 mL) was added. The mixture was stirred at r.t. for 16 h. After reaction completion, the mixture was filtered, and the filtrate was washed three times with a saturated solution of $NaHCO_3$ (3 x 10 mL) and two times with brine (2 x 10 mL). The organic phase was dried over Na_2SO_4, filtered, and the solvent evaporated under reduced pressure. The crude product was purified by flash chromatography (on a prepacked silica cartridge), using *n*-hexane:EtOAc (100:0→70:30) as eluent to afford 0.41 g of **22g** (91%) as a white powder.

All spectroscopic data are in agreement with published data.[176,178]

^{1}H-NMR (600 MHz, DMSO-*d6*) δ 7.93 – 7.87 (m, 3H), 7.84 (s, 1H), 7.54 – 7.45 (m, 3H), 6.11 (s, 2H), 4.74 (s, 2H).[176,178]

HPLC (Method B): Rt = 10.77 min, purity = 97.6%.

mp.: 56.3 °C, **Lit.**: 56.0 - 59.0 °C.[178]

O-Benzylhydroxylamine (**22h**)

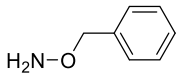

C_7H_9NO
[123.0684]

To a solution of 2-(benzyloxy)isoindoline- 1,3-dione (**21h**) (1.00 eq., 12.0 mmol, 3.00 g) in DCM (30 mL), hydrazine monohydrate (2.00 eq., 24.0 mmol, 1.20 g, 1.16 mL) was added. The mixture was stirred at r.t. for 16 h. After reaction completion, the mixture was filtered, and the filtrate was washed three times with a saturated solution of $NaHCO_3$ (3 x 10 mL) and two times with brine (2 x 10 mL). The organic phase was dried over Na_2SO_4, filtered, and the solvent evaporated under reduced pressure. The crude products were purified by flash chromatography (on a prepacked silica cartridge), using *n*-hexane:EtOAc (100:0→70:30) as eluent to afford 2.10 g of **22h** (68%) as a colorless oil.

All spectroscopic data are in agreement with published data.[182]

^{1}H-NMR (300 MHz, DMSO-*d6*) δ 7.41 – 7.24 (m, 5H), 6.05 (s, 2H), 4.59 (d, *J* = 1.5 Hz, 2H).[182]

HPLC (Method A): Rt = 4.58 min, purity = 98.7%.

General procedure **1** for the synthesis of the primary alcohols **57a-e**.

Lithium aluminum hydride 1.00 M in THF (2.00 eq.) was added dropwise to a solution of the corresponding carboxylic acid (1.00 eq.) in dry THF (1.00 mL/mmol) at 0°C. The resulting mixture was then refluxed for 2 h. After reaction completion, the reaction was cooled to 0°C, and EtOAc was added to the reaction mixture, followed by saturated Seignette salt solution to complex aluminum (until phase separation occurs). The mixture was then extracted with EtOAc (3 x 10 mL). The EtOAc phase was then washed with brine (1 x 10 mL), collected, dried over Na_2SO_4, filtered, and the solvent was removed under reduced pressure. The crude product was purified by flash chromatography (on a prepacked silica cartridge), using *n*-hexane:EtOAc (100:0→65:35) as eluent to afford the corresponding product.

3-(4-Fluorophenyl)propan-1-ol (**57a**)

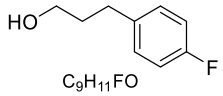

$C_9H_{11}FO$
[154.0794]

57a was synthesized from 3-(4-fluorophenyl)propanoic acid (**56a**) (1.00 eq., 20.0 mmol, 3.36 g), and Lithium aluminum hydride 1.00 M in THF (2.00 eq., 40.0 mmol, 40.0 mL) in dry THF (20.0 mL) according to general procedure **1**. 2.00 g of **57a** (65%) was obtained as a colorless oil.

All spectroscopic data are in agreement with published data.[183]

^{1}H-NMR (300 MHz, DMSO-*d6*) δ 7.27 – 7.15 (m, 2H), 7.07 (dd, J = 10.1, 7.7 Hz, 2H), 4.47 (t, J = 5.1 Hz, 1H), 3.46 – 3.36 (m, 2H), 2.59 (t, J = 8.3 Hz, 2H), 1.76 – 1.61 (m, 2H).[183]

^{13}C-NMR (75 MHz, DMSO-*d6*) δ 160.50 (d, $^1J_{C\text{-}F}$ = 240.7 Hz), 138.23 (d, $^4J_{C\text{-}F}$ = 3.0 Hz), 129.96 (d, $^3J_{C\text{-}F}$ = 7.9 Hz), 114.84 (d, $^2J_{C\text{-}F}$ = 20.9 Hz), 59.92, 34.35, 30.74.

3-(4-(Trifluoromethyl)phenyl)propan-1-ol (**57b**)

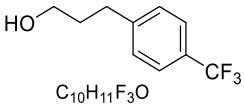

$C_{10}H_{11}F_3O$
[204.0762]

57b was synthesized from 3-(4-(trifluoromethyl)phenyl)propanoic acid (**56b**) (1.00 eq., 20.0 mmol, 4.36 g), and Lithium aluminum hydride 1.00 M in THF (2.00 eq., 40.0 mmol, 40.0 mL) in dry THF (20.0 mL) according to general procedure **1**. 3.50 g of **57b** (86%) was obtained as a colorless oil.

All spectroscopic data are in agreement with published data.[184,185]

^{1}H-NMR (300 MHz, DMSO-*d6*) δ 7.62 (d, J = 7.9 Hz, 2H), 7.45 – 7.38 (m, 2H), 4.49 (s, 1H), 3.47 – 3.35 (m, 2H), 2.78 – 2.62 (m, 2H), 1.81 – 1.63 (m, 2H).[184,185]

^{13}C-NMR (75 MHz, DMSO-*d6*) δ 147.23, 129.12, 126.42 (q, $^1J_{C\text{-}F}$ = 271.0 Hz), 125.05 (q, $^2J_{C\text{-}F}$ = 3.8 Hz), 122.68, 59.87, 33.88, 31.43.[185]

3-(*p*-Tolyl)propan-1-ol (**57c**)

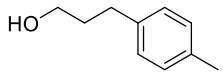

$C_{10}H_{14}O$
[150.1045]

57c was synthesized from 3-(*p*-tolyl)propanoic acid (**56c**) (1.00 eq., 30.5 mmol, 5.00 g), and Lithium aluminum hydride 1.00 M in THF (2.00 eq., 60.1 mmol, 61.0 mL) in dry THF (30.0 mL) according to general procedure **1**. 3.40 g of **57c** (74%) was obtained as a colorless oil.

All spectroscopic data are in agreement with published data.[185]

^{1}H-NMR (300 MHz, DMSO-*d6*) δ 7.07 (s, 4H), 4.46 (t, *J* = 5.1 Hz, 1H), 3.47 – 3.35 (m, 2H), 2.62 – 2.50 (m, 2H), 2.25 (s, 3H), 1.77 – 1.62 (m, 2H).[185]

^{13}C-NMR (75 MHz, MeOD-*d4*) δ 140.19, 136.17, 129.92, 129.30, 62.26, 35.57, 32.62, 21.05.[185]

3-(4-Methoxyphenyl)propan-1-ol (**57d**)

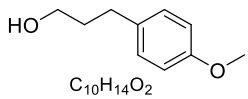

$C_{10}H_{14}O_2$
[166.0994]

57d was synthesized from 3-(*p*-methoxyphenyl)propanoic acid (**56d**) (1.00 eq., 30.5 mmol, 5.49 g), and Lithium aluminum hydride 1.00 M in THF (2.00 eq., 60.1 mmol, 61.0 mL) in dry THF (30.0 mL) according to general procedure **1**. 4.20 g of **57d** (83%) was obtained as a colorless oil.[185]

The product **57d** was used directly for the following reaction.

3-(3,5-Difluorophenyl)propan-1-ol (**57e**)

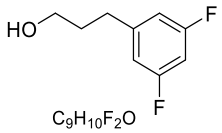

$C_9H_{10}F_2O$
[172.0700]

57e was synthesized from 3-(3,5-difluorophenyl)propanoic acid (**56e**) (1.00 eq., 24.7 mmol, 4.60 g), and Lithium aluminum hydride 1.00 M in THF (2.00 eq., 49.4 mmol, 49.0 mL) in dry THF (25.0 mL) according to general procedure **1**. 3.10 g of **57e** (73%) was obtained as a colorless oil.

^{1}H-NMR (300 MHz, DMSO-*d6*) δ 7.07 – 6.85 (m, 3H), 4.51 (t, *J* = 5.1 Hz, 1H), 3.46 – 3.34 (m, 2H), 2.63 (t, *J* = 7.0 Hz, 2H), 1.78 – 1.63 (m, 2H).

^{13}C-NMR (75 MHz, DMSO-*d6*) δ 162.35 (dd, $^{1}J_{C\text{-}F}$ = 258.8, $^{3}J_{C\text{-}F}$ = 13.4 Hz), 146.99, 111.37 (dd, $^{2}J_{C\text{-}F}$ = 22.4, $^{4}J_{C\text{-}F}$ = 6.6 Hz), 101.05 (t, $^{2}J_{C\text{-}F}$ = 25.8 Hz), 59.77, 33.55, 31.29.

Synthesis of phenylalkyl chlorides **41a,b**, and **58a-e**

(4-Chlorobutyl)benzene (**41a**)

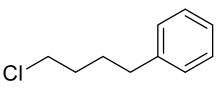

$C_{10}H_{13}Cl$
[168.0706]

41a was synthesized from 4-phenylbutan-1-ol (**40a**) according to the procedure reported by HATAE et al.[186]

All spectroscopic data are in agreement with published data. [186]

(5-Chloropentyl)benzene (**41b**)

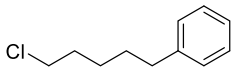

$C_{11}H_{15}Cl$
[182.0862]

41b was synthesized from 5-phenylpentan-1-ol (**40b**) according to the procedure reported by Hatae et al.[186]

All spectroscopic data are in agreement with published data.[186]

1-(3-Chloropropyl)-4-fluorobenzene (**58a**)

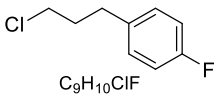

$C_9H_{10}ClF$
[172.0455]

Triphenylphosphine (1.30 eq., 13.0 mmol, 3.40 g) was added to a solution of 3-(4-fluorophenyl)propan-1-ol (**57a**) (1.00 eq., 10.0 mmol, 1.54 g) in CCl_4 (13 mL) at 0 °C under argon atmosphere and then refluxed for 1 h. After reaction completion, the mixture was quenched with water and extracted with hexane. The organic phase was collected, dried over Na_2SO_4 filtered, and the solvent was removed under reduced pressure. The crude product was purified by flash chromatography (on a prepacked silica cartridge), using *n*-hexane:EtOAc (100:0→10:90) as eluent to afford 0.92 g of **58a** (54%) as a colorless oil.

All spectroscopic data are in agreement with published data.[187]

^{1}H-NMR (300 MHz, DMSO-*d*$_6$) δ 7.69 – 7.60 (m, 2H), 7.49 - 7.41 (m, 2H), 3.62 (t, *J* = 6.5 Hz, 2H), 2.80 (dd, *J* = 8.7, 6.6 Hz, 2H), 2.12 – 1.96 (m, 2H).[187]

^{13}C-NMR (75 MHz, DMSO-*d*$_6$) δ 160.50 (d, $^1J_{C\text{-}F}$ = 240.7 Hz), 138.23 (d, $^4J_{C\text{-}F}$ = 3.0 Hz), 129.96 (d, $^3J_{C\text{-}F}$ = 7.9 Hz), 114.84 (d, $^2J_{C\text{-}F}$ = 20.9 Hz), 59.92, 34.35, 30.74.

1-(3-Chloropropyl)-4-(trifluoromethyl)benzene (**58b**)

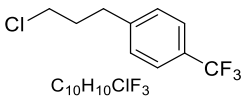

$C_{10}H_{10}ClF_3$
[222.0423]

Triphenylphosphine (1.30 eq., 6.50 mmol, 1.04 g) was added to a solution of 3-(4-fluorophenyl)propan-1-ol (**57a**) (1.00 eq., 5.00 mmol, 0.77 g) in CCl_4 (20 mL) at 0 °C under argon atmosphere and then refluxed for 1 h. After reaction completion, the mixture was quenched with water and extracted with hexane. The organic phase was collected, dried over Na_2SO_4 filtered, and the solvent was removed under reduced pressure. The crude product was purified by flash chromatography (on a prepacked silica cartridge), using *n*-hexane:EtOAc (100:0→10:90) as eluent to afford 0.60 g of **58b** (41%) as a colorless oil.

All spectroscopic data are in agreement with published data.[184]

^{1}H-NMR (300 MHz, DMSO-*d6*) δ 7.69 – 7.60 (m, 1H), 7.49 – 7.41 (m, 1H), 3.62 (t, *J* = 6.5 Hz, 1H), 2.80 (dd, *J* = 8.7, 6.6 Hz, 1H), 2.12 – 1.96 (m, 1H).[184]

^{13}C-NMR (75 MHz, DMSO-*d6*) δ 145.70, 129.19, 126.63(q, $^{1}J_{C\text{-}F}$ = 271.0 Hz), 125.19 (q, $^{2}J_{C\text{-}F}$ = 3.9 Hz), 122.60, 44.55, 33.23, 31.98.

1-(3-Chloropropyl)-4-methylbenzene (**58c**)

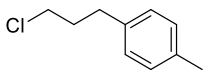

$C_{10}H_{13}Cl$
[168.0706]

Triphenylphosphine (1.30 eq., 26.0 mmol, 6.80 g) was added to a solution of 3-(*p*-tolyl)propan-1-ol (**57c**) (1.00 eq., 20.0 mmol, 3.00 g) in CCl_4 (26 mL) at 0 °C under argon atmosphere and then refluxed for 1 h. After reaction completion, the mixture was quenched with water and extracted with hexane. The organic phase was collected, dried over Na_2SO_4 filtered and the solvent was removed under reduced pressure. The crude product was purified by flash chromatography (on a prepacked silica cartridge), using *n*-hexane:EtOAc (100:0→10:90) as eluent to afford 2.01 g of **58c** (60%) as a colorless oil.

All spectroscopic data are in agreement with published data. [198]

^{1}H-NMR (300 MHz, DMSO-*d6*) δ 7.09 (s, 4H), 3.59 (t, *J* = 6.5 Hz, 2H), 2.65 (dd, *J* = 8.5, 6.6 Hz, 2H), 2.26 (s, 3H), 2.05 – 1.90 (m, 2H). [198]

^{13}C-NMR (75 MHz, MeOD-*d4*) δ 139.00, 136.58, 130.07, 129.41, 44.91, 35.52, 33.27, 21.05.[199]

1-(3-Chloropropyl)-4-methoxybenzene (**58d**)

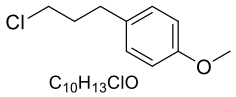

$C_{10}H_{13}ClO$
[184.0655]

58d was synthesized from 3-(4-methoxyphenyl)propan-1-ol (**57d**) according to the procedure reported by Fronza et al.[165]

All spectroscopic data are in agreement with published data.[165]

1-(3-Chloropropyl)-3,5-difluorobenzene (**58e**)

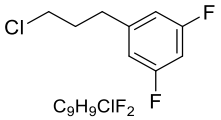

$C_9H_9ClF_2$
[190.0361]

Triphenylphosphine (1.30 eq.4.00 mmol, 1.04 g) was added to a solution of 3-(3,5-difluorophenyl)propan-1-ol (**57e**) (1.00 eq., 3.04 mmol, 0.52 g, 0.70 mL) in CCl_4 (20 mL) at 0 °C under argon atmosphere and then refluxed for 1 h. After reaction completion, the mixture was quenched with water and extracted with hexane. The organic phase was collected, dried over Na_2SO_4 filtered and the solvent was removed under reduced pressure. The crude product was purified by flash chromatography (on a prepacked silica cartridge), using *n*-hexane:EtOAc (100:0→10:90) as eluent to afford 0.29 g of **58e** (50%) as a colorless oil.

^{1}H-NMR (300 MHz, DMSO-*d6*) δ 7.05 – 6.84 (m, 3H), 3.40 (td, *J* = 6.3, 5.1 Hz, 2H), 2.63 (dd, *J* = 8.8, 6.7 Hz, 2H), 1.78 – 1.63 (m, 2H).

Synthesis of tert-butyl (benzyloxy)carbamate (**23**)

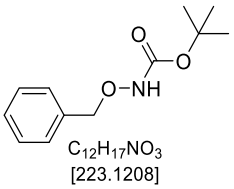

$C_{12}H_{17}NO_3$
[223.1208]

23 was synthesized from *O*-Benzylhydroxylamine (**22h**) according to the procedure reported by SULSKY et al.[188187]

All spectroscopic data are in agreement with published data.[188,189]

General procedure **2** for the synthesis of *N*-Boc and *O*-benzyl protected hydroxylamines **25a-e**, **42a,b**, and **59a-e**

To a solution of **23** (1.00 eq.) in dry DMF (1 mL/mmol) was added NaH (1.20 eq., 60% oil dispersion) portion-wise at 0˚C. After stirring for 1 h, the respective arylalkyl chloride **24a-e**, **41a,b**, and **58a-e** (1.00 eq.) was added and the reaction mixture was stirred for 16 h at r.t.. The reaction was quenched with water (10 mL) and extracted with EtOAc (3 x 10 mL). The combined EtOAc phase was washed with H_2O (3 x 10 mL) and brine (1 x 10 mL). The organic phase was dried over Na_2SO_4, filtered, and the solvent was evaporated under reduced pressure. The crude product was purified by flash chromatography (on a prepacked silica cartridge), using *n*-hexane/EtOAc (100:0-90:10%) as eluent to afford the corresponding product.

tert-Butyl (benzyloxy)(phenethyl)carbamate (**25a**)

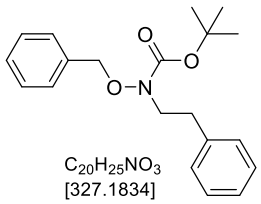

$C_{20}H_{25}NO_3$
[327.1834]

25a was synthesized from (2-bromoethyl)benzene (**24a**) (1.00 eq., 10.0 mmol, 1.84 g), *tert*-butyl (benzyloxy)carbamate (**23**) (1.00 eq., 10.0 mmol, 2.23 g) and NaH (1.20 eq., 12.00 mmol, 60% oil dispersion, 0.28 g) in dry DMF (10 mL) according to general procedure **2**. 2.58 g of **25a** (79%) was obtained as a colorless oil.

^{1}H-NMR (300 MHz, MeOD-*d4*) δ 7.38 – 7.05 (m, 10H), 4.03 (s, 2H), 2.90 (t, *J* = 6.7 Hz, 2H), 2.71 (t, *J* = 7.1 Hz, 2H), 1.34 (s, 9H).

^{13}C-NMR (75 MHz, MeOD-*d4*) δ 157.85, 140.15, 139.93, 130.06, 129.43, 127.34, 82.49, 76.10, 51.46, 35.65, 28.42.

HPLC (Method B): Rt = 19.39 min, purity > 99.0%.

tert-Butyl (benzyloxy)(3-phenylpropyl)carbamate (**25b**)

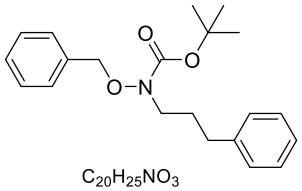

$C_{20}H_{25}NO_3$
[341.1991]

25b was synthesized from 3-bromopropyl)benzene (**24b**) (1.00 eq., 10.0 mmol, 1.99 g), *tert*-butyl (benzyloxy)carbamate (**23**) (1.00 eq., 10.0 mmol, 2.23 g) and NaH (1.20 eq., 12.00 mmol, 60% oil dispersion, 0.28 g) in dry DMF (10 mL) according to general procedure **2**. 2.5 g of **25b** (73%) was obtained as a colorless oil.

^{1}H-NMR (300 MHz, DMSO-*d6*) δ 7.42 – 7.32 (m, 5H), 7.31 – 7.22 (m, 2H), 7.21 – 7.13 (m, 3H), 4.78 (s, 2H), 3.44 – 3.34 (m, 10H), 2.56 (t, *J* = 7.6 Hz, 2H), 1.81 (p, *J* = 7.6 Hz, 2H), 1.41 (s, 9H).

^{13}C-NMR (75 MHz, DMSO-d_6) δ 155.19, 138.68, 138.42, 128.74, 128.70, 128.26, 128.21, 126.10, 80.18, 74.27, 49.98, 34.00, 32.53, 27.76.

HPLC (Method c): Rt = 20.99 min, purity > 99.0%.

tert-Butyl (benzyloxy)(4-isopropylbenzyl)carbamate (**25c**)

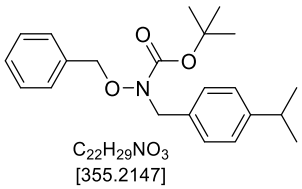

$C_{22}H_{29}NO_3$
[355.2147]

25c was synthesized from 1-(chloromethyl)-4-isopropylbenzene (**24c**) (1.00 eq., 10.0 mmol, 0.99 mL), *tert*-butyl (benzyloxy)carbamate (**23**) (1.00 eq., 10.0 mmol, 2.23 g) and NaH (1.20 eq., 12 mmol, 60% oil dispersion, 0.28 g) in dry DMF (10 mL) according to general procedure **2**. 2.41 g of **25c** (68%) was obtained as a colorless oil.

^{1}H-NMR (300 MHz, MeOD-*d4*) δ 7.36 – 7.25 (m, 5H), 7.20 (q, *J* = 8.2 Hz, 4H), 4.71 (s, 2H), 4.50 (s, 2H), 2.88 (p, *J* = 6.9 Hz, 1H), 1.47 (s, 9H), 1.23 (d, *J* = 6.9 Hz, 6H).

^{13}C-NMR (75 MHz, MeOD-*d4*) δ 158.13, 149.52, 136.89, 135.59, 130.61, 129.57, 129.33, 127.38, 82.89, 78.00, 54.22, 35.08, 28.55, 24.47.

HPLC (Method B): Rt = 20.30 min, purity = 96.2%.

tert-Butyl ([1,1'-biphenyl]-4-ylmethyl)(benzyloxy)carbamate (**25d**)

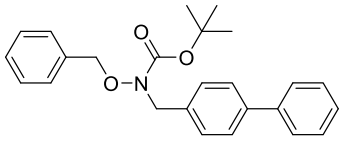

$C_{25}H_{27}NO_3$
[389.1991]

25d was synthesized from 4-(bromomethyl)-1,1'-biphenyl (1.00 eq., 10.0 mmol, 2.46 g) (**24d**), *tert*-butyl (benzyloxy)carbamate (**23**) (1.00 eq., 10.0 mmol, 2.23 g) and NaH (1.20 eq., 12.00 mmol, 60% oil dispersion, 0.28 g) in dry DMF (10 mL) according to general procedure **2**. 1.79 g of **25d** (46%) was obtained as a colorless oil.

^{1}H-NMR (300 MHz, DMSO-*d6*) *δ* 7.95 – 7.86 (m, 4H), 7.78 (d, *J* = 1.7 Hz, 1H), 7.59 – 7.42 (m, 4H), 7.33 (s, 5H), 4.78 (s, 2H), 4.76 (s, 2H), 1.43 (d, *J* = 1.2 Hz, 9H).

^{13}C-NMR (75 MHz, MeOD-*d4*) δ 158.20, 136.87, 135.73, 134.73, 134.32, 130.62, 129.54, 129.34, 129.15, 128.77, 128.68, 128.34, 127.31, 127.23, 126.96, 126.65, 83.06, 78.10, 54.74, 28.53.

tert-Butyl (benzyloxy)(naphthalen-2-ylmethyl)carbamate (**25e**)

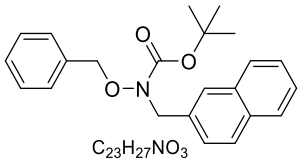

$C_{23}H_{27}NO_3$
[363.1834]

25e was synthesized from 2-(bromomethyl)naphthalene (1.00 eq., 10.0 mmol, 2.20 g) (**24e**), *tert*-butyl (benzyloxy)carbamate (**23**) (1.00 eq., 10.0 mmol, 2.23 g) and NaH (1.20 eq., 12.00 mmol, 60% oil dispersion, 0.28 g) in dry DMF (10 mL) according to general procedure **2**. 1.88 g of **25e** (52%) was obtained as a colorless oil.

^{1}H-NMR (300 MHz, DMSO-*d6*) *δ* 7.94 – 7.86 (m, 4H), 7.78 (d, *J* = 1.7 Hz, 1H), 7.53 – 7.48 (m, 2H), 7.45 (dd, *J* = 8.5, 1.8 Hz, 1H), 7.33 (s, 4H), 4.78 (s, 2H), 4.76 (s, 2H), 1.43 (s, 9H).

^{13}C-NMR (75 MHz, MeOD-*d4*) *δ* 148.72, 127.39, 126.26, 125.26, 124.85, 121.57, 121.14, 120.72, 120.02, 119.86, 119.68, 119.25, 118.86, 117.80, 117.49, 73.59, 68.62, 45.26, 18.91.

tert-Butyl (benzyloxy)(4-phenylbutyl)carbamate (**42a**)

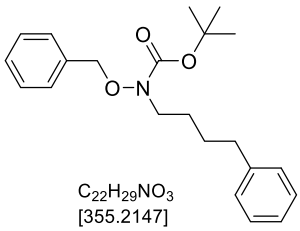

$C_{22}H_{29}NO_3$
[355.2147]

42a was synthesized from (4-chlorobutyl)benzene (**41a**) (1.00 eq., 13.5 mmol, 2.27 g), *tert*-butyl (benzyloxy)carbamate (**23**) (1.00 eq., 13.5 mmol, 3.01 g) and NaH (1.20 eq., 16.2 mmol, 60% oil dispersion, 0.37 g) in dry DMF (13.5 mL) according to general procedure **2**. 2.95 g of **42a** (68%) was obtained as a colorless oil.

^{1}H-NMR (300 MHz, DMSO-*d6*) δ 7.39 – 7.33 (m, 5H), 7.29 - 7.22 (m, 2H), 7.17 (d, *J* = 7.2 Hz, 3H), 4.75 (s, 2H), 3.44 – 3.36 (m, 2H), 2.62 – 2.53 (m, 2H), 1.53 (dt, *J* = 5.6, 2.4 Hz, 4H), 1.40 (s, 9H).

^{13}C-NMR (75 MHz, DMSO-*d6*) δ 155.57, 141.96, 135.60, 129.24, 128.34, 128.26, 128.20, 125.65, 80.27, 75.78, 48.26, 34.61, 28.05, 27.86, 26.00.

HPLC (Method A): Rt = 19.98 min, purity = 95.1%.

tert-Butyl (benzyloxy)(5-phenylpentyl)carbamate (**42b**)

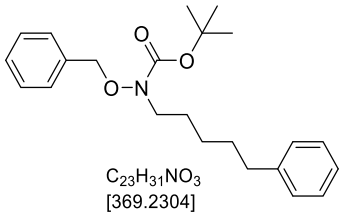

$C_{23}H_{31}NO_3$
[369.2304]

42b was synthesized from (5-chloropentyl)benzene (**41b**) (1.00 eq., 11.0 mmol, 2.00 g), *tert*-butyl (benzyloxy)carbamate (**23**) (1.00 eq., 11.0 mmol, 2.45 g) and NaH (1.20 eq., 13.2 mmol, 60% oil dispersion, 0.30 g) in dry DMF (11 mL) according to general procedure **2**. 2.50 g of **42b** (62%) was obtained as a colorless oil.

^{1}H-NMR (300 MHz, DMSO-*d6*) δ 7.40 – 7.34 (m, 5H), 7.28 - 7.22 (m, 2H), 7.16 (d, *J* = 7.2 Hz, 3H), 4.76 (s, 2H), 3.36 (t, *J* = 7.0 Hz, 2H), 2.55 (d, *J* = 7.6 Hz, 2H), 1.61 – 1.48 (m, 4H), 1.41 (s, 9H), 1.24 (t, *J* = 7.7 Hz, 2H).

^{13}C-NMR (75 MHz, DMSO-*d6*) δ 155.50, 142.10, 135.66, 129.22, 128.31, 128.25, 128.22, 128.17, 125.58, 80.22, 75.72, 48.33, 35.05, 30.57, 27.87, 26.33, 25.71.

HPLC (Method B): Rt = 21.93 min, purity = 95.0%.

tert-Butyl (benzyloxy)(3-(4-fluorophenyl)propyl)carbamate (**59a**)

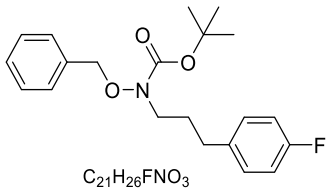

$C_{21}H_{26}FNO_3$
[359.1897]

59a was synthesized from 1-(3-chloropropyl)-4-fluorobenzene (**58a**) (1.00 eq., 4.00 mmol, 0.69 g), *tert*-butyl (benzyloxy)carbamate (**23**) (1.00 eq., 4.00 mmol, 0.89 g) and NaH (1.20 eq., 4.80 mmol, 60% oil dispersion, 0.11 g) in dry DMF (4.00 mL) according to general procedure **2**. 0.95 g of **59a** (66%) was obtained as a colorless oil.

^{1}H-NMR (300 MHz, DMSO-*d6*) δ 7.41 – 7.33 (m, 5H), 7.25 – 7.16 (m, 2H), 7.13 – 7.03 (m, 2H), 4.78 (s, 2H), 3.38 (t, *J* = 7.1 Hz, 2H), 2.55 (t, *J* = 7.6 Hz, 2H), 1.80 (p, *J* = 7.4 Hz, 2H), 1.41 (s, 9H).

^{13}C-NMR (75 MHz, MeOD-*d4*) δ 162.73 (d, $^{1}J_{C\text{-}F}$ = 242.1 Hz), 158.08, 138.71 (d, ^{3}J = 3.2 Hz), 137.04, 131.04, 130.94, 130.57, 129.58, 129.42, 115.92 (d, ^{2}J = 21.3 Hz), 82.67, 77.68, 49.78, 32.96, 29.83, 28.56.

tert-Butyl (benzyloxy)(3-(4-(trifluoromethyl)phenyl)propyl)carbamate (**59b**)

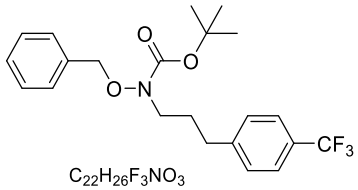

$C_{22}H_{26}F_3NO_3$
[409.1865]

59b was synthesized from 1-(3-chloropropyl)-4-(trifluoromethyl)benzene (**58b**) (1.00 eq., 3.10 mmol, 0.69 g), *tert*-butyl (benzyloxy)carbamate (**23**) (1.00 eq., 3.10 mmol, 0.69 g) and NaH (1.20 eq., 3.72 mmol, 60% oil dispersion, 0.09 g) in dry DMF (4.00 mL) according to general procedure **2**. 0.90 g of **59b** (70%) was obtained as a colorless oil.

^{1}H-NMR (300 MHz, DMSO-*d6*) δ 7.63 (d, *J* = 8.0 Hz, 2H), 7.46 – 7.30 (m, 7H), 4.79 (s, 2H), 3.39 (t, *J* = 7.1 Hz, 2H), 2.66 (t, *J* = 7.6 Hz, 2H), 1.84 (p, *J* = 7.4 Hz, 2H), 1.40 (s, 9H).

tert-Butyl (benzyloxy)(3-(*p*-tolyl)propyl)carbamate (**59c**)

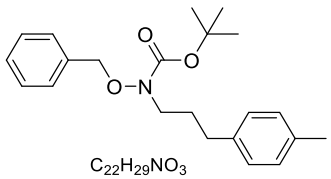

$C_{22}H_{29}NO_3$
[355.2147]

59c was synthesized from 1-(3-chloropropyl)-4-methylbenzene (**58c**) (1.00 eq., 5.00 mmol, 0.84 g), *tert*-butyl (benzyloxy)carbamate (**23**) (1.00 eq., 5.00 mmol, 1.11 g) and NaH (1.20 eq., 6.00 mmol, 60% oil dispersion, 0.14 g) in dry DMF (5.00 mL) according to general procedure **2**. 1.30 g of **59c** (73%) was obtained as a colorless oil.

^{1}H-NMR (300 MHz, CH_3OH+D_2O) δ 7.42 – 7.31 (m, 4H), 7.11 – 6.97 (m, 5H), 4.83 – 4.75 (m, 2H), 3.49 – 3.35 (m, 2H), 2.54 (t, *J* = 7.5 Hz, 2H), 2.28 (s, 3H), 1.85 (p, *J* = 7.6 Hz, 2H), 1.52 – 1.36 (m, 9H).

^{13}C-NMR (75 MHz, MeOD-*d4*) δ 158.08, 139.64, 137.03, 136.34, 130.54, 129.99, 129.54, 129.39, 129.30, 82.60, 77.66, 33.38, 29.80, 28.57, 21.07.

tert-Butyl (benzyloxy)(3-(4-methoxyphenyl)propyl)carbamate (**59d**)

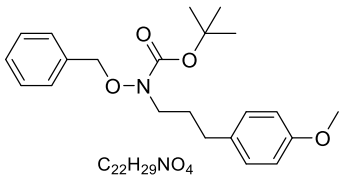

$C_{22}H_{29}NO_4$
[371.2097]

59d was synthesized from 1-(3-chloropropyl)-4-methoxybenzene (**58d**) (1.00 eq., 9.00 mmol, 1.66 g), *tert*-butyl (benzyloxy)carbamate (**23**) (1.00 eq., 9.00 mmol, 2.01 g) and NaH (1.20 eq., 10.8 mmol, 60% oil dispersion, 0.25 g) in dry DMF (9.00 mL) according to general procedure **2**. 2.50 g of **59d** (75%) was obtained as a colorless oil.

^{1}H-NMR (300 MHz, DMSO-*d6*) δ 7.45 – 7.33 (m, 5H), 7.17 - 7.07 (m, 2H), 6.91 – 6.82 (m, 2H), 4.81 (s, 2H), 3.74 (s, 3H), 3.40 (t, *J* = 7.2 Hz, 2H), 2.56 – 2.51 (m, 2H), 1.81 (p, *J* = 7.4 Hz, 2H), 1.44 (s, 9H).

^{13}C-NMR (75 MHz, MeOD-*d4*) δ 159.41, 158.12, 137.05, 134.76, 130.57, 130.31, 129.56, 129.41, 114.82, 82.64, 77.67, 55.63, 49.71, 32.93, 29.95, 28.57.

tert-Butyl (benzyloxy)(3-(3,5-difluorophenyl)propyl)carbamate (**59e**)

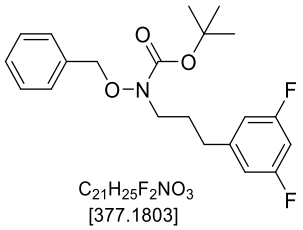

$C_{21}H_{25}F_2NO_3$
[377.1803]

59e was synthesized from 1-(3-chloropropyl)-3,5-difluorobenzene (**58e**) (1.00 eq., 3.70 mmol, 0.70 g), *tert*-butyl (benzyloxy)carbamate (**23**) (1.00 eq., 3.70 mmol, 0.83 g) and NaH (1.20 eq., 4.44 mmol, 60% oil dispersion, 0.10 g) in dry DMF (13.5 mL) according to general procedure **2**. 0.45 g of **59e** (32%) was obtained as a colorless oil.

^{1}H-NMR (300 MHz, DMSO-*d6*) δ 7.43 – 7.30 (m, 5H), 7.07 – 6.91 (m, 3H), 4.79 (s, 2H), 3.37 (t, *J* = 7.1 Hz, 2H), 2.60 (t, *J* = 7.5 Hz, 2H), 1.82 (p, *J* = 7.4 Hz, 2H), 1.41 (s, 9H).

^{13}C-NMR (75 MHz, MeOD-*d4*) δ 164.48 (dd, $^{1}J_{C\text{-}F}$ = 246.6, $^{3}J_{C\text{-}F}$ =13.0 Hz), 158.03, 147.45 (t, $^{3}J_{C\text{-}F}$ = 9.1 Hz), 137.02, 130.61, 129.61, 129.44, 112.35 (d, $^{2}J_{C\text{-}F}$ = 7.6 Hz), 112.12 (d, $^{2}J_{C\text{-}F}$ = 7.5 Hz), 102.06 (t, $^{2}J_{C\text{-}F}$ = 25.8 Hz), 82.77, 77.70, 33.42, 29.08, 28.55.

General procedure **3** for the Boc-deprotection to synthesize compounds **26a-e**, **43a,b**, and **60a-e**

N-Boc-deprotection was performed using two different experimental procedures:

Method I: using the procedure reported by SHENDAGE et al.[147]

1.00 eq. of the respective Boc-protected hydroxylamine (**25c-e**) was dissolved in a mixture of TFA/DCM (1:1, 10 mL/mmol) and stirred for 3 h at r.t.. The solvent was evaporated under reduced pressure. The resulting residue was neutralized with 2N KOH and extracted with DCM (3x10 mL). The DCM phase was dried over Na_2SO_4, filtered, and the solvent was evaporated under reduced pressure. The crude products were purified by flash chromatography (on a prepacked silica cartridge) using *n*-hexane/EtOAc (100:0-80:20) as eluent to afford the *N*-substituted *O*-benzyl protected hydroxylamine (**26c-e**).

O-Benzyl-*N*-(4-isopropylbenzyl)hydroxylamine (**26c**)

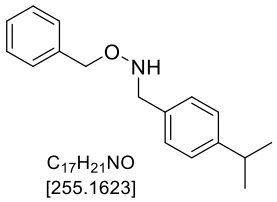

$C_{17}H_{21}NO$
[255.1623]

26c was synthesized from *tert*-butyl (benzyloxy)(4-isopropylbenzyl)carbamate (**25c**) (1.00 eq., 6.50 mmol, 2.30 g) and TFA/DCM (1:1, 10 mL/mmol, 65 mL) according to general procedure **3** Method I. 0.85 g of **26c** (70%) was obtained as a colorless oil.

^{1}H-NMR (300 MHz, DMSO-d_6) δ 7.38 – 7.20 (m, 7H), 7.17 (d, J = 8.1 Hz, 2H), 6.85 (t, J = 6.4 Hz, 1H), 4.57 (s, 2H), 3.89 (d, J = 6.3 Hz, 2H), 2.86 (p, J = 6.9 Hz, 1H), 1.19 (d, J = 7.0 Hz, 6H).

^{13}C-NMR (151 MHz, DMSO-d_6) δ 146.95, 138.37, 135.81, 128.72, 128.06, 127.35, 125.89, 74.91, 55.04, 33.12, 23.94.

HPLC (Method A): Rt = 12.47 min, purity = 98.4%.

N-([1,1'-Biphenyl]-4-ylmethyl)-O-benzylhydroxylamine (**26d**)

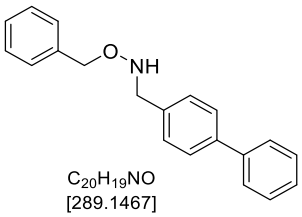

$C_{20}H_{19}NO$
[289.1467]

26d was synthesized from *tert*-butyl ([1,1'-biphenyl]-4-ylmethyl)(benzyloxy)carbamate (**25d**) (1.00 eq., 3.70 mmol, 1.40 g) and TFA/DCM (1:1, 10 mL/mmol, 37 mL) according to general procedure **3** Method I. 0.72 g of **26d** (70%) was obtained as a colorless oil.

^{1}H-NMR (300 MHz, DMSO-d_6) δ 7.68 – 7.58 (m, 4H), 7.49 – 7.41 (m, 4H), 7.39 – 7.23 (m, 6H), 6.98 (t, J = 6.2 Hz, 1H), 4.59 (s, 2H), 3.98 (d, J = 6.2 Hz, 2H).

^{13}C-NMR (151 MHz, DMSO-d_6) δ 140.05, 138.74, 138.35, 137.92, 129.29, 128.90, 128.09, 128.07, 127.38, 127.27, 126.56, 126.32, 74.97, 54.92.

HPLC (Method A): Rt = 13.31 min, purity = 97.3%.

mp.: 156.9 °C.

O-Benzyl-*N*-(naphthalen-2-ylmethyl)hydroxylamine (**26e**)

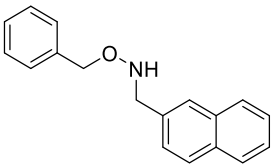

$C_{18}H_{18}ClNO$
[263.1310]

26e was synthesized from *tert*-butyl (benzyloxy)(naphthalen-2-ylmethyl)carbamate (**25e**) (1.00 eq., 3.70 mmol, 1.40 g) and TFA/DCM (1:1, 10 mL/mmol, 37 mL) according to general procedure **3** Method I. 1.12 g of **26e** (97%) was obtained as a white powder.

^{1}H-NMR (300 MHz, DMSO-d_6) δ 7.91 – 7.82 (m, 4H), 7.54 (dd, J = 8.4, 1.7 Hz, 1H), 7.51 – 7.46 (m, 2H), 7.34 – 7.21 (m, 5H), 7.07 (t, J = 6.0 Hz, 1H), 4.57 (s, 2H), 4.11 (d, J = 6.0 Hz, 2H).

^{13}C-NMR (75 MHz, DMSO-d_6) δ 138.33, 136.34, 132.87, 132.19, 128.07, 128.04, 127.52, 127.49, 127.43, 127.38, 127.20, 127.08, 125.98, 125.56, 75.03, 55.43.

HPLC (Method B): Rt = 17.20 min, purity = 98.3%.

mp.: 162.5 °C.

Method II:

1.00 eq. of the respective Boc-protected hydroxylamine (**25a,b**, **42a,b**, and **59a-e**) was dissolved in dioxane (2.00 mL/mmol), and 4 M HCl/dioxane (10.0 eq.) was added in one portion while stirring. The mixture was stirred at r.t for 4 h. The solvent was completely removed by rotary evaporation *in vacuo* at room temperature. The white solid was then washed with dry ether and separated by filtration to afford the *N*-substituted *O*-benzyl protected hydroxylamine hydrochloride (**26a,b**, **43a,b**, and **60a-e**).

O-Benzyl-*N*-phenethylhydroxylamine hydrochloride (**26a**)

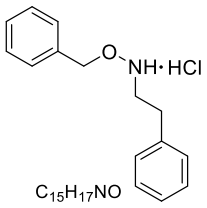

$C_{15}H_{17}NO$
[263.1077]

26a was synthesized from *tert*-butyl (benzyloxy)(phenethyl)carbamate (**25a**) (1.00 eq., 7.00 mmol, 2.30 g) and 4 M HCl/dioxane (10.0 eq.,70.0 mmol, 17.5 mL) in dioxane (15.0 mL) according to general procedure **3** Method II. 1.00 g of **26a** (63%) was obtained as a colorless oil.

^{1}H-NMR (300 MHz, DMSO-*d6*) δ 12.23 (s, 2H), 7.47 – 7.18 (m, 10H), 5.15 (s, 2H), 3.51 – 3.40 (m, 2H),3.07 – 2.95 (m, 2H).

^{13}C-NMR (75 MHz, DMSO-*d6*) δ 138.32, 136.33, 132.87, 128.03, 127.52, 127.43, 127.19, 125.97, 75.03, 55.43.

HPLC (Method B): Rt = 16.66 min, purity = 94.8%.

O-Benzyl-*N*-(3-phenylpropyl)hydroxylamine hydrochloride (**26b**)

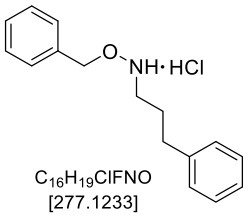

$C_{16}H_{19}ClFNO$
[277.1233]

26b was synthesized from *tert*-butyl (benzyloxy)(3-phenylpropyl)carbamate (**25b**) (1.00 eq., 7.50 mmol, 2.30 g) and 4 M HCl/dioxane (10.0 eq.,75.0 mmol, 18.8 mL) in dioxane (15.0 mL) according to general procedure **3** Method II. 2.00 g of **26b** (95%) was obtained as a white powder.

^{1}H-NMR (300 MHz, DMSO-d_6) δ 12.27 (s, 1H), 7.46 – 7.39 (m, 5H), 7.35 – 7.26 (m, 2H), 7.25 – 7.17 (m, 3H), 5.14 (s, 2H), 3.28 – 3.12 (m, 2H), 2.69 (t, J = 7.8 Hz, 2H), 2.05 – 1.89 (m, 2H).

^{13}C-NMR (75 MHz, MeOH-d_4) δ 142.36, 134.15, 130.76, 130.68, 129.96, 128.70, 128.62, 77.44, 39.99, 35.36.

HPLC (Method B): Rt = 16.25 min, purity = 98.1%.

mp.: 130.1 °C.

O-Benzyl-*N*-(4-phenylbutyl)hydroxylamine hydrochloride (**43a**)

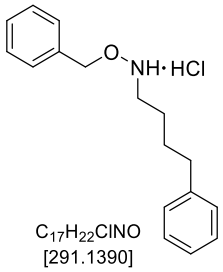

$C_{17}H_{22}ClNO$
[291.1390]

43a was synthesized from *tert*-butyl (benzyloxy)(4-phenylbutyl)carbamate (**42a**) (1.00 eq., 7.00 mmol, 2.48 g) and 4 M HCl/dioxane (10.0 eq.,70.0 mmol, 17.5 mL) in dioxane (15.0 mL) according to general procedure **3** Method II. 1.93 g of **43a** (62%) was obtained as white crystals.

^{1}H-NMR (300 MHz, DMSO-d_6) δ 12.23 (s, 1H), 7.41 (s, 5H), 7.32 – 7.23 (m, 2H), 7.23 – 7.13 (m, 3H), 5.13 (s, 2H), 3.22 (d, J = 13.2 Hz, 2H), 2.65 – 2.54 (m, 2H), 1.66 (p, J = 3.5 Hz, 4H).

^{13}C-NMR (75 MHz, DMSO-d_6) δ 141.61, 133.75, 129.22, 129.06, 128.61, 128.32, 128.27, 125.79, 74.47, 48.04, 34.53, 27.83, 22.90.

HPLC (Method B): Rt = 17.13 min, purity = 96.8%.

mp.: 118.0 ˚C.

O-Benzyl-*N*-(5-phenylpentyl)hydroxylamine hydrochloride (**43b**)

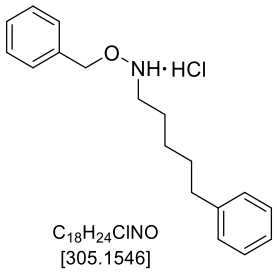

43b was synthesized from *tert*-butyl (benzyloxy)(5-phenylpentyl)carbamate (**42b**) (1.00 eq., 8.00 mmol, 2.95 g) and 4 M HCl/dioxane (10.0 eq.,80.0 mmol, 20.0 mL) in dioxane (15.0 mL) according to general procedure **3** Method II. 1.70 g of **43b** (67%) was obtained as white crystals.

^{1}H-NMR (300 MHz, MeOH-d_4) δ 7.42 (dq, J = 7.0, 3.6 Hz, 5H), 7.21 (d, J = 2.2 Hz, 2H), 7.19 – 7.09 (m, 3H), 5.13 (s, 2H), 3.30(d, J = 15.6 Hz, 2H), 2.61 (t, J = 7.5 Hz, 2H), 1.82 – 1.69 (m, 2H), 1.69 – 1.56 (m, 2H), 1.48 – 1.36 (m, 2H).

^{13}C-NMR (75 MHz, MeOH-d_4) δ 143.31, 134.12, 130.79, 130.52, 130.01, 129.42, 129.36, 126.85, 77.31, 50.65, 36.48, 32.06, 27.05, 24.68.

mp.: 126.8 ˚C.

HPLC (**Method B**): Rt = 11.11 min, purity > 99.0%.

O-Benzyl-*N*-(3-(4-fluorophenyl)propyl)hydroxylamine hydrochloride (**60a**)

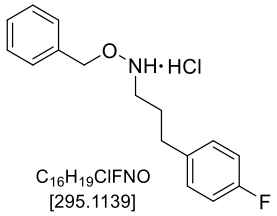

60a was synthesized from *tert*-butyl (benzyloxy)(3-(4-fluorophenyl)propyl)carbamate (**59a**) (1.00 eq., 2.30 mmol, 0.83 g) and 4 M HCl/dioxane (10.0 eq., 23.0 mmol, 5.75 mL) in dioxane (5.00 mL) according to general procedure **3** Method II. 0.62 g of **60a** (91%) was obtained as a white powder.

^{1}H-NMR (300 MHz, DMSO-d_6) δ 12.23 (s, 1H), 7.42 (d, J = 1.8 Hz, 5H), 7.32 – 7.18 (m, 2H), 7.18 – 7.04 (m, 2H), 5.13 (s, 2H), 3.16 (d, J = 7.5 Hz, 2H), 2.68 (t, J = 7.7 Hz, 2H), 1.94 (p, J = 7.7 Hz, 2H).

^{13}C-NMR (75 MHz, DMSO-d_6) δ 159.15, 136.19, 134.59, 130.05 (d, $^{3}J_{C\text{-}F}$ = 7.8 Hz), 129.49, 129.16, 128.60, 115.09 (d, $^{2}J_{C\text{-}F}$ = 21.0 Hz), 74.58, 38.19, 30.93, 28.81.

mp.: 135.4 ˚C.

HPLC (**Method B**): Rt = 10.47 min, purity > 99.0%.

O-Benzyl-*N*-(3-(4-(trifluoromethyl)phenyl)propyl)hydroxylamine hydrochloride (**60b**)

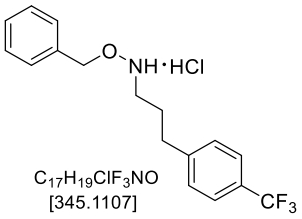

60b was synthesized from *tert*-butyl (benzyloxy)(3-(4-fluorophenyl)propyl)carbamate (**59b**) (1.00 eq., 2.10 mmol, 0.86 g) and 4 M HCl/dioxane (10.0 eq., 21.0 mmol, 5.25 mL) in dioxane (4.0 mL) according to general procedure **3** Method II. 0.59 g of **60b** (82%) was obtained as a white powder.

^{1}H-NMR (300 MHz, DMSO-*d6*) δ 12.19 (s, 1H), 7.66 (d, *J* = 8.0 Hz, 2H), 7.50 – 7.36 (m, 7H), 5.12 (s, 2H), 3.26 - 3.15 (m, 2H), 2.79 (t, *J* = 7.8 Hz, 2H), 1.98 (p, *J* = 7.8 Hz, 2H).

^{13}C-NMR (75 MHz, DMSO-*d6*) δ 145.86, 134.59, 129.49, 129.14, 128.59, 127.19 (q, $^{1}J_{C\text{-}F}$ = 197.8 Hz), 125.29, 125.24, 74.62, 38.18, 31.56, 28.36.

mp.: 138.3 ˚C.

O-Benzyl-*N*-(3-(*p*-tolyl)propyl)hydroxylamine hydrochloride (**60c**)

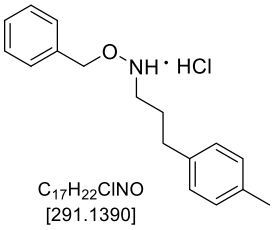

60c was synthesized from *tert*-butyl (benzyloxy)(3-(4-methoxyphenyl)propyl)carbamate (**59c**) (1.00 eq., 1.70 mmol, 0.60 g) and 4 M HCl/dioxane (10.0 eq.,17.0 mmol, 4.25 mL) in dioxane (3.50 mL) according to general procedure **3** Method II. 0.40 g of **60c** (82%) was obtained as a white powder.

^{1}H-NMR (300 MHz, MeOH-d_4) δ 7.46 – 7.43 (m, 4H), 7.11 (d, *J* = 1.2 Hz, 5H), 5.12 (s, 2H), 3.34 (d, *J* = 5.4 Hz, 2H), 2.71 (t, *J* = 7.6 Hz, 3H), 2.30 (s, 4H), 2.13 – 1.97 (m, 2H).

^{13}C-NMR (75 MHz, MeOH-d_4) δ 138.29, 137.11, 134.08, 130.81, 130.52, 130.28, 130.01, 129.29, 77.34, 50.16, 32.98, 26.60, 21.03.

mp.: 114.4 ˚C.

HPLC (**Method B**): Rt = 10.46 min, purity = 98.7%.

O-Benzyl-*N*-(3-(4-methoxyphenyl)propyl)hydroxylamine hydrochloride (**60d**)

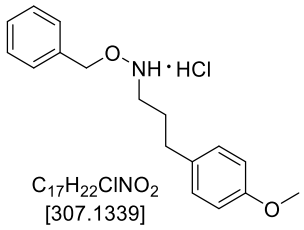

60d was synthesized from *tert*-butyl (benzyloxy)(3-(4-methoxyphenyl)propyl)carbamate (**59d**) (1.00 eq., 3.30 mmol, 1.22 g) and 4 M HCl/dioxane (10.0 eq.,33.0 mmol, 8.25 mL) in dioxane (7.0 mL) according to general procedure **3** Method II. 0.95 g of **60d** (94%) was obtained as a white powder.

^{1}H-NMR (300 MHz, DMSO-*d6*) δ 12.31 (s, 1H), 7.42 (d, *J* = 2.2 Hz, 5H), 7.17 – 7.07 (m, 2H), 6.91 – 6.80 (m, 2H), 5.14 (s, 2H), 3.72 (s, 3H), 3.17 (d, *J* = 7.6 Hz, 2H), 2.62 (t, *J* = 7.6 Hz, 2H), 1.92 (p, *J* = 7.8 Hz, 2H).

^{13}C-NMR (75 MHz, MeOH-*d4*) δ 159.81, 134.08, 133.32, 130.79, 130.54, 130.36, 130.00, 115.06, 77.33, 55.67, 50.14, 32.53, 26.73.

mp.: 124.1 ˚C.

HPLC (Method B): Rt = 10.37 min, purity = 97.0%.

O-Benzyl-*N*-(3-(3,5-difluorophenyl)propyl)hydroxylamine hydrochloride (**60e**)

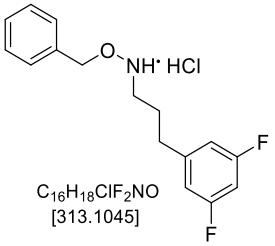

60e was synthesized from *tert*-butyl (benzyloxy)(3-(4-fluorophenyl)propyl)carbamate (**59e**) (1.00 eq., 1.06 mmol, 0.40 g) and 4 M HCl/dioxane (10.0 eq.,10.6 mmol, 2.65 mL) in dioxane (2.12 mL) according to general procedure **3** Method II. 0.53 g of **60e** (60%) was obtained as a white powder.

^{1}H-NMR (300 MHz, MeOD-*d4*) δ 7.45 (q, *J* = 2.1 Hz, 5H), 6.93 – 6.73 (m, 3H), 3.43 – 3.32 (m, 2H), 2.77 (t, *J* = 7.8 Hz, 2H), 2.15 – 1.99 (m, 2H).

mp.: 97.3 ˚C.

General procedure **4** for the synthesis of compounds **37a,b**

To a solution of 6-chloronicotinamide (**35**) (1.00 eq., 3.20 mmol, 0.50 g) in isoamyl alcohol (15.0 mL) at r.t. was added Na_2CO_3 (1.20 eq., 3.84 mmol, 0.40 g) followed by the corresponding diamine (1.20 eq.). The mixture was heated in MW 150 W at 130 ˚C for 2 h, cooled to r.t., and filtered through a medium glass-fritted filter. The resulting filtrate was concentrated under reduced pressure, and the resultant powder was triturated with diethyl ether (2 x 10 mL). The crude solid was dried *in vacuo* to afford the corresponding product.

4-((2-Aminoethyl)amino)benzamide (**37a**)

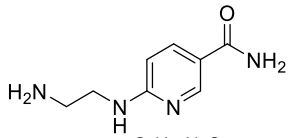

$C_8H_{12}N_4O$
[180.1011]

37a was synthesized from ethane-1,2-diamine (**36a**) (1.20 eq., 0.34 mL, 0.23 g) according to general procedure **4**. 1.20 g of **37a** (70%) was obtained as a yellow powder.

^{1}H-NMR (300 MHz, DMSO-*d6*) δ 8.50 (d, J = 2.5 Hz, 1H), 7.79 (dd, J = 8.8, 2.5 Hz, 1H), 7.64 (s, 1H), 7.03 (t, J = 5.8 Hz, 2H), 6.44 (d, J = 9.6 Hz, 1H), 3.26 (q, J = 6.4 Hz, 2H), 2.68 (t, J = 6.4 Hz, 2H), 1.55 (s, 2H).

^{13}C-NMR (75 MHz, DMSO-*d6*) δ 167.03, 160.33, 148.64, 135.84, 117.30, 106.73, 44.40, 41.16.

HPLC (Method C): Rt = 1.94 min, purity > 99.0%.

mp.: 153.8 ˚C.

4-((3-Aminopropyl)amino)benzamide (**37b**)

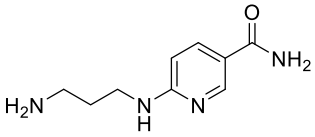

$C_9H_{14}N_4O$
[194.1168]

37b was synthesized from propane-1,3-diamine (**36b**) (1.20 eq., 0.32 mL, 0.28 g) according to general procedure **4**. 0.25 g of **37b** (44%) was obtained as a white powder.

^{1}H-NMR (300 MHz, DMSO-*d6*) δ 8.57 – 8.49 (m, 1H), 7.85 (dd, J = 8.9, 2.4 Hz, 1H), 6.57 – 6.46 (m, 1H), 3.46 – 3.37 (m, 2H), 2.74 (t, J = 7.1 Hz, 2H), 1.71 (s, 2H).

^{13}C-NMR (75 MHz, MeOD-*d4*) δ 171.32, 166.97, 154.84, 137.93, 126.22, 120.25, 41.01, 38.18, 27.17.

mp.: 194.5 ˚C

Synthesis of diethyl (3,4-difluorobenzyl)phosphonate (**49**)

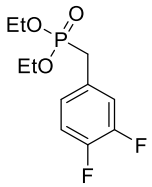

$C_{11}H_{15}F_2O_3P$
[264.0727]

49 was synthesized according to the procedures reported by LION et al.[163]

All spectroscopic data are in agreement with published data.[163]

Synthesis of diethyl (1-(3,4-difluorophenyl)-3-(1,3-dioxolan-2-yl)propyl)phosphonate (**50**)

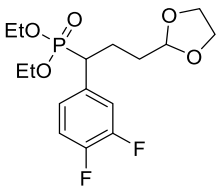

$C_{16}H_{23}F_2O_5P$
[364.1251]

Dioxolane **50** was synthesized according to the procedure reported by BEHRENDT et al. [134]

All spectroscopic data are in agreement with published data. [134]

Synthesis of diethyl (1-(3,4-difluorophenyl)-4-oxobutyl)phosphonate (**51**)

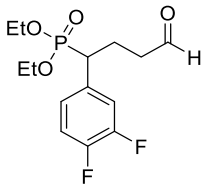

$C_{14}H_{19}F_2O_4P$
[320.0989]

Aldehyde **51** was synthesized according to the procedure reported by BEHRENDT et al. [134]

All spectroscopic data were in agreement with literature. [134]

4-(Diethoxyphosphoryl)-4-(3,4-difluorophenyl)butanoic acid (**52**)

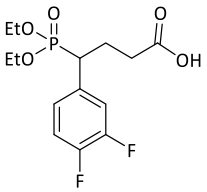

$C_{14}H_{19}F_2O_5P$
[336.09]

Carboxylic acid was **52** synthesized according to the procedure reported by BEHRENDT et al. [134]

All spectroscopic data are in agreement with published data. [134]

8.3.2 Synthesis of target compounds

8.3.2.1 Synthesis of phosphonate ester intermediates

General procedure **5** for HATU coupling reaction for the synthesis of **28a-g**, **29a-e**, **30a-c**, **38a**,**b**, **44a**,**b**, **35a-d**, **53a-d**, **61a-d**, and **64**.

To a solution of carboxylic acid **15** or **52** (1.00 eq.) in dry DMF (5 mL/mmol), HATU (1.00 eq.) and DIPEA were added (2.00 eq. DIPEA for the *O*-substituted hydroxylamines **22a-g**, amines **27a-c** and **37a,b**, and the free bases of hydroxylamines **26c-e** or 3.00 eq. DIPEA for the hydroxylamine hydrochlorides **26a,b**, **43a,b**, and **60a-e**). The mixture was allowed to stir for 15 min at r.t., the corresponding benzyl-protected hydroxylamine was added, and the reaction mixture was stirred for further 16 h at r.t.. The reaction was quenched with water and extracted with EtOAc (3 x 10 mL). The EtOAc phase was then washed with saturated Na_2CO_3 solution (3 x 10 mL), with 10% acetic acid (1 x 10 mL), and with brine (1 x 10 mL). The organic phase was then dried over anhydrous Na_2SO_4, filtered, and the solvent was evaporated under reduced pressure. The crude product was purified using flash chromatography (on a prepacked silica cartridge) using DCM:30% methanol/DCM (100:0→70:30) as eluent.

Diethyl (4-oxo-1-phenyl-4-(((2-phenyloxazol-4-yl)methoxy)amino)butyl)phosphonate (**28a**)

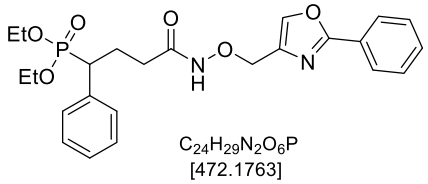

$C_{24}H_{29}N_2O_6P$
[472.1763]

28a was synthesized from **15** (1.00 eq, 1.80 mmol, 0.54 g), HATU (1.00 eq., 1.80 mmol, 0.68 g), and DIPEA (2.00 eq., 3.60 mmol, 0.47 g, 0.63 mL), and *O*-((2-phenyloxazol-4-yl)methyl)hydroxylamine (**22a**) (1.00 eq., 2.00 mmol, 0.34 g) in dry DMF (10 mL) according to general procedure **5**. 0.75 g of **28a** (88%) was obtained as a yellow oil.

^{1}H-NMR (300 MHz, DMSO-*d6*) δ 10.93 (s, 1H), 7.98 – 7.87 (m, 2H), 7.73 (s, 1H), 7.57 – 7.45 (m, 3H), 7.37 – 7.21 (m, 5H), 4.89 (s, 2H), 4.04 – 3.90 (m, 2H), 3.86 – 3.62 (m, 2H), 3.21 – 3.07 (m, 1H), 2.31 – 2.15 (m, 1H), 2.09 -1.95 (m, 1H), 1.84 (t, J = 7.5 Hz, 2H), 1.20 (t, J = 7.0 Hz, 3H), 1.01 (t, J = 7.0 Hz, 3H).

^{13}C-NMR (75 MHz, DMSO-*d6*) δ 168.63, 167.11, 152.32, 135.86 (d, $J_{c\text{-}p}$ = 6.6 Hz), 132.92, 130.33, 129.18, 128.32 (d, $J_{c\text{-}p}$ = 2.4 Hz), 126.99 (d, $J_{c\text{-}p}$ = 3.1 Hz), 126.12, 119.66, 71.84, 61.69 (d, $J_{c\text{-}p}$ = 6.9 Hz), 61.33 (d, $J_{c\text{-}p}$ = 6.9 Hz), 42.35 (d, $J_{c\text{-}p}$ = 136.1 Hz), 29.95 (d, $J_{c\text{-}p}$ = 15.7 Hz), 25.21, 16.27 (d, $J_{c\text{-}p}$ = 5.7 Hz), 16.04 (d, $J_{c\text{-}p}$ = 5.5 Hz).

HPLC (Method A): Rt = 12.20 min, purity = 95.4%.

Diethyl (4-oxo-1-phenyl-4-(((2-phenylthiazol-4-yl)methoxy)amino)butyl)phosphonate (**28b**)

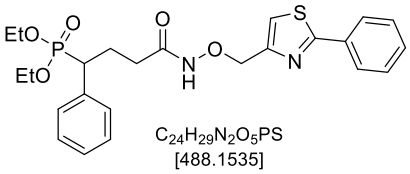

28b was synthesized from **15** (1.00 eq, 1.70 mmol, 0.51 g), HATU (1 eq., 1.70 mmol, 0.66 g), DIPEA (2.00 eq., 3.40 mmol, 0.44 g, 0.59 mL) and *O*-((2-phenylthiazol-4-yl)methyl)hydroxylamine (**22b**) (1.00 eq., 2.00 mmol, 0.38 g) in dry DMF (10 mL) according to general procedure **5**. 0.57 g of **28b** (69%) was obtained as an orange oil.

^{1}H-NMR (300 MHz, DMSO-*d6*) δ 10.88 (s, 1H), 8.23 (s, 1H), 8.04 – 7.90 (m, 2H), 7.62 – 7.46 (m, 3H), 7.37 – 7.19 (m, 5H), 4.73 (s, 2H), 4.09 – 3.89 (m, 2H), 3.89 – 3.60 (m, 2H), 3.25 – 3.06 (m, 1H), 2.32 – 1.97 (m, 2H), 1.84 (t, J = 7.6 Hz, 2H), 1.20 (t, J = 7.0 Hz, 3H), 1.01 (t, J = 7.0 Hz, 3H).

^{13}C-NMR (75 MHz, DMSO-*d6*) δ 168.61, 160.75, 139.14, 136.83, 135.88 (d, $J_{c\text{-}p}$ = 6.7 Hz), 130.75, 129.15 (d, $J_{c\text{-}p}$ = 5.8 Hz), 128.32 (d, $J_{c\text{-}p}$ = 2.4 Hz), 126.99 (d, $J_{c\text{-}p}$ = 3.0 Hz), 126.76, 125.93, 67.95, 61.70 (d, $J_{c\text{-}p}$ = 6.9 Hz), 61.33 (d, $J_{c\text{-}p}$ = 6.9 Hz), 42.38 (d, $J_{c\text{-}p}$ = 136.0 Hz), 29.97 (d, $J_{c\text{-}p}$ = 15.6 Hz), 25.21, 16.26 (d, $J_{c\text{-}p}$ = 5.6 Hz), 16.04 (d, $J_{c\text{-}p}$ = 5.6 Hz).

HPLC (Method A): Rt = 11.73 min, purity = 98.0%.

Diethyl (4-oxo-4-(phenethoxyamino)-1-phenylbutyl)phosphonate (**28c**)

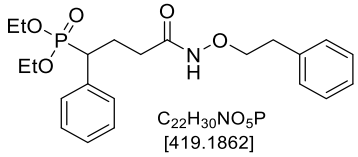

28c was synthesized from **15** (1.00 eq., 2.00 mmol, 0.60 g), HATU (1.00 eq., 2.00 mmol, 0.76 g), DIPEA (2.00 eq., 4.00 mmol, 0.52 g, 0.70 mL) and *O*-phenylethylhydroxylamine (**22c**) (1.00 eq., 2.00 mmol, 0.27 g) in dry DMF (10 mL) according to general procedure **5**. 0.66 g of **28c** (80%) was obtained as a colorless oil.

^{1}H-NMR (300 MHz, MeOD-*d4*) δ 10.86 (s, 1H), 7.40 – 7.08 (m, 10H), 4.06 – 3.61 (m, 6H), 3.26 – 3.07 (m, 1H), 2.83 (t, J = 6.8 Hz, 2H), 2.33 – 1.90 (m, 2H), 1.84 (t, J = 7.4 Hz, 2H), 1.21 (t, J = 7.0 Hz, 3H), 1.02 (t, J = 7.0 Hz, 3H).

^{13}C-NMR (75 MHz, MeOD-*d4*) δ 168.49, 138.34, 135.88 (d, $J_{c\text{-}p}$ = 6.6 Hz), 129.15 (d, $J_{c\text{-}p}$ = 6.7 Hz), 128.79, 128.34 (d, $J_{c\text{-}p}$ = 2.5 Hz), 128.24, 127.00 (d, $J_{c\text{-}p}$ = 3.0 Hz), 126.13, 75.55, 61.69 (d, $J_{c\text{-}p}$ = 6.9 Hz), 61.32 (d, $J_{c\text{-}p}$ = 7.0 Hz), 42.41 (d, $J_{c\text{-}p}$ = 136.1 Hz), 33.86, 29.97 (d, $J_{c\text{-}p}$ = 15.6 Hz), 25.22, 16.15 (dd, $J_{c\text{-}p}$ = 16.8, 5.6 Hz).

HPLC (Method B): Rt = 11.90 min, purity = 96.8%.

Diethyl (4-oxo-1-phenyl-4-((3-phenylpropoxy)amino)butyl)phosphonate (**28d**)

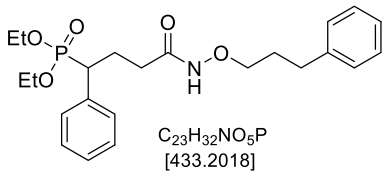

$C_{23}H_{32}NO_5P$
[433.2018]

28d synthesized from **15** (1.00 eq., 3.00 mmol, 0.90 g), HATU (1.00 eq., 3.00 mmol, 1.14 g), DIPEA (2.00 eq., 6.00 mmol, 0.78 g, 1.05 mL) and *O*-(3-phenylpropyl)hydroxylamine (**22d**) (1.00 eq., 3.00 mmol, 0.45 g) in dry DMF (10 mL) according to general procedure **5**. 0.70 g of **28d** (81%) was obtained as a colorless oil.

^{1}H-NMR (300 MHz, DMSO-*d*$_6$) δ 10.80 (s, 1H), 7.41 – 7.08 (m, 10H), 4.03 – 3.90 (m, 2H), 3.87 – 3.63 (m, 4H), 3.21 – 3.10 (m, 1H), 2.63 (t, J = 7.7 Hz, 2H), 2.28 – 2.15 (m, 1H), 2.08 – 1.94 (m, 1H), 1.89 – 1.64 (m, 4H), 1.20 (t, J = 7.0 Hz, 3H), 1.01 (t, J = 7.0 Hz, 3H).

^{13}C-NMR (151 MHz1 MHz, DMSO-*d*$_6$) δ 168.33, 141.58, 135.86 (d, $J_{C\text{-}P}$ = 7.0 Hz), 129.14 (d, $J_{C\text{-}P}$ = 6.7 Hz), 128.30 (d, $J_{C\ P}$ = 6.3 Hz), 127.00, 125.76, 74.28, 61.68 (d, $J_{C\text{-}P}$ = 7.0 Hz), 61.31 (d, $J_{C\text{-}P}$ = 6.7 Hz), 42.38 (d, $J_{C\text{-}P}$ = 135.7 Hz), 31.34, 29.95 (d, $J_{C\text{-}P}$ = 15.3 Hz), 29.48, 25.22, 16.26 (d, $J_{C\text{-}P}$ = 5.5 Hz), 16.04 (d, $J_{C\text{-}P}$ = 5.5 Hz).

HPLC (Method B): Rt = 12.41 min, purity = 97.0%.

Diethyl (4-(((4-isopropylbenzyl)oxy)amino)-4-oxo-1-phenylbutyl)phosphonate (**28e**)

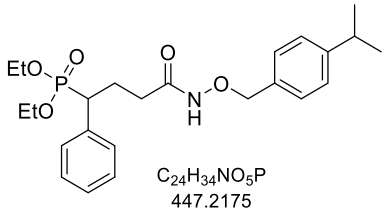

$C_{24}H_{34}NO_5P$
447.2175

28e was synthesized from **15** (1.00 eq., 2.00 mmol, 0.60 g), HATU (1.00 eq., 2.00 mmol, 0.76 g), DIPEA (2.00 eq., 4.00 mmol, 0.52 g, 0.70 mL) and *O*-(4-isopropylbenzyl)hydroxylamine (**22e**) (1.00 eq., 2.00 mmol, 0.33 g) according to general procedure **5**. 0.60 g of **28e** (70%) was obtained as a colorless oil.

^{1}H-NMR (300 MHz, DMSO-*d6*) δ 10.83 (s, 1H), 7.38 – 7.19 (m, 9H), 4.69 (s, 2H), 4.04 – 3.94 (m, 2H), 3.86 – 3.65 (m, 2H), 3.22 – 3.04 (m, 1H), 2.88 (p, J = 6.9 Hz, 1H), 2.30 – 1.99 (m, 2H), 1.81 (t, J = 7.6 Hz, 2H), 1.22 – 1.16 (m, 9H), 1.02 (t, J = 7.0 Hz, 3H).

^{13}C-NMR (75 MHz, DMSO-*d6*) δ 168.48, 148.44, 135.85 (d, $J_{c\text{-}p}$ = 6.6 Hz), 133.52, 129.16 (d, $J_{c\text{-}p}$ = 6.7 Hz), 128.89, 128.32 (d, $J_{c\text{-}p}$ = 2.5 Hz), 126.97 (d, $J_{c\text{-}p}$ = 3.0 Hz), 126.17, 76.49, 61.69 (d, $J_{c\text{-}p}$ = 6.8 Hz), 61.32 (d, $J_{c\text{-}p}$ = 6.9 Hz), 54.90, 42.34 (d, $J_{c\text{-}p}$ = 136.1 Hz), 33.21, 29.95 (d, $J_{c\text{-}p}$ = 15.6 Hz), 25.23, 23.84, 16.27 (d, $J_{c\text{-}p}$ = 5.6 Hz), 16.04 (d, $J_{c\text{-}p}$ = 5.6 Hz).

^{31}P-NMR (121 MHz, MeOD-*d4*) δ 28.63.

HPLC (Method C): Rt = 13.40 min, purity = 98.7%.

Diethyl (4-(([1,1'-biphenyl]-4-ylmethoxy)amino)-4-oxo-1-phenylbutyl)phosphonate (**28f**)

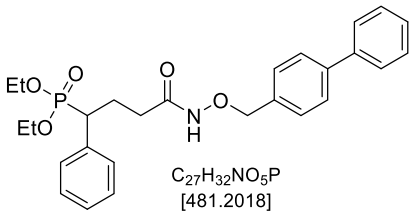

28f was synthesized from **15** (1.00 eq., 2.00 mmol, 0.60 g), HATU (1.00 eq., 2.00 mmol, 0.76 g), DIPEA (3.00 eq., 6.00 mmol, 0.78 g, 1.05 mL) and *O*-([1,1'-biphenyl]-4-ylmethyl)hydroxylamine (**22f**) (1.00 eq., 2.00 mmol, 0.40 g) in dry DMF (10 mL) according to general procedure **5**. 0.34 g of **28f** (32%) was obtained as a colorless oil.

^{1}H-NMR (300 MHz, DMSO-*d6*) δ 10.89 (s, 1H), 7.73 – 7.58 (m, 4H), 7.53 – 7.18 (m, 10H), 4.79 (s, 2H), 4.05 – 3.90 (m, 2H), 3.86 – 3.64 (m, 2H), 3.18 – 3.07 (m, 1H), 2.28 – 2.16 (m, 1H), 1.99 (s, 1H), 1.83 (t, J = 7.5 Hz, 2H), 1.20 (t, J = 7.1 Hz, 3H), 1.00 (t, J = 7.0 Hz, 3H).

^{13}C-NMR (75 MHz, MeOD-*d4*) δ 171.59, 142.80, 141.93, 136.10, 130.83, 130.60 (d, $J_{c\text{-}p}$ = 6.7 Hz), 129.91, 129.75 (d, $J_{c\text{-}p}$ = 3.0 Hz), 128.59 (d, $J_{c\text{-}p}$ = 4.7 Hz), 128.03 (d, $J_{c\text{-}p}$ = 4.6 Hz), 78.41, 64.14 (d, $J_{c\text{-}p}$ = 7.9 Hz), 63.66 (d, $J_{c\text{-}p}$ = 9.2 Hz), 44.20 (d, $J_{c\text{-}p}$ = 138.4 Hz), 31.27 (d, $J_{c\text{-}p}$ = 16.6 Hz), 26.45, 16.74 (d, $J_{c\text{-}p}$ = 7.3 Hz), 16.46 (d, $J_{c\text{-}p}$ = 6.8 Hz).

^{31}P-NMR (121 MHz, MeOD-*d4*) δ 28.85.

HPLC (Method C): Rt = 13.76 min, purity > 99.0%.

Diethyl (4-((naphthalen-2-ylmethoxy)amino)-4-oxo-1-phenylbutyl)phosphonate (**28g**)

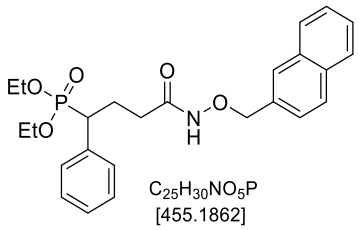

28g was synthesized from **15** (1.00 eq., 2.00 mmol, 0.60 g), HATU (1.00 eq., 2.00 mmol, 0.76 g), DIPEA (3.00 eq., 6.00 mmol, 0.78 g, 1.05 mL) and *O*-(naphthalen-2-ylmethyl)hydroxylamine (**22g**) (1.00 eq., 2.00 mmol, 0.35 g) in dry DMF (10 mL) according to general procedure **5**. 0.38 g of **28g** (42%) was obtained as an orange oil.

^{1}H-NMR (300 MHz, DMSO-*d6*) δ 10.90 (s, 1H), 8.07 – 7.75 (m, 4H), 7.61 – 7.42 (m, 3H), 7.38 – 7.14 (m, 5H), 4.91 (s, 2H), 4.04 – 3.88 (m, 2H), 3.88 – 3.63 (m, 2H), 3.16 – 3.03 (m, 1H), 2.02 (s, 3H), 1.82 (t, J = 7.5 Hz, 1H), 1.20 (t, J = 7.0 Hz, 3H), 1.01 (t, J = 7.0 Hz, 3H).

^{13}C-NMR (75 MHz, DMSO-*d6*) δ 168.57, 135.83 (d, $J_{c\text{-}p}$ = 6.7 Hz), 133.73, 132.71 (d, $J_{c\text{-}p}$ = 5.8 Hz), 129.14 (d, $J_{c\text{-}p}$ = 6.7 Hz), 128.30 (d, $J_{c\text{-}p}$ = 2.4 Hz), 127.85, 127.56, 126.96 (d, $J_{c\text{-}p}$ = 3.1 Hz), 126.61, 126.24, 76.74, 61.67 (d, $J_{c\,p}$ = 6.8 Hz), 61.32 (d, $J_{c\text{-}p}$ = 7.2 Hz), 42.31 (d, $J_{c\text{-}p}$ = 136.1 Hz), 29.94 (d, $J_{c\text{-}p}$ = 16.1 Hz), 25.21, 16.26 (d, $J_{c\text{-}p}$ = 5.6 Hz), 16.04 (d, $J_{c\text{-}p}$ = 5.6 Hz).

HPLC (Method A): Rt = 12.75 min, purity = 98.6%.

Diethyl (4-((benzyloxy)(phenethyl)amino)-4-oxo-1-phenylbutyl)phosphonate (**29a**)

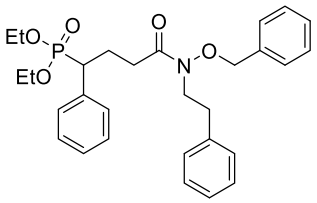

$C_{29}H_{36}NO_5P$
[509.2331]

29a was synthesized from **15** (1.00 eq., 2.20 mmol, 0.66 g), HATU (1.00 eq., 2.20 mmol, 0.84 g), DIPEA (3.00 eq., 6.60 mmol, 0.85 g, 1.15 mL) and *O*-benzyl-*N*-phenethylhydroxylamine hydrochloride (**26a**) (1.00 eq. 2.20 mmol, 0.50 g) according to general procedure **5**. 0.75 g of **29a** (67%) was obtained as a yellow oil.

^{1}H-NMR (300 MHz, MeOH-d_4) δ 7.45 – 7.09 (m, 15H), 4.72 – 4.47 (m, 2H), 4.12 – 4.00 (m, 2H), 3.94 – 3.83 (m, 2H), 3.79 – 3.67 (m, 2H), 3.18 – 3.04 (m, 1H), 2.86 (t, J = 7.2 Hz, 2H), 2.34 – 1.89 (m, 4H), 1.29 (t, J = 7.1 Hz, 3H), 1.11 (t, J = 7.1 Hz, 3H).

^{13}C-NMR (75 MHz, MeOH-d_4) δ 136.46, 132.80, 131.53, 130.69, 130.56 (d, $J_{C\text{-}P}$ = 5.6 Hz), 130.04, 129.89, 129.79, 129.61, 129.47, 128.68, 127.48, 77.08, 64.00 (d, $J_{C\text{-}P}$ = 7.2 Hz), 63.56 (d, $J_{C\text{-}P}$ = 7.6 Hz), 55.83, 43.79 (d, $J_{C\text{-}P}$ = 133.9 Hz), 18.69, 16.56 (dd, $J_{C\text{-}P}$ = 20.6, 7.0 Hz), 13.15.

HPLC (Method A): Rt = 16.23 min, purity = 96.9%.

Diethyl (4-((benzyloxy)(3-phenylpropyl)amino)-4-oxo-1-phenylbutyl)phosphonate (**29b**)

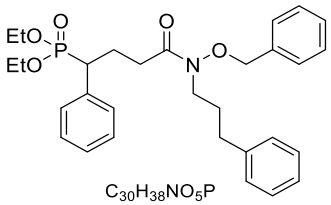

$C_{30}H_{38}NO_5P$
[523.2488]

29b was synthesized from **15** (1.00 eq., 1.50 mmol, 0.45 g), HATU (1.00 eq., 1.50 mmol, 0.57 g), DIPEA (3.00 eq., 4.50 mmol, 0.60 g, 0.79 mL) and *O*-benzyl-*N*-(3-phenylpropyl)hydroxylamine hydrochloride (**26b**) (1.00 eq., 1.50 mmol, 0.36 g) according to general procedure **5**. 0.73 g of **29b** (93%) was obtained as a colorless oil.

^{1}H-NMR (300 MHz, DMSO-d_6) δ 7.39 – 7.23 (m, 10H), 7.21 – 7.10 (m, 5H), 4.69 – 4.54 (m, 2H), 4.07 – 3.90 (m, 2H), 3.88 – 3.65 (m, 2H), 3.59 (s, 2H), 3.27 – 3.13 (m, 1H), 2.57 – 2.50 (m, 4H), 2.33 – 2.14 (m, 3H), 2.08 – 1.90 (m, 1H), 1.78 (p, J = 7.3 Hz, 2H), 1.19 (t, J = 7.0 Hz, 3H), 1.01 (t, J = 7.0 Hz, 3H).

^{13}C-NMR (75 MHz, MeOH-d_4) δ 175.30, 142.64, 136.40 (d, $J_{C\text{-}P}$ = 6.9 Hz), 135.64, 130.62 (d, $J_{C\text{-}P}$ = 6.8 Hz), 130.49, 129.90, 129.79 (d, $J_{C\text{-}P}$ = 2.6 Hz), 129.59, 129.40, 128.66 (d, $J_{C\text{-}P}$ = 3.2 Hz), 126.96, 77.04, 64.02 (d, $J_{C\text{-}P}$ = 7.2 Hz), 63.51 (d, $J_{C\text{-}P}$ = 7.4 Hz), 45.66, 44.23 (d, $J_{C\text{-}P}$ = 138.1 Hz), 33.89, 30.99 (d, $J_{C\text{-}P}$ = 16.2 Hz), 29.57, 25.64, 16.72 (d, $J_{C\text{-}P}$ = 6.0 Hz), 16.53 (d, $J_{C\text{-}P}$ = 5.8 Hz).

HPLC (Method A): Rt = 17.01 min, purity = 97.3%.

Diethyl (4-((benzyloxy)(4-isopropylbenzyl)amino)-4-oxo-1-phenylbutyl)phosphonate (**29c**)

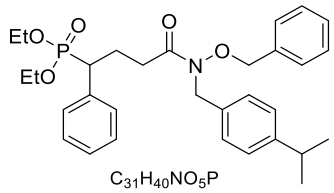

$C_{31}H_{40}NO_5P$
[537.2644]

29c was synthesized from **15** (1.00 eq., 3.50 mmol, 1.05 g), HATU (1.00 eq., 3.50 mmol, 1.33 g), DIPEA (2.00 eq., 7.0 mmol, 0.90, 1.22 mL) and *O*-benzyl-*N*-(4-isopropylbenzyl)hydroxylamine (**26c**) (1.00 eq., 3.50 mmol, 0.89 g) in dry DMF (17.5 mL) according to general procedure **5**. 1.69 g of **29c** (90%) was obtained as a yellow oil.

^{1}H-NMR (600 MHz, MeOH-d_4) δ 7.37 – 7.24 (m, 9H), 7.19 (d, J = 8.2 Hz, 4H), 7.07 (s, 2H), 4.75 (q, J = 15.4 Hz, 2H), 4.64 – 4.50 (m, 2H), 4.08 – 4.01 (m, 2H), 3.93 – 3.84 (m, 1H), 3.80 – 3.71 (m, 1H), 3.22 – 3.13 (m, 1H), 2.88 (p, J = 6.9 Hz, 1H), 2.43 – 2.34 (m, 1H), 2.33 – 2.29 (m, 2H), 2.21 – 2.10 (m, 1H), 1.28 (t, J = 7.0 Hz, 3H), 1.23 (d, J = 6.9 Hz, 6H), 1.09 (t, J = 7.1 Hz, 3H).

^{13}C-NMR (75 MHz, MeOH-d_4) δ 149.69, 136.38 (d, J_{C-P} = 6.9 Hz), 135.70, 135.18, 130.66 (d, J_{C-P} = 6.9 Hz), 130.52, 129.87, 129.79 (d, J_{C-P} = 2.6 Hz), 129.65, 129.54, 128.65 (d, J_{C-P} = 3.2 Hz), 127.54, 77.44, 64.01 (d, J_{C-P} = 8.1 Hz), 63.62 (d, J_{C-P} = 9.1 Hz), 58.54, 44.13 (d, J_{C-P} = 138.1 Hz), 38.87, 35.11, 30.95 (d, J_{C-P} = 16.3 Hz), 25.64, 24.44, 16.75 (d, J_{C-P} = 5.5 Hz), 16.52 (d, J_{C-P} = 5.8 Hz).

HPLC (Method A): Rt = 12.95 min, purity = 97.9%.

Diethyl (4-(([1,1'-biphenyl]-4-ylmethyl)(benzyloxy)amino)-4-oxo-1-phenylbutyl)phosphonate (**29d**)

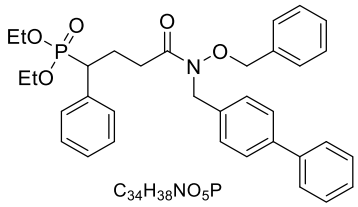

$C_{34}H_{38}NO_5P$
[571.2488]

29d was synthesized from **15** (1.00 eq., 1.80 mmol, 0.54 g), HATU (1.00 eq., 1.8 mmol, 0.68 g), DIPEA (2.00 eq, 3.60 mmol, 0.47 g, 0.63 mL) and *N*-([1,1'-biphenyl]-4-ylmethyl)-*O*-benzylhydroxylamine (**26d**) (1.00 eq., 1.8 mmol, 0.52 g) in dry DMF (9 mL) according to general procedure **5**. 0.87 g of **29d** (78%) was obtained as a colorless oil.

^{1}H-NMR (300 MHz, MeOH-d_4) δ 7.66 – 7.53 (m, 4H), 7.45 – 7.22 (m, 13H), 7.18 – 7.03 (m, 2H), 4.83 (d, J = 3.4 Hz, 2H), 4.73 – 4.53 (m, 2H), 4.14 – 3.96 (m, 2H), 3.96 – 3.65 (m, 2H), 3.25 – 3.11 (m, 1H), 2.49 – 2.29 (m, 3H), 2.27 – 2.08 (m, 1H), 1.27 (t, J = 7.0 Hz, 3H), 1.08 (t, J = 7.1 Hz, 3H).

^{13}C-NMR (75 MHz, MeOH-d_4) δ 141.95, 136.90, 136.42 (d, J_{C-P} = 6.9 Hz), 135.71, 130.67 (d, J_{C-P} = 6.6 Hz), 130.56, 130.07, 129.90 (d, J_{C-P} = 2.8 Hz), 129.80 (d, J_{C-P} = 2.6 Hz), 129.59, 128.65, 128.43, 128.12, 127.95, 77.52, 73.13, 64.02 (d, J_{C-P} = 6.8 Hz), 63.63 (d, J_{C-P} = 8.1 Hz), 44.14 (d, Jc-p = 138.0 Hz), 31.12 (d, J_{C-P} = 15.8 Hz), 25.63, 16.70 (d, J_{C-P} = 5.1 Hz), 16.54 (d, J_{C-P} = 5.2 Hz).

HPLC (Method A): Rt = 18.01 min, purity = 98.9%.

Diethyl (4-((benzyloxy)(naphthalen-2-ylmethyl)amino)-4-oxo-1-phenylbutyl)phosphonate (**29e**)

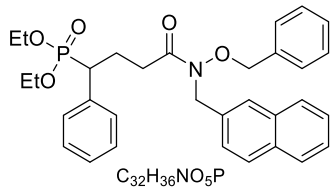

$C_{32}H_{36}NO_5P$
[545.2331]

29e was synthesized from **15** (1.00 eq., 4.00 mmol, 1.20 g), HATU (1.00 eq., 4.00 mmol, 1.52 g), DIPEA (3.00 eq., 12.00 mmol, 1.56 g, 2.10 mL) and *O*-benzyl-*N*-(naphthalen-2-ylmethyl)hydroxylamine hydrochloride (**26e**) (1.00 eq., 4.00 mmol,1.06 g) in dry DMF (10 mL) according to general procedure **5**. 1.95 g of **29e** (87%) was obtained as a yellow oil.

^{1}H-NMR (600 MHz, DMSO-d_6) δ 7.91 – 7.85 (m, 3H), 7.76 (s, 1H), 7.54 – 7.45 (m, 2H), 7.40 – 7.36 (m, 1H), 7.35 – 7.24 (m, 9H), 7.11 (d, J = 7.0 Hz, 2H), 5.01 – 4.92 (m, 2H), 4.73 – 4.60 (m, 2H), 4.01 – 3.92 (m, 2H), 3.86 – 3.76 (m, 1H), 3.76 – 3.66 (m, 1H), 3.27 – 3.19 (m, 1H), 2.38 – 2.22 (m, 2H), 2.08 – 1.99 (m, 1H), 1.19 (t, J = 7.0 Hz, 3H), 1.01 (t, J = 7.0 Hz, 3H).

^{13}C-NMR (75 MHz, MeOH-d_4) δ 136.35 (d, $J_{C\text{-}P}$ = 6.8 Hz), 135.69, 135.29, 134.75, 134.36, 130.63 (d, $J_{C\text{-}P}$ = 6.7 Hz), 130.54, 129.89, 129.77 (d, $J_{C\text{-}P}$ = 2.5 Hz), 129.56, 129.34, 128.84, 128.71, 127.33, 127.10, 77.57, 63.99 (d, $J_{C\text{-}P}$ = 7.2 Hz), 63.51 (d, $J_{C\text{-}P}$ = 7.1 Hz), 55.83, 44.10 (d, $J_{C\text{-}P}$ = 138.1 Hz), 30.91 (d, $J_{C\text{-}P}$ = 16.0 Hz), 25.65, 16.72 (d, $J_{C\text{-}P}$ = 5.3 Hz), 16.45 (d, $J_{C\text{-}P}$ = 5.5 Hz).

HPLC (Method A): Rt = 17.13 min, purity = 98.1%.

Diethyl (4-oxo-1-phenyl-4-((3-phenylpropyl)amino)butyl)phosphonate (**30a**)

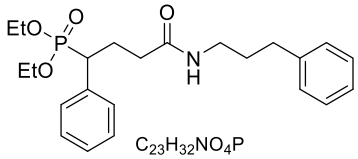

$C_{23}H_{32}NO_4P$
[417.2069]

30a was synthesized from **15** (1.00 eq., 2.00 mmol, 0.60 g), HATU (1.00 eq., 2.00 mmol, 0.76 g), DIPEA (2.00 eq., 4.00 mmol, 0.52 g, 0.70 mL) and 3-phenylpropan-1-amine (**27a**) (1.00 eq., 2.00 mmol, 0.27 g) in dry DMF (10 mL) according to general procedure **5**. 0.57 g of **30a** (68%) was obtained as an orange oil.

^{1}H-NMR (300 Hz, DMSO-*d6*) δ 7.74 (t, J = 5.5 Hz, 1H), 7.35 – 7.23 (m, 6H), 7.24 – 7.10 (m, 3H), 4.06 – 3.87 (m, 2H), 3.89 – 3.60 (m, 2H), 3.28 – 2.95 (m, 3H), 2.54 (d, J = 7.3 Hz, 2H), 2.32 – 2.12 (m, 1H), 2.10 – 1.87 (m, 3H), 1.71 – 1.56 (m, 2H), 1.20 (t, J = 7.0 Hz, 3H), 1.01 (t, J = 7.1 Hz, 3H).

^{13}C-NMR (75 MHz, DMSO-*d6*) δ 171.06, 141.73, 136.08 (d, $J_{c\text{-}p}$ = 6.6 Hz), 129.17 (d, $J_{c\text{-}p}$ = 6.7 Hz), 128.28 (d, $J_{c\text{-}p}$ = 2.7 Hz), 126.94 (d, $J_{c\text{-}p}$ = 3.0 Hz), 125.71, 61.65 (d, $J_{c\text{-}p}$ = 7.0 Hz), 61.29 (d, $J_{c\text{-}p}$ = 7.0 Hz), 42.53 (d, $J_{c\text{-}p}$ = 135.9 Hz), 38.03, 32.95 (d, $J_{c\text{-}p}$ = 15.4 Hz), 32.51, 30.88, 25.52, 16.27 (d, $J_{c\text{-}p}$ = 5.7 Hz), 16.05 (d, $J_{c\text{-}p}$ = 5.5 Hz).

HPLC (Method B): Rt = 12.55 min, purity = 95.1%.

Diethyl (4-oxo-1-phenyl-4-((4-phenylbutyl)amino)butyl)phosphonate (**30b**)

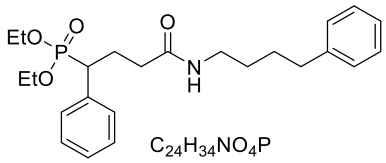

$C_{24}H_{34}NO_4P$
[431.2225]

30b was synthesized from **15** (1.00 eq., 2.00 mmol, 0.60 g), HATU (1.00 eq., 2.00 mmol, 0.76 g), DIPEA (2.00 eq., 4.00 mmol, 0.52 g, 0.70 mL) and 4-phenylbutan-1-amine (**27b**) (1.00 eq., 2.00 mmol, 0.32 g) in dry DMF (10 mL) according to general procedure **5**. 0.84 g of **30b** (97%) was obtained as a yellow oil.

^{1}H-NMR (300 MHz, DMSO-*d6*) δ 7.68 (t, J = 5.6 Hz, 1H), 7.35 – 7.23 (m, 6H), 7.20 – 7.12 (m, 3H), 3.96 (m, J = 7.8, 7.0, 1.0 Hz, 2H), 3.88 – 3.59 (m, 2H), 3.23 – 2.88 (m, 3H), 2.54 (t, J = 7.6 Hz, 2H), 2.31 – 1.85 (m, 4H), 1.59 – 1.43 (m, 2H), 1.42 – 1.28 (m, 2H), 1.20 (t, J = 7.1 Hz, 3H), 1.01 (t, J = 7.0 Hz, 3H).

^{13}C-NMR (75 MHz, DMSO-*d6*) δ 170.94, 142.13, 136.07 (d, $J_{c\text{-}p}$ = 6.6 Hz), 129.14 (d, $J_{c\text{-}p}$ = 6.7 Hz), 128.25 (t, $J_{c\text{-}p}$ = 3.8 Hz), 126.91 (d, $J_{c\text{-}p}$ = 3.2 Hz), 125.62, 61.62 (d, $J_{c\text{-}p}$ = 6.8 Hz), 61.26 (d, $J_{c\text{-}p}$ = 7.3 Hz), 42.49 (d, $J_{c\text{-}p}$ = 135.8 Hz), 38.10, 34.77, 32.91 (d, $J_{c\text{-}p}$ = 15.1 Hz), 28.74, 28.36, 25.52, 16.26 (d, $J_{c\text{-}p}$ = 5.6 Hz), 16.04 (d, $J_{c\text{-}p}$ = 5.6 Hz).

HPLC (Method B): Rt = 11.65 min, purity = 97.7%.

Diethyl (4-((2-(1H-indol-3-yl)ethyl)amino)-4-oxo-1-phenylbutyl)phosphonate (**30c**)

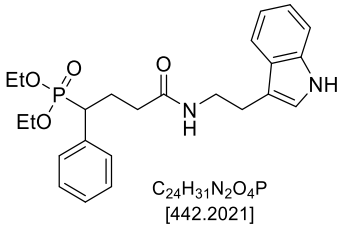

$C_{24}H_{31}N_2O_4P$
[442.2021]

30c was synthesized from **15** (1.00 eq., 2.00 mmol, 0.60 g), HATU (1.00 eq., 2.00 mmol, 0.76 g), DIPEA (2.00 eq., 4.00 mmol, 0.52 g, 0.70 mL) and 3-(2-aminoethyl)-1*H*-indol-6-ylium (**27c**) (1.00 eq., 2.00 mmol, 0.32 g) in dry DMF (10 mL) according to general procedure **5**. 0.84 g of **21c** (95%) was obtained as an orange oil.

^{1}H-NMR (300 MHz, DMSO-*d6*) δ 10.79 (s, 1H), 7.83 (t, J = 5.7 Hz, 1H), 7.49 (d, J = 7.8 Hz, 1H), 7.38 – 7.23 (m, 5H), 7.14 – 6.89 (m, 3H), 4.05 – 3.91 (m, 2H), 3.90 – 3.63 (m, 2H), 3.30 – 3.02 (m, 3H), 2.82 – 2.72 (m, 2H), 2.32 – 1.84 (m, 4H), 1.21 (t, J = 7.1 Hz, 3H), 1.02 (t, J = 7.0 Hz, 3H).

^{13}C-NMR (75 MHz, DMSO-*d6*) δ 171.31, 136.24, 136.05 (d, $J_{c\text{-}p}$ = 6.8 Hz), 129.20 (d, $J_{c\text{-}p}$ = 6.7 Hz), 128.34 (d, $J_{c\text{-}p}$ = 2.4 Hz), 127.26, 126.98, 122.54, 120.91, 118.22, 111.89, 111.36, 61.69 (d, $J_{c\text{-}p}$ = 6.7 Hz), 61.34 (d, $J_{c\text{-}p}$ = 7.2 Hz), 42.70, 42.53 (d, $J_{c\text{-}p}$ = 135.9 Hz), 33.05 (d, $J_{c\text{-}p}$ = 15.7 Hz), 25.52, 25.17, 16.31 (d, $J_{c\text{-}p}$ = 5.8 Hz), 16.08 (d, $J_{c\text{-}p}$ = 5.6 Hz).

HPLC (Method C): Rt = 11.68 min, purity = 96.3%.

Diethyl (4-((2-((5-carbamoylpyridin-2-yl)amino)ethyl)amino)-4-oxo-1-phenylbutyl)phosphonate (**38a**)

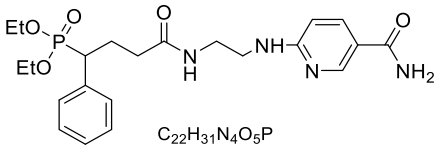

$C_{22}H_{31}N_4O_5P$
[462,2032]

38a was synthesized from **15** (1.00 eq., 1.00 mmol, 0.30 g), HATU (1.00 eq., 1.00 mmol, 0.38 g), DIPEA (2.00 eq., 2.00 mmol, 0.26 g, 0.35 mL) and 4-((2-aminoethyl)amino)benzamide (**37a**) (1.00 eq., 1.00 mmol, 0.18 g) in dry DMF (5 mL) according to general procedure **5**. 0.20 g of **38a** (43%) was obtained as a yellow oil.

^{1}H-NMR (300 MHz, MeOD-*d4*) δ 8.56 – 8.44 (m, 1H), 7.91 – 7.75 (m, 1H), 7.35 – 7.18 (m, 5H), 6.50 (dd, J = 8.9, 0.8 Hz, 1H), 4.13 – 3.96 (m, 2H), 3.96 – 3.64 (m, 2H), 3.43 (t, J = 6.3 Hz, 2H), 3.35 – 3.30 (m, 2H), 3.24 – 3.05 (m, 1H), 2.47 – 2.28 (m, 1H), 2.28 – 2.02 (m, 3H), 1.31 – 1.20 (m, 3H), 1.06 (dd, J = 7.1, 0.6 Hz, 3H).

^{13}C-NMR (151 MHz, MeOD-*d4*) δ 183.05, 178.83, 170.00, 157.73, 145.59, 144.27 (d, $J_{c\text{-}p}$ = 6.9 Hz), 138.50 (d, $J_{c\text{-}p}$ = 6.7 Hz), 137.63 (d, $J_{c\text{-}p}$ = 2.6 Hz), 136.53 (d, $J_{c\text{-}p}$ = 3.1 Hz), 126.67, 126.11, 116.74, 72.01 (d, $J_{c\text{-}p}$ = 7.1 Hz), 71.50 (d, $J_{c\text{-}p}$ = 7.3 Hz), 52.39 (d, $J_{c\text{-}p}$ = 137.8 Hz), 49.81, 42.53, 42.42, 34.65 (d, $J_{c\text{-}p}$ = 2.5 Hz), 24.67 (d, $J_{c\text{-}p}$ = 5.7 Hz), 24.48 (d, $J_{c\text{-}p}$ = 5.9 Hz), 8.78.

^{31}P-NMR (243 MHz, MeOD-*d4*) δ 28.77.

HPLC (Method C): Rt = 6.82 min, purity = 97.7%.

Diethyl (4-((3-((5-carbamoylpyridin-2-yl)amino)propyl)amino)-4-oxo-1-phenylbutyl)phosphonate (**38b**)

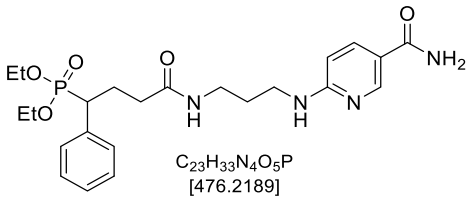

$C_{23}H_{33}N_4O_5P$
[476.2189]

38b was synthesized from **15** (1.00 eq., 2.00 mmol, 0.60 g), HATU (1.00 eq., 2.00 mmol, 0.76 g), DIPEA (2.00 eq., 4.00 mmol, 0.52 g, 0.70 mL) and 4-((3-aminopropyl)amino)benzamide (**37b**) (1.00 eq., 2.00 mmol, 0.39 g) in dry DMF (10 mL) according to general procedure **5**. 0.44 g of **38b** (46%) was obtained as a yellow oil.

^{1}H-NMR (300 MHz, MeOD-*d4*) δ 8.60 – 8.46 (m, 1H), 7.86 (dd, J = 9.0, 2.4 Hz, 1H), 7.33 – 7.28 (m, 3H), 7.27 – 7.16 (m, 1H), 6.52 (d, J = 8.1 Hz, 1H), 4.11 – 3.95 (m, 2H), 3.90 – 3.62 (m, 2H), 3.23 – 3.08 (m, 3H), 2.47 – 2.28 (m, 1H), 2.28 – 1.96 (m, 3H), 1.72 (p, J = 6.8 Hz, 2H), 1.33 (dd, J = 7.0, 3.8 Hz, 2H), 1.29 – 1.19 (m, 3H), 1.05 (t, J = 7.1 Hz, 3H).

^{13}CNMR (151 MHz, MeOD-*d4*) δ 170.56, 148.72, 137.90, 136.29, 130.57 (d, $J_{c\text{-}p}$ = 6.6 Hz), 129.70, 128.60, 118.47, 64.09, 63.55 (d, $J_{c\text{-}p}$ = 7.4 Hz), 44.48 (d, $J_{c\text{-}p}$ = 137.7 Hz), 39.87, 37.84, 34.56, 34.46, 29.93, 26.75, 16.71 (d, $J_{c\text{-}p}$ = 5.8 Hz), 16.52 (d, $J_{c\text{-}p}$ = 6.0 Hz).

HPLC (Method C): Rt = 6.84 min, purity = 92.8%.

HRMS (ESI$^+$): calculated. for $C_{23}H_{33}N_4O_5P$ 477.2271 $[M + H]^+$, found 477.2261.

Diethyl (4-((benzyloxy)(4-phenylbutyl)amino)-4-oxo-1-phenylbutyl)phosphonate (**44a**)

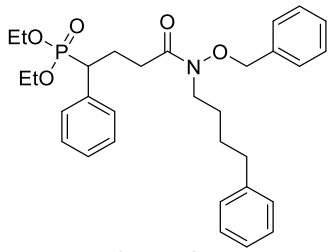

$C_{31}H_{40}NO_5P$
[537.2644]

44a was synthesized from **15** (1.00 eq., 3.00 mmol, 0.90 g), HATU (1.00 eq., 3.00 mmol, 1.14 g), DIPEA (3.00 eq., 9.00 mmol, 1.56 g) and *O*-benzyl-*N*-(4-phenylbutyl)hydroxylamine hydrochloride (**43a**) (1.00 eq., 3.00 mmol, 0.87 g) in dry DMF (15 mL) according to general procedure **5**. 1.10 g of **44a** (68%) was obtained as a colorless oil.

^{1}H-NMR (600 MHz, MeOH-*d*$_4$) δ 7.36– 7.27 (m, 9H), 7.25 – 7.20 (m, 2H), 7.16 – 7.09 (m, 4H), 4.64 – 4.52 (m, 2H), 4.12 – 3.99 (m, 2H), 3.93 – 3.84 (m, 1H), 3.82 – 3.71 (m, 1H), 3.70 – 3.65 (m, 2H), 3.23 – 3.16 (m, 1H), 2.60 (t, *J* = 7.2 Hz, 2H), 2.39 – 2.32 (m, 1H), 2.31 – 2.26 (m, 2H), 2.19 – 2.13 (m, 1H), 1.64 – 1.54 (m, 4H), 1.28 (t, *J* = 7.1 Hz, 3H), 1.09 (t, *J* = 7.1 Hz, 3H).

^{13}C-NMR (151 MHz, MeOH-*d*$_4$) δ 174.81, 143.42, 136.50, 135.81, 130.64 (d, $J_{C\text{-}P}$ = 6.7 Hz), 130.43 (d, $J_{C\text{-}P}$ = 4.5 Hz), 129.86, 129.78 (d, $J_{C\text{-}P}$ = 2.7 Hz), 129.58, 129.44, 129.32, 128.64 (d, $J_{C\text{-}P}$ = 3.4 Hz), 126.78, 77.06, 64.04 (d, $J_{C\text{-}P}$ = 7.1 Hz), 63.57 (d, $J_{C\text{-}P}$ = 7.3 Hz), 52.03, 45.26 (d, $J_{C\text{-}P}$ = 130.6 Hz), 43.90, 36.25, 31.03 (d, $J_{C\text{-}P}$ = 16.3 Hz), 29.54, 27.32, 16.69 (d, $J_{C\text{-}P}$ = 5.7 Hz), 16.50 (d, $J_{C\text{-}P}$ = 5.6 Hz).

HPLC (Method C): Rt = 17.42 min, purity = 95.4%.

Diethyl (4-((benzyloxy)(5-phenylpentyl)amino)-4-oxo-1-phenylbutyl)phosphonate (**44b**)

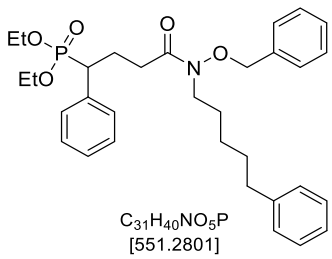

$C_{31}H_{40}NO_5P$
[551.2801]

44b was synthesized from **15** (1.00 eq., 1.50 mmol, 0.45 g), HATU (1.00 eq., 1.50 mmol, 0.57 g), DIPEA (3.00 eq., 4.50 mmol, 0.59 g, 0.79 m) and *O*-benzyl-*N*-(5-phenylpentyl)hydroxylamine hydrochloride (**43b**) (1.00 eq., 1.50 mmol, 0.46 g) in dry DMF (10 mL) according to general procedure **5**. 0.46 g of **44b** (56%) was obtained as a colorless oil.

^{1}H-NMR (600 MHz, MeOH-*d*$_4$) δ 7.40 – 7.27 (m, 9H), 7.25 – 7.20 (m, 2H), 7.13 (m, *J* = 12.6, 8.6, 1.3 Hz, 4H), 4.65 – 4.52 (m, 2H), 4.11 – 4.00 (m, 2H), 3.95 – 3.86 (m, 1H), 3.82 – 3.73 (m, 1H), 3.69 – 3.56 (m, 2H), 3.25 – 3.17 (m, 1H), 2.58 (t, *J* = 7.6 Hz, 2H), 2.40 – 2.22 (m, 3H), 2.20 – 2.09 (m, 1H), 1.67 – 1.56 (m, 4H), 1.67 – 1.56 (m, 4H), 1.29 (t, *J* = 7.0 Hz, 3H), 1.10 (t, *J* = 6.8 Hz, 3H)

^{13}C-NMR (151 MHz, MeOH-*d*$_4$) δ 175.40, 143.64, 136.52, 135.84, 130.64 (d, J_{C-P} = 6.7 Hz), 130.44, 129.87, 129.79, 129.59, 129.41, 129.26, 128.66, 126.67, 77.09, 64.05 (d, J_{C-P} = 7.1 Hz), 63.57 (d, J_{C-P} = 7.5 Hz), 45.93, 44.42 (d, J_{C-P} = 138.1 Hz), 36.68, 32.05, 31.06 (d, J_{C-P} = 16.1 Hz), 27.64, 27.20, 25.75, 16.70 (d, J_{C-P} = 5.8 Hz), 16.51 (d, J_{C-P} = 5.9 Hz).

HPLC (Method C): Rt = 20.89 min, purity = 95.4%.

Diethyl (4-((benzyloxy)(phenethyl)amino)-1-(3,4-difluorophenyl)-4-oxobutyl)phosphonate (**53a**)

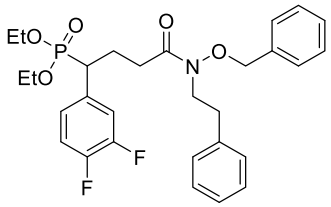

$C_{29}H_{34}F_2NO_5P$
[545.2143]

53a was synthesized from **52** (1.00 eq, 1.60 mmol, 0.54 g), HATU (1.00 eq., 1.60 mmol, 0.61 g), DIPEA (3.00 eq., 4.80 mmol, 0.62 g, 0.84 mL) and *O*-benzyl-*N*-phenethylhydroxylamine hydrochloride (**26a**) (1.00 eq., 1.60 mmol, 0.36 g) in dry DMF (8 mL) according to general procedure **5**. 0.49 g of **53a** (56%) was obtained as a yellow oil.

^{1}H-NMR (600 MHz, MeOD-*d4*) δ 7.32 (d, *J* = 6.6 Hz, 3H), 7.28 – 7.10 (m, 9H), 7.05 – 7.01 (m, 1H), 4.66 (q, *J* = 10.5 Hz, 2H), 4.11 – 4.02 (m, 2H), 3.99 – 3.80 (m, 4H), 3.17 – 3.08 (m, 1H), 2.91 – 2.79 (m, 2H), 2.28 – 2.13 (m, 3H), 2.00 – 1.83 (m, 1H), 1.28 (t, *J* = 7.0 Hz, 3H), 1.15 (t, *J* = 7.1 Hz, 3H).

^{13}C-NMR (151 MHz, MeOD-*d4*) δ 175.35, 151.98 (dd, J_{C-F} = 74.0, J_{C-F} = 10.9 Hz), 150.35 (dd, J_{C-F} = 78.5, J_{C-F} = 12.6 Hz), 139.84, 135.83, 134.17, 130.44, 129.99 (d, J_{C-P} = 19.5 Hz), 129.60, 129.46, 127.49, 127.11 (td, J_{C-F} = 6.7, J_{C-F} = 3.4 Hz), 119.30 (dd, J_{C-F} = 17.8, J_{C-F} = 6.5 Hz), 118.43 (dd, J_{C-F} = 17.5, J_{C-F} = 2.5 Hz), 77.06, 64.10 (d, J_{C-P} = 7.1 Hz), 63.77 (d, J_{C-P} = 7.3 Hz), 47.51, 43.41 (d, J_{C-P} = 139.2 Hz), 33.90, 30.92, 30.82, 16.71 (d, J_{C-P} = 5.8 Hz), 16.58 (d, J_{C-P} = 5.6 Hz).

HPLC (Method A): Rt = 16.50 min, purity = 97.5%.

Diethyl (4-((benzyloxy)(3-phenylpropyl)amino)-1-(3,4-difluorophenyl)-4-oxobutyl)phosphonate (**53b**)

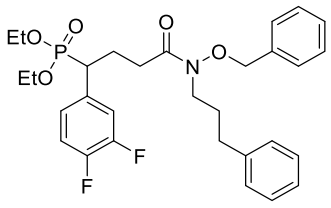

$C_{30}H_{36}F_2NO_5P$
[559.2299]

53b was synthesized from **52** (1.00 eq, 2.00 mmol, 0.67 g), HATU (1.00 eq., 2.00 mmol, 0.76 g), and DIPEA (3.00 eq., 6.00 mmol, 0.78 g, 1.05 mL) and *O*-benzyl-*N*-(3-phenylpropyl)hydroxylamine hydrochloride (**26b**) (1.00 eq., 2.00 mmol, 0.55 g) in dry DMF (10 mL) according to general procedure **5**. 0.69 g of **53b** (62%) was obtained as a yellow oil.

^{1}H-NMR (600 MHz, MeOH-*d*$_4$) *δ* 7.38 – 7.29 (m, 3H), 7.29 – 7.12 (m, 9H), 7.12 – 7.06 (m, 1H), 4.67 (q, *J* = 10.3 Hz, 2H), 4.13 – 4.02 (m, 2H), 4.00 – 3.82 (m, 2H), 3.68 (s, 2H), 3.27 – 3.21 (m, 1H), 2.59 (t, *J* = 7.8 Hz, 2H), 2.38 – 2.21 (m, 3H), 2.14 – 2.04 (m, 1H), 1.91 (h, *J* = 7.3 Hz, 2H), 1.28 (t, *J* = 7.0 Hz, 3H), 1.15 (t, *J* = 7.0 Hz, 3H).

^{13}C-NMR (151 MHz, MeOH-*d*$_4$) *δ* 175.27, 151.83 (dd, J_{C-F} = 83.3, J_{C-F} = 9.4 Hz), 150.49 (dd, J_{C-F} = 76.5, J_{C-F} = 10.9 Hz), 142.68, 135.73, 134.17, 130.48, 129.97, 129.62, 129.43 (d, J_{C-F} = 3.2 Hz), 127.19 (d, J_{C-P} = 8.7 Hz), 126.99, 119.35 (dd, J_{C-F} = 17.9, J_{C-F} = 6.4 Hz), 118.49 (dd, J_{C-F} = 16.0, J_{C-F} = 2.9 Hz), 77.08, 64.16 (d, J_{C-P} = 7.2 Hz), 63.82 (d, J_{C-P} = 7.3 Hz), 45.64, 43.47 (d, J_{C-P} = 139.4 Hz), 33.94, 31.01, 30.91 (d, J_{C-P} = 15.8 Hz), 29.57, 25.78, 16.69 (d, J_{C-P} = 6.0 Hz), 16.56 (d, J_{C-P} = 5.8 Hz).

^{31}P-NMR (243 MHz, MeOD-*d4*) *δ* 27.81.

HPLC (Method C): Rt = 17.19 min, purity = 98.9%.

Diethyl (4-((benzyloxy)(4-phenylbutyl)amino)-1-(3,4-difluorophenyl)-4-oxobutyl)phosphonate (**53c**)

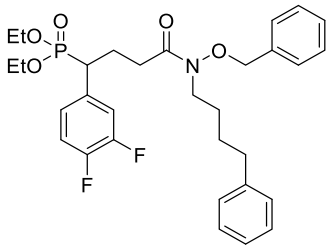

$C_{31}H_{38}F_2NO_5P$
[573.2456]

53c was synthesized from **52** (1.00 eq, 1.60 mmol, 0.54 g) HATU (1.00 eq., 1.60 mmol, 0.61 g) and DIPEA (3.00 eq., 4.80 mmol, 0.62 g, 0.84 mL) and *O*-benzyl-*N*-(4-phenylbutyl)hydroxylamine hydrochloride (**43a**) (1.00 eq., 1.60 mmol, 0.47 g) in dry DMF (10 mL) according to general procedure **5**. 0.57 g of **53c** (62%) was obtained as a yellow oil.

^{1}H-NMR (600 MHz, MeOD-*d4*) *δ* 7.37 – 7.28 (m, 3H), 7.27 – 7.12 (m, 9H), 7.08 – 7.03 (m, 1H), 4.67 (q, *J* = 10.2 Hz, 2H), 4.09 – 4.03 (m, 2H), 4.00 – 3.90 (m, 1H), 3.90 – 3.82 (m, 1H), 3.74 – 3.63 (m, 2H), 3.22 (q, *J* = 11.2 Hz, 1H), 2.62 (t, *J* = 7.1 Hz, 2H), 2.39 – 2.19 (m, 3H), 2.07 (s, 1H), 1.69 – 1.49 (m, 4H), 1.28 (t, *J* = 7.1 Hz, 3H), 1.15 (t, *J* = 7.1 Hz, 3H).

^{13}C-NMR (151 MHz, MeOD-*d4*) *δ* 175.24, 151.94 (dd, J_{C-F} = 64.7, J_{C-F} = 5.3 Hz), 150.36 (dd, J_{C-F} = 80.3, J_{C-F} = 6.6 Hz), 143.43, 135.77, 134.17, 130.45, 129.94, 129.61, 129.46, 129.36, 126.81, 127.17, 119.33 (dd, J_{C-F} = 17.9, J_{C-F} = 6.6 Hz), 118.47 (d, J_{C-F} = 17.1 Hz), 77.00, 64.15 (d, J_{C-P} = 7.2 Hz), 63.82 (d, J_{C-P} = 7.4 Hz), 52.11, 45.49, 43.44 (d, J_{C-P} = 139.4 Hz), 36.25, 30.89 (d, J_{C-P} = 15.6 Hz), 29.61, 27.27, 25.79, 16.70 (d, J_{C-P} = 5.7 Hz), 16.57 (d, J_{C-P} = 5.7 Hz).

HPLC (Method C): Rt = 17.77 min, purity = 95.4%.

Diethyl (4-((benzyloxy)(5-phenylpentyl)amino)-1-(3,4-difluorophenyl)-4-oxobutyl)phosphonate (**53d**)

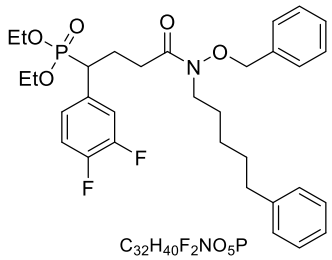

$C_{32}H_{40}F_2NO_5P$
[587.2612]

53d was synthesized from **52** (1.00 eq, 2.00 mmol, 0.67 g), HATU (1.00 eq., 2.00 mmol, 0.76 g), DIPEA (3.00 eq., 6.00 mmol, 0.78 g, 1.05 mL) and *O*-benzyl-*N*-(5-phenylpentyl)hydroxylamine hydrochloride (**43b**) (1.00 eq., 2.00 mmol, 0.61 g) in dry DMF (10 mL) according to general procedure **5**. 0.79 g of **53d** (62%) was obtained as a yellow oil.

^{1}H-NMR (600 MHz, MeOD-*d4*) δ 7.34 – 7.28 (m, 3H), 7.27 – 7.15 (m, 6H), 7.14 – 7.07 (m, 4H), 4.66 (q, J = 10.4 Hz, 2H), 4.12 – 4.00 (m, 4H), 4.00 – 3.82 (m, 2H), 3.69 – 3.58 (m, 2H), 3.28 – 3.22 (m, 1H), 2.56 (t, J = 7.7 Hz, 2H), 2.42 – 2.19 (m, 3H), 2.15 – 2.02 (m, 1H), 1.60 (t, J = 7.9 Hz, 4H), 1.26 (t, J = 7.0 Hz, 4H), 1.15 (t, J = 7.1 Hz, 3H).

^{13}C-NMR (151 MHz, MeOD-*d4*) δ 175.07, 152.37 , 151.2, 150.74, 149.7, 143.59, 135.75, 134.21 (d, $J_{C\text{-}P}$ = 10.2 Hz), 129.60, 129.41, 129.26, 127.49 (td, $J_{C\text{-}F}$ = 6.7, $J_{C\text{-}P}$ = 3.6 Hz), 126.90, 126.68, 119.94 – 119.15 (m), 118.47 (dd, $J_{C\text{-}F}$ = 17.4, $J_{C\text{-}f}$ = 2.5 Hz), 118.22 (dd, $J_{C\text{-}F}$ = 17.4, $J_{C\text{-}F}$ = 3.2 Hz), 76.99, 64.10 (d, $J_{C\text{-}P}$ = 7.2 Hz), 63.76 (d, $J_{C\text{-}P}$ = 7.0 Hz), 45.74, 43.45 (d, $J_{C\text{-}P}$ = 139.0 Hz), 36.67, 33.17, 32.25, 32.10, 30.88 (d, $J_{C\text{-}P}$ = 15.8 Hz), 27.58, 27.19, 25.74, 16.72 (d, $J_{C\text{-}P}$ = 5.9 Hz), 16.59 (d, $J_{C\text{-}P}$ = 6.1 Hz).

HPLC (Method A): Rt = 14.46 min, purity = 95.0%.

Diethyl (4-((benzyloxy)(3-(4-fluorophenyl)propyl)amino)-4-oxo-1-phenylbutyl)phosphonate (**61a**)

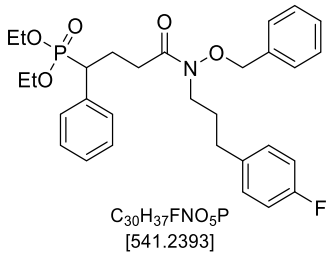

$C_{30}H_{37}FNO_5P$
[541.2393]

61a was synthesized from **15** (1.00 eq., 1.50 mmol, 0.45 g), HATU (1.00 eq., 1.50 mmol, 0.57 g), DIPEA (3.00 eq., 4.50 mmol, 0.58 g, 0.79 m) and *O*-benzyl-*N*-(3-(4-fluorophenyl)propyl)hydroxylamine hydrochloride (**60a**) (1.00 eq., 1.50 mmol, 0.44 g) in dry DMF (7.5 mL) according to general procedure **5**. 0.75 g of **61a** (93%) was obtained as a yellow oil.

^{1}H-NMR (600 MHz, MeOH-d_4) δ 7.37 – 7.27 (m, 8H), 7.21 – 7.06 (m, 4H), 7.00 – 6.93 (m, 2H), 4.65 – 4.51 (m, 2H), 4.10 – 4.01 (m, 2H), 3.93 – 3.85 (m, 1H), 3.80 – 3.74 (m, 1H), 3.65 (s, 2H), 3.25 – 3.18 (m, 1H), 2.59 – 2.53 (m, 2H), 2.40 – 2.24 (m, 3H), 2.21 – 2.12 (m, 1H), 1.87 (t, J = 7.5 Hz, 2H), 1.28 (t, J = 7.1 Hz, 3H), 1.10 (t, J = 7.1 Hz, 3H).

^{13}C-NMR (151 MHz, MeOH-*d*$_4$) δ 175.45, 162.76 (d, J_{C-F} = 242.1 Hz), 138.62, 136.43 (d, J_{C-P} = 6.8 Hz), 135.68, 131.01 (d, J_{C-P} = 7.7 Hz), 130.66 (d, J_{C-P} = 6.7 Hz), 130.53, 129.94, 129.83 (d, J_{C-P} = 2.6 Hz), 129.62, 128.70 (d, J_{C-P} = 3.2 Hz), 115.95 (d, J_{C-F} = 21.4 Hz), 77.11, 64.09 (d, J_{C-P} = 7.1 Hz), 63.57 (d, J_{C-P} = 7.2 Hz), 45.55, 44.30 (d, J_{C-P} = 138.5 Hz), 33.04, 31.04 (d, $J_{C P}$ = 14.9 Hz), 29.65, 25.66, 16.71 (d, J_{C-P} = 5.8 Hz), 16.51 (d, J_{C-P} = 5.8 Hz).

HPLC (Method c): Rt = 19.92 min, purity > 99.0%.

Diethyl (4-((benzyloxy)(3-(4-(trifluoromethyl)phenyl)propyl)amino)-4-oxo-1-phenylbutyl)phosphonate (**61b**)

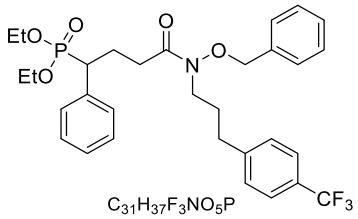

$C_{31}H_{37}F_3NO_5P$
[591.2361]

61b was synthesized from **15** (1.00 eq., 1.60 mmol, 0.48 g), HATU (1.00 eq., 1.60 mmol, 0.61 g), DIPEA (3.00 eq., 4.80 mmol, 0.62 g, 0.84 mL) and *O*-benzyl-*N*-(3-(4-(trifluoromethyl)phenyl)propyl)hydroxylamine hydrochloride (**60b**) (1.00 eq., 1.60 mmol, 0.55 g) in dry DMF (8 mL) according to general procedure 5. 0.80 g of **61b** (85%) was obtained as a yellow oil.

^{1}H-NMR (600 MHz, MeOD-*d4*) δ 7.55 (d, *J* = 8.0 Hz, 2H), 7.40 – 7.26 (m, 10H), 7.13 (d, *J* = 7.0 Hz, 2H), 4.60 (dd, *J* = 29.9, 11.4 Hz, 2H), 4.12 – 4.00 (m, 2H), 3.95 – 3.85 (m, 1H), 3.82 – 3.72 (m, 1H), 3.67 (s, 2H), 3.27 – 3.18 (m, 1H), 2.66 (t, *J* = 7.8 Hz, 2H), 2.45 – 2.22 (m, 3H), 2.22 – 2.12 (m, 1H), 2.01 – 1.83 (m, 2H), 1.28 (t, *J* = 7.0 Hz, 3H), 1.09 (d, *J* = 7.1 Hz, 3H).

^{13}C-NMR (151 MHz, MeOD-*d4*) δ 147.45, 136.44 (d, J_{C-P} = 6.8 Hz), 130.66 (d, J_{C-P} = 6.7 Hz), 130.54, 130.10, 129.96, 129.83 (d, J_{C-P} = 2.4 Hz), 129.63, 129.21, 128.71 (d, J_{C-P} = 3.3 Hz), 126.79, 126.37 – 126.18 (m), 124.99, 77.17, 64.09 (d, J_{C-P} = 7.1 Hz), 63.57 (d, J_{C-P} = 7.5 Hz), 45.54, 44.30 (d, J_{C-P} = 138.1 Hz), 33.66, 31.02 (d, J_{C-P} = 16.1 Hz), 29.20, 25.64, 25.25, 16.70 (d, J_{C-P} = 6.0 Hz), 16.51 (d, J_{C-P} = 5.9 Hz).

HPLC (Method A): Rt = 17.99 min, purity = 97.1%.

Diethyl (4-((benzyloxy)(3-(*p*-tolyl)propyl)amino)-4-oxo-1-phenylbutyl)phosphonate (**61c**)

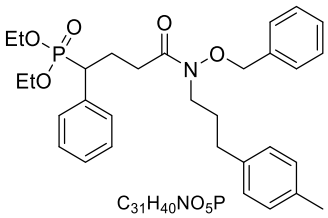

$C_{31}H_{40}NO_5P$
[537.2644]

61c was synthesized from **15** (1.00 eq., 2.00 mmol, 0.60 g), HATU (1.00 eq., 2.00 mmol, 0.76 g), DIPEA (3.00 eq., 6.00 mmol, 0.78 g, 1.05 mL) and *O*-benzyl-*N*-(3-(*p*-tolyl)propyl)hydroxylamine hydrochloride (**60c**) (1.00 eq., 2.00 mmol, 0.58 g) in dry DMF (10 mL) according to general procedure **5**. 0.90 g of **61c** (84%) was obtained as a yellow oil.

^{1}H-NMR (300 MHz, MeOH-d_4) δ 7.36 – 7.28 (m, 9H), 7.18 – 7.01 (m, 5H) , 4.57 (d, J = 13.3 Hz, 2H), 4.12 – 4.03 (m, 3H), 3.98 – 3.71 (m, 3H), 3.24 – 3.15 (m, 1H), 2.53 (t, J = 7.7 Hz, 2H), 2.45 – 2.31 (m, 2H), 2.28 (s, 3H), 2.26 – 2.16 (m, 2H), 1.86 (p, J = 7.2 Hz, 2H), 1.29 (d, J = 7.0 Hz, 3H), 1.13 – 1.08 (m, 3H).

^{13}C-NMR (75 MHz, MeOH-d_4) δ 174.79, 139.54, 136.44, 136.38, 130.70, 130.55 (d, $J_{C\text{-}P}$ = 9.4 Hz), 130.03, 129.91, 129.82 (d, $J_{C\text{-}P}$ = 2.5 Hz), 129.74 (d, $J_{C\text{-}P}$ = 2.6 Hz), 129.60, 129.31, 128.69 (d, $J_{C\text{-}P}$ = 3.3 Hz), 77.06, 64.11 (d, $J_{C\text{-}P}$ = 8.5 Hz), 63.61 (d, $J_{C\text{-}P}$ = 7.6 Hz), 52.07, 44.27 (d, $J_{C\text{-}P}$ = 138.4 Hz), 33.47, 31.03 (d, $J_{C\text{-}P}$ = 15.6 Hz), 29.64, 25.68, 21.07, 16.67 (d, $J_{C\text{-}P}$ = 5.9 Hz), 16.51 (d, $J_{C\text{-}P}$ = 5.8 Hz).

HPLC (Method C): Rt = 13.51 min, purity = 98.8%.

Diethyl (4-((benzyloxy)(3-(4-methoxyphenyl)propyl)amino)-4-oxo-1-phenylbutyl)phosphonate (**61d**)

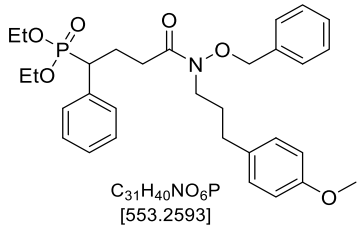

$C_{31}H_{40}NO_6P$
[553.2593]

61d was synthesized from **15** (1.00 eq, 3.00 mmol, 0.90 g), HATU (1.00 eq., 3.00 mmol, 1.14 g), DIPEA (3.00 eq., 9.00 mmol, 1.16 g, 1.57 mL) and *O*-benzyl-*N*-(3-(4-methoxyphenyl)propyl)hydroxylamine hydrochloride (**60d**) (1.00 eq., 3.00 mmol, 0.92 g)) in dry DMF (15 mL) according to general procedure **5**. 1.30 g of **61d** (79%) was obtained as a yellow oil.

^{1}H-NMR (300 MHz, MeOH-d_4) δ 7.44 – 7.22 (m, 9H), 7.19 – 6.99 (m, 3H), 6.87 – 6.74 (m, 2H), 4.58 (q, J = 10.2 Hz, 2H), 4.16 – 3.98 (m, 2H), 3.97 – 3.78 (m, 2H), 3.75 (s, 3H), 3.60 (d, J = 10.8 Hz, 2H), 3.26 – 3.15 (m, 1H), 2.51 (t, J = 7.6 Hz, 2H), 2.44 – 2.12 (m, 5H), 1.87 (q, J = 7.3 Hz, 2H), 1.28 (t, J = 7.0 Hz, 3H), 1.10 (t, J = 7.1 Hz, 4H).

^{13}C-NMR (151 MHz, MeOH-d_4) δ 174.72, 159.43, 136.50, 135.75, 134.603, 130.62 (d, $J_{C\text{-}P}$ = 6.8 Hz), 130.49 (d, $J_{C\text{-}P}$ = 7.0 Hz), 130.43 , 130.29, 129.86, 129.76, 129.69, 129.58, 128.63 (d, $J_{C\text{-}P}$ = 3.0 Hz), 114.89, 77.11, 64.01 (d, $J_{C\text{-}P}$ = 7.3 Hz), 63.54 (d, $J_{C\text{-}P}$ = 7.5 Hz), 52.02, 45.31 (d, $J_{C\text{-}P}$ = 145.5 Hz), 43.91, 32.98, 31.06 (d, $J_{C\text{-}P}$ = 16.2 Hz), 29.71, 26.18, 25.72, 16.70 (d, $J_{C\text{-}P}$ = 5.9 Hz), 16.51 (d, $^{3}J_{C\text{-}P}$ = 5.8 Hz).

HPLC (Method A): Rt = 16.55 min, purity = 95.6%.

Diethyl (4-((benzyloxy)(3-(3,5-difluorophenyl)propyl)amino)-4-oxo-1-phenylbutyl)phosphonate (**64**)

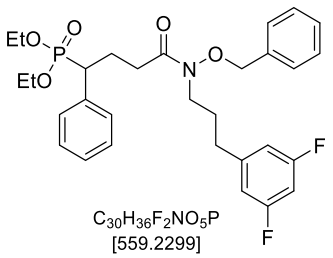

$C_{30}H_{36}F_2NO_5P$
[559.2299]

64 was synthesized from **15** (1.00 eq, 1.00 mmol, 0.30 g), HATU (1.00 eq., 1.00 mmol, 0.38 g), DIPEA (3.00 eq., 3.00 mmol, 0.39 g, 0.52 mL) and *O*-benzyl-*N*-(3-(3,5-difluorophenyl)propyl)hydroxylamine hydrochloride (**60e**)

(1.00 eq., 1.00 mmol, 0.31 g) in dry DMF (5 mL) according to general procedure **5**. 0.43 g of **64** (77%) was obtained as a yellow oil.

^{1}H-NMR (600 MHz, MeOD-*d4*) δ 7.38 – 7.27 (m, 8H), 7.14 (d, J = 6.8 Hz, 2H), 6.79 (d, J = 7.7 Hz, 2H), 6.74 (tt, J = 9.2, 2.3 Hz, 1H), 4.73 – 4.50 (m, 2H), 4.11 – 4.00 (m, 2H), 3.95 – 3.86 (m, 1H), 3.82 – 3.61 (m, 3H), 3.24 – 3.18 (m, 1H), 2.66 – 2.53 (m, 2H), 2.41 – 2.24 (m, 3H), 2.22 – 2.12 (m, 1H), 1.89 (d, J = 9.0 Hz, 2H), 1.29 (t, J = 7.1 Hz, 3H), 1.10 (t, J = 7.1 Hz, 3H).

^{13}C-NMR (151 MHz, MeOD-*d4*) δ 175.57, 164.51 (dd, $J_{C\text{-}F}$ = 246.9, $J_{C\text{-}F}$ = 13.0 Hz), 147.34, 136.52, 135.76, 130.65 (d, $J_{C\text{-}P}$ = 6.8 Hz), 130.50, 129.93, 129.80 (d, $J_{C\text{-}P}$ = 3.3 Hz), 129.62, 128.66, 112.23 (dd, $J_{C\text{-}F}$ = 19.9, $J_{C\text{-}F}$ = 4.9 Hz), 102.09 (t, $J_{C\text{-}F}$ = 26.0 Hz), 77.24, 64.07 (d, $J_{C\text{-}P}$ = 7.1 Hz), 63.59 (d, $J_{C\text{-}P}$ = 7.3 Hz), 55.90, 44.40 (d, $J_{C\text{-}P}$ = 134.9 Hz), 43.81, 33.55, 31.08 (d, $J_{C\text{-}P}$ = 15.4 Hz), 28.92, 25.72, 18.73, 16.68 (d, $J_{C\text{-}P}$ = 5.9 Hz), 16.49 (d, $J_{C\text{-}P}$ = 5.9 Hz), 13.10.

HPLC (Method A): Rt = 17.12 min, purity = 96.9%.

8.3.2.2 Conversion of the diethyl phosphonates to phosphonic acids

General procedure **6** for the cleavage of the diethyl phosphonates to give phosphonic acids.

The phosphonic acids were synthesized according to different experimental procedures:

Method I: using the procedure reported by KUMAR et al. for **31c-g**, **32a-e**, and **33a-c**.[154]

To a solution of the phosphonic acid diethyl ester (**28a-g**, **29a-e,** and **30a-c**, 1.00 eq.) in dry DCM (5 mL), trimethylsilyl bromide (2.00 eq.) was added in a septum-sealed microwave tube. The reaction mixture was irradiated in a microwave cavity at 150 W and 50 ˚C for 2 h. After reaction completion, the solvents and the volatiles were evaporated at r.t under reduced pressure and then kept for 16 h *in vacuo*. The residue was then dissolved in 10 mL THF and 0.1 mL H_2O and stirred at r.t. for 1 h. THF was then evaporated at r.t. under reduced pressure, and the product was dried for 16 h *in vacuo*.

The sodium salt of compounds **31c**, **31d**, **31f**, and **33a-c** was prepared by stirring (1.00 eq.) the residue with 1M NaOH (2.00 eq.) for another 16 h. The aqueous phase was then washed with DCM to remove organic impurities. Finally, the water was removed by lyophilization, and the crude product was recrystallized from ethanol.

Compounds **31e**, **31g** and **32a-e** were purified by reverse phase flash chromatography (on a prepacked silica cartridge), using water:acetonitrile (90:10→70:30) as eluent.

Method II: using the procedure reported by BEHRENDT et al. for **39a,b**, **46a,b**, and **62a-d**.[136]

To a solution of the appropriate phosphonic acid diethyl ester (1.00 eq.) in dry DCM (10 mL), trimethylsilyl bromide (5.00 eq.) was added at 0 °C. After 1 h, the solution was allowed to warm up to r.t. and stirred for further 24 h. After reaction completion, the solvents and the volatiles were evaporated at r.t. under reduced pressure and then kept for 16 h *in vacuo*. The residue was then dissolved in 10 mL THF and 0.1 mL H_2O and stirred at rt for 1 h. THF was then evaporated at r.t. *in vacuo* under reduced pressure, and the product was dried for 16 h *in vacuo*. The crude product was purified by reverse phase flash chromatography (on a prepacked silica cartridge), using water/acetonitrile (90:10-70:30) as eluent.

Sodium (4-oxo-4-(phenethoxyamino)-1-phenylbutyl)phosphonate (**31c**)

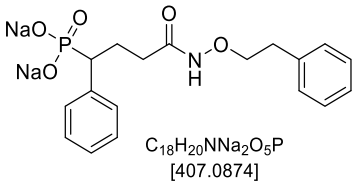

22c was synthesized from diethyl (4-oxo-4-(phenethoxyamino)-1-phenylbutyl)phosphonate (**28c**) (1.00 eq, 2.05 mmol, 1.26 g) and trimethylsilyl bromide (2.00 eq., 4.10 mmol, 0.63 g, 0.54 mL) according to general procedure **6** Method I. 1.14 g of **31c** (93%) was obtained as a white powder.

^{1}H-NMR (600 MHz, MeOD-*d4*) δ 7.42 (d, J = 7.5 Hz, 2H), 7.33 – 7.10 (m, 7H), 7.05 (t, J = 6.9 Hz, 1H), 3.94 (t, J = 7.5 Hz, 2H), 2.93 (t, J = 7.5 Hz, 2H), 2.75 – 2.66 (m, 1H), 2.46 – 2.41 (m, 1H), 2.17 – 2.08 (m, 1H), 2.01 – 1.88 (m, 2H).

^{13}C-NMR (151 MHz, DMSO-*d6*) δ 168.94, 138.41, 138.08 (d, $J_{c\text{-}p}$ = 6.6 Hz), 129.19 (d, $J_{c\text{-}p}$ = 6.2 Hz), 128.88, 128.33, 128.10, 126.32, 126.21, 75.61, 44.72 (d, $J_{c\text{-}p}$ = 133.5 Hz), 33.92, 30.56 (d, $J_{c\text{-}p}$ = 13.8 Hz), 25.88.

^{31}P-NMR (243 MHz, D_2O) δ 20.18, 19.95.

HPLC (Method A): Rt = 8.39 min, purity = 95.6%.

mp.: 60.0 ˚C.

Sodium (4-oxo-1-phenyl-4-((3-phenylpropoxy)amino)butyl)phosphonate (**31d**)

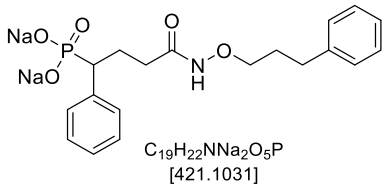

31d was synthesized from diethyl (4-oxo-1-phenyl-4-((3-phenylpropoxy)amino)butyl)phosphonate (**28d**) (1.00 eq., 2.90 mmol, 1.25 g) and trimethylsilyl bromide (2.00 eq., 5.80 mmol, 0.89 g, 0.77 mL) according to general procedure **6** Method I. 1.05 g of **31d** (86%) was obtained as a white powder.

^{1}H-NMR (600 MHz, MeOH-d_4) δ 7.40 (d, J = 8.1 Hz, 2H), 7.25 (t, J = 7.5 Hz, 2H), 7.22 – 7.11 (m, 6H), 7.06 (t, J = 8.2 Hz, 1H), 3.79 (t, J = 6.6 Hz, 2H), 2.74 – 2.67 (m, 3H), 2.47 – 2.40 (m, 1H), 2.18 – 2.09 (m, 1H), 2.07 – 1.95 (m, 2H), 1.95 – 1.87 (m, 2H).

^{13}C-NMR (151 MHz, MeOH-d_4) δ 173.25, 144.53, 143.05, 130.57 (d, $J_{C\text{-}P}$ = 5.8 Hz), 129.42, 128.71, 126.84, 125.94, 75.89, 49.19 (d, $J_{C\text{-}P}$ = 124.7 Hz), 33.93 (d, $J_{C\text{-}P}$ = 12.6 Hz), 33.00, 31.10, 30.05.

^{31}P-NMR (243 MHz, MeOD-*d4*) δ 20.90.

HPLC (Method A): Rt = 9.23 min, purity = 96.1%.

LCMS (ESI$^+$): Rt = 3.1 min, m/z = 378.14.

HRMS (ESI$^+$): calculated for $C_{19}H_{22}NNa_2O_5P$ = 378.1463 [M -2 Na^+ + 3 H]$^+$, found = 378.1465

mp.: 70.5 ˚C.

((4-(((4-Isopropylbenzyl)oxy)amino)-4-oxo-1-phenylbutyl)phosphonic acid(**31e**)

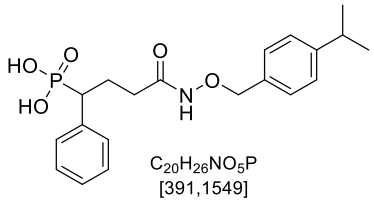

31e was synthesized from diethyl (4-(((4-isopropylbenzyl)oxy)amino)-4-oxo-1-phenylbutyl)phosphonate (**28e**) (1.00 eq., 2.02 mmol, 0.90 g) and trimethylsilyl bromide (2.00 eq., 4.04 mmol, 0.62 g, 0.53 mL) according to general procedure **6** Method I. 0.98 g of **31e** (90%) was obtained as a colorless oil.

^{1}H-NMR (600 MHz, MeOD-*d4*) δ 7.51 – 7.14 (m, 9H), 5.04 (s, 1H), 4.76 (s, 1H), 3.16 – 3.01 (m, 1H), 2.98 – 2.85 (m, 1H), 2.47 – 2.37 (m, 1H), 2.28 – 2.16 (m, 2H), 1.96 (s, 1H), 1.24 (t, J = 7.3 Hz, 6H).

^{13}C-NMR (151 MHz, MeOD-*d4*) δ 175.14, 151.85, 137.42 (d, $J_{c\text{-}p}$ = 7.0 Hz), 131.71, 130.80, 130.40 (d, $J_{c\text{-}p}$ = 6.9 Hz), 129.62 (d, $J_{c\text{-}p}$ = 2.6 Hz), 128.29 (d, $J_{c\text{-}p}$ = 3.2 Hz), 127.94, 78.04, 45.53 (d, $J_{c\text{-}p}$ = 136.6 Hz), 35.21, 32.71 (d, $J_{c\text{-}p}$ = 16.0 Hz), 26.37, 24.30.

HPLC (Method c): Rt = 10.16 min, purity = 97.5%.

Sodium (4-(([1,1'-biphenyl]-4-ylmethoxy)amino)-4-oxo-1-phenylbutyl)phosphonate (**31f**)

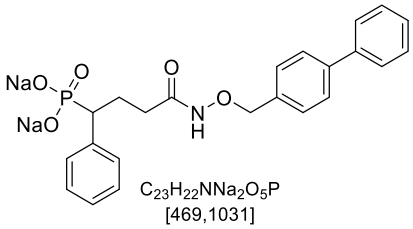

31f was synthesized from diethyl (4-(([1,1'-biphenyl]-4-ylmethoxy)amino)-4-oxo-1-phenylbutyl)phosphonate (**28f**) (1.00 eq., 3.00 mmol, 1.45 g) and trimethylsilyl bromide (2.00 eq., 6.00 mmol, 0.92 g, 0.79 mL) according to general procedure **6** Method I. 1.2 g of **31f** (94%) was obtained as a colorless oil.

^{1}H-NMR (600 MHz, MeOD-*d4*) δ 7.61 – 7.53 (m, 4H), 7.50 – 7.46 (m, 2H), 7.41 (t, J = 7.7 Hz, 4H), 7.34 – 7.28 (m, 1H), 7.16 (t, J = 7.6 Hz, 2H), 7.02 (t, J = 8.1 Hz, 1H), 4.82 (s, 2H), 2.74 – 2.65 (m, 1H), 2.46 – 2.39 (m, 1H), 2.18 – 2.03 (m, 1H), 1.91 – 1.77 (m, 2H).

^{13}C-NMR (151 MHz, D_2O) δ 171.41, 168.39, 140.36, 139.75, 137.93, 129.52 (d, $J_{c\text{-}p}$ = 5.5 Hz), 129.15, 128.54, 127.92, 127.68, 126.91 (d, $J_{c\text{-}p}$ = 5.7 Hz), 73.11, 47.64 (d, $J_{c\text{-}p}$ = 125.3 Hz), 32.48 (d, $J_{c\text{-}p}$ = 15.1 Hz), 28.16, 27.80.

^{31}P-NMR (243 MHz, D_2O) δ 20.30, 20.16.

HPLC (Method c): Rt = 8.32 min, purity = 98.4%.

mp.: 68.5 ˚C

(4-((Naphthalen-2-ylmethoxy)amino)-4-oxo-1-phenylbutyl)phosphonic acid (**31g**)

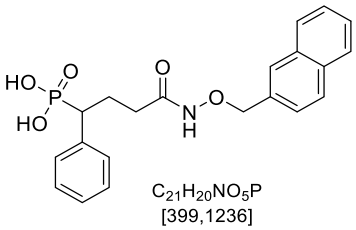

31g was synthesized from diethyl (4-((naphthalen-2-ylmethoxy)amino)-4-oxo-1-phenylbutyl)phosphonate (**28g**) (1.00 eq., 2.78 mmol, 1.26 g) and trimethylsilyl bromide (2.00 eq., 5.56 mmol, 0.85 g, 0.73 mL) according to general procedure **6** Method I. 1.0 g of **31g** (98%) was obtained as a colorless oil.

^{1}H-NMR (600 MHz, MeOD-*d4*) δ 7.95 – 6.89 (m, 12H), 4.84 (d, J = 14.3 Hz, 2H), 3.05 – 2.89 (m, 1H), 2.54 – 2.36 (m, 2H), 2.21 – 2.12 (m, 1H), 2.00 – 1.89 (m, 1H).

^{13}C-NMR (151 MHz, MeOD-*d4*) δ 173.25, 134.82,134.78, 134.66, 130.61 (d, $J_{c\text{-}p}$ = 5.6 Hz), 130.51 (d, $J_{c\text{-}p}$ = 5.6 Hz), 129.33, 129.14 (d, $J_{c\text{-}p}$ = 3.1 Hz), 128.87, 128.78, 128.66, 127.73, 127.30, 127.20, 126.39, 78.96, 48.11, 33.44 (d, $J_{c\text{-}p}$ = 12.4 Hz), 29.31.

^{31}P-NMR (243 MHz, DMSO-*d6*) δ 23.55.

HPLC (Method A): Rt = 9.37 min, purity = 98.9%.

(4-((Benzyloxy)(phenethyl)amino)-4-oxo-1-phenylbutyl)phosphonic acid (**32a**)

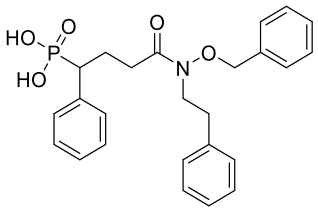

32a was synthesized from diethyl (4-((benzyloxy)(phenethyl)amino)-4-oxo-1-phenylbutyl)phosphonate (**29a**) (1.00 eq., 1.26 mmol, 0.64 g) and trimethylsilyl bromide (2.00 eq., 2.52 mmol, 0.39 g, 0.33 mL) according to general procedure **6** Method 1. 0.50 g of **32a** (87%) was obtained as a colorless oil.

^{1}H-NMR (600 MHz, MeOH-*d4*) δ 7.34 – 7.29 (m, 7H), 7.27 – 7.22 (m, 3H), 7.19 – 7.08 (m, 5H), 4.61 – 4.49 (m, 2H), 3.94 – 3.73 (m, 2H), 3.03 – 2.98 (m, 1H), 2.84 (d, J = 7.7 Hz, 2H), 2.38 – 2.17 (m, 3H), 2.09 (s, 1H).

^{13}C-NMR (151 MHz, MeOH-d_4) δ 164.85, 138.52, 130.56 (d, $J_{C\text{-}P}$ = 9.3 Hz), 129.99, 129.87, 129.59, 129.55 (d, $J_{C\text{-}P}$ = 2.3 Hz), 129.49, 127.98, 127.48, 77.17, 46.15 (d, $J_{C\text{-}P}$ = 135.6 Hz), 38.88, 36.95, 33.99, 31.64 (d, $J_{C\text{-}P}$ = 22.5 Hz).

^{31}P-NMR (243 MHz, MeOD-*d4*) δ 25.47.

HPLC (Method B): Rt = 12.10 min, purity = 96.20%.

(4-((Benzyloxy)(3-phenylpropyl)amino)-4-oxo-1-phenylbutyl)phosphonic acid (**32b**)

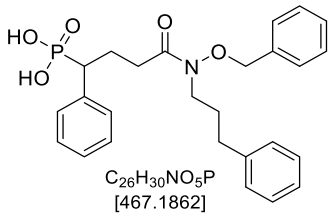

32b was synthesized from diethyl (4-((benzyloxy)(3-phenylpropyl)amino)-4-oxo-1-phenylbutyl)phosphonate (**29b**) (1.00 eq., 1.35 mmol, 0.70 g) and trimethylsilyl bromide (2.00 eq., 2.70 mmol, 0.41 g, 0.36 mL) according to general procedure **6** Method I. 0.53 g of **32b** (85%) was obtained as a white powder.

^{1}H-NMR (300 MHz, DMSO-*d*$_6$) 7.42 – 7.07 (m, 15H), 4.60 (d, *J* = 3.9 Hz, 2H), 3.58 (t, *J* = 7.1 Hz, 2H), 2.98 – 2.83 (m, 1H), 2.54 (s, 2H), 2.26 (d, *J* = 4.4 Hz, 3H), 1.99 (q, *J* = 10.3 Hz, 1H), 1.78 (p, *J* = 7.3 Hz, 2H).

^{13}C-NMR (75 MHz, DMSO-*d*$_6$) *δ* 173.06, 141.41, 138.30 (d, $J_{C\text{-}P}$ = 6.5 Hz), 134.49, 129.37, 129.18 (d, $J_{C\text{-}P}$ = 6.4 Hz), 128.67, 128.45, 128.29 (d, $J_{C\text{-}P}$ = 4.3 Hz), 128.08 (d, $J_{C\text{-}P}$ = 2.2 Hz), 126.25 (d, $J_{C\text{-}P}$ = 2.8 Hz), 125.83, 75.44, 44.57 (d, $J_{C\text{-}P}$ = 133.9 Hz), 44.14, 32.28, 30.09 (d, $J_{C\text{-}P}$ = 14.9 Hz), 28.22, 25.07.

^{31}P-NMR (243 MHz, MeOD-*d4*) *δ* 25.57.

HPLC (Method B): Rt = 12.86 min, purity = 97.7%.

mp.: 129.0 ˚C.

(4-((Benzyloxy)(4-isopropylbenzyl)amino)-4-oxo-1-phenylbutyl)phosphonic acid (**32c**)

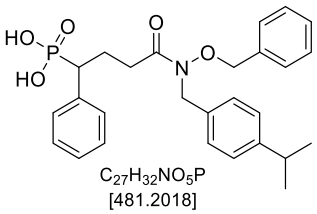

32c was synthesized from diethyl (4-((benzyloxy)(4-isopropylbenzyl)amino)-4-oxo-1-phenylbutyl)phosphonate (**29c**) (1.00 eq., 1.90 mmol, 1.00 g)) and trimethylsilyl bromide (2.00 eq., 3.80 mmol, 0.58 g, 0.50 mL) according to general procedure **6** Method I. 0.75 g of **32c** (84%) was obtained as a white powder.

^{1}H-NMR (600 MHz, MeOH-d4) *δ* 7.34 – 7.23 (m, 8H), 7.19 (s, 4H), 7.10 – 7.02 (m, 2H), 4.73 (t, *J* = 14.9 Hz, 2H), 4.63 – 4.50 (m, 2H), 3.10 – 3.01 (m, 1H), 2.88 (hept, *J* = 6.9 Hz, 1H), 2.48 – 2.40 (m, 1H), 2.33 (dd, *J* = 8.5, 6.3 Hz, 2H), 2.24 – 2.11 (m, 1H), 1.23 (d, *J* = 6.9 Hz, 6H).

^{13}C-NMR (151 MHz, MeOH-d4) *δ* 149.65, 138.17 (d, $J_{C\text{-}P}$ = 7.0 Hz), 135.69, 130.59 (d, $J_{C\text{-}P}$ = 6.5 Hz), 130.54, 129.86, 129.61 (d, $J_{C\text{-}P}$ = 2.5 Hz), 129.52, 128.09 (d, $J_{C\text{-}P}$ = 2.9 Hz), 127.54, 77.49, 45.91 (d, $J_{C\text{-}P}$ = 135.9 Hz), 35.12, 31.47 (d, $J_{C\text{-}P}$ = 18.3 Hz), 26.07, 24.43.

^{31}P-NMR (243 MHz, MeOD-*d4*) *δ* 25.90.

HPLC (Method C): Rt = 13.81 min, purity = 98.1%.

mp.: 153.7 ˚C.

(4-(([1,1'-Biphenyl]-4-ylmethyl)(benzyloxy)amino)-4-oxo-1-phenylbutyl)phosphonic acid (**32d**)

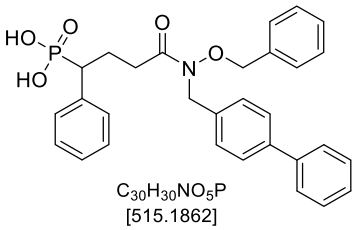

$C_{30}H_{30}NO_5P$
[515.1862]

32d was synthesized from diethyl(4-(([1,1'-biphenyl]-4-ylmethyl)(benzyloxy)amino)-4-oxo-1-phenylbutyl)phosphonate (**29d**) (1.00 eq., 1.26 mmol, 0.72 g) and trimethylsilyl bromide (2.00 eq., 2.52 mmol, 0.39 eq., 0.33 mL) according to general procedure **6** Method I. 0.58 g of **32d** (89%) was obtained as a white powder

^{1}H-NMR (600 MHz, MeOH-*d*$_4$) δ 7.68 (d, *J* = 7.9 Hz, 1H), 7.60 – 7.54 (m, 4H), 7.43 (t, *J* = 7.8 Hz, 2H), 7.39 – 7.24 (m, 11H), 7.04 (s, 1H), 4.66 – 4.49 (m, 2H), 3.12 – 2.99 (m, 1H), 2.43 (s, 1H), 2.32 (t, *J* = 7.3 Hz, 2H), 2.18 (s, 1H).

^{13}C-NMR (151 MHz, MeOH-*d*$_4$) 168.94, 138.41, 138.08 (d, *J* = 6.6 Hz), 129.19 (d, *J* = 6.2 Hz), 128.88, 128.33, 128.10, 126.32, 126.21, 75.61, 44.72 (d, $J_{C\text{-}P}$ = 133.5 Hz), 33.92, 30.56 (d, $J_{C\text{-}P}$ = 13.8 Hz), 25.88.

HPLC (Method C): Rt = 13.95 min, purity = 96.1%.

mp.: 167.6 ˚C.

(4-((Benzyloxy)(naphthalen-2-ylmethyl)amino)-4-oxo-1-phenylbutyl)phosphonic acid (**32e**)

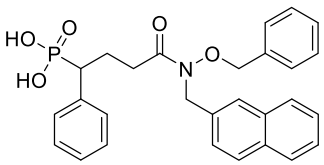

$C_{28}H_{28}NO_5P$
[489.1705]

32e was synthesized from diethyl (4-((benzyloxy)(naphthalen-2-ylmethyl)amino)-4-oxo-1-phenylbutyl)phosphonate (**29e**) (1.00 eq., 3.10 mmol, 1.70 g) and trimethylsilyl bromide (2.00 eq., 6.20 mmol, 0.95 g, 0.82 mL) according to general procedure **6** Method I. 1.28 g of **32e** (85%) was obtained as a white powder.

^{1}H-NMR (600 MHz, MeOH-*d*$_4$) δ 7.85 – 7.79 (m, 3H), 7.73 (s, 1H), 7.51 – 7.43 (m, 2H), 7.43 – 7.38 (m, 1H), 7.35 – 7.18 (m, 9H), 7.05 (s, 1H), 4.94 (s, 2H), 4.67 – 4.53 (m, 2H), 3.13 – 3.06 (m, 1H), 2.52 – 2.42 (m, 1H), 2.37 (t, *J* = 7.3 Hz, 2H), 2.25 – 2.14 (m, 1H).

^{13}C-NMR (151 MHz, DMSO-*d*$_6$) δ 176.06, 129.34, 129.12 (d, $J_{C\text{-}P}$ = 8.4 Hz), 128.55, 128.41, 128.27, 128.20, 127.37, 125.79, 81.40, 75.38, 43.02 (d, $J_{C\text{-}P}$ = 135.9 Hz), 32.24, 26.44 (t, $J_{C\text{-}P}$ = 6.3 Hz).

^{31}P-NMR (243 MHz, DMSO-*d6*) δ 28.50.

HPLC (Method A): Rt = 13.03 min, purity > 99.0%.

mp.: 151.5 ˚C.

Sodium (4-oxo-1-phenyl-4-((3-phenylpropyl)amino)butyl)phosphonate(**33a**)

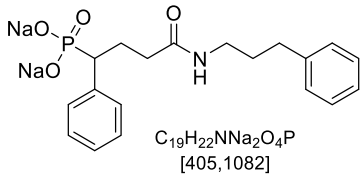

33a was synthesized from diethyl (4-oxo-1-phenyl-4-((3-phenylpropyl)amino)butyl)phosphonate (**30a**) (1.00 eq., 0.63 mmol, 0.96 g) and trimethylsilyl bromide (2.00 eq., 1.26 mmol, 0.19 g, 0.16 mL) according to general procedure **6** Method I. 0.90 g of **33a** (96%) was obtained as a yellow powder.

^{1}H-NMR (600 MHz, MeOD-*d4*) δ 7.40 (d, *J* = 8.1 Hz, 2H), 7.25 (t, *J* = 7.5 Hz, 2H), 7.22 – 7.11 (m, 5H), 7.06 (t, *J* = 8.2 Hz, 1H), 3.79 (t, *J* = 6.6 Hz, 2H), 2.77 – 2.65 (m, 3H), 2.50 – 2.38 (m, 1H), 2.18 – 2.08 (m, 1H), 2.07 – 1.88 (m, 4H).

^{13}C-NMR (75 MHz, MeOD-*d4*) *δ* 176.59, 144.07 (d, $J_{c\text{-}p}$ = 5.9 Hz), 143.00, 130.51 (d, $J_{c\text{-}p}$ = 5.8 Hz), 129.34 (d, $J_{c\text{-}p}$ = 2.1 Hz), 128.79 (d, $J_{c\text{-}p}$ = 2.1 Hz), 126.81, 126.07, 49.14 (d, $J_{c\text{-}p}$ = 124.3 Hz), 39.96, 34.17, 32.24, 29.65, 24.26.

^{31}P-NMR (243 MHz, MeOD-*d4*) *δ* 19.98.

HPLC (Method C): Rt = 9.21 min, purity = 96.9%.

HRMS (ESI^{+}): calculated for $C_{19}H_{22}Nna_2O_4P$ 362.1514 $[M - 2\ Na^{+} + 3\ H]^{+}$, found 362.1516.

mp.: 85.1 ˚C.

Sodium (4-oxo-1-phenyl-4-((4-phenylbutyl)amino)butyl)phosphonate (**33b**)

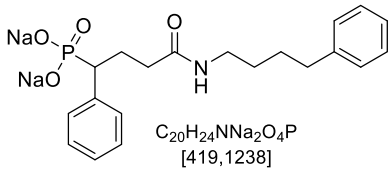

33b was synthesized from diethyl (4-oxo-1-phenyl-4-((4-phenylbutyl)amino)butyl)phosphonate (**30b**) (1.00 eq., 0.58 mmol, 1.00 g) and trimethylsilyl bromide (2.00 eq., 1.16 mmol, 0.18 g, 0.15 mL) according to general procedure **6** Method I. 1.084 g of **33b** (80%) was obtained as a yellow powder.

^{1}H-NMR (600 MHz, MeOD-*d4*) *δ* 8.55 (s, 1H), 7.41 – 7.36 (m, 2H), 7.26 – 7.10 (m, 7H), 7.09 – 7.03 (m, 1H), 3.18 – 3.06 (m, 2H), 2.73 – 2.65 (m, 1H), 2.60 (t, *J* = 7.6 Hz, 2H), 2.47 – 2.37 (m, 1H), 2.18 – 2.07 (m, 1H), 2.04 (t, *J* = 7.9 Hz, 2H), 1.65 – 1.57 (m, 2H), 1.52 – 1.44 (m, 2H).

^{13}C-NMR (151 MHz, DMSO-*d6*) *δ* 171.32, 142.13, 129.12 (d, $J_{c\text{-}p}$ = 6.6 Hz), 128.24 (d, $J_{c\text{-}p}$ = 8.6 Hz), 127.97, 126.15, 125.62, 44.80 (d, $J_{c\text{-}p}$ = 133.7 Hz), 38.11, 34.77, 33.60 (d, $J_{c\text{-}p}$ = 14.1 Hz), 28.75, 28.36, 26.10.

^{31}P-NMR (243 MHz, MeOD-*d4*) *δ* 20.18

HPLC (Method A): Rt = 9.24 min, purity = 96.8%.

HRMS (ESI^{+}): calculated for $C_{20}H_{24}Nna_2O_4P$ = 376.1671 $[M - 2\ Na^{+} + 3\ H]^{+}$, found 376.1672.

mp.: 60.6 ˚C.

Sodium (4-((2-(1*H*-indol-3-yl)ethyl)amino)-4-oxo-1 phenylbutyl)phosphonate (**33c**)

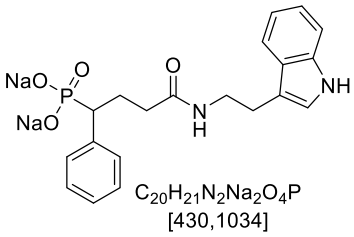

$C_{20}H_{21}N_2Na_2O_4P$
[430,1034]

33c was synthesized from diethyl (4-((2-(1*H*-indol-3-yl)ethyl)amino)-4-oxo-1-phenylbutyl)phosphonate (**30c**) (1.00 eq., 1.25 mmol, 0.55 g) and trimethylsilyl bromide (2.00 eq., 1.50 mmol, 0.23 g, 0.20 mL) according to general procedure **6** Method I. 0.43 g of **33c** (80%) was obtained as a yellow powder.

^{1}H-NMR (600 MHz, MeOD-*d4*) δ 7.52 (dd, *J* = 7.9, 1.0 Hz, 1H), 7.37 (d, *J* = 8.2 Hz, 2H), 7.32 (d, *J* = 8.1 Hz, 1H), 7.19 (t, *J* = 7.6 Hz, 2H), 7.10 – 7.03 (m, 3H), 6.99 – 6.94 (m, 1H), 3.46 – 3.37 (m, 2H), 2.93 – 2.87 (m, 2H), 2.73 – 2.64 (m, 1H), 2.49 – 2.39 (m, 1H), 2.17 – 2.08 (m, 1H), 2.07 – 1.98 (m, 2H).

^{13}C-NMR (151 MHz, MeOD-*d4*) δ 176.48, 138.20, 130.57 (d, *J* = 5.7 Hz), 128.79, 126.05, 123.43, 122.23, 119.50, 119.23, 113.29, 112.26, 49.67, 41.31, 36.65 (d, *J* = 13.7 Hz), 29.81, 26.36.

^{31}P-NMR (121 MHz, MeOD-*d4*) δ 26.33.

HPLC (Method A): Rt = 8.54 min, purity = 98.4%.

mp.: 55.1 ˚C.

(4-((2-((5-Carbamoylpyridin-2-yl)amino)ethyl)amino)-4-oxo-1-phenylbutyl)phosphonic acid (**39a**)

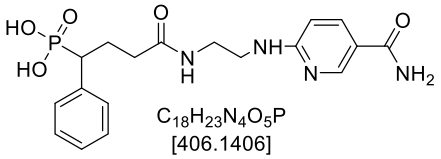

$C_{18}H_{23}N_4O_5P$
[406.1406]

39a was synthesized from diethyl (4-((2-((5-carbamoylpyridin-2-yl)amino)ethyl)amino)-4-oxo-1-phenylbutyl)phosphonate (**38a**) (1.00 eq., 0.73 mmol, 0.34 g) and trimethylsilyl bromide (5.00 eq., 3.65 mmol, 0.56 g, 0.48 mL) according to general procedure **6** Method II. 0.24 g of **39a** (81%) was obtained as a colorless oil.

^{1}H-NMR (300 MHz, MeOD-*d4*) δ 8.43 (dd, *J* = 2.2, 0.8 Hz, 1H), 8.39 – 8.26 (m, 1H), 7.39 – 7.20 (m, 5H), 7.15 (d, *J* = 9.4 Hz, 1H), 3.54 (t, *J* = 6.4 Hz, 2H), 3.46 – 3.36 (m, 2H), 3.19 – 3.08 (m, 1H), 2.51 – 2.07 (m, 4H).

^{13}C-NMR (151 MHz, DMSO-*d6*) δ 172.40, 163.81, 153.27, 138.07, 129.14 (d, $^{2}J_{c\text{-}p}$ = 6.5 Hz), 128.07, 126.29, 118.70, 44.65 (d, $^{1}J_{c\text{-}p}$ = 133.9 Hz), 41.65, 35.84, 33.61 (d, $^{2}J_{c\text{-}p}$ = 15.1 Hz), 25.95.

^{31}P-NMR (243 MHz, DMSO-*d6*) δ 23.72.

HPLC (Method B): Rt = 5.32 min, purity = 96.0%.

MS (ESI^{+}): 407.10 $[M + 1 H]^{+}$.

(4-((3-((5-Carbamoylpyridin-2-yl)amino)propyl)amino)-4-oxo-1-phenylbutyl)phosphonic acid (**39b**)

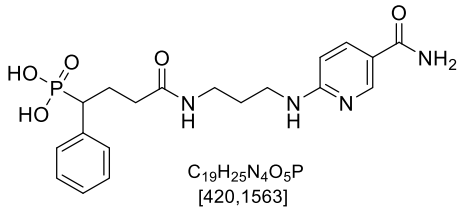

39b was synthesized from Diethyl (4-((3-((5-carbamoylpyridin-2-yl)amino)propyl)amino)-4-oxo-1-phenylbutyl)phosphonate (**38b**) (1.00 eq., 0.73 mmol, 0.35 g) and trimethylsilyl bromide (5.00 eq., 3.65 mmol, 0.56 g, 0.48 mL) according to general procedure **6** Method II. 0.29 g of **39b** (95%) was obtained as a colorless oil.

^{1}H-NMR (600 MHz, MeOD-*d4*) δ 8.68 – 8.59 (m, 1H), 8.48 – 8.42 (m, 1H), 7.43 – 7.29 (m, 5H), 7.28 – 7.21 (m, 1H), 3.58 (q, J = 7.1 Hz, 2H), 3.27 – 3.21 (m, 2H), 3.11 – 3.00 (m, 1H), 2.49 – 2.39 (m, 1H), 2.29 – 2.13 (m, 3H), 1.91 – 1.81 (m, 2H).

^{13}C-NMR (151 MHz, MeOD-*d4*) δ 176.02, 175.13, 164.74, 152.15, 145.22, 144.35, 137.98, 129.53, 130.46 (d, $^{2}J_{c\text{-}p}$ = 6.6 Hz), 128.11, 122.30, 114.03, 109.08, 46.15 (d, $^{1}J_{c\text{-}p}$ = 135.1 Hz), 43.92, 41.91, 35.54 (d, $^{2}J_{c\text{-}p}$ = 14.5 Hz), 29.35.

HPLC (Method B): Rt = 5.25 min, purity = 98.5%.

MS (ESI^{+}): 421.20 $[M + 1 H]^{+}$.

(4-((Benzyloxy)(4-phenylbutyl)amino)-4-oxo-1-phenylbutyl)phosphonic acid (**45a**)

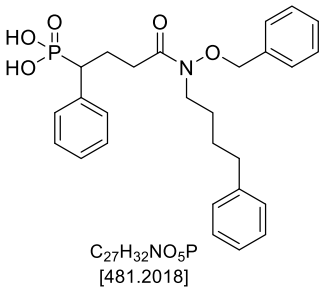

45a was synthesized from diethyl (4-((benzyloxy)(4-phenylbutyl)amino)-4-oxo-1-phenylbutyl)phosphonate (**44a**) (1.00 eq., 1.40 mmol, 0.80 g) and trimethylsilyl bromide (5.00 eq., 7.00 mmol, 1.07 g, 0.92 mL) according to general procedure **6** Method II. 0.70 g of **45a** (97%) was obtained as a colorless oil.

^{1}H-NMR (300 MHz, MeOH-d_4) δ 7.43 (s, 1H), 7.37 – 7.08 (m, 14H), 4.58 (q, J = 10.3 Hz, 2H), 3.75 – 3.70 (m, 2H), 3.12 – 3.01 (m, 1H), 2.61 (d, J = 7.2 Hz, 1H), 2.48 – 2.35 (m, 1H), 2.34 – 2.16 (m, 3H), 1.90 – 1.85 (m, 2H), 1.59 (s, 3H).

^{13}C-NMR (151 MHz, MeOH-d_4) δ 173.28, 142.09, 141.78, 139.05, 136.87, 130.50, 129.82, 129.38, 128.33, 128.06, 127.91, 127.75, 78.62, 52.72, 51.05, 46.62 (d, $J_{C\text{-}P}$ = 142.3 Hz), 35.23, 31.75, 27.34, 26.77, 17.50.

HPLC (Method C): Rt = 13.38 min, purity = 95.3%.

(4-((Benzyloxy)(5-phenylpentyl)amino)-4-oxo-1-phenylbutyl)phosphonic acid (**45b**)

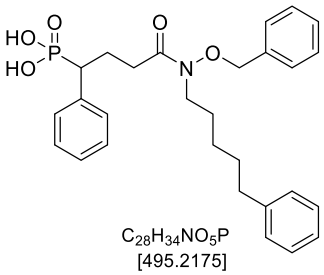

45b was synthesized from diethyl (4-((benzyloxy)(5-phenylpentyl)amino)-4-oxo-1-phenylbutyl)phosphonate (**44b**) (1.00 eq., 0.60 mmol, 0.33 g) and trimethylsilyl bromide (5.00 eq., 3.00 mmol, 0.46 g, 0.40 mL) according to general procedure **6** Method II. 0.27 g of **45b** (90%) was obtained as a yellow oil.

^{1}H-NMR (600 MHz, MeOH-d_4) δ 7.37 – 7.09 (m, 15H), 4.80 (d, J = 4.8 Hz, 1H), 4.61 – 4.47 (m, 1H), 3.64 – 3.54 (m, 1H), 2.91 (t, J = 7.5 Hz, 2H), 2.64 – 2.38 (m, 3H), 2.29 – 2.14 (m, 2H), 1.63 – 1.54 (m, 4H), 1.41 – 1.19 (m, 3H).

^{13}C-NMR (151 MHz, MeOH-d_4) δ 168.94, 138.41, 138.08, 129.19 (d, $J_{C\text{-}P}$ = 6.2 Hz), 128.88, 128.33, 128.10, 126.26, 75.61, 44.72 (d, $J_{C\text{-}P}$ = 133.5 Hz), 33.92, 30.61 (d, $J_{C\text{-}P}$ = 14.4 Hz), 25.88.

HPLC (Method C): Rt = 14.21 min, purity = 95.3%.

(4-((Benzyloxy)(3-(4-fluorophenyl)propyl)amino)-4-oxo-1-phenylbutyl)phosphonic acid (**62a**)

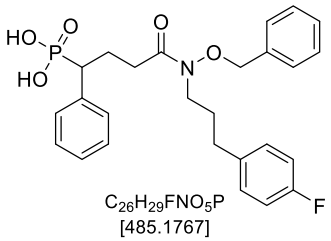

62a was synthesized from diethyl (4-((benzyloxy)(3-(4-fluorophenyl)propyl)amino)-4-oxo-1-phenylbutyl)phosphonate (**61a**) (1.00 eq., 0.54 mmol, 0.29 g) and trimethylsilyl bromide (5.00 eq., 3.00 mmol, 0.46 g, 0.40 mL) according to general procedure **6** Method II. 0.20 g of **62a** (77%) was obtained as a yellow oil.

^{1}H-NMR (600 MHz, MeOH-d_4) δ 7.34 – 7.29 (m, 7H), 7.24 – 7.20 (m, 1H), 7.19 – 7.09 (m, 4H), 6.98 – 6.94 (m, 2H), 4.65 – 4.52 (m, 2H), 3.63 (s, 2H), 3.06 – 2.96 (m, 1H), 2.71 – 2.60 (m, 1H), 2.54 (d, J = 7.9 Hz, 2H), 2.48 – 2.41 (m, 1H), 2.29 (s, 1H), 2.23 – 2.14 (m, 1H), 1.86 (q, J = 6.3 Hz, 2H).

^{13}C-NMR (151 MHz, MeOH-d_4) δ 162.75 (d, $J_{C\text{-}F}$ = 242.1 Hz), 139.13, 138.62, 131.01 (d, $J_{C\text{-}P}$ = 7.8 Hz), 130.58 (d, $J_{C\text{-}F}$ = 8.9 Hz), 129.89, 129.60, 129.50, 127.81 (d, $J_{C\text{-}P}$ = 2.5 Hz), 115.93 (d, $J_{C\text{-}F}$ = 21.3 Hz), 77.14, 46.58 (d, $J_{C\text{-}P}$ = 133.0 Hz), 45.56, 33.02, 31.69 (d, $J_{C\text{-}P}$ = 14.1 Hz), 29.66, 26.48.

HPLC (Method C): Rt = 12.82 min, purity = 97.2%.

(4-((Benzyloxy)(3-(4-(trifluoromethyl)phenyl)propyl)amino)-4-oxo-1-phenylbutyl)phosphonic acid (**62b**)

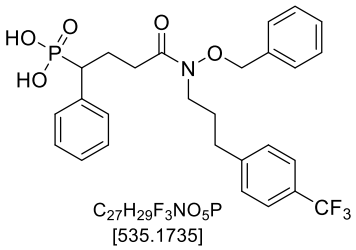

62b was synthesized from diethyl (4-((benzyloxy)(3-(4-(trifluoromethyl)phenyl)propyl)amino)-4-oxo-1-phenylbutyl)phosphonate (**61b**) (1.00 eq., 0.54 mmol, 0.32 g) and trimethylsilyl bromide (5.00 eq., 3.00 mmol, 0.46 g, 0.40 mL)according to general procedure **6** Method II. 0.15 g of **62b** (88%) was obtained as a yellow oil.

^{1}H-NMR (600 MHz, MeOD-*d4*) δ 7.55 (dd, *J* = 8.0, 5.0 Hz, 2H), 7.39 – 7.26 (m, 10H), 7.26 – 7.21 (m, 1H), 7.13 (s, 1H), 4.73 (s, 1H), 4.66 – 4.51 (m, 1H), 3.66 (s, 1H), 3.09 – 2.99 (m, 1H), 2.97 – 2.91 (m, 1H), 2.74 (t, *J* = 7.8 Hz, 1H), 2.66 (s, 1H), 2.44 (s, 1H), 2.30 (s, 1H), 2.19 (s, 1H), 1.96 – 1.83 (m, 3H).

^{13}C-NMR (151 MHz, MeOD-*d4*) δ 176.51, 147.43, 146.59, 141.20, 130.65, 130.49, 130.07, 129.83, 129.56, 129.23, 127.15, 126.73 (d, $J_{C\text{-}P}$ = 11.0 Hz), 126.54, 126.0, 124.94 (d, $J_{C\text{-}P}$ = 11.5 Hz), 77.29, 51.00, 47.39 (d, $J_{C\text{-}P}$ = 132.2 Hz), 40.11, 33.64, 33.29, 32.24, 29.87, 29.24, 27.34.

HPLC (Method C): Rt = 13.99 min, purity = 97.0%.

(4-((Benzyloxy)(3-(*p*-tolyl)propyl)amino)-4-oxo-1-phenylbutyl)phosphonic acid (**62c**)

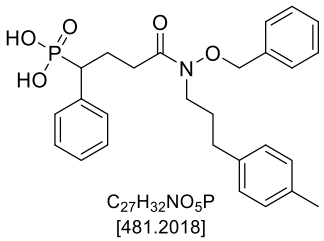

62c was synthesized from diethyl (4-((benzyloxy)(3-(*p*-tolyl)propyl)amino)-4-oxo-1-phenylbutyl)phosphonate (**61c**) (1.00 eq., 0.90 mmol, 0.48 g) and trimethylsilyl bromide (5.00 eq., 4.50 mmol, 0.69 g, 0.59 mL) according to general procedure **6** Method II. 0.35 g of **62c** (80%) was obtained as a yellow oil.

^{1}H-NMR (300 MHz, MeOH-d_4) δ 7.38 – 7.19 (m, 8H), 7.18 – 6.95 (m, 6H), 4.55 (q, *J* = 10.3 Hz, 2H), 3.72 – 3.47 (m, 2H), 3.14 – 2.97 (m, 1H), 2.51 (t, *J* = 7.6 Hz, 2H), 2.43 (s, 1H), 2.28 (s, 3H), 2.27 – 2.03 (m, 3H), 1.85 (p, *J* = 7.2 Hz, 2H).

^{13}C-NMR (75 MHz, MeOH-d_4) δ 175.76, 139.52, 138.25 (d, $J_{C\text{-}P}$ = 6.8 Hz), 136.40, 135.68, 130.57 (d, $J_{C\text{-}P}$ = 5.6 Hz), 130.01, 129.88, 129.58, 129.32, 128.06, 77.06, 46.97, 45.67, 33.44, 31.62 (d, $J_{C\text{-}P}$ = 16.9 Hz), 29.62, 26.16, 21.08.

HPLC (Method C): Rt = 13.51 min, purity = 98.8%.

(4-((Benzyloxy)(3-(4-methoxyphenyl)propyl)amino)-4-oxo-1-phenylbutyl)phosphonic acid (**62d**)

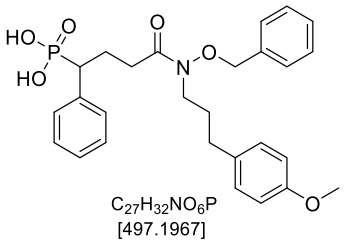

62d was synthesized from diethyl (4-((benzyloxy)(3-(4-(trifluoromethyl)phenyl)propyl)amino)-4-oxo-1-phenylbutyl)phosphonate (**61d**) (1.00 eq., 1.00 mmol, 0.55 g) and trimethylsilyl bromide (5.00 eq., 5.00 mmol, 0.77 g, 0.66 mL) according to general procedure **6** Method II. 0.31 g of **62d** (62%) was obtained as a yellow oil.

^{1}H-NMR (300 MHz, MeOH-d_4) δ 7.40 – 7.19 (m, 8H), 7.20 – 7.00 (m, 4H), 6.87 – 6.76 (m, 2H), 4.58 (t, J = 10.1 Hz, 2H), 3.75 (s, 3H), 3.62 (s, 2H), 3.11 – 2.98 (m, 1H), 2.51 (t, J = 7.6 Hz, 2H), 2.47 – 2.35 (m, 1H), 2.34 – 2.09 (m, 3H), 1.85 (p, J = 6.5 Hz, 2H).

^{13}C-NMR (75 MHz, MeOH-d_4) δ 159.43, 138.40, 134.63, 130.58 (d, $J_{C\text{-}P}$ = 5.4 Hz), 130.34, 129.89, 129.59, 128.08 (d, $J_{C\text{-}P}$ = 3.2 Hz), 114.83, 77.07, 55.65, 46.10 (d, $J_{C\text{-}P}$ = 135.6 Hz), 32.97, 31.44 (d, $J_{C\text{-}P}$ = 16.2 Hz), 29.75, 26.20.

HPLC (Method C): Rt = 10.07 min, purity = 99.0%.

8.3.2.3 Deprotection of the *O*-Bn-protected hydroxamic acids

General procedure **7** for the deprotection of the *O*-Bn-protected hydroxamic acids

The hydroxamic acids **34a-e**, **46a,b**, and **63a-d** were synthesized according to the procedure reported by BEHRENDT et al.[136]

The appropriate *O*-benzyl-protected hydroxamic acid (**32a-e**, **45a,b**, and **62a-d**) was dissolved in 10 mL of MeOH, and 10 mol% of 10 wt% Pd/C was added to the reaction solution. Catalytic hydrogenation was performed for 1-3 h, and the reaction solution was filtered through celite®. The solvent was removed under reduced pressure, and the product was purified by reverse phase flash chromatography (on a prepacked silica cartridge), using water:acetonitrile (90:10→80:20) as eluent.

(4-(Hydroxy(phenethyl)amino)-4-oxo-1-phenylbutyl)phosphonic acid (**34a**)

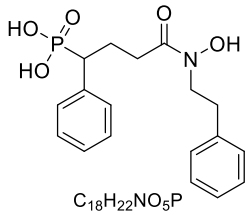

$C_{18}H_{22}NO_5P$
[363.1236]

34a was synthesized from (4-((benzyloxy)(phenethyl)amino)-4-oxo-1-phenylbutyl)phosphonic acid (**32a**) (1.00 eq., 1.25 mmol, 0.57 g) according to general procedure **7**. 0.43 g of **34a** (94%) was obtained as a yellow oil.

^{1}H-NMR (600 MHz, MeOH-*d*$_4$) δ 7.34 (d, J = 7.6 Hz, 2H), 7.30 – 7.24 (m, 4H), 7.19 (dd, J = 14.0, 7.2 Hz, 4H), 3.80 – 3.70 (m, 2H), 3.00 – 2.93 (m, 1H), 5.9 Hz, 1H), 2.86 (t, J = 7.6 Hz, 2H), 2.44 – 2.25 (m, 3H), 2.22 – 2.13 (m, 1H).

^{13}C-NMR (151 MHz, MeOH-*d*$_4$) δ 175.41, 140.01, 139.52 (d, $J_{C\text{-}P}$ = 6.6 Hz), 130.48 (d, $J_{C\text{-}P}$ = 6.4 Hz), 129.80, 129.44, 129.27, 127.54, 127.33, 50.57, 46.90 (d, $J_{C\text{-}P}$ = 133.9 Hz), 38.88, 33.83, 31.94 (d, $J_{C\text{-}P}$ = 15.2 Hz), 26.88.

^{31}P-NMR (243 MHz, MeOD-*d4*) δ 24.31.

HPLC (Method B): Rt = 8.56 min, purity = 97.3%.

LCMS (ESI$^+$): Rt = 2.86 min, m/z = 364.14.

HRMS (ESI$^-$): calculated for $C_{18}H_{22}NO_5P$: 362.1167 $[M - H]^-$, found 362.1163.

(4-(Hydroxy(3-phenylpropyl)amino)-4-oxo-1-phenylbutyl)phosphonic acid (**34b**)

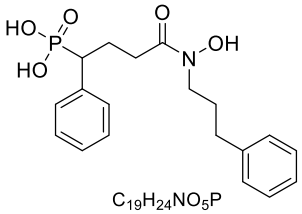

$C_{19}H_{24}NO_5P$
[377.1392]

34b was synthesized from (4-((benzyloxy)(3-phenylpropyl)amino)-4-oxo-1-phenylbutyl)phosphonic acid (**32b**) (1.00 eq., 0.65 mmol, 0.30 g) according to general procedure **7**. 0.19 g of **34b** (80%) was obtained as a yellow oil.

^{1}H-NMR (600 MHz, MeOH-*d*$_4$) δ 7.35 (d, J = 7.8 Hz, 2H), 7.29 (t, J = 7.6 Hz, 2H), 7.26 – 7.17 (m, 5H), 7.14 (t, J = 7.3 Hz, 1H), 3.65 – 3.52 (m, 2H), 3.07 – 3.00 (m, 1H), 2.58 (t, J = 7.8 Hz, 2H), 2.50 – 2.33 (m, 3H), 2.24 – 2.16 (m, 1H), 1.88 (p, J = 7.2 Hz, 2H).

^{13}C-NMR (151 MHz, MeOH-*d*$_4$) δ 175.58, 142.94, 139.70, 130.51 (d, $J_{C\text{-}P}$ = 5.8 Hz), 129.58, 129.36, 129.26, 127.50, 127.30, 126.85, 51.56, 47.02 (d, $J_{C\text{-}P}$ = 132.1 Hz), 33.94, 33.48, 31.98 (d, $J_{C\text{-}P}$ = 15.1 Hz), 29.55, 27.13, 26.28.

HPLC (Method C): Rt = 9.36 min, purity = 95.3%.

HRMS (ESI$^-$): calculated for $C_{18}H_{22}NO_5P$ 376.1312 $[M - H]^-$, found 376.1319.

(4-(Hydroxy(4-isopropylbenzyl)amino)-4-oxo-1-phenylbutyl)phosphonic acid (**34c**)

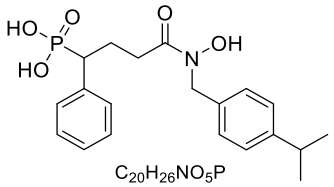

$C_{20}H_{26}NO_5P$
[391.1549]

34c was synthesized from (4-((benzyloxy)(4-isopropylbenzyl)amino)-4-oxo-1-phenylbutyl)phosphonic acid (**32c**) (1.00, 0.65 eq., 0.31 g) according to general procedure **7**. 0.24 g of **34c** (94%) was obtained as a colorless oil.

^{1}H-NMR (600 MHz, MeOH-d_4) δ 7.24 (d, J = 7.8 Hz, 2H), 7.19 (q, J = 7.9 Hz, 2H), 7.09 (d, J = 16.2 Hz, 5H), 4.65 – 4.48 (m, 2H), 2.99 – 2.91 (m, 1H), 2.77 (p, J = 6.9 Hz, 1H), 2.41 – 2.25 (m, 3H), 2.16 – 2.06 (m, 1H), 1.12 (d, J = 7.0 Hz, 6H), 1.10 (s, 1H).

^{13}C-NMR (151 MHz, MeOH-d_4) δ 175.35, 149.43, 138.86, 135.17, 130.52 (d, $J_{C\text{-}P}$ = 6.1 Hz), 129.41 (d, $J_{C\text{-}P}$ = 6.7 Hz), 127.78, 127.47, 52.65, 46.50 (d, $J_{C\text{-}P}$ = 137.5 Hz), 35.11, 31.69 (d, $J_{C\text{-}P}$ = 15.0 Hz), 26.63, 24.44.

HPLC (Method c): Rt = 10.37 min, purity = 95.5%.

HRMS (ESI$^+$): calculated for $C_{18}H_{22}NO_5P$ 392.1619 $[M + H]^+$, found 392.1621.

(4-(([1,1'-Biphenyl]-4-ylmethyl)(hydroxy)amino)-4-oxo-1-phenylbutyl)phosphonic acid (**34d**)

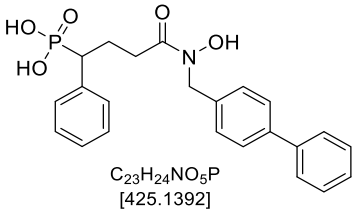

$C_{23}H_{24}NO_5P$
[425.1392]

34d was synthesized from (4-(([1,1'-biphenyl]-4-ylmethyl)(benzyloxy)amino)-4-oxo-1-phenylbutyl)phosphonic acid (**32d**) (1.00 eq., 0.15 mmol, 0.08 g) according to general procedure **7**. 0.07 g of **34d** (88%) and obtained as a white solid.

^{1}H-NMR (600 MHz, MeOH-d_4) δ 7.62 – 7.52 (m, 4H), 7.41 (t, J = 7.6 Hz, 2H), 7.37 – 7.26 (m, 7H), 7.21 (t, J = 7.4 Hz, 1H), 4.76 (q, J = 15.2 Hz, 2H), 3.11 – 3.02 (m, 1H), 2.52 – 2.41 (m, 3H), 2.30 – 2.15 (m, 1H).

^{13}C-NMR (151 MHz, MeOH-d_4) δ 142.09, 141.78, 139.05, 136.87, 130.51, 129.82, 129.38, 128.33, 128.06, 127.91, 127.75, 52.72, 46.63 (d, $J_{C\text{-}P}$ = 146.5 Hz), 31.75, 26.77.

HPLC (Method c): Rt = 10.66 min, purity = 96.4%.

LCMS (ESI$^+$): Rt = 3.6 min, m/z = 426.15.

HRMS (ESI$^+$): calculated for $C_{18}H_{22}NO_5P$ 426.1466 $[M + H]^+$, found 426.1465.

mp.: 121.4 ˚C.

(4-(Hydroxy(naphthalen-2-ylmethyl)amino)-4-oxo-1-phenylbutyl)phosphonic acid (**34e**)

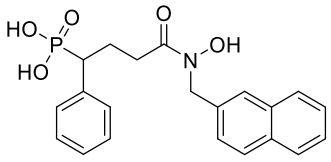

$C_{21}H_{22}NO_5P$
[399.1236]

34e was synthesized from (4-((benzyloxy)(naphthalen-2-ylmethyl)amino)-4-oxo-1-phenylbutyl)phosphonic acid (**32e**) (1.00 eq., 0.10 mmol, 0.05 g) according to general procedure **7**. 0.04 g of **34e** (98%) was obtained as a colorless oil.

^{1}H-NMR (600 MHz, MeOH-d_4) δ 7.90 – 7.82 (m, 4H), 7.54 (dd, J = 8.4, 1.7 Hz, 1H), 7.51 – 7.46 (m, 2H), 7.40 – 7.34 (m, 2H), 7.18 (t, J = 7.8 Hz, 2H), 7.07 (t, J = 7.4 Hz, 1H), 4.97 (s, 2H), 2.78 – 2.70 (m, 1H), 2.50 – 2.40 (m, 1H), 2.20 – 2.09 (m, 1H), 2.05 – 1.93 (m, 2H).

^{13}C-NMR (151 MHz, MeOH-d_4) δ 173.25, 134.82, 134.66, 130.61 (d, $J_{C\text{-}P}$ = 5.6 Hz), 130.51 (d, $J_{C\text{-}P}$ = 5.6 Hz), 129.33, 129.14 (d, $J_{C\text{-}P}$ = 3.1 Hz), 128.87, 128.78, 128.66, 127.73, 127.30, 127.20, 126.39, 78.96, 48.11, 33.44 (d, $J_{C\text{-}P}$ = 12.4 Hz), 29.31.

HPLC (Method C): Rt = 8.57 min, purity = 97.3%.

HRMS (ESI$^+$): calculated. for $C_{18}H_{22}NO_5P$ 400.1307 $[M + H]^+$, found 400.1308.

4-(Hydroxy(4-phenylbutyl)amino)-4-oxo-1-phenylbutyl)phosphonic acid (**46a**)

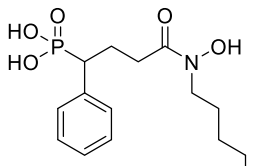

$C_{20}H_{26}NO_5P$
[391.1549]

46a was synthesized from (4-((benzyloxy)(4-phenylbutyl)amino)-4-oxo-1-phenylbutyl)phosphonic acid (**45a**) (1.00 eq., 0.40 mmol, 0.23 g) according to general procedure **7**. 0.17 g of **46a** (93%) was obtained as a colorless oil.

^{1}H-NMR (600 MHz, MeOH-d_4) δ 7.34 (dd, J = 7.7, 2.1 Hz, 2H), 7.29 – 7.21 (m, 4H), 7.20 – 7.11 (m, 4H), 3.63 – 3.51 (m, 1H), 3.05 – 2.84 (m, 2H), 2.67 – 2.58 (m, 2H), 2.46 – 2.29 (m, 2H), 2.26 – 2.14 (m, 1H), 1.74 – 1.52 (m, 5H).

^{13}C-NMR (151 MHz, MeOH-d_4) δ 175.43, 143.56, 142.86, 130.49 (d, $J_{C\text{-}P}$ = 6.1 Hz), 129.46, 129.43, 129.30, 127.47, 127.01, 126.73, 51.96, 47.12 (d, $J_{C\text{-}P}$ = 130.3 Hz), 36.40, 36.25, 32.03 (d, $J_{C\text{-}P}$ = 15.2 Hz), 29.64, 27.16, 24.18.

HPLC (Method C): Rt = 10.01 min, purity = 95.6%.

HRMS (ESI$^+$): calculated for $C_{20}H_{26}NO_5P$ 392.1626 $[M + H]^+$, found 392.1621.

(4-(Hydroxy(5-phenylpentyl)amino)-4-oxo-1-phenylbutyl)phosphonic acid (**46b**)

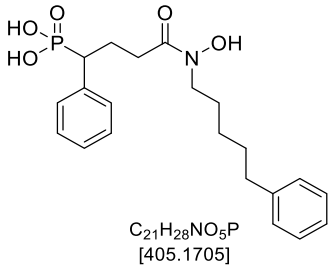

46b was synthesized from (4-((benzyloxy)(5-phenylpentyl)amino)-4-oxo-1-phenylbutyl)phosphonic acid (**45b**) (1.00 eq., 0.45 mmol, 0.22 g) according to general procedure **7**. 0.17 g of **46b** (92%) was obtained as a colorless oil.

^{1}H-NMR (600 MHz, MeOH-*d*$_4$) δ 7.35 (d, J = 7.6 Hz, 2H), 7.30 – 7.20 (m, 4H), 7.20 – 7.10 (m, 4H), 3.53 (h, J = 6.9 Hz, 2H), 3.02 – 2.88 (m, 1H), 2.65 – 2.56 (m, 2H), 2.45 – 2.29 (m, 2H), 2.24 – 2.12 (m, 1H), 1.68 – 1.49 (m, 5H), 1.39 – 1.27 (m, 2H).

^{13}C-NMR (151 MHz, MeOH-*d*$_4$) δ 175.37, 143.75, 139.72, 130.49 (d, $J_{C\text{-}P}$ = 6.0 Hz), 129.41 (d, $J_{C\text{-}P}$ = 5.2 Hz), 129.35, 129.26, 127.51, 126.82, 126.65, 51.98, 47.25 (d, $J_{C\text{-}P}$ = 134.4 Hz), 36.77, 32.31, 32.09, 27.47, 27.22, 24.44.

HPLC (Method C): Rt = 10.77 min, purity = 95.3%.

HRMS (ESI^{+}): calculated for $C_{21}H_{28}NO_5P$ 406.1772 $[M + H]^{+}$, found = 406.1778.

(4-((3-(4-Fluorophenyl)propyl)(hydroxy)amino)-4-oxo-1-phenylbutyl)phosphonic acid (**63a**)

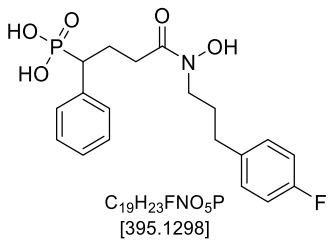

63a was synthesized from (4-((benzyloxy)(3-(4-fluorophenyl)propyl)amino)-4-oxo-1-phenylbutyl)phosphonic acid (**62a**) (1.00 eq., 0.25 mmol, 0.12 g) according to general procedure **7**. 0.09 g of **63a** (91%) was obtained as a colorless oil.

^{1}H-NMR (600 MHz, MeOH-*d*$_4$) δ 7.40 – 7.29 (m, 2H), 7.26 (t, J = 7.5 Hz, 2H), 7.17 (t, J = 6.9 Hz, 3H), 6.96 (t, J = 8.6 Hz, 2H), 3.58 (q, J = 6.5 Hz, 2H), 3.11 – 2.87 (m, 1H), 2.56 (t, J = 7.8 Hz, 2H), 2.52 – 2.31 (m, 3H), 2.27 – 2.08 (m, 1H), 1.86 (p, J = 7.2 Hz, 2H).

^{13}C-NMR (151 MHz, MeOH-*d*$_4$) δ 175.56, 162.69 (d, $^{1}J_{C\text{-}F}$ = 242.0 Hz), 139.86, 138.82, 131.01 (d, $J_{C\text{-}P}$ = 7.7 Hz), 130.55, 129.32, 129.25, 128.24, 127.97, 127.46, 115.94, 115.80, 65.20, 47.48 (d, $J_{C\text{-}P}$ = 141.2 Hz), 33.03, 31.82 (d, $J_{C\text{-}P}$ = 20.1 Hz), 29.66, 27.00.

^{19}F-NMR (565 MHz, MeOD-*d4*) δ -119.85 (d, J = 17.2 Hz).

HPLC (Method C): Rt = 9.54 min, purity = 97.4%.

HRMS (ESI$^+$): calculated for $C_{19}H_{23}FNO_5P$ 396.1372 $[M + H]^+$, found 396.1371.

(4-(Hydroxy(3-(4-(trifluoromethyl)phenyl)propyl)amino)-4-oxo-1-phenylbutyl)phosphonic acid (**63b**)

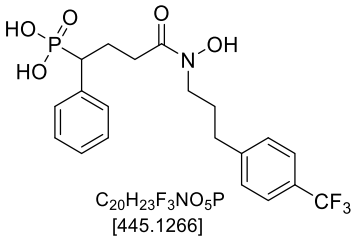

63b was synthesized from (4-((benzyloxy)(3-(4-(trifluoromethyl)phenyl)propyl)amino)-4-oxo-1-phenylbutyl)phosphonic acid (**62b**) (1.00 eq., 0.25 mmol, 0.13 g) according to general procedure **7**. 0.10 g of **63b** (91%) was obtained as a colorless oil.

^{1}H-NMR (600 MHz, MeOD-*d4*) δ 7.61 – 7.53 (m, 2H), 7.48 – 7.34 (m, 4H), 7.29 – 7.23 (m, 2H), 7.20 – 7.14 (m, 1H), 3.68 – 3.51 (m, 2H), 3.00 – 2.92 (m, 1H), 2.70 – 2.60 (m, 2H), 2.54 – 2.35 (m, 3H), 2.19 (s, 1H), 1.92 (q, J = 6.2 Hz, 2H).

^{13}C-NMR (151 MHz, MeOD-*d4*) δ 175.71, 147.68, 146.43, 140.36, 130.52, 130.07 (d, $J_{C\text{-}P}$ = 5.5 Hz), 129.22, 127.46, 127.36, 126.77, 126.61, 126.09, 124.97, 57.48, 49.55, 33.66, 33.03, 31.93, 31.51, 29.37, 29.20, 27.25.

^{19}F-NMR (282 MHz, MeOD-*d4*) δ -63.79, -63.91 (d, J = 9.2 Hz).

HPLC (Method C): Rt = 10.86 min, purity > 99.0%.

HRMS (ESI$^+$): calculated for $C_{20}H_{23}F_3NO_5P$ 446.1341 $[M + H]^+$, found 446.1339 $[M + H]^+$.

(4-(Hydroxy(3-(*p*-tolyl)propyl)amino)-4-oxo-1-phenylbutyl)phosphonic acid (**63c**)

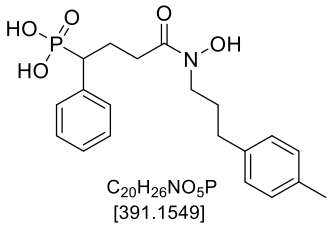

63c was synthesized from (4-((benzyloxy)(3-(*p*-tolyl)propyl)amino)-4-oxo-1-phenylbutyl)phosphonic acid (**62c**) (1.00 eq., 0.31 mmol, 0.149 g) according to general procedure **7**. 0.12 g of **63c** (94%) was obtained as a colorless oil.

^{1}H-NMR (300 MHz, MeOH-d_4) δ 7.43 – 7.16 (m, 5H), 7.06 (s, 4H), 3.56 (q, J = 4.6 Hz, 2H), 3.13 – 2.97 (m, 1H), 2.54 (t, J = 7.7 Hz, 2H), 2.39 (s, 2H), 2.28 (s, 3H), 2.26 – 2.04 (m, 2H), 1.85 (p, J = 7.1 Hz, 2H).

^{13}C-NMR (151 MHz, MeOH-d_4) δ 175.38, 143.81, 139.80, 138.84, 136.34, 130.51 (d, $J_{C\text{-}P}$ = 6.1 Hz), 129.96, 129.38, 129.29, 127.80, 47.01 (d, $J_{C\text{-}P}$ = 136.8 Hz), 33.50, 31.82 (d, $J_{C\text{-}P}$ = 15.6 Hz), 29.61, 26.69, 21.02.

HPLC (Method C): Rt = 10.09 min, purity = 96.8%.

LCMS (ESI$^+$): Rt = 3.40 min, , m/z = 392.16.

HRMS (ESI$^+$): calculated for $C_{20}H_{26}NO_5P$ 392.1624 $[M + H]^+$, found 392.1621 $[M + H]^+$.

(4-(Hydroxy(3-(4-methoxyphenyl)propyl)amino)-4-oxo-1-phenylbutyl)phosphonic acid (**63d**)

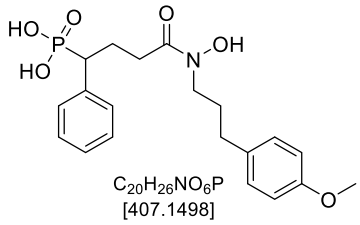

63d was synthesized from (4-((benzyloxy)(3-(4-methoxyphenyl)propyl)amino)-4-oxo-1-phenylbutyl)phosphonic acid (**62d**) (1.00 eq., 0.37 mmol, 0.18 g) according to general procedure **7**. 0.14 g of **63d** (89%) was obtained as a colorless oil.

^{1}H-NMR (300 MHz, MeOH-*d*$_4$) δ 7.39 – 7.17 (m, 5H), 7.09 (d, *J* = 8.1 Hz, 2H), 6.81 (d, *J* = 8.6 Hz, 2H), 3.74 (s, 3H), 3.57 (q, *J* = 6.6 Hz, 2H), 3.15 – 2.98 (m, 1H), 2.52 (t, *J* = 7.7 Hz, 2H), 2.39 (q, *J* = 9.4 Hz, 3H), 2.28 – 2.14 (m, 1H), 1.84 (p, *J* = 7.1 Hz, 2H).

^{13}C-NMR (75 MHz, MeOH-*d*$_4$) δ 175.23, 159.33, 138.51 (d, $J_{C\text{-}P}$ = 7.1 Hz), 134.85, 130.48 (d, $J_{C\text{-}P}$ = 6.1 Hz), 130.30, 129.41, 127.86, 114.76, 55.63, 46.39 (d, $J_{C\text{-}P}$ = 127.2 Hz), 32.97, 31.70 (d, $J_{C\text{-}P}$ = 15.8 Hz), 29.74, 26.50.

HPLC (Method C): Rt = 9.17 min, purity = 95.9%.

LCMS (ESI$^+$): Rt = 3.00 min, m/z = 408.16.

HRMS (ESI$^+$): calculated for $C_{20}H_{26}NO_6P$ 408.1572 $[M + H]^+$, found 408.1571.

Synthesis of hydroxamic acids **54a-d** and **65**

The hydroxamic acids **54a,b**, and **65** were synthesized according to general procedure **7** using the procedure reported by BEHRENDT et al.[136]

Diethyl (1-(3,4-difluorophenyl)-4-(hydroxy(phenethyl)amino)-4-oxobutyl)phosphonate (**54a**)

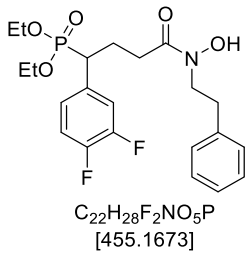

54a was synthesized from diethyl (4-((benzyloxy)(phenethyl)amino)-1-(3,4-difluorophenyl)-4-oxobutyl)phosphonate (**53a**) (1.00 eq., 0.50 mmol, 0.27 g) according to general procedure **7**. 0.20 g of **54a** (88%) was obtained as a yellow oil.

^{1}H-NMR (600 MHz, MeOD-*d4*) δ 7.71 – 7.58 (m, 7H), 7.55 – 7.49 (m, 1H), 4.54 – 4.45 (m, 2H), 4.44 – 4.34 (m, 1H), 4.35 – 4.27 (m, 1H), 4.20 (hept, *J* = 6.9 Hz, 2H), 3.71 – 3.62 (m, 1H), 3.30 (t, *J* = 7.4 Hz, 2H), 2.86 – 2.66 (m, 3H), 2.56 – 2.44 (m, 1H), 1.73 (t, *J* = 7.1 Hz, 3H), 1.60 (t, *J* = 7.1 Hz, 3H).

^{13}C-NMR (151 MHz, MeOD-*d4*) δ 174.45, 152.08 (dd, J_{C-F} = 85.8, J_{C-F} = 11.3 Hz), 150.41 (dd, J_{C-F} = 62.5, J_{C-F} = 7.8 Hz), 139.91, 134.29, 129.86, 129.45, 127.39, 127.16, 119.28 (dd, J_{C-F} = 18.0, J_{C-F} 6.5 Hz), 118.34 (d, J_{C-F} = 17.3 Hz), 64.11 (d, J_{C-P} = 7.1 Hz), 63.78 (d, J_{C-P} = 7.2 Hz), 50.36, 43.49 (d, J_{C-P} = 139.1 Hz), 33.76, 30.84 (d, J_{C-P} = 15.6 Hz), 25.87, 16.70 (d, J_{C-P} = 5.7 Hz), 16.57 (d, J_{C-P} = 5.7 Hz).

HPLC (Method C): Rt = 13.19 min, purity = 96.7%.

Diethyl (1-(3,4-difluorophenyl)-4-(hydroxy(3-phenylpropyl)amino)-4-oxobutyl)phosphonate (**54b**)

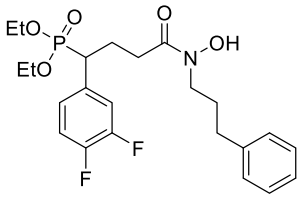

$C_{23}H_{30}F_2NO_5P$
[469.1830]

54b was synthesized from diethyl (4-((benzyloxy)(3-phenylpropyl)amino)-1-(3,4-difluorophenyl)-4-oxobutyl)phosphonate (**53b**) (1.00 eq., 0.20 mmol, 0.11 g) according to general procedure **7**. 0.09 g of **54b** (93%) was obtained as a yellow oil.

^{1}H-NMR (600 MHz, MeOH-d_4) δ 7.31 – 7.22 (m, 4H), 7.18 (d, J = 7.5 Hz, 2H), 7.17 – 7.13 (m, 2H), 4.11 – 4.05 (m, 2H), 4.00 – 3.93 (m, 1H), 3.94 – 3.86 (m, 1H), 3.58 (t, J = 7.0 Hz, 2H), 3.36 – 3.31 (m, 1H), 2.59 (t, J = 7.8 Hz, 2H), 2.45 – 2.27 (m, 3H), 2.21 – 2.10 (m, 1H), 1.88 (q, J = 7.4 Hz, 2H), 1.30 (t, J = 7.1 Hz, 3H), 1.17 (t, J = 7.0 Hz, 3H).

^{13}C-NMR (151 MHz, MeOH-d_4) δ 174.56, 152.08 (dd, J_{C-F} = 92.0, J_{C-F} = 10.4 Hz), 150.44 (dd, J_{C-F} = 89.4, J_{C-F} = 9.0 Hz), 142.87, 134.30, 129.39 (d, J_{C-F} = 4.4 Hz), 127.18 (d, J_{C-P} = 11.8 Hz), 126.91, 119.30 (dd, J_{C-F} = 17.9, J_{C-F} = 6.4 Hz), 118.37 (d, J_{C-F} = 17.7 Hz), 64.14 (d, J_{C-P} = 7.1 Hz), 63.80 (d, J_{C-P} = 7.2 Hz), 43.55 (d, J_{C-P} = 138.9 Hz), 33.93, 30.93 (d, J_{C-P} = 15.5 Hz), 29.57, 25.94, 16.69 (d, J_{C-P} = 5.9 Hz), 16.57 (d, J_{C-P} = 5.6 Hz).

HPLC (Method A): Rt = 18.52 min, purity = 95.2%.

Diethyl (1-(3,4-difluorophenyl)-4-(hydroxy(4-phenylbutyl)amino)-4-oxobutyl)phosphonate (**54c**)

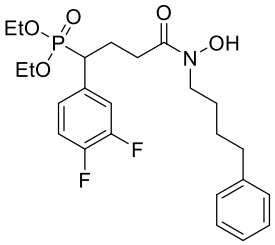

$C_{24}H_{32}F_2NO_5P$
[483.1986]

54c was synthesized from diethyl (4-((benzyloxy)(4-phenylbutyl)amino)-1-(3,4-difluorophenyl)-4-oxobutyl)phosphonate (**53c**) (1.00 eq., 0.30 mmol, 0.17 g) according to general procedure **7**. 0.13 g of **54c** (90%) was obtained as a yellow oil.

^{1}H-NMR (600 MHz, MeOD-*d4*) δ 7.29 – 7.08 (m, 8H), 4.11 – 4.04 (m, 2H), 3.99 – 3.84 (m, 2H), 3.65 – 3.53 (m, 2H), 3.30 – 3.21 (m, 1H), 2.62 (t, J = 7.2 Hz, 2H), 2.46 – 2.27 (m, 3H), 2.19 – 2.10 (m, 1H), 1.66 – 1.51 (m, 4H), 1.30 (t, J = 7.1 Hz, 4H), 1.16 (t, J = 7.1 Hz, 3H).

^{13}C-NMR (151 MHz, MeOD-*d4*) δ 174.40, 151.98 (dd, $J_{C\text{-}F}$ = 78.1, $J_{C\text{-}F}$ =14.1 Hz), 150.35 (dd, $J_{C\text{-}F}$ = 88.7, $J_{C\text{-}F}$ = 10.4 Hz), 143.54, 134.24 (d, $J_{C\text{-}P}$ = 8.6 Hz), 129.41, 129.32, 127.17 (td, $J_{C\text{-}P}$ = 6.7, $J_{C\text{-}F}$ = 3.4 Hz), 126.76, 119.27 (dd, $J_{C\text{-}F}$ = 17.9, $J_{C\text{-}F}$ = 6.5 Hz), 118.35 (dd, $J_{C\text{-}F}$ = 17.3, $J_{C\text{-}F}$ = 2.6 Hz), 64.12 (d, $J_{C\text{-}P}$ = 7.2 Hz), 63.79 (d, $J_{C\text{-}P}$ = 7.2 Hz), 43.50 (d, $J_{C\text{-}P}$ = 139.1 Hz), 36.35, 33.17, 30.82 (d, $J_{C\text{-}P}$ = 15.5 Hz), 29.61, 27.21, 25.92, 16.70 (d, $J_{C\text{-}P}$ = 5.8 Hz), 16.57 (d, $J_{C\text{-}P}$ = 5.6 Hz).

HPLC (Method C): Rt = 14.08 min, purity = 96.2%.

Diethyl (1-(3,4-difluorophenyl)-4-(hydroxy(5-phenylpentyl)amino)-4-oxobutyl)phosphonate (**54d**)

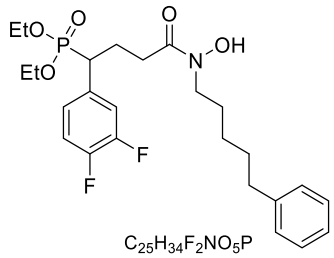

$C_{25}H_{34}F_2NO_5P$
[497.2143]

54d was synthesized from diethyl (4-((benzyloxy)(5-phenylpentyl)amino)-1-(3,4-difluorophenyl)-4-oxobutyl)phosphonate (**53d**) (1.00 eq., 0.55 mmol, 0.32 g) according to general procedure **7**. 0.25 g of **54d** (92%) was obtained as a yellow oil.

^{1}H-NMR (600 MHz, MeOD-*d4*) δ 7.31 – 7.20 (m, 4H), 7.18 – 7.10 (m, 4H), 4.15 – 4.02 (m, 2H), 4.02 – 3.85 (m, 2H), 3.54 (t, J = 7.0 Hz, 2H), 3.36 – 3.32 (m, 1H), 2.60 (t, J = 7.7 Hz, 2H), 2.45 – 2.30 (m, 3H), 2.19 – 2.08 (m, 1H), 1.62 (dp, J = 14.4, 7.4 Hz, 4H), 1.35 – 1.25 (m, 5H), 1.18 (t, J = 7.1 Hz, 3H).

^{13}C-NMR (151 MHz, MeOD-*d4*) δ 174.42, 152.25 (dd, $J_{C\text{-}F}$ = 74.0, $J_{C\text{-}F}$ = 11.5 Hz), 150.18 (dd, $J_{C\text{-}F}$ = 66.3, $J_{C\text{-}F}$ = 12.1 Hz), 143.74, 134.31, 129.41, 129.27, 127.20, 126.68, 119.33 (d, $J_{C\text{-}F}$ = 11.2 Hz), 118.38 (d, $J_{C\text{-}F}$ = 17.7 Hz), 64.15 (d, $J_{C\text{-}P}$ = 7.2 Hz), 63.82 (d, $J_{C\text{-}P}$ = 7.2 Hz), 49.57, 43.58 (d, $J_{C\text{-}P}$ = 139.1 Hz), 36.79, 32.27, 30.90 (d, $^{2}J_{C\text{-}P}$ = 15.7 Hz), 27.45, 27.21, 25.95, 16.71 (d, $J_{C\text{-}P}$ = 6.0 Hz), 16.58 (d, $J_{C\text{-}P}$ = 5.7 Hz).

HPLC (Method C): Rt = 14.84 min, purity = 97.2%.

Diethyl (4-((3-(3,5-difluorophenyl)propyl)(hydroxy)amino)-4-oxo-1-phenylbutyl)phosphonate (**65**)

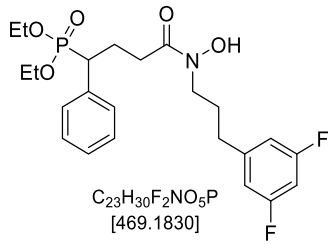

$C_{23}H_{30}F_2NO_5P$
[469.1830]

65 was synthesized from diethyl (4-((benzyloxy)(3-(3,5-difluorophenyl)propyl)amino)-4-oxo-1-phenylbutyl)phosphonate (**64**) (1.00 eq., 0.67 mmol, 0.38 g) according to general procedure **7**. 0.30 g of **65** (95%) was obtained as a colorless oil.

^{1}H-NMR (300 MHz, MeOD-*d4*) δ 7.45 – 7.23 (m, 5H), 6.86 – 6.78 (m, 2H), 6.78 – 6.67 (m, 1H), 4.17 – 4.00 (m, 2H), 3.96 – 3.67 (m, 2H), 3.58 (t, *J* = 6.9 Hz, 2H), 3.28 – 3.16 (m, 1H), 2.61 (t, *J* = 7.7 Hz, 2H), 2.45 – 2.12 (m, 4H), 1.88 (p, *J* = 7.1 Hz, 2H), 1.30 (t, *J* = 7.1 Hz, 3H), 1.12 (t, *J* = 7.1 Hz, 3H).

^{13}C-NMR (151 MHz, MeOD-*d4*) δ 175.04, 164.51 (dd, $J_{C\text{-}F}$ = 246.7, $J_{C\text{-}F}$ = 13.2 Hz), 147.58, 136.63, 130.60 (d, $J_{C\text{-}P}$ = 6.9 Hz), 129.67, 128.55, 112.21 (d, $J_{C\text{-}F}$ = 20.7 Hz), 102.01 (t, $J_{C\text{-}F}$ = 25.6 Hz), 64.06 (d, $J_{C\text{-}P}$ = 7.1 Hz), 63.58 (d, $J_{C\text{-}P}$ = 7.4 Hz), 55.93, 44.58 (d, $J_{C\text{-}P}$ = 141.4 Hz), 43.82, 33.54, 31.12 (d, $J_{C\text{-}P}$ = 15.7 Hz), 28.94, 25.99, 18.73, 16.67 (d, $J_{C\text{-}P}$ = 5.8 Hz), 16.49 (d, $J_{C\text{-}P}$ = 5.9 Hz).

HPLC (Method A): Rt = 13.35 min, purity = 95.7%.

8.3.2.4 Conversion of the diethyl phosphonates to phosphonic acids

General procedure **8** for the cleavage of the diethyl phosphonates **54a-d** and **65** to give phosphonic acids **55a-d** and **66**.

The phosphonic acids **55a-d** and **66** were synthesized using the procedure reported by BEHRENDT et al.[136]

To a solution of the appropriate phosphonic acid diethyl ester (**55a-d** and **66,** 1.00 eq.) in dry DCM (10 mL), trimethylsilyl bromide (5.00 eq.) was added at 0 °C. After 1 h, the solution was allowed to warm up to r.t. and stirred for further 24 h. After reaction completion, the solvents and the volatiles were evaporated at r.t. under reduced pressure and then kept for 16 h *in vacuo*. The residue was then dissolved in 10 mL THF and 0.1 mL H_2O and stirred at rt for 1 h. THF was then evaporated at r.t. *in vacuo* under reduced pressure, and the product was dried for 16 h *in vacuo*. The crude product was purified by reverse phase flash chromatography (on a prepacked silica cartridge), using water/acetonitrile (90:10-70:30) as eluent.

(1-(3,4-Difluorophenyl)-4-(hydroxy(phenethyl)amino)-4-oxobutyl)phosphonic acid (**55a**)

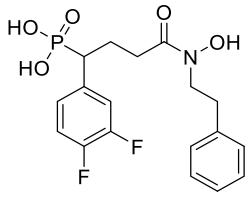

$C_{18}H_{20}F_2NO_5P$
[399.1047]

55a was synthesized from diethyl (1-(3,4-difluorophenyl)-4-(hydroxy(phenethyl)amino)-4 oxobutyl)phosphonate (**54a**) (1.00 eq., 0.15 mmol, 0.07 g) and trimethylsilyl bromide (2.00 eq., 0.30 mmol, 0.05 g, 0.04 mL)according to general procedure **8**. 0.05 g of **55a** (83%) was obtained as a yellow oil.

^{1}H-NMR (600 MHz, MeOD-*d4*) δ 7.31 – 7.12 (m, 8H), 7.11 – 7.06 (m, 1H), 3.76 (td, *J* = 7.3, 3.2 Hz, 2H), 3.09 – 2.98 (m, 1H), 2.87 (t, *J* = 7.6 Hz, 2H), 2.45 – 2.20 (m, 3H), 2.17 – 2.04 (m, 1H).

^{13}C-NMR (151 MHz, MeOD-*d4*) δ 174.92, 151.80 (dd, J_{C-F} = 97.4, J_{C-F} = 12.9 Hz), 150.14 (dd, J_{C-F} = 111.7, J_{C-F} = 11.9 Hz), 139.95, 136.21, 129.83, 129.46, 127.38, 127.01, 119.06 (d, J_{C-F} = 11.7 Hz), 117.99 (d, J_{C-F} = 17.1 Hz), 50.52, 45.46 (d, J_{C-P} = 136.2 Hz), 33.80, 31.44 (d, J_{C-P} = 15.4 Hz), 26.47.

^{19}F-NMR (565 MHz, MeOD-*d4*) δ -140.77 (d, *J* = 11.2 Hz), -143.48 (t, *J* = 14.8 Hz).

HPLC (Method C): Rt = 9.21 min, purity = 97.1%.

HRMS (ESI$^+$): calculated for $C_{18}H_{20}F_2NO_5P$ 400.1120 $[M + H]^+$, found 400.1120.

(1-(3,4-Difluorophenyl)-4-(hydroxy(3-phenylpropyl)amino)-4-oxobutyl)phosphonic acid (**55b**)

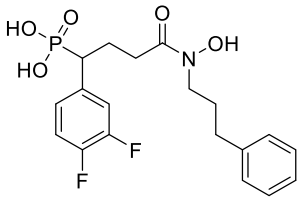

$C_{19}H_{22}F_2NO_5P$
[413.1204]

55b was synthesized from diethyl (1-(3,4-difluorophenyl)-4-(hydroxy(3-phenylpropyl)amino)-4-oxobutyl)phosphonate (**54b**) (1.00 eq., 0.22 mmol, 0.10 g) and trimethylsilyl bromide (2.00 eq., 0.44 mmol, 0.07 g, 0.06 mL) according to general procedure **8**. 0.08 g of **55b** (82%) was obtained as a colorless oil.

^{1}H-NMR (600 MHz, MeOH-d_4) δ 7.30 – 7.10 (m, 8H), 3.58 (h, *J* = 7.0 Hz, 2H), 3.11 – 3.03 (m, 1H), 2.59 (t, *J* = 7.8 Hz, 2H), 2.46 – 2.32 (m, 3H), 2.20 – 2.09 (m, 1H), 1.89 (p, *J* = 7.2 Hz, 2H).

^{13}C-NMR (151 MHz, MeOH-d_4) δ 175.05, 150.83 (dd, J_{C-F} = 129.2, J_{C-F} = 9.5 Hz), 149.33 (dd, $^1J_{C-F}$ = 128.51, $^2J_{C-F}$ = 12.30 Hz), 142.91, 129.67, 129.40 (d, J_{C-P} = 8.8 Hz), 126.94, 119.09 (dd, $^2J_{C-F}$ = 18.1, $^3J_{C-F}$ = 5.6 Hz), 117.97 (d, $^2J_{C-F}$ = 17.1 Hz), 51.65, 45.66 (d, J_{C-P} = 134.9 Hz), 33.93, 31.60 (d, J_{C-P} = 15.2 Hz), 29.60, 26.63, 20.89.

^{19}F-NMR (565 MHz, MeOD-*d4*) δ -140.77 (d, *J* = 82.8 Hz), -143.52 (d, *J* = 95.0 Hz).

HPLC (Method C): Rt = 9.94 min, purity = 95.3%.

HRMS (ESI$^+$): calculated for $C_{19}H_{22}F_2NO_5P$ 414.1283 $[M + H]^+$, found 414.1276.

(1-(3,4-Difluorophenyl)-4-(hydroxy(4-phenylbutyl)amino)-4-oxobutyl)phosphonic acid (**55c**)

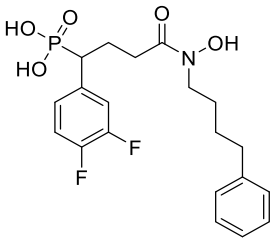

$C_{20}H_{24}F_2NO_5P$
[427.1360]

55c was synthesized from diethyl (1-(3,4-difluorophenyl)-4-(hydroxy(4-phenylbutyl)amino)-4-oxobutyl)phosphonate (**54c**) (1.00 eq., 0.30 mmol, 0.15 mg) and trimethylsilyl bromide (2.00 eq., 0.60 mmol, 0.09 g, 0.08 mL) according to general procedure **8**. 0.10 g of **55c** (78%) was obtained as a colorless oil.

^{1}H-NMR (600 MHz, MeOD-*d4*) δ 7.29 – 7.09 (m, 9H), 3.54 (td, J = 7.0, 3.1 Hz, 2H), 3.12 – 3.02 (m, 1H), 2.60 (t, J = 7.7 Hz, 2H), 2.47 – 2.30 (m, 3H), 2.19 – 2.09 (m, 1H), 1.67 – 1.57 (m, 4H), 1.35 – 1.27 (m, 3H).

^{13}C-NMR (151 MHz, MeOD-*d4*) δ 174.92, 152.42 (dd, $J_{C\text{-}F}$ = 112.3, $J_{C\text{-}F}$ = 19.5 Hz), 150.12 (dd, $J_{C\text{-}F}$ = 118.3, $J_{C\text{-}F}$ = 16.50Hz), 143.56, 129.44, 129.32, 126.75, 119.05 (dd, $J_{C\text{-}F}$ = 25.9, $J_{C\text{-}F}$ = 8.4 Hz), 117.91 (d, $J_{C\text{-}F}$ = 15.4 Hz), 45.66 (d, $J_{C\text{-}P}$ = 133.4 Hz), 36.38, 31.47 (d, $J_{C\text{-}P}$ = 15.1 Hz), 29.65, 27.23, 26.62.

HPLC (Method A): Rt = 11.40 min, purity = 95.2%.

HRMS (ESI^{+}): calculated for $C_{20}H_{24}F_2NO_5P$ 428.1436 $[M + H]^{+}$, found 428.1433.

(1-(3,4-Difluorophenyl)-4-(hydroxy(5-phenylpentyl)amino)-4-oxobutyl)phosphonic acid (**55d**)

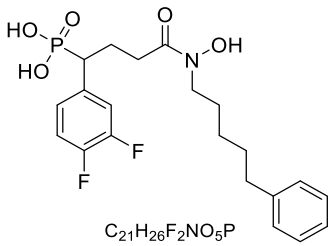

55d was synthesized from diethyl (1-(3,4-difluorophenyl)-4-(hydroxy(5-phenylpentyl)amino)-4-oxobutyl)phosphonate (**54d**) (1.00 eq., 0.22 mmol, 0.11 g) and trimethylsilyl bromide (2.00 eq., 0.44 mmol, 0.07, 0.06 mL)according to general procedure **8**. 0.09 g of **55d** (87%) was obtained as a colorless oil.

^{1}H-NMR (600 MHz, MeOD-*d4*) δ 7.26 – 7.11 (m, 8H), 3.54 (td, J = 6.9, 3.0 Hz, 2H), 3.12 – 3.03 (m, 1H), 2.60 (t, J = 7.7 Hz, 2H), 2.41 – 2.30 (m, 3H), 2.18 – 2.10 (m, 1H), 1.65 – 1.57 (m, 4H), 1.33 – 1.28 (m, 2H).

^{13}C-NMR (151 MHz, MeOD-*d4*) δ 174.84, 150.60 (dd, $J_{C\text{-}F}$ = 76.0, $J_{C\text{-}F}$ = 18.2 Hz), 149.83 (dd, $J_{C\text{-}F}$ = 77.2, $J_{C\text{-}F}$ = 21.5 Hz), 143.76, 129.41, 129.26, 126.67, 119.16 (dd, $J_{C\text{-}F}$ = 17.2, $J_{C\text{-}F}$ = 6.5 Hz), 118.07 (d, $J_{C\text{-}F}$ = 16.7 Hz), 49.57, 45.56 (d, $J_{C\text{-}P}$ = 135.9 Hz), 36.77, 32.30, 31.50 (d, $J_{C\text{-}F}$ = 15.8 Hz), 27.46, 27.21, 26.55.

HPLC (Method C): Rt = 11.40 min, purity = 96.2%.

HRMS (ESI^{+}): calculated for $C_{21}H_{26}F_2NO_5P$ 442.1590 $[M + H]^{+}$, found 442.1689.

4-((3-(3,5-Difluorophenyl)propyl)(hydroxy)amino)-4-oxo-1-phenylbutyl)phosphonic acid (**66**)

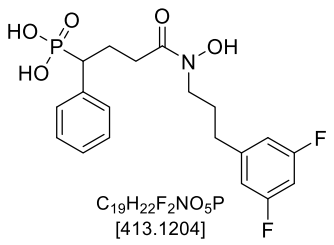

66 was synthesized from diethyl (4-((3-(3,5-difluorophenyl)propyl)(hydroxy)amino)-4-oxo-1-phenylbutyl)phosphonate (**65**) (1.00 eq., 0.34 mmol, 0.160 g) and trimethylsilyl bromide (2.00 eq., 0.68 mmol, 0.10 g, 0.09 mL) according to general procedure **8**. 0.10 g of **66** (71%) was obtained as a colorless oil.

^{1}H-NMR (300 MHz, MeOD-*d4*) δ 7.39 – 7.13 (m, 4H), 6.89 – 6.68 (m, 4H), 3.58 (t, J = 7.2 Hz, 2H), 3.09 – 2.92 (m, 1H), 2.77 – 2.55 (m, 3H), 2.39 (s, 2H), 2.28 – 2.14 (m, 1H), 1.99 – 1.80 (m, 2H).

^{13}C-NMR (151 MHz, MeOD-*d4*) δ 173.29, 164.52 (dt, $J_{C\text{-}F}$ = 259.0, $J_{C\text{-}F}$ = 10.5 Hz), 130.54, 129.30, 127.56, 112.25 (d, $J_{C\text{-}F}$ = 22.3 Hz), 51.03, 49.94, 33.56, 31.97, 29.02, 27.07.

HPLC (Method C): Rt = 9.90 min, purity = 97.9%.

HRMS (ESI^{+}): calculated for $C_{19}H_{22}F_2NO_5P$ 414.1272 $[M + H]^{+}$, found 414.1276.

8.3.3 Synthesis of bis(pivaloyloxymethyl)phosphonic acid (POM) esters

General procedure **9** for the synthesis of POM esters

The compounds were synthesized according to the procedure reported by BRÜCHER et al.[144]

A solution of the corresponding phosphonic acid (**32a-d**, and **69**, 1.00 eq.) in dry DMF (15 mL) was treated with TEA (3.00 eq.) after stirring for 10 min at r.t. chloromethyl pivalate (10.0 eq.) was added, and the solution was heated at 70 °C for 2 h. The mixture was treated again with TEA (1.00 eq.) and chloromethyl pivalate (1.50 eq.) and stirred for a further 2 h at 70 °C. The procedure of adding TEA and alkylating reagent was repeated once again. After two more hours at 70 °C, the reaction mixture was allowed to cool to room temperature and stirred for 16 h. The solution was diluted with diethyl ether (50 mL) and washed with water (60 mL), saturated aqueous solution of $NaHCO_3$ (2 × 60 mL), and once again with water (60 mL). The organic phase was dried over Na_2SO_4 and filtered, and the solvent was evaporated *in vacuo*. Crude products were purified by column chromatography on silica gel using diethyl ether as the eluent.

(((4-((Benzyloxy)(phenethyl)amino)-4-oxo-1-phenylbutyl)phosphoryl)bis(oxy))bis(methylene) bis(2,2-dimethylpropanoate) (**67a**)

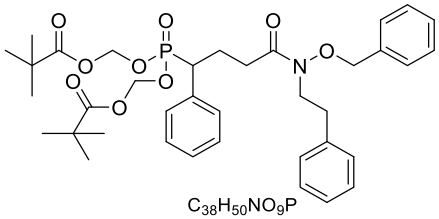

$C_{38}H_{50}NO_9P$
[681.3067]

67a was synthesized from (4-((benzyloxy)(phenethyl)amino)-4-oxo-1-phenylbutyl)phosphonic acid (**32a**) (1.00 eq, 1.07 mmol, 0.05 g) according to general procedure **9**. 0.31 g of **67a** (43%) was obtained as a colorless oil.

^{1}H-NMR (600 MHz, MeOD-*d4*) δ 7.37 – 7.29 (m, 7H), 7.25 (dd, J = 14.5, 7.3 Hz, 4H), 7.17 (dd, J = 15.1, 8.4 Hz, 4H), 5.66 – 5.59 (m, 2H), 5.51 – 5.42 (m, 2H), 4.63 – 4.46 (m, 2H), 3.95 – 3.69 (m, 2H), 3.28 – 3.19 (m, 1H), 2.87 – 2.74 (m, 2H), 2.25 – 2.12 (m, 3H), 2.04 (d, J = 7.6 Hz, 1H), 1.22 (d, J = 5.0 Hz, 9H), 1.18 (d, J = 5.1 Hz, 9H).

^{13}C-NMR (151 MHz, MeOD-*d4*) δ 178.02, 175.29, 139.84, 135.82, 135.36 (d, $J_{C\text{-}P}$ = 6.8 Hz), 130.65 (d, $J_{C\text{-}P}$ = 7.0 Hz), 130.53, 130.02, 129.95 (d, $J_{C\text{-}P}$ = 2.7 Hz), 129.91, 129.62, 129.48, 128.95 (d, $J_{C\text{-}P}$ = 3.4 Hz), 127.50, 83.05 (dd,

J_{C-P} = 12.1, 7.0 Hz), 77.11, 47.80, 44.65 (d, J_{C-P} = 138.1 Hz), 39.70 (d, J_{C-P} = 7.6 Hz), 33.95, 31.00, 30.89, 27.63, 27.27, 27.23, 25.24.

HPLC (method C): Rt: 19.63 min, Purity = 96.5%.

(((4-((Benzyloxy)(3-phenylpropyl)amino)-4-oxo-1-phenylbutyl)phosphoryl)bis(oxy))bis(methylene) bis(2,2-dimethylpropanoate) (**67b**)

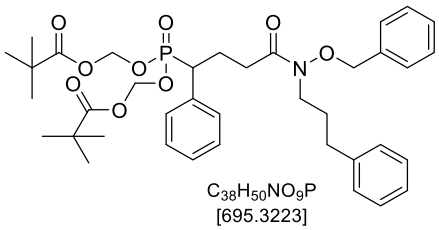

$C_{38}H_{50}NO_9P$
[695.3223]

67b was synthesized from (4-((benzyloxy)(3-phenylpropyl)amino)-4-oxo-1-phenylbutyl)phosphonic acid (**32b**) (1.00 eq., 1.07 mmol, 0.50 g) according to general procedure **9**. 0.30 g of **67b** (40%) was obtained as a colorless oil.

^{1}H-NMR (600 MHz, DMSO-*d6*) δ 7.38 – 7.22 (m, 11H), 7.16 (q, J = 10.8 Hz, 4H), 5.63 – 5.53 (m, 3H), 5.49 – 5.41 (m, 2H), 4.61 (q, J = 10.2 Hz, 2H), 3.58 (s, 2H), 3.38 (d, J = 10.1 Hz, 1H), 2.23 (s, 3H), 2.00 (d, J = 10.2 Hz, 1H), 1.81 – 1.72 (m, 2H), 1.16 – 1.13 (m, 9H), 1.11 (dd, J = 8.1, 2.6 Hz, 10H).

^{13}C-NMR (151 MHz, DMSO-*d6*) δ 176.09, 176.04, 141.36, 129.34, 129.15 (d, J_{C-P} = 7.2 Hz), 128.66, 128.56, 128.41, 128.27, 128.21, 127.37, 125.79, 81.43, 75.38, 42.56 (d, J_{C-P} = 136.6 Hz), 40.06, 38.17, 38.12, 32.24, 29.39 (d, J_{C-P} = 16.7 Hz), 28.15, 26.46, 26.42, 23.91.

HPLC (method C): Rt: 20.13 min, Purity = 96.2%.

(((4-((Benzyloxy)(4-isopropylbenzyl)amino)-4-oxo-1-phenylbutyl)phosphoryl)bis(oxy))bis(methylene) bis(2,2-dimethylpropanoate) (**67c**)

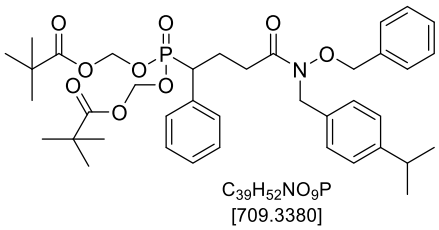

$C_{39}H_{52}NO_9P$
[709.3380]

67c was synthesized from (4-((benzyloxy)(4-isopropylbenzyl)amino)-4-oxo-1-phenylbutyl)phosphonic acid (**32c**) (1.00 eq., 0.85 mmol, 0.40 g) according to general procedure **9**. 0.19 g of **67c** (35%) was obtained as a colorless oil.

^{1}H-NMR (600 MHz, MeOD-*d4*) δ 7.34 – 7.24 (m, 9H), 7.21 – 7.13 (m, 4H), 7.06 (s, 1H), 5.68 – 5.57 (m, 1H), 5.54 – 5.40 (m, 1H), 4.77 – 4.63 (m, 2H), 4.62 – 4.46 (m, 2H), 3.22 – 3.00 (m, 1H), 2.93 – 2.83 (m, 1H), 2.49 – 2.29 (m, 3H), 2.21 – 2.14 (m, 1H), 1.23 (dd, J = 7.4, 1.0 Hz, 5H), 1.21 – 1.16 (m, 17H).

^{13}C-NMR (151 MHz, MeOD-*d4*) δ 182.53, 177.83, 130.86, 130.55, 129.53, 129.12, 127.54, 127.19, 93.43, 77.48, 50.68, 45.07 (d, $J_{C\text{-}P}$ = 131.9 Hz), 39.34, 35.10, 27.63, 27.29, 24.44.

HPLC (method C): Rt: 20.57 min, Purity = 99.0%.

(((4-(([1,1'-Biphenyl]-4-ylmethyl)(benzyloxy)amino)-4-oxo-1-phenylbutyl)phosphoryl)bis(oxy))bis(methylene) bis(2,2-dimethylpropanoate) (**67d**)

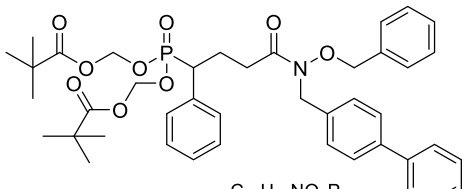

67d was synthesized from (4-(([1,1'-biphenyl]-4-ylmethyl)(benzyloxy)amino)-4-oxo-1-phenylbutyl)phosphonic acid (**32d**) (1.00 eq., 1.07 mmol, 0.55 g) according to general procedure **9**. 0.16 g of **67d** (20%) was obtained as a colorless oil.

^{1}H-NMR (600 MHz, MeOD-*d4*) δ 7.62 – 7.55 (m, 4H), 7.42 (t, *J* = 7.7 Hz, 3H), 7.38 – 7.24 (m, 11H), 7.12 (s, 1H), 5.65 – 5.57 (m, 2H), 5.51 – 5.41 (m, 2H), 4.79 (d, *J* = 15.2 Hz, 2H), 4.70 – 4.58 (m, 2H), 3.34 (d, *J* = 6.3 Hz, 1H), 2.37 (d, *J* = 8.2 Hz, 1H), 2.32 (t, *J* = 7.1 Hz, 2H), 2.21 – 2.12 (m, 1H), 1.20 – 1.18 (m, 10H), 1.15 (d, *J* = 1.4 Hz, 8H).

^{13}C-NMR (151 MHz, MeOD-*d4*) δ 182.50, 178.04, 141.93 (d, $J_{C\text{-}P}$ = 8.9 Hz), 130.68 (d, $J_{C\text{-}P}$ = 6.9 Hz), 130.58 (d, $J_{C\text{-}P}$ = 2.5 Hz), 130.13, 129.98 (d, $J_{C\text{-}P}$ = 2.7 Hz), 129.93, 129.87, 129.60, 129.15, 128.96, 128.41, 128.13, 127.96, 127.79, 38.13, 83.06, 77.51, 55.82, 44.56 (d, $J_{C\text{-}P}$ = 137.6 Hz), 39.69 (d, $^{2}J_{C\text{-}P}$ = 7.2 Hz), 39.33, 27.62, 27.26, 27.21, 18.70.

HPLC (method C): Rt: 20.63 min, Purity = 96.8%.

(((4-((benzyloxy)(methyl)amino)-4-oxo-1-phenylbutyl)phosphoryl)bis(oxy))bis(methylene) bis(2,2-dimethylpropanoate) (**70**)

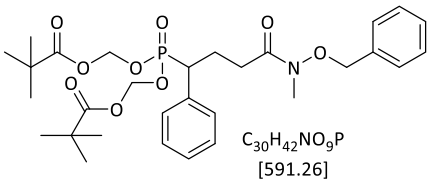

70 was synthesized from (4-((benzyloxy)(methyl)amino)-4-oxo-1-phenylbutyl)phosphonic acid (**69**) (2.10 eq., 1.07 mmol, 0.76 g) according to general procedure **9**. 0.31 g of **70** (25%) was obtained as a colorless oil.

The product **70** was used directly for the following reaction.

General procedure **10** for the deprotection of the *O*-Bn-protected POM ester prodrugs **67a-d**, and **70** to the hydroxamic acids **68a-d**, and **72**

Compounds **68a-d** and **72** were synthesized according to the procedure reported by BEHRENDT et al.[136]

The appropriate *O*-Bn-protected POM ester prodrugs **67a-d**, and **70** were dissolved in 10 mL of MeOH, and 10 mol% of 10 wt% Pd/C was added to the reaction solution. The catalytic hydrogenation was performed for 1-3 h, and the reaction solution was filtered through celite®. The solvent was removed under reduced pressure, and the products were purified by flash chromatography (on a prepacked silica cartridge), using *n*-hexane:EtOAc (100:0→50:50) as eluent.

(((4-(Hydroxy(phenethyl)amino)-4-oxo-1-phenylbutyl)phosphoryl)bis(oxy))bis(methylene) bis (2,2-dimethylpropanoate) (**68a**)

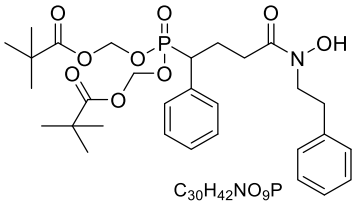

$C_{30}H_{42}NO_9P$
[591.2597]

68a was synthesized from (((4-((benzyloxy)(phenethyl)amino)-4-oxo-1-phenylbutyl)phosphoryl)bis(oxy))bis(methylene) bis(2,2-dimethylpropanoate) (**67a**) (1.00 eq., 0.10 mmol, 0.24 g) according to general procedure **10**. 0.20 g of **68a** (95%) was obtained as a colorless oil.

^{1}H-NMR (600 MHz, MeOD-*d4*) δ 7.38 – 7.33 (m, 2H), 7.33 – 7.27 (m, 4H), 7.26 (t, J = 7.5 Hz, 2H), 7.22 – 7.15 (m, 3H), 5.67 – 5.61 (m, 2H), 5.53 – 5.44 (m, 2H), 3.78 – 3.72 (m, 2H), 3.36 – 3.32 (m, 1H), 2.85 (t, J = 7.5 Hz, 2H), 2.37 – 2.22 (m, 3H), 2.14 (m, 1H), 1.22 (d, J = 3.1 Hz, 10H), 1.18 (s, 9H).

^{13}C-NMR (151 MHz, MeOD-*d4*) δ 178.07, 174.84, 145.16, 135.46, 130.66, 129.87, 129.47, 128.89, 127.40, 83.07, 45.00 (d, $J_{C\text{-}P}$ = 136.6 Hz), 39.72 (d, $J_{C\text{-}P}$ = 7.0 Hz), 33.80, 27.26, 27.23, 25.48.

HPLC (method C): Rt: 16.35 min, Purity > 99.0%.

(((4-(Hydroxy(3-phenylpropyl)amino)-4-oxo-1-phenylbutyl)phosphoryl)bis(oxy))bis(methylene) bis(2,2-dimethylpropanoate) (**68b**)

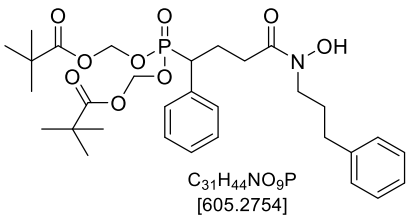

$C_{31}H_{44}NO_9P$
[605.2754]

68b was synthesized from (((4-((benzyloxy)(3-phenylpropyl)amino)-4-oxo-1-phenylbutyl)phosphoryl)bis(oxy))bis(methylene) bis(2,2-dimethylpropanoate) (**67b**) (1.00 eq., 0.10 mmol, 0.07 g) according to general procedure **10**. 0.06 g of **68b** (96%) was obtained as a colorless oil.

^{1}H-NMR (600 MHz, MeOD-*d4*) δ 5.85 – 5.52 (m, 10H), 4.12 – 4.05 (m, 2H), 3.98 – 3.89 (m, 2H), 3.31 (s, 11H), 2.01 (qt, J = 13.8, 6.9 Hz, 2H), 1.88 – 1.80 (m, 1H), 1.03 (t, J = 7.8 Hz, 2H), 0.86 – 0.78 (m, 2H), 0.66 (s, 2H), 0.32 (p, J = 7.1 Hz, 2H), -0.30 – -0.40 (m, 18H).

^{13}C-NMR (151 MHz, MeOD-*d4*) δ 178.11, 173.29, 142.92, 130.66, 130.60, 130.54, 129.88 (d, $J_{C\text{-}P}$ = 8.3 Hz), 129.38 (d, $J_{C\text{-}P}$ = 7.7 Hz), 129.29, 128.88, 126.88, 83.17, 57.40 (d, $J_{C\text{-}P}$ = 21.3 Hz), 44.22 (d, $J_{C\text{-}P}$ = 133.1 Hz), 39.72 (d, $J_{C\text{-}P}$ = 6.0 Hz), 33.95, 29.57, 27.62, 27.39, 27.25, 27.22, 25.70.

HPLC (method C): Rt: 20.63 min, Purity > 99.0%.

(((4-(Hydroxy(4-isopropylbenzyl)amino)-4-oxo-1-phenylbutyl)phosphoryl)bis(oxy))bis(methylene) bis(2,2-dimethylpropanoate) (**68c**)

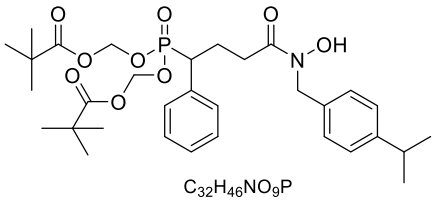

$C_{32}H_{46}NO_9P$
[619.2910]

68c was synthesized from (((4-((benzyloxy)(4-isopropylbenzyl)amino)-4-oxo-1-phenylbutyl)phosphoryl)bis(oxy)) bis(methylene) bis(2,2-dimethylpropanoate) (**67c**) (1.00 eq., 0.40 mmol, 0.28 g) according to general procedure **10**. 0.23 g of **68c** (93%) was obtained as a colorless oil.

^{1}H-NMR (600 MHz, MeOD-*d4*) δ 7.39 – 7.26 (m, 6H), 7.18 (s, 3H), 5.64 (td, J = 12.5, 5.3 Hz, 2H), 5.53 – 5.42 (m, 2H), 4.72 – 4.54 (m, 2H), 3.43 – 3.33 (m, 1H), 2.88 (p, J = 6.9 Hz, 1H), 2.44 – 2.35 (m, 3H), 2.27 – 2.17 (m, 1H), 1.25 – 1.21 (m, 16H), 1.18 (s, 12H).

^{13}C-NMR (151 MHz, MeOD-*d4*) δ 178.07, 174.49, 146.38, 130.63 (d, $J_{C\text{-}P}$ = 7.4 Hz), 129.88, 129.50, 127.48, 83.11, 52.64, 44.32 (d, $J_{C\text{-}P}$ = 125.7 Hz), 39.71 (d, $J_{C\text{-}P}$ = 7.6 Hz), 35.12, 27.26, 27.22, 25.51, 24.45.

HPLC (method C): Rt: 17.87 min, Purity = 97.1%.

(((4-(([1,1'-Biphenyl]-4-ylmethyl)(hydroxy)amino)-4-oxo-1phenylbutyl)phosphoryl)bis(oxy))bis(methylene) bis(2,2-dimethylpropanoate) (**68d**)

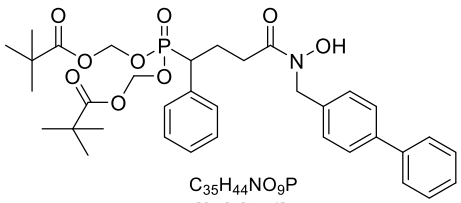

$C_{35}H_{44}NO_9P$
[653.2754]

68d was synthesized from (((4-(([1,1'-biphenyl]-4-ylmethyl)(benzyloxy)amino)-4-oxo-1-phenylbutyl)phosphoryl) bis(oxy))bis(methylene) bis(2,2-dimethylpropanoate) (**67d**) (1.00 eq., 0.40 mmol, 0.30 g) according to general procedure **10**. 0.24 g of **68d** (92%) was obtained as a colorless oil.

^{1}H-NMR (600 MHz, MeOD-*d4*) δ 7.64 – 7.51 (m, 4H), 7.42 (t, *J* = 7.6 Hz, 2H), 7.38 – 7.26 (m, 8H), 5.63 (td, *J* = 12.8, 5.2 Hz, 2H), 5.54 – 5.42 (m, 2H), 4.80 – 4.68 (m, 2H), 3.44 – 3.34 (m, 1H), 2.48 – 2.35 (m, 3H), 2.28 – 2.16 (m, 1H), 1.21 (d, *J* = 8.6 Hz, 9H), 1.18 (d, *J* = 11.3 Hz, 9H).

^{13}C-NMR (151 MHz, MeOD-*d4*) δ 178.07, 174.64, 142.05, 141.77, 136.87, 135.37 (d, *J* = 7.3 Hz), 130.63 (d, *J* = 7.1 Hz), 129.85, 128.89 (d, *J* = 3.3 Hz), 128.36, 128.06, 127.92, 83.09 (dd, *J* = 10.3, 7.0 Hz), 52.66, 44.79 (d, *J* = 137.5 Hz), 39.70 (d, *J* = 7.1 Hz), 31.01, 30.82 (d, *J* = 23.1 Hz), 27.25, 27.21, 25.51.

HPLC (method C): Rt: 17.77 min, Purity > 99.9%.

(((4-(Hydroxy(methyl)amino)-4-oxo-1-phenylbutyl)phosphoryl)bis(oxy))bis(methylene) bis(2,2-dimethylpropanoate) (**72**)

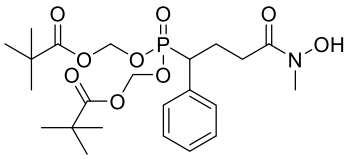

$C_{23}H_{36}NO_9P$
[501.2128]

72 was synthesized from (((4-((benzyloxy)(methyl)amino)-4-oxo-1-phenylbutyl)phosphoryl)bis(oxy))bis(methylene) bis(2,2-dimethylpropanoate) (**70**) (1.00 eq., 0.39 mmol, 0.23 g) according to general procedure **10**. 0.18 g of **72** (92%) was obtained as a colorless oil.

^{1}H-NMR (600 MHz, MeOD-*d4*) δ 7.39 – 7.28 (m, 5H), 5.70 – 5.59 (m, 2H), 5.56 – 5.43 (m, 2H), 3.41 – 3.32 (m, 1H), 3.13 (s, 3H), 2.41 – 2.30 (m, 2H), 2.25 – 2.17 (m, 1H), 1.82 – 1.71 (m, 1H), 1.23 (d, *J* = 3.0 Hz, 9H), 1.19 (d, *J* = 2.5 Hz, 9H).

^{13}C-NMR (151 MHz, MeOD-*d4*) δ 178.06, 174.57, 135.42 (d, $J_{C\text{-}P}$ = 7.5 Hz), 130.62 (d, $J_{C\text{-}P}$ = 3.4 Hz), 130.58 (d, $J_{C\text{-}P}$ = 3.7 Hz), 129.93 (t, $J_{C\text{-}P}$ = 2.8 Hz), 129.86 (d, $J_{C\text{-}P}$ = 2.7 Hz), 128.89, 83.10 (d, $J_{C\text{-}P}$ = 12.7Hz), 64.91, 44.51 (d, $J_{C\text{-}P}$ = 138.4 Hz), 39.71 (d, $J_{C\text{-}P}$ = 6.7 Hz), 36.21, 30.81, 30.34, 27.24, 27.21.

HPLC (method C): Rt: 17.77 min, Purity > 99.0%.

8.4 Biological evaluation

8.4.1 DXR enzyme assays

The *Pf*, *Ec,* and *Mtb* DXR inhibition assay was performed by the working group of Prof. Dr. MARKUS FISCHER

8.4.1.1 Gene expression and protein purification

The DXR of *P. falciparum* was expressed in *E. coli,* and the protein was purified as described earlier.[133] DXR orthologs of *E. coli* or *M. tuberculosis* were produced, isolated, and purified. The recombinant *E. coli* strain M15 pREP4 containing pQEispC-Ec (for the *E. coli* enzyme) or pQEispC-Mt (for the *M. tuberculosis* enzyme) was grown in shaking flasks with LB medium supplemented with ampicillin (70 mg L^{-1}) and kanamycin (30 mg L^{-1}) to an optical density of 0.4-0.6 at 37 ˚C. Isopropyl β-D-thiogalactoside was added to a final concentration of 1 mM, and the cell culture was incubated further for 36 h at 20 ˚C under shaking (140 rpm). Cells were harvested 16 hours thereafter by centrifugation, washed with 0.9% NaCl solution, and resuspended in loading buffer (50 mM Tris hydrochloride, pH 8.0, 0.5 M NaCl, 20 mM imidazole and 0.02% NaN3). The sample was passed through a cell disruption device (FrenchPress, Constant Cell Disruption Systems, Koenigswinter, Germany) and was then centrifuged (15,000 rpm, +4 ˚C, 1 h). The supernatant was applied onto a Ni^{2+}-chelating Sepharose fast flow column (1.5 cm × 15 cm) that had been pre-equilibrated with a loading buffer. The column was washed with 150 mL of the loading buffer and then developed with an imidazole gradient (20 mM - 500 mM) in the loading buffer. Fractions of DXR-containing eluent were combined and dialyzed overnight against 50 mM Tris-hydrochloride, pH 8.0, 2 mM DTT, 0.02% NaN3. DXR batches were approximately 95% pure, as estimated by SDS-PAGE analysis.

8.4.1.2 Photometric assay

Assays were conducted in 384-well plates with flat clear bottoms (Nunc, Wiesbaden, Germany). Dilution series (1:2) in DMSO for each tested compound were prepared in 10 wells of the 384-well plate so that at the end of the dilution series, each well contained the tested compound in 3 µl of DMSO. After that, 27 µL of assay buffer A containing 100 mM Tris-HCl pH 7.6 and 1.1 mM DXP were added to each assay well. The plate was centrifuged (3000 rpm, 10 sec, room temperature), and the assay was started by adding to each well 30 µl of assay buffer B containing 100 mM Tris-HCl, pH 7.6, 5 mM $MnCl_2$, 5 mM DTT, 0.5 mM NADPH, 0.02 U of DXR. The reaction was monitored photometrically (room temperature) at 340 nm using a plate reader (Spectra Max M5, Molecular Devices, Biberach a der Riss, Germany). IC_{50} values were estimated with the program Dynafit, as described earlier.[155,190]

8.4.2 Parasite *In Vitro* culture

The antiproliferative potential of the synthesized compounds against two *P. falciparum* strains, *Pf*Dd2 and *Pf*3D7, and the cytotoxicity against human HepG-2 cells were tested by the group of Dr. JANA HELD.

8.4.2.1 Chemicals

All tested drugs were first dissolved in their respective solvents (chloroquine in Milli-Q® water and the new compounds in DMSO) and subsequently further diluted in a complete culture medium to have the desired final concentration.

8.4.2.2 *Plasmodium* asexual stages

P. falciparum laboratory strains *Pf*3D7 (chloroquine-sensitive, provided by BEI resources, MRA-102) and *Pf*Dd2 (multidrug-resistant, provided by BEI resources, MRA-150 were cultivated *in vitro* as described before.[191,192] Briefly, the parasites were maintained in complete culture medium consisting of RPMI-1640 (Sigma-Aldrich) supplemented with 1M *N*-2-hydroxyethylpiperazine-*N*-2-ethane sulfonic acid (HEPES) solution (2.4% v/v) (Sigma-Aldrich), 200 mM L-glutamine (Gibco), 50 µg/ml gentamicin (Gibco), and 10% of AlbuMax II solution containing RPMI, hypoxanthine, $NaHCO_3$, HEPES, D-Glucose and 50 g/l of AlbuMax II (0.5% wt/vol in culture medium) at 2.5% hematocrit. The cultures were kept at 5% CO_2 and 5% O_2 at 37°C, with a change of medium every two days. *P. falciparum* parasites were synchronized using magnetic column separation (MACS) prior to the assays.[193]

8.4.2.3 Growth inhibition assays with asexual parasites

Growth inhibition assays of asexual stages of *P. falciparum* were performed as described before.[194] Briefly, the drugs were distributed in a 3-fold serial dilution in 96-well plates. The highest concentration of the solvent (<0.1%) did not interfere with parasite growth. Synchronized ring-stage parasites were diluted to a parasitemia of 0.05% with O Rh^+ erythrocytes in a complete RPMI medium and seeded at a hematocrit of 1.5% in a total volume of 225 µl per well. Plates were subsequently incubated at 5% CO_2 and 5% O_2 at 37°C before the plates were frozen and thawed three times. The growth inhibition of *P. falciparum* was measured using an enzyme-linked immunosorbent assay (ELISA) for histidine-rich protein 2 (HRP2) using a microplate reader (CLARIOstar BMG Labtech) (excitation filter: 450 nm).

8.4.3 Evaluation of cytotoxicity against human HepG2 cells

HepG2 cells (obtained from ATCC; HB-8065), a human hepatocyte carcinoma cell line, were maintained in DMEM medium (Sigma-Aldrich) supplemented with 10% of inactivated fetal bovine serum (Sigma-Aldrich), 200 mM L-glutamine (Gibco), 12 mL of HEPES buffer (Gibco), and 50 µg/ml penicillin/streptomycin solution (Gibco). Trypsin (Gibco) was used to detach the cells when they reached a semiconfluent layer. Cytotoxicity was evaluated using the neutral red assay as described previously by MISHRA et al. [195] Briefly,300,000 cells were seeded in supplemented Dulbecco´s Modified Eagle´s Medium (DMEM) medium as described above to 96-well plates. After 24 hours, the cells were incubated with a twofold serial dilution of the respective drug diluted in a supplemented DMEM medium for an additional 24 hours. The highest concentration of the solvent (<1%) did not interfere with cell viability. Subsequently, the drug-containing medium was replaced by a supplemented DMEM medium with 1.5% neutral red, and the cells were incubated for an additional 3 h at 37°C. Cells were then washed with phosphate-buffered saline (pH 7.2), and 100 µL of freshly prepared lysing buffer (50% methanol, 49% distilled

water, and 1% acetic acid) were added to the plates. Subsequently, the cells were shaken for 10 min, and the absorption was measured at a wavelength of 540 nm using CLARIOstar (BMG Labtech).[195]

9. References

(1) Michaud, C. M. Global Burden of Infectious Diseases. In *Encyclopedia of Microbiology*; Elsevier, 2009; pp 444–454. https://doi.org/10.1016/B978-012373944-5.00185-1.

(2) WHO. *World Malaria Report 2022*; 2022. https://www.who.int/teams/global-malaria-programme/reports/world-malaria-report-2022 (accessed 2023-08-01).

(3) WHO. *World Malaria Report 2021*; 2021. https://www.who.int/teams/global-malaria-programme/reports/world-malaria-report-2021 (accessed 2023-08-01).

(4) Tuteja, R. Malaria - An Overview. *FEBS Journal* **2007**, *274* (18), 4670–4679. https://doi.org/10.1111/j.1742-4658.2007.05997.x.

(5) Westling, J.; Yowell, C. A.; Majer, P.; Erickson, J. W.; Dame, J. B.; Dunn, B. M. Plasmodium Falciparum, P. Vivax,AndP. Malariae:A Comparison of the Active Site Properties of Plasmepsins Cloned and Expressed from Three Different Species of the Malaria Parasite. *Exp Parasitol* **1997**, *87* (3), 185–193. https://doi.org/10.1006/EXPR.1997.4225.

(6) White, N. J. Plasmodium Knowlesi: The Fifth Human Malaria Parasite. *Clinical Infectious Diseases* **2008**, *46* (2), 172–173. https://doi.org/10.1086/524889.

(7) MARTENS, P.; KOVATS, R.; NIJHOF, S.; DEVRIES, P.; LIVERMORE, M.; BRADLEY, D.; COX, J.; MCMICHAEL, A. Climate Change and Future Populations at Risk of Malaria. *Global Environmental Change* **1999**, *9*, S89–S107. https://doi.org/10.1016/S0959-3780(99)00020-5.

(8) Sato, S. Plasmodium—a Brief Introduction to the Parasites Causing Human Malaria and Their Basic Biology. *J Physiol Anthropol* **2021**, *40* (1), 1. https://doi.org/10.1186/s40101-020-00251-9.

(9) Putaporntip, C.; Kuamsab, N.; Pattanawong, U.; Yanmanee, S.; Seethamchai, S.; Jongwutiwes, S. Plasmodium Cynomolgi Co-Infections among Symptomatic Malaria Patients, Thailand. *Emerg Infect Dis* **2021**, *27* (2), 590–593. https://doi.org/10.3201/eid2702.191660.

(10) Imwong, M.; Madmanee, W.; Suwannasin, K.; Kunasol, C.; Peto, T. J.; Tripura, R.; von Seidlein, L.; Nguon, C.; Davoeung, C.; Day, N. P. J.; Dondorp, A. M.; White, N. J. Asymptomatic Natural Human Infections With the Simian Malaria Parasites *Plasmodium Cynomolgi* and *Plasmodium Knowlesi*. *J Infect Dis* **2019**, *219* (5), 695–702. https://doi.org/10.1093/infdis/jiy519.

(11) Grignard, L.; Shah, S.; Chua, T. H.; William, T.; Drakeley, C. J.; Fornace, K. M. Natural Human Infections With Plasmodium Cynomolgi and Other Malaria Species in an Elimination Setting in Sabah, Malaysia. *J Infect Dis* **2019**, *220* (12), 1946–1949. https://doi.org/10.1093/infdis/jiz397.

(12) Newton, C. R.; Taylor, T. E.; Whitten, R. O. Pathophysiology of Fatal Falciparum Malaria in African Children. *Am J Trop Med Hyg* **1998**, *58* (5), 673–683. https://doi.org/10.4269/ajtmh.1998.58.673.

(13) SNOW, R. W.; GOUWS, E.; KORENROMP, E. L. PEDIATRIC MORTALITY IN AFRICA: PLASMODIUM FALCIPARUM MALARIA AS A CAUSE OR RISK? *Am J Trop Med Hyg* **2004**, *71* (2_suppl), 16–24. https://doi.org/10.4269/ajtmh.2004.71.16.

(14) Anstey, N. M.; Douglas, N. M.; Poespoprodjo, J. R.; Price, R. N. Chapter Three - Plasmodium Vivax: Clinical Spectrum, Risk Factors and Pathogenesis; 2012; pp 151–201. https://doi.org/10.1016/B978-0-12-397900-1.00003-7.

(15) Baird, J. K. Neglect of Plasmodium Vivax Malaria. *Trends Parasitol* **2007**, *23* (11), 533–539. https://doi.org/10.1016/j.pt.2007.08.011.

(16) Sutherland, C. J.; Tanomsing, N.; Nolder, D.; Oguike, M.; Jennison, C.; Pukrittayakamee, S.; Dolecek, C.; Hien, T. T.; do Rosário, V. E.; Arez, A. P.; Pinto, J.; Michon, P.; Escalante, A. A.; Nosten, F.; Burke, M.; Lee, R.; Blaze, M.; Otto, T. D.; Barnwell, J. W.; Pain, A.; Williams, J.; White, N. J.; Day, N. P. J.; Snounou, G.; Lockhart, P. J.; Chiodini, P. L.; Imwong, M.; Polley, S. D. Two Nonrecombining Sympatric Forms of the Human Malaria Parasite Plasmodium Ovale Occur Globally. *Journal of Infectious Diseases* **2010**, *201* (10), 1544–1550. https://doi.org/10.1086/652240.

(17) Collins, W. E.; Jeffery, G. M. *Plasmodium Malariae* : Parasite and Disease. *Clin Microbiol Rev* **2007**, *20* (4), 579–592. https://doi.org/10.1128/CMR.00027-07.

(18) Vythilingam, I.; Tan, C. H.; Asmad, M.; Chan, S. T.; Lee, K. S.; Singh, B. Natural Transmission of Plasmodium Knowlesi to Humans by Anopheles Latens in Sarawak, Malaysia. *Trans R Soc Trop Med Hyg* **2006**, *100* (11), 1087–1088. https://doi.org/10.1016/j.trstmh.2006.02.006.

(19) Lee, K. S.; Divis, P. C. S.; Zakaria, S. K.; Matusop, A.; Julin, R. A.; Conway, D. J.; Cox-Singh, J.; Singh, B. Plasmodium Knowlesi: Reservoir Hosts and Tracking the Emergence in Humans and Macaques. *PLoS Pathog* **2011**, *7* (4). https://doi.org/10.1371/journal.ppat.1002015.

(20) Cox-Singh, J.; Singh, B. Knowlesi Malaria: Newly Emergent and of Public Health Importance? *Trends Parasitol* **2008**, *24* (9), 406–410. https://doi.org/10.1016/j.pt.2008.06.001.

(21) Singh, B.; Daneshvar, C. Human Infections and Detection of Plasmodium Knowlesi. *Clin Microbiol Rev* **2013**, *26* (2), 165–184. https://doi.org/10.1128/CMR.00079-12.

(22) Mayxay, M.; Pukrittayakamee, S.; Newton, P. N.; White, N. J. Mixed-Species Malaria Infections in Humans. *Trends Parasitol* **2004**, *20* (5), 233–240. https://doi.org/10.1016/j.pt.2004.03.006.

(23) Florens, L.; Washburn, M.; Muster, N.; Wolters, D.; Gardner, M.; Anthony, R.; Haynes, D.; Moch, K.; Sacci, J.; Witney, A.; Grainger, N.; Holder, A.; Wu, Y.; Yates, J.; Carucci, D. A Proteomic View of the Malaria Parasite Life Cycle. *Proceedings 50th ASMS Conference on Mass Spectrometry and Allied Topics* **2002**, *419* (October), 59–60.

(24) Karunaweera, N. D.; Grau, G. E.; Gamage, P.; Carter, R.; Mendis, K. N. Dynamics of Fever and Serum Levels of Tumor Necrosis Factor Are Closely Associated during Clinical Paroxysms in Plasmodium Vivax Malaria. *Proc Natl Acad Sci U S A* **1992**, *89* (8), 3200–3203. https://doi.org/10.1073/pnas.89.8.3200.

(25) Vijaykumar, M.; Naik, R. S.; Gowda, D. C. Plasmodium Falciparum Glycosylphosphatidylinositol-Induced TNF-α Secretion by Macrophages Is Mediated without Membrane Insertion or Endocytosis. *Journal of Biological Chemistry* **2001**, *276* (10), 6909–6912. https://doi.org/10.1074/jbc.C100007200.

(26) Wijesekera, S. K.; Carter, R.; Rathnayaka, L.; Mendis, K. N. A Malaria Parasite Toxin Associated with Plasmodium Vivax Paroxysms. *Clin Exp Immunol* **1996**, *104* (2), 221–227. https://doi.org/10.1046/j.1365-2249.1996.07699.x.

(27) *MMV Malaria parasite life cycle.* https://www.mmv.org/malaria/lifecycle-malaria-parasite (accessed 2023-10-08).

(28) Trampuz, A.; Jereb, M.; Muzlovic, I.; Prabhu, R. M. Clinical Review: Severe Malaria. *Crit Care* **2003**, *7* (4), 315. https://doi.org/10.1186/cc2183.

(29) Lis, B. Antigenic Diversity and Immune Evasion by Malaria Parasites. *Clin Diagn Lab Immunol* **2004**, *11* (6), 987–995. https://doi.org/DOI: 10.1128/CDLI.11.6.987–995.2004.

(30) Borst, P.; Genest, P.-A. Switching like for Like. *Nature* **2006**, *439* (7079), 926–927. https://doi.org/10.1038/439926b.

(31) FOWKES, F. J. I.; BOEUF, P.; BEESON, J. G. Immunity to Malaria in an Era of Declining Malaria Transmission. *Parasitology* **2016**, *143* (2), 139–153. https://doi.org/10.1017/S0031182015001249.

(32) Teo, A.; Feng, G.; Brown, G. v.; Beeson, J. G.; Rogerson, S. J. Functional Antibodies and Protection against Blood-Stage Malaria. *Trends Parasitol* **2016**, *32* (11), 887–898. https://doi.org/10.1016/j.pt.2016.07.003.

(33) DOBBS, K. R.; DENT, A. E. Plasmodium Malaria and Antimalarial Antibodies in the First Year of Life. *Parasitology* **2016**, *143* (2), 129–138. https://doi.org/10.1017/S0031182015001626.

(34) Mishra, M.; Mishra, V. K.; Kashaw, V.; Iyer, A. K.; Kashaw, S. K. Comprehensive Review on Various Strategies for Antimalarial Drug Discovery. *European Journal of Medicinal Chemistry*. Elsevier Masson SAS 2017, pp 1300–1320. https://doi.org/10.1016/j.ejmech.2016.11.025.

(35) WHO. *WHO Guidelines for Malaria 2022*; 2022. http://apps.who.int/bookorders.

(36) Kawamoto, F. Rapid Diagnosis of Malaria by Fluorescence Microscopy with Light Microscope and Interference Filter. *The Lancet* **1991**, *337* (8735), 200–202. https://doi.org/10.1016/0140-6736(91)92159-Y.

(37) Kawamoto, F.; Kumada, N. Fluorescent Probes for Detection of Protozoan Parasites. *Parasitology Today* **1987**, *3* (9), 284–286. https://doi.org/10.1016/0169-4758(87)90110-4.

(38) Trampuz, A.; Jereb, M.; Muzlovic, I.; Prabhu, R. M. Clinical Review: Severe Malaria. *Crit Care* **2003**, *7* (4), 315–323. https://doi.org/10.1186/cc2183.

(39) Ouédraogo, A. L.; Bastiaens, G. J. H.; Tiono, A. B.; Guelbéogo, W. M.; Kobylinski, K. C.; Ouédraogo, A.; Barry, A.; Bougouma, E. C.; Nebie, I.; Ouattara, M. S.; Lanke, K. H. W.; Fleckenstein, L.; Sauerwein, R. W.; Slater, H. C.; Churcher, T. S.; Sirima, S. B.; Drakeley,

C.; Bousema, T. Efficacy and Safety of the Mosquitocidal Drug Ivermectin to Prevent Malaria Transmission after Treatment: A Double-Blind, Randomized, Clinical Trial. *Clinical Infectious Diseases* **2015**, *60* (3), 357–365. https://doi.org/10.1093/cid/ciu797.

(40) Mahmoudi, S.; Keshavarz, H. Malaria Vaccine Development: The Need for Novel Approaches: A Review Article. *Iran J Parasitol* **2018**, *13* (1), 1–10.

(41) Lubanga, B.; Chemtai, A.; Kwaro, D. *The RTS,S/AS Malaria Vaccine Candidate: A Status Review*; 2016; Vol. 2. www.advancejournals.org.

(42) WHO. *WHO Guidelines for Malaria 2022*; 2022. http://apps.who.int/bookorders.

(43) Siddiqui, A. J.; Bhardwaj, J.; Saxena, J.; Jahan, S.; Snoussi, M.; Bardakci, F.; Badraoui, R.; Adnan, M. A Critical Review on Human Malaria and Schistosomiasis Vaccines: Current State, Recent Advancements, and Developments. *Vaccines (Basel)* **2023**, *11* (4), 792. https://doi.org/10.3390/vaccines11040792.

(44) Laurens, M. B. RTS,S/AS01 Vaccine (Mosquirix™): An Overview. *Hum Vaccin Immunother* **2020**, *16* (3), 480–489. https://doi.org/10.1080/21645515.2019.1669415.

(45) Efficacy and Safety of RTS,S/AS01 Malaria Vaccine with or without a Booster Dose in Infants and Children in Africa: Final Results of a Phase 3, Individually Randomised, Controlled Trial. *The Lancet* **2015**, *386* (9988), 31–45. https://doi.org/10.1016/S0140-6736(15)60721-8.

(46) Datoo, M. S.; Natama, H. M.; Somé, A.; Bellamy, D.; Traoré, O.; Rouamba, T.; Tahita, M. C.; Ido, N. F. A.; Yameogo, P.; Valia, D.; Millogo, A.; Ouedraogo, F.; Soma, R.; Sawadogo, S.; Sorgho, F.; Derra, K.; Rouamba, E.; Ramos-Lopez, F.; Cairns, M.; Provstgaard-Morys, S.; Aboagye, J.; Lawrie, A.; Roberts, R.; Valéa, I.; Sorgho, H.; Williams, N.; Glenn, G.; Fries, L.; Reimer, J.; Ewer, K. J.; Shaligram, U.; Hill, A. V. S.; Tinto, H. Efficacy and Immunogenicity of R21/Matrix-M Vaccine against Clinical Malaria after 2 Years' Follow-up in Children in Burkina Faso: A Phase 1/2b Randomised Controlled Trial. *Lancet Infect Dis* **2022**, *22* (12), 1728–1736. https://doi.org/10.1016/S1473-3099(22)00442-X.

(47) *World Health Organization (WHO) and the Malaria Vaccine Funders Group. The Malaria Vaccine Technology Roadmap. Nov, A.a. 2013. Available online: Accessed 24.04.2023. https://www.malariavaccine.org/sites/mvi/files/content/page/files/TRM_update_nov13.pdf*. https://www.malariavaccine.org/sites/mvi/files/content/page/files/TRM_update_nov13.pdf (accessed 2023-04-24).

(48) Müller, I. B.; Hyde, J. E. Antimalarial Drugs: Modes of Action and Mechanisms of Parasite Resistance. *Future Microbiol* **2010**, *5* (12), 1857–1873. https://doi.org/10.2217/fmb.10.136.

(49) Belete, T. M. Recent Progress in the Development of New Antimalarial Drugs with Novel Targets. *Drug Des Devel Ther* **2020**, *14*, 3875–3889. https://doi.org/10.2147/DDDT.S265602.

(50) Tse, E. G.; Korsik, M.; Todd, M. H. The Past, Present and Future of Anti-Malarial Medicines. *Malar J* **2019**, *18* (1), 93. https://doi.org/10.1186/s12936-019-2724-z.

(51) Foley, M. Quinoline Antimalarials Mechanisms of Action and Resistance and Prospects for New Agents. *Pharmacol Ther* **1998**, *79* (1), 55–87. https://doi.org/10.1016/S0163-7258(98)00012-6.

(52) Meshnick, S. R.; Thomas, A.; Ranz, A.; Xu, C.-M.; Pan, H.-Z. Artemisinin (Qinghaosu): The Role of Intracellular Hemin in Its Mechanism of Antimalarial Action. *Mol Biochem Parasitol* **1991**, *49* (2), 181–189. https://doi.org/10.1016/0166-6851(91)90062-B.

(53) Nzila, A.; Ward, S. A.; Marsh, K.; Sims, P. F. G.; Hyde, J. E. Comparative Folate Metabolism in Humans and Malaria Parasites (Part I): Pointers for Malaria Treatment from Cancer Chemotherapy. *Trends Parasitol* **2005**, *21* (6), 292–298. https://doi.org/10.1016/j.pt.2005.04.002.

(54) Fry, M.; Pudney, M. Site of Action of the Antimalarial Hydroxynaphthoquinone, 2-[Trans-4-(4'-Chlorophenyl) Cyclohexyl]-3- Hydroxy-1,4-Naphthoquinone (566C80). *Biochem Pharmacol* **1992**, *43* (7), 1545–1553. https://doi.org/10.1016/0006-2952(92)90213-3.

(55) Srivastava, I. K.; Rottenberg, H.; Vaidya, A. B. Atovaquone, a Broad Spectrum Antiparasitic Drug, Collapses Mitochondrial Membrane Potential in a Malarial Parasite. *Journal of Biological Chemistry* **1997**, *272* (7), 3961–3966. https://doi.org/10.1074/jbc.272.7.3961.

(56) Fichera, M. E.; Roos, D. S. A Plastid Organelle as a Drug Target in Apicomplexan Parasites. *Nature* **1997**, *390* (6658), 407–409. https://doi.org/10.1038/37132.

(57) *WHO Global Malaria Programme WHO Policy Recommendation: Seasonal Malaria Chemoprevention (SMC) for Plasmodium Falciparum Malaria Control in Highly Seasonal Transmission Areas of the Sahel Sub-Region in Africa*; 2012. http://www.who.int/malaria/publications/atoz/smc_report_teg_meetingmay2011.pdf .

(58) Phillips, M. A.; Burrows, J. N.; Manyando, C.; van Huijsduijnen, R. H.; van Voorhis, W. C.; Wells, T. N. C. Malaria. *Nat Rev Dis Primers* **2017**, *3* (1), 17050. https://doi.org/10.1038/nrdp.2017.50.

(59) Zongo, I.; Milligan, P.; Compaore, Y. D.; Some, A. F.; Greenwood, B.; Tarning, J.; Rosenthal, P. J.; Sutherland, C.; Nosten, F.; Ouedraogo, J. B. Randomized Noninferiority Trial of Dihydroartemisinin-Piperaquine Compared with Sulfadoxine-Pyrimethamine plus Amodiaquine for Seasonal Malaria Chemoprevention in Burkina Faso. *Antimicrob Agents Chemother* **2015**, *59* (8), 4387–4396. https://doi.org/10.1128/AAC.04923-14.

(60) Gutman, J.; Kovacs, S.; Dorsey, G.; Stergachis, A.; ter Kuile, F. O. Safety, Tolerability, and Efficacy of Repeated Doses of Dihydroartemisinin-Piperaquine for Prevention and Treatment of Malaria: A Systematic Review and Meta-Analysis. *Lancet Infect Dis* **2017**, *17* (2), 184–193. https://doi.org/10.1016/S1473-3099(16)30378-4.

(61) Elizabeth DeVos; Noel Dunn. *Malaria Prophylaxis. In: StatPearls [Internet]. Treasure Island (FL)* ; University of Florida, 2023.

(62) Nakato, H.; Vivancos, R.; Hunter, P. R. A Systematic Review and Meta-Analysis of the Effectiveness and Safety of Atovaquone Proguanil (Malarone) for Chemoprophylaxis

against Malaria. *Journal of Antimicrobial Chemotherapy* **2007**, *60* (5), 929–936. https://doi.org/10.1093/jac/dkm337.

(63) Daily, J. P. Malaria 2017: Update on the Clinical Literature and Management. *Curr Infect Dis Rep* **2017**, *19* (8), 28. https://doi.org/10.1007/s11908-017-0583-8.

(64) *Malaria: Artemisinin partial resistance 18 November 2022*. https://www.who.int/news-room/questions-and-answers/item/artemisinin-resistance (accessed 2023-10-08).

(65) Health Organization, W. *Guideline WHO Guidelines for Malaria - 14 March 2023*; 2023. http://apps.who.int/bookorders.

(66) Maiga, F. O.; Wele, M.; Toure, S. M.; Keita, M.; Tangara, C. O.; Refeld, R. R.; Thiero, O.; Kayentao, K.; Diakite, M.; Dara, A.; Li, J.; Toure, M.; Sagara, I.; Djimdé, A.; Mather, F. J.; Doumbia, S. O.; Shaffer, J. G. Artemisinin-Based Combination Therapy for Uncomplicated Plasmodium Falciparum Malaria in Mali: A Systematic Review and Meta-Analysis. *Malar J* **2021**, *20* (1), 356. https://doi.org/10.1186/s12936-021-03890-0.

(67) Premji, Z. G. Coartem®: The Journey to the Clinic. *Malar J* **2009**, *8* (S1), S3. https://doi.org/10.1186/1475-2875-8-S1-S3.

(68) Ravina, E. The Evolution of Drug Discovery : From Traditional Medicines to Modern Drugs; Weinheim: Wiley-VCH., 2015; p 139.

(69) Mohammed, H.; Sime, H.; Hailgiorgis, H.; Chernet, M.; Alebachew, M.; Solomon, H.; Assefa, G.; Haile, M.; Girma, S.; Bekele, W.; Tasew, G.; Gidey, B.; Commons, R. J.; Assefa, A. Efficacy and Safety of Pyronaridine-Artesunate (Pyramax®) for the Treatment of Uncomplicated Plasmodium Vivax Malaria in Northwest Ethiopia. *Malar J* **2022**, *21* (1), 401. https://doi.org/10.1186/s12936-022-04422-0.

(70) *Frequently asked questions about Eurartesim®*. https://www.mmv.org/access/products-projects/eurartesim-dihydroartemisinin-piperaquine/frequently-asked-questions-about (accessed 2023-10-08).

(71) Phillips, M. A.; Burrows, J. N.; Manyando, C.; Van Huijsduijnen, R. H.; Van Voorhis, W. C.; Wells, T. N. C. Malaria. *Nat Rev Dis Primers* **2017**, *3*. https://doi.org/10.1038/nrdp.2017.50.

(72) Singh Sidhu, A. B.; Verdier-Pinard, D.; Fidock, D. A. Chloroquine Resistance in Plasmodium Falciparum Malaria Parasites Conferred by Pfcrt Mutations. *Science (1979)* **2002**, *298* (5591), 210–213. https://doi.org/10.1126/science.1074045.

(73) Haldar, K.; Bhattacharjee, S.; Safeukui, I. Drug Resistance in Plasmodium. *Nat Rev Microbiol* **2018**, *16* (3), 156–170. https://doi.org/10.1038/nrmicro.2017.161.

(74) Blasco, B.; Leroy, D.; Fidock, D. A. Antimalarial Drug Resistance: Linking Plasmodium Falciparum Parasite Biology to the Clinic. *Nat Med* **2017**, *23* (8), 917–928. https://doi.org/10.1038/nm.4381.

(75) Lu, F.; Culleton, R.; Zhang, M.; Ramaprasad, A.; von Seidlein, L.; Zhou, H.; Zhu, G.; Tang, J.; Liu, Y.; Wang, W.; Cao, Y.; Xu, S.; Gu, Y.; Li, J.; Zhang, C.; Gao, Q.; Menard, D.; Pain, A.; Yang, H.; Zhang, Q.; Cao, J. Emergence of Indigenous Artemisinin-Resistant

Plasmodium Falciparum in Africa . *New England Journal of Medicine* **2017**, *376* (10), 991–993. https://doi.org/10.1056/nejmc1612765.

(76) Sutherland, C. J.; Lansdell, P.; Sanders, M.; Muwanguzi, J.; van Schalkwyk, D. A.; Kaur, H.; Nolder, D.; Tucker, J.; Bennett, H. M.; Otto, T. D.; Berriman, M.; Patel, T. A.; Lynn, R.; Gkrania-Klotsas, E.; Chiodini, P. L. *Pfk13* -Independent Treatment Failure in Four Imported Cases of Plasmodium Falciparum Malaria Treated with Artemether-Lumefantrine in the United Kingdom. *Antimicrob Agents Chemother* **2017**, *61* (3), e02382-16. https://doi.org/10.1128/AAC.02382-16.

(77) Taylor, A. R.; Flegg, J. A.; Holmes, C. C.; Guérin, P. J.; Sibley, C. H.; Conrad, M. D.; Dorsey, G.; Rosenthal, P. J. Artemether-Lumefantrine and Dihydroartemisinin-Piperaquine Exert Inverse Selective Pressure on Plasmodium Falciparum Drug Sensitivity-Associated Haplotypes in Uganda. *Open Forum Infect Dis* **2017**, *4* (1). https://doi.org/10.1093/ofid/ofw229.

(78) Health Organization, W. *Report on Antimalarial Drug Efficacy, Resistance and Response: 10 Years of Surveillance (2010–2019)*.

(79) Ward, K. E.; Fidock, D. A.; Bridgford, J. L. Plasmodium Falciparum Resistance to Artemisinin-Based Combination Therapies. *Curr Opin Microbiol* **2022**, *69*, 102193. https://doi.org/10.1016/j.mib.2022.102193.

(80) White, N. J. Antimalarial Drug Resistance. *Journal of Clinical Investigation* **2004**, *113* (8), 1084–1092. https://doi.org/10.1172/jci200421682.

(81) Wilson, C. M.; Volkman, S. K.; Thaithong, S.; Martin, R. K.; Kyle, D. E.; Milhous, W. K.; Wirth, D. F. Amplification of Pfmdr1 Associated with Mefloquine and Halofantrine Resistance in Plasmodium Falciparum from Thailand. *Mol Biochem Parasitol* **1993**, *57* (1), 151–160. https://doi.org/10.1016/0166-6851(93)90252-S.

(82) White, N. Antimalarial Drug Resistance and Combination Chemotherapy. *Philos Trans R Soc Lond B Biol Sci* **1999**, *354* (1384), 739–749. https://doi.org/10.1098/rstb.1999.0426.

(83) Srivastava, I. K.; Morrisey, J. M.; Darrouzet, E.; Daldal, F.; Vaidya, A. B. Resistance Mutations Reveal the Atovaquone-Binding Domain of Cytochrome b in Malaria Parasites. *Mol Microbiol* **1999**, *33* (4), 704–711. https://doi.org/10.1046/j.1365-2958.1999.01515.x.

(84) Mbugi, E. v; Mutayoba, B. M.; Malisa, A. L.; Balthazary, S. T.; Nyambo, T. B.; Mshinda, H. Drug Resistance to Sulphadoxine-Pyrimethamine in Plasmodium Falciparum Malaria in Mlimba, Tanzania. *Malar J* **2006**, *5* (1), 94–105. https://doi.org/10.1186/1475-2875-5-94.

(85) Yan, H.; Feng, J.; Yin, J.; Huang, F.; Kong, X.; Lin, K.; Zhang, T.; Feng, X.; Zhou, S.; Cao, J.; Xia, Z. High Frequency Mutations in Pfdhfr and Pfdhps of Plasmodium Falciparum in Response to Sulfadoxine-Pyrimethamine: A Cross-Sectional Survey in Returning Chinese Migrants From Africa. *Front Cell Infect Microbiol* **2021**, *11*. https://doi.org/10.3389/fcimb.2021.673194.

(86) Mbengue, A.; Bhattacharjee, S.; Pandharkar, T.; Liu, H.; Estiu, G.; Stahelin, R. v.; Rizk, S. S.; Njimoh, D. L.; Ryan, Y.; Chotivanich, K.; Nguon, C.; Ghorbal, M.; Lopez-Rubio, J. J.;

Pfrender, M.; Emrich, S.; Mohandas, N.; Dondorp, A. M.; Wiest, O.; Haldar, K. A Molecular Mechanism of Artemisinin Resistance in Plasmodium Falciparum Malaria. *Nature* **2015**, *520* (7549), 683–687. https://doi.org/10.1038/nature14412.

(87) *MMVs-pipeline-antimalarial-drugs (Last updated June 2022)*. https://www.mmv.org/research-development/mmvs-pipeline-antimalarial-drugs (accessed 2023-04-26).

(88) Gamo, F.-J.; Sanz, L. M.; Vidal, J.; de Cozar, C.; Alvarez, E.; Lavandera, J.-L.; Vanderwall, D. E.; Green, D. V. S.; Kumar, V.; Hasan, S.; Brown, J. R.; Peishoff, C. E.; Cardon, L. R.; Garcia-Bustos, J. F. Thousands of Chemical Starting Points for Antimalarial Lead Identification. *Nature* **2010**, *465* (7296), 305–310. https://doi.org/10.1038/nature09107.

(89) Biamonte, M. A.; Wanner, J.; le Roch, K. G. Recent Advances in Malaria Drug Discovery. *Bioorg Med Chem Lett* **2013**, *23* (10), 2829–2843. https://doi.org/10.1016/j.bmcl.2013.03.067.

(90) Wells, T. N. C.; Alonso, P. L.; Gutteridge, W. E. New Medicines to Improve Control and Contribute to the Eradication of Malaria. *Nat Rev Drug Discov* **2009**, *8* (11), 879–891. https://doi.org/10.1038/nrd2972.

(91) Burrows, J. N.; Duparc, S.; Gutteridge, W. E.; Hooft van Huijsduijnen, R.; Kaszubska, W.; Macintyre, F.; Mazzuri, S.; Möhrle, J. J.; Wells, T. N. C. New Developments in Anti-Malarial Target Candidate and Product Profiles. *Malar J* **2017**, *16* (1), 26. https://doi.org/10.1186/s12936-016-1675-x.

(92) Moehrle, J. J.; Duparc, S.; Siethoff, C.; van Giersbergen, P. L. M.; Craft, J. C.; Arbe-Barnes, S.; Charman, S. A.; Gutierrez, M.; Wittlin, S.; Vennerstrom, J. L. First-in-Man Safety and Pharmacokinetics of Synthetic Ozonide OZ439 Demonstrates an Improved Exposure Profile Relative to Other Peroxide Antimalarials. *Br J Clin Pharmacol* **2013**, *75* (2), 535–548. https://doi.org/10.1111/j.1365-2125.2012.04368.x.

(93) Phyo, A. P.; Jittamala, P.; Nosten, F. H.; Pukrittayakamee, S.; Imwong, M.; White, N. J.; Duparc, S.; Macintyre, F.; Baker, M.; Möhrle, J. J. Antimalarial Activity of Artefenomel (OZ439), a Novel Synthetic Antimalarial Endoperoxide, in Patients with Plasmodium Falciparum and Plasmodium Vivax Malaria: An Open-Label Phase 2 Trial. *Lancet Infect Dis* **2016**, *16* (1), 61–69. https://doi.org/10.1016/S1473-3099(15)00320-5.

(94) Abd-Rahman, A. N.; Zaloumis, S.; McCarthy, J. S.; Simpson, J. A.; Commons, R. J. Scoping Review of Antimalarial Drug Candidates in Phase I and II Drug Development. *Antimicrob Agents Chemother* **2022**, *66* (2). https://doi.org/10.1128/aac.01659-21.

(95) McCarthy, J. S.; Rückle, T.; Djeriou, E.; Cantalloube, C.; Ter-Minassian, D.; Baker, M.; O'Rourke, P.; Griffin, P.; Marquart, L.; Hooft van Huijsduijnen, R.; Möhrle, J. J. A Phase II Pilot Trial to Evaluate Safety and Efficacy of Ferroquine against Early Plasmodium Falciparum in an Induced Blood-Stage Malaria Infection Study. *Malar J* **2016**, *15* (1), 469. https://doi.org/10.1186/s12936-016-1511-3.

(96) Held, J.; Supan, C.; Salazar, C. L. O.; Tinto, H.; Bonkian, L. N.; Nahum, A.; Moulero, B.; Sié, A.; Coulibaly, B.; Sirima, S. B.; Siribie, M.; Otsyula, N.; Otieno, L.; Abdallah, A. M.; Kimutai, R.; Bouyou-Akotet, M.; Kombila, M.; Koiwai, K.; Cantalloube, C.; Din-Bell, C.; Djeriou, E.; Waitumbi, J.; Mordmüller, B.; Ter-Minassian, D.; Lell, B.; Kremsner, P. G.

Ferroquine and Artesunate in African Adults and Children with Plasmodium Falciparum Malaria: A Phase 2, Multicentre, Randomised, Double-Blind, Dose-Ranging, Non-Inferiority Study. *Lancet Infect Dis* **2015**, *15* (12), 1409–1419. https://doi.org/10.1016/S1473-3099(15)00079-1.

(97) Dini, S.; Zaloumis, S. G.; Price, D. J.; Gobeau, N.; Kümmel, A.; Cherkaoui, M.; Moehrle, J. J.; McCarthy, J. S.; Simpson, J. A. Seeking an Optimal Dosing Regimen for OZ439/DSM265 Combination Therapy for Treating Uncomplicated Falciparum Malaria. *Journal of Antimicrobial Chemotherapy* **2021**, *76* (9), 2325–2334. https://doi.org/10.1093/jac/dkab181.

(98) White, N. J.; Duong, T. T.; Uthaisin, C.; Nosten, F.; Phyo, A. P.; Hanboonkunupakarn, B.; Pukrittayakamee, S.; Jittamala, P.; Chuthasmit, K.; Cheung, M. S.; Feng, Y.; Li, R.; Magnusson, B.; Sultan, M.; Wieser, D.; Xun, X.; Zhao, R.; Diagana, T. T.; Pertel, P.; Leong, F. J. Antimalarial Activity of KAF156 in Falciparum and Vivax Malaria. *New England Journal of Medicine* **2016**, *375* (12), 1152–1160. https://doi.org/10.1056/nejmoa1602250.

(99) Leong, F. J.; Zhao, R.; Zeng, S.; Magnusson, B.; Diagana, T. T.; Pertel, P. A First-in-Human Randomized, Double-Blind, Placebo-Controlled, Single- and Multiple-Ascending Oral Dose Study of Novel Imidazolopiperazine KAF156 to Assess Its Safety, Tolerability, and Pharmacokinetics in Healthy Adult Volunteers. *Antimicrob Agents Chemother* **2014**, *58* (11), 6437–6443. https://doi.org/10.1128/AAC.03478-14.

(100) Kuhen, K. L.; Chatterjee, A. K.; Rottmann, M.; Gagaring, K.; Borboa, R.; Buenviaje, J.; Chen, Z.; Francek, C.; Wu, T.; Nagle, A.; Barnes, S. W.; Plouffe, D.; Lee, M. C. S.; Fidock, D. A.; Graumans, W.; van de Vegte-Bolmer, M.; van Gemert, G. J.; Wirjanata, G.; Sebayang, B.; Marfurt, J.; Russell, B.; Suwanarusk, R.; Price, R. N.; Nosten, F.; Tungtaeng, A.; Gettayacamin, M.; Sattabongkot, J.; Taylor, J.; Walker, J. R.; Tully, D.; Patra, K. P.; Flannery, E. L.; Vinetz, J. M.; Renia, L.; Sauerwein, R. W.; Winzeler, E. A.; Glynne, R. J.; Diagana, T. T. KAF156 Is an Antimalarial Clinical Candidate with Potential for Use in Prophylaxis, Treatment, and Prevention of Disease Transmission. *Antimicrob Agents Chemother* **2014**, *58* (9), 5060–5067. https://doi.org/10.1128/AAC.02727-13.

(101) *MMV medicines for malaria venture*. https://www.mmv.org/index.php/newsroom/news-resources-search/novartis-and-medicines-malaria-venture-announce-decision-move-phase (accessed 2023-04-26).

(102) White, N. J.; Pukrittayakamee, S.; Phyo, A. P.; Rueangweerayut, R.; Nosten, F.; Jittamala, P.; Jeeyapant, A.; Jain, J. P.; Lefèvre, G.; Li, R.; Magnusson, B.; Diagana, T. T.; Leong, F. J. Spiroindolone KAE609 for Falciparum and Vivax Malaria. *New England Journal of Medicine* **2014**, *371* (5), 403–410. https://doi.org/10.1056/nejmoa1315860.

(103) Huskey, S. E. W.; Zhu, C. Q.; Fredenhagen, A.; Kühnöl, J.; Luneau, A.; Jian, Z.; Yang, Z.; Miao, Z.; Yang, F.; Jain, J. P.; Sunkara, G.; Mangold, J. B.; Stein, D. S. KAE609 (Cipargamin), a New Spiroindolone Agent for the Treatment of Malaria: Evaluation of the Absorption, Distribution, Metabolism, and Excretion of a Single Oral 300-Mg Dose of [14C]KAE609 in Healthy Male Subjects. *Drug Metabolism and Disposition* **2016**, *44* (5), 672–682. https://doi.org/10.1124/dmd.115.069187.

(104) Ndayisaba, G.; Yeka, A.; Asante, K. P.; Grobusch, M. P.; Karita, E.; Mugerwa, H.; Asiimwe, S.; Oduro, A.; Fofana, B.; Doumbia, S.; Jain, J. P.; Barsainya, S.; Kullak-Ublick,

G. A.; Su, G.; Schmitt, E. K.; Csermak, K.; Gandhi, P.; Hughes, D. Hepatic Safety and Tolerability of Cipargamin (KAE609), in Adult Patients with Plasmodium Falciparum Malaria: A Randomized, Phase II, Controlled, Dose-Escalation Trial in Sub-Saharan Africa. *Malar J* **2021**, *20* (1), 478. https://doi.org/10.1186/s12936-021-04009-1.

(105) Schmitt, E. K.; Ndayisaba, G.; Yeka, A.; Asante, K. P.; Grobusch, M. P.; Karita, E.; Mugerwa, H.; Asiimwe, S.; Oduro, A.; Fofana, B.; Doumbia, S.; Su, G.; Csermak Renner, K.; Venishetty, V. K.; Sayyed, S.; Straimer, J.; Demin, I.; Barsainya, S.; Boulton, C.; Gandhi, P. Efficacy of Cipargamin (KAE609) in a Randomized, Phase II Dose-Escalation Study in Adults in Sub-Saharan Africa With Uncomplicated *Plasmodium Falciparum* Malaria. *Clinical Infectious Diseases* **2022**, *74* (10), 1831–1839. https://doi.org/10.1093/cid/ciab716.

(106) Sulyok, M.; Rückle, T.; Roth, A.; Mürbeth, R. E.; Chalon, S.; Kerr, N.; Samec, S. S.; Gobeau, N.; Calle, C. L.; Ibáñez, J.; Sulyok, Z.; Held, J.; Gebru, T.; Granados, P.; Brückner, S.; Nguetse, C.; Mengue, J.; Lalremruata, A.; Sim, B. K. L.; Hoffman, S. L.; Möhrle, J. J.; Kremsner, P. G.; Mordmüller, B. DSM265 for Plasmodium Falciparum Chemoprophylaxis: A Randomised, Double Blinded, Phase 1 Trial with Controlled Human Malaria Infection. *Lancet Infect Dis* **2017**, *17* (6), 636–644. https://doi.org/10.1016/S1473-3099(17)30139-1.

(107) McCarthy, J. S.; Lotharius, J.; Rückle, T.; Chalon, S.; Phillips, M. A.; Elliott, S.; Sekuloski, S.; Griffin, P.; Ng, C. L.; Fidock, D. A.; Marquart, L.; Williams, N. S.; Gobeau, N.; Bebrevska, L.; Rosario, M.; Marsh, K.; Möhrle, J. J. Safety, Tolerability, Pharmacokinetics, and Activity of the Novel Long-Acting Antimalarial DSM265: A Two-Part First-in-Human Phase 1a/1b Randomised Study. *Lancet Infect Dis* **2017**, *17* (6), 626–635. https://doi.org/10.1016/S1473-3099(17)30171-8.

(108) Coteron, J. M.; Marco, M.; Esquivias, J.; Deng, X.; White, K. L.; White, J.; Koltun, M.; el Mazouni, F.; Kokkonda, S.; Katneni, K.; Bhamidipati, R.; Shackleford, D. M.; Angulo-Barturen, I.; Ferrer, S. B.; Jiménez-Díaz, M. B.; Gamo, F. J.; Goldsmith, E. J.; Charman, W. N.; Bathurst, I.; Floyd, D.; Matthews, D.; Burrows, J. N.; Rathod, P. K.; Charman, S. A.; Phillips, M. A. Structure-Guided Lead Optimization of Triazolopyrimidine-Ring Substituents Identifies Potent Plasmodium Falciparum Dihydroorotate Dehydrogenase Inhibitors with Clinical Candidate Potential. *J Med Chem* **2011**, *54* (15), 5540–5561. https://doi.org/10.1021/jm200592f.

(109) Phillips, M. A.; Lotharius, J.; Marsh, K.; White, J.; Dayan, A.; White, K. L.; Njoroge, J. W.; el Mazouni, F.; Lao, Y.; Kokkonda, S.; Tomchick, D. R.; Deng, X.; Laird, T.; Bhatia, S. N.; March, S.; Ng, C. L.; Fidock, D. A.; Wittlin, S.; Lafuente-Monasterio, M.; Benito, F. J. G.; Alonso, L. M. S.; Martinez, M. S.; Jimenez-Diaz, M. B.; Bazaga, S. F.; Angulo-Barturen, I.; Haselden, J. N.; Louttit, J.; Cui, Y.; Sridhar, A.; Zeeman, A.-M.; Kocken, C.; Sauerwein, R.; Dechering, K.; Avery, V. M.; Duffy, S.; Delves, M.; Sinden, R.; Ruecker, A.; Wickham, K. S.; Rochford, R.; Gahagen, J.; Iyer, L.; Riccio, E.; Mirsalis, J.; Bathhurst, I.; Rueckle, T.; Ding, X.; Campo, B.; Leroy, D.; Rogers, M. J.; Rathod, P. K.; Burrows, J. N.; Charman, S. A. A Long-Duration Dihydroorotate Dehydrogenase Inhibitor (DSM265) for Prevention and Treatment of Malaria. *Sci Transl Med* **2015**, *7* (296), 111–123. https://doi.org/10.1126/scitranslmed.aaa6645.

(110) Ghidelli-Disse, S.; Lafuente-Monasterio, M. J.; Waterson, D.; Witty, M.; Younis, Y.; Paquet, T.; Street, L. J.; Chibale, K.; Gamo-Benito, F. J.; Bantscheff, M.; Drewes, G.

Identification of Plasmodium PI4 Kinase as Target of MMV390048 by Chemoproteomics. *Malar J* **2014**, *13* (S1), P38. https://doi.org/10.1186/1475-2875-13-S1-P38.

(111) Paquet, T.; le Manach, C.; Cabrera, D. G.; Younis, Y.; Henrich, P. P.; Abraham, T. S.; Lee, M. C. S.; Basak, R.; Ghidelli-Disse, S.; Lafuente-Monasterio, M. J.; Bantscheff, M.; Ruecker, A.; Blagborough, A. M.; Zakutansky, S. E.; Zeeman, A.-M.; White, K. L.; Shackleford, D. M.; Mannila, J.; Morizzi, J.; Scheurer, C.; Angulo-Barturen, I.; Martínez, M. S.; Ferrer, S.; Sanz, L. M.; Gamo, F. J.; Reader, J.; Botha, M.; Dechering, K. J.; Sauerwein, R. W.; Tungtaeng, A.; Vanachayangkul, P.; Lim, C. S.; Burrows, J.; Witty, M. J.; Marsh, K. C.; Bodenreider, C.; Rochford, R.; Solapure, S. M.; Jiménez-Díaz, M. B.; Wittlin, S.; Charman, S. A.; Donini, C.; Campo, B.; Birkholtz, L.-M.; Hanson, K. K.; Drewes, G.; Kocken, C. H. M.; Delves, M. J.; Leroy, D.; Fidock, D. A.; Waterson, D.; Street, L. J.; Chibale, K. Antimalarial Efficacy of MMV390048, an Inhibitor of *Plasmodium* Phosphatidylinositol 4-Kinase. *Sci Transl Med* **2017**, *9* (387), eaad9735. https://doi.org/10.1126/scitranslmed.aad9735.

(112) Mohammed, R.; Asres, M. S.; Gudina, E. K.; Adissu, W.; Johnstone, H.; Marrast, A. C.; Donini, C.; Duparc, S.; Yilma, D. Efficacy, Safety, Tolerability, and Pharmacokinetics of MMV390048 in Acute Uncomplicated Malaria. *Am J Trop Med Hyg* **2023**, *108* (1), 81–84. https://doi.org/10.4269/ajtmh.22-0567.

(113) Ge, J. F.; Arai, C.; Yang, M.; Bakar Md., A.; Lu, J.; Ismail, N. S. M.; Wittlin, S.; Kaiser, M.; Brun, R.; Charman, S. A.; Nguyen, T.; Morizzi, J.; Itoh, I.; Ihara, M. Discovery of Novel Benzo[a]Phenoxazine SSJ-183 as a Drug Candidate for Malaria. *ACS Med Chem Lett* **2010**, *1* (7), 360–364. https://doi.org/10.1021/ml100120a.

(114) Jiménez-Díaz, M. B.; Ebert, D.; Salinas, Y.; Pradhan, A.; Lehane, A. M.; Myrand-Lapierre, M.-E.; O'Loughlin, K. G.; Shackleford, D. M.; Justino de Almeida, M.; Carrillo, A. K.; Clark, J. A.; Dennis, A. S. M.; Diep, J.; Deng, X.; Duffy, S.; Endsley, A. N.; Fedewa, G.; Guiguemde, W. A.; Gómez, M. G.; Holbrook, G.; Horst, J.; Kim, C. C.; Liu, J.; Lee, M. C. S.; Matheny, A.; Martínez, M. S.; Miller, G.; Rodríguez-Alejandre, A.; Sanz, L.; Sigal, M.; Spillman, N. J.; Stein, P. D.; Wang, Z.; Zhu, F.; Waterson, D.; Knapp, S.; Shelat, A.; Avery, V. M.; Fidock, D. A.; Gamo, F.-J.; Charman, S. A.; Mirsalis, J. C.; Ma, H.; Ferrer, S.; Kirk, K.; Angulo-Barturen, I.; Kyle, D. E.; DeRisi, J. L.; Floyd, D. M.; Guy, R. K. (+)-SJ733, a Clinical Candidate for Malaria That Acts through ATP4 to Induce Rapid Host-Mediated Clearance of *Plasmodium*. *Proceedings of the National Academy of Sciences* **2014**, *111* (50). https://doi.org/10.1073/pnas.1414221111.

(115) Gaur, A. H.; Panetta, J. C.; Smith, A. M.; Dallas, R. H.; Freeman, B. B.; Stewart, T. B.; Tang, L.; John, E.; Branum, K. C.; Patel, N. D.; Ost, S.; Heine, R. N.; Richardson, J. L.; Hammill, J. T.; Bebrevska, L.; Gusovsky, F.; Maki, N.; Yanagi, T.; Flynn, P. M.; McCarthy, J. S.; Chalon, S.; Guy, R. K. Combining SJ733, an Oral ATP4 Inhibitor of Plasmodium Falciparum, with the Pharmacokinetic Enhancer Cobicistat: An Innovative Approach in Antimalarial Drug Development. *EBioMedicine* **2022**, *80*, 104065. https://doi.org/10.1016/j.ebiom.2022.104065.

(116) Chughlay, M. F.; Rossignol, E.; Donini, C.; el Gaaloul, M.; Lorch, U.; Coates, S.; Langdon, G.; Hammond, T.; Möhrle, J.; Chalon, S. First-in-Human Clinical Trial to Assess the Safety, Tolerability and Pharmacokinetics of P218, a Novel Candidate for Malaria

Chemoprotection. *Br J Clin Pharmacol* **2020**, *86* (6), 1113–1124. https://doi.org/10.1111/bcp.14219.

(117) Abbat, S.; Jain, V.; Bharatam, P. v. Origins of the Specificity of Inhibitor P218 toward Wild-Type and Mutant *Pf* DHFR: A Molecular Dynamics Analysis. *J Biomol Struct Dyn* **2015**, *33* (9), 1913–1928. https://doi.org/10.1080/07391102.2014.979231.

(118) Täubel, J.; Lorch, U.; Ferber, G.; Spencer, C. S.; Freier, A.; Coates, S.; El Gaaloul, M.; Donini, C.; Chughlay, M. F.; Chalon, S. Concentration-QT Modelling of the Novel DHFR Inhibitor P218 in Healthy Male Volunteers. *Br J Clin Pharmacol* **2022**, *88* (1), 128–137. https://doi.org/10.1111/bcp.14933.

(119) Baragaña, B.; Hallyburton, I.; Lee, M. C. S.; Norcross, N. R.; Grimaldi, R.; Otto, T. D.; Proto, W. R.; Blagborough, A. M.; Meister, S.; Wirjanata, G.; Ruecker, A.; Upton, L. M.; Abraham, T. S.; Almeida, M. J.; Pradhan, A.; Porzelle, A.; Martínez, M. S.; Bolscher, J. M.; Woodland, A.; Norval, S.; Zuccotto, F.; Thomas, J.; Simeons, F.; Stojanovski, L.; Osuna-Cabello, M.; Brock, P. M.; Churcher, T. S.; Sala, K. A.; Zakutansky, S. E.; Jiménez-Díaz, M. B.; Sanz, L. M.; Riley, J.; Basak, R.; Campbell, M.; Avery, V. M.; Sauerwein, R. W.; Dechering, K. J.; Noviyanti, R.; Campo, B.; Frearson, J. A.; Angulo-Barturen, I.; Ferrer-Bazaga, S.; Gamo, F. J.; Wyatt, P. G.; Leroy, D.; Siegl, P.; Delves, M. J.; Kyle, D. E.; Wittlin, S.; Marfurt, J.; Price, R. N.; Sinden, R. E.; Winzeler, E. A.; Charman, S. A.; Bebrevska, L.; Gray, D. W.; Campbell, S.; Fairlamb, A. H.; Willis, P. A.; Rayner, J. C.; Fidock, D. A.; Read, K. D.; Gilbert, I. H. A Novel Multiple-Stage Antimalarial Agent That Inhibits Protein Synthesis. *Nature* **2015**, *522* (7556), 315–320. https://doi.org/10.1038/nature14451.

(120) Arigoni, D.; Sagner, S.; Latzel, C.; Eisenreich, W.; Bacher, A.; Zenk, M. H. Terpenoid Biosynthesis from 1-Deoxy- <scp>d</Scp> -Xylulose in Higher Plants by Intramolecular Skeletal Rearrangement. *Proceedings of the National Academy of Sciences* **1997**, *94* (20), 10600–10605. https://doi.org/10.1073/pnas.94.20.10600.

(121) DISCH, A.; SCHWENDER, J.; MÜLLER, C.; LICHTENTHALER, H. K.; ROHMER, M. Distribution of the Mevalonate and Glyceraldehyde Phosphate/Pyruvate Pathways for Isoprenoid Biosynthesis in Unicellular Algae and the Cyanobacterium Synechocystis PCC 6714. *Biochemical Journal* **1998**, *333* (2), 381–388. https://doi.org/10.1042/bj3330381.

(122) Eisenreich, W.; Bacher, A.; Arigoni, D.; Rohdich, F. Biosynthesis of Isoprenoids via the Non-Mevalonate Pathway. *Cellular and Molecular Life Sciences* **2004**, *61* (12). https://doi.org/10.1007/s00018-004-3381-z.

(123) Rohmer, M.; Rohmer, M. The Discovery of a Mevalonate-Independent Pathway for Isoprenoid Biosynthesis in Bacteria, Algae and Higher Plants†. *Nat Prod Rep* **1999**, *16* (5), 565–574. https://doi.org/10.1039/a709175c.

(124) Holstein, S. A.; Hohl, R. J. Isoprenoids: Remarkable Diversity of Form and Function. *Lipids* **2004**, *39* (4), 293–309. https://doi.org/10.1007/s11745-004-1233-3.

(125) Buhaescu, I.; Izzedine, H. Mevalonate Pathway: A Review of Clinical and Therapeutical Implications. *Clin Biochem* **2007**, *40* (9–10), 575–584. https://doi.org/10.1016/j.clinbiochem.2007.03.016.

(126) Coppens, I. Targeting Lipid Biosynthesis and Salvage in Apicomplexan Parasites for Improved Chemotherapies. *Nat Rev Microbiol* **2013**, *11* (12), 823–835. https://doi.org/10.1038/nrmicro3139.

(127) Jomaa, H.; Wiesner, J.; Sanderbrand, S.; Altincicek, B.; Weidemeyer, C.; Hintz, M.; Türbachova, I.; Eberl, M.; Zeidler, J.; Lichtenthaler, H. K.; Soldati, D.; Beck, E. Inhibitors of the Nonmevalonate Pathway of Isoprenoid Biosynthesis as Antimalarial Drugs. *Science (1979)* **1999**, *285* (5433), 1573–1576. https://doi.org/10.1126/science.285.5433.1573.

(128) Takahashi, S.; Kuzuyama, T.; Watanabe, H.; Seto, H. A 1-Deoxy- d-Xylulose 5-Phosphate Reductoisomerase Catalyzing the Formation of 2-C-Methyl-d-Erythritol 4-Phosphate in an Alternative Nonmevalonate Pathway for Terpenoid Biosynthesis. *Proceedings of the National Academy of Sciences* **1998**, *95* (17), 9879–9884. https://doi.org/10.1073/pnas.95.17.9879.

(129) Tsuchiya, T.; Ishibashi, K.; Terakawa, M.; Nishiyama, M.; Itoh, N.; Noguchi, H. Pharmacokinetics and Metabolism of Fosmidomycin, a New Phosphonic Acid, in Rats and Dogs. *Eur J Drug Metab Pharmacokinet* **1982**, *7* (1), 59–64. https://doi.org/10.1007/BF03189544.

(130) Murakawa, T.; Sakamoto, H.; Fukada, S.; Konishi, T.; Nishida, M. Pharmacokinetics of Fosmidomycin, a New Phosphonic Acid Antibiotic. *Antimicrob Agents Chemother* **1982**, *21* (2), 224–230. https://doi.org/10.1128/AAC.21.2.224.

(131) *https://www.rcsb.org/structure/1onp*.

(132) Kurz, T. ; Geffken, D. ;; Kaula, U. Phosphororganische Verbindungen Und Deren Verwendung. . DE10356410A1, June 23, 2005.

(133) Konzuch, S.; Umeda, T.; Held, J.; Hähn, S.; Brücher, K.; Lienau, C.; Behrendt, C. T.; Gräwert, T.; Bacher, A.; Illarionov, B.; Fischer, M.; Mordmüller, B.; Tanaka, N.; Kurz, T. Binding Modes of Reverse Fosmidomycin Analogs toward the Antimalarial Target IspC. *J Med Chem* **2014**, *57* (21), 8827–8838. https://doi.org/10.1021/jm500850y.

(134) Behrendt, C. T.; Kunfermann, A.; Illarionova, V.; Matheeussen, A.; Pein, M. K.; Gräwert, T.; Kaiser, J.; Bacher, A.; Eisenreich, W.; Illarionov, B.; Fischer, M.; Maes, L.; Groll, M.; Kurz, T. Reverse Fosmidomycin Derivatives against the Antimalarial Drug Target IspC (Dxr). *J Med Chem* **2011**, *54* (19), 6796–6802. https://doi.org/10.1021/jm200694q.

(135) *https://www.rcsb.org/3d-view/3AU9/1*.

(136) Behrendt, C. T.; Kunfermann, A.; Illarionova, V.; Matheeussen, A.; Gräwert, T.; Groll, M.; Rohdich, F.; Bacher, A.; Eisenreich, W.; Fischer, M.; Maes, L.; Kurz, T. Synthesis and Antiplasmodial Activity of Highly Active Reverse Analogues of the Antimalarial Drug Candidate Fosmidomycin. *ChemMedChem* **2010**, *5* (10), 1673–1676. https://doi.org/10.1002/cmdc.201000276.

(137) Chofor, R.; Sooriyaarachchi, S.; Risseeuw, M. D. P.; Bergfors, T.; Pouyez, J.; Johny, C.; Haymond, A.; Everaert, A.; Dowd, C. S.; Maes, L.; Coenye, T.; Alex, A.; Couch, R. D.; Jones, T. A.; Wouters, J.; Mowbray, S. L.; Van Calenbergh, S. Synthesis and Bioactivity of β-Substituted Fosmidomycin Analogues Targeting 1-Deoxy-d-Xylulose-5-Phosphate

Reductoisomerase. *J Med Chem* **2015**, *58* (7), 2988–3001. https://doi.org/10.1021/jm5014264.

(138) Krebs, F. S.; Esque, J.; Stote, R. H. A Computational Study of the Molecular Basis of Antibiotic Resistance in a DXR Mutant. *J Comput Aided Mol Des* **2019**, *33* (10), 927–940. https://doi.org/10.1007/s10822-019-00229-5.

(139) Koppisch, A. T.; Fox, D. T.; Blagg, B. S. J.; Poulter, C. D. E. Coli MEP Synthase: Steady-State Kinetic Analysis and Substrate Binding. *Biochemistry* **2002**, *41* (1), 236–243. https://doi.org/10.1021/bi0118207.

(140) Masini, T.; Kroezen, B. S.; Hirsch, A. K. H. Druggability of the Enzymes of the Non-Mevalonate-Pathway. *Drug Discov Today* **2013**, *18* (23–24), 1256–1262. https://doi.org/10.1016/j.drudis.2013.07.003.

(141) San Jose, G.; Jackson, E. R.; Uh, E.; Johny, C.; Haymond, A.; Lundberg, L.; Pinkham, C.; Kehn-Hall, K.; Boshoff, H. I.; Couch, R. D.; Dowd, C. S. Design of Potential Bisubstrate Inhibitors against Mycobacterium Tuberculosis (Mtb) 1-Deoxy-d-Xylulose 5-Phosphate Reductoisomerase (Dxr)—Evidence of a Novel Binding Mode. *Medchemcomm* **2013**, *4* (7), 1099. https://doi.org/10.1039/c3md00085k.

(142) San Jose, G.; Jackson, E. R.; Haymond, A.; Johny, C.; Edwards, R. L.; Wang, X.; Brothers, R. C.; Edelstein, E. K.; Odom, A. R.; Boshoff, H. I.; Couch, R. D.; Dowd, C. S. Structure–Activity Relationships of the MEPicides: N-Acyl and O-Linked Analogs of FR900098 as Inhibitors of Dxr from Mycobacterium Tuberculosis and Yersinia Pestis. *ACS Infect Dis* **2016**, *2* (12), 923–935. https://doi.org/10.1021/acsinfecdis.6b00125.

(143) Jansson, A. M.; Więckowska, A.; Björkelid, C.; Yahiaoui, S.; Sooriyaarachchi, S.; Lindh, M.; Bergfors, T.; Dharavath, S.; Desroses, M.; Suresh, S.; Andaloussi, M.; Nikhil, R.; Sreevalli, S.; Srinivasa, B. R.; Larhed, M.; Jones, T. A.; Karlén, A.; Mowbray, S. L. DXR Inhibition by Potent Mono- and Disubstituted Fosmidomycin Analogues. *J Med Chem* **2013**, *56* (15), 6190–6199. https://doi.org/10.1021/jm4006498.

(144) Brücher, K.; Gräwert, T.; Konzuch, S.; Held, J.; Lienau, C.; Behrendt, C.; Illarionov, B.; Maes, L.; Bacher, A.; Wittlin, S.; Mordmüller, B.; Fischer, M.; Kurz, T. Prodrugs of Reverse Fosmidomycin Analogues. *J Med Chem* **2015**, *58* (4), 2025–2035. https://doi.org/10.1021/jm5019719.

(145) Zhao, Z.; Scarlato, G. R.; Armstrong, R. W. Synthesis of Trans-4-Alkenyl Oxazoles. *Tetrahedron Lett* **1991**, *32* (13), 1609–1612. https://doi.org/10.1016/S0040-4039(00)74284-5.

(146) Yodita Asfaha. Development of Class IIa Histone Deacetylase Inhibitors, in the Faculty of Mathematics and Natural Sciences at the Heinrich Heine University Düsseldorf, Düsseldorf, 2020.

(147) Shendage, D. M.; Fröhlich, R.; Haufe, G. Highly Efficient Stereoconservative Amidation and Deamidation of α-Amino Acids. *Org Lett* **2004**, *6* (21), 3675–3678. https://doi.org/10.1021/ol048771l.

(148) Dunetz, J. R.; Magano, J.; Weisenburger, G. A. Large-Scale Applications of Amide Coupling Reagents for the Synthesis of Pharmaceuticals. *Organic Process Research and*

Development. American Chemical Society February 19, 2016, pp 140–177. https://doi.org/10.1021/op500305s.

(149) Macmillan, D. S.; Murray, J.; Sneddon, H. F.; Jamieson, C.; Watson, A. J. B. Green Chemistry Evaluation of Alternative Solvents in Common Amide Coupling Reactions: Replacement of Dichloromethane and N,N-Dimethylformamide †. *Cite this: Green Chem* **2013**, *15*, 596. https://doi.org/10.1039/c2gc36900a.

(150) Harsági, N.; Keglevich, G. The Hydrolysis of Phosphinates and Phosphonates: A Review. *Molecules* **2021**, *26* (10), 2840. https://doi.org/10.3390/molecules26102840.

(151) McKenna, C. E.; Higa, M. T.; Cheung, N. H.; McKenna, M.-C. The Facile Dealkylation of Phosphonic Acid Dialkyl Esters by Bromotrimethylsilane. *Tetrahedron Lett* **1977**, *18* (2), 155–158. https://doi.org/10.1016/S0040-4039(01)92575-4.

(152) Conibear, A. C.; Lobb, K. A.; Kaye, P. T. 31P NMR Kinetic Study of the Tandem Cleavage of Phosphonate Esters by Bromotrimethylsilane. *Tetrahedron* **2010**, *66* (43), 8446–8449. https://doi.org/10.1016/j.tet.2010.08.058.

(153) Houghton, S. R.; Melton, J.; Fortunak, J.; Brown Ripin, D. H.; Boddy, C. N. Rapid, Mild Method for Phosphonate Diester Hydrolysis: Development of a One-Pot Synthesis of Tenofovir Disoproxil Fumarate from Tenofovir Diethyl Ester. *Tetrahedron* **2010**, *66* (41), 8137–8144. https://doi.org/10.1016/j.tet.2010.08.037.

(154) Kishore Kumar, G. D.; Saenz, D.; Lokesh, G. L.; Natarajan, A. Microwave-Assisted Cleavage of Phosphate, Phosphonate and Phosphoramide Esters. *Tetrahedron Lett* **2006**, *47* (35), 6281–6284. https://doi.org/10.1016/J.TETLET.2006.06.126.

(155) Kuzmič, P. *Program DYNAFIT for the Analysis of Enzyme Kinetic Data: Application to HIV Proteinase*; 1996; Vol. 237.

(156) Noedl, H.; Bronnert, J.; Yingyuen, K.; Attlmayr, B.; Kollaritsch, H.; Fukuda, M. Simple Histidine-Rich Protein 2 Double-Site Sandwich Enzyme-Linked Immunosorbent Assay for Use in Malaria Drug Sensitivity Testing. *Antimicrob Agents Chemother* **2005**, *49* (8), 3575–3577. https://doi.org/10.1128/AAC.49.8.3575-3577.2005.

(157) Press, H. W.; Teukolsky, A. S.; Vetterling, T. W.; Flannery, P. B. *Numerical Recipes: The Art of Scientific Computing*, 3rd ed.; Cambridge University Press: New York, 2007; Vol. Chapter 15.

(158) Brücher, K.; Illarionov, B.; Held, J.; Tschan, S.; Kunfermann, A.; Pein, M. K.; Bacher, A.; Gräwert, T.; Maes, L.; Mordmüller, B.; Fischer, M.; Kurz, T. α-Substituted β-Oxa Isosteres of Fosmidomycin: Synthesis and Biological Evaluation. *J Med Chem* **2012**, *55* (14), 6566–6575. https://doi.org/10.1021/jm300652f.

(159) Hatae, N.; Kujime, E.; Yano, K.; Kizuka, M.; Ashida, R.; Choshi, T.; Nishiyama, T.; Okada, C.; Iwamura, T.; Yoshimura, T. Synthesis of N-ω-Phenylalkyl-4-(p-Chlorophenyl)-Piperidin-4-Ol Analogues with Potent Antiproliferative Activity against HCT-116 Cells. *Heterocycles* **2018**, *97* (1), 560–568. https://doi.org/10.3987/COM-18-S(T)25.

(160) Wang, Z. Appel Reaction. In *Comprehensive Organic Name Reactions and Reagents*; John Wiley & Sons, Inc.: Hoboken, NJ, USA, 2010. https://doi.org/10.1002/9780470638859.conrr022.

(161) Bhattacharya, A. K.; Thyagarajan, G. Michaelis-Arbuzov Rearrangement. *Chem Rev* **1981**, *81* (4), 415–430. https://doi.org/10.1021/cr00044a004.

(162) Gerrard, W.; Green, W. J. 568. Mechanism of the Formation of Dialkyl Alkylphosphonates. *Journal of the Chemical Society (Resumed)* **1951**, 2550–2553. https://doi.org/10.1039/jr9510002550.

(163) Lion, C. J.; Matthews, C. S.; Stevens, M. F. G.; Westwell, A. D. Synthesis, Antitumor Evaluation, and Apoptosis-Inducing Activity of Hydroxylated (E)-Stilbenes. *J Med Chem* **2005**, *48* (4), 1292–1295. https://doi.org/10.1021/jm049238e.

(164) Patel, C. H.; Dhanani, S.; Owen, C. P.; Ahmed, S. Synthesis, Biochemical Evaluation and Rationalisation of the Inhibitory Activity of a Range of 4-Substituted Phenyl Alkyl Imidazole-Based Inhibitors of the Enzyme Complex 17α-Hydroxylase/17,20-Lyase (P45017α). *Bioorg Med Chem Lett* **2006**, *16* (18), 4752–4756. https://doi.org/10.1016/j.bmcl.2006.06.092.

(165) Fronza, G.; Fuganti, C.; Serra, S.; Cisero, M.; Koziet, J. Stable Isotope Labeling Pattern of Resveratrol and Related Natural Stilbenes. *J Agric Food Chem* **2002**, *50* (10), 2748–2754. https://doi.org/10.1021/jf011103j.

(166) Soo S. Ko; George V. DeLucca; John V. Duncia; Joseph B. Santella; Daniel S. Gardner. N-Ureidoalkyl-Piperidines as Modulators of Chemokine Receptor Activity. US6331541. **1999**.

(167) Halpern, L. THE TRANSFER OF INORGANIC PHOSPHORUS ACROSS THE RED BLOOD CELL MEMBRANE. *Journal of Biological Chemistry* **1936**, *114* (3), 747–770. https://doi.org/10.1016/s0021-9258(18)74803-5.

(168) LEIBMAN, K. C.; HEIDELBERGER, C. The Metabolism of P32-Labeled Ribonucleotides in Tissue Slices and Cell Suspensions. *J Biol Chem* **1955**, *216* (2), 823–830. https://doi.org/10.1016/s0021-9258(19)81436-9.

(169) Wiemer, A. J. Metabolic Efficacy of Phosphate Prodrugs and the Remdesivir Paradigm. *ACS Pharmacol Transl Sci* **2020**, *3* (4), 613–626. https://doi.org/10.1021/acsptsci.0c00076.

(170) Botté, C. Y.; Dubar, F.; McFadden, G. I.; Maréchal, E.; Biot, C. Plasmodium Falciparum Apicoplast Drugs: Targets or Off-Targets? *Chem Rev* **2012**, *112* (3), 1269–1283. https://doi.org/10.1021/cr200258w.

(171) Knak, T.; Abdullaziz, M. A.; Höfmann, S.; Alves Avelar, L. A.; Klein, S.; Martin, M.; Fischer, M.; Tanaka, N.; Kurz, T. Over 40 Years of Fosmidomycin Drug Research: A Comprehensive Review and Future Opportunities. *Pharmaceuticals* **2022**, *15* (12), 1553. https://doi.org/10.3390/ph15121553.

(172) Behrendt, C. T. *Synthese Und Biologische Evaluation Inverser α-Aryl-Substituierter Fosmidomycin-Analoga*; 2011.

(173) Mikati, M. O.; Miller, J. J.; Osbourn, D. M.; Barekatain, Y.; Ghebremichael, N.; Shah, I. T.; Burnham, C. A. D.; Heidel, K. M.; Yan, V. C.; Muller, F. L.; Dowd, C. S.; Edwards, R. L.; Odom John, A. R. Antimicrobial Prodrug Activation by the Staphylococcal Glyoxalase GloB. *ACS Infect Dis* **2020**, *6* (11), 3064–3075. https://doi.org/10.1021/acsinfecdis.0c00582.

(174) *https://www.rcsb.org/structure/3WQQ*.

(175) Marc, G.; Araniciu, C.; Dafina Oniga, S.; Vlase, L.; Pîrnău, A.; Duma, M.; Carmen Chifiriuc, M.; Oniga, O.; Barniol-Xicota, M.; Ruiz Santa Quiteria Saavedra, M.; Muñoz-Torrero, D. Molecules New N-(Oxazolylmethyl)-Thiazolidinedione Active against Candida Albicans Biofilm: Potential Als Proteins Inhibitors. **2018**. https://doi.org/10.3390/molecules23102522.

(176) Grottelli, S.; Annunziato, G.; Pampalone, G.; Pieroni, M.; Dindo, M.; Ferlenghi, F.; Costantino, G.; Cellini, B. Identification of Human Alanine–Glyoxylate Aminotransferase Ligands as Pharmacological Chaperones for Variants Associated with Primary Hyperoxaluria Type 1. *J Med Chem* **2022**, *65* (14), 9718–9734. https://doi.org/10.1021/acs.jmedchem.2c00142.

(177) Kim, I.-H.; Lee, I.-H.; Nishiwaki, H.; Hammock, B. D.; Nishi, K. Structure–Activity Relationships of Substituted Oxyoxalamides as Inhibitors of the Human Soluble Epoxide Hydrolase. *Bioorg Med Chem* **2014**, *22* (3), 1163–1175. https://doi.org/10.1016/j.bmc.2013.12.027.

(178) Jones, E. V.; Chen, D.; Wright, S. W.; Trujillo, J. I.; France, S. Elucidation of a Sequential Iminium Ion Cascade Reaction Triggered by a Silica Gel-Promoted Aza-Peterson Reaction. *J Org Chem* **2020**, *85* (23), 15660–15666. https://doi.org/10.1021/acs.joc.0c02102.

(179) Xie, J.; Xu, C.; Dai, Q.; Wang, X.; Xu, G.; Chen, Y.; Dai, L. Synthesis and Application of a Novel Asymmetric Azo Reagent: 1-(Tert -Butyl)-2-(4-Chlorobenzyl) Azodicarboxylate (TBCAD). *Tetrahedron* **2017**, *73* (35), 5321–5326. https://doi.org/10.1016/j.tet.2017.07.033.

(180) Terent'ev, A. O.; Krylov, I. B.; Lipatnikov, A. D. Oxidative Coupling of N-Hydroxyphthalimide with Toluene. *Russ J Gen Chem* **2014**, *84* (11), 2084–2087. https://doi.org/10.1134/S1070363214110061.

(181) Saczewski, J.; Hudson, A. L.; Rybczyńska, A. 2-[(Arylmethoxy)Imino]Imidazolidines with Potential Biological Activities. *Acta Pol Pharm* **2009**, *66* (6), 671–680.

(182) Wang, M.-Z.; Xu, H.; Liu, T.-W.; Feng, Q.; Yu, S.-J.; Wang, S.-H.; Li, Z.-M. Design, Synthesis and Antifungal Activities of Novel Pyrrole Alkaloid Analogs. *Eur J Med Chem* **2011**, *46* (5), 1463–1472. https://doi.org/10.1016/j.ejmech.2011.01.031.

(183) Shibuya, M.; Orihashi, T.; Li, Y.; Yamamoto, Y. N-Hydroxyphthalimide-Catalyzed Chemoselective Intermolecular Benzylic C–H Amination of Unprotected Arylalkanols. *Chemical Communications* **2021**, *57* (70), 8742–8745. https://doi.org/10.1039/D1CC03466A.

(184) Zhou, Y.; Li, J.; Yuan, H.; Su, R.; Huang, Y.; Huang, Y.; Li, Z.; Wu, Y.; Luo, H.; Zhang, C.; Huang, L. Design, Synthesis, and Evaluation of Dihydropyranopyrazole Derivatives as Novel PDE2 Inhibitors for the Treatment of Alzheimer's Disease. *Molecules* **2021**, *26* (10), 3034. https://doi.org/10.3390/molecules26103034.

(185) Kobayashi, M.; Itoh, S.; Yoshimura, K.; Tsukamoto, Y.; Obora, Y. Iridium Complex-Catalyzed C2-Extension of Primary Alcohols with Ethanol via a Hydrogen Autotransfer

Reaction. *J Org Chem* **2020**, *85* (18), 11952–11958. https://doi.org/10.1021/acs.joc.0c01540.

(186) Hatae, N.; Yoshimura, T.; Kujime, E.; Yano, K.; Kizuka, M.; Ashida, R.; Choshi, T.; Nishiyama, T.; Okada, C.; Iwamura, T. Synthesis of N-ω-Phenylalkyl-4-(p-Chlorophenyl)-Piperidin-4-Ol Analogues with Potent Antiproliferative Activity Against HCT-116 Cells. *Heterocycles* **2018**, *97* (1), 560. https://doi.org/10.3987/COM-18-S(T)25.

(187) Fyfe, T. J.; Kellam, B.; Sykes, D. A.; Capuano, B.; Scammells, P. J.; Lane, J. R.; Charlton, S. J.; Mistry, S. N. Structure–Kinetic Profiling of Haloperidol Analogues at the Human Dopamine D $_2$ Receptor. *J Med Chem* **2019**, *62* (21), 9488–9520. https://doi.org/10.1021/acs.jmedchem.9b00864.

(188) Sulsky, R.; Demers, J. P. Alkylation of N-Benzyloxyureas and Carbamates. *Tetrahedron Lett* **1989**, *30* (1), 31–34. https://doi.org/10.1016/S0040-4039(01)80314-2.

(189) Pflieger, M.; Sönnichsen, M.; Horstick-Muche, N.; Yang, J.; Schliehe-Diecks, J.; Schöler, A.; Borkhardt, A.; Hamacher, A.; Kassack, M. U.; Hansen, F. K.; Bhatia, S.; Kurz, T. Oxa Analogues of Nexturastat A Demonstrate Improved HDAC6 Selectivity and Superior Antileukaemia Activity. *ChemMedChem* **2021**, *16* (11), 1799–1804. https://doi.org/10.1002/cmdc.202001011.

(190) Kunfermann, A.; Lienau, C.; Illarionov, B.; Held, J.; Gräwert, T.; Behrendt, C. T.; Werner, P.; Hähn, S.; Eisenreich, W.; Riederer, U.; Mordmüller, B.; Bacher, A.; Fischer, M.; Groll, M.; Kurz, T. IspC as Target for Antiinfective Drug Discovery: Synthesis, Enantiomeric Separation, and Structural Biology of Fosmidomycin Thia Isosters. *J Med Chem* **2013**, *56* (20), 8151–8162. https://doi.org/10.1021/jm4012559.

(191) de Carvalho, L. P.; Sandri, T. L.; José Tenório de Melo, E.; Fendel, R.; Kremsner, P. G.; Mordmüller, B.; Held, J. Ivermectin Impairs the Development of Sexual and Asexual Stages of Plasmodium Falciparum *In Vitro*. *Antimicrob Agents Chemother* **2019**, *63* (8). https://doi.org/10.1128/AAC.00085-19.

(192) Trager, W.; Jensen, J. B. Human Malaria Parasites in Continuous Culture. *Science (1979)* **1976**, *193* (4254), 673–675. https://doi.org/10.1126/science.781840.

(193) Ribaut, C.; Berry, A.; Chevalley, S.; Reybier, K.; Morlais, I.; Parzy, D.; Nepveu, F.; Benoit-Vical, F.; Valentin, A. Concentration and Purification by Magnetic Separation of the Erythrocytic Stages of All Human Plasmodium Species. *Malar J* **2008**, *7* (1), 45. https://doi.org/10.1186/1475-2875-7-45.

(194) Noedl, H.; Bronnert, J.; Yingyuen, K.; Attlmayr, B.; Kollaritsch, H.; Fukuda, M. Simple Histidine-Rich Protein 2 Double-Site Sandwich Enzyme-Linked Immunosorbent Assay for Use in Malaria Drug Sensitivity Testing. *Antimicrob Agents Chemother* **2005**, *49* (8), 3575–3577. https://doi.org/10.1128/AAC.49.8.3575-3577.2005.

(195) Mishra, S. J.; Liu, W.; Beebe, K.; Banerjee, M.; Kent, C. N.; Munthali, V.; Koren, J.; Taylor, J. A.; Neckers, L. M.; Holzbeierlein, J.; Blagg, B. S. J. The Development of Hsp90β-Selective Inhibitors to Overcome Detriments Associated with *Pan* -Hsp90 Inhibition. *J Med Chem* **2021**, *64* (3), 1545–1557. https://doi.org/10.1021/acs.jmedchem.0c01700.